Michel O. Deville
Thomas B. Gatski

Mathematical Modeling for Complex Fluids and Flows

Springer

Mathematical Modeling for Complex Fluids and Flows

Michel O. Deville • Thomas B. Gatski

Mathematical Modeling for Complex Fluids and Flows

Springer

Michel O. Deville
Institute of Mechanical Engineering
Swiss Federal Institute of Technology
EPFL
Lausanne, Switzerland

Thomas B. Gatski
Institute PPRIME
CNRS-Université de Poitiers-ENSMA
Futuroscope Chasseneuil, France
and
Center for Coastal Physical Oceanography
and Ocean, Earth and Atmospheric
Sciences
Old Dominion University
Norfolk, USA

ISBN 978-3-642-25294-5 e-ISBN 978-3-642-25295-2
DOI 10.1007/978-3-642-25295-2
Springer Heidelberg Dordrecht London New York

Library of Congress Control Number: 2011945605

Mathematics Subject Classification (2010): 76A05, 76F55, 76F65

Printed on acid-free paper

Springer is part of Springer Science+Business Media (www.springer.com)

A theory has only the alternative of being right or wrong. A model has a third possibility: it may be right, but irrelevant.

Manfred Eigen

To our wives Christina and Rosann and our families

Preface

The book is intended to provide researchers and engineering practitioners in fluid flows with a state-of-the-art knowledge in continuum concepts and the associated fluid dynamics. It further exploits the implicit link between the turbulent flow of classical Newtonian fluids and the laminar and turbulent flow of non-Newtonian fluids needed in many applications such as food processing and polymeric flows. The underlying basis of the presentation will be primarily continuum modeling and will focus on tensorial constitutive relations needed to solve complex flow situations. The notion of complexity will be defined for both the fluids and the flows, and the interplay between the observed phenomena and the capabilities offered by the continuum theory will be highlighted where possible.

The reader is assumed to have a basic knowledge in standard continuum and fluid mechanics, that is, tensor algebra, and basic concepts of kinematics or dynamics of the fluid and flow stress tensor. The monograph will present the mathematical foundation to write meaningful constitutive equations and relevant fluid flow models. These equations are nonlinear most of the time and quite complicated to solve. In order to aid in the clarity, an effort has been made to conserve the usual topical mathematical notation within the complex fluid (viz. the continuum mechanics) and complex flow (viz. turbulent dynamics) communities. The solution methods require numerical methods and algorithms. However, this book does not address this topic as it deserves by itself a full manuscript. We refer the reader to the available specialized literature that covers these subjects.

The presentation of the material will range from the fundamental to the practical. For the fundamental, a focus on kinematic and dynamic considerations will prevail and related to the formation of constitutive relations for the fluid and flow stress fields. For the practical, current methods of solution including the direct numerical simulation, the scale-resolving simulation and the Reynolds-averaged method will be presented for both the Newtonian and non-Newtonian fluids. Some discussion will be presented on emerging technologies associated with multi-scale methods and a resurgence of the lattice-Boltzmann method.

Although numerical simulations are rapidly becoming the main tools for technological innovation and novel design, the book is aimed at the mathematical methodologies for the development of theoretical models needed to incorporate the requisite

physics, that in modern engineering, has to be predicted and understood before any manufacturing is involved. Important technologies associated with the global solutions for ground and air transportation including vehicular drag reduction, noise generation, and cabin ventilation and acoustics, are dependent on these models. Equally, or possibly more, important are the technologies associated with the understanding, and possible prediction, of the global environment.

We are grateful to our colleagues Nicolas Fiétier, Orestis Malaspinas, Rémi Manceau, Tim Phillips and Chris Rumsey who have provided valuable commentary on both the content and presentation of the material. We are also very appreciative of the financial support provided by the Région Poitou-Charentes, Programme Régional de Bourses de Chercheur Invité (MOD) and by the poste de Professeur Invité, École Polytechnique Fédérale de Lausanne, School of Engineering (TBG) during the preparation of this manuscript.

Lausanne, Switzerland — Michel O. Deville
Williamsburg, USA — Thomas B. Gatski

Contents

Nomenclature

Roman Letters

a	bead radius
$\mathbf{a}$	acceleration vector
a_i	coefficients
$\boldsymbol{A}_n$	n-th order Rivlin-Ericksen tensor
$\mathcal{A}$	generic variable
$\mathcal{A}_{ij}$	tensor function
b	length of rod (Rouse model)
b_{ij}, $\mathbf{b}$	Reynolds stress anisotropy tensor
$\boldsymbol{B}$	anisotropic mobility tensor, left Cauchy-Green tensor
$\mathcal{B}$	body
$\boldsymbol{b}_v$	viscoelastic extra-stress tensor anisotropy
$\mathbf{B}$	Brownian force
c_l	lattice speed of sound
c_s	speed of sound
c_v	specific heat at constant volume
$\mathbf{c}$	translation vector
C	Courant number
$\boldsymbol{C}$	right Cauchy-Green tensor
$\boldsymbol{c}$	conformation tensor
$\mathring{\boldsymbol{c}}$	Gordon-Schowalter convected derivative
$\boldsymbol{C}_{(t)}^{-1}$	relative Finger strain tensor
C_{ij}	cross tensor
C_s	Smagorinsky constant
$C_{\varepsilon 1}$	closure coefficient for production-of-dissipation rate term
$C_{\varepsilon 2}$	closure coefficient for destruction-of-dissipation rate term
$\mathcal{C}[\cdot,\cdot]$	collision operator
$\mathbf{d}$	dumbbell orientation vector
$\mathrm{d}\mathcal{V}$	volume element
$\boldsymbol{D}$	rate of deformation tensor
$\mathbf{D}$	Drag force

d_{ij}^t	turbulent transport anisotropy
d_{ij}^ε	dissipation rate anisotropy
De	Deborah number
D_{ij}^t	turbulent transport term
D_{pij}^t	polymeric turbulent transport term
D_ε^*	viscous diffusion of dissipation
$DxQy$	lattice denomination
e	internal energy
$\mathbf{e}$	unit vector
e_{ij}	Eulerian strain tensor
e_{ijk}	Levi-Civita permutation tensor
E	energy
E_{ij}	infinitesimal strain tensor
$\mathcal{E}$	subgrid dissipation term
$\boldsymbol{f}$	tangent correlation function
$\overline{f}$	filtered (resolved) or averaged part of f
F	Helmholtz free energy
$\mathfrak{F}$	stress functional
$\boldsymbol{\mathcal{F}}$	deformation gradient tensor
$\boldsymbol{\mathcal{F}}_{(t)}$	relative deformation gradient tensor
$\mathbf{g}$	external force
G	elastic modulus
$\boldsymbol{G}$	Oseen-Burgers tensor
$\mathcal{G}$	filter
$\mathfrak{S}$	constitutive functional
H	thermodynamic quantity
$\mathcal{H}$	Heaviside function
$\boldsymbol{\mathcal{H}}^{(n)}$	Hermite polynomials
$\boldsymbol{I}$	identity or unit tensor
I_d	identity operator
J	Jacobian
$\mathcal{J}$	invariant function
k	spring stiffness
k_B	Boltzmann constant ($1.381\,10^{-23}$ JK^{-1})
k_s	entropic spring stiffness
k_T	thermal conductivity
K	turbulent kinetic energy
Kn	Knudsen number
K_V	resolved scale kinetic energy
L	reference length
L	integral scale
$\boldsymbol{L}$	second-order tensor
L_{ij}	velocity gradient tensor, Leonard tensor
m	body mass
$\mathcal{M}_{ijkl}$	tensor function

n	number density
n_p	number of polymer chains
$\mathbf{n}$	unit normal vector
N_1, N_2	normal stress differences
m	molecular mass
$\boldsymbol{O}$	orthogonal matrix
O	symmetry group
$\mathcal{O}$	order of
P, p	pressure
P	Peterlin function
$\mathcal{P}$	turbulent kinetic energy production
$\boldsymbol{P}$	Boltzmann pressure tensor
$P_\varepsilon^{1,2,3}$	production terms in dissipation rate equation
$\boldsymbol{\mathcal{P}}$	stress functional
$\mathbf{q}$	heat flux, Boltzmann-BGK energy flux
$\boldsymbol{q}$	square root of the relative Finger tensor
$\mathcal{Q}_\mathcal{V}$	volumetric heat
$\boldsymbol{Q}$	proper orthogonal tensor, polymeric orientation tensor
$\boldsymbol{Q}$	Boltzmann-BGK internal energy flux tensor
$\mathcal{Q}_{D,E}^P$	Hermite quadrature rule
$\mathbf{r}$	end-to-end vector
R	gas constant
$\mathbf{R}$	stochastic position vector
$\boldsymbol{R}$	rotation tensor
R_{ij}	residual or subgrid stress tensor
Re	Reynolds number
s	entropy density
s_a	length of arm paths (pom-pom model)
s_b	model length of the backbone (pom-pom model)
s_c	model length of arm withdrawal (pom-pom model)
$\mathcal{S}_\mathrm{e}$	external source term
$\boldsymbol{S}$	strain rate tensor
$\mathcal{S}$	surface
$\mathscr{S}$	stress functional
$\mathbf{t}$	surface force
$\boldsymbol{T}_k$	tensor basis term
T_ε	dissipation rate equation transport term
Tr	Trouton ratio
u_i	velocity vector
$\mathbf{u}$	tangent unit vector
U	reference velocity
$\boldsymbol{U}$	right stretch tensor
$\mathbf{v}$	velocity field
$\boldsymbol{V}$	left stretch tensor
$\mathcal{V}$	volume

$\boldsymbol{W}$	vorticity tensor
We	Weissenberg number
$\boldsymbol{W}$	rate of rotation tensor, Wiener process
X_α	Lagrangian coordinates
x_i	Eulerian coordinates

Greek Letters

α_i	coefficients
$\dot{\gamma}$	shear rate
$\boldsymbol{\Gamma}_v$	deviatoric viscoelastic stress
δ_{ij}	identity tensor
δ	Dirac function
Δ	spatial mesh size, spectral filter cut-off length
Δ_t	temporal filter width
ε	energy dissipation rate
ζ	Brownian motion friction coefficient
η	Kolmogorov scale
$\eta_{\alpha\beta}$	Lagrangian strain tensor
θ	absolute temperature
κ	wavenumber
$\boldsymbol{\varkappa}$	relative deformation at time τ
λ	mean free path, extension or stretch ratio, material relaxation time
λ_d	diffusion time
λ_i	eigenvalues of a matrix
λ_R	Rouse relaxation time
Λ	stretch ratio
μ	dynamic viscosity
μ_E	extensional viscosity
ν	kinematic viscosity
ν	number of strands per unit volume (Doi-Edwards model)
$\boldsymbol{\xi}$	displacement vector, Boltzmann particle velocity
$\boldsymbol{\Xi}$	extra-stress tensor
$\boldsymbol{\Xi}_p$	polymeric stress
$\boldsymbol{\Xi}_v$	viscoelastic extra-stress
Π_{ij}	pressure-strain rate correlation
ρ	mass density
$\boldsymbol{\Sigma}$	Cauchy stress tensor
$\boldsymbol{\Sigma}_J$	Jaumann stress
$\boldsymbol{\Sigma}_O$	Oldroyd stress
τ	integral turbulent time scale
τ_{ij}	Reynolds stress tensor, unresolved stress tensor
Υ	destruction of dissipation
$\boldsymbol{\Phi}_k$	tensor basis term
φ_b	fraction of backbone molecular weight (pom-pom model)
$\boldsymbol{\chi}$	deformation function

$\boldsymbol{\chi}_{(t)}$	relative deformation function
ψ	probability density function
$\boldsymbol{\omega}$	vorticity vector
ω'_k	fluctuating vorticity vector
ω	specific dissipation rate
Ω_{ij}	infinitesimal rotation tensor
$\boldsymbol{\Omega}$	spin tensor

Notations

$[\cdot]$	matrix
$[\cdot]^T$	transpose of a matrix
$\lvert\cdot\rvert$	norm of a vector or a tensor
$\mathrm{I}_1(\cdot)$, $\mathrm{I}_2(\cdot)$, $\mathrm{I}_3(\cdot)$	first, second, and third invariants of a tensor
$<\cdot>$	ensemble average
$\dot{(\,)}$	time derivative
$\overline{(\,)}$	Reynolds mean or filtered (resolved) variable
$\overset{\triangledown}{(\cdot)}$	upper convective derivative

Operators

$\cdot$	scalar product
$\otimes$	tensor product of vectors
$:$	inner product of two second-order tensors
$\boldsymbol{\nabla}$	nabla
$\boldsymbol{\nabla}^2$	Laplace operator
div	divergence of a vector
det	determinant of a matrix
$\mathrm{tr}\cdot$, $\{\cdot\}$	trace of a tensor
$\frac{D}{Dt}$	material time derivative
$\frac{\mathcal{D}_B}{\mathcal{D}t}$	rate of change in phase space
$\frac{\mathcal{D}_H}{\mathcal{D}t}$	Harnoy derivative
$\frac{\mathcal{D}}{\mathcal{D}t}$	Jaumann or corotational derivative

Chapter 1
Introduction

Fluids and flows are pervading our daily lives without our conscious perception. The air we breathe, the shower in the bathroom with the shampoo, coffee or tea, the blood in our vascular tree including the heart and the brain, the ingredients of food like mayonnaise, oil, vinegar, yogurt, etc. The design and the engineering of new materials like polymers, plastics, ceramics, foams, etc., have produced complex fluids because the materials processing based on extrusion, molding, blowing, etc. is using them in the fluid state. Note that in polymers the presence of long molecular chains and their entanglement affect the mechanical behavior of the fluid. Therefore fluids are flowing around us in a swirl of natural events and of technological applications. Most flows in nature are complex due to their turbulent character: river and ocean currents, waves on a beach, storms, hurricanes, tsunamis, ... Many technological applications use turbulence to achieve the goal of the design, for example homogeneous mixing in materials processing. Moreover the understanding of the turbulent phenomena may lead to avoid them or reduce their intensity and thereby their effects, for example, in the design of hydraulic machines. These flows and fluids are reputed as complex. Therefore we need to better understand the meaning of this epithet.

Complexity is of course contrary to simplicity. A flow is simple when the associated geometrical patterns are simple themselves like the parallel streamlines in the so-called parallel flows as the plane Couette and Poiseuille flows. Here the physics is also simple and most of the time, the fluid dynamicist has an intuitive "a priori" feeling about how the solution will look like. In some sense the answer is rather obvious. But simplicity is also connected to linearity which implies that the observed effect is directly proportional to the cause coming either from pressure or shear. The Navier-Stokes equations that govern the dynamics of viscous fluid flows are non-linear from a mathematical standpoint. A linear combination of two (or several) solutions is no longer a solution. This non-linear character impedes our natural way of thinking based on reductionism to obtain a quick correct answer, because non-linearity has a deep (and sometimes, unexpected) influence on the resulting physics. Non-linear problems are extremely difficult to tackle through analytical tools. Numerical methods leading to numerical simulation constitute the state-of-the-art practice in physics and engineering. The demand for general and accurate

M.O. Deville, T.B. Gatski, *Mathematical Modeling for Complex Fluids and Flows*,
DOI 10.1007/978-3-642-25295-2_1,

models is very high and leads to the elaboration of advanced concepts that will be the major theme of this monograph.

Complexity not only comes from the physics of the flow or the fluid mechanical behavior, it may also be a consequence of the geometrical configuration. This is especially true in engineering where complicated shapes are involved like for example, airfoils, blades, runners, space shuttle, airplane body, wings, etc. The interplay between all parameters: geometry, flow and fluid renders the problems quite intricate and involved. We will address flow and fluid complexity separately leaving for case studies, the full aspect of the three complexity sources.

1.1 Complex Fluids

Complex fluids are designated as non-Newtonian or more generally as viscoelastic because their mechanical behavior does not fit the pattern of the classical Newtonian fluids represented, for example, by water in standard conditions. The Newtonian constitutive equation is given by the relationship

$$\boldsymbol{\Sigma} = -p\,\boldsymbol{I} + 2\mu\,\boldsymbol{D}\,, \tag{1.1}$$

where $\boldsymbol{\Sigma}$ denotes the Cauchy stress tensor, p the pressure, $\boldsymbol{I}$ the identity tensor, μ the dynamic shear viscosity, and $\boldsymbol{D}$ the rate of deformation tensor defined as the symmetric part of the velocity gradient

$$\boldsymbol{D} = \frac{1}{2}\left(\boldsymbol{\nabla}\mathbf{v} + (\boldsymbol{\nabla}\mathbf{v})^T\right)\,, \tag{1.2}$$

where $\mathbf{v}$ is the velocity field, $\boldsymbol{\nabla}\mathbf{v}$ is the velocity gradient, and the superscript T indicates the transpose. It is not surprising that when writing about two somewhat diverse topics that notational ambiguities arise. As just defined, the tensor $\boldsymbol{D}$ is termed the rate of deformation tensor in the rheology community; whereas, in the fluid mechanics community it is termed the rate of strain or strain rate tensor and denoted by $\boldsymbol{S}$.

The constitutive equation (1.1) is indeed linear as it is based only on the first power of $\boldsymbol{D}$. Water is clearly a good real world example of such a fluid responding to this kind of mechanical behavior.

A first class of non-Newtonian fluids is concerned with the generalized Newtonian fluids where the dynamic shear viscosity μ is dependent of the shear rate $\dot{\gamma}$ that is obtained from the second invariant of the tensor $\boldsymbol{D}$ such that $\dot{\gamma} = \sqrt{(2\boldsymbol{D} : \boldsymbol{D})}$. (In index notation, $\boldsymbol{D} : \boldsymbol{D}$ is given by $D_{ij}D_{ji}$ where the Einstein summation convention of repeated indices is used throughout unless otherwise noted.) This then leads to

$$\boldsymbol{\Sigma} = -p\boldsymbol{I} + 2\mu\,(\dot{\gamma})\,\boldsymbol{D}\,. \tag{1.3}$$

Shear-thinning or pseudo-plastic effects are present in most polymer flows or melts, and this is also the case of blood flow. A very popular relation is the power law

$$\mu(\dot{\gamma}) = K\,\dot{\gamma}^{n-1}\,, \tag{1.4}$$

where K is the consistency factor and n the power law index ($n = 1$ for the Newtonian case). For many polymers, the value of n lies between 0.3 and 0.6. Shear-thinning fluids have $n < 1$ while shear-thickening or dilating fluids are those with $n > 1$. When memory effects come into play, non-Newtonian fluids are called viscoelastic fluids that incorporate complicated and rather counter-intuitive physical phenomena.

1.1.1 Physical Considerations

The deviation of the flow field behavior of a non-Newtonian fluid from that of a Newtonian fluid is often quantified by normal stress field differences and characterized by fluid memory effects. The two are related and serve to identify key elements of the dynamic mechanisms responsible for the unique behavior of such fluids in even relatively simple geometric flow fields.

1.1.1.1 Normal Stress Effects

Newtonian fluids do not show imbalance in the first normal stress differences defined by the relations

$$N_1 = \Sigma_{11} - \Sigma_{22}, \quad N_2 = \Sigma_{22} - \Sigma_{33} \tag{1.5}$$

in simple shear flows. On the contrary for non-Newtonian fluids, $N_1 \neq 0$ and $N_2 \neq 0$. A spectacular experiment is the Weissenberg effect occurring in a cylindrical Couette device with a free surface when the inner cylinder rotates and the outer one is fixed. For the Newtonian case, under the centrifugal forces, the surface deforms and takes a paraboloid shape climbing along the exterior cylinder. A small trough is formed close to the inner cylinder. For the non-Newtonian case, the fluid rises up the inner shaft draining in some situations the container, Fig. 1.1. Another interesting effect is the swelling that is characteristic of the jet flowing out of a die. For the Newtonian fluid, the jet shape remains almost constant at the die outflow section. In the non-Newtonian test, the jet swells and can take three to four times the diameter of the orifice, see Fig. 1.2.

1.1.1.2 Memory Considerations

Memory effects are induced by the fact that the present time stresses depend on the history of deformation of the fluid. When submitted to a brief and intense force, the viscoelastic fluid behaves as an elastic solid while over very long time intervals, its response is that of a viscous fluid. Between these two situations, one gets the viscoelastic behavior. Viscoelastic fluids are characterized by stress relaxation. To maintain a constant deformation in the fluid, the applied force decreases over time in

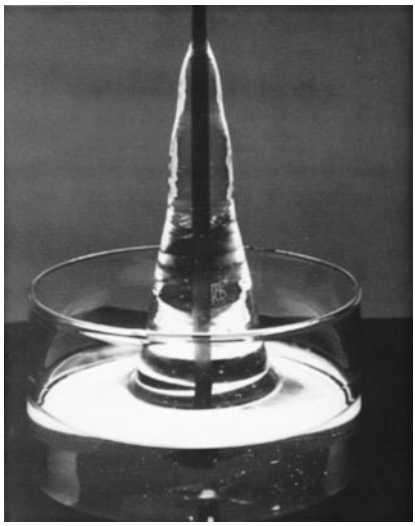

Fig. 1.1 Example of the Weissenberg effect with fluid rising up the inner cylinder of a Couette device[1]

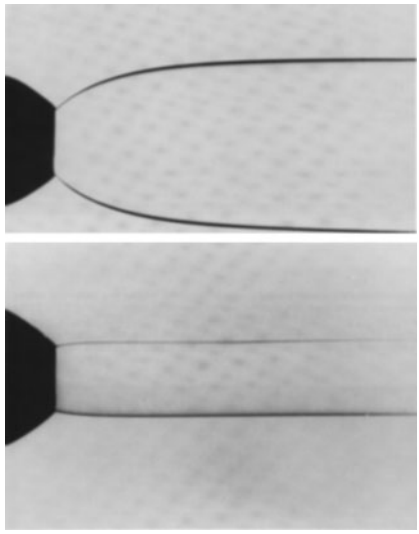

Fig. 1.2 Example of the die swell phenomenon: *top*, non-Newtonian fluid; *bottom*, Newtonian fluid

an exponential fashion. They present also the phenomenon of creep which produces under a constant force a permanent deformation depending on time. For example, it is well known that stained glass windows in cathedrals are thicker at the bottom than at the top because gravity has been acting over the centuries. On the other side if a glass pane is hit by a soft ball, it reacts as an elastic solid. This example shows that the choice of the constitutive relationship depends strongly on the physics to be modeled.

[1]Figures 1.1 and 1.2 reprinted with permission from: D.V. Boger, K. Walters (1993) Rheological Phenomena in Focus. Elsevier Science Ltd., Amsterdam.

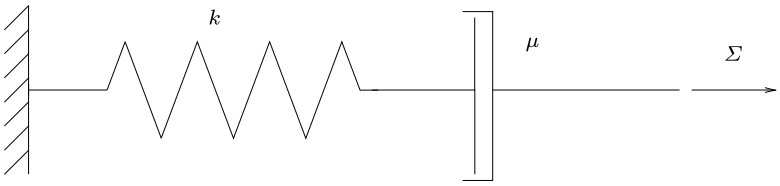

Fig. 1.3 Schematic of Maxwell linear viscoelastic mechanical model

1.1.2 Viscoelastic Fluids

Elementary models for viscoelastic fluids are easily described through mechanical analogs using springs and dashpots. A very simple viscoelastic model is made of a spring with constant stiffness k for the elastic part and a dashpot of viscosity μ (see Fig. 1.3). For example, the Maxwell model connects these two mechanical elements in series with an intrinsic characteristic time of the model being $\lambda = \mu/k$. The one-dimensional (1D) stress-strain relation for the spring is $\Sigma = k\,\epsilon_1$, and for the dashpot $\Sigma = \mu\,\dot{\epsilon}_2$. The same stress (force), Σ, applied to the model generates a displacement Σ/k in the spring and a velocity Σ/μ in the dashpot. The total velocity is then given by the sum

$$\dot{\epsilon} = \dot{\epsilon}_1 + \dot{\epsilon}_2 = \frac{\dot{\Sigma}}{k} + \frac{\Sigma}{\mu}\ , \tag{1.6a}$$

that is,

$$\Sigma + \lambda\dot{\Sigma} = \mu\dot{\epsilon}\ . \tag{1.6b}$$

With the aim of generalizing this relation to a viscoelastic fluid, the Cauchy stress tensor is split into two parts

$$\boldsymbol{\Sigma} = -p\boldsymbol{I} + \boldsymbol{\Xi}\ , \tag{1.7}$$

where the deviatoric tensor $\boldsymbol{\Xi}$ also called the extra-stress tensor is decomposed into a viscoelastic component $\boldsymbol{\Xi}_v$ and a purely viscous component

$$\boldsymbol{\Xi} = \boldsymbol{\Xi}_v + 2\mu_0\boldsymbol{D} \tag{1.8}$$

with μ_0 the Newtonian dynamic viscosity (e.g., the viscosity of the Newtonian solvent in which the polymer is diluted).

A straightforward three-dimensional extension of Eq. (1.6b) might be written as

$$\boldsymbol{\Xi}_v + \lambda\frac{d\boldsymbol{\Xi}_v}{dt} = 2\mu_1\boldsymbol{D}\ , \tag{1.9}$$

where μ_1 characterizes the viscoelastic viscosity. Unfortunately, as will be detailed later in Chap. 4, Eq. (1.9) cannot be accepted since the total derivative of the stress tensor is not objective and would violate the Principle of Material Indifference. As will be discussed in detail later, it is necessary to introduce the upper-convective derivative, denoted by $\overset{\nabla}{\boldsymbol{\Xi}}_v$, to resolve this difficulty,

$$\overset{\nabla}{\boldsymbol{\Xi}}_v = \frac{d\boldsymbol{\Xi}_v}{dt} - (\nabla\mathbf{v})\boldsymbol{\Xi}_v - \boldsymbol{\Xi}_v(\nabla\mathbf{v})^T\ . \tag{1.10}$$

The upper-convective derivative is one of the objective forms of the temporal derivative. The combination of Eqs. (1.7), (1.8) and (1.10) defines the Oldroyd-B fluid which incorporates many features of the Boger fluid that is used in experiments. For example, in steady state simple shear flow this model yields a constant viscosity, a N_1 that is quadratic in $\dot{\gamma}$ and $N_2 = 0$.

1.1.3 Viscometric Flows

In a viscometric flow, the fluid particle undergoes a history characterized by constant stretching. To investigate those flows it is necessary to introduce mathematical considerations on kinematics and of general principles on constitutive equations. This will be undertaken in later chapters, but the book by Coleman et al. (1966) constitutes a landmark of this theory. For the purposes of this introduction only the following simple nonlinear model will be considered:

$$\boldsymbol{\Sigma} = -p\boldsymbol{I} + K_1\left(\mathrm{I}_2\left(\boldsymbol{D}\right), \mathrm{I}_3\left(\boldsymbol{D}\right)\right)\boldsymbol{D} + K_2\left(\mathrm{I}_2\left(\boldsymbol{D}\right), \mathrm{I}_3\left(\boldsymbol{D}\right)\right)\boldsymbol{D}^2\,, \tag{1.11}$$

where K_1, K_2 are scalar functions of the second, $\mathrm{I}_2\left(\boldsymbol{D}\right)$, and third, $\mathrm{I}_3\left(\boldsymbol{D}\right)$, invariants of the tensor $\boldsymbol{D}$ defined by

$$\begin{aligned} \mathrm{I}_2\left(\boldsymbol{D}\right) &= \frac{1}{2}\left(\left(tr\,\boldsymbol{D}\right)^2 - tr\left(\boldsymbol{D}^2\right)\right) = -\frac{1}{2}\,tr\left(\boldsymbol{D}^2\right), \\ \mathrm{I}_3\left(\boldsymbol{D}\right) &= \det \boldsymbol{D}, \end{aligned} \tag{1.12}$$

and where for an incompressible fluid $tr(\boldsymbol{D})$, which is the first invariant $\mathrm{I}_1\left(\boldsymbol{D}\right)$, vanishes. The symbol tr represents the trace operator. This model is the Reiner-Rivlin fluid which is a particular case of the Rivlin-Ericksen fluid of second-order. Notice that if $K_2 \equiv 0$ and $K_1 = \mu$, the Newtonian case is recovered.

1.1.3.1 Plane Shear Flow

Let us consider the simple shear flow of the Reiner-Rivlin fluid (see Eq. (1.11)) in a Cartesian orthonormal coordinate system

$$v_1 = \dot{\gamma}\, x_2, \quad v_2 = v_3 = 0\,. \tag{1.13}$$

The components D_{ij} of the tensor $\boldsymbol{D}$ vanish except for $D_{12} = D_{21} = \dot{\gamma}/2$, which then leads to $\mathrm{I}_2\left(\boldsymbol{D}\right) = -\dot{\gamma}^2/4$ and $\mathrm{I}_3\left(\boldsymbol{D}\right) = 0$. We will denote the matrices associated with tensors by their symbol in between square brackets. Therefore the matrices $[D]$, $[D^2]$ are given by

$$[D] = \begin{pmatrix} 0 & \frac{\dot{\gamma}}{2} & 0 \\ \frac{\dot{\gamma}}{2} & 0 & 0 \\ 0 & 0 & 0 \end{pmatrix}, \quad \left[D^2\right] = \begin{pmatrix} \frac{\dot{\gamma}^2}{4} & 0 & 0 \\ 0 & \frac{\dot{\gamma}^2}{4} & 0 \\ 0 & 0 & 0 \end{pmatrix}. \tag{1.14}$$

The corresponding stress components are then

$$\Sigma_{11} = \Sigma_{22} = -p + K_2 \frac{\dot{\gamma}^2}{4}, \quad \Sigma_{33} = -p \,, \tag{1.15a}$$

$$\Sigma_{12} = \Sigma_{21} = K_1 \frac{\dot{\gamma}}{2} = \tau(\dot{\gamma}) \,, \tag{1.15b}$$

$$\Sigma_{13} = \Sigma_{23} = 0 \,, \tag{1.15c}$$

with the resulting normal stress differences being

$$N_1 = 0 \quad \text{and} \quad N_2 = K_2 \frac{\dot{\gamma}^2}{4} \,. \tag{1.16}$$

However, this does not correspond to the physical reality as experimental data show $N_1 \neq 0$ and $N_2 \neq 0$. We therefore need a different kind of model to resolve the right normal stress differences. It can be shown that the three functions N_1, N_2, τ do depend on the nature of the fluid, and are called the viscometric functions of the material.

1.1.3.2 Circular Couette Flow

The circular Couette flow occurs in the gap between two rotating concentric cylinders. The inner cylinder of radius R_1 has the angular velocity ω_1 while the outer cylinder of radius R_2 spins at ω_2. The apparatus has a height H which is much larger than either cylinder radii so that the apparatus height is assume infinite. If we refer to a cylindrical coordinates system r, θ, z (with r, θ and z, the radial, azimuthal and axial coordinates, respectively), the steady state velocity field is such that

$$v_r = 0, \quad v_\theta = v_\theta(r), \quad v_z = 0 \,. \tag{1.17}$$

This v_θ velocity field is then determined from the integration of the θ-momentum equation

$$\frac{1}{r^2} \frac{d}{dr} \left(r^2 \, \Sigma_{r\theta} \right) = 0 \,. \tag{1.18}$$

It can be shown that the velocity field for the constitutive equation (1.11) is then given by

$$v_\theta = \frac{\omega_2 R_2^2 - \omega_1 R_1^2}{R_2^2 - R_1^2} r - \frac{(\omega_2 - \omega_1) R_1^2 R_2^2}{R_2^2 - R_1^2} \frac{1}{r} \,. \tag{1.19}$$

In the case of a fixed outer cylinder $\omega_2 = 0$ and the velocity is given by

$$v_\theta = Ar + \frac{B}{r} = \frac{\omega_1 R_1^2}{R_2^2 - R_1^2} \left(\frac{R_2^2}{r} - r \right) \,. \tag{1.20}$$

With the stress component

$$\Sigma_{rr} = -p + \frac{K_2}{4} \left(\frac{\partial v_\theta}{\partial r} - \frac{v_\theta}{r} \right)^2$$

the r-momentum equation

$$\frac{d\,\Sigma_{rr}}{dr} + \frac{1}{r}\,(\Sigma_{rr} - \Sigma_{\theta\theta}) = -\rho\frac{v_\theta^2}{r} \tag{1.21}$$

yields

$$-\frac{\partial p}{\partial r} + K_2\frac{\partial}{\partial r}\left(\frac{B^2}{r^4}\right) = -\rho\frac{v_\theta^2}{r}\,. \tag{1.22}$$

As $\Sigma_{zz} = -p$, one obtains

$$-\Sigma_{zz} = p = K_2\,\frac{B^2}{r^4}\bigg|_{R_1}^{r} + \int_{R_1}^{r}\rho\frac{v_\theta^2}{r}\,dr + C \tag{1.23}$$

$$= p(R_1) + K_2\,\frac{B^2}{r^4} + \int_{R_1}^{r}\rho\frac{v_\theta^2}{r}\,dr\,. \tag{1.24}$$

If the fluid is Newtonian, $K_2 = 0$ and the pressure increases from the inner to the outer cylinder. The fluid rises along the outer cylinder under centrifugal forces. For the non-Newtonian fluid, if $K_2 > 0$ and if B is sufficiently large under a high shear due to a small gap between the cylinders, the pressure increases when one approaches the inner cylinder and this produces the so-called rod-climbing effect.

1.2 Complex Flows

In order to study flow complexity, we will now choose simple geometries, the fluid being assumed incompressible, viscous and Newtonian. The flow phenomena in classical viscous Newtonian fluid dynamics are globally characterized via the dimensionless Reynolds number, Re, defined by the relation

$$Re = \frac{UL}{\nu}\,, \tag{1.25}$$

where U and L are reference velocity and length, respectively, and $\nu = \mu/\rho$ the kinematic viscosity of the fluid expressed in $\mathrm{m^2\,s^{-1}}$ in the international unit system. The volumetric mass ρ is usually called in English texts density, but this is a misnomer as density is defined as the ratio of the volumetric mass of the considered fluid to that of water. Water density is consequently equal to 1 while its volumetric mass is $\rho = 1000\,\mathrm{kg\,m^{-3}}$. For water, it is interesting to note that $\nu_{water} = 10^{-6}\ \mathrm{m^2\,s^{-1}}$. If U and L are both of the order of unity, the Reynolds number will be $O(10^6)$. We will observe later that this value is typical of turbulence, one of the major topics that will be developed later.

1.2.1 Physical Considerations: Circular Couette Flow

Let us return now to the circular Couette flow. For the Couette flow it is usual to choose the inner angular velocity $U = \omega_1 R_1$ and the gap $L = R_2 - R_1$ as reference quantities for the Reynolds number definition. For creeping flows, at very low

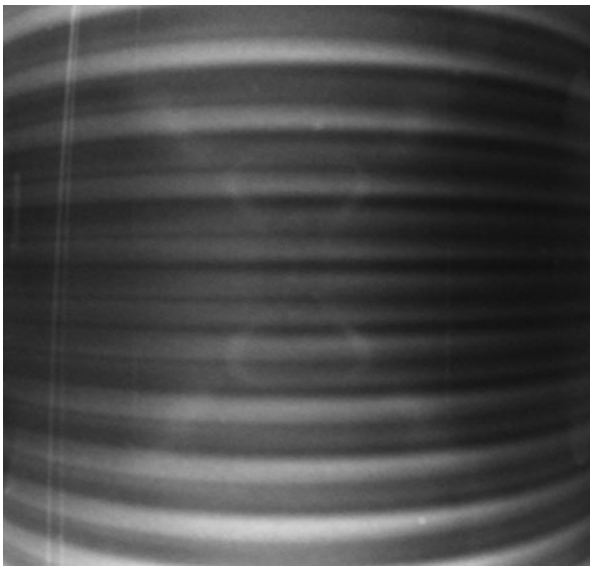

Fig. 1.4 Symmetric Taylor vortices. Courtesy of N. Borhani with permission

or vanishing Reynolds numbers, the flow is laminar. This indicates that the material fluid particles follow closed circles centered on the rotation axis. This situation is indeed simple and experimentally verified. When the Reynolds number increases, a first transition occurs and secondary flows are generated in the meridian r, z planes. They are superposed to the former Couette flow and we arrive at the situation of the Taylor vortices discovered in 1923 (Taylor 1923). Figure 1.4 shows the toroidal Taylor vortices pattern which is axisymmetric and steady-state, i.e. time independent. These vortices appear in counter rotating pairs and they are characterized by k_z, the axial wavenumber. The value at which the transition occurs is called the critical Reynolds number and will be denoted by Re_c. For example, Coles (1965) reports on a Couette flow where $\omega_2 = 0$ and the ratio of the radii $\eta = R_2/R_1 = 0.87$. For $Re < 41.5$ the flow is laminar and given by Eq. (1.19). The first critical Reynolds number $Re_{c,1}$ is reached at 42. Increasing the inner cylinder rotation, for $Re_{c,2} = 66$, a second transition occurs and the Taylor toruses are deformed in the azimuthal direction with k_θ the corresponding wavenumber. Figure 1.5 displays the steady-state wavy Taylor vortices pattern. Still increasing the Reynolds number, the geometrical vortices pattern is affected through changes in k_θ and k_z. At some Reynolds number value later transitions modify the number of vortex pairs and k_z accordingly in the axial direction, and the undulations of the azimuthal deformations, i.e. k_θ. These flows remain steady state.

The aspect ratio $\Gamma = H/(R_2 - R_1)$ has a significant influence on the physics of the Couette flow. Benjamin (1978) treats the case of short Couette cylinders with the end effects modifying the observations made on long devices. Koschmieder (1993) reviews the Taylor vortices state-of-the-art in the early nineties indicating the subsequent route to turbulence.

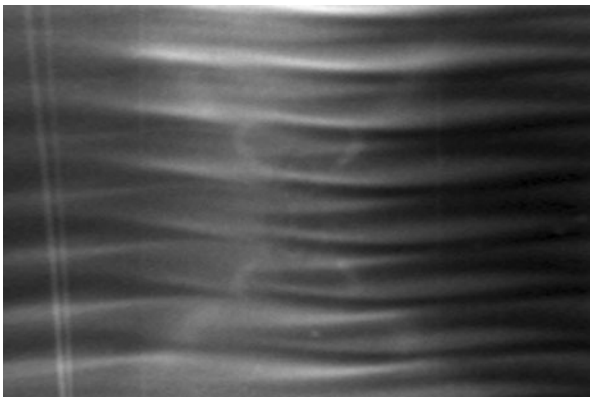

Fig. 1.5 Wavy Taylor vortices. Courtesy of N. Borhani with permission

1.2.2 Transitional Flows

It is difficult to quantify what is meant by transition. Broadly speaking, it is characterized by unsteady motion accompanied by a spectral broadening, in space and time, of the fluid motion. Flows that do transition between the laminar and turbulence state do have identifiable characteristics that mark the process.

For the Taylor-Couette flow, one can adopt the criterion that the flow will be in transition as soon as it becomes unsteady with or without small scale structures. Fenstermacher et al. (1979) carried out an experimental investigation of the time-dependent Taylor vortex and wavy vortex flows. Inspection of the velocity spectra showed that the first transition was a Hopf bifurcation, giving in phase space a limit cycle with a clearly identified period. The second transition was a quasi-periodic flow with two frequencies irrationally related. For higher Reynolds number, the sharp components and their subharmonics disappear and one gets a spectrum with a broad component and a background continuum. This feature is characteristic of weak turbulence also known as chaos, a theory that comes from nonlinear dynamics.

For flat plate boundary layer flows, the downstream transition to the turbulent state involves a sequence of linear to nonlinear instability mechanisms with an ever increasing broadening of the space-time spectral characteristics. Two types of transitions can occur (Schmid and Henningson 2001). One is a natural transition where unsteadiness in the oncoming flow or irregularities in the solid surface initiate this sequence of instabilities through a receptivity process. The other is a by-pass transition where strong disturbances (turbulence) in the oncoming flow void the naturally occurring sequence of instability and cause a sudden transition to the fully turbulent state on the plates. This latter type of transition often occurs in turbomachinery applications. Other factors significantly contribute to the detailed features of transitional flows including effects of pressure gradients, surface temperature, and Mach number.

The analysis and prediction of transitional flows has not developed as in the turbulent flow case. The formalisms have evolved from the study of the dynamics of

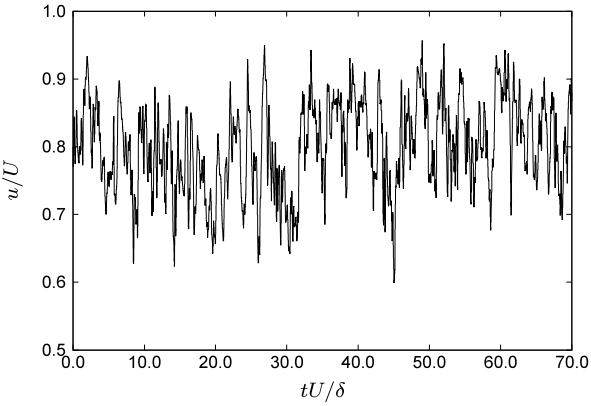

Fig. 1.6 Time variation of instantaneous velocity field at a fixed point within a turbulent boundary layer: U mean free-stream velocity and δ boundary layer thickness

deterministic disturbances rather than from the study of the dynamics of statistical quantities with associated probability density functions. In the latter case, constitutive equations are needed for higher-order (unknown) correlations. For this reason, the discussion of transitional flows will be minimal in the remainder of the text.

1.2.3 Turbulent Flows

Turbulence can be generated at (moderately) high value of the Reynolds number such that for many engineering flows, these values can range from $O(10^4 \ldots 10^6)$. Turbulence is rotational and three-dimensional, and is characterized by a high level of vorticity fluctuations. This is the reason why vorticity dynamics plays such an essential role in turbulence theory. Its origin comes from the flow instabilities engendered inside the governing equations by the interaction between the viscous and nonlinear terms of the acceleration. This interaction intensifies as the inertial effects dominate, that is for sufficiently high Reynolds numbers.

All turbulent flows have some general characterizing features that have varying degrees of prominence depending on particular conditions relative to each flow. The transient character of turbulent flows are never steady-state. They are irregular in space and time and present a random aspect (see Fig. 1.6) with an associated probability distribution. While all turbulent flows are unsteady, their statistical characteristics are not necessarily so. Such statistically steady, or stationary, flows are not uncommon and occur in many free shear and wall-bounded flows. Another important characteristic of a turbulent flow is the enhanced transport of energy brought on by the fluctuating velocity field. This enhanced transport implies high momentum and heat transfer, and brings a significant increase in passive scalar mixing. Such flow fields are important in materials processing in order to obtain better quality for the end product. A third feature is the dissipative character of the turbulence. Viscous shear stresses produce deformation work that increases the internal energy of the fluid at the expense of the turbulent kinetic energy. The turbulence will decrease

with time if energy is not provided to the fluid in order to counteract the friction losses which are more important than in the laminar case.

It is to be understood that turbulence is not an intrinsic feature of the fluid mechanical behavior, but is linked to the flow properties of the fluid. Thus, while in the description of complex (viscoelastic) fluids constitutive relations are necessary to characterize the fluid behavior, in the description of complex (turbulent) flows constitutive relations are necessary to characterize the flow behavior. This statement is a fundamental point in the developments to be presented and discussed throughout the book.

1.3 Elastic Turbulence

This topic has emerged about a decade and a half ago with the review paper of Shaqfeh (1996) on elastic instabilities in viscoelastic flows. At the beginning of this millennium Groisman and Steinberg (2000) showed experimentally in a plate-plate geometry that the velocity spectra were quite similar to the ones encountered in turbulence. This phenomenon was named elastic turbulence since it displayed characteristics of turbulence without dominant inertia since it occurred at very low Reynolds numbers. Groisman and Steinberg (2004) also confirmed the presence of elastic turbulence in curvilinear flows. In these situations the key parameter is the Weissenberg number, *We*, defined by the relation

$$We = \frac{\lambda U}{L} \,, \tag{1.26}$$

which plays a similar role as the Reynolds number for Newtonian fluids. The Weissenberg number measures the elasticity of the fluid as λ is the material relaxation time of the viscoelastic fluid and L/U is the inertial time of the flow ($We = 0$ corresponds to a Newtonian fluid). With increasing *We*, the flow physics changes drastically and the flow phenomena resembles classical turbulence. In the non-Newtonian case, the turbulence is built up by the elastic stresses that produce small-scale structures even at low Reynolds number. This is a consequence of the presence of the nonlinearities in constitutive equations such as the Oldroyd-B fluid. The elastic stresses induce anisotropy of the flow by the normal stress differences that cause the curvature of the streamlines. This mechanism leads to instability where some regions of high-shear generate and store locally elastic energy. By flow advection, this energy is transported to low shear zones where it enhances turbulence production. Recently Morozov and van Saarloos (2007) have assessed the state-of-the-art in a review (the authors call it an essay) about this complex physical phenomenon.

1.4 Examples of a Complex Fluid and Flow

To briefly illustrate the interesting type of phenomena that can be observed in studying complex fluids and flows, rebounding jets generated by an incoming jet falling

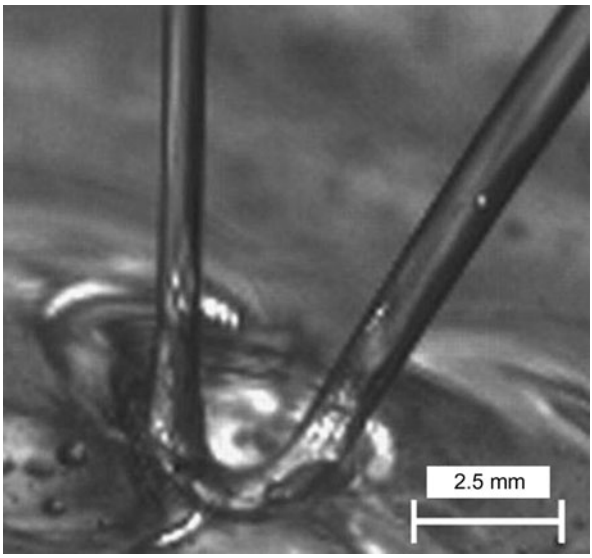

Fig. 1.7 Kaye effect: the geometry of the dimple inside the heap[2]

under gravity onto a bath made of the same liquid is shown. Two experiments have been investigated recently that yield similarly observed unique phenomena but with different dynamic mechanisms. The first one is the Kaye effect described in Kaye (1963), and the second one is a bouncing jet using a very common fluid—cooking oil.

1.4.1 The Kaye Effect: Shear-Thinning Evidence

In Versluis et al. (2006), the Kaye effect is revisited and explained. Indeed Kaye noticed that when shampoo is poured down from a height of ~ 20 cm on a thin layer of the same fluid, a viscous heap is formed as it would occur if one were using honey or silicone oil. After a very short time (< 1 s), the incoming jet will slip away from the heap, leading to the formation of a lasso type ring. Because shampoo is a shear-thinning non-Newtonian fluid, the departing jet creates a low viscosity layer that expels the jet at low inclination. At the same time, the falling jet exerts a vertical force that affects the shape of the heap where a dimple is formed. The dimple gets deeper and this geometrical change induces that the lower part of the lasso sticks to the thin bath and the outgoing jet straightens. Figure 1.7 illustrates the formation of the dimple in the heap. Observe in the figure that the lasso disappeared and the radii of the incoming and outgoing jets are clearly different. At some point the outgoing

[2]Figures 1.7, 1.8, 1.9 reprinted with permission from: M. Versluis, C. Blom, D. van der Meer, K. van der Weele, D. Lohse (2006) Leaping shampoo and the stable Kaye effect. J. Stat. Mech. P07007.

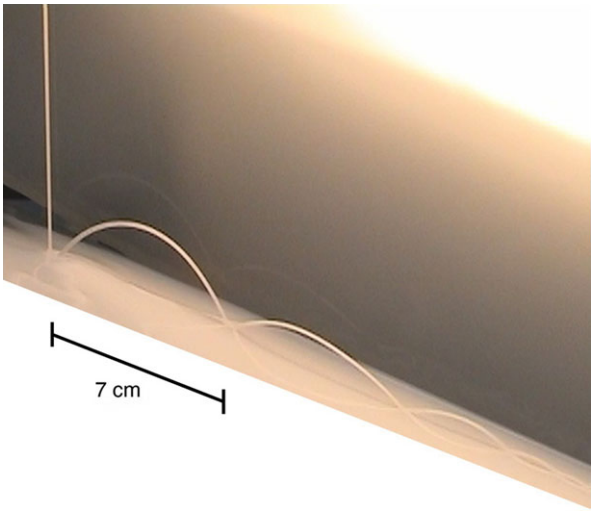

Fig. 1.8 Kaye effect: influence of a slanted wall

jet will reach the vertical jet in such a way that this disturbance may stop the Kaye effect. (The cited reference contains enticing videos of the phenomena.) Figure 1.8 exhibits the several bounced jets when they hit a thin layer on a slanted wall.

It is interesting to contrast that in Collyer and Fischer (1976), elasticity of the fluid was invoked to explain the physics of this flow; however, much later in Versluis et al. (2006) only shear-thinning viscosity arguments come into play. The experiments nevertheless show that the outgoing jet has a radius such that $R_{out} > R_{in}$. Therefore, the velocity of the outgoing jet is smaller than that of the incoming jet as global mass conservation enforces $V_{in} R_{in}^2 = V_{out} R_{out}^2$. The main reason for this decreasing velocity is the viscous dissipation in the dimple. Inspection of Fig. 1.9 shows that the jet in the dimple is in contact with the resting heap through a very thin shear layer of thickness δ. There the velocity profile may be taken as linear giving a constant shear rate $\dot{\gamma} = V/\delta$. The shear stress in this layer is given by (1.3) such that $\Sigma = \mu\dot{\gamma}$ ($\eta = \mu$ in the figure). The viscosity is chosen to follow Crow's relation

$$\mu(\dot{\gamma}) = \mu_\infty + \frac{\mu_0 - \mu_\infty}{1 + (\dot{\gamma}/\dot{\gamma}_c)^n} , \tag{1.27}$$

where μ_0 and μ_∞ are the zero-shear-rate and infinite-shear-rate viscosities, respectively, and $\dot{\gamma}_c$ is the critical shear rate. Versluis et al. (2006) found in their experiments $n = 1$ and $\dot{\gamma} \gg \dot{\gamma}_c$, so that the viscosity relationship could be approximated as

$$\mu(\dot{\gamma}) = \mu_\infty + \frac{\mu_0 \dot{\gamma}_c \delta}{V} . \tag{1.28}$$

A simple line of reasoning equating dissipation to the rate of change of kinetic energy provides a differential equation for the velocity that can be integrated over the interaction length L between the jet and the heap. From this equation, one obtains the threshold velocity of the incoming jet that ensures stability of the Kaye effect.

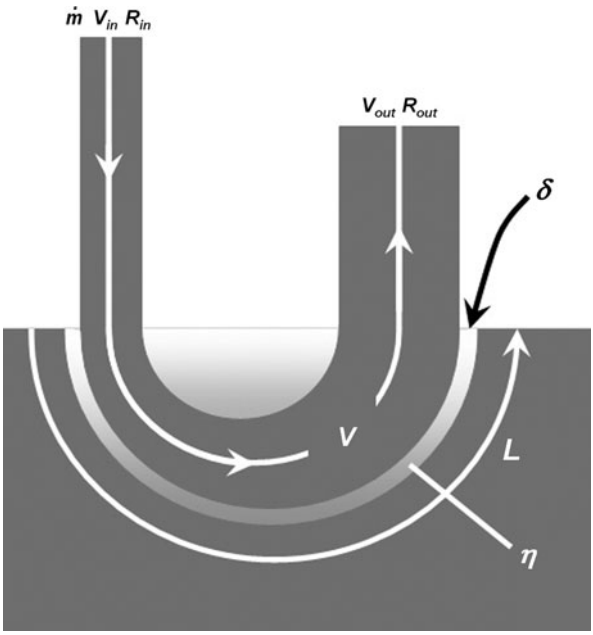

Fig. 1.9 Kaye effect: sketch of the flowing jet through the dimple

The developed model takes only shear-thinning into account, and obviously no elasticity is required to explain the observed physical phenomena.

1.4.2 Bouncing Newtonian Jet

Thrasher et al. (2007) have generated Newtonian bouncing jets when the incoming jets impact a thin, moving bath (see Fig. 1.10). The observed bouncing phenomenon is quite similar to the Kaye effect except that the liquids are typical classical Newtonian fluids (cooking oil). The observations show that the bouncing jet is separated from the surrounding bath by a sheath of air, while in the stable Kaye effect a shear-thinning layer played the lubricating role. Some energy arguments based on drag force of the impinging jet and the interfacial forces on the bouncing jet shed some light on the mechanisms involved in the transition between plunging and bouncing jets. Nonetheless, the physical situation is dynamically complex due to the interplay of viscous, inertial, surface and gravitational forces.

1.4.3 Turbulent Drag Reduction

Since the pioneering experiments by Toms (1949), it is known that the addition of minute amounts of long chain polymers to water or organic solvents can lead

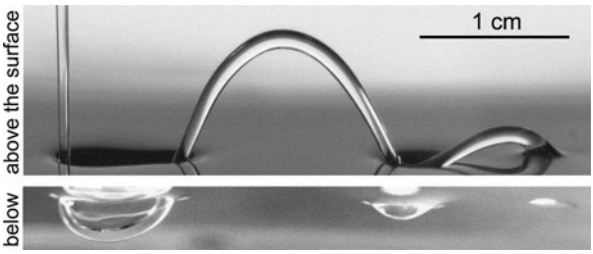

Fig. 1.10 Newtonian bouncing jet on a moving bath[3]

to significant turbulent drag reduction. However, it has only been within the last decade and a half that computational resources have been available to make it possible to perform (direct) numerical simulations of this phenomenon. As Fig. 1.11 illustrates, the fine-scale turbulence affects the polymer molecule and induces an extensive elongation of the molecular chain. The extended molecule then has an impact on the turbulent energy cascade which reduces the drag. The exact details of this interaction is as yet not known in detail.

The first such simulations considered a generalized Newtonian fluid (den Toonder et al. 1995; Orlandi 1995) in pipe and plane channel flow. Sureshkumar et al.

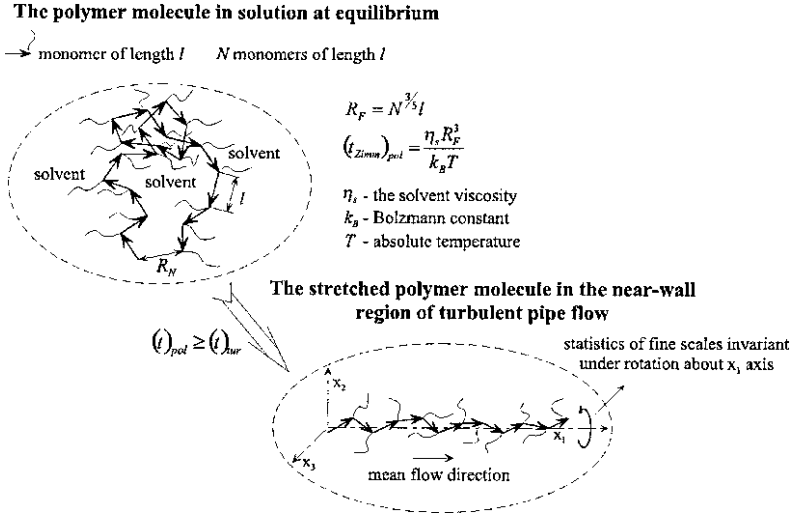

Fig. 1.11 Possible behavior of long chain macromolecule in proximity of wall in turbulent flow[4]

[3]Figure 1.10 reprinted with permission from: M. Thrasher, S. Jung, Y.K. Pang, C.-P. Chuu, H. Swinney (2007) The bouncing jet: a Newtonian liquid rebounding off a free surface. Phys. Rev. E 76:056319. Copyright 2007 by the American Physical Society.

[4]Figure 1.11 reprinted with permission from: J. Jovanović, M. Pashtrapanska, B. Frohnapfel, F. Durst, J. Koskinen, K. Koskinen (2006) On the mechanism responsible for turbulent drag reduction by dilute addition of high polymers: theory, experiments, simulations and predictions. J. Fluids Eng. 128:118–130.

(1997) were the first to perform direct numerical simulations (DNS) of drag reduction with a viscoelastic fluid and used the FENE-P model (Finitely Extensible Nonlinear Elastic in the Peterlin approximation) (see also Sureshkumar and Beris 1995; Dimitropoulos et al. 1998, 2001). More recently, other direct numerical simulations have been carried out (primarily with FENE-P fluid) (Housiadas and Beris 2003; Ptasinski et al. 2003; Dubief et al. 2004; Dimitropoulos et al. 2005, 2006) in order to better understand the drag reduction dynamics.

As with DNS of Newtonian fluids the numerical requirements for viscoelastic DNS makes them only amenable at relatively modest Reynolds numbers on large scale supercomputers. From the engineering point of view, it is necessary to envisage closures for viscoelastic turbulent flows. In this spirit, there has been recent attempts towards RANS (Reynolds Averaged Navier-Stokes) modeling (Cruz et al. 2004; Li et al. 2006; Pinho et al. 2008b). These models were generally low-order models, that is one- or two-equation linear eddy viscosity models. Unfortunately, such low-order models cannot properly capture anisotropy effects that certainly may be prevalent in drag reducing polymer flows due to the inherent viscoelastic effects.

An intermediate approach between direct numerical simulation and the Reynolds-averaged formulation, large eddy simulations (LES), has recently been applied to viscoelastic turbulent flows (Thais et al. 2010). This approach was based on a temporal formulation rather than the traditional spatial filtering approach. Nevertheless, the study showed that such a filtered methodology can be applied to viscoelastic fluids, but new considerations, such as differing filter widths associated with the velocity and extra-stress fields may need to be considered.

These studies have provided additional insight into the polymer-turbulent dynamics that include the effects on vortex stretching due to the high extensional viscosity. In addition, a change in the mean flow distribution across the boundary layer has been observed depending on the extent of drag reduction. At low drag reduction ($DR < 40\%$), the log law region is simply moved away from the wall; however, at high drag reduction, the log region is again moved away from the wall but its slope is increased with respect to the Newtonian flow.

1.5 The Modeling Map

This introductory chapter was intended to provide the reader with some context and physical examples of what was meant by complexity. To achieve our goals of modeling those complicated situations, it is necessary to build up in an axiomatic way a methodology capable of embracing all those physical phenomena. The concepts of continuum mechanics developed over the last half-century will help in that goal. From continuum mechanics (cf. Fig. 1.12), we derive fluid mechanics that covers both statics and dynamics of the fluids. The mechanical behavior of the fluids may be described as Newtonian or non-Newtonian. In this last case the modeler resorts also to rheology which is the science of "everything that flows", even mountains according to the prophet(ess) Deborah (see Reiner 1964 and Chap. 5). The complex

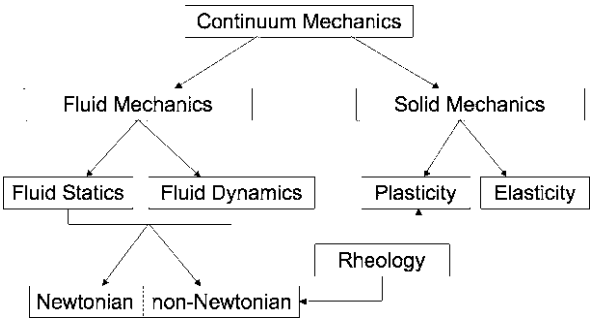

Fig. 1.12 Filiation of continuum mechanics

flows to be discussed are turbulent. Even with just the turbulent flow of a Newtonian fluid, the subject is not easily managed since external forces (e.g. buoyancy, magnetic fields, etc.) can be applied that make the complexity even greater. However, strides in the last decade have been made where numerical simulations of the fluid motion conservation equations coupled with viscoelastic constitutive equations have been made. This inherent link then between the complex fluid and complex flow can now be further explored.

Another route to generate the models for complex fluids starts from molecular dynamics (see Fig. 1.13) and goes through two possible branches. The left branch in Fig. 1.13 is based on kinetic theory (that can also be produced from continuum mechanics concepts). Kinetic theory mainly considers particles colliding and streaming and is primarily applied to gases. The random character of the particle motions is described by stochastic equations like the Fokker-Planck equations. These equations engender the micro-macro approach where the basic conservation laws of continuum mechanics are used, and the stress tensor is obtained from an ensemble average of solutions of the stochastic equations. An alternate choice consists in deriving the Boltzmann equation from kinetic theory and from there it is possible by the Chapman-Enskog analysis to build the classical hydrodynamic system within the framework of the lattice Boltzmann method (LBM). The right branch examines in detail the micro-macro structures of the fluid and rests upon the concept of dumbbells. Differential equations are then deduced and lead to the writing of constitutive equations involving partial differential operators.

Chapter 2 provides the reader with the tensorial tools in exploring the various models. Invariant theory and integrity bases will play an essential role in the design of the representation of tensor-valued functions. Chapter 3 will develop the basics of kinematics and dynamics of continua with conservation laws of mass, momentum, moment of momentum obtained. Chapter 4 yields the general principles to write the constitutive equations that relate the stress tensor to the other relevant variables as pressure, velocity gradients, etc. In addition, a section will be devoted to the principle of objectivity and its consequences. In Chap. 5 we start by the simple fluids model. Then we address the nonlinear constitutive equations: Oldroyd-B, Maxwell, and Phan-Thien Tanner. The popular Finite Extensible Nonlinear Elastic (FENE) models that are based on the representation of long polymer chains by dumbbells is also discussed. These developments will be linked to the so- called micro-macro ap-

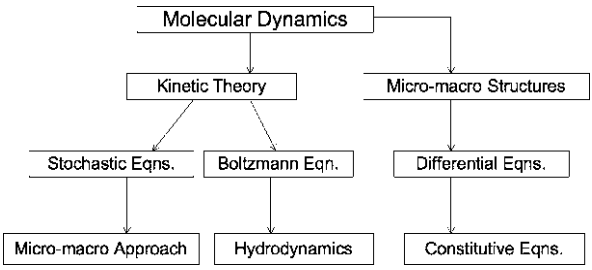

Fig. 1.13 Filiation of molecular dynamics

proach. Polymer melts are treated by the Doi-Edwards model, the (extended) pom-pom approach and finally the Rolie-Poly equation. For the turbulent case, the closure problem is addressed with Chap. 6 then devoted to averaged and filtered conservation laws. The Reynolds-averaged Navier-Stokes equations, the large eddy simulation, the various explicit algebraic models will be discussed. The final chapter will bring another view of the Navier-Stokes equations by the lattice Boltzmann method (LBM) where virtual particles collide and stream. The Chapman-Enskog multi-scale analysis leads to the compressible Navier-Stokes equations at low Mach number. This LBM will be put in perspective with the continuum mechanics methodology to emphasize the broad scope of the latter.

At the end of this intellectual trip through the mathematical models aimed at the understanding and prediction of the complicated physics of fluid behavior and intricate flows, the major challenge and task that remain are to solve them. As nonlinearity dominates these models, there is little hope to build up analytical solutions in closed forms. This imposes linearization procedures that are severely restricted by convergence assumptions. The resort to numerical simulation is therefore unavoidable and the numericist faces the choice of the discretization method. There is no doubt that the former century brought to the scientific computing community the weak formulation of the problem as the essential tool for high performance computing. The availability of huge parallel machines and the speed-up provided by the use of graphics processing units opens the door to unknown territory of simulations that practitioners could not dream of until recently.

The production of this myriad of numerical databases calls for the development of new tools to accurately and deeply analyze the results. Plots of vector fields are not enough and new routes based on sound models are needed. Furthermore, the comparison of theory and computations with experimental data is also a source of concern. This triad forms the tripod of modern science and engineering in a feedback loop that endlessly improves each discipline.

Chapter 2
Tensor Analysis, Invariants, and Representations

In this chapter, the concepts necessary to formulate the vector and tensor representations needed in the construction of viscoelastic and turbulent constitutive equations are introduced. The material is generally adapted from the review article of Spencer (1971) who summarized the research work of Ronald Rivlin and colleagues, and with the goal to present to the reader a description more familiar to a fluid dynamicist. Probably the most general presentation of the theory leading to the appropriate form of constitutive equations resulting from invariance conditions is given in the book by Smith (1994); however such a general presentation is not needed here and would be more mathematically intense than desired. Nevertheless, it is assumed at the outset that the reader, at a minimum, is familiar with elements of tensor and matrix algebra. The numerous citations within this chapter will guide the reader to the relevant publications.

One of the inherent drawbacks in attempting to present a mathematical description of polynomial invariants and polynomial representations is the rapid increase in notational complexity. At the least, the reader becomes rapidly discouraged in following the discussion, or more seriously can incorrectly interpret what is presented. While cognizant of the problem, there are instances where notational complexity is inherent in the material being presented. Nevertheless, there are some rules that can be adhered to that hopefully will alleviate some of the problems. In what follows some notational guidelines that will be followed are presented.

In the following: scalar fields will be denoted by f for a scalar-valued function; vectors will be bold-faced like $\mathbf{v}$, the components of which being v_i in an orthonormal Cartesian coordinate system; second-order tensors will also be bold-faced as $\boldsymbol{L}$ with components L_{ij}, and the matrix associated with the components of the tensor will contain the elements L_{ij}. It is important to distinguish between the vector $\mathbf{v}$ with an associated (column) matrix $[v] = [v_1, v_2, v_3]$, or the tensor $\boldsymbol{L}$ with the corresponding 3×3 matrix. In a given coordinate system, the matrices serve to describe the corresponding vector $\mathbf{v}$ and tensor $\boldsymbol{L}$. However, the vector is represented by different matrices in different coordinate systems; whereas, the vec-

M.O. Deville, T.B. Gatski, *Mathematical Modeling for Complex Fluids and Flows*,
DOI 10.1007/978-3-642-25295-2_2,

tor itself is independent of the coordinate system. Similarly, a 3×3 matrix with elements L_{ij}

$$[L] = \begin{pmatrix} L_{11} & L_{12} & L_{13} \\ L_{21} & L_{22} & L_{23} \\ L_{31} & L_{32} & L_{33} \end{pmatrix} \tag{2.1}$$

describes the tensor $\boldsymbol{L}$ in a given coordinate system, but $\boldsymbol{T}$ has different matrix representations in different coordinates; although $\boldsymbol{T}$ itself is independent of the coordinate system. The following example further illustrates the distinction.

Assume there is a linear mapping $\boldsymbol{L}$ in a real Euclidean vector space that transforms a vector into another one. For example, if $\boldsymbol{L}$ transforms $\mathbf{u}_1$ into $\mathbf{v}_1$ and $\mathbf{u}_2$ into $\mathbf{v}_2$ through the relations

$$\begin{aligned} \boldsymbol{L}\mathbf{u}_1 &= \mathbf{v}_1 \,, \\ \boldsymbol{L}\mathbf{u}_2 &= \mathbf{v}_2 \,, \end{aligned}$$

and if $\boldsymbol{L}$ has the properties

$$\begin{aligned} \boldsymbol{L}(\mathbf{u}_1 + \mathbf{u}_2) &= \boldsymbol{L}\mathbf{u}_1 + \boldsymbol{L}\mathbf{u}_2 \,, \\ \boldsymbol{L}(\alpha \mathbf{u}_1) &= \alpha \boldsymbol{L}\mathbf{u}_1 \,, \end{aligned} \tag{2.2}$$

with $\mathbf{u}_1$ and $\mathbf{u}_2$ two arbitrary vectors in the real Euclidean vector space and α real, then $\boldsymbol{L}$ is a linear transformation. It is also a tensor of second order or simply a tensor.

For every vector $\mathbf{u}$, the vector $\mathbf{v}$ is such that we write

$$\mathbf{v} = \boldsymbol{L}\mathbf{u} = \boldsymbol{L}u_i\mathbf{e}_i = u_i \boldsymbol{L}\mathbf{e}_i \tag{2.3}$$

where the $\mathbf{e}_i$ are the basis vectors of the coordinate system. The components of $\mathbf{v}$ are obtained by taking the scalar product

$$v_i = \mathbf{e}_i \cdot \mathbf{v} \,. \tag{2.4}$$

Combining Eqs. (2.3) and (2.4), one gets

$$v_i = \mathbf{e}_i \cdot (u_j \boldsymbol{L}\mathbf{e}_j) = u_j \mathbf{e}_i \cdot \boldsymbol{L}\mathbf{e}_j \,. \tag{2.5}$$

In general, one has

$$L_{ij} = \mathbf{e}_i \cdot \boldsymbol{L}\mathbf{e}_j \,. \tag{2.6}$$

The elements L_{ij} are the tensor components of $\boldsymbol{L}$. With (2.5) and (2.6), one obtains

$$v_i = L_{ij}u_j \,. \tag{2.7}$$

This last relation can be written in matrix form as

$$\begin{pmatrix} v_1 \\ v_2 \\ v_3 \end{pmatrix} = \begin{pmatrix} L_{11} & L_{12} & L_{13} \\ L_{21} & L_{22} & L_{23} \\ L_{31} & L_{32} & L_{33} \end{pmatrix} \begin{pmatrix} u_1 \\ u_2 \\ u_3 \end{pmatrix} \,, \qquad [v] = [L][u] \,. \tag{2.8}$$

The matrix array $[L]$ is the matrix associated with the tensor $\boldsymbol{L}$ with respect to the basis vectors $\{\mathbf{e}_i\}$. Although the focus here will primarily require second-order

tensors (3×3 matrices), generalized discussions may require the specification of higher-order tensors. In this case, for nth-order tensors the index notation $A_{i_1 i_2 \cdots i_n}$ will be used.

It should be apparent at this point that, if left unconstrained, the notational distinctions required between vectors and tensors and their corresponding matrices could lead to a proliferation of symbols. We feel that this is undesirable since it burdens the reader with the task of recognizing subtle font deviations between symbols for vectors, tensors and matrices. For this reason, we will take the notational liberty of using the same symbol to designate both vectors, tensors and their corresponding matrices when the discussion is based within the same coordinate system and the components of the vector or tensor are the elements of the corresponding matrix. When the component notation is used, mathematical relations are written so that they preserve their form under coordinate transformations. Of course, in considering specific problems it is always necessary to introduce a coordinate system and components, and this will be followed here where necessary.

If the component form of a vector or tensor is written any superscript notation will refer to a vector or tensor element in a set. If the bold-face form is used then any subscript notation will refer to an element in some vector or tensor set. In some instances, it may be necessary to utilize both notational conventions. If this occurs, such as in the case of a tensor element $\boldsymbol{T}_k$ for example, the component form will then be written as $T_{ij}^{(k)}$. Such instances are unavoidable when polynomial representations or tensor (vector) products arise. It is always a difficult task not to deviate from a set of notational rules to be followed in such a text, especially when the topics span such a wide range. Nevertheless, some guidelines (rules) do need to be set but, when necessary deviations do occur, the reader will be duly alerted.

2.1 Symmetries and Transformations

Two main principles constitute the backbone for the methodological process generating constitutive relationships: objectivity and material invariance. In this chapter we will focus on material invariance deferring objectivity to later developments.

Solid materials draw their symmetry properties from their crystallographic characteristics: solids with triclinic, rhombic, tetragonal, hexagonal, cubic networks. Some fluids also possess those types of properties, for example, the nematic fluids. For example, the material properties of a solid with hexagonal symmetry will be similar (invariant) with respect to a $\pi/3$ rotation of the reference configuration. The material equations, namely the constitutive relations, will reflect this property through the condition that the change of reference configuration involves a matrix denoted e.g. by $\boldsymbol{H}$ such that $\det \boldsymbol{H} = 1$. This matrix is a proper unimodular matrix.

The principle of material symmetry is used to set up the mathematical framework in such a way that the constitutive functionals do not change their formulation under symmetry transformation like central inversion, reflections and various rotations.

These symmetry transformations are represented by a set of orthogonal matrices $\boldsymbol{O}$ such that

$$\boldsymbol{O}\,\boldsymbol{O}^T = \boldsymbol{O}^T\,\boldsymbol{O} = \boldsymbol{I} \quad \text{and} \quad \det \boldsymbol{O} = \pm 1\ . \tag{2.9}$$

For example, the reflection transformation across a symmetry plane passing through the origin and orthogonal to the unit vector $\mathbf{n}$ is defined by the tensor $\boldsymbol{\mathscr{R}}$ with the components

$$\mathscr{R}_{ij} = \delta_{ij} - 2n_i n_j \quad \text{with} \quad \det[\boldsymbol{\mathscr{R}}] = -1\ . \tag{2.10}$$

This set of orthogonal matrices form the symmetry group O. When O is the proper orthogonal group with a matrix $[O]$ such that $\det[O] = +1$, the material is called hemitropic, and when O is the full group, $\det[O] = \pm 1$, the material is called isotropic.

These orthogonal transformations change a vector $\mathbf{x}$ with components x_i $(i = 1, 2, 3)$ into a new vector $\overline{\mathbf{x}}$ by the relation

$$\overline{\mathbf{x}} = \boldsymbol{O}\mathbf{x}\ , \tag{2.11a}$$

and a tensor $\boldsymbol{T}$ with components T_{ij} $(i, j = 1, 2, 3)$ into a new tensor $\overline{\boldsymbol{T}}$ by the relation

$$\overline{\boldsymbol{T}} = \boldsymbol{O}\boldsymbol{T}\,\boldsymbol{O}^T\ . \tag{2.11b}$$

When dealing with polynomial invariants and the subsequent vector (and tensor) representations, it is necessary to sometimes distinguish between *axial* and *absolute* vectors. For an *axial* (*or dual*) vector $\mathbf{w}$, the components are associated with the three (non-zero) components of a skew-symmetric tensor $\boldsymbol{W}$ $(\boldsymbol{W} = -\boldsymbol{W}^T)$, through the relation

$$w_i = \frac{1}{2} e_{ijk} W_{jk} \quad \text{with} \quad W_{jk} = e_{jki} w_i\ , \tag{2.12}$$

where the tensor e_{ijk} is the third-order, Levi-Civita permutation tensor with $e_{ijk} = 1$ or -1 for i, j, k, an even or an odd permutation of 1, 2, 3; and $e_{ijk} = 0$ otherwise. The axial vector is then transformed according to the rule

$$\overline{\mathbf{w}} = \det[O]\,\boldsymbol{O}\mathbf{w}\ . \tag{2.13}$$

In obtaining the traces of the matrix products comprising the invariant bases, such vectors are replaced with the corresponding skew-symmetric tensors. For the proper orthogonal group all vectors are assumed to be axial vectors so that the integrity basis for this group need only contain symmetric and skew-symmetric tensors (see Sect. 2.3.3.1). For an *absolute* vector $\mathbf{v}$ under an orthogonal transformation, it becomes

$$\overline{\mathbf{v}} = \boldsymbol{O}\mathbf{v}\ . \tag{2.14}$$

In obtaining the traces of the matrix products comprising the invariant bases, outer (tensor) products of such vectors are formed and both symmetric and skew-symmetric tensors derived. These elements are then coupled with the axial vectors

(skew-symmetric tensors) to form the invariants under the full orthogonal group (see Sect. 2.3.3.2).

Fluids are obviously isotropic materials. The symmetry group includes all the possible rotations and reflections and therefore is the full three-dimensional orthogonal group. Let us mention that this conclusion is not shared by every fluid mechanist as they do not involve reflections in the symmetry group. Huilgol and Phan-Thien (1997) and Fosdick and Serrin (1979) note that: "The body cannot be expected to ever take on configurations which would require the vanishing of the local volume elements or mirror reflections of the reference configuration. This point cannot be too strongly emphasized." However, if reflections are taken into account in the symmetry group, their presence do not place any new conditions on the design of the constitutive equations.

2.2 Invariants and Traces of Matrix Polynomials

The fundamental element in the construction of tensor and vector polynomial representations is the identification of a suitable set of invariants associated with the dependent vectors and tensors relative to the fluid and flow dynamics.

The starting point in this section is then to define an invariant. Consider an algebraic function $\phi(\mathbf{u}, \mathbf{v}, \mathbf{w}, \ldots, \boldsymbol{D}, \boldsymbol{E}, \ldots)$ of the vectors $\mathbf{u}, \mathbf{v}, \mathbf{w}, \ldots$ and the tensors $\boldsymbol{D}, \boldsymbol{E}, \ldots$, then it is an invariant of these vectors and tensors under the group of transformations O, if

$$\phi(\mathbf{u}, \mathbf{v}, \mathbf{w}, \ldots, \boldsymbol{D}, \boldsymbol{E}, \ldots) = \phi(\overline{\mathbf{u}}, \overline{\mathbf{v}}, \overline{\mathbf{w}}, \ldots, \overline{\boldsymbol{D}}, \overline{\boldsymbol{E}}, \ldots) \,. \tag{2.15}$$

It is useful to present some terminology often used when discussing invariants. An invariant is termed *even* if it is unchanged under all orthogonal transformations (such as the scalar product), and *odd* if it changes sign under an orthogonal transformation with negative determinant (such as the scalar triple product). Even invariants are *absolute* invariants for both the full and proper orthogonal transformation groups; however, odd invariants are only absolute invariants for the proper orthogonal group and *relative* invariants for the full orthogonal group. Such distinctions become important as invariants comprising the integrity basis for combinations of vectors and tensors are discussed.

A related and useful identifying property of tensor fields is that of *isotropy*. Recall in Chap. 1, the concept of stress on a fluid element was introduced in order to highlight some characterizing features of complex fluids. Let us assume here that the constitutive equation for the stress field, $\boldsymbol{\Sigma}$, is given by

$$\boldsymbol{\Sigma} = \boldsymbol{\varphi}(\mathbf{u}, \mathbf{v}, \mathbf{w}, \ldots, \boldsymbol{D}, \boldsymbol{E}, \ldots) \,. \tag{2.16}$$

Then, under the invariance principle for the group O,

$$\begin{aligned} \boldsymbol{O}\boldsymbol{\Sigma}\boldsymbol{O}^T &= \boldsymbol{\varphi}(\boldsymbol{O}\mathbf{u}, \boldsymbol{O}\mathbf{v}, \boldsymbol{O}\mathbf{w}, \ldots, \boldsymbol{O}\boldsymbol{D}\boldsymbol{O}^T, \boldsymbol{O}\boldsymbol{E}\boldsymbol{O}^T, \ldots) \\ \overline{\boldsymbol{\Sigma}} &= \boldsymbol{\varphi}(\overline{\mathbf{u}}, \overline{\mathbf{v}}, \overline{\mathbf{w}}, \ldots, \overline{\boldsymbol{D}}, \overline{\boldsymbol{E}}, \ldots) \,, \end{aligned} \tag{2.17}$$

and the tensor function $\boldsymbol{\varphi}$, satisfying Eq. (2.17), is then an *isotropic function* of the vectors $\boldsymbol{O}\mathbf{u}$, $\boldsymbol{O}\mathbf{v}$, $\boldsymbol{O}\mathbf{w}$, ..., and the tensors $\boldsymbol{O}\boldsymbol{D}\boldsymbol{O}^T$, $\boldsymbol{O}\boldsymbol{E}\boldsymbol{O}^T$, ...

As will be seen in the following sections, the invariants formed from the vector and tensor products will ultimately be used in the formation of polynomials of invariants used in the generation of vector and tensor bases.

2.2.1 Polynomial Invariants

A way of dealing with invariant functions such as $\boldsymbol{\varphi}$ is to use algebraic polynomial functions expressed in terms of basic invariants. For example, a polynomial invariant $\mathcal{I}$ of a combination of n vectors $\mathbf{u}_\mathbf{r}$ ($\mathbf{r} = r_1, \ldots, r_n$) and m tensors $\boldsymbol{P}_\mathbf{s}$ ($\mathbf{s} = s_1, \ldots, s_m$) can be written in the form

$$\mathcal{I} = \beta_{i_1 i_2 \ldots i_n j_1 k_1 j_2 k_2 \ldots j_m k_m} u_{i_1}^{(r_1)} u_{i_2}^{(r_2)} \cdots u_{i_n}^{(r_n)} P_{j_1 k_1}^{(s_1)} P_{j_2 k_2}^{(s_2)} \cdots P_{j_m k_m}^{(s_m)} \tag{2.18}$$

where $\beta_{i_1 i_2 \ldots i_n j_1 k_1 j_2 k_2 \ldots j_m k_m}$ are the components of an isotropic tensor. This isotropic tensor can be expressed as a linear combination of terms consisting of Kronecker deltas if the integer order of $\beta_{i_1 i_2 \ldots i_n j_1 k_1 j_2 k_2 \ldots j_m k_m}$ is even, and a linear combination of terms consisting of Kronecker deltas and one permutation tensor if the integer order of $\beta_{i_1 i_2 \ldots i_n j_1 k_1 j_2 k_2 \ldots j_m k_m}$ is odd (Spencer 1971). Some example cases will show how Eq. (2.18) can be expanded.

When $\beta_{i_1 i_2 \ldots i_n j_1 k_1 j_2 k_2 \ldots j_m k_m}$ is even, it is clear that if vectors are included in the invariant relationship for $\mathcal{I}$ they must enter in even numbers. For example, for the case of two vectors $u_{i_1}^{(1)}$ and $u_{i_2}^{(2)}$ and no tensors, the corresponding isotropic tensor $\beta_{i_1 i_2}$ is a scalar multiple of the Kronecker delta itself $\delta_{i_1 i_2}$ such that $\mathcal{I} = u_{i_1}^{(1)} u_{i_1}^{(2)}$; or for the case of a single tensor $P_{j_1 k_1}^{(1)}$, the corresponding isotropic tensor is $\beta_{j_1 k_1} \propto \delta_{j_1 k_1}$ such that $\mathcal{I} = P_{j_1 j_1}^{(1)}$. For the case of four vectors, two vectors and a tensor, or two tensors, the corresponding fourth-order isotropic tensors are a sum of products of Kronecker deltas (e.g. Jeffreys 1965),

$$\begin{aligned}
\beta_{i_1 i_2 i_3 i_4} &= \mu_0 \delta_{i_1 i_2} \delta_{i_3 i_4} + \mu_1 \left(\delta_{i_1 i_3} \delta_{i_2 i_4} + \delta_{i_1 i_4} \delta_{i_2 i_3} \right) \\
&\quad + \mu_2 \left(\delta_{i_1 i_3} \delta_{i_2 i_4} - \delta_{i_1 i_4} \delta_{i_2 i_3} \right) && \text{(2.19a)} \\
\beta_{i_1 i_2 j_1 k_1} &= \mu_0 \delta_{i_1 i_2} \delta_{j_1 k_1} + \mu_1 \left(\delta_{i_1 j_1} \delta_{i_2 k_1} + \delta_{i_1 k_1} \delta_{i_2 j_1} \right) \\
&\quad + \mu_2 \left(\delta_{i_1 j_1} \delta_{i_2 k_1} - \delta_{i_1 k_1} \delta_{i_2 j_1} \right) && \text{(2.19b)} \\
\beta_{j_1 k_1 j_2 k_2} &= \mu_0 \delta_{j_1 k_1} \delta_{j_2 k_2} + \mu_1 \left(\delta_{j_1 j_2} \delta_{k_1 k_2} + \delta_{j_1 k_2} \delta_{k_1 j_2} \right) \\
&\quad + \mu_2 \left(\delta_{j_1 j_2} \delta_{k_1 k_2} - \delta_{j_1 k_2} \delta_{k_1 j_2} \right) , && \text{(2.19c)}
\end{aligned}$$

respectively, and with the corresponding invariants

$$\begin{aligned}
\mathcal{I} &= \mu_0 u_{i_1}^{(1)} u_{i_1}^{(2)} u_{i_3}^{(3)} u_{i_3}^{(4)} + \mu_1 \left(u_{i_1}^{(1)} u_{i_1}^{(3)} u_{i_2}^{(2)} u_{i_2}^{(4)} + u_{i_1}^{(1)} u_{i_1}^{(4)} u_{i_2}^{(2)} u_{i_2}^{(3)} \right) \\
&\quad + \mu_2 \left(u_{i_1}^{(1)} u_{i_1}^{(3)} u_{i_2}^{(2)} u_{i_2}^{(4)} - u_{i_1}^{(1)} u_{i_1}^{(4)} u_{i_2}^{(2)} u_{i_2}^{(3)} \right) && \text{(2.20a)}
\end{aligned}$$

$$\mathcal{I} = \mu_0 u_{i_1}^{(1)} u_{i_1}^{(2)} P_{j_1 j_1}^{(1)} + \mu_1 \left(u_{i_1}^{(1)} u_{i_2}^{(2)} P_{i_1 i_2}^{(1)} + u_{i_1}^{(1)} u_{i_2}^{(2)} P_{i_1 i_2}^{(1)} \right) + \mu_2 \left(u_{i_1}^{(1)} u_{i_2}^{(2)} P_{i_1 i_2}^{(1)} - u_{i_1}^{(1)} u_{i_2}^{(2)} P_{i_1 i_2}^{(1)} \right) \tag{2.20b}$$

$$\mathcal{I} = \mu_0 P_{j_1 j_1}^{(1)} P_{j_2 j_2}^{(2)} + \mu_1 \left(P_{j_1 k_1}^{(1)} P_{j_1 k_1}^{(2)} + P_{j_1 k_1}^{(1)} P_{k_1 j_1}^{(2)} \right) + \mu_2 \left(P_{j_1 k_1}^{(1)} P_{j_1 k_1}^{(2)} - P_{j_1 k_1}^{(1)} P_{k_1 j_1}^{(2)} \right) , \tag{2.20c}$$

respectively. In general, substitution of these linear combinations of Kronecker deltas for $\boldsymbol{\beta}$ will result in $\mathcal{I}$ being expressed as polynomials consisting of expressions of the following two types:

$$\Pi_{kk}^{(1)} \tag{2.21a}$$

$$u_i^{(r_1)} \Pi_{ij}^{(2)} u_j^{(r_2)} \tag{2.21b}$$

where $\Pi_{ij}^{(1)}$ and $\Pi_{ij}^{(2)}$ each represent matrix products of the form

$$\Pi_{ij}^{(k)} = P_{il}^{(s_1)} P_{ln}^{(s_2)} \cdots P_{pj}^{(s_m)} , \tag{2.22}$$

and each having a different number of factors s_m. Additionally, each or both of $\Pi_{ij}^{(1)}$ and $\Pi_{ij}^{(2)}$ can degenerate to the Kronecker delta δ_{ij}. The invariants formed from Eqs. (2.21a), (2.21b) and (2.22) are not necessarily a minimal set. Oftentimes, reductions are possible through a utilization of the properties of the tensors and two fundamental identities relating matrix products.

When the isotropic tensor $\beta_{i_1 i_2 \ldots i_n j_1 k_1 j_2 k_2 \ldots j_m k_m}$ is odd, it consists of a linear combination of terms containing Kronecker deltas and one permutation tensor (which is a third-order isotropic tensor—there is no first-order isotropic tensor, Jeffreys 1965). The restriction to a single permutation tensor follows from the relationship,

$$e_{ijk} e_{rst} = \begin{vmatrix} \delta_{ir} & \delta_{is} & \delta_{it} \\ \delta_{jr} & \delta_{js} & \delta_{jt} \\ \delta_{kr} & \delta_{ks} & \delta_{kt} \end{vmatrix} \tag{2.23}$$

between the permutation tensor and the determinant of a matrix with Kronecker delta elements. In its simplest form, an invariant containing the isotropic tensor e_{ijk} can be written as

$$e_{i_1 i_2 i_3} u_{i_1}^{(r_1)} u_{i_2}^{(r_2)} u_{i_3}^{(r_3)} , \tag{2.24}$$

where $\mathbf{u}_{r_1}$, $\mathbf{u}_{r_2}$, and $\mathbf{u}_{r_3}$ are three distinct vector quantities. If tensors are included, this form can be generalized and written in the form

$$e_{i_1 j_1 k_1} \Pi_{i_1 i_2}^{(3,1)} u_{i_2}^{(r_1)} \Pi_{j_1 k_1}^{(3,2)} , \tag{2.25a}$$

where $\Pi_{i_1 i_2}^{(3,1)}$ and $\Pi_{j_1 k_1}^{(3,2)}$ are matrix products of the form given in Eq. (2.22) with each having a different number of factors s_m. Although $\Pi_{j_1 k_1}^{(3,2)}$ cannot be the Kronecker delta $\delta_{j_1 k_1}$, the product $\Pi_{i_1 i_2}^{(3,1)}$ can degenerate to $\delta_{i_1 i_2}$. It follows from these relationships that the number of vectors included in the invariant relationship for $\mathcal{I}$

must then be odd when $\beta_{i_1 i_2 \ldots i_n j_1 k_1 j_2 k_2 \ldots j_m k_m}$ is odd. Finally, an obvious generalization of Eq. (2.25a) consistent with Eq. (2.24) leads to the invariant

$$e_{i_1 j_1 k_1} \Pi^{(4,1)}_{i_1 i_2} u^{(r_1)}_{i_2} \Pi^{(4,2)}_{j_1 i_3} u^{(r_2)}_{i_3} \Pi^{(4,3)}_{k_1 i_4} u^{(r_3)}_{i_4} \tag{2.25b}$$

where $\Pi^{(4,1)}_{i_1 i_2}$, $\Pi^{(4,2)}_{i_1 i_2}$, and $\Pi^{(4,3)}_{i_1 i_2}$ each represent matrix products of the form given in Eq. (2.22) with each having a different number of factors s_m. In addition, since the relation in (2.24) is also an invariant, it follows that each or all of $\Pi^{(4,1)}_{i_1 i_2}$, $\Pi^{(4,2)}_{i_1 i_2}$, and $\Pi^{(4,3)}_{i_1 i_2}$ can degenerate to Kronecker deltas.

2.2.2 Traces of Matrix Polynomials

Up to this point the discussion has focused on vectors and tensors such as $\mathbf{v}$ and $\boldsymbol{L}$; however, as was discussed in Sect. 2.1 and shown in Eq. (2.8) for example, the components comprising these vectors and tensors are also the elements used in the corresponding matrix representations. As such, the invariants that have just been discussed can also be expressed in terms of invariants associated with matrix elements and matrix products.

If $\boldsymbol{T}$ denotes a matrix product such that

$$[T] = [A][B] \ldots [R][S] \quad \text{and} \quad T_{ij} = A_{ik} B_{kl} \ldots R_{pq} S_{qj} \tag{2.26}$$

then

$$\operatorname{tr} \boldsymbol{T} = \{\boldsymbol{T}\} = \operatorname{tr}[A][B] \ldots [R][S] \quad \text{and} \quad T_{ii} = A_{ik} B_{kl} \ldots R_{pq} S_{qi} \; . \tag{2.27}$$

It is simple to show that the trace of a matrix product does not change if the factors of the product are interchanged cyclically, so that the trace of a matrix product is equal to the trace of the product transpose. Note also in Eq. (2.27) that the trace of $\boldsymbol{T}$ has been represented by three equivalent, but different notations, that is, $\operatorname{tr} \boldsymbol{T}$, $\{\boldsymbol{T}\}$, and T_{ii}. Each designation of the trace will be used throughout and the particular form used will depend on the context and space allowed.

Traces of matrices (tensors) appear in the principal invariants of a matrix (tensor) when it is referred to the principal basis given in the eigenspace. The eigenvalues λ_1, λ_2, λ_3 of the matrix $\boldsymbol{D}$, for example, are computed as the roots of the cubic characteristic equation of the matrix $\boldsymbol{D}$,

$$\det(\boldsymbol{D} - \lambda \boldsymbol{I}) = 0 \; , \tag{2.28}$$

with $\boldsymbol{I}$ the identity matrix, that yields the characteristic equation

$$\lambda^3 - \mathrm{I}_1(\boldsymbol{D})\, \lambda^2 + \mathrm{I}_2(\boldsymbol{D})\, \lambda - \mathrm{I}_3(\boldsymbol{D}) = 0 \; . \tag{2.29}$$

The coefficients in (2.29) are termed the principal invariants of $\boldsymbol{D}$ and are given by

$$\mathrm{I}_1(\boldsymbol{D}) = \operatorname{tr} \boldsymbol{D} = \lambda_1 + \lambda_2 + \lambda_3 \tag{2.30}$$

$$\mathrm{I}_2(\boldsymbol{D}) = \frac{1}{2}\left[(\operatorname{tr} \boldsymbol{D})^2 - \operatorname{tr} \boldsymbol{D}^2 \right] = \lambda_1 \lambda_2 + \lambda_2 \lambda_3 + \lambda_3 \lambda_1 \tag{2.31}$$

$$\mathrm{I}_3(\boldsymbol{D}) = \det \boldsymbol{D} = \lambda_1 \lambda_2 \lambda_3 \; . \tag{2.32}$$

From the Cayley-Hamilton theorem, which states that a matrix satisfies its own characteristic equation, $\boldsymbol{D}$ then satisfies

$$\boldsymbol{D}^3 - \mathrm{I}_1(\boldsymbol{D})\,\boldsymbol{D}^2 + \mathrm{I}_2(\boldsymbol{D})\,\boldsymbol{D} - \mathrm{I}_3(\boldsymbol{D})\,\boldsymbol{I} = 0\,. \tag{2.33}$$

$\boldsymbol{D}$ is now expressible as a matrix polynomial in terms of lower degree matrices. In general, all matrices $\boldsymbol{D}^n$, $n \geq 3$, can be expressed as linear combinations of $\boldsymbol{D}^2$, $\boldsymbol{D}$ and $\boldsymbol{I}$. By taking the trace of Eq. (2.33), $\det \boldsymbol{D}$ can be expressed as a polynomial in $\mathrm{tr}\,\boldsymbol{D}$, $\mathrm{tr}\,\boldsymbol{D}^2$, and $\mathrm{tr}\,\boldsymbol{D}^3$,

$$\{\boldsymbol{D}^3\} = \frac{3}{2}\{\boldsymbol{D}^2\}\{\boldsymbol{D}\} - \frac{1}{2}(\{\boldsymbol{D}\})^3 + 3\,\det \boldsymbol{D} \tag{2.34}$$

and, consequently,

$$\mathrm{I}_3(\boldsymbol{D}) = \det \boldsymbol{D} = \frac{1}{6}\left[\{\boldsymbol{D}\}^3 - 3\{\boldsymbol{D}\}\{\boldsymbol{D}^2\} + 2\{\boldsymbol{D}^3\}\right]\,. \tag{2.35}$$

Tensor representations are directly derivable from invariants, and it is important to know that invariant bases from which the various tensor bases are obtained do not have any redundant members. Such an invariant basis should not contain any members that can be expressed in terms of other invariants, that is, be reducible. For example, if Eq. (2.33) is multiplied by $\boldsymbol{P}$, and the trace of this relation then taken, one gets

$$\begin{aligned}\{\boldsymbol{D}^3\boldsymbol{P}\} &= \left\{\left[\mathrm{I}_1(\boldsymbol{D})\,\boldsymbol{D}^2 - \mathrm{I}_2(\boldsymbol{D})\,\boldsymbol{D} + \mathrm{I}_3(\boldsymbol{D})\,\boldsymbol{I}\right]\boldsymbol{P}\right\} \\ &= \{\mathcal{G}(\boldsymbol{D})\boldsymbol{P}\}\,,\end{aligned} \tag{2.36}$$

which shows that $\{\boldsymbol{D}^3\boldsymbol{P}\}$ is reducible since the trace of the matrix product of degree four and having a factor with maximum degree three can be expressed as a polynomial of matrix products of degree three or less and having a maximum degree of two or less. Similar results may be generated by evaluating the traces of matrix products of higher degree.

The invariant bases to be introduced in this chapter contain only members that are irreducible; however, it is informative where possible to show the procedure followed in determining the reducibility of such invariants. The identification of such irreducible invariants for both 2×2 and 3×3 matrices and matrix products was initiated over a half-century ago by Spencer and Rivlin (1959) (see also Spencer 1971). Although there is no attempt here to discuss this in detail, it is necessary, even in the simpler examples, to introduce a notation that significantly simplifies the presentation. Consider the invariant relation in Eq. (2.36) where each term in the polynomial invariant on the right is of lower total degree than the invariant on the left and the (partial) degree of the factor $\boldsymbol{D}$ also differs. This is sufficient to identify $\{\boldsymbol{D}^3\boldsymbol{P}\}$ as a reducible invariant and the exact form of the polynomial invariant on the right is not of particular concern. Spencer and Rivlin (1959) used the notation

$$\{\boldsymbol{D}^3\boldsymbol{P}\} \equiv 0\,, \tag{2.37}$$

to denote that $\{\boldsymbol{D}^3\boldsymbol{P}\}$ could be expressed as a polynomial in terms of traces of matrix products of lower degree than $\boldsymbol{D}^3\boldsymbol{P}$. As some further examples are shown shortly, the benefits of such an abbreviated form will become clear.

The Cayley-Hamilton theorem has been generalized by Rivlin (1955) (see also Rivlin and Smith 1975) and can be written as

$$\begin{aligned}
&\boldsymbol{DEF}+\boldsymbol{DFE}+\boldsymbol{EFD}+\boldsymbol{EDF}+\boldsymbol{FED}+\boldsymbol{FDE}\\
&\quad=\operatorname{tr}\boldsymbol{D}\,(\boldsymbol{EF}+\boldsymbol{FE})+\operatorname{tr}\boldsymbol{E}\,(\boldsymbol{FD}+\boldsymbol{DF})+\operatorname{tr}\boldsymbol{F}\,(\boldsymbol{DE}+\boldsymbol{ED})\\
&\qquad-(\operatorname{tr}\boldsymbol{E}\operatorname{tr}\boldsymbol{F}-\operatorname{tr}\boldsymbol{EF})\,\boldsymbol{D}-(\operatorname{tr}\boldsymbol{F}\operatorname{tr}\boldsymbol{D}-\operatorname{tr}\boldsymbol{FD})\,\boldsymbol{E}-(\operatorname{tr}\boldsymbol{D}\operatorname{tr}\boldsymbol{E}-\operatorname{tr}\boldsymbol{DEF})\\
&\qquad+[\operatorname{tr}\boldsymbol{D}\operatorname{tr}\boldsymbol{E}\operatorname{tr}\boldsymbol{F}-\operatorname{tr}\boldsymbol{D}\operatorname{tr}\boldsymbol{EF}-\operatorname{tr}\boldsymbol{E}\operatorname{tr}\boldsymbol{FD}-\operatorname{tr}\boldsymbol{F}\operatorname{tr}\boldsymbol{DE}\\
&\qquad\qquad+\operatorname{tr}\boldsymbol{DEF}+\operatorname{tr}\boldsymbol{FED}]\boldsymbol{I}\,,
\end{aligned}\tag{2.38}$$

where $\boldsymbol{D}$, $\boldsymbol{E}$, $\boldsymbol{F}$ are arbitrary second-order tensors. Equation (2.38) can be obtained in different ways (Rivlin and Smith 1975), but one method is to insert (2.35) in (2.33) and then to replace $\boldsymbol{D}$ with $\alpha\boldsymbol{D}+\beta\boldsymbol{E}+\gamma\boldsymbol{F}$ $(\alpha,\beta,\gamma)\in R$. The generalized equation (2.38) is then obtained by imposing the condition that the coefficient of $\alpha\beta\gamma$ vanishes. This ensures that each term in the resulting polynomial is of degree 3 and the matrices $\boldsymbol{D}$, $\boldsymbol{E}$, and $\boldsymbol{F}$ each appear in every term of the polynomial linearly. The Cayley-Hamilton relation (2.33) is then recovered for $\boldsymbol{D}=\boldsymbol{E}=\boldsymbol{F}$.

An invariant relationship analogous to Eq. (2.36) can be similarly obtained from Eq. (2.38), and can be written in the notation introduced in Eq. (2.37) as

$$\operatorname{tr}(\boldsymbol{DEF}+\boldsymbol{DFE}+\boldsymbol{EFD}+\boldsymbol{EDF}+\boldsymbol{FED}+\boldsymbol{FDE})\,\boldsymbol{P}\equiv 0\,. \tag{2.39}$$

Obviously, if the trace of the product of the right-side of Eq. (2.38) with $\boldsymbol{P}$ were formed, and then coupled with the other matrix products being introduced, there would be a rapid increase in notational complexity. If, however, the interest is only in whether an invariant is reducible or not, the details of the contracted expression is not relevant. Such is the interest here and questions pertaining to the reducibility of invariants will employ the notation used in Eqs. (2.36) and (2.39).

Equation (2.38) is one of two fundamental identities that can be associated with three (3×3) matrices. The other was originally obtained by Spencer and Rivlin (1962) (see also Rivlin and Smith 1975) and involves two skew-symmetric matrices, $\mathbf{V}$, $\mathbf{W}$. It is given by

$$\begin{aligned}
\boldsymbol{VAW}+\boldsymbol{A}^{\mathrm{T}}\boldsymbol{VW}+\boldsymbol{VWA}^{\mathrm{T}}&=\operatorname{tr}\boldsymbol{A}(\boldsymbol{VW})+\frac{1}{2}(\operatorname{tr}\boldsymbol{VW})\boldsymbol{A}^{\mathrm{T}}\\
&\quad+\left[\operatorname{tr}(\boldsymbol{VWA}^{\mathrm{T}})-\frac{1}{2}\operatorname{tr}(\boldsymbol{VW})\operatorname{tr}\mathbf{A}\right]\boldsymbol{I}\,.
\end{aligned}\tag{2.40}$$

As Rivlin and Smith (1975) have shown, neither Eq. (2.38) nor Eq. (2.40) are consequences of one another. They both have been used in the literature extensively in generating minimal invariant bases for tensor and vector products.

The following theorem gives the essential and summarizing results of this section pertaining to invariants of matrix products:

Theorem 2.1 *The trace of a matrix polynomial using k three-dimensional matrices* $\boldsymbol{A}_{\mathbf{s}}$ $(\mathbf{s}=s_1,\ldots,s_k)$ *can be written as a polynomial in traces of matrix products that satisfy the following conditions*:

1. *The matrix product is made of factors involving* $\boldsymbol{A}_{\mathbf{s}}$, $\boldsymbol{A}_{\mathbf{s}}^2$, $\boldsymbol{A}_{\mathbf{s}}^3$.
2. *The first and last factors are not powers of the same matrix.*
3. *If the matrix product incorporates* $\boldsymbol{A}_{\mathbf{s}}^3$ *as a factor, it contains no other factors.*
4. *No two factors are identical.*
5. $\boldsymbol{A}_{\mathbf{s}}$ *comes before* $\boldsymbol{A}_{\mathbf{s}}^2$ *in any product if these two factors appear.*
6. *When* $\boldsymbol{A}_{s_i}^2$ *and* $\boldsymbol{A}_{s_j}^2$ $(s_i \neq s_j)$ *are present, they must be consecutive factors or the first and last factors of the product.*
7. *The highest total degree reached in the product of the matrices* $\boldsymbol{A}_{\mathbf{s}}$ *is six.*

2.3 Integrity Bases for Vectors and Tensors

The discussion in Sect. 2.2 focused on the construction of matrix invariants since this has been the historical path followed within the continuum mechanics community as evidenced by the extensive literature base cited. However, our interest in the development of constitutive equations for fluids and flows is to provide some specification for either the material stress or the turbulent stress field. Both these stress fields are necessarily represented by second-order tensors. These second-order tensors can in turn be functionals of second-order tensors, and in cases with heat transfer effects, for example, also functions of vector scalar fluxes for heat (and possibly mass). It is then a matter of relating the results of matrix invariants to those for vectors and tensors. As highlighted at the beginning of this chapter, the matrices containing the components of a tensor serve to describe the corresponding tensor, but the tensor is represented by different matrices in different coordinate systems; although the tensor itself is independent of the coordinate system (the same is true for a column (or row) matrix for a vector). Thus an invariant formed from a tensor quantity or an invariant formed from the corresponding matrix of the components yield equivalent information.

Let us assume that a set of vectors and tensors and a group of transformations are given. Oftentimes a task requires obtaining a set of basic invariants capable of generating all other invariants with no redundancies. (For the purposes here, only polynomial invariants will be considered.) Following Spencer (1971), such a polynomial invariant will be called irreducible if it cannot be expressed as a polynomial in other invariants. If the set comprising these polynomial invariants is such that any polynomial invariant can be written as a polynomial using only members of this given set, then this set is termed an *integrity basis*. One of the goals for building such a basis is to avoid redundant terms in a way that the basis is minimal, i.e. it contains the minimum number of elements. Of course, all members of a minimal integrity basis should be irreducible. In addition, there sometimes exist polynomial relations between invariants that prevent an invariant from being expressed as a polynomial in terms of the integrity basis. These polynomial relations are called *syzygies* and are useful in assessing the minimality of the integrity basis. The interested reader is referred to Spencer (1971) and associated references for additional discussion on this topic. Thus, polynomial invariants (the integrity bases) formed from the matrix products discussed in Sect. 2.2 apply equally to the corresponding tensor quantities.

In the remainder of this chapter, the integrity bases (irreducible invariants) for the vector and tensor quantities will be formed directly from the results of the previous section.

2.3.1 Integrity Basis for Vectors

The invariants of vectors are well known and include both their length and relative orientation. For example, for the simple case of two vectors $\mathbf{u}$ and $\mathbf{v}$, the associated invariants are

$$\mathbf{u}\cdot\mathbf{u},\ \mathbf{u}\cdot\mathbf{v},\ \mathbf{v}\cdot\mathbf{v} \qquad \text{or} \qquad u_i u_i,\ u_i v_i,\ v_i v_i\ . \tag{2.41}$$

From the definitions at the beginning of Sect. 2.2, these are even invariants of the vectors $\mathbf{u}$ and $\mathbf{v}$. For the case of three vectors, $\mathbf{u}$, $\mathbf{v}$, $\mathbf{w}$, the triple scalar product

$$\mathbf{u}\cdot(\mathbf{v}\times\mathbf{w}) \qquad \text{or} \qquad e_{ijk}u_i v_j w_k\ , \tag{2.42}$$

is also an invariant—an odd invariant due to the sign change with the permutation of indices; however, it can be shown (e.g. see Spencer 1971, page 256) that this scalar quantity is related to the vector scalar products. If the product of two triple scalar products is considered, the relationship with the scalar products in Eq. (2.41) can be found using Eq. (2.23),

$$(e_{ijk}u_i v_j w_k)\,(e_{lmn}x_l y_m z_n) = \begin{vmatrix} u_i x_i & u_i y_i & u_i z_i \\ v_i x_i & v_i y_i & v_i z_i \\ w_i x_i & w_i y_i & w_i z_i \end{vmatrix}\ , \tag{2.43}$$

which relates the invariants in Eq. (2.41) with those in Eq. (2.42). Such a functional relationship is an example of a syzygy introduced in the last section. Both these invariant relations can be easily extended to larger numbers of vectors, so that the corresponding generalized invariant relations are given by

$$\mathbf{u_r}\cdot\mathbf{u_s},\quad \mathbf{u_r}\cdot(\mathbf{u_s}\times\mathbf{u_t}) \quad (r_i,\ s_i,\ t_i,\ i=1,2,\ldots)\ . \tag{2.44}$$

For the odd invariants generated by the triple scalar product, $\mathbf{r}$, $\mathbf{s}$, and $\mathbf{t}$ are necessarily all different. If absolute invariants are only considered (see end of Sect. 2.2), then both types of invariants need to be considered for the proper orthogonal group; however, for the full orthogonal group only the scalar product should be retained. In either group, the elements generated consist of the (minimal) integrity basis for vectors.

2.3.2 Integrity Bases for Symmetric Second-Order Tensors

From the principal invariants (2.30)–(2.32) and Theorem 2.1, it is not difficult to deduce that the integrity basis for a single symmetric tensor $\boldsymbol{D}$ is given by the associated matrix invariants

$$\operatorname{tr}\boldsymbol{D},\ \operatorname{tr}\boldsymbol{D}^2,\ \operatorname{tr}\boldsymbol{D}^3\ . \tag{2.45}$$

Recalling that the trace of a matrix product is equal to the trace of its transpose, the trace of a matrix product composed of symmetric matrices is equal to the trace of the matrix product built on the factors taken in reverse order. For the case of two tensors $\boldsymbol{D}$, $\boldsymbol{E}$, each of the associated matrices them has the invariants listed in Eq. (2.45), and according to Theorem 2.1, the additional matrix products to be considered are

$$\boldsymbol{DE},\ \boldsymbol{DE}^2,\ \boldsymbol{ED}^2,\ \boldsymbol{D}^2\boldsymbol{E}^2,\ \boldsymbol{DED}^2\boldsymbol{E}^2\ , \tag{2.46}$$

and the invariants associated with the matrix products of $\boldsymbol{D}$ and $\boldsymbol{E}$ are

$$\operatorname{tr}\boldsymbol{DE},\ \operatorname{tr}\boldsymbol{DE}^2,\ \operatorname{tr}\boldsymbol{ED}^2,\ \operatorname{tr}\boldsymbol{D}^2\boldsymbol{E}^2,\ \operatorname{tr}\boldsymbol{DED}^2\boldsymbol{E}^2 \tag{2.47}$$

Of these five invariants, the first four are irreducible, but the last one is reducible. It is useful to show how this last invariant $\operatorname{tr}\boldsymbol{DED}^2\boldsymbol{E}^2$ can be expressed in terms of irreducible invariants.

The generalized Cayley-Hamilton theorem, Eq. (2.38) is used to show the reducibility of an invariant. Since $\operatorname{tr}\boldsymbol{DED}^2\boldsymbol{E}^2$ contains matrix factors of degree two, Eq. (2.39) is rewritten for the case $\boldsymbol{F} = \boldsymbol{D}$ such that

$$\operatorname{tr}\left(\boldsymbol{DED} + \boldsymbol{D}^2\boldsymbol{E} + \boldsymbol{ED}^2\right)\boldsymbol{P} \equiv 0\ , \tag{2.48a}$$

and with $\boldsymbol{P} = \boldsymbol{DE}^2$ as

$$\operatorname{tr}\left(\boldsymbol{DED}^2\boldsymbol{E}^2 + \boldsymbol{D}^2\boldsymbol{EDE}^2 + \boldsymbol{ED}^3\boldsymbol{E}^2\right) \equiv 0\ , \tag{2.48b}$$

where the notation introduced in Sect. 2.2.2 has been used. Since the last term on the left in Eq. (2.48b), $\operatorname{tr}\boldsymbol{ED}^3\boldsymbol{E}^2 = \operatorname{tr}\boldsymbol{D}^3\boldsymbol{E}^3$ is reducible by a repeated application of Eq. (2.36), Eq. (2.48b) then reduces to

$$\operatorname{tr}\boldsymbol{DED}^2\boldsymbol{E}^2 = -\operatorname{tr}\boldsymbol{D}^2\boldsymbol{EDE}^2\ . \tag{2.49}$$

Since a cyclic interchange of factors leaves the trace of the matrix product unchanged and since the matrices are symmetric, a transposition of indices also leaves the trace of the matrix product unchanged. It follows that $\operatorname{tr}\boldsymbol{D}^2\boldsymbol{EDE}^2 = \operatorname{tr}\boldsymbol{DED}^2\boldsymbol{E}^2$ and

$$\operatorname{tr}\boldsymbol{DED}^2\boldsymbol{E}^2 \equiv 0\ , \tag{2.50}$$

so that $\operatorname{tr}\boldsymbol{DED}^2\boldsymbol{E}^2$ can be expressed in terms of invariants of lower degree and is therefore reducible. Relating this to the symmetric second-order tensors, the resulting integrity basis then consists of

$$\operatorname{tr}\boldsymbol{D},\ \operatorname{tr}\boldsymbol{D}^2,\ \operatorname{tr}\boldsymbol{D}^3,\ \operatorname{tr}\boldsymbol{E},\ \operatorname{tr}\boldsymbol{E}^2,\ \operatorname{tr}\boldsymbol{E}^3,\ \operatorname{tr}\boldsymbol{DE},\ \operatorname{tr}\boldsymbol{DE}^2,\ \operatorname{tr}\boldsymbol{ED}^2,\ \operatorname{tr}\boldsymbol{D}^2\boldsymbol{E}^2\ . \tag{2.51}$$

Spencer (1971) has summarized the development of these six factor products in Art. 2.5 of this reference and the list is given here in Table 2.1. Since, as Theorem 2.1 states, no invariant can involve more than six distinct matrices, cases where more than six matrices are involved simply requires taking bases for matrices six at a time in all possible combinations.

Table 2.1 Matrix products of symmetric matrices whose traces form the integrity basis for the full and proper orthogonal group. An *asterisk* ($*$) indicates that in addition to the trace of any matrix product, the integrity basis includes traces of matrix products formed by cyclic permutation of the symmetric matrices. (Adapted from Spencer 1971, Table II, page 288)

Matrices	Matrix products
A	$\mathbf{A}$; $\mathbf{A}^2$; $\mathbf{A}^3$
A, **B**	$\mathbf{AB}$; $\mathbf{AB}^{2*}$; $\mathbf{A}^2\mathbf{B}^2$
A, **B**, **C**	$\mathbf{ABC}$; $\mathbf{A}^2\mathbf{BC}^*$; $\mathbf{A}^2\mathbf{B}^2\mathbf{C}^*$
A, **B**, **C**, **D**	$\mathbf{ABCD}$, $\mathbf{ABDC}$; $\mathbf{A}^2\mathbf{BCD}^*$, $\mathbf{A}^2\mathbf{BDC}^*$; $\mathbf{A}^2\mathbf{B}^2\mathbf{CD}$, $\mathbf{A}^2\mathbf{C}^2\mathbf{BD}$, $\mathbf{A}^2\mathbf{D}^2\mathbf{BC}$, $\mathbf{B}^2\mathbf{C}^2\mathbf{AD}$, $\mathbf{B}^2\mathbf{D}^2\mathbf{AC}$, $\mathbf{C}^2\mathbf{D}^2\mathbf{AB}$; $\mathbf{A}^2\mathbf{BACD}^*$
A, **B**, **C**, **D**, **E**	$\mathbf{ABCDE}$, $\mathbf{ABDEC}$, $\mathbf{ABECD}$, $\mathbf{ACBED}$, $\mathbf{ACDBE}$, $\mathbf{ADBCE}$; $\mathbf{A}^2\mathbf{BCDE}^*$, $\mathbf{A}^2\mathbf{BCED}^*$, $\mathbf{A}^2\mathbf{CBDE}^*$, $\mathbf{A}^2\mathbf{BEDC}^*$
A, **B**, **C**, **D**, **E**, **F**	$\mathbf{ACFEBD}$, $\mathbf{ADCBFE}$, $\mathbf{ADCFBE}$, $\mathbf{ADFBCE}$, $\mathbf{ADFCBE}$, $\mathbf{AEBDCF}$, $\mathbf{AECBDF}$, $\mathbf{AECDBF}$, $\mathbf{AEDBCF}$, $\mathbf{AEDCBF}$

2.3.3 Integrity Bases for Vectors and Second-Order Tensors

In determining the invariants and integrity basis associated with vectors and second-order (symmetric and skew-symmetric) tensors it is necessary to further delineate the discussion by identifying the transformation group. The reason for this is the nature of the invariants formed depending on whether absolute or axial vectors are involved. These vectors and their corresponding transformation properties were shown in Eqs. (2.14) and (2.13).

2.3.3.1 Proper Orthogonal Group

For this transformation group, the distinction between absolute and axial vectors does not exist so all invariants can be considered as absolute invariants. Recall from Sect. 2.1 that an axial vector can be associated with a skew-symmetric tensor. The invariants formed from combinations of symmetric $(\boldsymbol{A}, \boldsymbol{B}, \boldsymbol{C}, \ldots)$ and skew-symmetric $(\boldsymbol{X}, \boldsymbol{Y}, \boldsymbol{Z}, \ldots)$ matrices have been obtained previously (Spencer and Rivlin 1962; Spencer 1965, 1971) and the associated integrity bases are a combination of those listed in Table 2.1 and those listed in Table 2.2. Once again, from Theorem 2.1 the highest total degree in the matrices is six, so that from Eq. (2.25b) the maximum number of vectors (that is, skew-symmetric matrices) is limited to three.

2.3.3.2 Full Orthogonal Group

Unlike the proper group, a distinction needs to be made here between absolute and axial vectors. However, since axial vectors can be associated with skew-symmetric

Table 2.2 Matrix products of symmetric and skew-symmetric matrices whose traces form part of the integrity basis for the proper orthogonal group. An *asterisk* ($*$) indicates that in addition to the trace of any matrix product, the integrity basis includes traces of matrix products formed by cyclic permutation of the symmetric matrices. A *dagger* ($\dagger$) indicates that in addition to the trace of any matrix product, the integrity basis includes traces of matrix products formed by cyclic permutation of the skew-symmetric matrices. (Adapted from Spencer 1971, Table II, page 288)

Matrices	Matrix products
$\mathbf{X}$	$\mathbf{X}^2$
$\mathbf{X}$, $\mathbf{A}$	$\mathbf{X}^2\mathbf{A}$; $\mathbf{X}^2\mathbf{A}^2$; $\mathbf{X}^2\mathbf{A}\mathbf{X}\mathbf{A}^2$
$\mathbf{X}$, $\mathbf{A}$, $\mathbf{B}$	$\mathbf{X}\mathbf{A}\mathbf{B}$; $\mathbf{X}\mathbf{A}^2\mathbf{B}^*$; $\mathbf{X}\mathbf{A}^2\mathbf{B}^2$; $\mathbf{X}\mathbf{A}^2\mathbf{B}\mathbf{A}^*$; $\mathbf{X}\mathbf{A}^2\mathbf{B}^2\mathbf{A}^*$; $\mathbf{X}^2\mathbf{A}\mathbf{B}$; $\mathbf{X}^2\mathbf{A}^2\mathbf{B}^*$; $\mathbf{X}^2\mathbf{A}\mathbf{X}\mathbf{B}$; $\mathbf{X}^2\mathbf{A}\mathbf{X}\mathbf{B}^{2*}$
$\mathbf{X}$, $\mathbf{A}$, $\mathbf{B}$, $\mathbf{C}$	$\mathbf{X}\mathbf{A}\mathbf{B}\mathbf{C}$, $\mathbf{X}\mathbf{A}\mathbf{C}\mathbf{B}$, $\mathbf{X}\mathbf{B}\mathbf{A}\mathbf{C}$; $\mathbf{X}\mathbf{A}^2\mathbf{B}\mathbf{C}^*$, $\mathbf{X}\mathbf{A}^2\mathbf{C}\mathbf{B}^*$, $\mathbf{X}\mathbf{B}\mathbf{A}^2\mathbf{C}^*$; $\mathbf{X}\mathbf{A}^2\mathbf{B}\mathbf{C}\mathbf{A}^*$; $\mathbf{X}\mathbf{A}^2\mathbf{B}^2\mathbf{C}^*$, $\mathbf{X}\mathbf{B}^2\mathbf{A}^2\mathbf{C}^*$; $\mathbf{X}^2\mathbf{A}\mathbf{B}\mathbf{C}$, $\mathbf{X}^2\mathbf{B}\mathbf{C}\mathbf{A}$; $\mathbf{X}^2\mathbf{A}^2\mathbf{B}\mathbf{C}^*$; $\mathbf{X}^2\mathbf{A}\mathbf{X}\mathbf{B}\mathbf{C}$
$\mathbf{X}$, $\mathbf{A}$, $\mathbf{B}$, $\mathbf{C}$, $\mathbf{D}$	$\mathbf{X}\mathbf{A}\mathbf{B}\mathbf{C}\mathbf{D}$, $\mathbf{X}\mathbf{A}\mathbf{B}\mathbf{D}\mathbf{C}$, $\mathbf{X}\mathbf{A}\mathbf{C}\mathbf{D}\mathbf{B}$, $\mathbf{X}\mathbf{B}\mathbf{A}\mathbf{C}\mathbf{D}$, $\mathbf{X}\mathbf{C}\mathbf{A}\mathbf{B}\mathbf{D}$; $\mathbf{X}\mathbf{B}\mathbf{A}^2\mathbf{C}\mathbf{D}^*$, $\mathbf{X}\mathbf{C}\mathbf{A}^2\mathbf{D}\mathbf{B}^*$, $\mathbf{X}\mathbf{D}\mathbf{A}^2\mathbf{B}\mathbf{C}$; $\mathbf{X}^2\mathbf{A}\mathbf{C}\mathbf{D}\mathbf{B}$, $\mathbf{X}^2\mathbf{A}\mathbf{B}\mathbf{D}\mathbf{C}$, $\mathbf{X}^2\mathbf{A}\mathbf{B}\mathbf{C}\mathbf{D}$
$\mathbf{X}$, $\mathbf{A}$, $\mathbf{B}$, $\mathbf{C}$, $\mathbf{D}$, $\mathbf{E}$	$\mathbf{X}\mathbf{B}\mathbf{D}\mathbf{A}\mathbf{C}\mathbf{E}$, $\mathbf{X}\mathbf{A}\mathbf{C}\mathbf{B}\mathbf{D}\mathbf{E}$, $\mathbf{X}\mathbf{A}\mathbf{B}\mathbf{C}\mathbf{E}\mathbf{D}$, $\mathbf{X}\mathbf{A}\mathbf{B}\mathbf{D}\mathbf{C}\mathbf{E}$, $\mathbf{X}\mathbf{A}\mathbf{C}\mathbf{E}\mathbf{B}\mathbf{D}$
$\mathbf{X}$, $\mathbf{Y}$	$\mathbf{X}\mathbf{Y}$
$\mathbf{X}$, $\mathbf{Y}$, $\mathbf{A}$	$\mathbf{X}\mathbf{Y}\mathbf{A}$; $\mathbf{X}\mathbf{Y}\mathbf{A}^2$; $\mathbf{X}^2\mathbf{Y}\mathbf{A}^\dagger$; $\mathbf{X}^2\mathbf{Y}\mathbf{A}^{2\dagger}$; $\mathbf{X}^2\mathbf{A}\mathbf{Y}\mathbf{A}^{2\dagger}$
$\mathbf{X}$, $\mathbf{Y}$, $\mathbf{A}$, $\mathbf{B}$	$\mathbf{X}\mathbf{Y}\mathbf{A}\mathbf{B}$, $\mathbf{X}\mathbf{Y}\mathbf{B}\mathbf{A}$; $\mathbf{X}\mathbf{Y}\mathbf{A}^2\mathbf{B}^*$, $\mathbf{X}\mathbf{Y}\mathbf{B}\mathbf{A}^{2*}$; $\mathbf{X}\mathbf{Y}\mathbf{A}^2\mathbf{B}^2$; $\mathbf{X}\mathbf{Y}\mathbf{A}^2\mathbf{B}\mathbf{A}^*$; $\mathbf{X}^2\mathbf{Y}\mathbf{A}\mathbf{B}^\dagger$; $\mathbf{X}^2\mathbf{A}\mathbf{Y}\mathbf{B}^\dagger$; $\mathbf{X}^2\mathbf{B}\mathbf{Y}\mathbf{A}^{*\dagger}$
$\mathbf{X}$, $\mathbf{Y}$, $\mathbf{A}$, $\mathbf{B}$, $\mathbf{C}$	$\mathbf{X}\mathbf{Y}\mathbf{A}\mathbf{B}\mathbf{C}$, $\mathbf{X}\mathbf{Y}\mathbf{A}\mathbf{C}\mathbf{B}$, $\mathbf{X}\mathbf{Y}\mathbf{B}\mathbf{A}\mathbf{C}$, $\mathbf{X}\mathbf{Y}\mathbf{B}\mathbf{C}\mathbf{A}$, $\mathbf{X}\mathbf{Y}\mathbf{C}\mathbf{A}\mathbf{B}$; $\mathbf{X}\mathbf{Y}\mathbf{A}^2\mathbf{B}\mathbf{C}^*$, $\mathbf{X}\mathbf{Y}\mathbf{A}^2\mathbf{C}\mathbf{B}^*$, $\mathbf{X}\mathbf{Y}\mathbf{B}\mathbf{C}\mathbf{A}^{2*}$; $\mathbf{X}^2\mathbf{A}\mathbf{Y}\mathbf{B}\mathbf{C}^\dagger$
$\mathbf{X}$, $\mathbf{Y}$, $\mathbf{A}$, $\mathbf{B}$, $\mathbf{C}$, $\mathbf{D}$	$\mathbf{X}\mathbf{Y}\mathbf{A}\mathbf{C}\mathbf{D}\mathbf{B}$, $\mathbf{X}\mathbf{Y}\mathbf{A}\mathbf{B}\mathbf{D}\mathbf{C}$, $\mathbf{X}\mathbf{Y}\mathbf{A}\mathbf{B}\mathbf{C}\mathbf{D}$, $\mathbf{X}\mathbf{Y}\mathbf{B}\mathbf{C}\mathbf{D}\mathbf{A}$, $\mathbf{X}\mathbf{Y}\mathbf{B}\mathbf{A}\mathbf{D}\mathbf{C}$, $\mathbf{X}\mathbf{Y}\mathbf{C}\mathbf{B}\mathbf{D}\mathbf{A}$
$\mathbf{X}$, $\mathbf{Y}$, $\mathbf{Z}$	$\mathbf{X}\mathbf{Y}\mathbf{Z}$
$\mathbf{X}$, $\mathbf{Y}$, $\mathbf{Z}$, $\mathbf{A}$	$\mathbf{X}\mathbf{Y}\mathbf{Z}\mathbf{A}$, $\mathbf{X}\mathbf{Z}\mathbf{Y}\mathbf{A}$; $\mathbf{X}\mathbf{Y}\mathbf{Z}\mathbf{A}^2$, $\mathbf{X}\mathbf{Z}\mathbf{Y}\mathbf{A}^2$; $\mathbf{X}\mathbf{Y}\mathbf{A}\mathbf{Z}\mathbf{A}^2$
$\mathbf{X}$, $\mathbf{Y}$, $\mathbf{Z}$, $\mathbf{A}$, $\mathbf{B}$	$\mathbf{X}\mathbf{Y}\mathbf{Z}\mathbf{A}\mathbf{B}$, $\mathbf{Y}\mathbf{Z}\mathbf{X}\mathbf{A}\mathbf{B}$, $\mathbf{X}\mathbf{Y}\mathbf{A}\mathbf{Z}\mathbf{B}$; $\mathbf{X}\mathbf{Y}\mathbf{B}\mathbf{Z}\mathbf{A}^{2*}$
$\mathbf{X}$, $\mathbf{Y}$, $\mathbf{Z}$, $\mathbf{A}$, $\mathbf{B}$, $\mathbf{C}$	$\mathbf{X}\mathbf{Y}\mathbf{A}\mathbf{Z}\mathbf{B}\mathbf{C}$

tensors (see Eq. (2.12)), and these skew-symmetric tensors transform as second-order tensors, they do not have to be included directly. Thus, it is only necessary to obtain integrity bases for arbitrary numbers of absolute vectors, symmetric tensors, and skew-symmetric tensors. Such integrity bases for this transformation group were first obtained by Smith (1965). Since the full group contains the proper group, invariants contained in the proper group are invariants in the full group (although invariants that are irreducible under the full group may not be irreducible under the proper group). This allows for the invariants given in Tables 2.1 and 2.2 to be included in obtaining the invariants in the full group.

The identification of the integrity basis becomes clearer by associating symmetric and skew-symmetric tensors with the absolute vectors. Consider the matrices

quantities

$$[u_i u_j], \qquad [u_i v_j], \qquad [u_j v_i] = [u_i v_j]^T \tag{2.52}$$

from which the following tensor components

$$M_{ij}^{(u)} = [u_i u_j], \quad M_{ij}^{(u,v)} = \frac{1}{2}\left([u_i v_j] + [u_j v_i]^T\right), \quad N_{ij}^{(u,v)} = \frac{1}{2}\left([u_i v_j] - [u_j v_i]^T\right) \tag{2.53}$$

can be constructed, and where $M_{ij}^{(u)}$ and $M_{ij}^{(u,v)}$ are symmetric tensors and $N_{ij}^{(u,v)}$ is a skew-symmetric tensor. The determination of the integrity basis for a single vector $\mathbf{u}$ and the tensors $\boldsymbol{A}, \boldsymbol{B}, \boldsymbol{C}, \ldots, \boldsymbol{X}, \boldsymbol{Y}, \boldsymbol{Z}, \ldots$ now reduces to finding an integrity basis for the symmetric matrices $\boldsymbol{A}, \boldsymbol{B}, \boldsymbol{C}, \ldots, [u_i u_j]$, and the skew-symmetric matrices $\boldsymbol{X}, \boldsymbol{Y}, \boldsymbol{Z}, \ldots$. This is the case that was just treated in the previous section for the proper orthogonal group and so the results can be obtained from Tables 2.1 and 2.2. Since the invariants are formed from Eq. (2.21b), it is clear that only those invariants linear in $\boldsymbol{M}$ should be retained. An integrity basis for two vectors, $\mathbf{u}$ and $\mathbf{v}$, and symmetric and skew-symmetric tensors is obtained by combining with the integrity bases that involve the vectors singly, the integrity basis for the symmetric matrices $\boldsymbol{A}, \boldsymbol{B}, \boldsymbol{C}, \ldots, ([u_i v_j] + [u_j v_i])/2$ and skew-symmetric tensors $\boldsymbol{X}, \boldsymbol{Y}, \boldsymbol{Z}, \ldots, ([u_i v_j] - [u_j v_i])/2$. This integrity basis can also be read from Tables 2.1 and 2.2, where once again all invariants that are of degree two or higher in $([u_i v_j] + [u_j v_i])/2$ and $([u_i v_j] - [u_j v_i])/2$ should be discarded since the invariant is of the form given in Eq. (2.21b).

In summary, for the case of a single vector the invariants are of the form

$$u_i (\boldsymbol{\Pi}_k)_{ij} u_j \ , \tag{2.54a}$$

and for the case of two vectors, there are contributions from symmetric and skew-symmetric parts,

$$u_i (\boldsymbol{\Pi}_k)_{ij} v_j + v_i (\boldsymbol{\Pi}_k)_{ij} u_j \tag{2.54b}$$

$$u_i (\boldsymbol{\Theta}_k)_{ij} v_j - v_i (\boldsymbol{\Theta}_k)_{ij} u_j \ , \tag{2.54c}$$

respectively, with $\boldsymbol{\Pi}_k$ and $\boldsymbol{\Theta}_k$ representing an invariant entry in Tables 2.3a and 2.3b that form the integrity bases under the full orthogonal group for one or two vectors and up to three symmetric or skew-symmetric tensors. The notation $(\boldsymbol{\Pi}_k)_{ij}$ and $(\boldsymbol{\Theta}_k)_{ij}$ is used to define the matrices $[\Pi_{ij}^{(k)}]$ and $[\Theta_{ij}^{(k)}]$ extracted from the invariant entries $\boldsymbol{\Pi}_k$ and $\boldsymbol{\Theta}_k$. For example, let $\boldsymbol{\Pi}_k$ be the invariant $\mathrm{tr}\,\boldsymbol{ABC}$ $(= A_{kl} B_{ln} C_{nk})$ given in Table 2.3a (set $\boldsymbol{A}$, $\boldsymbol{B}$, $\boldsymbol{C}$, first entry), then $[\Pi_{ij}^{(k)}]$ is given by $[A_{il} B_{ln} C_{nj}]$, or let $\boldsymbol{\Theta}_k$ be the invariant $\mathrm{tr}\,\boldsymbol{AXY}$ $(= X_{kl} Y_{ln} A_{nk})$ given in Table 2.3b (set $\boldsymbol{X}$, $\boldsymbol{Y}$, $\boldsymbol{A}$, first entry), then $[\Theta_{ij}^{(k)}]$ is given by $[X_{il} Y_{ln} A_{nj}]$

Additionally, the results involving invariants formed with vectors and given in Table 2.3 must be combined with the invariants obtained from Tables 2.1 and 2.2 involving only the symmetric $\boldsymbol{A}, \boldsymbol{B}, \boldsymbol{C}, \ldots$ and skew-symmetric $\boldsymbol{X}, \boldsymbol{Y}, \boldsymbol{Z}, \ldots$ tensor components. While Table 2.3 only gives the cases of one and two vectors and a total

Table 2.3 Integrity bases for the full orthogonal group: (**a**) Invariants for one vector and symmetric part of two vectors; (**b**) Invariants for skew-symmetric part of two vectors. (Adapted from Spencer 1971, Table III, page 293)

Matrices	$\mathbf{\Pi}_k$
None	$\mathbf{I}$
$\mathbf{X}$	$\mathbf{X}^2$
$\mathbf{A}$	$\mathbf{A}, \mathbf{A}^2$
$\mathbf{X}, \mathbf{Y}$	$\mathbf{XY}, \mathbf{X}^2\mathbf{Y}, \mathbf{XY}^2$
$\mathbf{X}, \mathbf{A}$	$\mathbf{XA}, \mathbf{XA}^2, \mathbf{AXA}^2, \mathbf{X}^2\mathbf{A}, \mathbf{X}^2\mathbf{A}^2, \mathbf{X}^2\mathbf{AX}, \mathbf{XA}^2\mathbf{X}^2$
$\mathbf{A}, \mathbf{B}$	$\mathbf{AB}, \mathbf{A}^2\mathbf{B}, \mathbf{AB}^2, \mathbf{A}^2\mathbf{B}^2$
$\mathbf{X}, \mathbf{Y}, \mathbf{Z}$	$\mathbf{XYZ}, \mathbf{XZY}$
$\mathbf{X}, \mathbf{Y}, \mathbf{A}$	$\mathbf{XYA}, \mathbf{AXY}, \mathbf{XYA}^2, \mathbf{YXA}^2, \mathbf{AXYA}^2, \mathbf{X}^2\mathbf{YA}, \mathbf{Y}^2\mathbf{XA}, \mathbf{X}^2\mathbf{AY}, \mathbf{Y}^2\mathbf{AX}, \mathbf{YA}^2\mathbf{X}^2, \mathbf{XA}^2\mathbf{Y}^2$
$\mathbf{X}, \mathbf{A}, \mathbf{B}$	$\mathbf{XAB}, \mathbf{AXB}, \mathbf{ABX}, \mathbf{XA}^2\mathbf{B}, \mathbf{AXB}^2, \mathbf{BXA}^2, \mathbf{XB}^2\mathbf{A}, \mathbf{XBA}^2, \mathbf{B}^2\mathbf{AX}, \mathbf{AXA}^2\mathbf{B}, \mathbf{ABXB}^2, \mathbf{XA}^2\mathbf{B}^2, \mathbf{XB}^2\mathbf{A}^2, \mathbf{X}^2\mathbf{AB}, \mathbf{BX}^2\mathbf{A}, \mathbf{X}^2\mathbf{A}^2\mathbf{B}, \mathbf{AX}^2\mathbf{B}^2, \mathbf{X}^2\mathbf{AXB}$
$\mathbf{A}, \mathbf{B}, \mathbf{C}$	$\mathbf{ABC}, \mathbf{CAB}, \mathbf{A}^2\mathbf{BC}, \mathbf{AB}^2\mathbf{C}, \mathbf{ABC}^2, \mathbf{CA}^2\mathbf{B}, \mathbf{B}^2\mathbf{CA}, \mathbf{BAC}^2, \mathbf{A}^2\mathbf{B}^2\mathbf{C}, \mathbf{A}^2\mathbf{C}^2\mathbf{B}, \mathbf{B}^2\mathbf{C}^2\mathbf{A}, \mathbf{A}^2\mathbf{BAC}, \mathbf{AB}^2\mathbf{CB}, \mathbf{CABC}^2$

(a) Invariants are products of the forms $u_i(\mathbf{\Pi}_k)_{ij}u_j$, $u_i(\mathbf{\Pi}_k)_{ij}v_j + v_i(\mathbf{\Pi}_k)_{ij}u_j$

Matrices	$\mathbf{\Theta}_k$
$\mathbf{X}$	$\mathbf{X}$
$\mathbf{X}, \mathbf{Y}$	$\mathbf{XY}$
$\mathbf{X}, \mathbf{A}$	$\mathbf{AX}, \mathbf{A}^2\mathbf{X}, \mathbf{AX}^2, \mathbf{A}^2\mathbf{X}^2, \mathbf{A}^2\mathbf{X}^2\mathbf{A}$
$\mathbf{A}, \mathbf{B}$	$\mathbf{AB}, \mathbf{A}^2\mathbf{B}, \mathbf{B}^2\mathbf{A}, \mathbf{A}^2\mathbf{B}^2, \mathbf{A}^2\mathbf{BA}, \mathbf{B}^2\mathbf{AB}, \mathbf{A}^2\mathbf{B}^2\mathbf{A}, \mathbf{B}^2\mathbf{A}^2\mathbf{B}$
$\mathbf{X}, \mathbf{Y}, \mathbf{A}$	$\mathbf{AXY}, \mathbf{YAX}, \mathbf{A}^2\mathbf{XY}, \mathbf{YA}^2\mathbf{X}, \mathbf{A}^2\mathbf{XYA}$
$\mathbf{X}, \mathbf{A}, \mathbf{B}$	$\mathbf{ABX}, \mathbf{BAX}, \mathbf{A}^2\mathbf{BX}, \mathbf{B}^2\mathbf{AX}, \mathbf{XA}^2\mathbf{B}, \mathbf{XB}^2\mathbf{A}, \mathbf{A}^2\mathbf{B}^2\mathbf{X}, \mathbf{A}^2\mathbf{BAX}, \mathbf{B}^2\mathbf{ABX}, \mathbf{ABX}^2, \mathbf{BX}^2\mathbf{A}, \mathbf{A}^2\mathbf{X}^2\mathbf{B}, \mathbf{B}^2\mathbf{X}^2\mathbf{A}$
$\mathbf{A}, \mathbf{B}, \mathbf{C}$	$\mathbf{ABC}, \mathbf{BCA}, \mathbf{CAB}, \mathbf{A}^2\mathbf{BC}, \mathbf{B}^2\mathbf{CA}, \mathbf{C}^2\mathbf{AB}, \mathbf{A}^2\mathbf{CB}, \mathbf{B}^2\mathbf{AC}, \mathbf{C}^2\mathbf{BA}, \mathbf{BA}^2\mathbf{C}, \mathbf{CB}^2\mathbf{A}, \mathbf{AC}^2\mathbf{B}, \mathbf{A}^2\mathbf{BCA}, \mathbf{B}^2\mathbf{CAB}, \mathbf{C}^2\mathbf{ABC}, \mathbf{A}^2\mathbf{B}^2\mathbf{C}, \mathbf{B}^2\mathbf{C}^2\mathbf{A}, \mathbf{C}^2\mathbf{A}^2\mathbf{B}, \mathbf{B}^2\mathbf{A}^2\mathbf{C}, \mathbf{C}^2\mathbf{B}^2\mathbf{A}, \mathbf{A}^2\mathbf{C}^2\mathbf{B}$

(b) Invariants are products of the form $u_i(\mathbf{\Theta}_k)_{ij}v_j - v_i(\mathbf{\Theta}_k)_{ij}u_j$

of three matrices of tensor components, a more complete list for the cases of one and two vectors and a total of six matrices of tensor components can be found in Smith (1965).

2.4 Polynomial Representations for Tensors and Vectors

Since the fluids and flows under discussion will require a specification of a material or turbulent stress tensor as well as vector scalar fluxes, it is often necessary to provide models, or closure, for these and other quantities. At its lowest level, this requires representing tensor and vector functions, that possess certain transformation properties, by known tensor and vector functions that possess the same transformation properties.

The results of the previous section have provided a list of the various integrity (invariant) bases that can be associated with polynomial invariants. From these, it is possible to construct, from the dependent tensors and vectors (and their associated matrices), polynomial representations of tensor and vector functions. The discussion to follow is best divided between polynomial representations within the proper orthogonal group and those within the full orthogonal group. Similarities, of course, exist between the two but differ in detail sufficiently to warrant a separate discussion. While it will be possible in the following to identify the various basis tensors for the respective polynomial representations as well as the functional dependencies of the corresponding expansion coefficients, the determination of these coefficients will be left to later and discussed within the particular context in which the representation is used.

2.4.1 Proper Orthogonal Group

As alluded to at the beginning of this chapter, one of the important topics to be discussed is the development of constitutive equations for viscoelastic fluids and turbulent flows. A common feature in both cases is the need to prescribe a (symmetric) stress tensor. For the viscoelastic fluid this entails an extra-stress tensor, and a turbulent stress tensor for the turbulent flow. Polynomial representations for second-order tensors within this group will be the focus of this section, and the cases examined, while not exhaustive, will provide the framework for the procedure to follow in constructing such a tensor representation.

Consider a tensor polynomial function $\boldsymbol{P}$, and the scalar invariant $\mathcal{J}$ formed from $\boldsymbol{P}$ and an arbitrary second-order tensor $\boldsymbol{\psi}$,

$$\mathcal{J} = \operatorname{tr} \boldsymbol{P}\boldsymbol{\psi} = P_{ij}\psi_{ij}^T = \psi_{ij}P_{ij}^T \,, \tag{2.55}$$

where as shown a distinction is necessarily made between ψ_{ij} and ψ_{ij}^T in order to properly account for both symmetric and skew-symmetric tensor functions $\boldsymbol{P}$. The tensor components P_{ij} and P_{ij}^T are then directly obtained from Eq. (2.55) as

$$P_{ij} = \frac{\partial \mathcal{J}}{\partial \psi_{ij}^T} \quad \text{and} \quad P_{ij}^T = \frac{\partial \mathcal{J}}{\partial \psi_{ij}} \,. \tag{2.56}$$

For a symmetric tensor function $\boldsymbol{P}$, Eq. (2.56) yields

$$P_{ij} = P_{ij}^T = P_{ji} = \frac{\partial \mathcal{J}}{\partial \psi_{ij}^T} = \frac{\partial \mathcal{J}}{\partial \psi_{ij}} \,, \tag{2.57a}$$

where $\boldsymbol{\psi}$ is a symmetric tensor function, and for s skew-symmetric tensor function $\boldsymbol{P}$, Eq. (2.56) yields

$$P_{ij} = -P_{ij}^T = -P_{ji} = \frac{\partial \mathcal{J}}{\partial \psi_{ij}^T} = -\frac{\partial \mathcal{J}}{\partial \psi_{ij}} , \tag{2.57b}$$

where $\boldsymbol{\psi}$ is now a skew-symmetric tensor function.

In Sect. 2.3, integrity bases comprising combinations of tensors and vectors were presented. These invariant basis elements can be used to construct polynomial invariants for $\mathcal{J}$ through

$$\mathcal{J} = \sum_k I_k \mathcal{J}_k = \frac{1}{2} \sum_k I_k \, \mathrm{tr} \left(\boldsymbol{\Phi}_k \boldsymbol{\psi}^T + \boldsymbol{\psi} \boldsymbol{\Phi}_k^T \right) , \tag{2.58}$$

where I_k are expansion coefficients that can also be polynomials in the integrity basis of the tensor dependencies of $\boldsymbol{P}$, and $\mathcal{J}_k$ are the invariants listed in Tables 2.1 and 2.2 formed from the tensor $\boldsymbol{\psi}$ and the tensor dependencies of $\boldsymbol{P}$. Using Eq. (2.58), the tensor representations for the symmetric tensor polynomial function

$$\begin{aligned} \frac{1}{2} \left(P_{ij} + P_{ij}^T \right) &= \frac{1}{2} \sum_k I_k \left(\frac{\partial \mathcal{J}_k}{\partial \psi_{ij}^T} + \frac{\partial \mathcal{J}_k}{\partial \psi_{ij}} \right) \\ &= \frac{1}{2} \sum_k I_k \left(\Phi_{ij}^{(k)} + \Phi_{ij}^{(k)T} \right) , \end{aligned} \tag{2.59a}$$

and the skew-symmetric tensor polynomial function

$$\begin{aligned} \frac{1}{2} \left(P_{ij} - P_{ij}^T \right) &= \frac{1}{2} \sum_k I_k \left(\frac{\partial \mathcal{J}_k}{\partial \psi_{ij}^T} - \frac{\partial \mathcal{J}_k}{\partial \psi_{ij}} \right) \\ &= \frac{1}{2} \sum_k I_k \left(\Phi_{ij}^{(k)} - \Phi_{ij}^{(k)T} \right) , \end{aligned} \tag{2.59b}$$

can be obtained from Eqs. (2.57a) and (2.57b), respectively. The tensor component basis elements $\Phi_{ij}^{(k)}$ ($\boldsymbol{\Phi}_k$) are thus identified with the algebraic differentiation of the invariant (integrity) basis given previously. As pointed out by Spencer (1971), these tensor functions are polynomials so that the differentiation operation shown here can be regarded as an algebraic process. Since the $\mathcal{J}_k$ are each matrix products involving tensor components, the differentiation process yields k tensor products that then form the tensor representation for $\boldsymbol{P}$.

For the proper orthogonal group, there is no distinction between absolute and axial vectors and all vectors are assumed related to second-order tensor quantities through Eq. (2.12). As such, results for vector functions of tensors are extracted from the cases where skew-symmetric functions are considered. However, since the primary interest is in the stress tensor which is a symmetric tensor for both the fluids and flows considered, the case of a skew-symmetric tensor function is not pursued here. The interested reader is referred to Spencer (1971) for some additional examples. Of course, representations for vector functions are of interest, particularly

in the case of scalar flux representations that often occur in turbulence modeling, but these are absolute vector functions and would be considered as representations under the full orthogonal group and will be discussed in Sect. 2.4.2.

2.4.1.1 Symmetric Tensor Function of Symmetric Tensors

In this first example, consider the symmetric, polynomial tensor function $\boldsymbol{\Sigma}$ which is assumed to be a function of two symmetric tensors, such that

$$\boldsymbol{\Sigma} = \boldsymbol{\Phi}\left(\boldsymbol{A}, \boldsymbol{B}\right), \quad \text{or} \quad \Sigma_{ij} = \Phi_{ij}\left(A_{pq}, B_{pq}\right) . \tag{2.60}$$

Now, the invariant function $\mathcal{J}$ given in Eq. (2.55) can be constructed from Σ_{ij} and an arbitrary symmetric second-order tensor ψ_{ij}. Using Eqs. (2.55) and (2.58), it follows that

$$\Sigma_{ij} = \sum_k I_k \frac{\partial \mathcal{J}_k}{\partial \psi_{ij}} \quad \text{and} \quad \Sigma_{ji} = \sum_k I_k \frac{\partial \mathcal{J}_k}{\partial \psi_{ji}} \tag{2.61a}$$

$$\Sigma_{ij} = \frac{1}{2} \sum_k I_k \left(\frac{\partial \mathcal{J}_k}{\partial \psi_{ij}} + \frac{\partial \mathcal{J}_k}{\partial \psi_{ji}} \right) . \tag{2.61b}$$

Since the representation for Σ_{ij} is a polynomial, Eq. (2.58) is assumed to apply and the expansion coefficients I_k are functions of the invariants formed from the functional dependencies of $\boldsymbol{\Sigma}$, that is $\boldsymbol{A}$, $\boldsymbol{B}$. The invariants formed from $\boldsymbol{A}$ and $\boldsymbol{B}$ are obtained directly from Table 2.1 and are given by

$$\begin{gathered} \operatorname{tr}\boldsymbol{A}, \quad \operatorname{tr}\boldsymbol{A}^2, \quad \operatorname{tr}\boldsymbol{A}^3, \quad \operatorname{tr}\boldsymbol{B}, \quad \operatorname{tr}\boldsymbol{B}^2, \quad \operatorname{tr}\boldsymbol{B}^3 \\ \operatorname{tr}\boldsymbol{A}\boldsymbol{B}, \quad \operatorname{tr}\boldsymbol{A}\boldsymbol{B}^2, \quad \operatorname{tr}\boldsymbol{B}\boldsymbol{A}^2, \quad \operatorname{tr}\boldsymbol{A}^2\boldsymbol{B}^2 . \end{gathered} \tag{2.62}$$

The $\mathcal{J}_k$ are then invariants formed from these same functional dependencies of Σ_{ij}, and ψ_{ij}. The $\mathcal{J}_k$ are then expressible in terms of the invariants $\operatorname{tr}\boldsymbol{\Phi}_k\boldsymbol{\psi}$, where $\boldsymbol{\Phi}_k$ are symmetric basis tensors extracted from the associated matrix products involving the associated matrices of the symmetric tensors $\boldsymbol{A}$ and $\boldsymbol{B}$. From Table 2.1, the integrity basis $\mathcal{J}_k$ involving $\boldsymbol{A}$, $\boldsymbol{B}$, $\boldsymbol{\psi}$, and by construction linear in $\boldsymbol{\psi}$, consists of the following eight elements

$$\begin{gathered} \operatorname{tr}\boldsymbol{A}\boldsymbol{\psi}, \quad \operatorname{tr}\boldsymbol{A}^2\boldsymbol{\psi}, \quad \operatorname{tr}\boldsymbol{B}\boldsymbol{\psi}, \quad \operatorname{tr}\boldsymbol{B}^2\boldsymbol{\psi} \\ \operatorname{tr}\boldsymbol{A}\boldsymbol{B}\boldsymbol{\psi}, \quad \operatorname{tr}\boldsymbol{A}^2\boldsymbol{B}\boldsymbol{\psi}, \quad \operatorname{tr}\boldsymbol{A}\boldsymbol{B}^2\boldsymbol{\psi}, \quad \operatorname{tr}\boldsymbol{A}^2\boldsymbol{B}^2\boldsymbol{\psi} . \end{gathered} \tag{2.63}$$

Equation (2.61b) can then be written as

$$\Sigma_{ij} = \frac{1}{2} \sum_k I_k \left(\boldsymbol{\Phi}_k + \boldsymbol{\Phi}_k^T \right) , \tag{2.64}$$

where

$$\Phi_{ij}^{(k)} = \frac{\partial \mathcal{J}_k}{\partial \psi_{ij}} \quad \text{and} \quad \Phi_{ji}^{(k)} = \frac{\partial \mathcal{J}_k}{\partial \psi_{ji}} , \tag{2.65}$$

and the resulting set of eight basis tensors are given by

$$\begin{aligned} \boldsymbol{\Phi}_1 &= \boldsymbol{A} & \boldsymbol{\Phi}_5 &= \boldsymbol{A}\boldsymbol{B} \\ \boldsymbol{\Phi}_2 &= \boldsymbol{B} & \boldsymbol{\Phi}_6 &= \boldsymbol{A}^2\boldsymbol{B} \\ \boldsymbol{\Phi}_3 &= \boldsymbol{A}^2 & \boldsymbol{\Phi}_7 &= \boldsymbol{A}\boldsymbol{B}^2 \\ \boldsymbol{\Phi}_4 &= \boldsymbol{B}^2 & \boldsymbol{\Phi}_8 &= \boldsymbol{A}^2\boldsymbol{B}^2 \end{aligned} \tag{2.66}$$

Although the example here is for a symmetric tensor function of two symmetric tensors, it should be recalled from Theorem 2.1 that no matrix product, used in representing the trace of a matrix product such as $\operatorname{tr}\boldsymbol{\Phi}\boldsymbol{\psi}$ in Eq. (2.55), can be greater than six. This then would inherently limit the discussion in this example to five symmetric tensors $\boldsymbol{A}$, $\boldsymbol{B}$, $\boldsymbol{C}$, $\boldsymbol{D}$, $\boldsymbol{E}$ and the arbitrary symmetric tensor $\boldsymbol{\psi}$. The trace of tensor component products with a higher number of functional dependencies can then be expressed in terms of traces of tensor component products of lower degree.

2.4.1.2 Symmetric Tensor Function of Symmetric and Skew-Symmetric Tensors

In the second example, a symmetric, polynomial tensor function $\boldsymbol{\Sigma}$ is considered which is now assumed to be a function of one symmetric and one skew-symmetric tensor, such that

$$\boldsymbol{\Sigma} = \boldsymbol{\Phi}(\boldsymbol{A}, \boldsymbol{X}), \quad \text{or} \quad \Sigma_{ij} = \Phi_{ij}\left(A_{pq}, X_{pq}\right). \tag{2.67}$$

The invariant function $\mathcal{J}$ is again given by Eq. (2.55) so that using Eq. (2.59a), the equalities given in Eqs. (2.61a) and (2.61b) hold.

In this example, the expansion coefficients I_k are functions of invariants formed from the functional dependencies of $\boldsymbol{\Sigma}$, that is $\boldsymbol{A}$, $\boldsymbol{X}$. The invariants formed from $\boldsymbol{A}$ and $\boldsymbol{X}$ are obtained directly from Table 2.2 and are given by

$$\operatorname{tr}\boldsymbol{A}, \quad \operatorname{tr}\boldsymbol{A}^2, \quad \operatorname{tr}\boldsymbol{X}^2, \quad \operatorname{tr}\boldsymbol{A}^3, \quad \operatorname{tr}\boldsymbol{X}^2\boldsymbol{A}, \quad \operatorname{tr}\boldsymbol{X}^2\boldsymbol{A}^2, \quad \operatorname{tr}\boldsymbol{X}^2\boldsymbol{A}\boldsymbol{X}\boldsymbol{A}^2. \tag{2.68}$$

The $\mathcal{J}_k$ are then expressible in terms of the invariants $\operatorname{tr}\boldsymbol{\Phi}_k\boldsymbol{\psi}$, where $\boldsymbol{\Phi}_k$ are symmetric basis tensors formed from products involving the symmetric tensor $\boldsymbol{A}$ and skew-symmetric tensor $\boldsymbol{X}$. From Tables 2.1 and 2.2, the integrity basis $\mathcal{J}_k$ involving $\boldsymbol{A}$, $\boldsymbol{X}$, and $\boldsymbol{\psi}$, and linear in $\boldsymbol{\psi}$, consists of the following ten elements

$$\begin{aligned} &\operatorname{tr}\boldsymbol{A}\boldsymbol{\psi}, \quad \operatorname{tr}\boldsymbol{\psi}\boldsymbol{A}^2, \quad \operatorname{tr}\boldsymbol{X}^2\boldsymbol{\psi}, \quad \operatorname{tr}\boldsymbol{X}\boldsymbol{A}\boldsymbol{\psi}, \quad \operatorname{tr}\boldsymbol{X}\boldsymbol{A}^2\boldsymbol{\psi}, \quad \operatorname{tr}\boldsymbol{A}\boldsymbol{X}\boldsymbol{A}^2\boldsymbol{\psi}, \\ &\operatorname{tr}\boldsymbol{X}^2\boldsymbol{A}\boldsymbol{\psi}, \quad \operatorname{tr}\boldsymbol{X}^2\boldsymbol{A}^2\boldsymbol{\psi}, \quad \operatorname{tr}\boldsymbol{X}^2\boldsymbol{A}\boldsymbol{X}\boldsymbol{\psi}, \quad \operatorname{tr}\boldsymbol{\psi}\boldsymbol{X}\boldsymbol{A}^2\boldsymbol{X}^2. \end{aligned} \tag{2.69}$$

The corresponding ten-term basis $\boldsymbol{\Phi}_k$, defined by Eq. (2.65), is given by

$$\begin{aligned} \boldsymbol{\Phi}_1 &= \boldsymbol{A} & \boldsymbol{\Phi}_6 &= \boldsymbol{X}^2\boldsymbol{A} \\ \boldsymbol{\Phi}_2 &= \boldsymbol{A}\boldsymbol{X} & \boldsymbol{\Phi}_7 &= \boldsymbol{X}\boldsymbol{A}\boldsymbol{X}^2 \\ \boldsymbol{\Phi}_3 &= \boldsymbol{A}^2 & \boldsymbol{\Phi}_8 &= \boldsymbol{A}\boldsymbol{X}\boldsymbol{A}^2 \\ \boldsymbol{\Phi}_4 &= \boldsymbol{X}^2 & \boldsymbol{\Phi}_9 &= \boldsymbol{X}^2\boldsymbol{A}^2 \\ \boldsymbol{\Phi}_5 &= \boldsymbol{X}\boldsymbol{A}^2 & \boldsymbol{\Phi}_{10} &= \boldsymbol{X}\boldsymbol{A}^2\boldsymbol{X}^2 \end{aligned} \tag{2.70}$$

Once again, the example could be generalized to more dependent tensors with, of course, a rapid increase in the number of basis tensors. Inclusion of absolute vectors in the list of dependent functions requires a slightly more detailed accounting of the invariants for both tensors and vectors. This topic will be taken up next.

2.4.2 Full Orthogonal Group

Since there was no need to distinguish between absolute and axial vectors under the proper orthogonal group, it was possible to account for any vector function or vector dependency by considering the corresponding skew-symmetric tensor function. Under the full orthogonal group, a distinction exists and it is necessary to obtain the additional invariants, and subsequent basis tensors, generated by these vectors. Two cases are of interest here under this transformation group. The first case includes vector functions that are functions of both vectors and tensors, and the second case includes tensor functions that are now functions of both vectors and tensors. The integrity bases in each have their origins in Tables 2.1–2.3.

First consider a vector polynomial function $\mathbf{p}$, and the scalar invariant $\mathcal{L}$ formed from $\mathbf{p}$ and an arbitrary vector function $\boldsymbol{\phi}$,

$$\mathcal{L} = \mathbf{p} \cdot \boldsymbol{\phi} = p_i \phi_i \ . \tag{2.71}$$

The vector function component p_i can then be directly obtained from Eq. (2.71) as

$$p_i = \frac{\partial \mathcal{L}}{\partial \phi_i} \ . \tag{2.72}$$

A polynomial expansion analogous to the form given in Eq. (2.58),

$$\mathcal{L} = \sum_k I_k \mathcal{L}_k = \sum_k I_k \left(\boldsymbol{\chi}_k \cdot \boldsymbol{\phi} \right) \ , \tag{2.73}$$

can be assumed so that

$$p_i = \sum_k I_k \frac{\partial \mathcal{L}_k}{\partial \phi_i} = \sum_k I_k \chi_i^{(k)} \ , \tag{2.74}$$

where I_k are expansion coefficients that can also be polynomials in the integrity basis of the tensor and vector dependencies of $\mathbf{p}$ listed in Tables 2.2 and 2.3 and $\mathcal{L}_k$ are the invariants formed from the vector $\boldsymbol{\phi}$ and the tensor and vector dependencies of $\mathbf{p}$ also listed in Tables 2.2 and 2.3.

The invariants $\mathcal{L}_k$ are of a form discussed in Sect. 2.3.3.2 and given by Eqs. (2.54a), (2.54b), (2.54c). For the case of two vectors, $\mathbf{u}$ and $\boldsymbol{\phi}$, the invariant forms are

$$u_i (\boldsymbol{\Pi}_k)_{ij} \phi_j + \phi_i (\boldsymbol{\Pi}_k)_{ij} u_j \tag{2.75a}$$

$$u_i (\boldsymbol{\Theta}_k)_{ij} \phi_j - \phi_i (\boldsymbol{\Theta}_k)_{ij} u_j \ , \tag{2.75b}$$

where $\boldsymbol{\Pi}_k$ and $\boldsymbol{\Theta}_k$ are given in Table 2.3. Using Eqs. (2.74), (2.75a) and (2.75b), the vector basis for $\boldsymbol{\chi}_k$ is found to be composed of contributions from

$$\left(\boldsymbol{\Pi}_k + \boldsymbol{\Pi}_k^T \right) \cdot \mathbf{u} \quad \text{and} \quad \left(\boldsymbol{\Theta}_k - \boldsymbol{\Theta}_k^T \right) \cdot \mathbf{u} \ . \tag{2.76}$$

Using Eq. (2.74), the integrity basis for the polynomial representation of $\mathbf{p}$ is then given by

$$\mathbf{p} = \sum_k I_k \left[\left(\boldsymbol{\Pi}_k + \boldsymbol{\Pi}_k^T \right) \cdot \mathbf{u} + \left(\boldsymbol{\Theta}_k - \boldsymbol{\Theta}_k^T \right) \cdot \mathbf{u} \right] . \tag{2.77}$$

The next case to be considered is the construction of the representation for a tensor polynomial function $\boldsymbol{P}$ of vectors and tensors. Although the primary interest here is in symmetric tensor functions (that is, the stress tensor field), the discussion that follows will include both symmetric and skew-symmetric tensor functions for completeness. The invariant $\mathcal{J}$ formed between the polynomial function $\boldsymbol{P}$ and the arbitrary second-order tensor $\boldsymbol{\psi}$ is once again given by Eq. (2.55), and its polynomial expansion given by

$$\mathcal{J} = \operatorname{tr} \boldsymbol{P}\boldsymbol{\psi} = \sum_k I_k \mathcal{J}_k , \tag{2.78}$$

where the expansion coefficients I_k are now invariants of the argument vectors and tensors of $\boldsymbol{P}$, and the invariants $\boldsymbol{\Pi}_k$ to be constructed consist of three distinct types of polynomial invariants formed from the vector and tensor dependencies of $\boldsymbol{P}$ and $\boldsymbol{\psi}$. The first type is composed of the invariants formed solely from the tensor dependencies of $\boldsymbol{P}$ and $\boldsymbol{\psi}$ and the other two types are composed of invariants that include both the vector and tensor dependencies of $\boldsymbol{P}$ and $\boldsymbol{\psi}$.

For the first type, the invariant $\mathcal{J}_k$ is analogous to the form given in Eq. (2.58),

$$\mathcal{J}_k = \operatorname{tr} \boldsymbol{\Phi}_k^{(1,1)} \boldsymbol{\psi} , \tag{2.79}$$

where the $\boldsymbol{\Phi}_k^{(1,1)}$ are extracted from Tables 2.1 and 2.2 (the superscripts in the matrix product $\boldsymbol{\Phi}_k^{(m,n)}$ are introduced in order to distinguish between the $m = 3$ distinct polynomial invariants that are to be introduced and the number n of factors appearing with each m polynomial invariants).

In Eqs. (2.54a), (2.54b), (2.54c) the expressions for the invariants formed from the product of one and two vectors and tensor products $\boldsymbol{\Pi}_k$ and $\boldsymbol{\Theta}_k$ were given. For the determination of the tensor basis, the tensor $\boldsymbol{\psi}$ is introduced and the products $\boldsymbol{\Pi}_k \boldsymbol{\psi}^T$ and $\boldsymbol{\Theta}_k \boldsymbol{\psi}^T$ formed. As was the case when representations for the proper orthogonal group were being considered in Sect. 2.4.1, the construction varies slightly when symmetric or skew-symmetric tensor functions are being considered, and the same holds for the full orthogonal group. For symmetric tensor functions, each invariant entry in Table 2.3 can be written in the form,

$$\boldsymbol{\Pi}_k = \boldsymbol{\Phi}_k^{(2,1)} \left(\boldsymbol{\psi} + \boldsymbol{\psi}^T \right) \boldsymbol{\Phi}_k^{(2,2)T} \tag{2.80a}$$

$$\boldsymbol{\Theta}_k = \boldsymbol{\Phi}_k^{(3,1)} \left(\boldsymbol{\psi} + \boldsymbol{\psi}^T \right) \boldsymbol{\Phi}_k^{(3,2)T} . \tag{2.80b}$$

with $\boldsymbol{\psi}$ a symmetric tensor, and for skew-symmetric tensor functions, each invariant entry in Table 2.3 can be written in the form

$$\boldsymbol{\Pi}_k = \boldsymbol{\Phi}_k^{(2,1)} \left(\boldsymbol{\psi} - \boldsymbol{\psi}^T \right) \boldsymbol{\Phi}_k^{(2,2)T} \tag{2.81a}$$

$$\boldsymbol{\Theta}_k = \boldsymbol{\Phi}_k^{(3,1)} \left(\boldsymbol{\psi} - \boldsymbol{\psi}^T \right) \boldsymbol{\Phi}_k^{(3,2)T} , \tag{2.81b}$$

with $\boldsymbol{\psi}$ a skew-symmetric tensor. The products $\boldsymbol{\Phi}^{(2,1)}$, $\boldsymbol{\Phi}^{(2,2)}$, $\boldsymbol{\Phi}^{(3,1)}$, and $\boldsymbol{\Phi}^{(3,2)}$ represent the different products combinations that can be associated with each element of $\boldsymbol{\Pi}_k$ and $\boldsymbol{\Theta}_k$.

From the invariants listed in Eq. (2.79) and formed using Eqs. (2.54a), (2.54b), (2.54c) with Eqs. (2.80a), (2.80b) or (2.81a), (2.81b), a polynomial representation for a symmetric tensor function $\boldsymbol{P}$ can be constructed. The basis tensors are obtained by the differentiation process described in Sect. 2.4.1 that yield

$$\boldsymbol{P} = \sum I_k \left[\boldsymbol{P}_k^1 + \boldsymbol{P}_k^2 + \boldsymbol{P}_k^3 + \boldsymbol{P}_k^4 \right] \tag{2.82}$$

$$\boldsymbol{P}_k^1 = (\boldsymbol{\Phi}_k^{(1,1)})_{ij} + (\boldsymbol{\Phi}_k^{(1,1)})_{ji} \tag{2.83a}$$

$$\boldsymbol{P}_k^2 = (\mathbf{u}\cdot\boldsymbol{\Phi}_k^{(2,1)})_i(\mathbf{u}\cdot\boldsymbol{\Phi}_k^{(2,2)})_j + (\mathbf{u}\cdot\boldsymbol{\Phi}_k^{(2,1)})_j(\mathbf{u}\cdot\boldsymbol{\Phi}_k^{(2,2)})_i \tag{2.83b}$$

$$\begin{aligned}\boldsymbol{P}_k^3 = {} & (\mathbf{u}\cdot\boldsymbol{\Phi}_k^{(2,1)})_i(\mathbf{v}\cdot\boldsymbol{\Phi}_k^{(2,2)})_j + (\mathbf{u}\cdot\boldsymbol{\Phi}_k^{(2,1)})_j(\mathbf{v}\cdot\boldsymbol{\Phi}_k^{(2,2)})_i \\ & + (\mathbf{v}\cdot\boldsymbol{\Phi}_k^{(2,1)})_i(\mathbf{u}\cdot\boldsymbol{\Phi}_k^{(2,2)})_j + (\mathbf{v}\cdot\boldsymbol{\Phi}_k^{(2,1)})_j(\mathbf{u}\cdot\boldsymbol{\Phi}_k^{(2,2)})_i\end{aligned} \tag{2.83c}$$

$$\begin{aligned}\boldsymbol{P}_k^4 = {} & (\mathbf{u}\cdot\boldsymbol{\Phi}_k^{(3,1)})_i(\mathbf{v}\cdot\boldsymbol{\Phi}_k^{(3,2)})_j + (\mathbf{u}\cdot\boldsymbol{\Phi}_k^{(3,1)})_j(\mathbf{v}\cdot\boldsymbol{\Phi}_k^{(3,2)})_i \\ & - (\mathbf{v}\cdot\boldsymbol{\Phi}_k^{(3,1)})_i(\mathbf{u}\cdot\boldsymbol{\Phi}_k^{(3,2)})_j - (\mathbf{v}\cdot\boldsymbol{\Phi}_k^{(3,1)})_j(\mathbf{u}\cdot\boldsymbol{\Phi}_k^{(3,2)})_i\,.\end{aligned} \tag{2.83d}$$

The polynomial representation for a skew-symmetric tensor function $\boldsymbol{P}$ can be constructed similarly, and yield for $\boldsymbol{P}_k^1$, $\boldsymbol{P}_k^2$, $\boldsymbol{P}_k^3$ and $\boldsymbol{P}_k^4$

$$\boldsymbol{P}_k^1 = (\boldsymbol{\Phi}_k^{(1,1)})_{ij} - (\boldsymbol{\Phi}_k^{(1,1)})_{ji} \tag{2.84a}$$

$$\boldsymbol{P}_k^2 = (\mathbf{u}\cdot\boldsymbol{\Phi}_k^{(2,1)})_i(\mathbf{u}\cdot\boldsymbol{\Phi}_k^{(2,2)})_j - (\mathbf{u}\cdot\boldsymbol{\Phi}_k^{(2,1)})_j(\mathbf{u}\cdot\boldsymbol{\Phi}_k^{(2,2)})_i \tag{2.84b}$$

$$\begin{aligned}\boldsymbol{P}_k^3 = {} & (\mathbf{u}\cdot\boldsymbol{\Phi}_k^{(2,1)})_i(\mathbf{v}\cdot\boldsymbol{\Phi}_k^{(2,2)})_j - (\mathbf{u}\cdot\boldsymbol{\Phi}_k^{(2,1)})_j(\mathbf{v}\cdot\boldsymbol{\Phi}_k^{(2,2)})_i \\ & + (\mathbf{v}\cdot\boldsymbol{\Phi}_k^{(2,1)})_i(\mathbf{u}\cdot\boldsymbol{\Phi}_k^{(2,2)})_j - (\mathbf{v}\cdot\boldsymbol{\Phi}_k^{(2,1)})_j(\mathbf{u}\cdot\boldsymbol{\Phi}_k^{(2,2)})_i\end{aligned} \tag{2.84c}$$

$$\begin{aligned}\boldsymbol{P}_k^4 = {} & (\mathbf{u}\cdot\boldsymbol{\Phi}_k^{(3,1)})_i(\mathbf{v}\cdot\boldsymbol{\Phi}_k^{(3,2)})_j - (\mathbf{u}\cdot\boldsymbol{\Phi}_k^{(3,1)})_j(\mathbf{v}\cdot\boldsymbol{\Phi}_k^{(3,2)})_i \\ & - (\mathbf{v}\cdot\boldsymbol{\Phi}_k^{(3,1)})_i(\mathbf{u}\cdot\boldsymbol{\Phi}_k^{(3,2)})_j + (\mathbf{v}\cdot\boldsymbol{\Phi}_k^{(3,1)})_j(\mathbf{u}\cdot\boldsymbol{\Phi}_k^{(3,2)})_i\end{aligned} \tag{2.84d}$$

The skew-symmetric construction will not be pursued further since its use is, of course, limited in the development of physical constitutive equations such as those discussed here. The following examples will help illustrate the construction of such vector and tensor polynomial representations under this transformation group.

2.4.2.1 Vector Function of Vectors and Tensors

Consider a vector function of a vector, one symmetric and one skew-symmetric tensor, that is

$$\mathbf{p}(\mathbf{u}, \boldsymbol{A}, \boldsymbol{X}), \quad \text{or} \quad p_i(u_r, A_{rs}, X_{rs})\,. \tag{2.85}$$

The invariant of the argument vectors and tensors formed is given in Eq. (2.71) and the corresponding invariant polynomial is given in Eq. (2.73). In this example, the

expansion coefficients I_k are functions of the invariants formed from the vector $\mathbf{u}$, and the tensors $\boldsymbol{A}$ and $\boldsymbol{X}$. These are obtained directly from Table 2.3 by collecting the number of invariants associated with one symmetric and one skew-symmetric tensor. The resulting eleven elements are of the form

$$\mathrm{tr}\,\mathbf{u}^T \boldsymbol{\Pi}_k \mathbf{u}\,, \tag{2.86a}$$

where the $\boldsymbol{\Pi}_k$ are

$$\begin{aligned} &\boldsymbol{I}, \quad \boldsymbol{A}, \quad \boldsymbol{A}^2, \quad \boldsymbol{X}^2, \quad \boldsymbol{X}\boldsymbol{A}, \quad \boldsymbol{X}\boldsymbol{A}^2, \quad \boldsymbol{A}\boldsymbol{X}\boldsymbol{A}^2, \\ &\boldsymbol{X}^2\boldsymbol{A}, \quad \boldsymbol{X}^2\boldsymbol{A}^2, \quad \boldsymbol{X}^2\boldsymbol{A}\boldsymbol{X}, \quad \boldsymbol{X}\boldsymbol{A}^2\boldsymbol{X}^2\,. \end{aligned} \tag{2.86b}$$

The $\boldsymbol{\chi}_k$ can be obtained from the polynomial representations given in Eq. (2.76) with the $\boldsymbol{\Pi}_k$ and $\boldsymbol{\Theta}_k$ obtained from Table 2.3 for the case of a single symmetric and skew-symmetric tensor. There are eleven matrix products associated with $\boldsymbol{\Pi}_k + \boldsymbol{\Pi}_k^T$, and these are given by

$$\begin{aligned} \boldsymbol{\Pi}_1 &= \boldsymbol{I} & \boldsymbol{\Pi}_7 &= \boldsymbol{X}^2\boldsymbol{A} \\ \boldsymbol{\Pi}_2 &= \boldsymbol{A} & \boldsymbol{\Pi}_8 &= \boldsymbol{X}\boldsymbol{A}\mathbf{X}^2 \\ \boldsymbol{\Pi}_3 &= \boldsymbol{A}\boldsymbol{X} & \boldsymbol{\Pi}_9 &= \boldsymbol{A}\boldsymbol{X}\mathbf{A}^2 \\ \boldsymbol{\Pi}_4 &= \boldsymbol{A}^2 & \boldsymbol{\Pi}_{10} &= \boldsymbol{X}^2\boldsymbol{A}^2 \\ \boldsymbol{\Pi}_5 &= \boldsymbol{X}^2 & \boldsymbol{\Pi}_{11} &= \boldsymbol{X}\boldsymbol{A}^2\mathbf{X}^2 \\ \boldsymbol{\Pi}_6 &= \boldsymbol{X}\boldsymbol{A}^2 \end{aligned} \tag{2.87}$$

and there are six matrix products associated with $\boldsymbol{\Theta}_k - \boldsymbol{\Theta}_k^T$, and these are given by

$$\begin{aligned} \boldsymbol{\Theta}_1 &= \boldsymbol{X} & \boldsymbol{\Theta}_4 &= \boldsymbol{A}\boldsymbol{X}^2 \\ \boldsymbol{\Theta}_2 &= \boldsymbol{A}\boldsymbol{X} & \boldsymbol{\Theta}_5 &= \boldsymbol{A}^2\boldsymbol{X}^2 \\ \boldsymbol{\Theta}_3 &= \boldsymbol{A}^2\boldsymbol{X} & \boldsymbol{\Theta}_6 &= \boldsymbol{A}^2\boldsymbol{X}^2\boldsymbol{A} \end{aligned} \tag{2.88}$$

Such vector representations are required, for example, in the development of models for scalar flux quantities that arise when heat and mass transfer effects are included in turbulent flow computations.

2.4.2.2 Symmetric Tensor Function of Vectors and Tensors

Another example under the full orthogonal group, and an extension of the example in Sect. 2.4.1.2, is the case of a symmetric tensor function which is a function of a vector $\mathbf{u}$, and one symmetric tensor $\boldsymbol{A}$ and one skew-symmetric tensor $\boldsymbol{X}$,

$$\boldsymbol{P}\,(\mathbf{u}, \boldsymbol{A}, \boldsymbol{X})\,, \quad \text{or} \quad P_{ij}\,(u_r, A_{rs}, X_{rs})\,. \tag{2.89}$$

The invariants comprising $\boldsymbol{\Pi}_k$ have the forms given in Eqs. (2.79) and (2.80a), (2.80b). The first set given by Eq. (2.79) consists of ten invariants and these are obtained directly from Tables 2.1 and 2.2 and have been listed previously in Eq. (2.69). Correspondingly, the seven invariants associated with the expansion coefficients I_k are listed in Eq. (2.68).

Another set consists of invariants given by $u_i \Pi_{ij}^{(k)} u_j$ in Eq. (2.54a) with the product $\boldsymbol{\Pi}$ in Eq. (2.80a) given by

$$\boldsymbol{\Pi}_k = \boldsymbol{\Phi}_k^{(2,1)} \boldsymbol{\psi} \boldsymbol{\Phi}_k^{(2,2)T} + \boldsymbol{\Phi}_k^{(2,1)} \boldsymbol{\psi}^T \boldsymbol{\Phi}_k^{(2,2)T} \ . \tag{2.90}$$

The products comprising $\boldsymbol{\Phi}_k^{(2,1)}$ and $\boldsymbol{\Phi}_k^{(2,2)}$ can be obtained directly from Table 2.3a (in the Table only the first term in Eq. (2.90) need be used in identifying $\boldsymbol{\Phi}_k^{(2,1)}$ and $\boldsymbol{\Phi}_k^{(2,2)}$), and are given by

$$\begin{aligned}
&(\boldsymbol{\Phi}_1^{(2,1)}, \boldsymbol{\Phi}_1^{(2,2)}) = (\boldsymbol{I}, \boldsymbol{I}) && (\boldsymbol{\Phi}_{10}^{(2,1)}, \boldsymbol{\Phi}_{10}^{(2,2)}) = (\boldsymbol{X}\boldsymbol{A}^2, \boldsymbol{I}) \\
&(\boldsymbol{\Phi}_2^{(2,1)}, \boldsymbol{\Phi}_2^{(2,2)}) = (\boldsymbol{A}, \boldsymbol{I}) && (\boldsymbol{\Phi}_{11}^{(2,1)}, \boldsymbol{\Phi}_{11}^{(2,2)}) = (\boldsymbol{A}^2\boldsymbol{X}, \boldsymbol{I}) \\
&(\boldsymbol{\Phi}_3^{(2,1)}, \boldsymbol{\Phi}_3^{(2,2)}) = (\boldsymbol{A}^2, \boldsymbol{I}) && (\boldsymbol{\Phi}_{12}^{(2,1)}, \boldsymbol{\Phi}_{12}^{(2,2)}) = (\boldsymbol{A}^2, \boldsymbol{X}) \\
&(\boldsymbol{\Phi}_4^{(2,1)}, \boldsymbol{\Phi}_4^{(2,2)}) = (\boldsymbol{X}, \boldsymbol{I}) && (\boldsymbol{\Phi}_{13}^{(2,1)}, \boldsymbol{\Phi}_{13}^{(2,2)}) = (\boldsymbol{A}\boldsymbol{X}\boldsymbol{A}^2, \boldsymbol{I}) \\
&(\boldsymbol{\Phi}_5^{(2,1)}, \boldsymbol{\Phi}_5^{(2,2)}) = (\boldsymbol{X}^2, \boldsymbol{I}) && (\boldsymbol{\Phi}_{14}^{(2,1)}, \boldsymbol{\Phi}_{14}^{(2,2)}) = (\boldsymbol{X}^2\boldsymbol{A}, \boldsymbol{I}) \\
&(\boldsymbol{\Phi}_6^{(2,1)}, \boldsymbol{\Phi}_6^{(2,2)}) = (\boldsymbol{X}^2, \boldsymbol{X}) && (\boldsymbol{\Phi}_{15}^{(2,1)}, \boldsymbol{\Phi}_{15}^{(2,2)}) = (\boldsymbol{A}\boldsymbol{X}^2, \boldsymbol{I}) \\
&(\boldsymbol{\Phi}_7^{(2,1)}, \boldsymbol{\Phi}_7^{(2,2)}) = (\boldsymbol{X}\boldsymbol{A}, \boldsymbol{I}) && (\boldsymbol{\Phi}_{16}^{(2,1)}, \boldsymbol{\Phi}_{16}^{(2,2)}) = (\boldsymbol{X}^2\boldsymbol{A}^2, \boldsymbol{I}) \\
&(\boldsymbol{\Phi}_8^{(2,1)}, \boldsymbol{\Phi}_8^{(2,2)}) = (\boldsymbol{A}\boldsymbol{X}, \boldsymbol{I}) && (\boldsymbol{\Phi}_{17}^{(2,1)}, \boldsymbol{\Phi}_{17}^{(2,2)}) = (\boldsymbol{X}^2\boldsymbol{A}\boldsymbol{X}, \boldsymbol{I}) \\
&(\boldsymbol{\Phi}_9^{(2,1)}, \boldsymbol{\Phi}_9^{(2,2)}) = (\boldsymbol{A}, \boldsymbol{X})
\end{aligned} \tag{2.91}$$

Associated with these seventeen invariants comprising the $\mathcal{J}_k$ for this set, are the invariants associated with the corresponding expansion coefficients I_k. These eleven invariants have already been given in Eqs. (2.86a), (2.86b) for the case of a tensor function having the same functional arguments.

In summary, the invariants $\mathcal{J}_k$ consist of ten invariants obtained from $\mathrm{tr}\, \boldsymbol{\Phi}_k^{(1)} \boldsymbol{\psi}$ and seventeen invariants from $\mathrm{tr}\, \mathbf{u}^T \boldsymbol{\Pi}_k \mathbf{u}$. The corresponding expansion coefficients I_k are then functions of the seven invariants listed in (2.68), and the eleven invariants listed in (2.86a), (2.86b).

The basis tensors are constructed from contributions from both $\mathrm{tr}\, \boldsymbol{\Phi}^{(1)} \boldsymbol{\phi}$ and $\mathrm{tr}\, \mathbf{u}^T \boldsymbol{\Pi}_k \mathbf{u}$ (with Eq. (2.90)). For $\mathrm{tr}\, \boldsymbol{\Phi}^{(1)} \boldsymbol{\phi}$, the basis tensors are represented by Eq. (2.83a),

$$\boldsymbol{P}_k^1 = (\boldsymbol{\Phi}_k^{(1)})_{ij} + (\boldsymbol{\Phi}_k^{(1)})_{ji} \tag{2.92}$$

with $\boldsymbol{\Phi}_k^{(1)}$ given in Eq. (2.70). The remaining set of basis tensors are constructed from the invariants $\mathrm{tr}\, \mathbf{u}^T \boldsymbol{\Pi}_k \mathbf{u}$ and are represented by Eq. (2.83b) for a single vector as

$$(\mathbf{u}\boldsymbol{\Phi}_k^{(2,1)})_i (\mathbf{u}\boldsymbol{\Phi}_k^{(2,2)})_j + (\mathbf{u}\boldsymbol{\Phi}_k^{(2,1)})_j (\mathbf{u}\boldsymbol{\Phi}_k^{(2,2)})_i \ , \tag{2.93}$$

where the $\boldsymbol{\Phi}_k^{(2,1)}$ and $\boldsymbol{\Phi}_k^{(2,2)}$ are given in Eq. (2.91). This yields an additional seventeen basis bringing the total number of basis tensors to twenty-six for this example. These results have been extended up to two symmetric or skew-symmetric tensors and are given in Spencer (1971) (see page 331, Table IX).

Chapter 3
Kinematics and Dynamics

Underlying the study of fluid flow are the mechanical concepts of kinematics and dynamics, where kinematics applies to the description of the motion, and dynamics applies to the causes of the motion. It is first necessary to develop how to describe the motion and then examine the various forces involved in the motion and energy balance.

The discussion here is rather general and reflects a continuum mechanics slant. Such a bias is intentional and seeks to emphasize that fluid mechanics is a direct subset of the broader continuum mechanics field that also includes solid mechanics (see Fig. 1.12). Of course this assumes the flow can be viewed as a continuum, with the exclusions being fluids and flows where the continuum hypothesis no longer applies, such as in rarefied gas flows. Such assessments of a continuum can be quantified and are based on the Knudsen number parameter, $\mathrm{Kn} \ll 1$, which is the ratio between the molecular mean free path and a characteristic length scale of the motion. This non-dimensional parameter will surface again in Chap. 7 in the development of the lattice Boltzmann method.

3.1 Material Elements and Deformation

Since material elements in fluids are deformable, their movement is the aggregate of a rigid-body motion and a deformation, and as such the discussion here will focus on the elements of stretch, that is the change in distance between fluid particles. Consider the motion of a material element of fluid undergoing an arbitrary deformation. Let the material or Lagrangian coordinates of a particle within the element at some reference state be represented by X_α, and the spatial or Eulerian (Cartesian) coordinates of the particle at some later time t be represented by x_i (see Fig. 3.1). (In the discussion to follow, the component Lagrangian coordinates will be designated by Greek letters, and the component Eulerian coordinates by Latin letters.) A continuous deformation, from some reference time $t = 0$, of this material element

M.O. Deville, T.B. Gatski, *Mathematical Modeling for Complex Fluids and Flows*,
DOI 10.1007/978-3-642-25295-2_3, © Springer-Verlag Berlin Heidelberg 2012

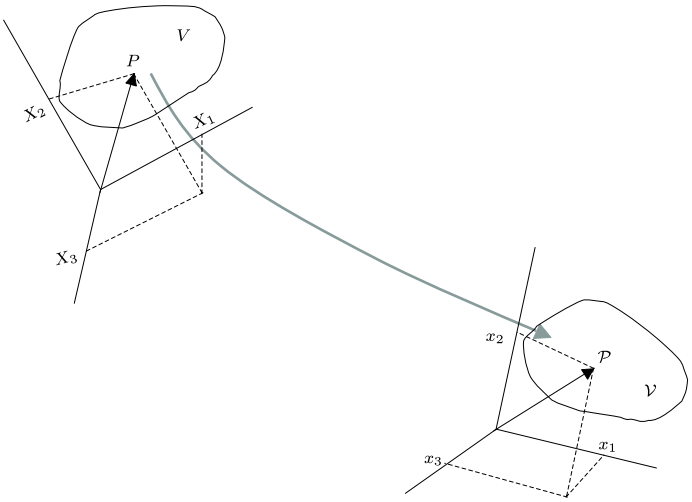

Fig. 3.1 Mapping of deformation from reference state to state at time t

to a state at the present time t is assumed. This mapping, as sketched in Fig. 3.1, can be expressed as[1]

$$x_i = \chi_i(\mathbf{X}, t) \qquad (i = 1, 2, 3), \qquad \mathbf{x} = \boldsymbol{\chi}(\mathbf{X}, t) \ , \tag{3.1a}$$

where $\boldsymbol{\chi}(\mathbf{X}, t)$ is the deformation function, or by the inverse,

$$X_\alpha = \chi_\alpha^{-1}(\mathbf{x}, t) \qquad (\alpha = 1, 2, 3), \qquad \mathbf{X} = \boldsymbol{\chi}^{-1}(\mathbf{x}, t) \ . \tag{3.1b}$$

In the present context, a continuous deformation implies that the transformations in Eqs. (3.1a) and (3.1b) possess continuous partial derivatives with respect to their arguments. With the particle motion described by Eq. (3.1a), the evolution of a material line element $\mathrm{d}X_\alpha$, composed of several fluid particles, from its reference state to its state at some time t can be determined from

$$\mathrm{d}x_i = \frac{\partial \chi_i(\mathbf{X}, t)}{\partial X_\alpha} \mathrm{d}X_\alpha = \mathcal{F}_{i\alpha}(t) \mathrm{d}X_\alpha \ , \tag{3.2}$$

where the second-order tensor $\mathcal{F}_{i\alpha}(t) (= \partial x_i / \partial X_\alpha)$ is called the deformation gradient tensor, and in the absence of any motion is simply the identity tensor $\delta_{i\alpha}$. If $\boldsymbol{\mathcal{F}}$ is assumed to be only a function of time, integration of Eq. (3.2) between the reference state and the state at time t yields,

$$x_i = \chi_i(\mathbf{X}, t) = \mathcal{F}_{i\alpha}(t) \, (X_\alpha - X_{\alpha 0}) + x_{i0}(t) \ . \tag{3.3}$$

[1] In this chapter both index and boldface notation will be used in the mathematical description and formulation. In subsequent chapters, the index notation will prevail for the most part, since the algebraic manipulations of the equations are easier. However, the boldface notation will be retained where compactness of the mathematical expression is paramount.

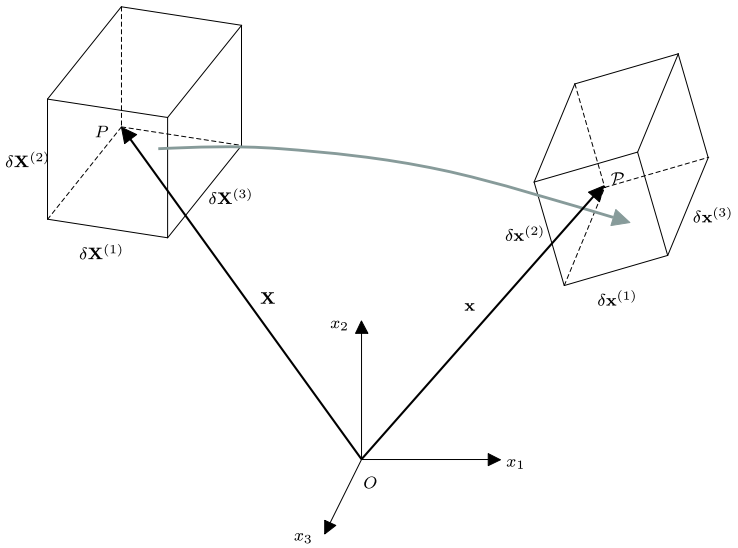

Fig. 3.2 Deforming motion of a box structure from the reference time with sides ($\delta X_\alpha^{(1)}$, $\delta X_\alpha^{(2)}$, $\delta X_\alpha^{(3)}$; $\alpha = 1, 2, 3$) to a time t with sides ($\delta x_i^{(1)}$, $\delta x_i^{(2)}$, $\delta x_i^{(3)}$; $i = 1, 2, 3$)

Since such a motion is homogeneous ($\mathcal{F}(t)$ having the same value at all places), it can be observed that a straight line segment in the reference state is carried over to a straight line segment in the state at time t (Truesdell 1991). In the formulation of constitutive equations for viscoelastic fluids, the underlying functional relations for the stress field are derived for such homogeneous motions. In turbulent flows, homogeneous flow fields are often used in the development and calibration of closure models (e.g. Sagaut and Cambon 2008).

In general, the deformation gradient tensor is not a symmetric tensor, but its inverse does exist (provided its determinant is nonzero—which will be the case since it will be shown shortly that it is related to the Jacobian of the transformation). Correspondingly, the evolution of a material element follows directly so that at time t, the volume of this element with edges $\mathrm{d}\mathbf{x}^{(1)}$, $\mathrm{d}\mathbf{x}^{(2)}$, and $\mathrm{d}\mathbf{x}^{(3)}$ is (see Fig. 3.2 where the material element is a simple box structure for illustrative purposes)

$$\mathrm{d}\mathcal{V} = \underbrace{\left(e_{ijk}\mathrm{d}x_j^{(1)}\mathrm{d}x_k^{(2)}\right)}_{n_i\mathrm{d}\mathcal{S}}\mathrm{d}x_i^{(3)}, \qquad \mathrm{d}\mathcal{V} = \left(\mathrm{d}\mathbf{x}^{(1)} \times \mathrm{d}\mathbf{x}^{(2)}\right) \cdot \mathrm{d}\mathbf{x}^{(3)}\ , \tag{3.4a}$$

where n_i is the unit surface normal with element surface area $\mathrm{d}\mathcal{S}$. This can be related to the volume, $\mathrm{d}V\,(= e_{\alpha\beta\gamma}\mathrm{d}X_\beta^{(1)}\mathrm{d}X_\gamma^{(2)}\mathrm{d}X_\alpha^{(3)})$ at the reference time by using Eq. (3.2), so that

$$\mathrm{d}\mathcal{V} = J\mathrm{d}V\ , \tag{3.4b}$$

where J is the Jacobian of the transformation,

$$J = e_{ijk}\frac{\partial x_1}{\partial X_i}\frac{\partial x_2}{\partial X_j}\frac{\partial x_3}{\partial X_k} = \det\boldsymbol{\mathcal{F}} = \mathrm{I}_3\,(\boldsymbol{\mathcal{F}})$$
$$= \frac{1}{6}\left(\{\boldsymbol{\mathcal{F}}\}^3 - 3\{\boldsymbol{\mathcal{F}}\}\{\boldsymbol{\mathcal{F}}^2\} + 2\{\boldsymbol{\mathcal{F}}^3\}\right)\,, \tag{3.5}$$

with $\mathrm{I}_3\,(\boldsymbol{\mathcal{F}})$ the third invariant of the deformation gradient (cf. Eq. (2.35)).

The description just provided is based on a configuration at $\mathbf{X}$ fixed at a reference time $t = t_r$. An alternative to this would be to describe this motion relative to the present one when the particle $(\mathbf{X}, t_r)$ is at $(\mathbf{x}, t)$. Consider the two times τ and t, and the corresponding deformations given by

$$\boldsymbol{\varkappa} = \boldsymbol{\chi}(\mathbf{X}, \tau) \quad \text{and} \quad \mathbf{x} = \boldsymbol{\chi}(\mathbf{X}, t)\,, \tag{3.6}$$

respectively. As illustrated in Fig. 3.3, the motion represented by $\boldsymbol{\chi}(\mathbf{X}, t)$ describes the motion from $t = t_r$ to t or $t + s$ with $s \geq 0$. For $\tau = t - s$, the motion represented by $\boldsymbol{\chi}_{(t)}$ is from an earlier time τ to the present time t and for $\tau = t + s$, the motion represented by $\boldsymbol{\chi}_{(t)}$ is from the present time t to the later time τ. From this, a new deformation can be obtained and written as

$$\boldsymbol{\varkappa} = \boldsymbol{\chi}(\boldsymbol{\chi}^{-1}(\mathbf{x}, t), \tau) := \boldsymbol{\chi}_{(t)}(\mathbf{x}, \tau)\,, \tag{3.7}$$

where the relative deformation function $\boldsymbol{\chi}_{(t)}(\mathbf{x}, \tau)$ is defined. Figure 3.3 illustrates that the motion represented by $\boldsymbol{\chi}_{(t)}(\mathbf{x}, t)$ can describe the motion from t to τ (either $t - s$ or $t + s$). The question can now be asked about the deformation of the material line element at time τ and the corresponding deformation gradient tensor $\mathcal{F}_{i\alpha}(\tau)(= \partial\varkappa_i/\partial X_\alpha)$. The deformation gradient tensor $\mathcal{F}_{i\alpha}(\tau)$ can be written as a succession of mappings given by

$$\frac{\partial\varkappa_i(\mathbf{X}, \tau)}{\partial X_\alpha} = \frac{\partial\chi_{(t)i}(\mathbf{x}, \tau)}{\partial\chi_j(\mathbf{X}, t)}\frac{\partial\chi_j(\mathbf{X}, t)}{\partial X_\alpha}\,, \tag{3.8}$$

or rewriting solely in terms of the deformation gradients as,

$$\mathcal{F}_{i\alpha}(\tau) = \mathcal{F}_{(t)ij}(\tau)\mathcal{F}_{j\alpha}(t), \qquad \boldsymbol{\mathcal{F}}(\tau) = \boldsymbol{\mathcal{F}}_{(t)}(\tau)\boldsymbol{\mathcal{F}}(t)\,, \tag{3.9}$$

where $\mathcal{F}_{(t)ij}$ is defined as the relative deformation gradient tensor,

$$\mathcal{F}_{(t)ij}(\tau) := \frac{\partial\chi_{(t)i}(\mathbf{x}, \tau)}{\partial\chi_j(\mathbf{X}, t)} = \frac{\partial\varkappa_i}{\partial x_j}\,, \tag{3.10}$$

so that at $\tau = t$, $\mathcal{F}_{(t)ij} = \delta_{ij}$.

Analogous to Eq. (3.2), the evolution of a material line element $\mathrm{d}\varkappa_i$ from its state at time τ to its state, $\mathrm{d}x_i$, at some time t can be determined from

$$\mathrm{d}x_i = \frac{\partial x_i}{\partial\varkappa_k}\mathrm{d}\varkappa_k = \mathcal{F}_{(t)ik}\mathrm{d}\varkappa_k, \qquad \mathrm{d}\mathbf{x} = \boldsymbol{\mathcal{F}}_{(t)}\mathrm{d}\boldsymbol{\varkappa}\,. \tag{3.11}$$

Thus, the relative deformation gradient provides information on the transformation of line, surface, and volume elements (see Fig. 3.3).

Returning now to the reference and present states, $\mathbf{X}$ and $\mathbf{x}$, respectively, let us additionally assume that the vectors representing both the material line element $\mathrm{d}X_\alpha$

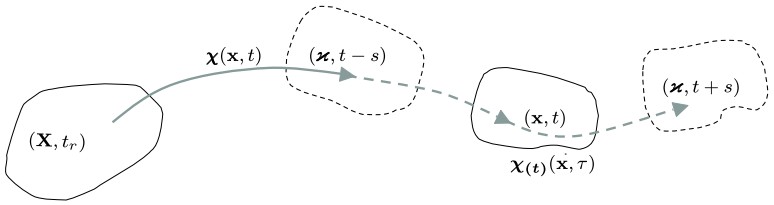

Fig. 3.3 Motion of a material element from a reference frame at $t = t_r$ to frames at times t and τ ($\tau = t - s$ or $\tau = t + s$, $s \geq 0$)

and the material line element $\mathrm{d}x_i$ are each aligned with their respective unit vector such that

$$\mathrm{d}X_\alpha = \delta l e_\alpha, \qquad \mathrm{d}\mathbf{X} = \delta l \mathbf{e}_{(\mathrm{r})} \tag{3.12a}$$

$$\mathrm{d}x_i = \delta \ell e_i, \qquad \mathrm{d}\mathbf{x} = \delta \ell \mathbf{e}\ , \tag{3.12b}$$

where $\mathbf{e}_{(\mathrm{r})}$ and $\mathbf{e}$ are unit vectors in the reference and present states, respectively, and δl and $\delta \ell$ are material line element lengths in the reference and present states, respectively. Substituting Eqs. (3.12a), (3.12b) into Eq. (3.2) then yields an expression for the extension or stretch ratio, λ, of the material line element given by

$$\lambda e_i = \frac{\delta \ell}{\delta l} e_i = \mathcal{F}_{i\alpha} e_\alpha\ . \tag{3.13}$$

An analogous derivation, originating with Eq. (3.1b), would then yield the alternative relation,

$$e_\alpha = \lambda \mathcal{F}^{-1}_{\alpha i} e_i\ . \tag{3.14}$$

Since the extension ratio, λ, represents the ratio of the length of the material line element after deformation relative to its length in the reference state, the corresponding elongation, or strain, is given by $\lambda - 1$. If a displacement vector between the reference and present state, ξ_i, is defined as

$$\xi_i = x_i - X_\alpha \qquad (\alpha = i)\ , \tag{3.15}$$

then differentiation with respect to either material or spatial coordinates leads to

$$\frac{\partial \xi_i}{\partial X_\beta} = \mathcal{F}_{i\beta} - \delta_{\alpha\beta} \qquad (\alpha = i)\ , \tag{3.16}$$

or

$$\frac{\partial \xi_i}{\partial x_j} = \delta_{ij} - \mathcal{F}^{-1}_{\alpha j} \qquad (\alpha = i)\ , \tag{3.17}$$

respectively, and $\partial \xi_i / \partial X_\beta$ is the displacement gradient tensor defined in terms of the material coordinates and $\partial \xi_i / \partial x_j$ is the displacement gradient tensor defined in terms of the spatial coordinates. The relevance of this quantity to the calculation of strain will be discussed shortly.

Although the deformation gradient tensor is a fundamental quantity in the description of material element deformation and displacement, it is not directly applicable as a measure of either extension or strain. This is easily seen when the limiting case of rigid-body motion (no deformation) is considered. A comparison of Eqs. (2.11a) and (3.2) shows that in this limit the deformation gradient tensor $\mathcal{F}_{i\alpha}$ reduces to the orthogonal tensor $\boldsymbol{O}$. Thus $\mathcal{F}_{i\alpha}$ is no longer a measure of deformation (or displacement) but rather a measure of rigid-body motion (e.g. rotation). This change of "measure" precludes $\mathcal{F}_{i\alpha}$ itself from being a useful measuring function. Fortunately, it is relatively straightforward to construct suitable measures of extension and strain from the relations just obtained.

Since $\mathbf{e}$ is a unit vector ($e_i e_i = 1$), an expression for λ in terms of the orientation in the reference configuration is easily extracted from Eq. (3.13) by forming the square,

$$\begin{aligned} \lambda^2 &= e_\alpha \mathcal{F}_{i\alpha} \mathcal{F}_{i\beta} e_\beta, \qquad & \lambda^2 &= \mathbf{e}_{(\mathrm{r})}^T \boldsymbol{\mathcal{F}}^T \boldsymbol{\mathcal{F}} \mathbf{e}_{(\mathrm{r})} \\ &= e_\alpha C_{\alpha\beta} e_\beta, \qquad & \boldsymbol{C} &= \boldsymbol{\mathcal{F}}^T \boldsymbol{\mathcal{F}} \,. \end{aligned} \tag{3.18}$$

Equation (3.18) shows that the extension ratio of the material line element from its reference state length is directly related to the tensorial product of the deformation gradient tensors $\mathcal{F}_{i\alpha}\mathcal{F}_{i\beta}$, and this tensor product is called the right Cauchy-Green tensor, $C_{\alpha\beta}$.

An analogous derivation, originating with Eq. (3.1b), would then yield the alternative extension ratio relation,

$$\begin{aligned} \lambda^{-2} &= e_i \mathcal{F}_{\alpha i}^{-1} \mathcal{F}_{\alpha j}^{-1} e_j, \qquad & \lambda^{-2} &= \mathbf{e}^T (\boldsymbol{\mathcal{F}}^{-1})^T (\boldsymbol{\mathcal{F}}^{-1}) \mathbf{e} \\ &= e_i B_{ij}^{-1} e_j, \qquad & \mathbf{B}^{-1} &= (\boldsymbol{\mathcal{F}}^{-1})^T (\boldsymbol{\mathcal{F}}^{-1}) \,, \end{aligned} \tag{3.19}$$

and as Eq. (3.19) shows, the extension ratio is directly related to the tensorial product of the inverses of the deformation gradient tensors $\mathcal{F}_{\alpha i}^{-1}\mathcal{F}_{\alpha j}^{-1}$. Correspondingly, the tensor product, $B_{ij} = \mathcal{F}_{i\alpha}\mathcal{F}_{j\alpha}$ ($\mathbf{B} = \boldsymbol{\mathcal{F}}\boldsymbol{\mathcal{F}}^T$), is called the left Cauchy-Green tensor.

In contrast to $\mathcal{F}_{i\alpha}$, the combination of deformation gradient tensors represented by the Cauchy-Green tensors does provide a consistent measure of deformation. As shown in Eqs. (3.18) and (3.19), both the left and right Cauchy-Green tensors provide a consistent measure by degenerating, in the case of a rigid-body motion, to the identity tensor $\boldsymbol{I}$.

Similarly, the displacement gradient tensor $\partial \xi_i / \partial X_\alpha$ retains the same characteristics as the deformation gradient tensor (cf. Eqs. (3.16) or (3.17)), and as such is also not directly useful as a measure of strain. However, just as the Cauchy-Green tensors were the basis for a quantitative measure of the extension ratio, they can be equally applied to the measure of strain. This is done through the defining relations

$$\eta_{\alpha\beta} = \frac{1}{2}\left(C_{\alpha\beta} - \delta_{\alpha\beta}\right) \,, \tag{3.20}$$

$$e_{ij} = \frac{1}{2}\left(\delta_{ij} - B_{ij}^{-1}\right) \,, \tag{3.21}$$

where $\eta_{\alpha\beta}$ is called the Lagrangian strain tensor and e_{ij} is called the Eulerian strain tensor. In the former case, the relationship with the right Cauchy-Green tensor $C_{\alpha\beta}$

indicates a dependence on the material coordinates X_α; whereas, in the latter case the relationship with the (inverse of) the left Cauchy-Green tensor B_{ij} indicates a dependence on the spatial coordinates x_i.

3.1.1 Decomposition of the Deformation

It is a useful exercise to further decompose the deformation gradient tensor using the polar decomposition theorem. The starting point is the partitioning of $\mathcal{F}_{i\alpha}$ into the forms

$$\mathcal{F}_{i\alpha} = R_{ij} U_{j\alpha}, \qquad \boldsymbol{\mathcal{F}} = \boldsymbol{R}\boldsymbol{U} \ , \tag{3.22a}$$

or alternately,

$$\mathcal{F}_{i\alpha} = V_{i\beta} R_{\beta\alpha}, \qquad \boldsymbol{\mathcal{F}} = \boldsymbol{V}\boldsymbol{R} \ , \tag{3.22b}$$

where R_{ij} is an orthogonal tensor, and $U_{i\alpha}$ and $V_{i\beta}$ are symmetric, positive-definite tensors. From the transformation described in Eq. (3.2), Eq. (3.22a) shows that the deformation gradient tensor can be decomposed into a stretching action represented locally by the $U_{i\alpha}$ followed by a (local) rigid-body rotation represented by R_{ij} (since $\boldsymbol{R}$ is an orthogonal tensor), or alternately by a rigid-body rotation, $R_{\beta\alpha}$, followed by a stretching action represented by $V_{i\beta}$. It is then not surprising that the stretch ratio, deduced earlier in Eqs. (3.18) and (3.19), can be related to the right and left Cauchy-Green tensors. From the relations,

$$C_{\alpha\beta} = \mathcal{F}_{k\alpha}\mathcal{F}_{k\beta} = U_{i\alpha} R_{ki} R_{kj} U_{j\beta} = U_{i\alpha} U_{i\beta}, \quad \boldsymbol{C} = \boldsymbol{\mathcal{F}}^T\boldsymbol{\mathcal{F}} = \boldsymbol{U}^2 \ , \tag{3.23a}$$

$$B_{ij} = \mathcal{F}_{i\gamma}\mathcal{F}_{j\gamma} = V_{i\alpha} R_{\alpha\gamma} R_{\beta\gamma} V_{j\beta} = V_{i\alpha} V_{j\alpha}, \quad \mathbf{B} = \boldsymbol{\mathcal{F}}\boldsymbol{\mathcal{F}}^T = \boldsymbol{V}^2 \ . \tag{3.23b}$$

The orthogonal tensor $\boldsymbol{R}$ is called the rotation tensor and the tensors $\boldsymbol{U}$ and $\boldsymbol{V}$ are called the right stretch tensor and left stretch tensor, respectively. It can be shown (Spencer 2004; Truesdell and Rajagopal 2000) that in the absence of rotation, the stretch tensors represent the principal stretches of the material element, and the rotation tensor $\boldsymbol{R}$ represents the rotation through which the principal directions of $\boldsymbol{U}$ are moved to align with the principal directions of $\boldsymbol{V}$. Other physical consequences of these component motions will be discussed in the next section. Additionally, it should be recognized that the polar decomposition can be applied as well to the relative deformation gradient tensor. The corresponding relative rotation and stretch tensors and relative Cauchy-Green tensors would then be obtained.

3.1.2 Infinitesimal Strain and Rotation

Up to this point, there has been no reference to the magnitude of the deformation or displacement under consideration. In addition, no reference has been made to the

type of material, solid or fluid, under deformation. In this section, a link will be established here that will bridge this broad continuum mechanics discussion to one specialized to fluid mechanics.

Consider now the limiting case of an infinitesimal displacement gradient tensor, $|\partial\xi_i/\partial X_\beta| \ll 1$. In this case to lowest order, the right hand sides of Eqs. (3.16) and (3.17) are equal so that

$$\mathcal{F}_{i\beta} \approx \delta_{\alpha\beta}, \quad \text{and} \quad \mathcal{F}^{-1}_{\alpha j} \approx \delta_{ij} \quad (\alpha = i,\ \beta = j)\ , \tag{3.24}$$

with

$$\frac{\partial\xi_i}{\partial x_j} \approx \frac{\partial\xi_i}{\partial X_\beta} \qquad (\beta = j)\ . \tag{3.25}$$

A consequence of this equality is that the Lagrangian and Eulerian strain tensors given in Eqs. (3.20) and (3.21) are approximately equal to this order of approximation, that is

$$\eta_{\alpha\beta} \approx e_{ij} \approx \frac{1}{2}\left(\frac{\partial\xi_i}{\partial X_\beta} + \frac{\partial\xi_j}{\partial X_\alpha}\right) \approx \frac{1}{2}\left(\frac{\partial\xi_i}{\partial x_j} + \frac{\partial\xi_j}{\partial x_i}\right) \quad (\alpha = i,\ \beta = j) \tag{3.26}$$

and

$$E_{ij} = \frac{1}{2}\left(\frac{\partial\xi_i}{\partial X_\beta} + \frac{\partial\xi_j}{\partial X_\alpha}\right), \tag{3.27a}$$

$$= \frac{1}{2}\left(\mathcal{F}_{i\beta} + \mathcal{F}_{j\alpha}\right) - \delta_{ij} \quad (\alpha = i,\ \beta = j)\ . \tag{3.27b}$$

The tensor E_{ij} is called the infinitesimal strain tensor. It is easily seen that the tensor E_{ij} is the symmetric part of the displacement gradient tensor $\partial\xi_i/\partial X_\beta$ given in Eq. (3.16). The skew-symmetric part is called the infinitesimal rotation tensor, Ω_{ij}, and is given by

$$\Omega_{ij} = \frac{1}{2}\left(\frac{\partial\xi_i}{\partial X_\beta} - \frac{\partial\xi_j}{\partial X_\alpha}\right) \tag{3.28a}$$

$$= \frac{1}{2}\left(\mathcal{F}_{i\beta} - \mathcal{F}_{j\alpha}\right) \qquad (\alpha = i,\ \beta = j)\ . \tag{3.28b}$$

With the defining relations given in Eqs. (3.27a), (3.27b) and (3.28a), (3.28b), it has now been shown that any infinitesimal motion can be decomposed into an infinitesimal strain, $\mathbf{E}$, and infinitesimal rotation, $\boldsymbol{\Omega}$. However, an analogous partitioning was found in Sect. 3.1.1 using the polar decomposition theorem. Equations (3.27a), (3.27b) and (3.28a), (3.28b) show that the deformation gradient tensor can be written as

$$\mathcal{F}_{i\beta} = \delta_{ij} + E_{ij} + \Omega_{ij} \qquad (\beta = j)\ , \tag{3.29}$$

and Eqs. (3.20) and (3.23a) shows that the right Cauchy-Green tensor can be written as

$$C_{\alpha\beta} = U_{k\alpha}U_{k\beta} = \delta_{\alpha\beta} + 2E_{ij} \qquad (\alpha = i,\ \beta = j)\ . \tag{3.30}$$

Consistent with the level of approximation in this analysis where quadratic terms are neglected, the right stretch tensor is then given by

$$U_{i\beta} = \delta_{i\beta} + E_{ij} \qquad (\beta = j) \,, \tag{3.31}$$

and similarly for $V_{i\beta}$,

$$V_{i\beta} = \delta_{i\beta} + E_{ij} \qquad (\beta = j) \,. \tag{3.32}$$

The results in Eqs. (3.31) and (3.32) show that the stretch tensors are related to the infinitesimal strain tensor. From Eq. (3.22a), the rotation tensor R_{ij} can be extracted from the deformation gradient tensor and the right stretch tensor using

$$R_{ij} = \mathcal{F}_{i\alpha} U^{-1}_{\alpha j} \,, \tag{3.33}$$

where the inverse of the right stretch tensor $U_{i\beta}$ is given, to this order of approximation, by

$$U^{-1}_{i\beta} = \delta_{i\beta} - E_{ij} \qquad (\beta = j) \,. \tag{3.34}$$

Using Eq. (3.34) in Eq. (3.33) leads to

$$R_{ij} = \delta_{i\beta} + \Omega_{ij} \qquad (\beta = j) \,. \tag{3.35}$$

Just as the stretch tensors were related to the infinitesimal strain tensors, Eq. (3.35) shows that the rotation tensor R_{ij} can be related to the infinitesimal rotation tensor.

Having now established measures for quantities related to material line element extension, strain, and rotation, it is now possible to begin to focus on the kinematics related to fluid flows. As will be seen in the next section where rate of deformation is discussed, a useful link with this limiting case of infinitesimal displacements will be developed. This link provides an insightful physical relevance to the properties associated with the rate of deformation.

3.2 Rate of Deformation

In solid mechanics, the primary interest is on the change of shape of the material body so that kinematic quantities associated with the strain imposed on material elements of a body will be of interest. In fluid mechanics, however, the primary interest is the rate at which this change of shape is taking place so the relevant kinematic quantity will be the rate of deformation. Additionally, the overall conservation principles associated with mass, momentum, and energy in fluid flows also require a knowledge of the time rate variation within the flow domain.

3.2.1 Time Rate of Change

It suffices in the discussion here to consider some scalar function f which is associated with some particle whose motion is described by Eq. (3.1a) or inversely by

Eq. (3.1b). Using Eq. (3.1a), this scalar function could be written as $f(x_i(X_\alpha, t), t)$ or, using Eq. (3.1b), as $f(X_\alpha(x_i, t), t)$. In the former case, the scalar function f has some value at the particle position $x_i(X_\alpha, t)$ in space, and in the latter case, it has a value that is associated with the particle located at $X_\alpha(x_i, t)$. From the discussion up to this point, the time rate of change of interest is the variation associated with a particle which can be written as

$$\frac{Df}{Dt} = \left.\frac{\partial f(X_\alpha(\mathbf{x}, t), t)}{\partial t}\right|_{\mathbf{X}} , \tag{3.36}$$

where D/Dt is called the material derivative. As noted above the same function f can be alternately described by $f(x_i(\mathbf{X}, t), t)$, so that the same time rate of change can be written as

$$\begin{aligned} \frac{Df}{Dt} &= \frac{\partial f(x_i(\mathbf{X}, t), t)}{\partial t} \\ &= \left.\frac{\partial f}{\partial x_i}\frac{\partial x_i(\mathbf{X}, t)}{\partial t}\right|_{\mathbf{X}} + \left.\frac{\partial f}{\partial t}\right|_{\mathbf{x}} \\ &= v_i \frac{\partial f}{\partial x_i} + \frac{\partial f}{\partial t} , \end{aligned} \tag{3.37}$$

where the velocity component $v_i(x_i(\mathbf{X}, t), t)$ is, from Eq. (3.36), the material derivative of the position of the particle. The material derivative is an essential element in the description of viscoelastic fluids and dynamics of turbulent flows.

3.2.2 Strain Rate and Rotation Rate Tensors

It is worth emphasizing at this point the kinematic nature of these results so far, that is, there has been no distinction between fluid or solid up to this point; however, a distinction can now begin to be made. In fluid mechanics, an important kinematic quantity in analyzing the fluid motion is the rate of deformation. Although the ultimate aim is to determine this rate of deformation in some region of space in terms of x_i, the convenient starting point is the extension ratio expressed in terms of the material coordinates X_α fixed in time and given by Eq. (3.18). The time rate of change of the extension ratio can then be written as

$$2\lambda\frac{D\lambda}{Dt} = e_\alpha \left(\mathcal{F}_{i\alpha}\frac{D\mathcal{F}_{i\beta}}{Dt} + \frac{D\mathcal{F}_{i\alpha}}{Dt}\mathcal{F}_{i\beta}\right) e_\beta , \tag{3.38}$$

where

$$\frac{D\mathcal{F}_{i\beta}}{Dt} = \frac{\partial}{\partial X_\beta}\left[\frac{D}{Dt}x_i(\mathbf{X}, t)\right] = \frac{\partial v_i}{\partial x_k}\mathcal{F}_{k\beta}, \qquad \frac{D\boldsymbol{\mathcal{F}}}{Dt} = \boldsymbol{L}\boldsymbol{\mathcal{F}} , \tag{3.39}$$

with $v_i(\mathbf{X}, t) = Dx_i(\mathbf{X}, t)/Dt$ the particle velocity at constant $\mathbf{X}$, and $\boldsymbol{L}$ the velocity gradient tensor. Equation (3.38) can then be rewritten as

$$\lambda \frac{D\lambda}{Dt} = \frac{1}{2}\left(\frac{\partial v_i}{\partial x_j} + \frac{\partial v_j}{\partial x_i}\right) e_\alpha \mathcal{F}_{i\alpha} \mathcal{F}_{j\beta} e_\beta \ , \tag{3.40}$$

and if Eq. (3.13) is used, can be expressed in terms of the unit vectors at the time t of the deformation as

$$\lambda^{-1} \frac{D\lambda}{Dt} = D_{ij} e_i e_j \ , \tag{3.41}$$

where the rate of deformation tensor D_{ij} $(= S_{ij})$ is given by

$$D_{ij} = \frac{1}{2}\left(\frac{\partial v_i}{\partial x_j} + \frac{\partial v_j}{\partial x_i}\right) . \tag{3.42}$$

With D_{ij} a symmetric tensor, it can be associated with the velocity gradient tensor $\partial v_i / \partial x_j$, and a corresponding skew-symmetric part, called the vorticity tensor, given by

$$W_{ij} = \frac{1}{2}\left(\frac{\partial v_i}{\partial x_j} - \frac{\partial v_j}{\partial x_i}\right) . \tag{3.43}$$

Since the vorticity tensor is a skew-symmetric tensor involving velocity gradients it is a measure of a rate of rotation.

It is useful to point out that these elementary relationships associated with the deformation gradient of the fluid element and the velocity gradient field can have significant consequences concerning the development of constitutive equations for complex fluids and flows in Chaps. 5 and 6. For example, consider the simple case of a constant velocity gradient, the time rate of change of $\boldsymbol{\mathcal{F}}$ given by Eq. (3.36) along the fluid element path, can be readily obtained from Eq. (3.39) as

$$\boldsymbol{\mathcal{F}}(t) = e^{t\boldsymbol{L}} \ , \tag{3.44}$$

where $\boldsymbol{\mathcal{F}}(0) = \boldsymbol{I}$ since there is no stretch initially. The associated relative deformation gradient $\boldsymbol{\mathcal{F}}_{(t)}$ can be obtained from Eq. (3.9) and is

$$\boldsymbol{\mathcal{F}}_{(t)}(\tau) = e^{(\tau - t)\boldsymbol{L}} \ . \tag{3.45}$$

More complex situations can occur when the velocity gradient is a function of time; however, many useful and relevant motions follow from the simple case of $\boldsymbol{L}$ constant.

With the introduction of the velocity gradient tensor, which is of fundamental importance in the description and dynamics of fluid motion, it is useful to provide some linkage with some of the other quantities introduced in this chapter.

Consider first the relative deformation tensor introduced in Eq. (3.9). The time rate of change of this expression yields

$$\frac{D\mathcal{F}_{i\beta}(\tau)}{D\tau} = \frac{D\mathcal{F}_{(t)ik}(\tau)}{D\tau} \mathcal{F}_{k\beta}(t) \ , \tag{3.46}$$

which, when evaluated at $\tau = t$ and compared with Eq. (3.39), shows that the time rate of change of the relative deformation gradient tensor is just the velocity gradient tensor, that is

$$\left.\frac{D\mathcal{F}_{(t)ik}(\tau)}{D\tau}\right|_{\tau=t} = \frac{\partial v_i}{\partial x_k}, \qquad \left.\frac{D\boldsymbol{\mathcal{F}}_{(t)}}{D\tau}\right|_{\tau=t} = \boldsymbol{L}\ , \tag{3.47}$$

where $\boldsymbol{L}$ can be decomposed into symmetric, $\boldsymbol{D}$, and skew-symmetric, $\boldsymbol{W}$, parts as

$$\boldsymbol{L} = \boldsymbol{D} + \boldsymbol{W}\ . \tag{3.48}$$

Additionally, the polar decomposition theorem can be applied to the relative deformation gradient, that is $\mathcal{F}_{(t)ik}(\tau) = \boldsymbol{R}_{(t)ij}(\tau)\boldsymbol{U}_{(t)jk}(\tau)$. Substituting this decomposition into Eq. (3.47), then yields the defining relations

$$\left.\frac{D\boldsymbol{U}_{(t)}}{D\tau}\right|_{\tau=t} = \boldsymbol{D} \quad \text{and} \quad \left.\frac{D\boldsymbol{R}_{(t)}}{D\tau}\right|_{\tau=t} = \boldsymbol{W}\ , \tag{3.49}$$

where the symmetric tensor $\boldsymbol{D}$ is the rate of strain of the fluid element, and the skew-symmetric tensor $\boldsymbol{W}$ is a rate of rotation, or spin, of a fluid element.

Next consider the results from Sect. 3.1.2 where the elements of the infinitesimal strain and rotation were discussed. It was shown in Sect. 3.1.2 that in the limit of small displacements $\mathcal{F}^{-1}_{\alpha j} \approx \delta_{ij}$ $(\alpha = i)$. In this limit, Eq. (3.39) simply reduces to

$$\frac{D\mathcal{F}_{i\beta}}{Dt} = \frac{\partial v_i}{\partial x_j} \qquad (\beta = j)\ , \tag{3.50a}$$

and the rate of strain and the rate of rotation tensors are

$$D_{ij} = \frac{DE_{ij}}{Dt} \quad \text{and} \quad W_{ij} = \frac{D\Omega_{ij}}{Dt}\ , \tag{3.50b}$$

from Eqs. (3.27b) and (3.28b), respectively. Equations (3.50a), (3.50b) then show that in the limit of infinitesimal displacements the velocity gradient tensor is the rate of deformation tensor.

3.2.3 Dilatation Rate

Consider the material derivative of the Jacobian definition given in Eq. (3.5),

$$\begin{aligned}
\frac{DJ}{Dt} &= \frac{\partial J}{\partial \mathcal{F}_{i\beta}}\frac{D\mathcal{F}_{i\beta}}{Dt} = \text{tr}\left[\frac{\partial J}{\partial \boldsymbol{\mathcal{F}}}\frac{D\boldsymbol{\mathcal{F}}^T}{Dt}\right] \\
&= J\ \mathcal{F}^{-1}_{\beta i}\frac{D\mathcal{F}_{i\beta}}{Dt} = J\ \text{tr}\left[\left(\boldsymbol{\mathcal{F}}^{-1}\right)^T\frac{D\boldsymbol{\mathcal{F}}^T}{Dt}\right] = J\ \text{tr}\left[\left(\frac{D\boldsymbol{\mathcal{F}}}{Dt}\,\boldsymbol{\mathcal{F}}^{-1}\right)^T\right] \\
&= J\left[\mathcal{F}^{-1}_{\beta i}\frac{\partial v_i}{\partial x_k}\mathcal{F}_{k\beta}\right] = J\ \text{tr}\left[(\nabla\mathbf{v})^T\,\boldsymbol{I}\right] \\
&= J\left[\delta_{ki}\frac{\partial v_i}{\partial x_k}\right] = J\ \frac{\partial v_i}{\partial x_i} = J\ \text{div}\,\mathbf{v}\ ,
\end{aligned} \tag{3.51}$$

where $\mathrm{I}_3(\boldsymbol{\mathcal{F}}) = J$ has been used.[2] With the material volume relationship given in Eq. (3.4b), Eq. (3.51) can be rewritten as

$$\frac{1}{\mathcal{V}}\frac{\mathrm{d}\mathcal{V}}{\mathrm{d}t} = \frac{\partial v_i}{\partial x_i} = \operatorname{div}\mathbf{v}\,. \tag{3.52}$$

Equation (3.52) shows that the divergence of the velocity is a measure of the relative rate of change of the dilatation J. Thus, when the condition $\operatorname{div}\mathbf{v} = 0$ holds the fluid can be considered as incompressible and the motion is isochoric.

3.2.4 Rivlin-Ericksen Tensors

Higher rates of change of the deformation can be developed and among these, the most useful, are the Rivlin-Ericksen tensors which are extracted from the relative right Cauchy-Green tensor,

$$C_{(t)ij}(\tau) = \mathcal{F}_{(t)ki}(\tau)\mathcal{F}_{(t)kj}(\tau), \quad \boldsymbol{C}_{(t)}(\tau) = \boldsymbol{\mathcal{F}}^T_{(t)}(\tau)\boldsymbol{\mathcal{F}}_{(t)}(\tau)\,. \tag{3.53}$$

The n-th order Rivlin-Ericksen tensors are then defined as

$$\boldsymbol{A}_n(t) = \left.\frac{\partial^n \boldsymbol{C}_{(t)}(\tau)}{\partial\tau^n}\right|_{\mathbf{X},\tau=t}, \quad n = 1, 2, \ldots \tag{3.54a}$$

or

$$A^{(n)}_{ij}(t) = \left.\frac{\partial^n C_{(t)ij}(\tau)}{\partial\tau^n}\right|_{\mathbf{X},\tau=t}, \quad n = 1, 2, \ldots\,. \tag{3.54b}$$

Alternatively, it is often times useful to introduce a time shift variable s such that the reference time τ can be related to the present time t through the relation $\tau = t - s$, with $0 \le s < \infty$. Equations (3.54a), (3.54b) can then be rewritten as

$$\boldsymbol{A}_n(t) = (-1)^n \left.\frac{\partial^n \boldsymbol{C}_{(t)}(t-s)}{\partial s^n}\right|_{\mathbf{X},s=0}, \quad n = 1, 2, \ldots \tag{3.55a}$$

or

$$A^{(n)}_{ij}(t) = (-1)^n \left.\frac{\partial^n C_{(t)ij}(t-s)}{\partial s^n}\right|_{\mathbf{X},s=0}, \quad n = 1, 2, \ldots \tag{3.55b}$$

where the time rate of change is once again the material derivative given by Eq. (3.36). Both $A^{(0)}_{ij}(t)$ and $A^{(1)}_{ij}(t)$ have been identified previously and are given by

$$A^{(0)}_{ij}(t) = \delta_{ij}\,, \tag{3.56}$$

[2] The differentiation $\partial \mathrm{I}_3(\boldsymbol{\mathcal{F}})/\partial\boldsymbol{\mathcal{F}}$ can be expressed as

$$\frac{\partial \mathrm{I}_3(\boldsymbol{\mathcal{F}})}{\partial\boldsymbol{\mathcal{F}}}\boldsymbol{\mathcal{F}}^T = \mathrm{I}_3(\boldsymbol{\mathcal{F}})\,\boldsymbol{I}.$$

since $\mathcal{F}_{(t)ki}(\tau = t) = \delta_{ki}$, and

$$\begin{aligned} A^{(1)}_{ij}(t) &= \left.\frac{\partial \mathcal{F}_{(t)ki}}{\partial \tau}\right|_{\mathbf{X},\tau=t} \mathcal{F}_{(t)kj}(t) + \mathcal{F}_{(t)ki}(t) \left.\frac{\partial \mathcal{F}_{(t)kj}}{\partial \tau}\right|_{\mathbf{X},\tau=t} \\ &= \left.\frac{D\mathcal{F}_{(t)ji}}{D\tau}\right|_{\tau=t} + \left.\frac{D\mathcal{F}_{(t)ij}}{D\tau}\right|_{\tau=t} \\ &= 2D_{ij} \ , \end{aligned} \tag{3.57}$$

where Eq. (3.47) has also been used. The next order, which will be the last shown here, is useful in the development of constitutive equations. Following directly from Eqs. (3.54a), (3.54b) it can be written as

$$\begin{aligned} A^{(2)}_{ij}(t) &= \frac{\partial}{\partial \tau}\left[\frac{\partial \mathcal{F}_{(t)ki}}{\partial \tau}\mathcal{F}_{(t)kj}(\tau) + \mathcal{F}_{(t)ki}(\tau)\frac{\partial \mathcal{F}_{(t)kj}}{\partial \tau}\right]\Bigg|_{\mathbf{X},\tau=t} \\ &= \frac{\partial}{\partial \tau}\left[\mathcal{F}_{l\alpha}(\tau)\mathcal{F}^{-1}_{\alpha i}(t)A^{(1)}_{lk}(\tau)\mathcal{F}_{k\beta}(\tau)\mathcal{F}^{-1}_{\beta j}(t)\right]\Bigg|_{\mathbf{X},\tau=t} \\ &= \left.\frac{\partial A^{(1)}_{ij}}{\partial \tau}\right|_{\mathbf{X},\tau=t} + \left.\frac{\partial \mathcal{F}_{l\alpha}(\tau)}{\partial \tau}\right|_{\mathbf{X},\tau=t} \mathcal{F}^{-1}_{\alpha i}(t)A^{(1)}_{lj}(t) \\ &\qquad + A^{(1)}_{ik}(t) \left.\frac{\partial \mathcal{F}_{k\alpha}(\tau)}{\partial \tau}\right|_{\mathbf{X},\tau=t} \mathcal{F}^{-1}_{\alpha j}(t) \\ &= \frac{DA^{(1)}_{ij}}{Dt} + \frac{\partial v_l}{\partial x_i}A^{(1)}_{lj} + A^{(1)}_{ik}\frac{\partial v_k}{\partial x_j} \ , \end{aligned} \tag{3.58}$$

where Eqs. (3.9), (3.39) and (3.46) have been used.

If the concept of acceleration is generalized so that the n-th acceleration and associated spatial gradient can be defined as

$$\mathbf{a}_n = \left.\frac{D^n \boldsymbol{\varkappa}(\mathbf{X},t)}{D\tau^n}\right|_{\tau=t} \quad \text{and} \quad \boldsymbol{L}_n = \boldsymbol{\nabla}\mathbf{a}_n \ , \tag{3.59a}$$

or

$$a^{(n)}_i = \left.\frac{D^n \varkappa_i(\mathbf{X},t)}{D\tau^n}\right|_{\tau=t} \quad \text{and} \quad L^{(n)}_{ij} = \frac{\partial}{\partial x_j}\left(\left.\frac{D^n \varkappa_i(\mathbf{X},t)}{D\tau^n}\right|_{\tau=t}\right) \ , \tag{3.59b}$$

respectively. For $n = 0$, $\mathbf{a}_0 = \mathbf{x}(\mathbf{X},t)$ and $\boldsymbol{L}_0 = \boldsymbol{I}$, and for $n = 1$, $\mathbf{a}_1 = \mathbf{v}$ and $\boldsymbol{L}_1 = \boldsymbol{\nabla}\mathbf{v}$ are obtained. A kinematic recursion relation for the Rivlin-Ericksen tensors can then be obtained and given by

$$\boldsymbol{A}_n(t) = \boldsymbol{L}_n + \boldsymbol{L}_n^T + \sum_{m=1}^{n-1}\binom{n}{m}\boldsymbol{L}_i\boldsymbol{L}^T_{n-i} = \sum_{m=0}^{n}\binom{n}{m}\boldsymbol{L}_m\boldsymbol{L}^T_{n-m} \ , \tag{3.60}$$

where the binomial coefficient is defined in the usual way,

$$\binom{n}{m} = \frac{n!}{(n-m)!\,m!} \ . \tag{3.61}$$

In particular, for $\boldsymbol{A}_1$ and $\boldsymbol{A}_2$ one has

$$\boldsymbol{A}_1 = \boldsymbol{L} + \boldsymbol{L}^T = 2\boldsymbol{D} \,, \tag{3.62}$$

$$\boldsymbol{A}_2 = \dot{\boldsymbol{L}}_2 + \boldsymbol{L}_2^T + 2\boldsymbol{L}^T\boldsymbol{L} \,, \tag{3.63}$$

which are consistent with the results in Eqs. (3.57) and (3.58).

With the introduction of the time shift variable s, it is possible to formally consider the past history of the deformation. A Taylor series expansion about the present time t can then be written as

$$\begin{aligned} C_{(t)ij}(t-s) &= C_{(t)ij}(t) - s\left.\frac{\partial C_{(t)ij}(t-s)}{\partial s}\right|_{s=0} + \frac{s^2}{2}\left.\frac{\partial^2 C_{(t)ij}(t-s)}{\partial s^2}\right|_{s=0} + \cdots \\ &= \delta_{ij} + sA_{ij}^{(1)} + \frac{s^2}{2}A_{ij}^{(2)} + \cdots \end{aligned} \tag{3.64}$$

where Eqs. (3.56), (3.57), and (3.58) have been used. For small values of s, that a short interval over which the deformation occurs, Eq. (3.64) shows that the deformation can be measured through the Rivlin-Ericksen tensors which are functions of the (local) velocity gradient tensor.

3.3 Reynolds Transport Theorem

A final kinematic result that is a prerequisite for obtaining the various conservation equations in the next section can be extracted using the result in Eq. (3.52). Of interest in the study of any fluid flow is the evolution of physical variables. Within a volume element $\mathcal{V}$ moving with the fluid, the evolution of these physical variables can be obtained from a knowledge of a corresponding density function of space and time, $\mathscr{F}(\mathbf{x}, t)$, and would be given by

$$\int_{\mathcal{V}(t)} \mathscr{F}(\mathbf{x}, t)\mathrm{d}\mathcal{V} \,. \tag{3.65}$$

The term density function is used in a broad context. Up to this point, the mass density (mass per unit volume) has only been considered. As noted previously, the study of fluid flows in general is focused on rate of change of variables so the interest is actually in the rate of change of this integral. Unfortunately, in its present form the integral is not readily amenable to differentiation since the volume $\mathcal{V}$ varies with time and the differentiation cannot be taken through the integral sign. However, recall from Eq. (3.4b) that this changing volume $\mathrm{d}\mathcal{V}$ can be related to a volume in $\boldsymbol{\xi}$-space, and that $\mathrm{d}/\mathrm{d}t$ is differentiation with respect to time with $\boldsymbol{\xi}$ constant. With these relations,

$$\begin{aligned} \frac{\mathrm{d}}{\mathrm{d}t}\int_{\mathcal{V}(t)} \mathscr{F}(\mathbf{x}, t)\mathrm{d}\mathcal{V} &= \frac{\mathrm{d}}{\mathrm{d}t}\int_V \mathscr{F}[\boldsymbol{\xi}_{(t)}(\boldsymbol{\xi}, t'), t]J\mathrm{d}V \\ &= \int_V \left(\frac{\mathrm{d}\mathscr{F}}{\mathrm{d}t}J + \mathscr{F}\frac{\mathrm{d}J}{\mathrm{d}t}\right)\mathrm{d}V \\ &= \int_{\mathcal{V}} \left(\frac{\mathrm{d}\mathscr{F}}{\mathrm{d}t} + \mathscr{F}\frac{\partial v_i}{\partial x_i}\right)\mathrm{d}\mathcal{V} \,. \end{aligned} \tag{3.66}$$

The material derivative $\mathrm{d}/\mathrm{d}t$ can be re-expressed in an Eulerian frame by the relation (cf. Eqs. (3.36) and (3.37))

$$\left.\frac{\mathrm{d}}{\mathrm{d}t}\right|_{\xi} = \frac{D}{Dt} = \left.\frac{\partial}{\partial t}\right|_{\xi} + \left.\frac{\partial}{\partial x_j}\frac{\partial x_j}{\partial t}\right|_{\xi} = \frac{\partial}{\partial t} + v_j\frac{\partial}{\partial x_j}\,, \tag{3.67}$$

so that Eq. (3.66) can be written as

$$\frac{\mathrm{d}}{\mathrm{d}t}\int_{\mathcal{V}(t)} \mathscr{F}(\mathbf{x},t)\mathrm{d}\mathcal{V} = \int_{\mathcal{V}}\left[\frac{\partial \mathscr{F}}{\partial t} + \frac{\partial}{\partial x_j}(\mathscr{F}v_j)\right]\mathrm{d}\mathcal{V}\,. \tag{3.68}$$

A clearer physical interpretation of this relation is obtained by rewriting the last term on the right-side using Green's theorem. The resulting expression,

$$\frac{\mathrm{d}}{\mathrm{d}t}\int_{\mathcal{V}(t)} \mathscr{F}(\mathbf{x},t)\mathrm{d}\mathcal{V} = \int_{\mathcal{V}}\frac{\partial \mathscr{F}}{\partial t}\mathrm{d}\mathcal{V} + \int_{\mathcal{S}}\mathscr{F}v_j n_j \mathrm{d}\mathcal{S}\,, \tag{3.69}$$

where $\mathcal{S}(t)$ is the surface of $\mathcal{V}(t)$, and n_i is the unit normal to the surface, shows that the rate of change of the integral of $\mathscr{F}$ within the moving volume $\mathcal{V}$ is the rate of change at a point plus the net flow of $\mathscr{F}$ over the surface of $\mathcal{V}$.

3.4 Conservation Equations

The primary focus in this book will be on the incompressible motion of fluid flows; however, in fully exploiting the usefulness of the Reynolds transport theorem, the development of the full set of conservation laws for mass, momentum, and energy will be derived. As such these conservation equations are applicable to fully compressible flows and with the added assumption of a constant density field readily reduce to the corresponding incompressible form. Both the modeled statistical transport equations (RANS) and the filtered transport equations (LES) used in numerical simulation of incompressible flows have their origin in these equations.

The starting point in the development of a mathematical description of incompressible flows is the mass, momentum, and energy conservation equations. The derivation of these equations can be found in almost all fluid dynamic texts so it will not be necessary here to go into their detailed formulation. However, each will be presented to introduce the reader to the notational convention used as well as highlight the various assumptions used in deriving the commonly used forms.

The mathematical basis for these balance equations lies in the Reynolds transport theorem which simply equates the time rate of change of an arbitrary moving material element, characterized by some physical property (e.g. mass density, momentum density, etc.), to the sum of the time change of the physical property within the volume, the rate of change of the surface of the element, and the cumulative effect of (body) forces on the element.

3.4.1 Mass Conservation

Consider a body of fluid whose mass density is $\rho(\mathbf{x}, t)$. The total mass of the body is given by (cf. Eq. (3.65))

$$m(t) = \int_{\mathcal{V}(t)} \rho(\mathbf{x}, t) \mathrm{d}\mathcal{V} \,. \tag{3.70}$$

If it is assumed that during the motion the total mass is unchanged within the volume (there are no sources or sinks within the material volume), the rate of change of mass is then

$$\frac{\mathrm{d}m}{\mathrm{d}t} = \int_{\mathcal{V}} \left[\frac{\partial \rho}{\partial t} + \frac{\partial}{\partial x_j}(\rho v_j) \right] \mathrm{d}\mathcal{V} = 0 \,, \tag{3.71}$$

where Eq. (3.68) has been used with $\rho(\mathbf{x}, t) = \mathscr{F}(\mathbf{x}, t)$. Since $\mathcal{V}$ is an arbitrary volume, the integrand must vanish everywhere, so that the mass conservation equation is

$$\frac{\partial \rho}{\partial t} + \frac{\partial}{\partial x_j}(\rho v_j) = 0 \qquad \text{or} \qquad \frac{D\rho}{Dt} = -\rho \frac{\partial v_j}{\partial x_j} \,. \tag{3.72}$$

Equation (3.72) is also known as the continuity equation, and it shows that if the fluid volume (cf. Eq. (3.52)) is density preserving $D\rho/Dt = 0$, then the velocity field is solenoidal (source free),

$$\frac{\partial v_j}{\partial x_j} = 0 \,, \tag{3.73}$$

and the fluid is incompressible. Only incompressible fluids will be considered here so that the density field ρ is also constant.

3.4.2 Momentum Conservation

The conservation equation for the linear momentum of a body can be stated as a balance between the time rate of change of the momentum of the body and the resultant force acting on the body,

$$\int_{\mathcal{V}} \left[\frac{\partial \rho v_i}{\partial t} + \frac{\partial}{\partial x_j}(\rho v_i v_j) \right] \mathrm{d}\mathcal{V} = \mathcal{F}_i \,, \tag{3.74}$$

where Eq. (3.68) has been used with $\mathscr{F}(\mathbf{x}, t)$ replaced with the linear momentum density ρv_i. The vector total force $\mathcal{F}_i$ consists of the sum of all the forces acting on the body. This total force can be partitioned into a surface force and a body force,

$$\mathcal{F}_i(\mathbf{x}, t) = \oint_{\mathcal{S}} \Sigma_{ij} n_j \mathrm{d}\mathcal{S} + \int_{\mathcal{V}} \rho f_i \mathrm{d}\mathcal{V} \,, \tag{3.75}$$

where $\Sigma_{ij} n_j \mathrm{d}\mathcal{S}$ is the surface force exerted across an element of area $\mathrm{d}\mathcal{S}$, and f_i is the body force per unit mass. The surface force is proportional to the amount of

surface area acted upon; whereas, the body force is assumed to act uniformly on all elements within the fluid volume.

In integral form over the material boundary, the balance equation given in Eq. (3.74) can be written as

$$\int_{\mathcal{V}} \left[\frac{\partial \rho v_i}{\partial t} + \frac{\partial}{\partial x_j}(\rho v_i v_j) - \frac{\partial}{\partial x_j}\Sigma_{ij} - \rho f_i \right] \mathrm{d}\mathcal{V} = 0 \,, \tag{3.76}$$

where the divergence theorem has been used on the integral of the surface forces. Since Eq. (3.76) holds for all choices of the material volume $\mathcal{V}$, and the integrands are continuous functions in space, then the corresponding differential form can be written as

$$\rho \frac{Dv_i}{Dt} = \frac{\partial(\rho v_i)}{\partial t} + \frac{\partial(v_j \rho v_i)}{\partial x_j} = \frac{\partial}{\partial x_j}\Sigma_{ij} + \rho f_i \,. \tag{3.77}$$

An alternate form of this equation, that can be useful in the subsequent analysis, can be obtained. It is easily extracted by introducing the vorticity vector $\boldsymbol{\omega}$ $(= \nabla \times \mathbf{v})$ or $\omega_i = (e_{ijk}(\partial v_k / \partial x_j))$ into the formulation using the vector identity

$$\boldsymbol{\omega} \times \mathbf{v} = \mathbf{v} \cdot \nabla \mathbf{v} - \nabla \left(\frac{|v|^2}{2} \right) \,, \tag{3.78a}$$

or, in Cartesian tensor notation

$$e_{ijk}\omega_j v_k = e_{ijk} e_{jlm} \left(\frac{\partial v_m}{\partial x_l} \right) v_k = v_j \frac{\partial v_i}{\partial x_j} - \frac{\partial}{\partial x_i}\left(\frac{v_j v_j}{2} \right) \,, \tag{3.78b}$$

where the (two-dimensional) tensor identity $e_{ijk}e_{jlm} = \delta_{kl}\delta_{im} - \delta_{km}\delta_{il}$ is also used. The alternate form for the linear momentum conservation equation can then be written as

$$\frac{\partial v_i}{\partial t} + e_{ijk}\omega_j v_k = -\frac{\partial}{\partial x_i}\left(\frac{v_j v_j}{2} \right) + \frac{1}{\rho}\frac{\partial}{\partial x_j}\Sigma_{ij} + f_i \,. \tag{3.79}$$

It is also straightforward to derive the corresponding vorticity equation from Eq. (3.77), by simply taking the curl, in order to obtain

$$\frac{D\omega_i}{Dt} = \frac{\partial v_i}{\partial x_k}\omega_k - \frac{\partial v_k}{\partial x_k}\omega_i + \frac{1}{\rho}\left[e_{ijk}\frac{\partial}{\partial x_j}\left(\frac{\partial \Sigma_{kl}}{\partial x_l} \right) \right] + e_{ijk}\frac{\partial f_k}{\partial x_j} \,, \tag{3.80}$$

where for an incompressible fluid the second term on the right-side vanishes. It remains to identify the exact forms of both the surface and body forces acting on a material element. This requires the specification of the local stress field Σ_{ij}, and the applicable body force (per unit volume) ρf_i.

The conservation equation for the angular momentum of a body can be stated as a balance between the time rate of change of the angular momentum of the body and the total torque acting on the body,

$$\int_{\mathcal{V}} \left[\frac{\partial \rho m_i}{\partial t} + \frac{\partial}{\partial x_l}(\rho m_i v_l) \right] \mathrm{d}\mathcal{V} = \mathcal{T}_i \,, \tag{3.81}$$

where Eq. (3.68) has been used with $\mathscr{F}(\mathbf{x}, t)$ replaced with the angular momentum density $\rho m_i = e_{ijk} r_j \rho v_k$ (where r_k is a position vector from some chosen axis). The vector $\mathcal{T}_i$ represents the total torque acting on the body which can be partitioned into contribution from the same surface and body forces that contributed to the linear momentum balance as well as any other applied torques T_i^a,

$$\mathcal{T}_i(\mathbf{x}, t) = \oint_{\mathcal{S}} e_{ijk} r_j \Sigma_{kl} n_l \mathrm{d}\mathcal{S} + \int_{\mathcal{V}} e_{ijk} r_j \rho f_k \mathrm{d}\mathcal{V} + \int_{\mathcal{V}} \rho T_i^a \mathrm{d}\mathcal{V} \,. \tag{3.82}$$

Applying the same arguments to Eq. (3.81) as for the mass and linear momentum integral relations, yields the differential form for conservation of angular momentum,

$$\rho \frac{Dm_i}{Dt} = \frac{\partial(\rho m_i)}{\partial t} + \frac{\partial(\rho m_i v_l)}{\partial x_l} = \frac{\partial}{\partial x_l}\left(e_{ijk} r_j \Sigma_{kl}\right) + \rho e_{ijk} r_j f_k + \rho T_i^a \,. \tag{3.83}$$

Analogously, an equation for the angular momentum can be formed from the linear equation balance, given in Eq. (3.77), by taking the vector cross product with the position vector $\boldsymbol{r}$. The resulting angular momentum equation can be written as

$$\frac{\partial(\rho m_i)}{\partial t} + \frac{\partial(\rho m_i v_l)}{\partial x_l} = e_{ijk} r_j \frac{\partial}{\partial x_l} \Sigma_{kl} + \rho e_{ijk} r_j f_k \,. \tag{3.84}$$

A comparison of Eqs. (3.83) and (3.84) shows that the two equations are equivalent if

$$\rho T_i^a = e_{ikl} \Sigma_{kl} \,. \tag{3.85}$$

In the absence of any (external) applied torque on the fluid flow, the stress tensor Σ_{kl} must be symmetric.

3.4.2.1 Surface Forces: The Stress Tensor

In the discussion of the stress tensor, it is assumed that no applied torques are imposed on the fluid so that as just shown from the conservation of angular momentum that the symmetry of the stress tensor Σ_{ij} $(= \Sigma_{ji})$ holds.

In a fluid at rest, the only non-zero stresses are the normal stresses and these are independent of the surface normals on which they act. Thus, the stress tensor Σ_{ij} can be written in the isotropic form

$$\Sigma_{ij} = -p\delta_{ij} \,, \tag{3.86}$$

where p is the static-fluid or equilibrium pressure and is equal to the mean normal stress acting on an element of fluid. For a fluid in motion, the pressure can in general be different than the static-fluid pressure shown, but for incompressible Newtonian fluids it is generally assumed equal to the equilibrium pressure. In addition, the stress not only consists of an isotropic part but also a non-isotropic or deviatoric part Ξ_{ij} to account for the fluid motion. The total stress tensor can then be written as (cf. Eq. (1.7))

$$\Sigma_{ij} = -p\delta_{ij} + \Xi_{ij} \ . \tag{3.87}$$

Equation (3.87) then requires the specification of a constitutive relation for the stress tensor Ξ_{ij}.

A defining relation for the viscous stress tensor Ξ_{ij} for a Newtonian fluid is obtained by first assuming that it is solely a function of the mean velocity gradient. The most general linear tensor representation for Ξ_{ij} in terms of the mean velocity gradient can be written as

$$\Xi_{ij} = \alpha_{ijkl} \frac{\partial v_k}{\partial x_l} = \alpha_{ijkl} \left(S_{kl} + W_{kl} \right) \ , \tag{3.88}$$

where the mean velocity gradient has been partitioned into its symmetric and skew-symmetric parts given previously in Eqs. (3.42) and (3.43). Since the molecular structure of the fluid is statistically isotropic, α_{ijkl} is a fourth order isotropic tensor function (81 components) and as such can be written as the sum of products of the Kronecker delta δ_{ij} given in Eqs. (2.19a), (2.19b). The scalar coefficients, μ_0, μ_1, and μ_2, given in Eqs. (2.19a), (2.19b) can now depend on the local thermodynamic state. Since the stress tensor is symmetric, it immediately follows from Eqs. (2.19a), (2.19b) that $\mu_2 = 0$. Substituting the remaining two terms of the isotropic tensor expansion into Eq. (3.88) yields

$$\Xi_{ij} = 2\mu S_{ij} \ , \tag{3.89}$$

where $\mu (= \mu_1)$ is the shear viscosity, and the solenoidal condition on the velocity field has been used for incompressible flow. Equation (3.89) is the Newtonian constitutive equation for the deviatoric part of the viscous stress tensor Ξ_{ij}, and the remaining contribution to the total stress acting on a moving fluid element is the isotropic part $-p\delta_{ij}$.

3.4.2.2 Body Forces

As noted previously, body forces act uniformly on all elements within the fluid volume. Their action is a result of the fluid (volume) being embedded in a force field that acts directly on the fluid elements within the fluid. Common examples are gravitational, electrostatic and (electro)magnetic effects. Of these only the former gravitational force will be considered further here. A convenient feature of the gravitational force is that it can be written in terms of a force potential, that is,

$$\rho f_i = -\rho g_i = -\rho \frac{\partial \mathcal{F}_p}{\partial x_i} \ , \tag{3.90}$$

where $\mathcal{F}_p = g_k x_k$ is the force potential or potential energy per unit mass (the negative sign accounts for proper orientation of the gravitational force). In this form, the body force contribution can be directly assimilated into the pressure gradient and a modified pressure defined.

3.4.3 Energy Conservation

As with the conservation of mass and momentum equations obtained previously in this chapter, the conservation of total energy, ρE, can be obtained through the Reynolds transport theorem. The total energy in the system is a sum of the internal and kinetic energies. However, the interest here is in incompressible, isothermal flows, so that the consideration of the internal energy contribution is unnecessary. Although a kinetic energy equation could be obtained from the total energy equation by subtracting out the internal energy contribution, this would require the introduction of thermodynamic relations which we feel is unnecessary here. Thus, the kinetic energy equation will be obtained directly from the linear momentum equation, and is a balance between the time rate of change of the kinetic energy and rate at which energy is transferred to the body through work. The equation for $\rho v_i v_i/2$ can be derived from Eq. (3.77) by simply forming the scalar product, that is, multiplying by v_i, which then yields

$$\begin{aligned}\rho \frac{D}{Dt}\left(\frac{v_i v_i}{2}\right) &= \frac{\partial}{\partial t}\left(\rho \frac{v_i v_i}{2}\right) + \frac{\partial}{\partial x_j}\left(v_j \rho \frac{v_i v_i}{2}\right) \\ &= v_i \frac{\partial}{\partial x_j} \Sigma_{ij} + \rho v_i f_i \\ &= \frac{\partial}{\partial x_j}\left[v_i \left(-p\delta_{ij} + \Xi_{ij}\right)\right] - \left(-p\delta_{ij} + \Xi_{ij}\right) S_{ij} + \rho v_i f_i \,. \end{aligned} \tag{3.91}$$

With this, the fundamental conservation laws governing incompressible, isothermal fluid motion have been specified. Irrespective of whether the fluid is Newtonian or non-Newtonian, or the flow is laminar or turbulent, these equations are the basis for any numerical or theoretical solution.

Chapter 4
Constitutive Equations: General Principles

4.1 Introduction

The general principles of continuous media apply to a large variety of materials. Over the last half-century the development and production of new materials, initially linked to oil derivatives like polymers, but further on to composites, bio-materials, food and drugs, etc. launched the need to describe mathematically the mechanical behavior of those products. The principles of writing relevant constitutive equations were elaborated step by step by generalization of the concepts of mechanics to continua and by a constant interplay between theory and experiments. This lengthy process gave rise to the first nonlinear models that constituted the cornerstone for the development of numerical simulations. The theory of constitutive equations elaborates relations linking the stress tensor to the motion. These constitutive relationships quantify the mechanical behavior of these materials. In this monograph this concept of constitutive equations will also be used, but also extended and adapted to represent the behavior of a turbulent flow. Rivlin (1957) suggested such an analogy between a non-Newtonian fluid and turbulent Newtonian flow over a half-century ago. The analogy was primarily based on the appearance of secondary motions in both the laminar flow of a non-Newtonian fluid and the turbulent flow of a Newtonian fluid in a pipe with elliptical cross-section; whereas, for the laminar flow of a Newtonian fluid the flow is rectilinear. Such behavior is induced through the appearance of normal stress effects, that is, normal stresses associated with the extra-stress of the non-Newtonian fluid in a laminar flow and the turbulent stress of the Newtonian fluid in a turbulent flow.

Later Liepmann (1962), in attempting to describe the dynamics of free turbulent shear flows, proposed an heuristic non-Newtonian model for the apparent stress, induced by the fine-scale turbulence, on the large scale motion that required a viscosity dependent on the rate of strain. This concept was more rigorously pursued by Crow (1967, 1968), Lumley (1970b) who, cognizant of the diverse perspectives of Rivlin (1957) and Liepmann (1962), attempted to qualitatively describe the behavior of turbulence by regarding it as a viscoelastic medium acting on a mean flow field. These early studies provided the necessary incentive to further pursue and quantify

M.O. Deville, T.B. Gatski, *Mathematical Modeling for Complex Fluids and Flows*,
DOI 10.1007/978-3-642-25295-2_4,

this analogy. Over the decades numerous studies have been conducted in connection with the development of constitutive equations for the turbulent stress tensor. These constitutive equations are used in numerical calculations where the transport equations are solved in conjunction with the corresponding conservation equations. Thus, it is within this context that the discussion throughout this chapter is placed.

While the phenomenological similarity in the behavior of the type of flows Rivlin considered was established as well as the underlying dynamic similarity—a normal stress effect—the nature of the stress fields under consideration, as exemplified by Liepmann (1962), are fundamentally different. For example, for a viscoelastic fluid of macromolecules, the extra-stress is related to the second-moment of the end-to-end vector of a macromolecule, and for a turbulent flow the turbulent stress is related to the second-moment of the fluctuating velocity field. Thus, in the laminar flow of a non-Newtonian fluid, the extra-stress is linked to fluid properties; whereas, in the turbulent flow of a Newtonian fluid, the turbulent stress is linked to flow properties. It is related to the fluctuating velocity field as will be discussed in detail in Chap. 6. The fluctuating velocity referred to here, for example, is a consequence of a mathematical partitioning of the instantaneous velocity field into either an ensemble mean and fluctuating part or a filtered (resolved) part and an unresolved part (see Sect. 6.2). In the case of a filtered velocity partitioning, the filtered velocity field can also have a fluctuating component; however, this fluctuation is part of the resolved (known) field and does not require a constitutive (closure) relationship with the resolved field. The basis for any attempt at correspondence between the behavior of the stress fields of the non-Newtonian fluid and the turbulent flow can only be simply based on the fact that both stress fields are related to the motion and each is associated with a probability density function associated with the stochastic component of each.

4.2 Methodological Principles

The founding methodological principles in writing constitutive equations of continuous media are: determinism, local action and material frame-indifference. The mathematical framework and applicability of these principles in forming constitutive equations for non-Newtonian fluids have been extensively developed for well over a half-century and these have been extensively discussed in a variety of texts (e.g. Truesdell 1991; Huilgol and Phan-Thien 1997; Truesdell and Rajagopal 2000). Their extension and relevance to turbulent stress constitutive equations has been considered less extensively. In the next section, some of the well-known consequences of the fundamental principles on the formulation of constitutive equations for materials will be discussed, and in Sect. 4.2.2 some distinctive aspects of these principles when applied to turbulent flows will be discussed.

4.2.1 Material Stress Field

From the first two principles, it is possible to write a general functional form for the stress constitutive equations of such media. The principle of determinism requires that the stress $\boldsymbol{\Sigma}(\mathbf{X}, t)$ be determined by the history of the deformation of the body,

$$\boldsymbol{\Sigma}(\mathbf{X}, t) = \mathscr{S}(\boldsymbol{\chi}(t - s); \mathbf{X}, t), \qquad s \geq 0\,, \tag{4.1}$$

where $\boldsymbol{\chi}$ is the deformation function whose influence is restricted to all past times up to the present time t. Additionally, the notion of contact forces in such material limits the effect of long distance forces. This leads to the local action principle which prevents events that occur far from the present position $\boldsymbol{x}$ from affecting the stress at $\boldsymbol{x}$. This means that the deformation function needed in the determination of the stress field is always assumed limited to a small neighborhood of the present position $\boldsymbol{x}$.

Up to this point, the class of functionals satisfying these first two principles can be rather large. The class can be delimited, but yet sufficiently general to include the constitutive equations relevant to the discussion in this monograph. For this purpose, the discussion will focus on *simple materials* and, in particular, the relevant subset of *simple fluids*. This terminology may, at first, seem contradictory since the monograph is focused on so-called complex fluids and flows. In some ways, this is an example of the disconnect in terminology that often occurs among the continuum mechanics, and fluid mechanics communities. It is, of course, useful to clarify this here. The deformation function of the motion, $\boldsymbol{\chi}(\mathbf{X}, t)$, can be related to the deformation gradient, $\boldsymbol{\mathcal{F}}$ by the relation shown in Eq. (3.3). As noted, the motion defined in this way is termed *homogeneous*. If the behavior of a material (fluid) can be determined from this homogeneous motion described by Eq. (3.3) through $\boldsymbol{\mathcal{F}}$, then the material (fluid) is called simple. Within this context, the continuum mechanics description of a simple fluid is appropriate. In contrast, as will be shown in the remainder of this monograph, this simple functional description of a material element motion, when extrapolated to the behavior of practical fluid flows, can lead to a complex observed behavior. This complex behavior was exemplified throughout Chap. 1.

Taking into account the two principles of determinism and local action, a constitutive equation for the stress field of a *simple material* would then take the form

$$\boldsymbol{\Sigma}(\mathbf{X}, t) = \boldsymbol{\mathcal{S}}(\boldsymbol{\mathcal{F}}(t - s); \mathbf{X}, t), \qquad s \geq 0\,. \tag{4.2}$$

Thus, the stress in the simple material is related to a fundamental descriptor of the motion, that is, the deformation gradient tensor. In Sect. 4.4.2, it will be shown that objectivity constraints imposed on material constitutive equations further refines the functional dependency of Eq. (4.2) to the right Cauchy-Green tensor, $\mathbf{C}$. Of course, the focus here is on fluids, so it is natural to ask what further modifications to the stress dependency can be achieved by considering only fluids, or more specifically incompressible fluids where no change of material volume is allowed ($\det \boldsymbol{\mathcal{F}} = J = 1$). Within the continuum mechanics context, the corresponding question is the functional behavior of a *simple fluid*. It follows immediately

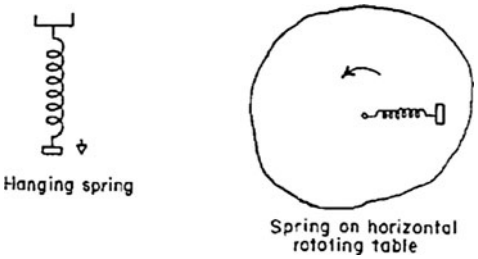

Fig. 4.1 Example of material frame-indifference principle: demonstration of centrifugal force. From Truesdell (1965)

from Eq. (3.9) that a functional dependency on $\mathcal{F}(\tau)$ leads also to a dependency on $\mathcal{F}_{(t)}(\tau)$ and $\mathcal{F}(t)$. Symmetry restrictions (e.g. Huilgol and Phan-Thien 1997), further limits the dependence on $\mathcal{F}(t)$ to $\det\mathcal{F}$ or the Jacobian.[1] For incompressible fluids no changes of element volume ($J = 1$) are encountered so that Eq. (4.2) for such a simple fluid can be recast in terms of the relative motion and written as,

$$\boldsymbol{\Sigma}(\mathbf{X}, t) = \mathfrak{S}'(\mathcal{F}_{(t)}(t-s); \mathbf{X}, t), \qquad s \geq 0\,. \tag{4.3}$$

Within the context of Eq. (4.3), the stress field can be determined by the history of the relative deformation gradient tensor of the fluid element up to the present time t. As with Eq. (4.2), objectivity constraints introduce a functional dependency on the right relative Cauchy-Green tensor, $\boldsymbol{C}_{(t)}$, in Eq. (4.3) (see Sect. 4.4.2).

The remaining principle yet to be discussed is that of material frame-indifference (MFI). Details on the mathematical constraints imposed by this principle will be deferred until Sect. 4.4.2 so that the necessary frame transformation rules can be introduced. Here, as a prelude, a well-known example is presented which describes the physical basis for imposing the principle of MFI on fluid constitutive equations.

The principle of material frame-indifference is related to the notion of frame that is different from that of a simple coordinates system. The frame is linked to an observer and the MFI states that the material properties do not depend on the choice of the observers, that is, "the response of a material is the same for all observers" (Truesdell and Noll 1992). Truesdell (1960, 1965) has an example for this principle and which is a demonstration of centrifugal force. A spring is taken as a one-dimensional elastic body. (In the following description we have taken the liberty of paraphrasing the description in Truesdell (1965). As the reader will see the choice of unit system is unique.) First, the spring is suspended in the laboratory (see Fig. 4.1 with a one pound weight and its deformation (one inch) recorded). Then, the experimental set-up is placed on a rotating table, and the rotational speed of the table is adjusted in such a way that the same deformation of the spring occurs (one inch) as in the fixed laboratory frame. For the same extension, the force exerted on the spring in the rotating frame is the same as in the fixed laboratory frame, that is one poundal, and thus independent of the frame. The principle of MFI has consequences in the behavior of the material stress field which impose constraints on the

[1] Through such arguments, the density field is introduced into the functional relationship for the stress field for compressible fluids.

form of the constitutive equations. Some examples of these constraints are given in Sect. 4.4.2.

4.2.2 Turbulent Stress Field

It is apparent that the various principles associated with the formulation of material stress constitutive equations need not apply to the turbulent stress constitutive equations. In general, the determinism principle should apply to any functional describing the turbulent stress field. The wide spectral scales of motion that make help a high Reynolds number turbulent flow depend on the flow history through both the boundary conditions and the time scales associated with the spectral cascade inherent in the turbulence dynamics. The degree to which a constitutive equation for the turbulent stress should adhere to the determinism principle can depend on the type of turbulent flow being described (for example, through numerical calculation or simulation). Neglecting any initial transients, if the flow becomes statistically steady (stationary), the dependence on the past is removed, and the turbulent field adjusts to a time independent mean motion, since the functional relationships that are used in turbulent constitutive equations are often based on the local mean values at the present time. A more general situation can occur when the ensemble mean is time dependent. This time dependent motion can be periodic, or possibly cyclic, which introduces some past mean flow history effects into the constitutive equation. The extent to which this occurs depends on the memory functional of the stress constitutive equation. Interestingly, in developing a constitutive equation for incompressible fine-grained turbulence, Crow (1968) made the assumption that the "...Reynolds stress evolves in a continuously changing mean field according to a viscoelastic constitutive law, relating stress to deformation history by means of a scalar memory function...." Lumley (1970b) further exploited the relationship as well as the mathematical formalism in the formulation of a turbulent stress constitutive equation applicable to homogeneous sheared turbulence (in this context homogeneous shear to an ensemble mean velocity field independent of spatial orientation). For approaches where a resolved field is determined, the determinism principle is inherent since any constitutive equation for the turbulent stress necessarily includes a time dependent resolved field motion. It should be recognized, of course, that inclusion of an instantaneous mean velocity gradient field has only a limited past history effect. A more direct influence would require a dependence on a time integral related to the mean velocity field.

The principle of local action is certainly not applicable to a turbulent flow. It is well-known from (spatial) multi-point correlation results, that the turbulence is spatially correlated over distances comparable to integral scales of the flow (scales consistent with the domain boundaries) and as such easily violate any restriction based on arbitrarily small neighborhoods of the present position $\mathbf{x}$. Nevertheless, even though the local action principle should not apply in the development of turbulent stress constitutive equations, the vast majority of all single-point constitutive

equations inherently satisfy this principle by the nature of the fact that the constitutive equations are dependent almost exclusively on the mean or resolved field through the local mean velocity gradient tensor. Where the contradiction is most apparent is in the pressure-strain rate correlation term that appears in any constitutive equation for the turbulent stress field. The details of which are deferred until Chap. 6.

In developing constitutive equations, for the turbulent stress field, one needs to impose constraints, either mathematical or physical, on the constitutive equation in order to determine the various closure coefficients that appear. The principle of material frame-indifference would be appealing in this regard since it introduces constraints on the functional forms of the stress fields based on vector and tensorial Euclidean transformations. As a reminder, a distinction is made here between form-invariance and (material) frame-indifference. Form-invariance requires that the structural form of the constitutive equation used by each observer be the same, and frame-indifference requires that the constitutive equation be independent of any frame of reference properties (Sadiki and Hutter 1996). As has been just pointed out, the turbulent stress field is a consequence of the dynamics of the fluid motion rather than the fluid (material) itself. Thus, it is not surprising that the MFI principle cannot apply in the same fashion for the turbulent stress field as it can for the material stress field. Skepticism of the applicability of MFI to turbulent flows was first raised by Lumley (1970b) (see also Lumley 1983) who argued that the turbulence consists of scales of motion consistent with those of the non-inertial frame, and thus negating the requirement that variable transformations be independent of frame rotation. Since all material has inertia, for MFI to be valid the inertia of the material causing the stress must be neglected. As noted this is highly unlikely in a turbulent flow. Nevertheless, objectivity of vector and tensor transformations does impose constraints on the functional forms of turbulent closures and it is within this context the principles associated with constitutive equation development will be discussed for such turbulent flows. The MFI principle was further explored by Speziale (1981, 1998b) who also showed that MFI was not applicable for three-dimensional turbulence, but was able to show that in the limit of two-dimensional turbulence, the turbulent stress field did satisfy MFI. An excellent, recent historical survey of the long-standing debate concerning MFI is given in Frewer (2009). There are aspects of the applicability of the material frame-indifference principle that remain unresolved and have been and continue to be debated. It is outside of the scope of this text to enter into this discussion, but it is intended here to alert the reader to the ongoing debate and to point out some relevant literature.

Nevertheless, other constraints can be imposed on the turbulent stress field that can aid in the formulation of constitutive equations. The constraint of realizability is one such example (see Sect. 6.3.1) and requires that a turbulent stress model yield non-negative component energies in all turbulent flows, with the Schwarz inequality satisfied for each off-diagonal component of the turbulent stress tensor (Schumann 1977). Lumley (1978) further exploited these ideas by examining the limiting behavior of the second and third invariants of the Reynolds stress anisotropy tensor. This invariant map constraint will be discussed further in Sect. 6.4. While these

constraints have been formulated in the context of turbulence model development, they can also be adapted to the material stress field. In this case, rather than being used for constitutive equation development, they have been used as a diagnostic and have provided physical insight into the behavior of the extra-stress field (Thais et al. 2010) induced by the viscoelastic fluid.

4.3 Frames, Transformations and Objectivity

An inertial frame of reference is one where the classical laws of Newtonian mechanics hold and one which is void of any reference frame accelerations. More precisely, it is a frame such that if the body momentum is constant over a finite time interval, then this corresponds to a vanishing force during that interval. Another way of looking at the physical situation in this frame, consists in observing that the center of mass of the body $\mathcal{B}$ moves along a straight line with a uniform speed if there is no force exerted on the body. This is the definition of an inertial frame. A non-inertial frame is, of course, a frame that is not inertial. It introduces into the describing equations fictitious forces like the Coriolis force or the centripetal (centrifugal) force that are generated by the non-objectivity of the acceleration vector. Changes of frame require transformations of tensor quantities of varying order (zero, first, second ...). These transformations can be objective or non-objective, but for the material frame-indifference principle to hold, only objective transformations—those independent of the motion of the observer—are allowed. In the next section, the transformation rules for both kinematic and dynamic variables will be examined.

4.3.1 Transformations and Objectivity

As is well known, the physical properties of a fluid should not be dependent on the frame of the observer. The consequence of having such a property is that measurements of fluid properties made in one reference frame will apply in all other reference frames that are in rigid motion relative to one another (see the discussion in Sect. 3.1). It then follows to formulate equations describing such property variations through variables that are independent of the motion of the observer, that is, objective variables.

Assume there are two frames, with the position and time in each characterized by $(\mathbf{x}, t)$ and $(\mathbf{x}^*, t^*)$, respectively. The two frames are in relative time-dependent motion such that the following bijective mapping exists

$$\mathbf{x}^*(t^*) = \boldsymbol{Q}(t)\,[\mathbf{x} - \mathbf{x}_0] + \mathbf{c}(t)\ , \tag{4.4}$$

and

$$t^* = t - t_s\ , \tag{4.5}$$

where $\boldsymbol{Q}(t)$ is a proper orthogonal tensor with the time t as parameter, $\mathbf{c}(t)$ a translation vector and t_s a constant time shift. Of course in general inhomogeneous flow

fields, the dependency on time is augmented with a spatial dependency so that differentiation in an Eulerian frame will require material derivatives. The relation (4.4) is an Euclidean transformation as it leaves unchanged the structure of the Euclidean vector space we are dealing with. In particular, in this case vector lengths do not change in the frame transformation. Equation (4.4) can also be interpreted as a rigid body motion where the orthogonal tensor $\boldsymbol{Q}$ corresponds to the rotation and the vector $\mathbf{c}$ is the translation. An important subset of this general transformation is the case when $\boldsymbol{Q}(t) = \boldsymbol{Q}_0$ is constant. The transformation in Eq. (4.4) is then representative of the extended Galilean group, and with the further assumption that $\mathbf{c}(t)$ is linear in time, that is $\mathbf{c}(t) = \mathbf{c}_0 + \boldsymbol{V}_0 t$ this transformation is then representative of the Galilean group. It is under this latter transformation group that the Navier-Stokes equations are form-invariant. It follows from the general transformation given in Eq. (4.4) that both the length between two points and the angle between two directions are independent of the rigid motion of the coordinate frame (see Eringen 1980; Spencer 2004).

The transformation of the velocity and acceleration vectors are obtained by taking the (material) time derivative(s) of (4.4), and can be written as

$$\mathbf{v}^* = \boldsymbol{Q}\mathbf{v} + \dot{\boldsymbol{Q}}\left[\mathbf{x} - \mathbf{x}_0\right] + \dot{\mathbf{c}}\,, \tag{4.6}$$

$$\mathbf{a}^* = \boldsymbol{Q}\mathbf{a} + 2\dot{\boldsymbol{Q}}\mathbf{v} + \ddot{\boldsymbol{Q}}\left[\mathbf{x} - \mathbf{x}_0\right] + \ddot{\mathbf{c}}\,, \tag{4.7}$$

where the material time differentiation of a variable is represented by $\dot{(\,)}$ for brevity. If Eq. (4.4) is used in Eq. (4.6), then the velocity transformation is given by

$$\mathbf{v}^* = \boldsymbol{Q}\mathbf{v} + \dot{\mathbf{c}} + \dot{\boldsymbol{Q}}\boldsymbol{Q}^T\left(\mathbf{x}^* - \mathbf{c}\right)\,, \tag{4.8}$$

and if Eqs. (4.4) and (4.6) are used in Eq. (4.7), the acceleration transformation becomes

$$\mathbf{a}^* = \boldsymbol{Q}\mathbf{a} + \ddot{\mathbf{c}} + 2\dot{\boldsymbol{Q}}\boldsymbol{Q}^T\left(\mathbf{v}^* - \dot{\mathbf{c}}\right) - 2\left(\dot{\boldsymbol{Q}}\boldsymbol{Q}^T\right)^2\left(\mathbf{x}^* - \mathbf{c}\right) + \ddot{\boldsymbol{Q}}\boldsymbol{Q}^T\left(\mathbf{x}^* - \mathbf{c}\right)\,. \tag{4.9}$$

Since $\boldsymbol{Q}\boldsymbol{Q}^T = \boldsymbol{Q}^T\boldsymbol{Q} = \boldsymbol{I}$ are orthogonal tensors that are only a function of time, it immediately follows that $\dot{\boldsymbol{Q}}\boldsymbol{Q}^T$ is skew-symmetric, and is denoted by

$$\dot{Q}_{ik}Q_{jk} = -Q_{ik}\dot{Q}_{jk} = \Omega_{ij}, \qquad \dot{\boldsymbol{Q}}\boldsymbol{Q}^T = -\boldsymbol{Q}\dot{\boldsymbol{Q}}^T = \boldsymbol{\Omega}\,, \tag{4.10}$$

where $\boldsymbol{\Omega}$ is sometimes called the spin tensor, and is the spin of the $\mathbf{x}^*$ frame with respect to the $\mathbf{x}$ frame (Truesdell and Rajagopal 2000). Using the spin tensor, Eqs. (4.8) and (4.9) can be written as

$$\mathbf{v}^* - \boldsymbol{Q}\mathbf{v} = \dot{\mathbf{c}} + \boldsymbol{\Omega}\left(\mathbf{x}^* - \mathbf{c}\right)\,, \tag{4.11}$$

where the two terms on the right side represents the relative translational and rotational velocities between the two frames, and

$$\mathbf{a}^* - \boldsymbol{Q}\mathbf{a} = \ddot{\mathbf{c}} + 2\boldsymbol{\Omega}\left(\mathbf{v}^* - \dot{\mathbf{c}}\right) + \left(\dot{\boldsymbol{\Omega}} - \boldsymbol{\Omega}^2\right)\left(\mathbf{x}^* - \mathbf{c}\right)\,, \tag{4.12}$$

where the first term on the right represents the frame translational acceleration, and the remaining contributions on the right are due to Coriolis acceleration, frame rotational and centripetal acceleration, respectively.

With this set of transformation rules, let us investigate how objective scalars, vectors, and tensors transform when there is a change of frame. It easily follows that a scalar quantity ϕ would be objective if and only if $\phi^* = \phi$, that is, its value does not change through a change of frame. A vector quantity would be required to show that $\mathbf{u}^* \cdot \mathbf{u}^* = \mathbf{u} \cdot \mathbf{u}$ because this would correspond to the geometrical vector length, that is, the norms of $\mathbf{u}^*$ and $\mathbf{u}$ are the same and the transformation corresponds to a rigid body rotation. Thus, such a vector $\mathbf{u}$ is objective if and only if

$$\mathbf{v}^* = \boldsymbol{Q}(t)\mathbf{v} \,. \tag{4.13}$$

Thus, only in the case of a Galilean transformation will the acceleration reduce to an objective transformation, $\mathbf{a}^* = \boldsymbol{Q}(t)\mathbf{a}$. As such, the force balance described by the Navier-Stokes equations is then objective under this Galilean transformation group. From this, it is possible to deduce the tensor transformation rules. Consider the Cauchy stress field as an example. The corresponding surface force $\mathbf{t}$ on a surface with unit normal $\mathbf{n}$ is given by

$$\mathbf{t} = \boldsymbol{\Sigma}\mathbf{n} \,. \tag{4.14}$$

Following the objective vector transformation rule in Eq. (4.13) yields

$$\begin{aligned} \mathbf{t}^* = \boldsymbol{Q}(t)\mathbf{t} &= \boldsymbol{Q}(t)\boldsymbol{\Sigma}\boldsymbol{Q}^T(t)\mathbf{n}^* \\ &= \boldsymbol{\Sigma}^*\mathbf{n}^* \end{aligned} \tag{4.15}$$

so that an objective second-order tensor should transform as

$$\boldsymbol{\Sigma}^*(\boldsymbol{X}, t^*) = \boldsymbol{Q}(t)\boldsymbol{\Sigma}(\boldsymbol{X}, t)\boldsymbol{Q}^T(t) \,. \tag{4.16}$$

Transformation properties of other descriptors of the motion can also be identified. For example, as was shown in Chap. 3, the motion of the material element is described by the deformation gradient or relative deformation gradient tensors. These play an important role in formulating properly invariant constitutive equations through the formulation of objective rates of the stress tensor. Using Eqs. (3.9) and (3.53), the right Cauchy-Green tensor can be related to the relative right Cauchy-Green tensor by

$$\boldsymbol{C}(\tau) = \boldsymbol{\mathcal{F}}^T(t)\boldsymbol{C}_t(\tau)\boldsymbol{\mathcal{F}}(t) \,. \tag{4.17}$$

Recall from Eq. (3.6), $\mathbf{x} = \boldsymbol{\chi}(\mathbf{X}, t)$, and by using Eq. (4.4) the transformation of the deformation gradient $\boldsymbol{\mathcal{F}}$ can be described by the transformation,

$$\boldsymbol{\mathcal{F}}^* = \boldsymbol{Q}(t)\boldsymbol{\mathcal{F}} \,. \tag{4.18}$$

which is not an objective tensor transformation (note here that $\boldsymbol{\mathcal{F}}$ is a tensor, but it transforms as a vector since one of index identifiers is associated with a particle and the other with the frame).

The relative deformation gradient, given by Eq. (3.9), can be written in the transformed frame as $\boldsymbol{\mathcal{F}}^*_{(t)}(\tau) = \boldsymbol{\mathcal{F}}^*(\tau)\boldsymbol{\mathcal{F}}^{-1*}$ so that

$$\begin{aligned} \boldsymbol{\mathcal{F}}^*_{(t)}(\tau) &= \boldsymbol{Q}(\tau)\boldsymbol{\mathcal{F}}(\tau)\left[\boldsymbol{Q}(t)\boldsymbol{\mathcal{F}}(t)\right]^{-1} \\ &= \boldsymbol{Q}(\tau)\boldsymbol{\mathcal{F}}(\tau)\boldsymbol{\mathcal{F}}(t)^{-1}\boldsymbol{Q}(t)^T \\ &= \boldsymbol{Q}(\tau)\boldsymbol{\mathcal{F}}_{(t)}(\tau)\boldsymbol{Q}(t)^T \,. \end{aligned} \tag{4.19}$$

Equation (4.19) shows that the relative deformation gradient tensor is also not objective. Since $\mathbf{C} = \boldsymbol{\mathcal{F}}^T \boldsymbol{\mathcal{F}}$ from Eq. (3.18), Eq. (4.18) immediately leads to $\mathbf{C}^* = \mathbf{C}$, which shows that the right Cauchy-Green tensor is not objective. With $\mathbf{C}^* = \mathbf{C}$, Eq. (4.17) can be written as

$$\boldsymbol{\mathcal{F}}^{T*}(t)\boldsymbol{C}^*_{(t)}(\tau)\boldsymbol{\mathcal{F}}^*(t) = \boldsymbol{\mathcal{F}}^T(t)\boldsymbol{C}_{(t)}(\tau)\boldsymbol{\mathcal{F}}(t) \; . \tag{4.20}$$

so that using Eq. (4.18), the transformation property of the relative right Cauchy-Green tensor is given by

$$\boldsymbol{C}^*_{(t)}(\tau) = \boldsymbol{Q}(t)\boldsymbol{C}_{(t)}(\tau)\,\boldsymbol{Q}^T(t) \; , \tag{4.21}$$

which shows $\boldsymbol{C}_{(t)}(\tau)$ to be objective.

These results can be easily generalized to the Rivlin-Ericksen tensors, $\boldsymbol{A}_n(t)$ (see Sect. 3.2.4) by taking the n-th derivative with respect to τ of both sides of Eq. (4.21) and evaluating at $\tau = t$ (see Eqs. (3.54a), (3.54b))

$$\boldsymbol{A}_n(t)^* = \boldsymbol{Q}\boldsymbol{A}_n(t)\,\boldsymbol{Q}^T \; . \tag{4.22}$$

This then shows that the Rivlin-Ericksen tensors are objective.

Of particular relevance in developing constitutive equations is the rate of change of the stress. Since a fundamental quantity associated with the stress motion is the relative deformation gradient tensor, let us first examine transformation properties of its rate of change. In Eq. (3.47), it was shown that the velocity gradient tensor $\nabla\mathbf{v}$ is simply the time rate of change of the relative deformation gradient tensor evaluated at the present time t. From Eqs. (3.47) and (4.6), the velocity gradient tensor $\boldsymbol{L}^*$ can be calculated to obtain

$$\left.\frac{D\mathcal{F}_{(t)ij}(\tau)}{D\tau}\right|^*_{\tau=t} = L^*_{ij} = \frac{\partial v^*_i}{\partial x_k}\frac{\partial x_k}{\partial x^*_j} = Q_{il}\frac{\partial v_l}{\partial x_k}Q_{jk} + \dot{Q}_{ik}Q_{jk} \; , \tag{4.23a}$$

$$\left.\frac{D\boldsymbol{\mathcal{F}}_{(t)}(\tau)}{D\tau}\right|^*_{\tau=t} = \boldsymbol{L}^* = \boldsymbol{Q}\boldsymbol{L}\,\boldsymbol{Q}^T + \dot{\boldsymbol{Q}}\,\boldsymbol{Q}^T \; . \tag{4.23b}$$

Thus, from Eq. (3.48) the symmetric part, the rate of deformation tensor, is objective while the second part, the rate of rotation tensor, is not, and consequently

$$\boldsymbol{D}^* = \boldsymbol{Q}\boldsymbol{D}\,\boldsymbol{Q}^T \; , \tag{4.24}$$

$$\boldsymbol{W}^* = \boldsymbol{Q}\boldsymbol{W}\,\boldsymbol{Q}^T + \boldsymbol{\Omega} \; . \tag{4.25}$$

The relation (4.25) indicates that if two observers register the rotation rate of a continuous media for the same material point, the observed quantities will differ by their relative rotation rate and this is the reason why the tensor $\boldsymbol{W}$ is not objective. Only under a (extended) Galilean transformation (a translational transformation) will $\boldsymbol{W}$ be objective. Equation (4.25) can be rewritten in the form

$$\boldsymbol{W} = \boldsymbol{Q}^T\left(\boldsymbol{W}^* - \boldsymbol{\Omega}\right)\boldsymbol{Q} \; . \tag{4.26}$$

Equation (4.26) shows that the rotation rate tensor $\boldsymbol{W}^*$ can be made objective by adding a measure of the non-inertial frame rotation rate $\boldsymbol{\Omega}$. This modification of $\boldsymbol{W}^*$ is not surprising since objective variables are quantities independent of the motion of

the observer (Eringen 1980). For this reason, $\mathbf{W}_a^* = \mathbf{W}^* - \boldsymbol{\Omega}$ is sometimes called the absolute vorticity tensor. If the orthogonal transformation matrices are associated with the eigenvectors of the principle axes of $\boldsymbol{D}$, then $\mathbf{W}_a^*$ is a measure of the rate of rotation of a material element with respect to the rate of strain principle axes (Astarita 1979).

4.3.2 Objective Rates of the Stress Tensor

As shown in Eq. (4.16), the stress tensor $\boldsymbol{\Sigma}$ transforms as an objective tensor, as well as, the relative right Cauchy-Green tensor, Eq. (4.21), and the Rivlin-Ericksen tensors, Eq. (4.22). However, the relative deformation gradient tensor, Eq. (4.19), and the rate of change of the relative deformation gradient tensor, Eqs. (4.23a), (4.23b), did not. Since the stress rate plays a pivotal role in constitutive equation development, it is worthwhile to investigate whether there are other objective rate operators in addition to the Rivlin-Ericksen tensors that can be used in material and turbulent stress constitutive equations of both complex fluids and flows.

The rate of change of the stress tensor follows directly from the transformation rules just established and can be written as

$$\frac{D\boldsymbol{\Sigma}^*}{Dt} - \boldsymbol{Q}\frac{D\boldsymbol{\Sigma}}{Dt}\boldsymbol{Q}^T = \boldsymbol{\Omega}\boldsymbol{\Sigma}^* - \boldsymbol{\Sigma}^*\boldsymbol{\Omega} \ , \tag{4.27}$$

or

$$\boldsymbol{Q}\frac{D\boldsymbol{\Sigma}}{Dt}\boldsymbol{Q}^T = \frac{D\boldsymbol{\Sigma}^*}{Dt} - \boldsymbol{\Omega}\boldsymbol{\Sigma}^* + \boldsymbol{\Sigma}^*\boldsymbol{\Omega} \ . \tag{4.28}$$

Equation (4.27) (or Eq. (4.28)) is clearly a non-objective transformation that can be linked to the fact that it is associated with an applied force acting on a material element undergoing an arbitrary deformation inclusive of a rigid-body motion and a stretching motion. Of course, this can be problematic when used in constitutive equations describing the evolution of the stress tensor which transforms objectively. As was first proposed by Oldroyd (1950), it is desirable to express the constitutive equations in terms of tensor quantities in a fixed frame. A simple practical reason for this is the fact that references to position required in any flow field solution are fixed relative to some choice of boundary conditions. As a consequence, alternative rate operators need to be formulated that account for material moving in space, but which introduce no dependence on the fixed reference frame. There have been a variety of stress-rates proposed to remedy this deficiency and these have included Jaumann (1911), Oldroyd (1950), Truesdell (1955), Green and Naghdi (1965), and Harnoy (1976). For the purposes here, the Oldroyd upper convective derivative, Jaumann, or co-rotational, derivative and the Harnoy derivative will be discussed.

4.3.2.1 Oldroyd Stress Rate

In order to ensure the invariance of a transformation for either the stress or stress rate, the starting point needs to be independent of any frame of reference. The most

general situation is then to start with the stress field and stress rate associated with a fluid element undergoing an arbitrary deformation. Such a stress and rate concept was first proposed by J.G. Oldroyd in a series of papers over a half-century ago (e.g. Oldroyd 1950, 1958) in order to develop properly invariant forms for rheological equations of state. Since the fluid element is undergoing an arbitrary deformation, the transformation of the stress to another frame of reference would be given by

$$\boldsymbol{\Sigma}(\mathbf{x},t) = \boldsymbol{\mathcal{F}}(t)\boldsymbol{\Sigma}_O(X,t)\boldsymbol{\mathcal{F}}^T(t) \tag{4.29}$$

where the stress in the element undergoing the arbitrary deformation is $\boldsymbol{\Sigma}_O(t)$ (the Oldroyd stress), and the transformation tensor is identified with the deformation gradient tensor $\boldsymbol{\mathcal{F}}$. Since the Oldroyd stress and associated Oldroyd stress rate, $D\boldsymbol{\Sigma}_O/Dt$, are defined in a frame fixed in the material element undergoing an arbitrary deformation, the question that arises is what form does this stress rate take in some transformed frame. This transformation is directly given by

$$\boldsymbol{\mathcal{F}}(t)\frac{D\boldsymbol{\Sigma}_O}{Dt}\boldsymbol{\mathcal{F}}^T(t) = \boldsymbol{\mathcal{F}}\frac{D}{Dt}\left[\boldsymbol{\mathcal{F}}^{-1}\boldsymbol{\Sigma}(\boldsymbol{\mathcal{F}}^{-1})^T\right]\boldsymbol{\mathcal{F}}^T \ . \tag{4.30}$$

The transformation on the left of the Oldroyd stress rate is defined as $\overset{\triangledown}{\boldsymbol{\Sigma}}$ and given by

$$\overset{\triangledown}{\boldsymbol{\Sigma}} = \frac{D\boldsymbol{\Sigma}}{Dt} + \boldsymbol{\mathcal{F}}(\dot{\boldsymbol{\mathcal{F}}^{-1}})\boldsymbol{\Sigma} + \boldsymbol{\Sigma}((\dot{\boldsymbol{\mathcal{F}}^{-1}})^T)\boldsymbol{\mathcal{F}}^T \ , \tag{4.31}$$

with $\boldsymbol{\mathcal{F}}\boldsymbol{\mathcal{F}}^{-1} = \boldsymbol{I}$. Analogous to Eq. (4.10), the rate of change associated with $\boldsymbol{\mathcal{F}}\boldsymbol{\mathcal{F}}^{-1}$ leads to the relation

$$\begin{aligned}\dot{\boldsymbol{\mathcal{F}}}\boldsymbol{\mathcal{F}}^{-1} &= -\boldsymbol{\mathcal{F}}\dot{\boldsymbol{\mathcal{F}}}^{-1} = \dot{\boldsymbol{\mathcal{F}}}_{(t)} \\ &= \boldsymbol{L} \ ,\end{aligned} \tag{4.32}$$

where Eqs. (3.46) and (3.47) have been used. Equation (4.31) can then be written in the usual form as

$$\overset{\triangledown}{\boldsymbol{\Sigma}} = \frac{D\boldsymbol{\Sigma}}{Dt} - \boldsymbol{L}\boldsymbol{\Sigma} - \boldsymbol{\Sigma}\boldsymbol{L}^T \ , \tag{4.33a}$$

$$\overset{\triangledown}{\boldsymbol{\Sigma}} = \frac{D\boldsymbol{\Sigma}}{Dt} - (\boldsymbol{D}\boldsymbol{\Sigma} + \boldsymbol{\Sigma}\boldsymbol{D}) + (\boldsymbol{\Sigma}\boldsymbol{W} - \boldsymbol{W}\boldsymbol{\Sigma}) \ , \tag{4.33b}$$

or in index notation as

$$\overset{\triangledown}{\Sigma}_{ij} = \frac{D\Sigma_{ij}}{Dt} - (L_{ik}\Sigma_{kj} + L_{jk}\Sigma_{ki}) \ , \tag{4.34a}$$

$$\overset{\triangledown}{\Sigma}_{ij} = \frac{D\Sigma_{ij}}{Dt} - \left(D_{ik}\Sigma_{kj} + \Sigma_{ik}D_{kj}\right) + \left(\Sigma_{ik}W_{kj} - W_{ik}\Sigma_{kj}\right) \ , \tag{4.34b}$$

where the operator $\overset{\triangledown}{\boldsymbol{\Sigma}}$ is the Oldroyd, or upper convective, derivative. It yields an interesting relationship between the identity tensor $\boldsymbol{I}$ and the rate of strain tensor $\boldsymbol{D}$, that is

$$\overset{\triangledown}{\boldsymbol{I}} = -2\boldsymbol{D} \ . \tag{4.35}$$

It is now straightforward to show that the Oldroyd derivative transforms in an objective fashion. From Eqs. (4.33a), (4.33b), the Oldroyd derivative $\overset{\nabla}{\boldsymbol{\Sigma}}$ transforms as

$$\begin{aligned}
\overset{\nabla}{\boldsymbol{\Sigma}}^{*} &= \boldsymbol{Q}(t)\,\overset{\nabla}{\boldsymbol{\Sigma}}\,\boldsymbol{Q}^{T}(t) \\
&= \boldsymbol{Q}(t)\left[\frac{D\boldsymbol{\Sigma}}{Dt} - \boldsymbol{L}\boldsymbol{\Sigma} - \boldsymbol{\Sigma}\boldsymbol{L}^{T}\right]\boldsymbol{Q}^{T}(t) \\
&= \left(\frac{D\boldsymbol{\Sigma}^{*}}{Dt} + \boldsymbol{\Omega}^{*}\boldsymbol{\Sigma}^{*} - \boldsymbol{\Sigma}^{*}\boldsymbol{\Omega}^{*}\right) \\
&\quad - \left(\boldsymbol{L}^{*} + \boldsymbol{\Omega}^{*}\right)\boldsymbol{\Sigma}^{*} - \boldsymbol{\Sigma}^{*}\left(\boldsymbol{L}^{*T} - \boldsymbol{\Omega}^{*}\right) \\
&= \frac{D\boldsymbol{\Sigma}^{*}}{Dt} - \boldsymbol{L}^{*}\boldsymbol{\Sigma}^{*} - \boldsymbol{\Sigma}^{*}\boldsymbol{L}^{*T}\,,
\end{aligned} \tag{4.36}$$

where Eqs. (4.23a), (4.23b) and (4.28) have been used. Equation (4.36) confirms the objectivity of the transformation of the Oldroyd upper-convective derivative.

4.3.2.2 Jaumann Stress Rate

While the Oldroyd stress rate provides an objective measure that accounts for an arbitrary deformation of a fluid element, the Jaumann stress rate provides a similar objective measure that is based solely on the rate of rotation or spin of the fluid element $\boldsymbol{W}$. Note that the rate of rotation of the fluid element is distinct from the rotation tensor $\boldsymbol{R}$ defined in connection with the polar decomposition of the deformation gradient tensor. As discussed in Sect. 3.1.1, the rotation tensor $\boldsymbol{R}$ represents a rotation of the principal axes of the fluid element stretch. In addition, since $\boldsymbol{R}$ is orthogonal $\boldsymbol{R}\boldsymbol{R}^{T} = \boldsymbol{I}$, the corresponding rate of change then represents the rate of the principal axes of rotation.

This distinction between $\boldsymbol{W}$ and $\boldsymbol{R}$ is exemplified by further considering Eq. (4.32). Since the velocity gradient tensor $\boldsymbol{L}$ can be partitioned into a symmetric and skew-symmetric parts, Eq. (4.32) can be expanded using the polar decomposition theorem (3.22a) to yield

$$\underbrace{\frac{1}{2}\boldsymbol{R}\left(\dot{\boldsymbol{U}}\boldsymbol{U}^{-1} + \boldsymbol{U}^{-1}\dot{\boldsymbol{U}}\right)\boldsymbol{R}^{T}}_{\boldsymbol{D}} + \underbrace{\dot{\boldsymbol{R}}\boldsymbol{R}^{T} + \frac{1}{2}\boldsymbol{R}\left(\dot{\boldsymbol{U}}\boldsymbol{U}^{-1} - \boldsymbol{U}^{-1}\dot{\boldsymbol{U}}\right)\boldsymbol{R}^{T}}_{\boldsymbol{W}} = \boldsymbol{L}\,. \tag{4.37}$$

As noted, when in a coordinate system aligned with the principal axes $\boldsymbol{W} = \boldsymbol{R}$ since $\dot{\boldsymbol{U}}\boldsymbol{U}^{-1} = \boldsymbol{U}^{-1}\dot{\boldsymbol{U}}$. Additionally, since the polar decomposition can also be applied to the relative deformation gradient $\boldsymbol{\mathcal{F}}_{(t)}$,

$$\boldsymbol{\mathcal{F}}_{(t)}(\tau) = \boldsymbol{R}_{(t)}(\tau)\boldsymbol{U}_{(t)}(\tau)\,, \tag{4.38}$$

so that the rate of change $\dot{\boldsymbol{\mathcal{F}}}_{(t)}$

$$\dot{\boldsymbol{\mathcal{F}}}_{(t)} = \dot{\boldsymbol{R}}_{(t)}\boldsymbol{U}_{(t)} + \boldsymbol{R}_{(t)}\dot{\boldsymbol{U}}_{(t)}\,, \tag{4.39}$$

evaluated at $\tau = t$ can be written as

$$\begin{aligned}\dot{\boldsymbol{\mathcal{F}}}_{(t)}|_{\tau=t} &= \dot{\boldsymbol{R}}_{(t)}|_{\tau=t} + \dot{\boldsymbol{U}}_{(t)}|_{\tau=t} \\ &= \boldsymbol{W} + \boldsymbol{D} = \boldsymbol{L} \ . \end{aligned} \tag{4.40}$$

Since $\boldsymbol{U}_{(t)}$ is a symmetric tensor and associated with the deformation motion, then $\dot{\boldsymbol{U}}_{(t)} = \boldsymbol{D}$ and $\dot{\boldsymbol{R}}_{(t)} = \boldsymbol{W}$.

Since the non-objectivity of the stress rates is due to the skew-symmetric contribution to the velocity gradient tensor, it is only necessary to account for this non-objective fluid element rate of rotation contribution in constructing an objective stress rate measure. The applicable stress transformation then utilizes the orthogonal relative rotation tensor $\boldsymbol{R}_{(t)}(\tau)$ to transform from the present configuration at t to one at time τ

$$\boldsymbol{\Sigma}(\boldsymbol{X}, \tau) = \boldsymbol{R}_{(t)}(\tau)\boldsymbol{\Sigma}_J(\boldsymbol{X}, \tau)\boldsymbol{R}^T_{(t)}(\tau) \ , \tag{4.41}$$

where $\boldsymbol{\Sigma}_J(\boldsymbol{X}, \tau)$ is the (Jaumann) stress in the fluid element with rotational motion characterized by $\boldsymbol{W}$. We observe that at time $\tau = t$, $\boldsymbol{\Sigma}_J = \boldsymbol{\Sigma}$. The Jaumann, or corotational, derivative $\mathcal{D}/\mathcal{D}t$ is then defined by

$$\begin{aligned}\frac{\mathcal{D}\boldsymbol{\Sigma}}{\mathcal{D}t} &= \boldsymbol{R}_{(t)}(\tau)\frac{D\boldsymbol{\Sigma}_J}{D\tau}\boldsymbol{R}^T_{(t)}(\tau)\bigg|_{\tau=t} = \frac{D}{D\tau}\left[\boldsymbol{R}^{-1}_{(t)}\boldsymbol{\Sigma}\boldsymbol{R}^{-T}_{(t)}\right]\bigg|_{\tau=t} \\ &= \frac{D\boldsymbol{\Sigma}}{D\tau}\bigg|_{\tau=t} + \frac{D\boldsymbol{R}^{-1}_{(t)}}{D\tau}\bigg|_{\tau=t}\boldsymbol{\Sigma}(\boldsymbol{X}, t) + \boldsymbol{\Sigma}(\boldsymbol{X}, t)\frac{D\boldsymbol{R}^{-T}_{(t)}}{D\tau}\bigg|_{\tau=t} \ , \end{aligned} \tag{4.42}$$

where $\boldsymbol{R}_{(t)}(\tau = t) = \boldsymbol{I}$ has been used. Since the rate of change of the inverse of the relative rotation tensor is given by,

$$\frac{D\boldsymbol{R}^{-1}_{(t)}}{D\tau}\bigg|_{\tau=t} = -\left[\boldsymbol{R}^{-2}_{(t)}\frac{D\boldsymbol{R}_{(t)}}{D\tau}\right]\bigg|_{\tau=t} = -\boldsymbol{W} \ , \tag{4.43}$$

the Jaumann derivative can then be written as

$$\frac{\mathcal{D}\boldsymbol{\Sigma}}{\mathcal{D}t} = \frac{D\boldsymbol{\Sigma}}{D\tau}\bigg|_{\tau=t} - \boldsymbol{W}\boldsymbol{\Sigma} + \boldsymbol{\Sigma}\boldsymbol{W} \ , \tag{4.44}$$

or in index notation as

$$\frac{\mathcal{D}\Sigma_{ij}}{\mathcal{D}t} = \frac{D\Sigma_{ij}}{D\tau}\bigg|_{\tau=t} - W_{ik}\Sigma_{kj} + \Sigma_{ik}W_{kj} \ . \tag{4.45}$$

It only remains now to determine whether the Jaumann derivative is objective. From Eq. (4.44), the corotational derivative $\mathcal{D}\boldsymbol{\Sigma}/\mathcal{D}t$ transforms as

$$\begin{aligned}\frac{\mathcal{D}\boldsymbol{\Sigma}^*}{\mathcal{D}t} &= \boldsymbol{Q}(t)\frac{\mathcal{D}\boldsymbol{\Sigma}}{\mathcal{D}t}\boldsymbol{Q}^T(t) \\ &= \boldsymbol{Q}(t)\left[\frac{D\boldsymbol{\Sigma}}{Dt} - \boldsymbol{W}\boldsymbol{\Sigma} + \boldsymbol{\Sigma}\boldsymbol{W}\right]\boldsymbol{Q}^T(t) \\ &= \left(\frac{D\boldsymbol{\Sigma}^*}{Dt} + \boldsymbol{\Omega}^*\boldsymbol{\Sigma}^* - \boldsymbol{\Sigma}^*\boldsymbol{\Omega}^*\right) \end{aligned}$$

$$
\begin{aligned}
&- \left(\boldsymbol{W}^* + \boldsymbol{\Omega}^*\right) \boldsymbol{\Sigma}^* + \boldsymbol{\Sigma}^* \left(\boldsymbol{W}^* + \boldsymbol{\Omega}^*\right) \\
&= \frac{D\boldsymbol{\Sigma}^*}{Dt} - \boldsymbol{W}^* \boldsymbol{\Sigma}^* + \boldsymbol{\Sigma}^* \boldsymbol{W}^* \,, \qquad (4.46)
\end{aligned}
$$

where Eqs. (4.25) and (4.28) have been used. Equation (4.46) confirms the objectivity of the transformation of the Jaumann corotational derivative.

4.3.2.3 Harnoy Stress Rate

The discussion in this section will focus on a stress rate whose objectivity is based on the rotation of the principal axes of the strain rate. Although the Green and Naghdi (1965) and Harnoy (1976) stress rates are similar in form, the Harnoy stress rate was formulated with specific reference to a frame of reference in a fluid element associated with the principal axes of the strain rate tensor.

It is easy to show from Eq. (4.37) that the principal stretches associated with the $\boldsymbol{U}$, $\boldsymbol{\lambda}_U$, are related to the strain rate $\boldsymbol{D}$ (or $\dot{\boldsymbol{U}}_{(t)}$) and given by $\dot{\boldsymbol{\lambda}}_U \boldsymbol{\lambda}_U^{-1}$, such that

$$
\begin{aligned}
\dot{\boldsymbol{U}}_{(t)}|_{\tau=t} = \boldsymbol{D} &= (\boldsymbol{R}\boldsymbol{P}^T) \left[\dot{\boldsymbol{\lambda}}_U \boldsymbol{\lambda}_U^{-1} + \boldsymbol{\lambda}_U^{-1} \dot{\boldsymbol{\lambda}}_U\right] (\boldsymbol{P}\boldsymbol{R}^T) \\
&= \boldsymbol{R}_H \left[\dot{\boldsymbol{\lambda}}_U \boldsymbol{\lambda}_U^{-1} + \boldsymbol{\lambda}_U^{-1} \dot{\boldsymbol{\lambda}}_U\right] \boldsymbol{R}_H^T \,, \qquad (4.47)
\end{aligned}
$$

where $\boldsymbol{P}$ is an orthogonal matrix comprised of the eigenvectors associated with the principal stretches (eigenvalues) $\boldsymbol{\lambda}_U$ and, $\boldsymbol{R}_H$ and $\boldsymbol{R}_H^T$ represent the rotation factor associated with the deformation gradient and the diagonalizing transformation of the rate of strain to the principal directions of stretch. As Eq. (4.47) shows, the diagonal transformation differs and is a composite of first the diagonal transformation of $\boldsymbol{U}$ and then a rotation by $\boldsymbol{R}$ (from the polar decomposition of the deformation gradient associated with the motion). However, from Eq. (4.37) the rate of rotation associated with the relative deformation gradient simply reduces to

$$
\dot{\boldsymbol{R}}_{(t)}|_{\tau=t} = \boldsymbol{W} = \dot{\boldsymbol{R}}_H \boldsymbol{R}_H^T = \boldsymbol{\Omega} \,, \qquad (4.48)
$$

where $\boldsymbol{\Omega}$ represents the rotation rate of the eigenvectors associated with the rate of strain $\boldsymbol{D}$. Correspondingly, the derivation just outlined for the Jaumann derivative directly applies, but now with the rotation rate tensor identified with the rotation rate $\boldsymbol{\Omega}$ of the principle axes of the strain rate tensor. This is the Harnoy (1976) derivative and given by

$$
\frac{\mathcal{D}_H \boldsymbol{\Sigma}}{\mathcal{D}t} = \left.\frac{D\boldsymbol{\Sigma}}{D\tau}\right|_{\tau=t} - \boldsymbol{\Omega}\boldsymbol{\Sigma} + \boldsymbol{\Sigma}\boldsymbol{\Omega} \,, \qquad (4.49)
$$

or in index notation as

$$
\frac{\mathcal{D}_H \Sigma_{ij}}{\mathcal{D}t} = \left.\frac{D\Sigma_{ij}}{D\tau}\right|_{\tau=t} - \Omega_{ik}\Sigma_{kj} + \Sigma_{ik}\Omega_{kj} \,. \qquad (4.50)
$$

Although both the Jaumann and Harnoy derivatives account is some form for the fluid element rotation, the underlying basis is different. In the development of explicit polynomial representations for both the viscoelastic extra-stress and the turbulent stress, the Harnoy stress rate will be used in establishing equilibrium conditions for the various differential viscoelastic and turbulent stress rate equations.

4.4 Restrictions on Constitutive Relationships

Both the exact functional form and material (model) coefficients associated with the various constitutive equations are subject to restrictions imposed by the various principles discussed earlier in this chapter. Since the interest here is on incompressible fluid dynamics, there has been little need to discuss thermodynamic aspects of constitutive model development; however, it is worthwhile to mention briefly in the subsection to follow the origin of such a constraint that originate in an entropy inequality. For material frame-indifference, some examples will be used to show how this principle can influence the functional form of non-Newtonian stress field.

4.4.1 A Thermodynamic Constraint for Constitutive Relationships

So far the second principle of thermodynamics has not been considered since the focus has been on isothermal flows. However, this principle has to be taken into account when the modeler faces the final stage of constructing the constitutive equation. The last step consists in checking that the constitutive equation satisfies the Clausius-Duhem inequality. From statistical physics considerations, it is well known that physical events evolve in an irreversible way. This is one of the major discoveries of the twentieth century. The physical variable measuring the irreversibility is the entropy. In the continuum theory framework, the Clausius-Duhem inequality expresses that the rate of change of entropy is greater than the heat received by the material volume $\mathcal{V}$ divided by the (absolute) temperature θ. The amount of heat received by the material may be split in two parts, $\mathcal{Q}_\mathcal{V}$ a volumetric part resulting, for example, from chemical reactions, heat sources, etc., and the heat transported $\mathbf{q}$ across the surface resulting mainly from conduction. We will discard all thermal radiation effects resulting. One obtains

$$\frac{\mathrm{d}}{\mathrm{d}t}\int_\mathcal{V}(\rho s)\,\mathrm{d}\mathcal{V} \geq \int_\mathcal{V}\frac{\mathcal{Q}_\mathcal{V}}{\theta}\mathrm{d}\mathcal{V} - \int_{\partial\mathcal{V}}\frac{\mathbf{q}\cdot\mathbf{n}}{\theta}\mathrm{d}\mathcal{S}\,, \tag{4.51}$$

where ρs is the entropy density, and $\mathbf{q}$ is the heat flux (positive into volume $\mathrm{d}\mathcal{V}$ with surface unit outward normal $\mathbf{n}$). Using the Reynolds transport theorem, divergence theorem and localization (see Sect. 3.3), Eq. (4.51) becomes

$$\rho\frac{Ds}{Dt} \geq \frac{\mathcal{Q}_\mathcal{V}}{\theta} - \mathrm{div}\left(\frac{\mathbf{q}}{\theta}\right)\,, \tag{4.52}$$

where the mass conversation equation Eq. (3.72) has also been used. Eliminating the volumetric contribution $\mathcal{Q}_\mathcal{V}$ by the internal energy equation,

$$\rho\frac{De}{Dt} = \mathcal{Q}_\mathcal{V} + \{\boldsymbol{\Sigma}\boldsymbol{D}\} - \mathrm{div}\,\mathbf{q}\,, \tag{4.53}$$

where e is the internal energy, the local Clausius-Duhem inequality is then

$$\rho\frac{Ds}{Dt} \geq \frac{1}{\theta}\left(\rho\frac{De}{Dt} - \{\boldsymbol{\Sigma}\boldsymbol{D}\}\right) + \frac{1}{\theta^2}\left(\mathbf{q}\cdot\boldsymbol{\nabla}\theta\right)\,. \tag{4.54}$$

If the fluid has the properties of a perfect gas, then the internal energy is given by

$$e = c_v \theta \ , \tag{4.55}$$

where c_v is (constant) specific heat of the fluid at constant volume. Additionally, the Fourier law for heat conduction,

$$\mathbf{q} = -k_T \nabla \theta \ , \tag{4.56}$$

can also be assumed where k_T is the thermal conductivity. Then the inequality in Eq. (4.54) takes the form

$$\rho \frac{Ds}{Dt} \geq \frac{1}{\theta} \left(\rho c_v \frac{D\theta}{Dt} - \{ \boldsymbol{\Sigma} \boldsymbol{D} \} \right) - \frac{k_T}{\theta^2} (\nabla \theta)^2 \ , \tag{4.57}$$

or in terms of the Helmholtz free energy, $F \ (= e - \theta s)$, as

$$\rho \frac{DF}{Dt} \leq \{ \boldsymbol{\Sigma} \boldsymbol{D} \} + \frac{k_T}{\theta} (\nabla \theta)^2 \ . \tag{4.58}$$

The presence of the stress tensor in (4.57) indicates that for a thermodynamic process built upon a history of the deviatoric part of the rate of deformation tensor, the heat flux and other relevant variables the inequality should hold for the chosen constitutive relationship. As we will see later, this can impose conditions on the material constants used in non-Newtonian constitutive relations. For a turbulent flow of an isothermal, Newtonian viscous fluid, the instantaneous field satisfies the Clausius-Duhem inequality identically since

$$\{ \boldsymbol{\Sigma} \boldsymbol{D} \} = 2\mu \{ \boldsymbol{D}^2 \} \geq 0 \ . \tag{4.59}$$

However, for filtered or Reynolds-averaged fields, Eq. (4.59) then becomes a relationship involving resolved or mean quantities and unresolved/fluctuating correlations. A more complete analysis of the consequences of such thermodynamic constraints on a turbulent fluid flow is given in Marshall and Naghdi (1991).

4.4.2 Objectivity Constraints on Material Constitutive Equations

Although it has been known for over a century that responses of a material is invariant to superimposed rigid body motions, it was Truesdell and Noll (1992, 1st edition, 1965) who raised the concept to a guiding principle in the development of material constitutive equations. It is from this origin that the debate has continued for almost a half-century (see Frewer 2009 for an historical review). The foundation of the debate lies in the interpretation of whether the rigid-body motion is with respect to a given observer, or whether there is relative motion between two observers with respect to the same body (Frewer 2009). Truesdell and Noll then postulated that the response of the material should be independent of the observer.

Recall in Sect. 3.1 and Eq. (3.1a), that the deformation function was introduced as a mapping of the motion of a material element in space. Using Eq. (3.1a), the transformation given in Eq. (4.4) can be written as

$$\boldsymbol{\chi}^*(\mathbf{X}, t^*) = \boldsymbol{Q}(t) \boldsymbol{\chi}(\mathbf{X}, t) + \mathbf{c}(t), \qquad t^* = t - t_s \ , \tag{4.60}$$

where, for the purposes of discussion here, it is assumed that there is no spatial shift, $\boldsymbol{x}_0 = 0$. Additionally, if the stress tensor $\boldsymbol{\Sigma}$ transforms in an objective manner as given in Eq. (4.16), then the two motions given by Eqs. (4.60) and (4.16) are termed equivalent (e.g. Truesdell and Rajagopal 2000). For material frame-indifference to hold, the dynamical processes described by $\boldsymbol{\chi}$ and $\boldsymbol{\Sigma}$ must be equivalent and the functional constitutive relation for a material, Eq. (4.1), must satisfy

$$\boldsymbol{\Sigma}^*(\mathbf{X}, t^*) = \mathscr{S}(\boldsymbol{\chi}^*(t^* - s); \mathbf{X}, t^*), \qquad s \geq 0\,, \tag{4.61a}$$

and for a simple material, Eq. (4.2),

$$\boldsymbol{\Sigma}^*(\mathbf{X}, t^*) = \boldsymbol{\mathcal{S}}(\boldsymbol{\mathcal{F}}^*(t^* - s); \mathbf{X}, t^*), \qquad s \geq 0 \tag{4.61b}$$

and for a simple fluid, Eq. (4.3),

$$\boldsymbol{\Sigma}^*(\mathbf{X}, t^*) = \mathfrak{S}(\boldsymbol{\mathcal{F}}^*_{(t)}(t^* - s); \mathbf{X}, t^*), \qquad s \geq 0\,. \tag{4.61c}$$

It is with Eq. (4.61c) for a simple (incompressible) fluid, that further analysis of the effect of the MFI principle on the form of the constitutive functional $\mathfrak{S}$ will be primarily focused.

For a given material, the material frame-indifference principle holds if the stress tensorial functional is invariant for a change of frame. Some consequences of this principle are easily illustrated in the following rigid-body motions and time shifts (see e.g. Botsis and Deville 2006).

Consider first a simple rigid-body translation for all time, $\boldsymbol{Q}(t) = \boldsymbol{I}$, with no shift of origin, $\mathbf{c} = \mathbf{0}$, but with a time shift $t_s = t$ so that $t^* = 0$ and $\tau^* = \tau - t = -s$. The material deformation function and stress, for some neighborhood $\boldsymbol{Z}$ close to $\boldsymbol{X}$, are then given by

$$\boldsymbol{\chi}^*(\mathbf{Z}, \tau^*) = \boldsymbol{\chi}(\mathbf{Z}, t - s)\,, \tag{4.62}$$

and

$$\begin{aligned} \boldsymbol{\Sigma}^*(\mathbf{X}, t^*) &= \boldsymbol{\Sigma}^*(\mathbf{X}, 0) = \boldsymbol{\Sigma}(\mathbf{X}, t) \\ &= \mathscr{S}(\boldsymbol{\chi}(\mathbf{Z}, t - s); \mathbf{X}, 0), \qquad s \geq 0\,, \end{aligned} \tag{4.63}$$

respectively. As Eq. (4.63) shows, there is no explicit dependence of the stress functional $\mathscr{S}$ on the time t, so that the stress $\boldsymbol{\Sigma}(\mathbf{X}, t)$ only depends on the present time through the history of the motion introduced through $t - s$. For a simple fluid, the stress relationship then becomes

$$\boldsymbol{\Sigma}^*(\mathbf{X}, 0) = \boldsymbol{\Sigma}(\mathbf{X}, t) = \mathfrak{S}(\boldsymbol{\mathcal{F}}_{(t)}(\mathbf{Z}, t - s); \mathbf{X}), \qquad s \geq 0 \tag{4.64}$$

which then shows the dependence of the stress functional and the relative deformation gradient on the history of the motion.

A variation of this first example is to retain the rigid-body translation, $\boldsymbol{Q}(t) = \boldsymbol{I}$, but with a shift of origin $\mathbf{c}(t) = -\boldsymbol{\chi}(\mathbf{X}, t)$, and no time shift $t_s = 0$ so that $t^* = t$. Then for the deformation function

$$\boldsymbol{\chi}^*(\mathbf{Z}, t - s) = \boldsymbol{\chi}(\mathbf{Z}, t - s) - \boldsymbol{\chi}(\mathbf{X}, t - s), \qquad s \geq 0\,, \tag{4.65}$$

where the material points $\boldsymbol{Z}$ satisfy the local action principle, and for the stress functional,

$$\boldsymbol{\Sigma}^*(\mathbf{X},t)=\boldsymbol{\Sigma}(\mathbf{X},t)=\mathscr{S}(\boldsymbol{\chi}(\mathbf{Z},t-s)-\boldsymbol{\chi}(\mathbf{X},t-s);\mathbf{X},t),\qquad s\geq 0\,. \tag{4.66}$$

In such a translating frame, the material point $\mathbf{X}$ is at the frame origin, and the stress is unchanged in the transformed frame. Since the deformation function $\boldsymbol{\chi}(\mathbf{X},t)$ is associated with a point in space as shown in Eq. (3.1a), Eq. (4.66) shows that the stress field is simply a function of the corresponding relative motion of the material points. This can be explored further by exploiting the local action principle and expanding the deformation function in a Taylor series about the vector function $\mathbf{X}$ of material particles, that is,

$$\begin{aligned}\boldsymbol{\chi}(\mathbf{Z},t-s)&=\boldsymbol{\chi}(\mathbf{X},t-s)+(\mathbf{Z}-\mathbf{X})\left.\frac{\partial\boldsymbol{\chi}(\mathbf{Z},t-s)}{\partial\mathbf{X}}\right|_{\mathbf{Z}=\mathbf{X}}+\mathcal{O}\left(\|\,\mathbf{Z}-\mathbf{X}\,\|^2\right)\\&=\boldsymbol{\chi}(\mathbf{X},t-s)+(\mathbf{Z}-\mathbf{X})\boldsymbol{\mathcal{F}}(\mathbf{X},t-s)+\mathcal{O}\left(\|\,\mathbf{Z}-\mathbf{X}\,\|^2\right)\,.\end{aligned} \tag{4.67}$$

Using Eq. (4.67) in Eq. (4.66), it is seen that the stress functional then reduces to the behavior of a simple material or fluid given by

$$\begin{aligned}\boldsymbol{\Sigma}^*(\mathbf{X},t)&=\boldsymbol{\Sigma}(\mathbf{X},t)\\&=\boldsymbol{\mathcal{S}}(\boldsymbol{\mathcal{F}}_{(t)}(\mathbf{X},t-s);\mathbf{X},t),\qquad s\geq 0\,,\end{aligned} \tag{4.68}$$

or

$$\begin{aligned}\boldsymbol{\Sigma}^*(\mathbf{X},t)&=\boldsymbol{\Sigma}(\mathbf{X},t)\\&=\mathfrak{S}(\boldsymbol{\mathcal{F}}_{(t)}(\mathbf{X},t-s);\mathbf{X},t),\qquad s\geq 0\,.\end{aligned} \tag{4.69}$$

respectively. (Note that explicit dependence on $\mathbf{Z}-\mathbf{X}$ has been suppressed since the particles represented by the vectors $\mathbf{Z}$ and $\mathbf{X}$ lie within the same frame and share the same basis so that it is sufficient to simply retain the explicit functional dependence on $\mathbf{X}$.) These equations show that a simple rigid-frame translation, with a shift of origin, can leave a stress field unchanged and subsequently reduce the stress to that described by a simple material or fluid.

A final example is that of a rigid-body rotation, $\boldsymbol{Q}$ arbitrary, with no shift of origin, $\boldsymbol{c}=\mathbf{0}$, or time shift, $t_s=0$ ($t^*=t$). The deformation function and stress field transformations are given by

$$\boldsymbol{\chi}^*(\mathbf{Z},\tau)=\boldsymbol{Q}(t)\boldsymbol{\chi}(\mathbf{Z},\tau)\,, \tag{4.70}$$

and

$$\begin{aligned}\boldsymbol{\Sigma}^*(\mathbf{X},t)&=\boldsymbol{Q}(t)\boldsymbol{\Sigma}(\mathbf{X},t)\,\boldsymbol{Q}^T(t)\\&=\boldsymbol{Q}(t)\mathscr{S}(\boldsymbol{\chi}(\mathbf{Z},t-s);\mathbf{X},t)\,\boldsymbol{Q}^T(t),\qquad s\geq 0\,,\end{aligned} \tag{4.71}$$

respectively. If Eq. (4.70) is used, the stress in the transformed frame $\boldsymbol{\Sigma}^*(\mathbf{X},t)$ can be written in terms of the stress functional as

$$\begin{aligned}\boldsymbol{\Sigma}^*(\mathbf{X},t)&=\mathscr{S}(\boldsymbol{\chi}^*(\mathbf{Z},t-s);\mathbf{X},t)\\&=\mathscr{S}(\boldsymbol{Q}(t)\boldsymbol{\chi}(\mathbf{Z},t-s);\mathbf{X},t),\qquad s\geq 0\,,\end{aligned} \tag{4.72}$$

and when combined with Eq. (4.71) yields

$$\boldsymbol{Q}(t)\mathscr{S}(\boldsymbol{\chi}(\mathbf{Z},t-s);\mathbf{X},t)\,\boldsymbol{Q}^T(t)=\mathscr{S}(\boldsymbol{Q}(t)\boldsymbol{\chi}(\mathbf{Z},t-s);\mathbf{X},t)\;. \tag{4.73}$$

For a simple fluid this stress relationship becomes,

$$\boldsymbol{Q}(t)\mathfrak{S}(\boldsymbol{\mathcal{F}}_{(t)}(\mathbf{Z},t-s);\mathbf{X},t)\,\boldsymbol{Q}^T(t)=\mathfrak{S}(\boldsymbol{Q}(t)\boldsymbol{\mathcal{F}}_{(t)}(\mathbf{Z},t-s);\mathbf{X},t),\qquad s\geq 0\;. \tag{4.74}$$

Both Eqs. (4.73) and (4.74) show that the functionals $\mathscr{S}$ and $\mathfrak{S}$ behave like isotropic functions. Thus, the stress field behaves as a isotropic tensor-valued function as it should for material frame-indifference.

As was shown in Eq. (4.2), for simple materials the stress tensor is a function of the deformation gradient tensor, and as such the transformation property for the stress tensor given in Eq. (4.61b) requires that

$$\boldsymbol{Q}(t)\boldsymbol{\Sigma}(\mathbf{X},t)\,\boldsymbol{Q}^T(t)=\boldsymbol{\mathcal{S}}(\boldsymbol{Q}(t-s)\boldsymbol{\mathcal{F}}(t-s)),\qquad s\geq 0\;, \tag{4.75}$$

where Eq. (4.18) has been used. If the polar decomposition in Eq. (3.22a) is now applied to the deformation gradient tensor, so that

$$\boldsymbol{Q}(t)\boldsymbol{\Sigma}(\mathbf{X},t)\,\boldsymbol{Q}^T(t)=\boldsymbol{\mathcal{S}}(\boldsymbol{Q}(t-s)\boldsymbol{R}(t-s)\boldsymbol{U}(t-s)\,\boldsymbol{Q}^T(t)),\quad s\geq 0\;, \tag{4.76}$$

and if the orthogonal matrix $\boldsymbol{Q}(t)$ is now associated with the rotational motion of the polar decomposition, $\boldsymbol{R}^T(t)$, Eq. (4.76) becomes

$$\begin{aligned}\boldsymbol{\Sigma}(\mathbf{X},t)&=\boldsymbol{R}(t)\boldsymbol{\mathcal{S}}(\boldsymbol{U}(t-s))\boldsymbol{R}^T(t)\\&=\boldsymbol{\mathcal{F}}(t)\boldsymbol{U}^{-1}(t)\boldsymbol{\mathcal{S}}(\boldsymbol{U}(t-s))\boldsymbol{U}^{-1}(t)\boldsymbol{\mathcal{F}}^T(t)\\&=\boldsymbol{\mathcal{F}}(t)\boldsymbol{\mathcal{P}}(\boldsymbol{C}(t-s))\boldsymbol{\mathcal{F}}^T(t),\qquad s\geq 0\;,\end{aligned} \tag{4.77}$$

where

$$\boldsymbol{\mathcal{P}}(\boldsymbol{C}(t-s))=\boldsymbol{U}^{-1}(t)\boldsymbol{\mathcal{S}}(\boldsymbol{U}(t-s))\boldsymbol{U}^{-1}_{(t)}(t)\;, \tag{4.78}$$

since $\boldsymbol{C}(t-s)=\boldsymbol{U}^2(t-s)$. As Eq. (4.77) shows, a consequence of this result for constitutive equation development is the fact that only the present state of the rotational motion is required; whereas, the deformation history of the fluid, expressed through $\boldsymbol{U}_{(t)}(t-s)$, influences the state of the stress. Unfortunately, since the right Cauchy-Green tensor does not transform objectively, the expression for the stress field, Eq. (4.77), is not generally useful. However, the relative right Cauchy-Green tensor is objective, as shown in Eq. (4.21), and $\boldsymbol{C}_{(t)}$ can be related to the Cauchy-Green tensor by the relation

$$\boldsymbol{C}(\tau)=\boldsymbol{\mathcal{F}}^T(t)\boldsymbol{C}_{(t)}(\tau)\boldsymbol{\mathcal{F}}(t)\;. \tag{4.79}$$

With Eq. (4.79), the stress field functional can be written in the general form for a simple material as

$$\begin{aligned}\boldsymbol{\Sigma}(\mathbf{X},t)&=\boldsymbol{\mathcal{F}}(t)\boldsymbol{\mathcal{P}}(\boldsymbol{\mathcal{F}}^T(t)\boldsymbol{C}_{(t)}(t-s)\boldsymbol{\mathcal{F}}^T(t))\boldsymbol{\mathcal{F}}^T(t)\\&=\boldsymbol{\mathfrak{P}}(\boldsymbol{C}_{(t)}(t-s),\boldsymbol{\mathcal{F}}(t)),\qquad s\geq 0\;.\end{aligned} \tag{4.80}$$

For a simple fluid, it was shown in Eq. (4.3) that the stress field is a functional of the relative deformation gradient. Since the history of $\boldsymbol{\mathcal{F}}_{(t)}$ can be given by the relative right Cauchy-Green tensor, a comparison of Eq. (4.3) and Eq. (4.80) shows that the stress field for an incompressible simple fluid is given by

$$\boldsymbol{\Sigma}(\mathbf{X}, t) = \mathfrak{F}(\boldsymbol{C}_{(t)}(t-s)), \qquad s \geq 0\,, \tag{4.81}$$

which yields an objective functional relationship that satisfies the constraints imposed by material frame-indifference (see Huilgol and Phan-Thien 1997).

The form of the stress field given in Eq. (4.81), is extracted from conditions based on the motion of the material (fluid), and as such is only determined only up to its isotropic part. In the absence of motion, this isotropic part is identified with the hydrostatic pressure p, so that in general, the stress power is such that $\{\boldsymbol{\Sigma}\,\boldsymbol{D}\} = 0$. Thus, the constitutive relation for the incompressible fluid is built such that the representation for the Cauchy stress tensor $\boldsymbol{\Sigma}$ should include an isotropic part that is represented of this arbitrary (hydrostatic) pressure p. The resultant form for $\boldsymbol{\Sigma}$ is then given by

$$\boldsymbol{\Sigma} = -p\boldsymbol{I} + \mathfrak{F}(\boldsymbol{C}_{(t)}(t-s))\,. \tag{4.82}$$

The generalized incompressible viscous fluids have an extremely short memory, i.e. the stress depends on $\boldsymbol{C}_{(t)}(t-s)$ with $0 \leq s \leq \epsilon$ for $\epsilon \to 0$, and the stress tensor has a quasi-instantaneous memory. If it is assumed that the history of the deformation is smooth enough to allow $\boldsymbol{C}_{(t)}(t-s)$ to be developed in Taylor series with respect to s, the final result being evaluated at $s = 0$, the stress field functional can be approximated so that

$$\boldsymbol{\Sigma} = -p\boldsymbol{I} + \mathfrak{F}(\boldsymbol{C}_{(t)}, \dot{\boldsymbol{C}}_{(t)}, \ldots)\,. \tag{4.83}$$

From Eqs. (3.55a), (3.55b), the dependence of the stress functional then reduces further to a dependence on the Rivlin-Ericksen tensors.

4.5 Deformation and Constant Stretch History Motion

Up to this point, an extensive basis of kinematic variables have been introduced that act as descriptors of the fluid motion. Before proceeding onto the development of (material) fluid and (turbulent) flow constitutive relationships, an analysis of some simple deformations will further identify the physical relevance of the various kinematic variables that have been introduced. Such motions have a constant stretch history (or monotonous motion, Truesdell and Rajagopal 2000), and are exemplified by viscometric flows in the study of non-Newtonian and viscoelastic fluids, and homogeneous flows in turbulent flows.

Flows with constant stretch history (Noll 1962) are defined as flows resulting from a motion where the present deformation is obtained through a sequence of past deformations that remain constant. This means that $\boldsymbol{C}_{(t)}(t-s)$ may be expressed by

$$\boldsymbol{C}_{(t)}(t-s) = \boldsymbol{Q}(t)\boldsymbol{C}_{(0)}(0-s)\,\boldsymbol{Q}(t)^T, \qquad 0 \leq s < \infty \tag{4.84}$$

with $\boldsymbol{C}_{(0)}(0-s)$ being $\boldsymbol{C}_{(t)}(t-s)$ at time $t=0$ and $\boldsymbol{Q}(0)=\boldsymbol{I}$. Equation (4.84) is motivated by the fact that the two tensors $\boldsymbol{C}_{(t)}(t-s)$ and $\boldsymbol{C}_{(0)}(-s)$ have the same eigenvalues, that is the same principal relative stretches, and the principal axes of one of the tensor are allowed to rotate with respect to those of the other, the rotation $\boldsymbol{Q}(t)$ being the rotation at the present time t. A theorem due to Noll (1976) then applies

Theorem 4.1 *A motion has a constant stretch history iff* (*if and only if*) *there exist an orthogonal tensor* $\boldsymbol{Q}(t)$, *a scalar* $\dot{\gamma}$ *and a constant tensor* $\boldsymbol{N}_0$ *such that*[2]

$$\boldsymbol{\mathcal{F}}(\tau)=\boldsymbol{Q}(\tau)e^{\tau\dot{\gamma}\boldsymbol{N}_0},\quad \boldsymbol{Q}(0)=\boldsymbol{I},\quad |\boldsymbol{N}_0|=1\,, \tag{4.85}$$

where the matrix norm $|\boldsymbol{N}_0|$ is given by $\sqrt{\{\boldsymbol{N}_0\boldsymbol{N}_0^T\}}$. In the form given in Eq. (4.85), it is clear that $\boldsymbol{Q}(t)$ is the rate of rotation tensor $\boldsymbol{R}(t)$ associated with the deformation gradient, and $e^{\tau\dot{\gamma}\boldsymbol{N}_0}$ is the corresponding (right) stretch tensor $\boldsymbol{U}(t)$ associated with the deformation gradient (cf. Eq. (3.22a)). In terms of the principal stretches, it is the principal stretch histories that remain constant but allows for rotation of the principal axes.

Applying Eq. (3.9) to $\boldsymbol{\mathcal{F}}(\tau)$ ($\boldsymbol{\mathcal{F}}_{(t)}(\tau)=\boldsymbol{\mathcal{F}}(\tau)\boldsymbol{\mathcal{F}}(t)^{-1}$), one can write for a constant stretch history motion,

$$\boldsymbol{\mathcal{F}}_{(t)}(\tau)=\boldsymbol{Q}(\tau)\,\boldsymbol{Q}(t)^T e^{(\tau-t)\dot{\gamma}\boldsymbol{N}}=\boldsymbol{Q}(\tau)e^{(\tau-t)\dot{\gamma}\boldsymbol{N}_0}\,\boldsymbol{Q}(t)^T\,, \tag{4.86}$$

where the tensor $\boldsymbol{N}$, defined by

$$\boldsymbol{N}=\boldsymbol{Q}(t)\boldsymbol{N}_0\,\boldsymbol{Q}(t)^T,\quad |\boldsymbol{N}|=1\,, \tag{4.87}$$

has been introduced. The relative right Cauchy-Green tensor, defined in Eq. (3.53), is then given by

$$\begin{aligned}\boldsymbol{C}_{(t)}(t-s)&=e^{-s\dot{\gamma}(\boldsymbol{N}+\boldsymbol{N}^T)}\\&=\boldsymbol{Q}(t)e^{-s\dot{\gamma}(\boldsymbol{N}_0+\boldsymbol{N}_0^T)}\,\boldsymbol{Q}(t)^T\,.\end{aligned} \tag{4.88}$$

The corresponding (right) stretch tensor, $\boldsymbol{U}_{(t)}$, and rate of rotation tensor, $\boldsymbol{R}_{(t)}$, associated with the relative deformation gradient follow directly from Eqs. (4.86) and (4.88) and are given by

$$\begin{aligned}\boldsymbol{U}_{(t)}(t-s)&=e^{-s\frac{\dot{\gamma}}{2}(\boldsymbol{N}+\boldsymbol{N}^T)}\\&=\boldsymbol{Q}(t)\boldsymbol{U}_{(0)}(0-s)\,\boldsymbol{Q}(t)^T\,,\end{aligned} \tag{4.89}$$

$$\begin{aligned}\boldsymbol{R}_{(t)}(t-s)&=\boldsymbol{Q}(t-s)\,\boldsymbol{Q}(t)^T e^{-s\frac{\dot{\gamma}}{2}(\boldsymbol{N}-\boldsymbol{N}^T)}\\&=\boldsymbol{Q}(t-s)\boldsymbol{R}_{(0)}(0-s)\,\boldsymbol{Q}(t)^T\,.\end{aligned} \tag{4.90}$$

[2]Recall the definition of the exponential of a tensor $\boldsymbol{T}$ is given as

$$e^{\boldsymbol{T}}=\boldsymbol{I}+\sum_{n=1}^{\infty}\frac{1}{n!}\boldsymbol{T}^n.$$

The rate of change of the relative deformation gradient (see Eq. (3.46)) is the velocity gradient which, when coupled with Eq. (4.86) yields

$$\boldsymbol{L} = \dot{\gamma}\boldsymbol{N} + \dot{\boldsymbol{Q}}(t)\,\boldsymbol{Q}(t)^T \,. \tag{4.91}$$

Using Eq. (3.55a), the Rivlin-Ericksen tensors $\boldsymbol{A}_n$ follow from the right relative Cauchy-Green tensor

$$\boldsymbol{A}_1 = \dot{\gamma}\left(\boldsymbol{N} + \boldsymbol{N}^T\right) , \tag{4.92a}$$

$$\boldsymbol{A}_2 = \dot{\gamma}\left(\boldsymbol{N}^T\boldsymbol{A}_1 + \boldsymbol{A}_1\boldsymbol{N}\right) = \dot{\gamma}^2\left[2\boldsymbol{N}^T\boldsymbol{N} + \boldsymbol{N}^2 + (\boldsymbol{N}^T)^2\right] , \tag{4.92b}$$

$$\boldsymbol{A}_3 = \dot{\gamma}\left(\boldsymbol{N}^T\boldsymbol{A}_2 + \boldsymbol{A}_2\boldsymbol{N}\right), \tag{4.92c}$$

$$\vdots$$

$$\boldsymbol{A}_n = \dot{\gamma}\left(\boldsymbol{N}^T\boldsymbol{A}_{n-1} + \boldsymbol{A}_{n-1}\boldsymbol{N}\right) \,. \tag{4.92d}$$

From this, a monotonous motion is isochoric (incompressible flow) iff

$$\{\boldsymbol{N}\} = 0 \,. \tag{4.93}$$

As was discussed in Sect. 4.3.2.2, the rate of change of the relative rate of rotation in Eq. (4.90) and the relative (right) stretch in Eq. (4.89) are related to the rate of rotation and the rate of strain of the fluid element and for a monotonous motion are given by

$$\boldsymbol{W} = \dot{\boldsymbol{Q}}(t)\,\boldsymbol{Q}(t)^T + \frac{\dot{\gamma}}{2}\boldsymbol{Q}(t)\left(\boldsymbol{N}_0 - \boldsymbol{N}_0^T\right)\boldsymbol{Q}(t)^T \,, \tag{4.94a}$$

$$\boldsymbol{D} = \frac{\dot{\gamma}}{2}\boldsymbol{Q}(t)\left(\boldsymbol{N}_0 + \boldsymbol{N}_0^T\right)\boldsymbol{Q}(t)^T \,. \tag{4.94b}$$

These results are consistent with those given in Eq. (4.37) where, from Eq. (4.85), $\boldsymbol{R}(t) = \boldsymbol{Q}(t)$ and $\boldsymbol{U}(t) = e^{\frac{\dot{\gamma}}{2}t(\boldsymbol{N}_0 + \boldsymbol{N}_0^T)}$.

If, additionally, the velocity gradient $\boldsymbol{L}$ is constant with a vanishing material derivative, so that the relative deformation gradient is given by Eq. (3.45), then the right relative Cauchy-Green tensors simply reduces to

$$\boldsymbol{C}_{(t)}(t-s) = \boldsymbol{C}_{(0)}(0-s) \,. \tag{4.95}$$

When compared to Eq. (4.84), it then requires that $\boldsymbol{Q}(t) = \mathbf{I}$ and consequently that $\boldsymbol{L} = \dot{\gamma}\boldsymbol{N}_0$. Equation (4.95) then describes a motion along a fluid element path with a constant stretch history. A useful consequence of this type of motion is seen from Eq. (4.48). If $\boldsymbol{Q}(t) = \boldsymbol{I}$ then the rate of rotation of the relative deformation gradient reduces to the rotation rate of the eigenvectors associated with the rate of strain.

Two important examples of motions with constant stretch history, viscometric flow and extensional flows, will be further examined.

4.5.1 Viscometric Flow

Within the class of monotonous motions falls the viscometric flows. These are motions that possess a so-called viscometric basis whose matrix is given by

$$[N_0] = \begin{pmatrix} 0 & 1 & 0 \\ 0 & 0 & 0 \\ 0 & 0 & 0 \end{pmatrix} , \tag{4.96}$$

which results in

$$\boldsymbol{N}_0^2 = \boldsymbol{0} . \tag{4.97}$$

From Eqs. (4.85) and (4.86), the deformation gradient and relative deformation gradient for a viscometric flow are given by

$$\boldsymbol{\mathcal{F}}(\tau) = e^{\tau\dot{\gamma}\boldsymbol{N}} = \boldsymbol{I} + \tau\dot{\gamma}\boldsymbol{N}_0 , \tag{4.98}$$

and

$$\boldsymbol{\mathcal{F}}_{(t)}(\tau) = \boldsymbol{Q}(\tau)\,\boldsymbol{Q}(t)^T \left[\boldsymbol{I} + (\tau - t)\dot{\gamma}\,\boldsymbol{Q}(t)\boldsymbol{N}_0\,\boldsymbol{Q}(t)^T\right] , \tag{4.99}$$

where Eq. (4.97) has been used.

In a viscometric flow, the only Rivlin-Ericksen tensors remaining are,

$$\boldsymbol{A}_1 = \dot{\gamma}\left(\boldsymbol{N} + \boldsymbol{N}^T\right) \quad \text{and} \quad \boldsymbol{A}_2 = 2\dot{\gamma}^2\boldsymbol{N}^T\boldsymbol{N} , \tag{4.100}$$

and since all the Rivlin-Ericksen tensors vanish from the third-order and higher, the relative right Cauchy-Green tensor (see Eq. (3.64)) then becomes

$$\boldsymbol{C}_{(t)}(t - s) = \boldsymbol{I} - s\boldsymbol{A}_1 + \frac{s^2}{2}\boldsymbol{A}_2 . \tag{4.101}$$

The corresponding rate of rotation tensor, $\boldsymbol{R}_{(t)}$, and stretch tensor, $\boldsymbol{U}_{(t)}$, of the relative deformation gradient are

$$\boldsymbol{R}_{(t)}(t - s) = \boldsymbol{Q}(t - s)\,\boldsymbol{Q}(t)^T \left[\boldsymbol{I} - s\frac{\dot{\gamma}}{2}(\boldsymbol{N} - \boldsymbol{N}^T)\right] , \tag{4.102}$$

$$\boldsymbol{U}_{(t)}(t - s) = \boldsymbol{I} - s\frac{\dot{\gamma}}{2}(\boldsymbol{N} + \boldsymbol{N}^T) , \tag{4.103}$$

with the rate of rotation and rate of strain tensors given by Eqs. (4.94a), (4.94b).

$$\dot{\boldsymbol{R}}_{(t)}|_{s=0} = \dot{\boldsymbol{Q}}(t)\,\boldsymbol{Q}(t)^T + \frac{\dot{\gamma}}{2}(\boldsymbol{N}_0 - \boldsymbol{N}_0^T) , \tag{4.104}$$

$$\dot{\boldsymbol{U}}_{(t)}|_{s=0} = \frac{\dot{\gamma}}{2}(\boldsymbol{N}_0 + \boldsymbol{N}_0^T) . \tag{4.105}$$

Viscometric flows are basically shear flows, and one of the most fundamental is plane shear flow which has been briefly described in Sect. 1.1.3.1. This simple shear flow has a shear rate in the cross-stream direction and is uniform in perpendicular planes. It is a flow field amenable to analysis in the development of material stress constitutive equations, and when interpreted as a mean flow field in turbulent flows

is pivotal in assessing the dynamics of turbulent statistical correlations. The constant velocity gradient matrix is given by

$$[L] = \begin{pmatrix} 0 & \dot{\gamma} & 0 \\ 0 & 0 & 0 \\ 0 & 0 & 0 \end{pmatrix}, \quad \boldsymbol{L} = \dot{\gamma}\boldsymbol{N}_0 \,. \tag{4.106}$$

The matrices associated with the Rivlin-Ericksen tensors are then

$$[A_1] = \begin{pmatrix} 0 & \dot{\gamma} & 0 \\ \dot{\gamma} & 0 & 0 \\ 0 & 0 & 0 \end{pmatrix}, \quad \left[A_1^2\right] = \begin{pmatrix} \dot{\gamma}^2 & 0 & 0 \\ 0 & \dot{\gamma}^2 & 0 \\ 0 & 0 & 0 \end{pmatrix}, \quad [A_2] = \begin{pmatrix} 0 & 0 & 0 \\ 0 & 2\dot{\gamma}^2 & 0 \\ 0 & 0 & 0 \end{pmatrix} \tag{4.107}$$

and $\boldsymbol{A}_n = \boldsymbol{0}$, $n = 3, \ldots$. With the constant velocity gradient, this is a motion with a constant stretch history so that $\boldsymbol{C}_{(t)}(t-s) = \boldsymbol{C}_{(0)}(0-s)$. Since this type of deformation behavior will be shown to be important in formulating equilibrium conditions for explicit representations of constitutive equations for both material stress and turbulent stress fields. Due to this, it is worth probing further the kinematic characteristics of this flow.

From Eqs. (4.104) and (4.105), the rate of rotation and the rate of strain for a constant stretch history motion are given by

$$\boldsymbol{W} = \frac{\dot{\gamma}}{2}\left(\boldsymbol{N}_0 - \boldsymbol{N}_0^T\right), \qquad [W] = \frac{\dot{\gamma}}{2}\begin{pmatrix} 0 & 1 & 0 \\ -1 & 0 & 0 \\ 0 & 0 & 0 \end{pmatrix}, \tag{4.108a}$$

$$\boldsymbol{D} = \frac{\dot{\gamma}}{2}\boldsymbol{Q}(t)\left(\boldsymbol{N}_0 + \boldsymbol{N}_0^T\right), \qquad [D] = \frac{\dot{\gamma}}{2}\begin{pmatrix} 0 & 1 & 0 \\ 1 & 0 & 0 \\ 0 & 0 & 0 \end{pmatrix}. \tag{4.108b}$$

In Astarita and Marucci (1974), a full description of viscometric flows is covered and includes plane flows: linear Couette and channel flows; helical flows like Poiseuille flow, flow between concentric cylinders (Couette, annular, etc.), cone and plate flow, torsional flow. A more elaborate viscometric flow is the cone- torsional flow occurring in a domain located between a flat plate and a rotating cone, the rotation axis of which being orthogonal to the plate.

4.5.2 Extensional Flow

Another important subset of constant stretch history flows are extensional flows. These are motions such that $\boldsymbol{N} = \boldsymbol{N}^T$ so that the matrix associated with this symmetry condition reads

$$[N_0] = \begin{pmatrix} n_1 & 0 & 0 \\ 0 & n_2 & 0 \\ 0 & 0 & n_3 \end{pmatrix}, \tag{4.109}$$

where n_i, $i = 1, 2, 3$ are constant and unequal, with a normalization such that

$$\{\boldsymbol{N}_0^2\} = 1 \tag{4.110}$$

($\dot{\gamma} = 1$ here). It then immediately follows that the relative right Cauchy-Green tensor can be written as

$$\boldsymbol{C}_{(t)}(t-s) = \boldsymbol{C}_{(0)}(0-s) = e^{-2s\boldsymbol{N}_0} , \tag{4.111}$$

and yielding Rivlin-Ericksen tensors of the form

$$\boldsymbol{A}_1 = 2\boldsymbol{N}_0 , \tag{4.112a}$$

$$\boldsymbol{A}_2 = \left(\boldsymbol{N}_0^T\boldsymbol{A}_1 + \boldsymbol{A}_1\boldsymbol{N}_0\right) = (2\boldsymbol{N}_0)^2 = \boldsymbol{A}_1^2 , \tag{4.112b}$$

$$\vdots$$

$$\boldsymbol{A}_n = (2\boldsymbol{N}_0)^n = \boldsymbol{A}_1^n . \tag{4.112c}$$

The velocity gradient $\boldsymbol{L}$ is $\boldsymbol{N}_0$ and for an isochoric motion is

$$\{\boldsymbol{L}\} = (n_1 + n_2 + n_3) = 0 . \tag{4.113}$$

4.5.3 Viscometric Functions

From the study of the planar shear flow, let us consider the shear stress Σ_{xy}. The stress component is an odd function of the shear rate and therefore may be written as

$$\Sigma_{xy} = \dot{\gamma}\mu(\dot{\gamma}) , \tag{4.114}$$

where the shear viscosity $\mu = \Sigma_{xy}/\dot{\gamma}$ is an even function of the shear rate. The normal stress differences defined in Eq. (1.5) are not modified by the reversal of the shear direction and should be even functions of $\dot{\gamma}$. They should also vanish when $\dot{\gamma}$ goes to zero. Consequently the normal stress differences are written as

$$N_1 = \dot{\gamma}^2\Psi_1(\dot{\gamma}), \qquad N_2 = \dot{\gamma}^2\Psi_2(\dot{\gamma}) , \tag{4.115}$$

with Ψ_1 and Ψ_2 the normal stress difference coefficients. The viscometric functions are defining the material behavior of the fluid.

The continuum approach that has been described so far does not bring micro-scale information of the fluid intrinsic structure. In the following chapters, when need be, we will resort to kinetic theory and a stochastic description to take that information into account.

Chapter 5
Non-Newtonian and Viscoelastic Fluids

5.1 Introduction

The theory of non-Newtonian and viscoelastic fluids flourished in the second half of last century with the developments of (molten and dilute) polymers and the growth of materials science and engineering that generated many new products and applications. The mathematical setting of the constitutive equations required new tools from tensor analysis and algebra that have already been exposed in previous chapters. Here the concentration will be on the various constitutive relations that became dominant over time because of their generality and/or their physical relevance. Despite the major effort carried out by numericists over the last four decades, numerical simulations at high Weissenberg number values (and zero Reynolds number) are not always feasible and this poses deep questions and concerns about getting the appropriate models for those fluids. However the log-formulation introduced by Fattal and Kupferman (2004) has eased that difficulty. Nonetheless in problems where experimental data are available, numerical results based on non-Newtonian models may sometimes be in error by an order of magnitude. This situation is detrimental in the long run to engineering and should be tackled by all means: theory, experiments and computations.

The major physical phenomena have been described in Chap. 1, and the dimensionless Weissenberg number defined by Eq. (1.26). Another useful dimensionless number is the Deborah number De

$$\mathrm{De} = \frac{\lambda}{T}\,, \tag{5.1}$$

that compares the material relaxation time to a characteristic time of the flow, which might be a particle residence time, a time scale related to the geometrical configuration or to the main physical phenomenon like the core vortex in a cavity. Relevant Weissenberg numbers for industrial applications are of the order of one hundred and beyond, a value that is possible to reach by present day computations avoiding the traditional Oldroyd-B or UCM constitutive equations in favor of, for example, Giesekus models and resorting to very stable finite elements in the framework of the discontinuous Galerkin method.

M.O. Deville, T.B. Gatski, *Mathematical Modeling for Complex Fluids and Flows*,
DOI 10.1007/978-3-642-25295-2_5,

Modern constitutive equations take into account more and more often the microscopic features of polymeric fluids. The interplay between micro- and macro-scale is of prime importance and leads to a multiscale approach that is a major step forward towards the goal of incorporating more physics into the models. The starting point here will be with linear constitutive equations and then build up to nonlinear equations and more sophisticated relationships. The development of an explicit representation of the extra-stress tensor will then be proposed. Then the dumbbell theory, where the polymer chains are modeled by springs connecting two beads, will be presented and followed by a stochastic approach with the Fokker-Planck equation. The micro-macro approach is the starting point for another way of building up the stress tensor. A full section is then devoted to the modeling of polymer melts where the Doi-Edwards, (extended) pom-pom and Rolie-Poly models are explored.

The theory of constitutive equations for non-Newtonian and viscoelastic fluids has been described in numerous books. Without being exhaustive, the reader is referred to the following references for further study: Barnes et al. (1987), Bird et al. (1987a, 1987b), Doi and Edwards (1988), Joseph (1990), Larson (1988), Öttinger (1996), Phan-Thien (2002), Tanner (1989). A complete state-of-the-art review for numerical methods applied to viscoelastic fluids has been published by Owens and Phillips (2002). The recent review article by Lozinski et al. (2011) brings forward modern views to the computational landscape.

5.2 Classical and Generalized Newtonian Models

As a starting point in the discussion of constitutive equations, the fundamental linear tensorial relationship of stress proportional to strain rate is first examined. Such relations hold for Newtonian fluids with constant shear viscosity and those displaying a relationship with the shear rate.

5.2.1 Newtonian Fluids

The classical viscous Newtonian incompressible fluid is characterized by the linear constitutive equation

$$\boldsymbol{\Sigma} = -p\,\boldsymbol{I} + 2\mu\,\boldsymbol{D}\,, \tag{5.2}$$

where the coefficient μ is the dynamic or shear viscosity, and can be expressed in Pa s. This material coefficient is obtained, for example, by the measurement of the torque applied to a circular Couette flow in a rheometer. The kinematic viscosity is defined by $\nu = \mu/\rho$, can be expressed in $\mathrm{m}^2\,\mathrm{s}^{-1}$ units. If $\mu = 0$, one obtains the inviscid or perfect fluid

$$\boldsymbol{\Sigma} = -p\,\boldsymbol{I}\,. \tag{5.3}$$

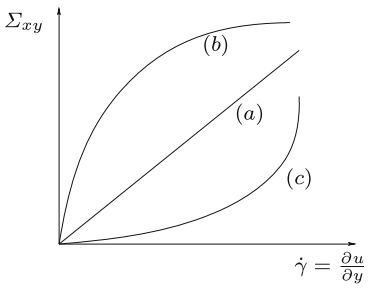

Fig. 5.1 Shear stress component as a function of the shear rate

Unlike the compressible case, the incompressible fluid has no equation of state for the pressure. This variable is obtained by imposing the continuity constraint. In problems where analytical solutions are sought, either the pressure gradient is given, as in a channel or Poiseuille flow, or the pressure is obtained once the velocity field is computed. The pressure is the physical variable responsible for the incompressibility and in the framework of variational principles the pressure occurs as the Lagrange parameter associated with $\nabla \cdot \mathbf{v} = 0$.

5.2.2 Generalized Newtonian Fluids

The constitutive equation of generalized Newtonian fluids is generated by allowing the dynamic viscosity in Eq. (5.2) to depend on the shear rate $\dot{\gamma}$ such that $\mu = \mu(\dot{\gamma})$ where $\dot{\gamma} = \sqrt{2\{\boldsymbol{D}^2\}}$ (cf. Sect. 1.1). A very common model is the power law

$$\mu(\dot{\gamma}) = K\dot{\gamma}^{m-1} \tag{5.4}$$

with K the consistency factor and m the index of the power law ($m = 1$, $K = \mu$ for the Newtonian case). For many polymers, blood or food liquids, m is between 0.3 and 0.6. Fluids with $m < 1$ are pseudo-plastic fluids; those with $m > 1$ are dilating fluids. Figure 5.1 displays the evolution of the shear stress in a plane Couette flow versus $\dot{\gamma}$ for various m values. Curve (a) corresponds to the Newtonian case; curve (b) is pseudo-plastic fluids ($m < 1$) and curve (c) belongs to dilating fluids. The viscosity variation with respect to the shear rate for a pseudo-plastic fluid is shown in Fig. 5.2. One observes that μ decreases when $\dot{\gamma}$ increases and the viscosity is shear thinning. In the opposite case, where μ increases with increasing $\dot{\gamma}$, the viscosity is shear thickening. The power law model does not allow the presence of a Newtonian plateau; furthermore the viscosity becomes infinite for a vanishing shear rate. For industrial applications the Bird-Carreau (Carreau 1972) law is preferred

$$\mu - \mu_\infty = \frac{\mu_0 - \mu_\infty}{[1 + (\lambda\dot{\gamma})^2]^{(m-1)/2}} \tag{5.5}$$

where μ_0 is the viscosity of the Newtonian plateau at low shear rate, μ_∞ the viscosity of the second Newtonian plateau at very high shear rate, and λ a characteristic

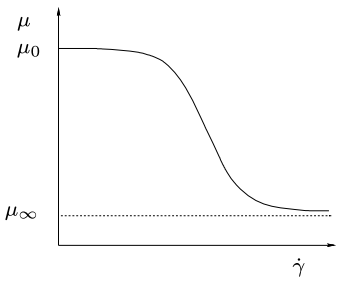

Fig. 5.2 Viscosity variation with respect to the shear rate for a pseudo-plastic fluid

relaxation time of the material. The generalized form of this equation is due to Yasuda and Cross (1965)

$$\mu - \mu_\infty = \frac{\mu_0 - \mu_\infty}{[1 + (\lambda\dot{\gamma})^a]^{(m-1)/a}} \tag{5.6}$$

with a a curve-fit parameter.

The yield fluids contain a yield stress Σ_y. This means that the shear stress has to be higher than a threshold for the fluid to flow. Below this threshold, the fluid behaves like a solid, and above it may behave as Newtonian or power-law like. These are the Bingham (1916) fluid (everybody uses it in the bathroom: toothpaste)

$$\mu = \begin{cases} \infty & \text{if } |\Sigma| < |\Sigma_y| \\ \mu_0 + \frac{\Sigma_y}{\dot{\gamma}} & \text{if } |\Sigma| \geq |\Sigma_y| \end{cases}, \tag{5.7}$$

and the Herschel and Bulkley (1926) fluid

$$\mu = \begin{cases} \infty & \text{if } |\Sigma| < |\Sigma_y| \\ K\dot{\gamma}^{m-1} + \frac{\Sigma_y}{\dot{\gamma}} & \text{if } |\Sigma| \geq |\Sigma_y| \end{cases}. \tag{5.8}$$

These yield fluids produce so-called plug flows in channels or pipes since near the symmetry axis the shear stress vanishes and therefore does not reach the threshold value.

5.3 Linear Viscoelasticity

The concepts for the design of linear viscoelastic models were framed with the aid of mechanical parts involving springs and dashpots. The number of combinations of these elementary pieces is infinite; however, obvious examples emerged and are proposed in the sequel. In the example models to follow, the discussion is restricted to the simple 1D case where the motion is homogeneous. The strain ϵ and associated $\dot{\epsilon}$ are relative measures of an extensional motion. Since all the models are linear, the superposition principle can provide the user with more complicated and elaborate assemblages.

5.3.1 Maxwell Model

Consider again the Maxwell model of Sect. 1.1.2 composed of a spring of stiffness k and a dashpot of viscosity μ connected in series. With a relaxation time defined as $\lambda = \mu/k$, the relation between stress and strain rate was given as

$$\Sigma + \lambda \dot{\Sigma} = \mu \dot{\epsilon} \ . \tag{5.9}$$

If this relation is rewritten as

$$\frac{\mathrm{d}}{\mathrm{d}t}(\Sigma e^{t/\lambda}) = \left(\frac{\mu}{\lambda}\dot{\epsilon}\right) e^{t/\lambda} \ , \tag{5.10}$$

and if the constraint that Σ remains finite when $t \to -\infty$ is imposed, the integration in time yields

$$\Sigma(t) = \int_{\tau=-\infty}^{t} \frac{\mu}{\lambda} \exp\left[-\frac{(t-\tau)}{\lambda}\right] \dot{\epsilon}(\tau)\mathrm{d}\tau \ . \tag{5.11}$$

The quantity in the integrand,

$$G(t-\tau) := \frac{\mu}{\lambda} \exp\left[-\frac{(t-\tau)}{\lambda}\right] \ , \tag{5.12}$$

is called the relaxation modulus. This expression shows that in the Maxwell model the stress at the present time depends on the history of the deformation through the strain rate. In addition, the fluid possesses an intrinsic property of fading memory that gives more weight to the recent past than to the distant past, with the decay rate driven by the material relaxation time. Although several forms of G may be found in the literature, the exponential $G = G_0 \exp^{-(t-\tau)/\lambda}$ is the most used. It may also be generalized to multi-mode exponential which is characteristic of polymers with $G = \sum_{i=1}^{n} G_i \exp^{-(t-\tau)/\lambda_i}$. The Newtonian case is recovered with $G = \mu\delta(t-\tau)$, δ being the Dirac function and the linear elastic solid for $G = G_0$.

As an example, a creep experiment where the model is subject to a constant force (per unit area) Σ_0 for $t \geq 0$ can be carried out. Since $\dot{\Sigma} = 0$ in Eq. (5.9), one easily gets

$$\epsilon = \epsilon_0 + \frac{\Sigma_0}{\mu} t \ , \tag{5.13}$$

showing that the deformation will increase linearly in time forever. On the other hand, one can look at a stress relaxation experiment, where now the strain ϵ_0 (at $t = 0$) remains constant for $t > 0$. The resulting stress is readily given by

$$\Sigma = k\,\epsilon_0\, e^{-t/\lambda} = \frac{\mu}{\lambda}\,\epsilon_0\, e^{-t/\lambda} \ , \tag{5.14}$$

which shows that the relaxation time is the time for the stress to decrease by a factor e^{-1} from its initial value.

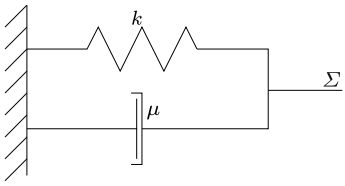

Fig. 5.3 Kelvin-Voigt mechanical model

5.3.2 Kelvin-Voigt Model

The Kelvin-Voigt model is composed of a spring and a dashpot in parallel as is shown in Fig. 5.3, and is described by the relation

$$\Sigma = k\epsilon + \mu\dot{\epsilon} \tag{5.15}$$

which shows that the force associated with Σ applies at the same time to both elements.

Under constant strain $\dot{\epsilon} = 0$, the stress remains constant and there is no stress relaxation. If the stress is loaded through a Heaviside function, the resulting strain is given as

$$\epsilon(t) = \frac{\Sigma_0}{k}\left[1 - \exp(-t/\lambda)\right] \tag{5.16}$$

This shows that the deformation will be damped by the dashpot viscosity and in the long run the system will be in equilibrium with $\Sigma_0 = k\epsilon$, the force in the elastic solid. Therefore, this model is more applicable to viscoelastic solids than fluids.

5.3.3 Jeffreys Model

Here a dashpot of viscosity μ_1 and a Kelvin-Voigt model of stiffness k and of viscosity μ_2 are put in series (see Fig. 5.4). The total strain rate is given by

$$\dot{\epsilon} = \dot{\epsilon}_1 + \dot{\epsilon}_2 \,, \tag{5.17}$$

while the stress is expressed as

$$\Sigma = \mu_1\dot{\epsilon}_1 = k\epsilon_2 + \mu_2\dot{\epsilon}_2 \,. \tag{5.18}$$

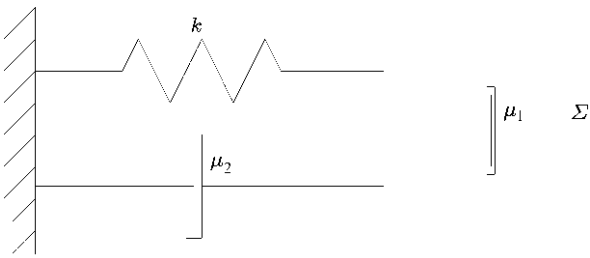

Fig. 5.4 Jeffreys mechanical model

In terms of the total strain rates, Eqs. (5.17) and (5.18) can be combined to yield

$$\frac{\mu_2+\mu_2}{k}\dot{\Sigma}+\Sigma=\mu_1\left(\dot{\epsilon}+\frac{\mu_2}{k}\ddot{\epsilon}\right)\ . \tag{5.19}$$

If a constant stress is applied to the model, the isolated dashpot will never stop the deformation as in the Maxwell model, so that the Jeffreys model will never reach equilibrium under a constant force. Consequently it is more amenable to fluids than solids. If a relaxation time is defined as $\lambda_1=(\mu_1+\mu_2)/k$ and a retardation time as $\lambda_2=\mu_2/k$ the Jeffreys model takes the form

$$\Sigma+\lambda_1\dot{\Sigma}=\mu_1\left(\dot{\epsilon}+\lambda_2\ddot{\epsilon}\right)\ . \tag{5.20}$$

5.4 From a Simple Fluid to Viscoelasticity

It is best now to come back to the general framework of multi-dimensional constitutive equations, and start from the simple fluid model and investigating viscoelastic models. For the viscoelastic models, two limiting behaviors, the viscous fluid and the elastic "fluid", will be examined.

5.4.1 Reiner-Rivlin Fluid

The constraints considered in Sect. 4.4 led to the stress expression given by Eq. (4.83). If the first-order time derivative is the only one required in the development, the constitutive relation reduces to

$$\boldsymbol{\Sigma}=-p\boldsymbol{I}+\mathfrak{F}(\mathbf{C}_{(t)},\dot{\mathbf{C}}_{(t)})\ . \tag{5.21}$$

Adding the assumption of a regular and smooth history of deformation, and an instantaneous memory, one can express the dependency of the functional by the Rivlin-Ericksen tensors and obtain the relation

$$\boldsymbol{\Sigma}=-p\boldsymbol{I}+\boldsymbol{K}(\boldsymbol{D})\ , \tag{5.22}$$

with the isotropy condition (see Sect. 4.4)

$$\boldsymbol{Q}\boldsymbol{\Sigma}\boldsymbol{Q}^T=\boldsymbol{K}(\boldsymbol{Q}\boldsymbol{D}\boldsymbol{Q}^T)\ , \tag{5.23}$$

where the former functional $\mathfrak{F}$ of Eq. (5.21) has become an isotropic tensorial function $\boldsymbol{K}$ of the symmetric tensor $\boldsymbol{D}$. Applying the results of Table 2.1 on isotropic tensorial functions of symmetric tensors, one gets

$$\boldsymbol{\Sigma}=K_0\,\boldsymbol{I}+K_1\,\boldsymbol{D}+K_2\,\boldsymbol{D}^2\ , \tag{5.24}$$

where the scalar functions K_i $(i=0,1,2)$ are functions of the integrity bases (2.45) expressed as functions of the invariants of $\boldsymbol{D}$. For the incompressible fluid

$\mathrm{I}_1(\boldsymbol{D}) = 0$, and the function K_0 is identified with the pressure. Equation (5.24) is then written as

$$\boldsymbol{\Sigma} = -p\,\boldsymbol{I} + K_1(\mathrm{I}_2(\boldsymbol{D}), \mathrm{I}_3(\boldsymbol{D}))\,\boldsymbol{D} + K_2(\mathrm{I}_2(\boldsymbol{D})), \mathrm{I}_3(\boldsymbol{D})\;\boldsymbol{D}^2 \,. \tag{5.25}$$

This nonlinear non-Newtonian constitutive relation describes the stress field of the Reiner-Rivlin fluid (see Eq. (1.11)).

5.4.2 Elasticity as the Limit Case

It was discussed in Sect. 4.2.1 that the stress in a simple fluid can be described by a functional relationship dependent on the relative deformation gradient tensor $\boldsymbol{\mathcal{F}}_{(t)}$ (see Eq. (4.2)). From the principle of local action, this means that if the deformation acts for a long time (De $<$ 1), the fluid behaves as a Newtonian fluid, and if the deformation is rapid (De $>$ 1), the fluid behaves elastically. In this latter case, the stress tensor depends solely on the deformation (through $\boldsymbol{\mathcal{F}}_{(t)}$) and not on the rate of deformation, and such a constitutive relationship was presented in Eq. (4.69). In that discussion, the relative deformation gradient $\boldsymbol{\mathcal{F}}_{(t)}$ described the motion from the earlier time τ $(= t - s)$ relative to the present time t. In evaluating the elastic limit, the interest lies in the result of the deformation at the present time t relative to the earlier time τ $(= t - s)$. As such, the inverse relative deformation gradient is relevant $\boldsymbol{\mathcal{F}}^{-1}_{(t)}$, and the material stress field can be written as

$$\boldsymbol{\Sigma} = \mathfrak{S}'(\boldsymbol{\mathcal{F}}^{-1}_{(t)}(t - s_\epsilon)) = G\boldsymbol{\mathcal{F}}^{-1}_{(t)}(t - s_\epsilon) \,, \tag{5.26}$$

where $t - s_\epsilon$ is used to emphasize the short memory $s_\epsilon \longrightarrow 0$ of the fluid, with G a constant. If before the (rapid) deformation the material was in an isotropic state and the relative deformation described by a simple rotation through some fixed angle, it follows from Eq. (5.26) that an anisotropic stress would be induced in the fluid; although, for an elastic material an isotropic stress is expected. For this simple example, one can appeal to the objectivity constraints discussed in Sect. 4.4.2 (cf. Eqs. (4.81) and (4.82)), and rewrite the stress field relationship in Eq. (5.26) as

$$\boldsymbol{\Sigma} = G\boldsymbol{C}^{-1}_{(t)}(t - s_\epsilon) \,, \tag{5.27}$$

where $\boldsymbol{C}_{(t)} = \boldsymbol{\mathcal{F}}^T_{(t)}\boldsymbol{\mathcal{F}}_{(t)}$ and

$$\boldsymbol{C}^{-1}_{(t)} = \boldsymbol{\mathcal{F}}^{-1}_{(t)}\boldsymbol{\mathcal{F}}^{-T}_{(t)} \,, \tag{5.28}$$

the relative Finger strain tensor. Now, for the rapid deformation considered here, the definition of the relative right Cauchy-Green tensor leads to $\boldsymbol{C}^{-1}_{(t)} \approx \boldsymbol{I}$ for vanishing s_ϵ. As such, the stress field remains isotropic before and after the deformation.

5.4.3 Design of a Viscoelastic Constitutive Equation

The Maxwell model (5.11) can be generalized by considering the quantity Σ as being the shear component Σ_{12} of the full tensor $\boldsymbol{\Sigma}$. This leads to

$$\Sigma_{12} = \frac{G}{\lambda}\int_{-\infty}^{t} e^{-\frac{(t-\tau)}{\lambda}}\epsilon(\tau)d\tau = \frac{G}{\lambda}\int_{-\infty}^{t} e^{-\frac{(t-\tau)}{\lambda}} C^{-1}_{(t)12}(\tau)d\tau \ , \tag{5.29}$$

where $C^{-1}_{(t)12} = \epsilon(\tau) = \int_{\tau}^{t}\dot{\epsilon}dt'$ has been used. The general tensorial form is the Lodge equation written as

$$\boldsymbol{\Sigma} = \frac{G}{\lambda}\int_{-\infty}^{t} e^{-\frac{(t-\tau)}{\lambda}} \boldsymbol{C}^{-1}_{(t)}(\tau)\mathrm{d}\tau \ . \tag{5.30}$$

Two limiting cases of Eq. (5.30) are of interest. In one case, if the deformation is extremely rapid, $\boldsymbol{C}^{-1}_{(t)}$ is constant and Eq. (5.27) is recovered. In the other case, if the deformation is slow, the approximation

$$\boldsymbol{C}^{-1}_{(t)} \approx \boldsymbol{I} + \delta\boldsymbol{C}^{-1}_{(t)} \ , \tag{5.31a}$$

holds to within a small perturbation term. A first-order Taylor series expansion with respect to time then yields

$$\begin{aligned}\boldsymbol{C}^{-1}_{(t)} &\approx \boldsymbol{I} - (t-\tau)\left.\frac{\partial \boldsymbol{C}^{-1}_{(t)}}{\partial\tau}\right|_{\tau=t} \\ &\approx \boldsymbol{I} - 2(t-\tau)\boldsymbol{D} \ ,\end{aligned} \tag{5.31b}$$

where Eq. (3.57) has been used.

The Lodge equation, when integrated with (5.31a), (5.31b), yields

$$\boldsymbol{\Sigma} = G\boldsymbol{I} + 2G\lambda\boldsymbol{D} \ , \tag{5.32}$$

which is the Newtonian fluid stress equation with $G = -p$ and $G\lambda = \mu$.

5.5 Rivlin-Ericksen and Order Fluids

The book by Truesdell and Rajagopal (2000) contains a thorough discussion of Rivlin-Ericksen fluids and the various associated models such as the fluids of grade n that will not be considered here for the sake of conciseness. If all the terms present in the development of the history of $\boldsymbol{C}_{(t)}$ (cf. Eq. (3.64)) are now incorporated, the constitutive equation for the simple fluid leads to the relation

$$\boldsymbol{\Sigma} = -p\boldsymbol{I} + \boldsymbol{f}(\boldsymbol{A}_1, \boldsymbol{A}_2, \ldots, \boldsymbol{A}_N, \ldots) \ , \tag{5.33}$$

involving the Rivlin-Ericksen tensors.

5.5.1 Rivlin-Ericksen Fluids

Truncation of the Taylor series to order N yields the Rivlin-Ericksen fluid of complexity N and the requirement of the MFI condition imposes the constraint that

$$\boldsymbol{Q}\boldsymbol{f}(\boldsymbol{A}_1, \boldsymbol{A}_1, \ldots, \boldsymbol{A}_N)\boldsymbol{Q}^T = \boldsymbol{f}(\boldsymbol{Q}\boldsymbol{A}_1\boldsymbol{Q}^T, \boldsymbol{Q}\boldsymbol{A}_2\boldsymbol{Q}^T, \ldots, \boldsymbol{Q}\boldsymbol{A}_N\boldsymbol{Q}^T) , \tag{5.34}$$

for any arbitrary orthogonal tensor $\boldsymbol{Q}$. Therefore, the function $\boldsymbol{f}$ is an isotropic tensor function. Although the general solution for the polynomial representation is known (cf. Wang 1970), the Rivlin-Ericksen fluid of complexity 2 is the most popular constitutive equation. Using the results given in Sect. 2.4.1.1, that is Eqs. (2.62) and (2.66), it can be written as

$$\begin{aligned}\boldsymbol{\Sigma} = &-p\boldsymbol{I} + K_1\boldsymbol{A}_1 + K_2\boldsymbol{A}_1^2 + K_3\boldsymbol{A}_2 + K_4\boldsymbol{A}_2^2 \\ &+ K_5(\boldsymbol{A}_1\boldsymbol{A}_2 + \boldsymbol{A}_2\boldsymbol{A}_1) + K_6\left(\boldsymbol{A}_1\boldsymbol{A}_2^2 + \boldsymbol{A}_2^2\boldsymbol{A}_1\right) \\ &+ K_7\left(\boldsymbol{A}_1^2\boldsymbol{A}_2 + \boldsymbol{A}_2\boldsymbol{A}_1^2\right) + K_8\left(\boldsymbol{A}_1^2\boldsymbol{A}_2^2 + \boldsymbol{A}_2^2\boldsymbol{A}_1^2\right) ,\end{aligned} \tag{5.35}$$

where the functions K_i are scalar functions of the invariants (cf. Table 2.1),

$$\operatorname{tr}\boldsymbol{A}_1^2,\ \operatorname{tr}\boldsymbol{A}_1^3,\ \operatorname{tr}\boldsymbol{A}_2,\ \operatorname{tr}\boldsymbol{A}_2^2,\ \operatorname{tr}\boldsymbol{A}_2^3,\ \operatorname{tr}\boldsymbol{A}_1\boldsymbol{A}_2,\ \operatorname{tr}\boldsymbol{A}_1^2\boldsymbol{A}_2,\ \operatorname{tr}\boldsymbol{A}_1\boldsymbol{A}_2^2,\ \operatorname{tr}\boldsymbol{A}_1^2\boldsymbol{A}_2^2 , \tag{5.36}$$

since $\{A_1\} = 0$ for an incompressible fluid. This model is rather complicated to construct as the K_i have to be obtained through calibration with experiments.

5.5.2 Order Fluids

The so-called second-order fluid is a particular case of the Rivlin-Ericksen fluid of complexity two. As the tensors $\boldsymbol{A}_i$ have a dimension of t^{-i}, Eq. (5.35) is truncated to the second-order approximation in terms of the intrinsic time scale given by the $\boldsymbol{A}_i$. This is a valid procedure if it is assumed that the fluid has a fading memory and that the flow is slow. Consequently, Eq. (5.35) simplifies and becomes

$$\boldsymbol{\Sigma} = -p\boldsymbol{I} + K_1\boldsymbol{A}_1 + K_2\boldsymbol{A}_1^2 + K_3\boldsymbol{A}_2 , \tag{5.37}$$

with K_i, $i = 1, 2, 3$ being the material constants. Note that the Newtonian fluid constitutes the first-order approximation, while the perfect fluid is the zeroth-order approximation.

A third-order fluid is given by the relation

$$\begin{aligned}\boldsymbol{\Sigma} = &-p\boldsymbol{I} + \left(K_1 + K_2\left(\operatorname{tr}\boldsymbol{A}_1^2\right)\right)\boldsymbol{A}_1 + K_3\boldsymbol{A}_1^2 + K_4\boldsymbol{A}_2 \\ &+ K_5(\boldsymbol{A}_1\boldsymbol{A}_2 + \boldsymbol{A}_2\boldsymbol{A}_1) + K_6\boldsymbol{A}_3 ,\end{aligned} \tag{5.38}$$

where the coefficient K_2 depends on an invariant. Coleman and Noll (1960) introduced the concept of retarded motion and proved that the order fluids can be considered as retarded motion expansions of the simple fluid model. This then shows that order fluids, that have no memory, should only be used for slow motions.

5.5.3 Plane Shear Flow of a Second-Order Fluid

Consider the plane shear flow discussed in Sect. 4.5.1 and described by the second-order fluid equation (5.37). With the velocity components given by (1.13), and the matrices associated with the Rivlin-Ericksen tensors given in Eq. (4.107), the stress components are then

$$\Sigma_{11} = -p + K_2\dot{\gamma}^2,\ \Sigma_{22} = -p + (K_2 + 2K_3)\,\dot{\gamma}^2,\ \Sigma_{33} = -p\,, \tag{5.39a}$$

$$\Sigma_{12} = \Sigma_{21} = K_1\,\dot{\gamma} = \tau(\dot{\gamma})\,, \tag{5.39b}$$

$$\Sigma_{13} = \Sigma_{23} = 0\,, \tag{5.39c}$$

with the resulting normal stress differences being

$$N_1 = -2K_3\dot{\gamma}^2, \qquad N_2 = K_2\,\dot{\gamma}^2 + 2K_3\dot{\gamma}^2\,. \tag{5.40}$$

For a second-order fluid to flow under shear, normal forces (i.e. to push) have to be exerted on the bounding walls to generate non-vanishing normal stress differences.

For the third-order fluid, the matrix corresponding to the tensor product $\boldsymbol{A}_1\boldsymbol{A}_2$ is given as

$$[A_1A_2] = \begin{pmatrix} 0 & 2\dot{\gamma}^3 & 0 \\ 0 & 0 & 0 \\ 0 & 0 & 0 \end{pmatrix}\,. \tag{5.41}$$

The stress components are then

$$\Sigma_{11} = -p + K_2\dot{\gamma}^2,\ \Sigma_{22} = -p + (K_2 + 2K_3)\,\dot{\gamma}^2,\ \Sigma_{33} = -p\,, \tag{5.42a}$$

$$\Sigma_{12} = \Sigma_{21} = K_1\,\dot{\gamma} + 2\dot{\gamma}^3(K_4 + K_5), \tag{5.42b}$$

$$\Sigma_{13} = \Sigma_{23} = 0\,, \tag{5.42c}$$

with the same normal stress differences as in (5.40). Rewriting the shear stress component as

$$\Sigma_{12} = \dot{\gamma}\left[K_1 + 2\dot{\gamma}^2(K_4 + K_5)\right]\,, \tag{5.43}$$

the viscosity is deduced to be

$$\mu = \mu(0) + 2\dot{\gamma}^2(K_4 + K_5)\,, \tag{5.44}$$

where $\mu(0)$ is the shear viscosity at vanishing shear rate. If the fluid shows shear-thinning effects (viscosity decrease with increasing shear rate), one requires that $K_4 + K_5 < 0$.

5.6 Constant Stretch History Flows

In Sect. 4.5 the kinematic characteristics of monotonous motions or motions with constant stretch history were discussed including two subset motions, viscometric

flows and extensional flows. As a consequence of Noll's theorem, Wang (1965) proved that "in a motion with constant stretch history, the relative Cauchy-Green tensor, regarded as a function of s, is uniquely determined by the first three Rivlin-Ericksen tensors $\boldsymbol{A}_i(t)$, $i = 1, 2, 3$ at the present time t", and this was shown in Eqs. (4.92a)–(4.92d). Therefore, the stress tensor for this class of motions is represented by

$$\boldsymbol{\Sigma} = -p\boldsymbol{I} + \boldsymbol{f}(\boldsymbol{A}_1, \boldsymbol{A}_2, \boldsymbol{A}_3) \,, \tag{5.45}$$

and the behavior of the simple fluid is exactly the same as the Rivlin-Ericksen fluid of third-order.

Viscometric Flows By definition, viscometric flows are motions such that $\boldsymbol{N}_0^2 = \boldsymbol{0}$. Viscometric flows possess a so-called viscometric basis which was given in Eq. (4.96) so that the only remaining Rivlin-Ericksen tensors are $\boldsymbol{A}_1$ and $\boldsymbol{A}_2$ given in Eq. (4.100). This shows that a viscometric flow of a simple fluid behaves in the same way as a Rivlin-Ericksen fluid of second-order. Note also that it is possible to prove that in a viscometric flow, the stress components Σ_{13} and Σ_{23} are always zero. Viscometric flows are basically shear flows, and the example of the plane shear flow was described in Sect. 5.5.3. As was shown in Sect. 4.5.1, all the Rivlin-Ericksen tensors vanish from the third order, with the relative Cauchy-Green tensor given by Eq. (4.101).

Extensional Flows For an extensional flow the motion is dependent only on the first Rivlin-Ericksen tensor (see Sect. 4.5.2) so that the stress tensor will also only depend on the first Rivlin-Ericksen tensor. The off-diagonal stress components will then vanish, and the stress tensor would be

$$\boldsymbol{\Sigma} = -p\boldsymbol{I} + K_1\boldsymbol{A}_1 + K_2\boldsymbol{A}_1^2 \,, \tag{5.46}$$

where K_i, $i = 1, 2$ are functions of the invariants $\{\boldsymbol{A}_1^2\}$, $\{\boldsymbol{A}_1^3\}$.

For a steady velocity field given by,

$$v_1 = \dot{\epsilon}x_1, \quad v_2 = -\frac{\dot{\epsilon}}{2}x_2, \quad v_3 = -\frac{\dot{\epsilon}}{2}x_3 \,, \tag{5.47}$$

where $\dot{\epsilon}$ is the constant elongational rate and replaces the shear rate $\dot{\gamma}$ parameter. This flow field corresponds to the extension of a small cylindrical bar (like a fiber) that is stretched out in the x_1 direction while a contraction occurs in the cross plane (x_2, x_3). It is trivially confirmed that the motion is isochoric. The diagonal stress components are

$$\Sigma_{11} = -p + 2K_1\dot{\epsilon} + 4K_2\dot{\epsilon}^2 \,, \tag{5.48a}$$

$$\Sigma_{22} = -p - K_1\dot{\epsilon} + K_2\dot{\epsilon}^2 \,, \tag{5.48b}$$

$$\Sigma_{33} = -p - K_1\dot{\epsilon} + K_2\dot{\epsilon}^2 \,. \tag{5.48c}$$

A very important material property of this flow is the extensional viscosity μ_E defined as the ratio

$$\mu_E = \frac{\Sigma_{11} - \Sigma_{22}}{\dot{\epsilon}} = 3(K_1 + K_2\dot{\epsilon}) \,. \tag{5.49}$$

Note that for a Newtonian fluid, $K_2 = 0$ and the extensional viscosity is $\mu_E = 3K_1 = 3\mu_0$, i.e. three times the shear viscosity. This was first noticed by Trouton (1906), and the Trouton ratio

$$\mathrm{Tr} = \frac{\mu_E}{\mu_0} , \tag{5.50}$$

which is equal to 3 for a Newtonian fluid, undergoes strong variations (several orders of magnitude) for non-Newtonian fluids.

5.7 Constitutive Equations of the Rate Type

In this section, stress rate models like the Oldroyd-B fluid, used for dilute solutions, as well as various extensions are presented. The plane channel flow of an Oldroyd-B model yields a quadratic first normal stress difference and a constant viscosity. This is one of the reasons why this model has been extensively employed in numerical calculations since it is well suited to represent one of the characteristic features of the Boger fluids (James 2009): constant viscosity. As such, the Boger fluids allow the user to look for the influence of elasticity on the fluid behavior. Boger fluids may be used to obtain extensional data but their main interest is in producing shear data. Although the Oldroyd-B and Boger fluids are far from the industrial fluids of polymer type that offer shear-thinning viscosity, they are nonetheless satisfactory in many problems. A major drawback of the Oldroyd-B type models resides in their wrong behavior for extensional flows.

5.7.1 Oldroyd-B Models

The Oldroyd-B equation is a fundamental building block of non-Newtonian modeling. Here it is assumed that the polymers are diluted in a Newtonian solvent so that the Cauchy stress tensor is split into two parts

$$\boldsymbol{\Sigma} = -p\boldsymbol{I} + 2\mu_0\boldsymbol{D} + \boldsymbol{\Xi}_v , \tag{5.51}$$

where the first part is the Newtonian solvent which consists of an isotropic part and a deviatoric part characterized by viscosity μ_0 and the second part, the viscoelastic stress, characterized by the viscosity μ_1 (cf. Eq. (1.9)). Now consider a generalization of the simple 1D Maxwell model in Eq. (5.9) by replacing $\boldsymbol{\Sigma}$ with the stress $\boldsymbol{\Xi}_v$ and the strain rate by the rate of deformation tensor $\boldsymbol{D}$. This yields a transport equation for $\boldsymbol{\Xi}_v$ given by

$$\boldsymbol{\Xi}_v + \lambda\frac{D\boldsymbol{\Xi}_v}{Dt} = 2\mu_1\boldsymbol{D} . \tag{5.52}$$

In order to ensure the objectivity of Eq. (5.52), an objective stress rate needs to be introduced. The Oldroyd-B fluid constitutive equation is obtained by replacing

the material time derivative of the extra-stress in (5.52) with the Oldroyd upper-convected derivative (4.33a),

$$\boldsymbol{\Xi}_v + \lambda \overset{\nabla}{\boldsymbol{\Xi}}_v = 2\mu_1 \boldsymbol{D} \,, \tag{5.53}$$

or

$$\boldsymbol{\Xi}_v + \lambda \left(\frac{D\boldsymbol{\Xi}_v}{Dt} - \boldsymbol{L}\boldsymbol{\Xi}_v - \boldsymbol{\Xi}_v \boldsymbol{L}^T \right) = 2\mu_1 \boldsymbol{D} \,, \tag{5.54}$$

where $\boldsymbol{L}$ is the velocity gradient tensor $\nabla \mathbf{v}$.

Maxwell only wrote a model for linear viscoelasticity; however it is customary to call the model corresponding to the relation (5.51), with $\mu_0 = 0$, and coupled with Eq. (5.54), the upper-convected Maxwell (UCM) model. It has the same drawbacks as the Oldroyd-B model, but since it contains one parameter less, it is sometimes more tractable from an analytical and/or numerical standpoint.

5.7.1.1 Jeffreys Model

A more general Oldroyd-B fluid is based on the objective tensor representation of the Jeffreys fluid (Jeffreys 1976). Generalizing Eq. (5.20), one obtains

$$\boldsymbol{\Xi}_v + \lambda_1 \overset{\nabla}{\boldsymbol{\Xi}}_v = 2\mu_1 \left(\boldsymbol{D} + \lambda_2 \overset{\nabla}{\boldsymbol{D}} \right) \,. \tag{5.55}$$

For the problem of steady plane shear flow (see Sect. 5.5.3), Eq. (5.55) yields the stress components

$$\Xi_{v,xx} = 2\mu_1(\lambda_1 - \lambda_2)\dot{\gamma}^2, \quad \Xi_{v,yy} = \Xi_{v,zz} = 0, \quad \Xi_{v,xy} = \mu_1 \dot{\gamma} \,, \tag{5.56}$$

which show a quadratic first normal stress difference $N_1 = 2\mu_1(\lambda_1 - \lambda_2)\dot{\gamma}^2$ in the shear rate and a vanishing second normal stress difference $N_2 = 0$ (cf. Eq. (5.40)). The corresponding normal stress differences for Eq. (5.54) follow immediately with $\lambda_2 = 0$ and $\lambda_1 = \lambda$.

5.7.1.2 Explicit Algebraic Extra-stress Model

In Sect. 5.5 it was shown that a viable constitutive equation for a simple fluid could be extracted from a polynomial representation for the deviatoric part of the stress field using the Rivlin-Ericksen tensors. In this section a procedure is outlined that can be used to generate another explicit polynomial representation of the material stress field but now directly from differential constitutive equations.

The starting point is a differential rate equation describing the evolution of the material stress field, such as for the Oldroyd-B fluid. In principle, extension to other differential stress rate equations is possible; although, each may require some added approximations/assumptions in order to construct a viable polynomial representation. The foundation for the procedure to be followed is analogous to that followed

in turbulence modeling, and requires the imposition of a suitably defined equilibrium condition on a measure of the anisotropy of the material stress rate. The procedure to be shown here has its origins in an initial study by Pope (1975) for two-dimensional flows. It was extended to three-dimensional flows by Gatski and Speziale (1993) and has subsequently been further refined in turbulent flow modeling studies that will be discussed in Sect. 6.5. For viscoelastic fluids, it was originally applied by Mompean et al. (1998) and has been further analyzed in numerous other studies (Mompean 2002, Mompean et al. 2003, 2011; Jongen and Gatski 2005; Mompean and Thais 2007) for the case of two-dimensional flow fields.

For the Oldroyd-B fluid, Eq. (5.54) can be written as

$$\boldsymbol{\Xi}_v + \lambda \left[\frac{D\boldsymbol{\Xi}_v}{Dt} - (\boldsymbol{\Xi}_v \boldsymbol{D} + \boldsymbol{D}\boldsymbol{\Xi}_v) + (\boldsymbol{\Xi}_v \boldsymbol{W} - \boldsymbol{W}\boldsymbol{\Xi}_v) \right] = 2\mu_1 \boldsymbol{D} \,, \tag{5.57}$$

where the velocity gradient tensor has been partitioned into its symmetric, $\boldsymbol{D}$, and skew-symmetric, $\mathbf{W}$, parts. The associated deviatoric part of the viscoelastic stress is then given by

$$\boldsymbol{\Gamma}_v = \boldsymbol{\Xi}_v - \frac{\{\boldsymbol{\Xi}_v\}}{3} \boldsymbol{I} \,. \tag{5.58}$$

The corresponding equation for the trace, $\{\boldsymbol{\Xi}_v\}$, then immediately follows from Eq. (5.57) as

$$\frac{D\{\boldsymbol{\Xi}_v\}}{Dt} = -\frac{\{\boldsymbol{\Xi}_v\}}{\lambda} + 2\{\boldsymbol{\Gamma}_v \boldsymbol{D}\} \,, \tag{5.59}$$

where $\{\mathbf{D}\} = 0$ has been used due to the restriction to incompressible (isochoric) motions. In terms of $\boldsymbol{\Gamma}_v$, Eq. (5.57) can be rewritten as

$$\begin{aligned} \frac{D\boldsymbol{\Gamma}_v}{Dt} = &-\frac{\boldsymbol{\Gamma}_v}{\lambda} + \left(\boldsymbol{D}\boldsymbol{\Gamma}_v + \boldsymbol{\Gamma}_v \boldsymbol{D} - \frac{2}{3}\{\boldsymbol{\Gamma}_v \boldsymbol{D}\}\boldsymbol{I} \right) - (\boldsymbol{\Gamma}_v \boldsymbol{W} - \boldsymbol{W}\boldsymbol{\Gamma}_v) \\ &+ 2\left(\frac{\{\boldsymbol{\Xi}_v\}}{3} + \frac{\mu_1}{\lambda} \right) \boldsymbol{D} \,, \end{aligned} \tag{5.60}$$

where Eq. (5.59) has been used. Although the viscoelastic extra-stress tensor anisotropy can be easily formed from the deviatoric tensor $\boldsymbol{\Gamma}$,

$$\boldsymbol{b}_v = \frac{\boldsymbol{\Gamma}}{\{\boldsymbol{\Xi}_v\}} \,, \tag{5.61}$$

it should be cautioned that, as Eqs. (5.59) and (5.60) show, in the absence of any mean velocity gradients, the anisotropy rate $D\boldsymbol{b}_v/Dt$ vanishes leaving $\boldsymbol{b}_v$ constant and only dependent on the initial value of $\boldsymbol{\Xi}_v$. In light of this initial value dependence, the formulation is based on the deviatoric viscoelastic $\boldsymbol{\Gamma}_v$, but with reference and utilization of the anisotropy $\boldsymbol{b}_v$ where necessary.

Implicit Algebraic Formulation: Equilibrium Condition As a practical matter, useful explicit algebraic representations for the viscoelastic extra-stress can only be constructed in the limit of a suitable equilibrium state that eliminates the dependence on the convective transport of the extra-stress field. Additionally, an underlying constraint is to retain the objectivity of any equation describing the behavior of

the viscoelastic stress since the MFI principle needs to hold and no frame-dependent influences can be introduced. This suggests that Eq. (5.60) be recast using only objective rate operators so that the imposition of equilibrium conditions would not violate any objectivity requirements.

As was discussed in Sect. 4.3.2, a variety of objective rate operators exist including the convective rate, $\overset{\nabla}{\boldsymbol{\Xi}}_v$ used in Eq. (5.57) for the Oldroyd-B fluid. It is easy to see from Eq. (4.36) that imposition of an equilibrium condition associated with the non-objective material rate operator D/Dt could be problematic since it could render the modified rate operator $\overset{\nabla}{\boldsymbol{\Xi}}_v$ non-objective. This potential problem can be avoided by recasting the material rate operator D/Dt in terms of an objective rate operator that can account for frame rotation effects. In Sect. 4.3.2, three objective rate operators where presented. Both the Oldroyd upper convective rate and the Jaumann rate operators have a basis in the relative deformation rate tensor and inherently both involve a measure of the rate of change of rotation of a fluid element $\mathbf{W}$. In light of this, any recasting of the material D/Dt in terms of the Jaumann rate would not introduce an independent rate measure into the formulation. As Eq. (4.37) showed, the rate of change of rotation given by $\boldsymbol{W}$ is a composite of the rate of rotation and the rate of stretch of the fluid element. These effects of stretch and rotation are isolated in the third objective rate operator discussed, the Harnoy stress rate. This is done by considering a frame fixed in the principal axes of the rate of strain tensor. In such axes, the fluid element motion is divided between the rate of change of the principal stretches and the rate of rotation of the principal directions. Recasting material rate D/Dt in terms of the Harnoy rate operator then introduces an independent measure (the rate of rotation of the principal directions) into the formulation.

Rewriting Eq. (4.49) as

$$\frac{D\boldsymbol{\Xi}_v}{Dt} = \frac{\mathcal{D}_H \boldsymbol{\Xi}_v}{\mathcal{D}t} + \boldsymbol{\Omega}\boldsymbol{\Xi}_v - \boldsymbol{\Xi}_v\boldsymbol{\Omega} \tag{5.62}$$

and substituting into Eq. (5.60) yields

$$\begin{aligned}\frac{\mathcal{D}_H \boldsymbol{\Gamma}_v}{\mathcal{D}t} = &-\frac{\boldsymbol{\Gamma}_v}{\lambda} + \left(\boldsymbol{D}\boldsymbol{\Gamma}_v + \boldsymbol{\Gamma}_v\boldsymbol{D} - \frac{2}{3}\{\boldsymbol{\Gamma}_v\boldsymbol{D}\}\boldsymbol{I}\right) - \left(\boldsymbol{\Gamma}_v\overline{\boldsymbol{W}} - \overline{\boldsymbol{W}}\boldsymbol{\Gamma}_v\right) \\ &+ 2\left(\frac{\{\boldsymbol{\Xi}_v\}}{3} + \frac{\mu_1}{\lambda}\right)\boldsymbol{D}\,,\end{aligned} \tag{5.63}$$

where $\overline{\boldsymbol{W}} = \boldsymbol{W} - \boldsymbol{\Omega}$ is an objective intrinsic rate of rotation tensor, and $\boldsymbol{\Omega}$ is the rate of rotation of the rate of strain eigenvectors. As formulated, Eq. (5.63) retains its objective transformation properties.

In developing algebraic representations, some approximation has to be made to the stress rate appearing in Eq. (5.63). As dynamically weak a condition on the stress rate is optimal since it will hopefully yield the least constrained constitutive equation. In developing algebraic representations for the turbulent stress tensor (Pope 1975), an equilibrium condition on the turbulent anisotropy stress rate has been applied (vanishing of the anisotropy stress rate). This condition is representative of the dynamic behavior of the turbulent anisotropy stress in homogeneous flow

when subjected to a constant mean shear over several turbulent time scales, and is weaker than imposing a similar constraint on the stress field itself.

In terms of the Harnoy extra-stress rate, Eq. (5.63) can be written as

$$\{\boldsymbol{\Xi}_v\}\frac{\mathcal{D}_H \boldsymbol{b}_v}{\mathcal{D}t} = -2\left(\frac{\{\boldsymbol{\Gamma}_v \boldsymbol{D}\}}{\{\boldsymbol{\Xi}_v\}}\right)\boldsymbol{\Gamma}_v + \left(\boldsymbol{D}\boldsymbol{\Gamma}_v + \boldsymbol{\Gamma}_v\boldsymbol{D} - \frac{2}{3}\{\boldsymbol{\Gamma}_v\boldsymbol{D}\}\boldsymbol{I}\right) - \left(\boldsymbol{\Gamma}_v\overline{\boldsymbol{W}} - \overline{\boldsymbol{W}}\boldsymbol{\Gamma}_v\right) + 2\left(\frac{\{\boldsymbol{\Xi}_v\}}{3} + \frac{\mu_1}{\lambda}\right)\boldsymbol{D}\,, \tag{5.64}$$

where $\mathcal{D}_H\{\boldsymbol{\Xi}_v\}/\mathcal{D}t = D\{\boldsymbol{\Xi}_v\}/Dt$ has been used as well as Eq. (5.59). As suggested, it is assumed that a dynamic equilibrium is reached when $\mathcal{D}_H \boldsymbol{b}_v/\mathcal{D}t = 0$, and the equilibrium extra-stress represented by $\boldsymbol{\Gamma}_v$ is described by the implicit algebraic equation

$$a_0\boldsymbol{\Gamma}_v - a_1\boldsymbol{D} - \left(\boldsymbol{D}\boldsymbol{\Gamma}_v + \boldsymbol{\Gamma}_v\boldsymbol{D} - \frac{2}{3}\{\boldsymbol{\Gamma}_v\boldsymbol{D}\}\boldsymbol{I}\right) + \left(\boldsymbol{\Gamma}_v\overline{\boldsymbol{W}} - \overline{\boldsymbol{W}}\boldsymbol{\Gamma}_v\right) = 0\,, \tag{5.65}$$

where

$$a_0 = 2\{\boldsymbol{b}_v\boldsymbol{D}\} \qquad \text{and} \qquad a_1 = 2\left(\frac{\{\boldsymbol{\Xi}_v\}}{3} + \frac{\mu_1}{\lambda}\right)\,. \tag{5.66}$$

The vanishing of $\mathcal{D}_H \boldsymbol{b}_v/\mathcal{D}t$ implies that the extra-stress anisotropy reaches an equilibrium (constant) value in a frame moving with the principal directions of the rate of strain. In this context, it is important to recall that the Harnoy derivative is only dependent on the rate of the change of the principal directions, and that in flow fields where the principal directions remain fixed $\mathcal{D}_H/\mathcal{D}t = D/Dt$. The relation between $\boldsymbol{\Gamma}_v$, $\boldsymbol{D}$ and $\overline{\boldsymbol{W}}$ remains isotropic and material frame indifferent, so that the construction of an explicit representation for $\boldsymbol{\Gamma}_v$ will depend on the objective tensors $\boldsymbol{D}$ and $\overline{\boldsymbol{W}}$.

Extra-stress Representation from Invariant Basis From Eq. (5.65), the requirement is to identify a suitable invariant basis from which to construct a representation for a symmetric tensor function, $\boldsymbol{\Gamma}_v$, of a symmetric, $\boldsymbol{D}$, and (objective) skew-symmetric tensor, $\overline{\boldsymbol{W}}$. Such an invariant and associated tensor basis have been identified in Sect. 2.4.1.2. It was shown that the expansion coefficient integrity basis invariants were given in Eq. (2.68), and the associated basis tensors given in Eq. (2.70) (for the particular case here, $\mathbf{A} = \boldsymbol{D}$ and $\mathbf{X} = \overline{\boldsymbol{W}}$). As noted previously, the development of explicit extra-stress representations has been based on the exact relationships established for two-dimensional velocity fields with

$$[D] = \begin{pmatrix} D_{11} & D_{12} & 0 \\ D_{12} & -D_{11} & 0 \\ 0 & 0 & 0 \end{pmatrix}, \quad \left[\overline{W}\right] = \begin{pmatrix} 0 & \overline{W}_{12} & 0 \\ -\overline{W}_{12} & 0 & 0 \\ 0 & 0 & 0 \end{pmatrix}, \tag{5.67}$$

where the trace of each vanishes, and the symmetric and skew-symmetric properties of $\boldsymbol{D}$ and $\overline{\boldsymbol{W}}$ have been introduced. For such a two-dimensional flow, the higher-degree basis tensors $k \geq 4$ in Eq. (2.70) can be rewritten in terms of the basis tensors $\boldsymbol{\Phi}_1$, $\boldsymbol{\Phi}_2$, and $\boldsymbol{\Phi}_3$. In terms of $\boldsymbol{D}$ and $\overline{\boldsymbol{W}}$ and the two-dimensional case here,

the expansion coefficients can be functions of the 3 invariants ($\{\boldsymbol{D}\} = 0$, isochoric motions)

$$\operatorname{tr} \boldsymbol{D}^2, \quad \operatorname{tr} \overline{\boldsymbol{W}}^2, \quad \operatorname{tr}(\boldsymbol{D}^2 \overline{\boldsymbol{W}}^2) \,, \tag{5.68}$$

with the corresponding three-term tensor basis $\boldsymbol{\Phi}_k$[1] given by

$$\boldsymbol{\Phi}_1 = \boldsymbol{D}, \qquad \boldsymbol{\Phi}_2 = \boldsymbol{D}\overline{\boldsymbol{W}}, \qquad \boldsymbol{\Phi}_3 = \boldsymbol{D}^2 - \frac{\{\boldsymbol{D}^2\}}{3}\boldsymbol{I} \,, \tag{5.69}$$

where the trace has been subtracted out to ensure that each basis tensor term is traceless. For a complete representation of $\boldsymbol{b}_v$ for a two-dimensional flow, the polynomial representation will include the basis tensors in Eq. (5.69) such that

$$\boldsymbol{\Gamma} = \frac{I_k}{2} \sum_{k=1}^{3} \left(\boldsymbol{\Phi}_k + \boldsymbol{\Phi}_k^T \right) = I_k \sum_{k=1}^{3} \boldsymbol{T}_k \,, \tag{5.70}$$

with the expansion coefficients I_k, in general, being functions of the three invariants given in Eq. (5.68). There are different, though equivalent, approaches that can be followed in obtaining the respective expansion coefficients I_k. Here, the approach used by Pope (1975) is applied, but the reader is referred to Mompean et al. (1998, 2003) for an alternative approach.

Since the basis tensors formed from those in Eq. (5.69) are linearly independent, each term in Eq. (5.65) can be represented by a polynomial expansion, so that in addition to the representation for $\boldsymbol{\Gamma}_v$ given in Eq. (5.70), the representation for the remaining two terms are

$$\boldsymbol{T}_k \boldsymbol{D} + \boldsymbol{D}\boldsymbol{T}_k - \frac{2}{3}\{\boldsymbol{T}_k \boldsymbol{D}\}\boldsymbol{I} = \sum_{\gamma=1}^{3} H_{k\gamma} \boldsymbol{T}_\gamma \,, \tag{5.71a}$$

$$\boldsymbol{T}_k \overline{\boldsymbol{W}} - \overline{\boldsymbol{W}} \boldsymbol{T}_k = \sum_{\gamma=1}^{3} J_{k\gamma} \boldsymbol{T}_\gamma \,. \tag{5.71b}$$

Substitution of the polynomial expansions given in Eqs. (5.70) and (5.71a), (5.71b) into Eq. (5.65) yields a 3×3 linear system of equations for the expansion coefficients given by

$$a_0 \sum_{k=1}^{3} I_k \boldsymbol{T}_k - \sum_{k=1}^{3} I_k \sum_{\gamma=1}^{3} H_{k\gamma} \boldsymbol{T}_\gamma + \sum_{k=1}^{3} I_k \sum_{\gamma=1}^{3} J_{k\gamma} \boldsymbol{T}_\gamma = a_1 \boldsymbol{D} \,, \tag{5.72}$$

or in the form

$$\left[a_0 \delta_{\gamma k} - H_{\gamma k} + J_{\gamma k} \right] I_k = a_1 \delta_{\gamma 1}, \qquad k, \gamma = 1, 2, 3 \,, \tag{5.73}$$

[1] For the two-dimensional case, the basis tensor $\boldsymbol{\Phi}_3$ is reduced to the form

$$\boldsymbol{\Phi}_3 \propto \frac{\boldsymbol{I}^{(2)}}{2} - \frac{\boldsymbol{I}}{3} \,,$$

by the Cayley-Hamilton theorem where $\boldsymbol{I}^{(2)}$ is the two-dimensional Kronecker delta.

with

$$[H_{k\gamma}] = \begin{pmatrix} 0 & 0 & -\frac{1}{3}\{\boldsymbol{D}^2\} \\ 0 & 0 & 0 \\ -2 & 0 & 0 \end{pmatrix}, \quad [J_{k\gamma}] = \begin{pmatrix} 0 & 2\{\overline{\boldsymbol{W}}^2\} & 0 \\ 1 & 0 & 0 \\ 0 & 0 & 0 \end{pmatrix}. \tag{5.74}$$

The solution of this system of equations gives

$$I_1 = a_0 a_1 \left[a_0^2 - 2\{\overline{\boldsymbol{W}}^2\} - \frac{2}{3}\{\boldsymbol{D}^2\} \right]^{-1}, \quad I_2 = -\frac{I_1}{a_0}, \quad I_3 = \frac{2I_1}{a_0}. \tag{5.75}$$

It is important to recognize at this point that the representation, as constructed, using the I_k values just obtained is not fully explicit. From Eq. (5.66), it is seen that the coefficient a_0 has a dependency on the extra-stress anisotropy $\boldsymbol{b}_v$ and is then inherently coupled to the representation just extracted for $\boldsymbol{\Gamma}_v$. The representation can be made fully explicit by forming the invariant $\{\boldsymbol{b}_v \boldsymbol{D}\}$ using the representation given in Eq. (5.70),

$$\{\boldsymbol{\Xi}_v\}\{\boldsymbol{b}_v \boldsymbol{D}\} = \sum_{k=1}^{3} I_k \{\boldsymbol{T}_k \boldsymbol{D}\}, \tag{5.76}$$

and solving the resulting polynomial equation for $\{\boldsymbol{b}_v \boldsymbol{D}\}$ in terms of the flow invariants given in Eq. (5.68). This results in a quadratic equation for $\{\boldsymbol{b}_v \boldsymbol{D}\}$ given by

$$2\{\boldsymbol{\Xi}_v\}\{\boldsymbol{b}_v \boldsymbol{D}\}^2 - \left[\{\boldsymbol{\Xi}_v\}\{\overline{\boldsymbol{W}}^2\} + \{\boldsymbol{\Xi}_v\}\{\boldsymbol{D}^2\} + \frac{2\mu_1}{\lambda}\{\boldsymbol{D}^2\} \right] = 0, \tag{5.77}$$

where Eqs. (5.66) and (5.75) have been used. It follows that

$$\{\boldsymbol{\Xi}_v\}\{\boldsymbol{b}_v \boldsymbol{D}\} = +\sqrt{\frac{\{\boldsymbol{\Xi}_v\}^2}{2}\left(\{\overline{\boldsymbol{W}}^2\} + \{\boldsymbol{D}^2\}\right) + \left(\frac{\mu_1}{\lambda}\right)\{\boldsymbol{\Xi}_v\}\{\boldsymbol{D}^2\}}, \tag{5.78}$$

where the positive root is chosen (Mompean et al. 1998) based on the analogy with the turbulent stress anisotropy equations and using a dynamical systems analysis of the corresponding equilibrium states (Jongen and Gatski 1999).

5.7.2 Improved Rate Type Models

The Oldroyd-B type models presented in Sect. 5.7.1 suffer from several deficiencies: such as lack of shear-thinning behavior and unbounded extensional viscosity. There have been many constitutive equations that add an extra term to the Oldroyd-B fluid in order to overcome these defects, and these have the generic form

$$\boldsymbol{\Xi}_v + \lambda \overset{\nabla}{\boldsymbol{\Xi}}_v + \boldsymbol{f}(\boldsymbol{\Xi}_v, \boldsymbol{D}) = 2\mu_1 \boldsymbol{D}. \tag{5.79}$$

5.7.2.1 Giesekus Model

The Giesekus model (Giesekus 1966, 1982) introduces a quadratic nonlinearity that represent a drag force in order to keep the extensional viscosity at a finite level when the extensional rate increases, namely

$$\boldsymbol{f}(\boldsymbol{\Xi}_v, \boldsymbol{D}) = \alpha\, \boldsymbol{\Xi}_v^2 \,, \tag{5.80}$$

where $0 \leq \alpha \leq 1$.

5.7.2.2 Phan-Thien Tanner Model

The Phan-Thien Tanner (PTT) model (Phan-Thien and Tanner 1977) is written with

$$\boldsymbol{f}(\boldsymbol{\Xi}_v, \boldsymbol{D}) = (Y\{\boldsymbol{\Xi}_v\} - \boldsymbol{I})\, \boldsymbol{\Xi}_v + \lambda\xi\, (\boldsymbol{\Xi}_v \boldsymbol{D} + \boldsymbol{D}\boldsymbol{\Xi}_v) \,, \tag{5.81}$$

where $Y\{\boldsymbol{\Xi}_v\}$ takes the exponential form

$$Y\{\boldsymbol{\Xi}_v\} = \exp\left[\frac{\varepsilon\lambda}{\mu_1}\{\boldsymbol{\Xi}_v\}\right] \,, \tag{5.82}$$

or the linearized version (LPPT)

$$Y\{\boldsymbol{\Xi}_v\} = 1 + \frac{\varepsilon\lambda}{\mu_1}\{\boldsymbol{\Xi}_v\} \,. \tag{5.83}$$

The two parameters ξ and ε control the shear-thinning effect and, additionally, ε removes the singularity of the extensional viscosity.

5.7.3 Relation Between Rate Type and Integral Models

Numericists prefer to tackle differential equations rather than integral equations, and for these constitutive equations it is possible to transform one form into another. As an example, consider the Lodge equation, Eq. (5.30). To this end, the rate of change of Eq. (5.30) is taken,

$$\begin{aligned}
\frac{\mathrm{d}\boldsymbol{\Sigma}}{\mathrm{d}t} &= \frac{\mathrm{d}}{\mathrm{d}t}\left[\frac{G}{\lambda}\int_{-\infty}^{t} e^{-\frac{(t-\tau)}{\lambda}} \boldsymbol{C}_{(t)}^{-1}(\tau)\mathrm{d}\tau\right] \\
&= \frac{G}{\lambda}\boldsymbol{C}_{(t)}^{-1}(t) - \frac{G}{\lambda^2}\int_{-\infty}^{\tau} e^{-\frac{(t-\tau)}{\lambda}} \boldsymbol{C}_{(t)}^{-1}\mathrm{d}\tau + \frac{G}{\lambda}\int_{-\infty}^{\tau} e^{-\frac{(t-\tau)}{\lambda}} \frac{\partial\, \boldsymbol{C}_{(t)}^{-1}}{\partial t} d\tau \\
&= \frac{G}{\lambda}\boldsymbol{I} - \frac{\boldsymbol{\Sigma}}{\lambda} + \boldsymbol{L}\boldsymbol{\Sigma} + \boldsymbol{\Sigma}\boldsymbol{L}^T \,,
\end{aligned} \tag{5.84}$$

where $\boldsymbol{C}_{(t)}^{-1}(t) = \boldsymbol{I}$ and

$$\frac{\partial\, \boldsymbol{C}_{(t)}^{-1}}{\partial t} = \boldsymbol{L}\boldsymbol{C}_{(t)}^{-1} + \boldsymbol{C}_{(t)}^{-1}\boldsymbol{L}^T \,, \tag{5.85}$$

have been used. Collecting all the terms in (5.84), the upper convected Maxwell model is retrieved

$$\boldsymbol{\Sigma} + \lambda \overset{\nabla}{\boldsymbol{\Sigma}} = G\boldsymbol{I} \ , \tag{5.86}$$

and the Oldroyd-B model, Eq. (5.53), results from the change of variables $\boldsymbol{\Xi}_v = \boldsymbol{\Sigma} - G\boldsymbol{I}$ in Eq. (5.86), with $G\lambda = \mu_1$ and the use of Eq. (4.35).

5.8 Dumbbell Models

Soon after the introduction of the models presented up to this point, it was recognized that they were too "mechanical"—in the sense they were tensor generalizations of simple (crude?) mechanical structures made by assembling springs and dashpots. Therefore, the conclusion was quite evident: let us go down, for example, to the nanoscale. Even though some researchers invoking the small values of the Knudsen number claim that the continuum approach holds until a scale close to 10 nm, it does not make sense to work at this level. The intent consists indeed in designing a model that is computationally tractable and efficient, and that takes some microstructure peculiarities into account, say, at a mesoscopic level. This criterion automatically precludes all attempts to perform a molecular dynamics simulation, since it would be out of reach even to attempt the evolution of a single polymer chain. The complexity of the micro-structural description is reduced by a statistical mechanics argument. In this section, pedestrian approach that was first presented by Wilson (2011) is deliberately adopted leaving a more rigorous presentation for a later section.

5.8.1 Rouse Model

Assume that at position $\mathbf{x}$, a polymer chain is composed of $N+1$ beads connected by simple rods (without mass), each of length b (see Fig. 5.5). This simple model resembles a surveyor's chain. The beads may rotate with respect to each other but they do not deform. The end-to-end vector, denoted by $\mathbf{r}$ connects the extreme beads at the end of the chain, and is the relevant variable expressing the statistical behavior of the complete chain. It can be proved (Phan-Thien 2002) that the probability to have a chain of length $\mathbf{r}$ is given by a Gaussian function

$$P(\mathbf{r}) = \left(\frac{3}{2\pi N b^2}\right)^{3/2} \exp\left(\frac{-3r^2}{2Nb^2}\right) \ , \tag{5.87}$$

where the connector has zero mean, $<\mathbf{r}> = 0$ ($< >$ implies a mean or ensemble average of the statistical variable), and a mean square such that $<\mathbf{r}\cdot\mathbf{r}> = <r^2> = Nb^2$.

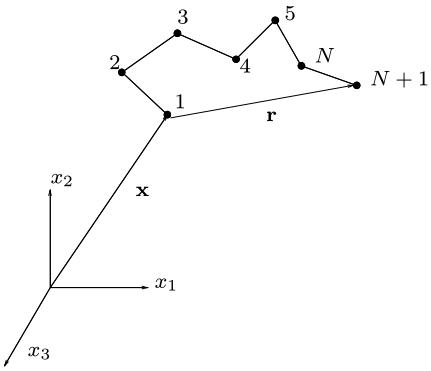

Fig. 5.5 Polymer as chain of beads

5.8.2 The Hookean Dumbbell

The elastic dumbbell model corresponds to the particular case of the Rouse model with $N = 1$ (two beads) as shown in Fig. 5.6. In order to obtain a deformable structure, it is assumed that the two beads are spheres connected by a linear spring. This spring is no longer of a mechanical nature since the Newton forces are exerted at the (lower) atomic level, but this is now an entropic spring. Indeed, if the chain is extended to full length $|\mathbf{r}| = Nb$, the polymer will try to recoil and to collapse to a zero end-to-end vector. Therefore, the number of possible chain configurations is by far more numerous than the one case of full extension. This physical process is driven by entropy, which by the second law of thermodynamics, always increases. Entropy will, therefore, produce shorter chains than longer ones. With the definition of the free energy F given by (cf. Sect. 4.4.1)

$$F(\mathbf{r}) = e(\theta) - k_B\theta \ln P(\mathbf{r}) \tag{5.88}$$

where e is the internal energy, k_B the Boltzmann constant and θ the absolute temperature, a variation $\mathrm{d}\mathbf{r}$ of chain length changes the free energy by the amount

$$\mathrm{d}F = -k_B\,\theta\,\mathrm{d}\ln P(\mathbf{r}) = \frac{3k_B\theta}{Nb^2}\mathbf{r}\cdot\mathrm{d}\mathbf{r}\,, \tag{5.89}$$

where the second equality is obtained using Eq. (5.87), and the phenomenon occurs at a constant temperature giving a constant e. Thus, the chain free energy F changes only through the spring force, that is

$$\mathrm{d}F = \mathbf{f}(\mathbf{r})\cdot\mathrm{d}\mathbf{r}\,, \tag{5.90}$$

such that the spring force is

$$\mathbf{f}(\mathbf{r}) = \frac{3k_B\theta}{Nb^2}\mathbf{r} := k_s\mathbf{r}\,, \tag{5.91}$$

with stiffness $k_s = 3k_B\,\theta/Nb^2$. A careful inspection of the previous relations, particularly Eqs. (5.88) and (5.91), shows that the entropic spring force is proportional to the gradient of $\ln P$ with respect to $\mathbf{r}$; more precisely, for bead i,

$$\mathbf{f}_i = -k_B\,\theta\frac{\partial \ln P}{\partial \mathbf{r}_i}\,. \tag{5.92}$$

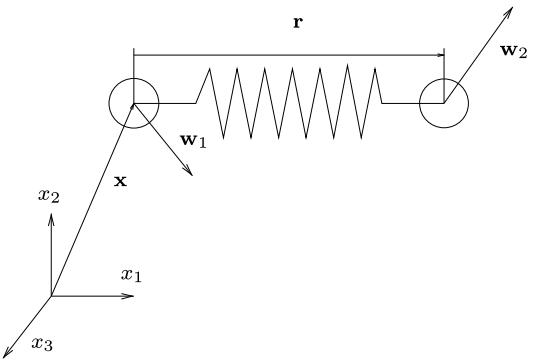

Fig. 5.6 Elastic dumbbell

This is completely consistent at this stage since P is the stationary solution of the dynamic equation written for the pdf of $\mathbf{r}$ when the surrounding solvent flows around the polymer chain and generates a velocity field.

5.8.3 Drag Force

As the polymer chain is immersed in the Newtonian solvent, the two spherical beads of radius a are subjected to Stokes drag forces. By assuming a low Reynolds number flow, the drag force is the result of the integration of the pressure and viscous forces on the spherical surface yielding the relation

$$F_D = 6\pi\mu_0 a U \ , \tag{5.93}$$

where U represents the free stream velocity approaching the solid body. The first bead at position $\mathbf{x}$ moves with the velocity $\mathbf{w}_1$ in the surrounding fluid flowing with the local velocity $\mathbf{v}(\mathbf{x})$, while the second bead at $\mathbf{x}+\mathbf{r}$ travels at velocity $\mathbf{w}_2$ in a fluid at velocity $\mathbf{v}(\mathbf{x}+\mathbf{r})$. The total force on the first bead is given by

$$\frac{3k_B\theta}{a^2}\mathbf{r} + 6\pi\mu_0 a(\mathbf{v}(\mathbf{x}) - \mathbf{w}_1) = 0 \ , \tag{5.94}$$

since the bead is in mechanical equilibrium. This yields for the bead velocity

$$\mathbf{w}_1 = \frac{k_B\theta}{2\pi\mu_0 a^3}\mathbf{r} + \mathbf{v}(\mathbf{x}) \ . \tag{5.95}$$

On the second bead, the spring force has the opposite sign and this leads to

$$\mathbf{w}_2 = -\frac{k_B\theta}{2\pi\mu_0 a^3}\mathbf{r} + \mathbf{v}(\mathbf{x}+\mathbf{r}) \ . \tag{5.96}$$

Using the definition $\mathbf{w}_i = \mathrm{d}(\mathbf{x} + (i-1)\mathbf{r})/\mathrm{d}t$, $i = 1, 2$, the dynamic equation for $\mathbf{r}$ reads

$$\frac{\mathrm{d}\mathbf{r}}{\mathrm{d}t} = \mathbf{w}_2 - \mathbf{w}_1 = -\frac{k_B\theta}{\pi\mu_0 a^3}\mathbf{r} + \mathbf{v}(\mathbf{x}+\mathbf{r}) - \mathbf{v}(\mathbf{x}) \ . \tag{5.97}$$

By truncating the Taylor series of $\mathbf{v}(\mathbf{x}+\mathbf{r})$ with respect to $\mathbf{r}$ at second-order ($\mathbf{r}$ is small compared to the macroscopic scales involved by the changing velocity $\mathbf{v}$), the following relation ensues

$$\frac{\mathrm{d}\mathbf{r}}{\mathrm{d}t} = -\frac{k_B\theta}{\pi\mu_0 a^3}\mathbf{r} + \mathbf{r}\cdot\nabla\mathbf{v} = -\frac{k_B\theta}{\pi\mu_0 a^3}\mathbf{r} + \mathbf{r}\boldsymbol{L}\ . \tag{5.98}$$

If the spring force in Eq. (5.98) is discarded for the moment, the equation for $\mathbf{r}$ reduces to

$$\frac{\mathrm{d}\mathbf{r}}{\mathrm{d}t} = \mathbf{r}\boldsymbol{L}\ , \tag{5.99}$$

which defines the affine motion of the connector.

Since the constant $k_B\theta/\pi\mu_0 a^3$ has a dimension of an inverse time, one can write

$$\frac{k_B\theta}{\pi\mu_0 a^3} = \frac{1}{2\lambda}\ , \tag{5.100}$$

where λ is the relaxation time of the dumbbell. Equation (5.98) can then be written as

$$\frac{\mathrm{d}\mathbf{r}}{\mathrm{d}t} = -\frac{\mathbf{r}}{2\lambda} + \mathbf{r}\boldsymbol{L}\ . \tag{5.101}$$

It should be noted that in this analysis the influence of one bead over the flow next to the other one has been completely discarded so that the approach considered here is a one way coupling where the beads do not influence the flow field.

5.8.4 Brownian Motion

Up to now only deterministic forces have been considered. However, due to thermal motion, the beads undergo the impact of the solvent molecules and this phenomenon creates the Brownian force that is highly random and must be represented by a stochastic variable. Consequently, a Brownian motion is included in the model given in Eq. (5.101).

Recall that a Brownian motion is defined through a Wiener process $\mathbf{W}(t)$ with a Gaussian pdf of zero mean and covariance $<\mathbf{W}(t)\mathbf{W}(t')> = \min(t,t')\boldsymbol{I}$. Thermal agitation may be expressed by a diffusion equation with a diffusion coefficient given by the Einstein relation

$$D = \frac{k_B\theta}{N\zeta}\ , \tag{5.102}$$

which is proportional to the variance of the pdf, and ζ is a friction coefficient which for a single particle in a Stokes flow is given by $\zeta = 6\pi\mu_0 a$. The reader may consult the book of Nelson (2001) for a straightforward derivation of the Einstein diffusion equation.

Normalizing the Brownian motion to the identity matrix for the covariance and adopting the convention that the dumbbell length will be unity for a solvent at rest, Eq. (5.101) with the Brownian motion incorporated becomes

$$\mathrm{d}\mathbf{r} = \left(-\frac{\mathbf{r}}{2\lambda} + \mathbf{r}\boldsymbol{L}\right)\mathrm{d}t + \frac{\mathrm{d}\mathbf{W}(t)}{\sqrt{\lambda}}\,, \tag{5.103}$$

where the coefficient $\sqrt{\lambda}$ is a consequence of the normalization.

5.8.5 Dumbbell Stress

In order to obtain the stress in the fluid for the general case of a Newtonian solvent containing a large number of polymer chains, the solvent is assumed to be homogeneous and the polymer chain is regarded as a continuous media. The Cauchy stress is computed as the ensemble average on a volume $\mathcal{V}$

$$<\boldsymbol{\Sigma}(\mathbf{x},t)> = \frac{1}{\mathcal{V}}\int_{\mathcal{V}} \boldsymbol{\Sigma}(\mathbf{x},t)\mathrm{d}\mathcal{V}\,, \tag{5.104}$$

where $\mathcal{V}$ may be decomposed into the solvent volume $\mathcal{V}_s$, and the polymeric volume $\mathcal{V}_p$. It can be shown that the solvent part leads to the classical Newtonian stress tensor involving the pressure, the rate of deformation tensor and the viscosity μ_0. With the chain being considered as a continuum in equilibrium, and with gravity neglected, the condition $\boldsymbol{\nabla}\cdot\boldsymbol{\Sigma} = \mathbf{0}$ must be satisfied.

Now consider the polymeric part, $\boldsymbol{\Xi}_p$ ($\boldsymbol{\Xi}_v$), of the stress tensor $\boldsymbol{\Xi}$. Observing that $\boldsymbol{\Sigma} = \boldsymbol{\nabla}\cdot(\mathbf{x}\boldsymbol{\Sigma})$, the stress induced by the polymer chains is

$$\begin{aligned}\frac{1}{\mathcal{V}}\sum_p\int_{\mathcal{V}_p}\boldsymbol{\Xi}_p\,\mathrm{d}\mathcal{V} &= \frac{1}{\mathcal{V}}\sum_p\int_{\mathcal{V}_p}\boldsymbol{\nabla}\cdot(\mathbf{x}\boldsymbol{\Xi}_p)\,\mathrm{d}\mathcal{V} = \frac{1}{\mathcal{V}}\sum_p\int_{\mathcal{S}_p}\mathbf{x}\boldsymbol{\Xi}_p\cdot\mathbf{n}\mathrm{d}\mathcal{S}\\ &= n_p\int_{\mathcal{S}_p}\mathbf{x}\boldsymbol{\Xi}_p\cdot\mathbf{n}\mathrm{d}\mathcal{S}\,,\end{aligned} \tag{5.105}$$

where the last equality is allowed by the homogeneity hypothesis, with n_p designating the number of polymer chains (per unit volume). The symbol $\mathcal{S}_p$ is the surface area of the beads. Since the product $\boldsymbol{\Xi}_p\cdot\mathbf{n} = \mathbf{t}_p$ is the density of the polymeric contact forces, one can take into account the deterministic and Brownian forces.

The contribution of the average Brownian forces to the polymeric stress is represented by an isotropic tensor that is merged into the pressure term. For the deterministic forces, it is customary to neglect the inertia term so that the spring forces are only left, namely

$$\begin{aligned}\boldsymbol{\Xi}_p &= \sum_{i=1}^{n_p}<\mathbf{f}_i\otimes\mathbf{r}_i> = n_p\,k_s<\mathbf{r}\otimes\mathbf{r}>\\ &= \frac{3\pi\mu_0 b n_p}{2\lambda N}<\mathbf{r}\otimes\mathbf{r}> := H<\mathbf{r}\otimes\mathbf{r}>\,.\end{aligned} \tag{5.106}$$

where Eq. (5.100) has been used, and $\otimes$ denotes the tensor product of two vectors. Introducing the conformation tensor,

$$\boldsymbol{c}(\mathbf{x},t) := <\mathbf{r}(\mathbf{x},t)\otimes\mathbf{r}(\mathbf{x},t)> , \tag{5.107}$$

the constitutive relation for the polymeric stress becomes

$$\boldsymbol{\Xi}_p = H\boldsymbol{c} , \quad H = \frac{3k_B\theta n_p}{Nb^2} . \tag{5.108}$$

To close the system of equations, a dynamic relation is needed for $\boldsymbol{c}$. Based on Itô's lemma (Itô 1951), a first order time scheme is sufficient to carry out the developments of the relevant variables. Considering the conformation tensor at the new position $\mathbf{x}+\mathrm{d}\mathbf{x}$ at the time level $t+dt$, i.e. $\boldsymbol{c}(\mathbf{x}+\mathrm{d}\mathbf{x},t+dt)$ and defining $\mathrm{d}\mathbf{x}=\mathbf{v}(\mathbf{x},t)\mathrm{d}t$, the time scheme is evaluated to order $\mathrm{d}t$

$$\begin{aligned}\boldsymbol{c}(\mathbf{x}+\mathbf{v}(\mathbf{x},t)\mathrm{d}t,t+\mathrm{d}t) &= <\mathbf{r}+\mathrm{d}\mathbf{r}\otimes\mathbf{r}+\mathrm{d}\mathbf{r}> \\ &= <\mathbf{r}\otimes\mathbf{r}> + <\mathbf{r}\otimes\mathrm{d}\mathbf{r}> + <\mathrm{d}\mathbf{r}\otimes\mathbf{r}> + <\mathrm{d}\mathbf{r}\otimes\mathrm{d}\mathbf{r}> .\end{aligned} \tag{5.109}$$

By the definition (5.108), the first term on the right side of Eq. (5.109) is the conformation tensor itself, and using (5.103), the second term yields

$$\begin{aligned}<\mathbf{r}\otimes\mathrm{d}\mathbf{r}> &= <\mathbf{r}\otimes\left(-\frac{\mathbf{r}}{2\lambda}+\mathbf{r}\boldsymbol{L}\right)\mathrm{d}t+\frac{\mathrm{d}\boldsymbol{W}(t)}{\sqrt{\lambda}}> \\ &= <\mathbf{r}\otimes\left(-\frac{\mathbf{r}}{2\tau}+\mathbf{r}\boldsymbol{L}\right)\mathrm{d}t> \\ &= -\frac{\boldsymbol{c}}{2\lambda}\mathrm{d}t+\boldsymbol{c}\boldsymbol{L}^T\mathrm{d}t ,\end{aligned} \tag{5.110}$$

and a similar computation for the third term gives $<\mathrm{d}\mathbf{r}\otimes\mathbf{r}> = -[(\boldsymbol{c}/2\lambda)-\boldsymbol{L}\boldsymbol{c}]\mathrm{d}t$. The fourth term is approximated (neglecting second-order terms in $\mathrm{d}t$) as

$$<\mathrm{d}\mathbf{r}\otimes d\mathbf{r}> = <\frac{\mathrm{d}\boldsymbol{W}(t)}{\sqrt{\lambda}}\otimes\frac{\mathrm{d}\boldsymbol{W}(t)}{\sqrt{\lambda}}> = \frac{\boldsymbol{I}}{\lambda}\mathrm{d}t . \tag{5.111}$$

Correspondingly, expand the left side of Eq. (5.109) as a first-order series in $\mathrm{d}t$ to obtain

$$\boldsymbol{c}(\mathbf{x}+\mathbf{v}(\mathbf{x},t)\mathrm{d}t,t+\mathrm{d}t) = \boldsymbol{c}+\frac{\partial\boldsymbol{c}}{\partial t}\mathrm{d}t+(\mathbf{v}\cdot\nabla)\boldsymbol{c}\,\mathrm{d}t . \tag{5.112}$$

When combined with the previous relations for the right side of Eq. (5.109), the evolution of the conformation tensor is given by the relation

$$\frac{\partial\boldsymbol{c}}{\partial t}+(\mathbf{v}\cdot\nabla)\boldsymbol{c}-\boldsymbol{L}\boldsymbol{c}-\boldsymbol{c}\boldsymbol{L}^T = \overset{\nabla}{\boldsymbol{c}} = -\frac{1}{\lambda}(\boldsymbol{c}-\boldsymbol{I}) . \tag{5.113}$$

The steady-state case ($\mathbf{v}=\mathbf{0}$) yields $\boldsymbol{c}=\boldsymbol{I}$ which, recall, was one of the normalization assumptions. With $\boldsymbol{c}$ known, the polymeric stress $\boldsymbol{\Xi}_p$ is then obtained using Eq. (5.108).

Finally, the dumbbell model, specifically Eq. (5.113), is able to reconstruct the Oldroyd-B model; although, with a different meaning for the main terms of the constitutive relationship. Of course, this new model that would be constructed, would have the same shortcomings as the original Oldroyd-B model.

5.8.6 The Giesekus Model Revisited

Giesekus (1966) dropped the assumption of an isotropic influence of neighboring dumbbells on the dumbbell at hand, and proposed that the environment of the adjacent dumbbells induces an anisotropic drag that is dependent on the orientation. To take this effect into account, one replaces the λ parameter, which is proportional to the drag friction coefficient, in Eqs. (5.100) and (5.113) with an anisotropic mobility tensor $\boldsymbol{B}$ such that

$$\lambda \overset{\nabla}{\boldsymbol{c}} + \boldsymbol{B}\,(\boldsymbol{c} - \boldsymbol{I}) = \boldsymbol{0}\,. \tag{5.114}$$

Since at equilibrium the stress is isotropic, this would imply that $\boldsymbol{B} = \boldsymbol{I}$ with $\boldsymbol{c} = \boldsymbol{I}$. The simplest representation for the anisotropy would be obtained by choosing $\boldsymbol{B}$ proportional to $\boldsymbol{c} - \boldsymbol{I}$,

$$\boldsymbol{B} = \boldsymbol{I} + \alpha(\boldsymbol{c} - \boldsymbol{I})\,. \tag{5.115}$$

Taking Eq. (4.35) into account, and setting $\boldsymbol{\Xi}_v = H(\boldsymbol{c} - \boldsymbol{I})$, one gets

$$\boldsymbol{\Xi}_v + \lambda \overset{\nabla}{\boldsymbol{\Xi}}_v + \frac{\alpha}{H}\boldsymbol{\Xi}_v^2 = 2\lambda H \boldsymbol{D}\,. \tag{5.116}$$

As Eq. (5.116) shows, this Giesekus model is a UCM model comprising a quadratic term that stabilize the model. For $\alpha = 0$, the UCM model is recovered, and for $\alpha = 1$, there is full anisotropy.

5.9 Dumbbells and Stochastic Differential Equations

Dumbbells are in some sense moving particles that are subject to random collisions produced by the neighboring particles and the solvent molecules. The relevant theory to build the methodological framework is related to stochastic differential equations.

5.9.1 The Fokker-Planck Equation

The design of the stochastic differential equation(s) (SDE) starts from the Langevin equation written for each bead of mass m_i and of radius a_i at position $\mathbf{x}_i$, $i = 1, 2$, respectively

$$m_i \frac{\mathrm{d}^2\mathbf{x}_i}{\mathrm{d}t^2} = -\zeta_i \left(\frac{\mathrm{d}\mathbf{x}_i}{\mathrm{d}t} - (\mathbf{v}_0 + \boldsymbol{L}\mathbf{x}_i) \right) + \mathbf{f}_i + \mathbf{B}_i\,, \tag{5.117}$$

where the friction coefficients ζ_i come from the Stokes drag law, $\mathbf{f}_i$ are the spring forces applied to the beads, $\mathbf{B}_i$ the Brownian forces. The homogeneous velocity field is approximated by $\mathbf{v} = \mathbf{v}_0 + \boldsymbol{L}\mathbf{x}_i$, with $\mathbf{v}_0$ a constant velocity field. The connector

length is obtained readily as $\mathbf{r} = \mathbf{x}_2 - \mathbf{x}_1$. The probability of finding the dumbbell length in the interval $[\mathbf{r}, \mathbf{r} + \mathrm{d}\mathbf{r}]$ is provided by $\psi(\mathbf{r}, \mathbf{x}, t)\mathrm{d}\mathbf{r}$ where ψ is the pdf. As suggested by Chandrasekhar (1943), the Brownian forces are obtained from the gradient of the logarithm of the pdf as

$$\mathbf{B}_i = -k_B\theta\nabla_i \ln\psi \ . \tag{5.118}$$

Neglecting the inertia of the beads (i.e. the left side of Eq. (5.117)), and also assuming equal diameters for the beads $a_1 = a_2 = a$, $\mathbf{f}_1 = -\mathbf{f}_2 = \mathbf{f}$ and $\zeta_1 = \zeta_2 = \zeta$, the subtraction of the Langevin equation (5.117) for each bead, yields the dynamic equation for the connector,

$$\frac{\mathrm{d}\mathbf{r}}{\mathrm{d}t} = \boldsymbol{L}\mathbf{r} - 2\frac{k_B\theta}{\zeta}\frac{\partial}{\partial\mathbf{r}}\ln\psi - \frac{2}{\zeta}\mathbf{f} \ . \tag{5.119}$$

Assuming again that the polymer chains behave like a continuum, and taking into account that

$$\int \psi(\mathbf{r}, t)\,\mathrm{d}\mathbf{r} = 1 \ , \tag{5.120}$$

the application of the Reynolds transport theorem produces a conservation law for the probability flux $\dot{\mathbf{r}}\psi$ analogous to the mass conservation law in Eq. (3.72) (for example Larson 1988, Sect. 2.6.1 for a proof),

$$\frac{\partial\psi}{\partial t} + \frac{\partial}{\partial\mathbf{r}}\cdot(\dot{\mathbf{r}}\psi) = 0 \ . \tag{5.121}$$

Multiplying through (5.119) by ψ, taking the derivative with respect to $\mathbf{r}$, and using (5.121), the Smoluchowski equation is obtained

$$\frac{\partial\psi}{\partial t} + \frac{\partial}{\partial\mathbf{r}}\cdot\left(\boldsymbol{L}\mathbf{r}\psi - 2\frac{k_B\theta}{\zeta}\frac{\partial\psi}{\partial\mathbf{r}} - \psi\frac{2}{\zeta}\mathbf{f}\right) = 0 \ . \tag{5.122}$$

Carrying out the divergence evaluation in Eq. (5.122), a diffusion equation for ψ, the Fokker-Planck equation, is then generated

$$\frac{\partial\psi}{\partial t} + \boldsymbol{L}\mathbf{r}\cdot\frac{\partial\psi}{\partial\mathbf{r}} - 2\frac{k_B\theta}{\zeta}\frac{\partial^2\psi}{\partial\mathbf{r}^2} - \frac{2}{\zeta}\frac{\partial}{\partial\mathbf{r}}\cdot(\psi\mathbf{f}) = 0 \ . \tag{5.123}$$

The equation is solved in the so-called configuration space $(\mathbf{r}, t)$ with $\mathbf{x}$ being a parameter. The case of the linear spring corresponds to the fact that every point in the configuration space can be reached. Therefore, the boundary condition is simply $\psi = 0$ for $|\mathbf{r}| \to \infty$. Notice that there is no need to solve the Fokker-Planck equation for ψ. Indeed what is required is a formal solution for $<\mathbf{r}\otimes\mathbf{r}>$ as this quantity leads to the stress tensor.

The stress tensor is again split into the Newtonian solvent part and the polymeric part. The extra-stress is then provided by the following relation known as Kramers equation, where the ensemble average involves the pdf of ψ,

$$\begin{aligned}\boldsymbol{\Xi}(\mathbf{x}, t) &= -n_p k_B\theta\boldsymbol{I} + 2\mu_0\boldsymbol{D} + n_p\int(\mathbf{r}\otimes\mathbf{f}(\mathbf{r}))\,\psi(\mathbf{r}, \mathbf{x}, t)\mathrm{d}\mathbf{r} \\ &= -n_p k_B\theta\boldsymbol{I} + 2\mu_0\boldsymbol{D} + n_p<\mathbf{r}\otimes\mathbf{f}(\mathbf{r})> \ .\end{aligned} \tag{5.124}$$

The isotropic term may be incorporated into the pressure term.

5.9.2 Hookean Dumbbell

The Hookean model built so far may be transformed to obtain a solution in closed form. Indeed, Eq. (5.122) can be multiplied by $\mathbf{r} \otimes \mathbf{r}$ and then ensemble averaged so that the transient term becomes $\partial <\mathbf{r} \otimes \mathbf{r}> / \partial t$. The other terms are transformed using the divergence theorem as many times as necessary, and the surface integral vanishes because of the homogeneous boundary condition. It then follows that

$$\int \mathbf{r} \otimes \mathbf{r} \frac{\partial^2 \psi}{\partial \mathbf{r}^2} \mathrm{d}\mathbf{r} = 2\boldsymbol{I} \,, \tag{5.125}$$

and for the second-order tensor $\boldsymbol{L}$,

$$\int (\mathbf{r} \otimes \mathbf{r}) \frac{\partial}{\partial \mathbf{r}} \cdot (\boldsymbol{L}\mathbf{r}\psi) \, \mathrm{d}\mathbf{r} = -\int \left[\boldsymbol{L}(\mathbf{r} \otimes \mathbf{r}) + (\mathbf{r} \otimes \mathbf{r})\boldsymbol{L}^T \right] \psi \, \mathrm{d}\mathbf{r} \,. \tag{5.126}$$

Finally, taking into account the Eulerian representation of the time derivative this leads to the relation

$$\frac{D}{Dt} <\mathbf{r} \otimes \mathbf{r}> - \boldsymbol{L} <\mathbf{r} \otimes \mathbf{r}> - <\mathbf{r} \otimes \mathbf{r}> \boldsymbol{L}^T - \frac{4k_B\theta}{\zeta}\boldsymbol{I} + \frac{4}{\zeta} <\mathbf{r} \otimes \mathbf{f}> = 0 \,. \tag{5.127}$$

The first three terms of Eq. (5.127) are the upper-convective derivative $<\mathbf{r} \overset{\nabla}{\otimes} \mathbf{r}>$. Solving (5.127) for $<\mathbf{r} \otimes \mathbf{f}>$ and inserting the expression into Kramers equation, Eq. (5.124), the Giesekus form of the viscoelastic stress tensor is obtained,

$$\boldsymbol{\Xi}_v(\mathbf{x}, t) = -\frac{n_p \zeta}{4} <\mathbf{r} \overset{\nabla}{\otimes} \mathbf{r}> \,. \tag{5.128}$$

From Eq. (5.91), the spring force (for one bead) can be written as

$$\mathbf{f} = \left(\frac{3k_B\theta}{Nb^2} \right) \mathbf{r} = H\mathbf{r} \,, \tag{5.129}$$

with the extra-stress tensor now given by

$$\boldsymbol{\Xi} = -n_p k_B \theta \boldsymbol{I} + 2\mu_0 \boldsymbol{D} + n_p \left(\frac{3k_B\theta}{Nb^2} \right) <\mathbf{r} \otimes \mathbf{r}> \quad \text{(Kramers)} \tag{5.130}$$

$$\boldsymbol{\Xi} = 2\mu_0 \boldsymbol{D} - \frac{n_p \zeta}{4} <\mathbf{r} \overset{\nabla}{\otimes} \mathbf{r}> \quad \text{(Giesekus)} \tag{5.131}$$

If Eqs. (5.130) and (5.131) are equated with $Nb^2 = 3$ assumed, the dynamic equation for $<\mathbf{r} \otimes \mathbf{r}>$ in Eq. (5.113) is recovered with a relaxation time λ given by $\zeta / 4k_B\theta$. Alternatively, it is possible to eliminate the conformation tensor from those two equations by applying the upper-convective derivative to Eq. (5.130), and taking into account the relation in Eq. (4.35). This yields

$$\boldsymbol{\Xi} - 2\mu_0 \boldsymbol{D} = -\frac{\zeta}{4H} \left(\overset{\nabla}{\boldsymbol{\Xi}} - 2n_p k_B \theta \boldsymbol{D} - 2\mu_0 \overset{\nabla}{\boldsymbol{D}} \right) \,. \tag{5.132}$$

Defining the viscoelastic viscosity μ_1 and the characteristic relaxation and retardation times, λ_1 and λ_2, respectively as

$$\mu_1 = \frac{n_p k_B \theta \zeta}{4H}, \quad \lambda_1 = \frac{n_p \zeta}{4H}, \quad \lambda_2 = \frac{n_p \zeta \mu_0}{4H(\mu_0 + \mu_1)} = \frac{\mu_0 \lambda_1}{\mu_0 + \mu_1} \,, \tag{5.133}$$

Equation (5.132) can be written as

$$\boldsymbol{\Xi} + \lambda_1 \overset{\nabla}{\boldsymbol{\Xi}} = 2\mu_T (\boldsymbol{D} + \lambda_2 \overset{\nabla}{\boldsymbol{D}}) \,, \tag{5.134}$$

with $\mu_T = \mu_0 + \mu_1$, the total viscosity. Using the splitting of the stress tensor ($\boldsymbol{\Xi} = \boldsymbol{\Xi}_N + \boldsymbol{\Xi}_v$), the Newtonian solvent yields

$$\boldsymbol{\Xi}_N = 2\mu_0 \boldsymbol{D} \,, \tag{5.135}$$

and the polymeric extra-stress obeys the Oldroyd-B equation

$$\boldsymbol{\Xi}_v + \lambda \overset{\nabla}{\boldsymbol{\Xi}}_v = 2\mu_1 \boldsymbol{D} \,. \tag{5.136}$$

5.9.3 Nonlinear Dumbbells

The Oldroyd-B model has well known shortcomings such as an infinite elongational viscosity for a finite value of the extension rate and the inability of reproducing shear-thinning effects. These defects are generated by the possibility of the polymer chains in the linear dumbbell approach to extend to infinity. A remedy is found in the adoption of a nonlinear spring force (Warner 1972)

$$\mathbf{f} = \frac{H\mathbf{r}}{1 - r^2/r_0^2} \,, \tag{5.137}$$

where $r^2 = \{\mathbf{r} \otimes \mathbf{r}\}$, r_0^2 is a constant, and Warner's law shows that the spring cannot be extended further than the length r_0. Beris and Edwards (1994) notice that Warner law is an approximation of the more general spring law

$$\mathbf{f} = \frac{k_B \theta}{b} L^{-1}\left(\frac{r}{r_0}\right) \,, \tag{5.138}$$

where the Langevin function L is defined as

$$L(x) = \coth(x) - \frac{1}{x} \,. \tag{5.139}$$

With Warner law, the topic of finitely extendable (extensible) nonlinear elastic (FENE) models is now introduced and will be investigated in the next subsections. Observe, that if $r_0 \to \infty$, Warner's law becomes the linear Hookean law. Unfortunately, Warner's law prevents obtaining a solution of the diffusion equation Eq. (5.123), in closed form, so an approximation is needed to close the problem.

5.9.3.1 The FENE-P Model

The FENE-P model follows the proposal of Peterlin (1966) which replaces the spring force (5.137) by a pre-averaged form, namely

$$\mathbf{f} = \frac{H\mathbf{r}}{1 - <r^2/r_0^2>} \,. \tag{5.140}$$

With Eq. (5.140) inserted into (5.124), the stress field is given by

$$\boldsymbol{\Xi}(\mathbf{x},t) = -n_p k_B \theta \boldsymbol{I} + 2\mu_0 \boldsymbol{D} + \frac{n_p H}{1 - <r^2/r_0^2>} <\mathbf{r} \otimes \mathbf{r}> . \tag{5.141}$$

By computing the trace of $\boldsymbol{\Xi}$, the Peterlin function

$$\frac{1}{1 - <r^2/r_0^2>} = 1 + \frac{3k_B\theta}{Hr_0^2}\left(1 + \frac{\{\boldsymbol{\Xi}\}}{3n_p k_B \theta}\right) := \mathrm{P}(\boldsymbol{\Xi}) \tag{5.142}$$

is obtained, and yielding the spring force

$$\mathbf{f} = H\mathrm{P}(\boldsymbol{\Xi})\mathbf{r} . \tag{5.143}$$

The extra-stress tensor may be obtained from the Kramers and Giesekus relations as

$$\boldsymbol{\Xi} = -n_p k_B \theta \boldsymbol{I} + 2\mu_0 \boldsymbol{D} + n_p H \mathrm{P}(\boldsymbol{\Xi}) <\mathbf{r} \otimes \mathbf{r}> \quad \text{(Kramers)} \tag{5.144}$$

$$\boldsymbol{\Xi} = 2\mu_0 \boldsymbol{D} - \frac{n_p \zeta}{4} <\mathbf{r} \overset{\nabla}{\otimes} \mathbf{r}> \quad \text{(Giesekus)} \tag{5.145}$$

The elimination of $<\mathbf{r} \otimes \mathbf{r}>$ between Eqs. (5.144) and (5.145) gives, after some algebra,

$$\frac{\zeta}{4H} \overset{\nabla}{\boldsymbol{\Xi}} + \mathrm{P}(\boldsymbol{\Xi})\boldsymbol{\Xi} - \frac{\zeta}{4H}\left(\boldsymbol{\Xi} + n_p k_B \theta \boldsymbol{I}\right) \frac{D}{Dt} \ln(\mathrm{P}(\boldsymbol{\Xi})) = n_p k_B \theta \frac{\zeta}{4H} \boldsymbol{D} , \tag{5.146}$$

with the relaxation time and polymer viscosity defined as

$$\lambda = \frac{\zeta}{4H}, \quad \mu_1 = n_p k_B \theta \lambda . \tag{5.147}$$

A FENE-P model can be generated by equating Eqs. (5.144) and (5.145), and can be expressed as the two equations

$$\lambda <\mathbf{r} \overset{\nabla}{\otimes} \mathbf{r}> + \frac{1}{\left(1 - <\frac{r^2}{r_0^2}>\right)} <\mathbf{r} \otimes \mathbf{r}> = \frac{k_B \theta}{H} \boldsymbol{I} \tag{5.148}$$

and

$$\boldsymbol{\Xi}_p = \frac{n_p H}{\left(1 - <\frac{r^2}{r_0^2}>\right)} <\mathbf{r} \otimes \mathbf{r}> . \tag{5.149}$$

If the conformation tensor is introduced, the FENE-P model becomes

$$\lambda \overset{\nabla}{\boldsymbol{c}} + \frac{r_0^2}{\left(r_0^2 - \{\boldsymbol{c}\}\right)} \boldsymbol{c} = \frac{k_B \theta}{H} \boldsymbol{I} , \tag{5.150}$$

$$\boldsymbol{\Xi}_p = n_p \frac{r_0^2 H}{\left(r_0^2 - \{\boldsymbol{c}\}\right)} \boldsymbol{c} . \tag{5.151}$$

Note that some authors incorporate the isotropic part of the stress field into the definition of the polymeric stress (instead of merging it into the pressure computation). This practice yields the same dynamical equation for the conformation tensor (5.150), while the second relation becomes

$$\boldsymbol{\Xi}_p = n_p \left[\frac{r_0^2 H}{\left(r_0^2 - \{\boldsymbol{c}\}\right)} \boldsymbol{c} - k_B \theta \boldsymbol{I} \right] . \tag{5.152}$$

A last variant of the FENE-P model (Beris and Edwards 1994) is built on a dimensionless conformation tensor $\tilde{\boldsymbol{c}}$ defined by the relation

$$\tilde{\boldsymbol{c}} = 3 \frac{\boldsymbol{c}}{r_e^2}, \quad r_e^2 = 3 \frac{k_B \theta}{\mathrm{P}(r_e^2)} , \tag{5.153}$$

with r_e a dumbbell reference length. The FENE-P constitutive equation reads

$$\lambda \left(1 - \frac{\{\tilde{\boldsymbol{c}}\}}{r_0^2} \right) \overset{\nabla}{\tilde{\boldsymbol{c}}} + \tilde{\boldsymbol{c}} = \frac{1 - \frac{\{\tilde{\boldsymbol{c}}\}}{r_0^2}}{1 - \frac{3}{r_0^2}} \boldsymbol{I} , \tag{5.154}$$

$$\boldsymbol{\Xi}_p = \frac{\mu_p}{\lambda} \frac{1}{1 - \frac{\{\tilde{\boldsymbol{c}}\}}{r_0^2}} \left(\tilde{\boldsymbol{c}} - \frac{1 - \frac{\{\tilde{\boldsymbol{c}}\}}{r_0^2}}{1 - \frac{3}{r_0^2}} \right) \boldsymbol{I} . \tag{5.155}$$

The FENE-P model produces elongational viscosity for all deformation rates and generates shear-thinning effects; although, the predicted shear rates are lower than the experimental values. However, it has been observed from the computational standpoint that the FENE-P model is less stiff than the Oldroyd-B model and this is the reason why it has been used widely over the last two decades. This aspect will be discussed further in Chap. 6.

5.9.3.2 The FENE-CR Model

Another FENE model was proposed by Chilcott and Rallison (1988). Here, the spring force is still given by (5.140), but in the form

$$f(r) = \frac{1}{1 - <r^2/r_0^2>} , \tag{5.156}$$

such that $\mathbf{f} = H f(r) \mathbf{r}$. Then, the combination of Eqs. (5.156), (5.124) and (5.128) leads to the constitutive relationship

$$\overset{\nabla}{\boldsymbol{c}} = -\frac{1}{\lambda} \left[f(r) \boldsymbol{c} - \boldsymbol{I} \right] , \tag{5.157}$$

with the viscoelastic stress obtained from Kramers expression as

$$\boldsymbol{\Xi}_p = n_p k_B \theta \left[f(r) \boldsymbol{c} - \boldsymbol{I} \right] . \tag{5.158}$$

The FENE-CR approximation of this last equation yields

$$\boldsymbol{\Xi}_p = n_p k_B \theta f(r) \left[\boldsymbol{c} - \boldsymbol{I} \right] . \tag{5.159}$$

This model is capable of reproducing constant shear viscosity and therefore able to handle Boger fluids. Computations for steady state problems produce reasonable results; however, for transient problems the FENE-CR model offers dismal performance.

5.9.4 Dumbbells with Hydrodynamic Interactions

Up to this point, the dumbbell models built use one way coupling. The two way coupling, where the hydrodynamic interaction is taken into account in the model, is now incorporated. The local velocity field at the bead 1 is now given by

$$\mathbf{v}_1 = \mathbf{v}_0 + \boldsymbol{L}\mathbf{x}_1 + \mathbf{v}_{p,1} \tag{5.160}$$

where $\mathbf{v}_{p,1}$ is the perturbed velocity induced by the presence of the neighboring second bead. This velocity can be evaluated by the relation

$$\mathbf{v}_{p,1} = \boldsymbol{G}\mathbf{D}_2 \,, \tag{5.161}$$

where $\boldsymbol{G}$ is the Oseen-Burgers tensor (or Stokeslet) (Hasimoto and Sano 1980)

$$\boldsymbol{G} = \frac{1}{8\pi\mu_0 r}\left(\boldsymbol{I} + \frac{\mathbf{r}\otimes\mathbf{r}}{r^2}\right) . \tag{5.162}$$

The Stokeslet corresponds to the solution of the Stokes flow around a sphere with the assumption that the effect of a translating sphere in a fluid at rest is equivalent to the effect of a unit pointwise force centered on the sphere. Furthermore this flow field is asymptotically independent of the sphere's radius if the solution is considered at distances sufficiently far from the sphere. In Eq. (5.161), $\mathbf{D}_2$ is the drag force exerted by the second bead on the solvent, namely

$$\mathbf{D}_2 = -\zeta\left(\mathbf{v}_2 + \mathbf{v}_{p,2} - \frac{\mathrm{d}\mathbf{x}_2}{\mathrm{d}t}\right) = -m\frac{\mathrm{d}^2\mathbf{x}_2}{\mathrm{d}t^2} - \mathbf{f}_2 + \mathbf{B}_2 \,. \tag{5.163}$$

The corresponding Langevin equation for the beads ($\zeta_i = \zeta$) is

$$m\frac{\mathrm{d}^2\mathbf{x}_i}{\mathrm{d}t^2} = -\zeta_i\left(\frac{\mathrm{d}\mathbf{x}_i}{\mathrm{d}t} - (\mathbf{v}_0 + \boldsymbol{L}\mathbf{x}_i + \mathbf{v}_{p,i})\right) + \mathbf{f}_i + \mathbf{B}_i, \quad i = 1, 2 \,. \tag{5.164}$$

Setting

$$(\boldsymbol{I} - \zeta\boldsymbol{G}) := \boldsymbol{H} = \boldsymbol{I} - \frac{\zeta}{8\pi\mu_0 r}\left(\boldsymbol{I} + \frac{\mathbf{r}\otimes\mathbf{r}}{r^2}\right) , \tag{5.165}$$

the connector equation obtained by subtraction is given by

$$m\boldsymbol{H}\frac{\mathrm{d}^2\mathbf{r}}{\mathrm{d}t^2} = \zeta\left(\boldsymbol{L}\mathbf{r} - \frac{\mathrm{d}\mathbf{r}}{\mathrm{d}t}\right) - 2\boldsymbol{H}\mathbf{f} + \boldsymbol{H}\mathbf{B} \,. \tag{5.166}$$

Neglecting again the inertia of the beads, the Smoluchowski equation in the configuration space now becomes

$$\frac{\partial\psi}{\partial t} + \frac{\partial}{\partial\mathbf{r}}\cdot\left(\boldsymbol{L}\mathbf{r}\psi - 2\frac{k_B\theta}{\zeta}\boldsymbol{H}\frac{\partial\psi}{\partial\mathbf{r}} - \psi\frac{2}{\zeta}\boldsymbol{H}\mathbf{f}\right) = 0 \,. \tag{5.167}$$

Note that the factor $\zeta/8\pi\mu_0$ in Eq. (5.165) is a characteristic length of the hydrodynamic interaction. With an integration by parts and use of the divergence theorem, it is possible to derive a dynamic equation for the average quantity $<\mathbf{r}\otimes\mathbf{r}>$ given by

$$<\mathbf{r}\overset{\nabla}{\otimes}\mathbf{r}> - (\boldsymbol{I}-\zeta<\boldsymbol{G}>)\left(\frac{4k_B\theta}{\zeta}\boldsymbol{I}-\frac{4H}{\zeta}<\mathbf{r}\otimes\mathbf{r}>\right)=0\,, \tag{5.168}$$

where an average value for $\boldsymbol{G}$ has been used. Carrying through the algebra, the following constitutive equation is obtained

$$\boldsymbol{\Xi}+\lambda_1\,(\boldsymbol{I}-\zeta<\boldsymbol{G}>)^{-1}\overset{\nabla}{\boldsymbol{\Xi}}=2\mu_T(\boldsymbol{D}+\lambda_2\overset{\nabla}{\boldsymbol{D}})\,, \tag{5.169}$$

and which is very similar to Eq. (5.134). The material relaxation time $\lambda_1(\boldsymbol{I}-\zeta<\boldsymbol{G}>)^{-1}$ is greater than the former λ_1 as the denominator is less than unity. For example, if the shear rate of the flow increases, then this induces a reduction of the connector length r and the real relaxation time decreases. Since from physical experiments, it is known that the viscosity is proportional to the relaxation time, this quantity diminishes also. It can then be concluded that the hydrodynamic interaction affects the model in such a way that the shear-thinning effects are incorporated.

5.10 The Micro-Macro Description

The micro-macro approach combines the use of conservation laws at the macroscopic level, while at the mesoscopic level, the kinetic theory provides the model of the polymer behavior. This procedure avoids the painful step of closure approximations. However this nice feature has a major drawback, namely the blow-up of the computational cost. The book by Öttinger (1996) constitutes a cornerstone of this two-level modeling. At the micro level, the integration of an SDE for a large number of different polymeric configurations is undertaken. An ensemble average of the resulting stresses is obtained and this average contributes as a source term in the macro momentum equations. This methodology was first designed in the CONNFFESSIT approach: **C**alculation **o**f **N**on-**N**ewtonian **F**low: **F**inite **E**lements and **S**tochastic **Si**mulation **T**echniques. A recent review of the micro-macro approach has been given by Keunings (2004).

As has been described over the last few sections, the macro description solves a generalized Navier-Stokes problem that takes into account the splitting of the stress tensor into a Newtonian part of viscosity μ_0 and a viscoelastic, or polymeric part, associated with the tensor $\boldsymbol{\Xi}_p$. The resulting form of the mass and momentum conservation equations were

$$\boldsymbol{\nabla}\cdot\mathbf{v}=0 \quad \text{and} \quad \rho\frac{D\mathbf{v}}{Dt}=-\boldsymbol{\nabla}p+\mu_0\boldsymbol{\nabla}^2\mathbf{v}+\boldsymbol{\nabla}\cdot\boldsymbol{\Xi}_p\,. \tag{5.170}$$

The classical macro-macro description closes the system with a constitutive equation, e.g. the Oldroyd-B model in Eq. (5.136). In the micro-macro approach, the

Fokker-Planck equation (5.123) is used and the polymeric stress is given by Kramers equation (5.124). The spring force in Kramers definition may be chosen among either the Hookean law (5.129) (corresponding to Oldroyd-B), the nonlinear law (5.137), or the FENE-P law (5.140). The link between the macro-macro and the micro-macro descriptions is made by the relation (5.147).

5.10.1 Solving the Fokker-Planck Equation

The solution of the Fokker-Planck equation is detailed by Itô calculus which yields the following SDE

$$\mathrm{d}\mathbf{r} = \left(\boldsymbol{L}\mathbf{r} - \frac{2}{\zeta}\mathbf{f} \right) \mathrm{d}t + 2\sqrt{\frac{k_B\theta}{\zeta}}\mathrm{d}\boldsymbol{W}(t) \, . \tag{5.171}$$

Note that Eq. (5.171) corresponds to a Lagrangian formulation. In a Brownian dynamics simulation, this equation will be integrated for a large number of dumbbells—the larger, the better. Assuming that the initial condition $\mathbf{r}(0)$ is given at time $t = 0$, the numerical time integration of (5.171) is performed using an explicit Euler-Maruyama scheme. Defining the local time step by $\Delta t^n = t^{n+1} - t^n$, the algorithm computes the successive approximations

$$\mathbf{r}^{n+1} = \mathbf{r}^n + \left(\boldsymbol{L}^n\mathbf{r}^n - \frac{2}{\zeta}\mathbf{f} \right) \Delta t^n + 2\sqrt{\frac{k_B\theta}{\zeta}}\boldsymbol{W}^n(\Delta t^n)^{1/2} \, . \tag{5.172}$$

As soon as the configurations at the new time level are known, the polymeric stress is computed by the approximation

$$\boldsymbol{\Xi}_p = -n_p k_B\theta\boldsymbol{I} + n_p H \frac{1}{N_d}\sum_{i=1}^{N_d} r_i r_i \, , \tag{5.173}$$

where N_d is the total number of dumbbells and the sum is carried out over all dumbbells in order to compute the ensemble average. The solution method is, therefore, built up through the four steps. First, the macro equations in (5.170) are solved to compute the pressure and velocity fields at the new time level t^{n+1}. In the second step, the trajectory of the center of mass of each transported polymer configuration is integrated using the definition $\mathrm{d}\mathbf{r}/\mathrm{d}t = \mathbf{v}(\mathbf{r}, t)$. The third step tackles the discretized SDE (5.172) and the final step evaluates the average stress through a local set of configurations whose size depends on the numerical method that has been chosen.

The micro-macro approach is extremely computationally intensive and unfortunately suffers from several drawbacks: number of dumbbells and the costly computations of their trajectories, presence of boundaries, localization of the dumbbells to sort out, and control of the statistical error.

5.10.2 Brownian Configuration Fields

The burden of calculating the particle trajectories is alleviated by resorting to Brownian configuration fields treated using an Eulerian representation. The method was first described by Hulsen et al. (1997). For this purpose, an ensemble of N_f configuration fields $\mathbf{r}_i(\mathbf{x}, t)$, $i = 1, \ldots, N_f$ is set up, and at time $t = 0$, the field $\mathbf{r}_i^0$ is uniformly distributed and sampled from the equilibrium distribution function of the dumbbell model (e.g. Hookean). The dynamic equation governing the evolution of the field $\mathbf{r}_i$ is given by

$$\mathrm{d}\mathbf{r} = \left(-\mathbf{v}(\mathbf{x}, t) \cdot \nabla \mathbf{r}(\mathbf{x}, t) + \boldsymbol{L}\mathbf{r} - \frac{2}{\zeta}\mathbf{f} \right) \mathrm{d}t + 2\sqrt{\frac{k_B\theta}{\zeta}}\mathrm{d}\boldsymbol{W}(t) \,, \tag{5.174}$$

which is very similar to Eq. (5.171) except for the first term on the right-side that takes the convection of the configuration field by the advection flow into account. The Wiener process, depending only on time, influences spatially the configuration fields in a uniform way, thereby allowing for smooth and well behaved gradients of these fields.

For the stress computation, the present procedure is very similar to the former particle tracking. The polymeric stress again reads

$$\boldsymbol{\Xi}_p = -n_p k_B \theta \boldsymbol{I} + n_p H \frac{1}{N_f} \sum_{i=1}^{N_f} r_i r_i \,, \tag{5.175}$$

with N_d now replaced by N_f. Although the Brownian configuration fields method reduces the computational complexity, it is still a major undertaking. These simulations are indeed more expensive than the full continuum approach.

5.11 Consequences of Non-affine Motion

Unlike the affine motions given by Eq. (5.99), non-affine motions induce strain softening, that is, the transient viscosity in a shear flow is lower than the values predicted by the theory of linear viscoelasticity for large strains. Conversely, the growth rate for the first normal stress is well above the prediction given by the linear viscoelasticity; this is the so-called strain hardening.

5.11.1 Dumbbells with Non-affine Motion and the Gordon-Schowalter Model

Based on a continuum theory for anisotropic fluids developed by Ericksen (1960), Gordon and Schowalter (1972) formulated a dumbbell model that incorporates a

non-affine motion of the connector vector. Ericksen had proposed that the Cauchy stress be a function of the velocity gradient and of an orientation vector $\mathbf{d}$

$$\boldsymbol{\Sigma} = -p\boldsymbol{I} + \mathbf{f}(\boldsymbol{D}, \mathbf{d} \otimes \mathbf{d}) \,, \tag{5.176}$$

with the governing equation for the orientation vector given by

$$\frac{\mathrm{d}}{\mathrm{d}t}\mathbf{d} - \boldsymbol{W}\mathbf{d} = \mathbf{g}(\boldsymbol{D}, \mathbf{d}) \,, \tag{5.177}$$

$\boldsymbol{W}$ being the vorticity tensor defined in Eq. (3.43). Equation (5.177) shows that the material time derivative depends on both the velocity gradient and the value of $\mathbf{d}$.

The dumbbell theory used a similar approach where the orientation vector $\mathbf{d}$ was replaced by the connector $\mathbf{r}$, and the stress tensor took the form

$$\boldsymbol{\Xi} = -p\boldsymbol{I} + 2\mu_0\boldsymbol{D} + \boldsymbol{h}<\mathbf{r} \otimes \mathbf{r}> \,, \tag{5.178}$$

with a Newtonian part $2\mu_0\boldsymbol{D}$, and a polymeric part based on the average of the orientation tensor $<\mathbf{r} \otimes \mathbf{r}>$ defined by the relation

$$<\mathbf{r} \otimes \mathbf{r}> = \int (\mathbf{r} \otimes \mathbf{r})\, \psi \mathrm{d}\mathbf{r} \tag{5.179}$$

where the pdf ψ in the case of homogeneous flow depends only on $\mathbf{r}$ and the time t (cf. Eq. (5.124)). The evolution of the connector results from (5.177) written now for the end-to-end vector $\mathbf{r}$,

$$\frac{\mathrm{d}\mathbf{r}}{\mathrm{d}t} - \boldsymbol{W}\mathbf{r} = \dot{\mathbf{r}} - \boldsymbol{W}\mathbf{r} = \mathbf{g}(\boldsymbol{D}, \mathbf{r}) \,. \tag{5.180}$$

The next step consists in choosing an expression for the function $\mathbf{g}$. A polynomial expansion in terms of $\boldsymbol{D}$ and $\mathbf{r}$ is constructed. If all terms of second-order, such as $\boldsymbol{D}^2$ and $\mathbf{r} \otimes \mathbf{r}$, and higher are neglected, Eq. (5.180) becomes

$$\frac{\mathrm{d}\mathbf{r}}{\mathrm{d}t} - \boldsymbol{W}\mathbf{r} = (1 - \xi)\boldsymbol{D}\mathbf{r} - \alpha\mathbf{r} \,, \tag{5.181}$$

where the coefficients $1 - \xi$ and α are used for the sake of convenience. Equation (5.181) yields the non-affine motion

$$\frac{\mathrm{d}\mathbf{r}}{\mathrm{d}t} = \mathbf{L}\mathbf{r} - \xi\boldsymbol{D}\mathbf{r} - \alpha\mathbf{r} \,, \tag{5.182}$$

where for $\xi = 0$ the affine motion is recovered. The second term on the right side of (5.182) is interpreted as representative of the slip of the dumbbell with respect to the neighboring continuum.

For the non-affine motion, the polymeric stress given by Eq. (5.106) is no longer valid. A very simple argument obtained from the principle of energy conservation shows that the polymeric stress now becomes

$$\boldsymbol{\Xi}_p = (1 - \xi)H\boldsymbol{c} \,, \tag{5.183}$$

with the physical interpretation being that because of the slip, the tension built in the strands is not completely transmitted to the neighboring continuum. Using

$\alpha = (2\lambda)^{-1}$ in Eq. (5.182), and taking the Brownian motion into account the following relation is obtained

$$\mathrm{d}\mathbf{r} = \left(-\frac{\mathbf{r}}{2\tau} + \mathbf{r}\cdot(\boldsymbol{L} - \xi\boldsymbol{D})\right)\mathrm{d}t + \frac{\mathrm{d}\boldsymbol{W}(t)}{\sqrt{\lambda}}\ , \tag{5.184}$$

and which generalizes Eq. (5.103). Carrying through the same calculation as in Sect. 5.8, it can be shown that the evolving dynamics for the conformation tensor obeys the relationship

$$\frac{\partial \boldsymbol{c}}{\partial t} + \mathbf{v}\cdot\nabla\boldsymbol{c} - \boldsymbol{c}(\boldsymbol{L} - \xi\boldsymbol{D})^T - (\boldsymbol{L} - \xi\boldsymbol{D})\boldsymbol{c} := \mathring{\boldsymbol{c}} = -\frac{1}{\tau}(\boldsymbol{c} - \boldsymbol{I})\ , \tag{5.185}$$

where $\mathring{\boldsymbol{c}}$ defines the Gordon-Schowalter non-affine convected derivative (cf. Gordon and Schowalter 1972). The special case $\xi = 0$ corresponds to the upper-convected derivative, i.e. $\mathring{\boldsymbol{c}} = \overset{\nabla}{\boldsymbol{c}}$ and Eq. (5.185) reduces to the standard relation (5.113).

5.11.2 Modeling Polymeric Networks

Before embarking in the next section on models built to treat polymer melts, it is useful to focus briefly on the theory of polymeric networks. Here, the entangled polymers are supposed to form a network of polymers strands where each strand has, from a statistical point of view, the same behavior. This network possesses junction points ensuring that the whole structure will not collapse through a breaking phenomena. The first attempt to model such a network was put forth by Yamamoto (1956), who generalized the conservation law (5.121) for the pdf

$$\frac{\partial\psi}{\partial t} + \frac{\partial}{\partial\mathbf{r}}\cdot(\dot{\mathbf{r}}\psi) = g(\mathbf{r}) - h(\mathbf{r})\psi\ , \tag{5.186}$$

where the scalar functions f and g are source and sink terms related to the rate of creation and destruction of strands in the network geometry, respectively, and in general, are functions of $\mathbf{r}$. For the rate of creation g, the equilibrium condition is applied which is obtained from Eq. (5.186) by assuming the vanishing of the left side,

$$g(\mathbf{r}) = h(\mathbf{r})\psi_{eq}\ . \tag{5.187}$$

With the same non-affine motion as described by Eq. (5.184), the transient equation for the conformation tensor in Eq. (5.183) becomes

$$\mathring{\boldsymbol{c}} = \int g\,\mathbf{r}\otimes\mathbf{r}\mathrm{d}\mathbf{r} - <h\mathbf{r}\otimes\mathbf{r}> \tag{5.188}$$

Yamamoto proposed that h be constant such that the rate of strand destruction is directly proportional to the number of strands composing the network. Therefore $g = h\psi_{eq}$, and if the equilibrium function is Gaussian as usual, the right side of Eq. (5.188) yields

$$\frac{hNb^2}{2}\boldsymbol{I} - h\boldsymbol{c}\ . \tag{5.189}$$

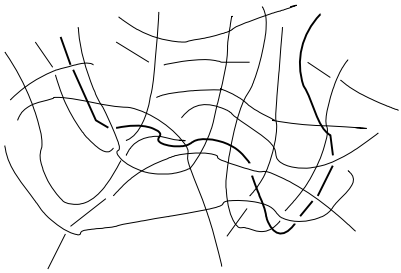

Fig. 5.7 Entanglement of a polymer molecule in a network composed of polymer chains

If the slip term is neglected ($\xi = 0$) and the polymeric stress tensor is given by Eq. (5.108), it is easy to show that the dynamic equation reduces to (5.86) with $h = 1/\lambda$. For a better model, the slip term needs to be considered in full; however, the major difficulty of the complete model is the term $<h\mathbf{r} \otimes \mathbf{r}>$. To circumvent this drawback, Phan-Thien and Tanner (1977) proposed a closure approximation that makes h depend on $<r^2>$ instead of $\mathbf{r} \otimes \mathbf{r}$. The governing equation for the conformation tensor then becomes

$$\mathring{\boldsymbol{c}} = h<r^2>\left(\frac{Nb^2}{2}\boldsymbol{I} - \boldsymbol{c}\right) . \tag{5.190}$$

With the constitutive relation (5.183), the polymeric stress obeys the evolution equation

$$\mathring{\boldsymbol{\Xi}}_p = -h(\{\boldsymbol{\Xi}_p\})\left(\boldsymbol{\Xi}_p - \frac{H}{1-\xi}\boldsymbol{I}\right) , \tag{5.191}$$

which, by introducing the change of variable $\boldsymbol{\Xi}_v = \boldsymbol{\Xi}_p - H\boldsymbol{I}/(1-\xi)$, gives

$$\lambda\mathring{\boldsymbol{\Xi}}_v + Y(\{\boldsymbol{\Xi}_v\})\boldsymbol{\Xi}_v = 2\mu_1\boldsymbol{D} \tag{5.192}$$

where $Y(\{\boldsymbol{\Xi}_v\}) = \lambda h(\{\boldsymbol{\Xi}_p\})$, and $\mu_1 = \lambda H$. This is the Phan-Thien Tanner equation previously considered in Sect. 5.7.2.2.

5.12 Modeling of Polymer Melts

Polymer melts offer a different rheological behavior than the dilute polymers as each polymer molecule interacts with its many surrounding neighbors. It has been shown, and confirmed by experiments, that the distribution of the chain configuration in the melt is Gaussian (Larson 1988). The first theory where the polymer chain was considered as part of a chain network (Fig. 5.7) was developed by de Gennes (1971) under the name of reptation theory. In this theory, it was assumed that the polymer chain changes by reptation, i.e. a snake like movement and that the motion of the other molecules orthogonal to the chain backbone is impeded by the neighboring molecules as if they were creating an environment in shape of a tube (this is shown in Fig. 5.8). The chain then deforms essentially with the tube. Therefore, the transverse motion of the tube is reduced and the chain can rearrange itself by a creeping motion termed—longitudinal reptation.

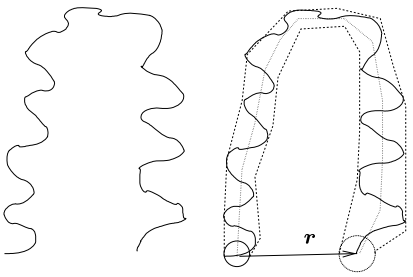

Fig. 5.8 Entangled polymer chain (*left*) imbedded by the neighboring molecules in a tubular region (*right*)

5.12.1 Doi-Edwards Model

Following the lead of de Gennes, Doi and Edwards in a series of seminal papers (1978a, 1978b, 1978c, 1979) developed their reptation model known as the Doi-Edwards model.

The axis of symmetry of the chain in the tube (Fig. 5.8, right) is the primitive chain. The modeling is focused on this particular chain even though the real polymer has a more complicated geometrical shape. This assumption relieves many of the difficulties that could occur due to the complexity of the geometry. For the sake of simplicity, consider that at time $t = 0$ the polymer melt, subjected to some force, deforms homogeneously. The fluid will return after some time to the initial configuration, namely the one before deformation. The motion of a chain may be decomposed into three steps: an instantaneous deformation; followed by a quick return (retraction) toward the initial length; and then a slow creeping motion outside the tube where the chain was before. The first two steps are mainly kinematical, as they reorient the chain without stretching or compression; the final step is a relaxation process dominated by diffusion. In Fig. 5.9 is shown how the chain moves with this simplified topology. From the initial configuration, the chain slips away from one end, and then from the other one. When one end of the tube is free, this part of the tube no longer has an effect on the deformation. The tube ends are not subjected to the same constraints when the chain changes direction so that by these back and forth movements, the chain forgets more and more of the initial ends of the tube. A new conformation diffuses the ends of the chain inside the interior of a new tube. Observe that the cross motion of the tube is assumed to be so small, compared to the longitudinal motion, that it can be completely discarded.

As the chain movement continues, the orientation of each strand is not given by the tube the polymeric chain leaves, but by the new one it moves into. Therefore, the orientation of the chain is extremely difficult to predict through a general deformation history. Doi and Edwards proposed to avoid this difficulty by assuming that each strand deforms independently. This is the hypothesis of the independent alignment approximation. As a consequence, the deformation of the tube and the chain is supposed to be affine in such a way that the end-to-end vector $\mathbf{r}$ (cf. Fig. 5.8) is given by the relation

$$\mathbf{r} = \boldsymbol{\mathcal{F}}\mathbf{r}_0 \,, \tag{5.193}$$

where $\boldsymbol{\mathcal{F}}$ is the imposed deformation gradient and $\mathbf{r}_0$ the initial vector.

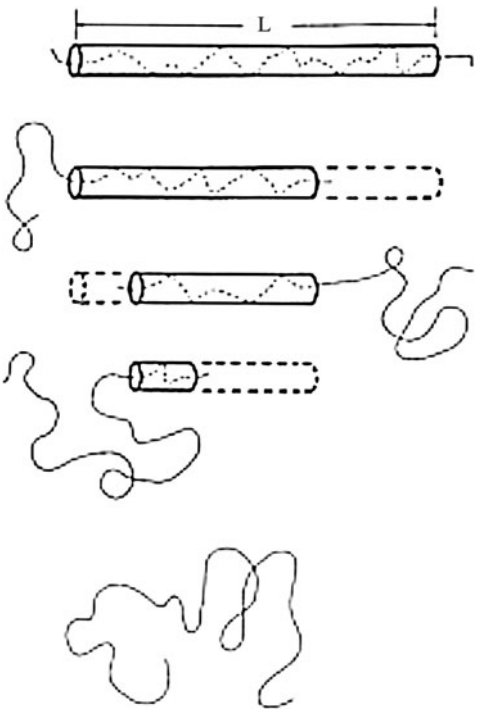

Fig. 5.9 Reptant motion of the polymer chain outside the confining tube[2]

Let us introduce the variable $\mathbf{u}$, which is a unit vector tangent to the primitive chain and the dimensionless curvilinear abscissa s along the chain with $s = 0$ and $s = 1$ corresponding to the inlet and outlet ends of the tube. The configuration pdf $\psi(\mathbf{u}, s, \mathbf{x}, t)$ is such that the increment $\psi(\mathbf{u}, s, \mathbf{x}, t)\mathrm{d}\mathbf{u}\mathrm{d}s$ is the joint probability that for the position $\mathbf{x}$ at time t, a strand of the chain has its orientation comprised in the range $[\mathbf{u}, \mathbf{u} + \mathrm{d}\mathbf{u}]$ with the chain label in the interval $[s, s + ds]$. The Doi-Edwards model yields the Fokker-Planck relation

$$\frac{\partial \psi}{\partial t} = -\frac{\partial}{\partial \mathbf{u}} \cdot \left[(\boldsymbol{I} - \mathbf{u} \otimes \mathbf{u}) \boldsymbol{L}\mathbf{u}\psi \right] + \frac{1}{\pi^2 \lambda_d} \frac{\partial^2 \psi}{\partial s^2} , \tag{5.194}$$

where λ_d is the diffusion time related to the reptation motion or more precisely the time spent by a chain to escape by reptation from the tube where it is located. The boundary conditions are

$$\psi(\mathbf{u}, 0, \mathbf{x}, t) = \psi(\mathbf{u}, 1, \mathbf{x}, t) = \frac{1}{4\pi} \delta(|\mathbf{u}| - 1) , \tag{5.195}$$

and arise from the requirement that ψ is isotropic at $s = 0$ and 1. In Eq. (5.195), δ is the Dirac function.

[2]Figure 5.9 reprinted with permission from: R.G. Larson (1988) Constitutive Equations for Polymer Melts and Solutions. Butterworth, Boston. Copyright Elsevier 1988.

Because of the joint probability, two differential equations can be built that decouple the stochastic processes $\mathbf{u}$ and $s(t)$. The first stochastic process $\mathbf{u}(t)$ evolves according to a deterministic differential equation,

$$\frac{D\mathbf{u}(t)}{Dt} = \boldsymbol{L}\mathbf{u} - \{\boldsymbol{L}\mathbf{u}\otimes\mathbf{u}\}\mathbf{u} = (\boldsymbol{I} - \mathbf{u}\otimes\mathbf{u})\,\boldsymbol{L}\mathbf{u}\,, \tag{5.196}$$

where Eq. (5.194) has been used. In the previous equation, the term $\boldsymbol{L}\mathbf{u}$ shows that the vector $\mathbf{u}$ is transported by the flow field, while the quantity $(\boldsymbol{I} - \mathbf{u}\otimes\mathbf{u})$ enforces the constraint $(|\mathbf{u}\otimes\mathbf{u}| - 1)$ which ensures that the unit vector conserves its magnitude at every instant. This means also that the unit vector has the only capability of rotation inside the flow.

The stochastic process $s(t)$ describing the Brownian motion is given by the diffusion SDE

$$\mathrm{d}s(t) = (2/\pi^2\lambda_d)^{1/2}\mathrm{d}W(t)\,. \tag{5.197}$$

The coupling between the two variables $\mathbf{u}$ and s is made through the boundary conditions (5.195).

The polymeric stress is computed by the relation

$$\boldsymbol{\Xi}_p = 5G<\mathbf{u}\otimes\mathbf{u}>\,, \tag{5.198}$$

where G is an elastic modulus and the orientation tensor is defined as

$$<\mathbf{u}\otimes\mathbf{u}> = \int_{s=0}^{1}\int_{B(0,1)}(\mathbf{u}\otimes\mathbf{u})\psi\,\mathrm{d}\mathbf{u}\mathrm{d}s\,, \tag{5.199}$$

where $B(0,1)$ is the unit sphere centered at the origin.

The Doi-Edwards model may be written in an equivalent integral constitutive equation form. Using the Lagrangian representation, and following the trajectory of a fluid particle, the polymeric stress can be written as

$$\boldsymbol{\Xi}_p = G\int_{-\infty}^{t} m(t,t')\,\boldsymbol{Q}(\boldsymbol{x},t,t')\,\mathrm{d}t'\,, \tag{5.200}$$

where the integral is carried out on the past history of the deformation parameterized with the auxiliary variable t'. The memory function is given by the one-dimensional solution of the diffusion equation with the diffusion coefficient (5.102)

$$\frac{\partial\psi}{\partial t} = D\frac{\partial^2\psi}{\partial x^2}\,, \tag{5.201}$$

namely

$$m(t,t') = \frac{8}{\pi^2\lambda_d}\sum_{k=0}^{\infty}\exp\left(-\frac{(2k+1)^2(t-t')}{\lambda_d}\right) \tag{5.202}$$

and $\boldsymbol{Q}$ is an orientation tensor based on the average of the orientation vectors of the tube segments

$$\boldsymbol{Q}(\boldsymbol{x},t,t') = <\mathbf{u}\otimes\mathbf{u}>_{t'} = <\frac{(\boldsymbol{\mathcal{F}}_{(t)}(t')\mathbf{u}(t'))(\boldsymbol{\mathcal{F}}_{(t)}(t')\mathbf{u}(t'))}{|\boldsymbol{\mathcal{F}}_{(t)}(t')\mathbf{u}(t')|^2}>_{t'}\,, \tag{5.203}$$

with the constant G a modulus of rigidity. With L the length of the tube, it is possible to obtain that $\lambda_d = L^2/(\pi^2 D)$.

5.12.2 Differential Form of the Doi-Edwards Model

There are obvious numerical difficulties associated with the discretization of the integral model, Eq. (5.200), of Doi-Edwards due to the presence of several time integrals. To circumvent such difficulties, differential forms have been produced as they are more amenable to finite difference, finite element and finite volume algorithms.

5.12.2.1 Non-extensible Non-affine Motion

Suppose the end-to-end vector $\mathbf{r}$ satisfies the equation of affine motion (5.99). If the connector is related to the unit vector $\mathbf{u}$ that is aligned with the local direction of the chain, $\mathbf{r} = r\mathbf{u}$, we have that $\dot{\mathbf{r}} = r\dot{\mathbf{u}} + \dot{r}\mathbf{u}$. Since $\mathbf{u}\cdot\mathbf{u} = 1$ and $\dot{\mathbf{u}}\cdot\mathbf{u} = 0$,

$$\dot{r} = r\{\boldsymbol{L}(\mathbf{u}\otimes\mathbf{u})\} \tag{5.204}$$

and

$$\dot{\mathbf{u}} = \boldsymbol{L}\mathbf{u} - \{\boldsymbol{L}(\mathbf{u}\otimes\mathbf{u})\}\mathbf{u} = \boldsymbol{L}\mathbf{u} - \{\boldsymbol{D}(\mathbf{u}\otimes\mathbf{u})\}\mathbf{u}\,. \tag{5.205}$$

If it is now assumed that the polymer chain behaves like a rigid rod, i.e. the strand may rotate but cannot extend, the motion is non-affine. Larson (1983) then proposed for $\dot{\mathbf{r}}$ the following relation

$$\dot{\mathbf{r}} = \boldsymbol{L}\mathbf{r} - \{\boldsymbol{D}(\mathbf{u}\otimes\mathbf{u})\}\mathbf{r}\,, \tag{5.206}$$

which yields $\dot{r} = 0$.

If the time derivative of r^2 is taken, namely $\dot{\mathbf{r}}\cdot\mathbf{r} + \mathbf{r}\cdot\dot{\mathbf{r}}$, and averaged in configuration space by multiplying by ψ, a relation very similar to Eq. (5.127)

$$\frac{D}{Dt}<\mathbf{r}\otimes\mathbf{r}> - \boldsymbol{L}<\mathbf{r}\otimes\mathbf{r}> - <\mathbf{r}\otimes\mathbf{r}>\boldsymbol{L}^T - 2\boldsymbol{D}<\mathbf{u}\otimes\mathbf{u}\otimes\mathbf{r}\otimes\mathbf{r}> = 0 \tag{5.207}$$

is obtained. The fourth-order moment can be approximated by the product of two second-order moments

$$<\mathbf{u}\otimes\mathbf{u}\otimes\mathbf{r}\otimes\mathbf{r}> \simeq <\mathbf{u}\otimes\mathbf{u}><\mathbf{r}\otimes\mathbf{r}> = \frac{1}{a^2}<\mathbf{r}\otimes\mathbf{r}><\mathbf{r}\otimes\mathbf{r}>\,, \tag{5.208}$$

with a the strand length. Defining the polymeric tensor as

$$\boldsymbol{\Xi}_p = \frac{3\nu k_B\theta}{a^2}<\mathbf{r}\otimes\mathbf{r}>\,, \tag{5.209}$$

Eq. (5.207) becomes

$$\overset{\nabla}{\boldsymbol{\Xi}}_p + \frac{2}{3G}\{\boldsymbol{D}\boldsymbol{\Xi}_p^2\} = 0\,, \tag{5.210}$$

with $G = 3\nu k_B\theta$, ν being the number of strands per unit of volume. Equation (5.210) constitutes the instantaneous response to a step strain. If the effect of material relaxation is incorporated, the former relation generates the differential model of Doi-Edwards

$$\overset{\nabla}{\boldsymbol{\Xi}}_p + \frac{2}{3G}\{\boldsymbol{D}\boldsymbol{\Xi}_p^2\} + \frac{1}{\lambda}\left(\boldsymbol{\Xi}_p - G\boldsymbol{I}\right) = 0\,. \tag{5.211}$$

5.12.2.2 Convective Constraint Release

Another major defect of the Doi-Edwards model is the excessive shear-thinning in steady shear flows. Among the many improvements that have been proposed, the convective constraint release (CCR) is worth noting. The CCR occurs when the convection rate reaches the order of the shear rate and therefore sweeps away the tube constraints that were present at the end of the relaxation process described by Doi and Edwards (cf. Ianniruberto and Marrucci 1996, 2000, 2001).

A model incorporating CCR and also a force balance on the entanglement nodes of the polymer chain is due to Marrucci et al. (2001). To model the force balance, a simple three-chain network is worked out. This implies that the orientation tensor $\boldsymbol{Q}$ now depends on the relative Finger tensor $\boldsymbol{C}_{(t)}^{-1}$ as

$$\boldsymbol{Q} = \frac{\boldsymbol{C}_{(t)}^{-1/2}}{\{\boldsymbol{C}_{(t)}^{-1/2}\}} , \tag{5.212}$$

where $\boldsymbol{C}_{(t)}^{-1/2}$ is the square root of the relative Finger tensor. The insertion of (5.212) in (5.200) leads to $\{\boldsymbol{\Xi}_p\} = G$. The only remaining difficulty for using the model lies in the computation of the memory function that depends on the relaxation time λ of the flow. Within the CCR framework, this is given by the relation

$$\frac{1}{\lambda} = \frac{1}{\lambda_d(\mathbf{x}, \tau)} + \frac{C}{G}\{\boldsymbol{L}\boldsymbol{\Xi}\} \tag{5.213}$$

where C is a numerical constant, and consequently the memory function becomes

$$m = \frac{1}{\lambda} \exp\left(- \int_\tau^t \frac{\mathrm{d}t'}{\lambda(\mathbf{x}, t')} \right) \tag{5.214}$$

Substituting Eq. (5.214) into (5.200) yields a double integral representation for the stress with all the numerical pitfalls lurking the unaware numericist.

5.12.2.3 The Marrucci-Greco-Ianniruberto Differential Equation

Marrucci et al. (2001) designed an approximate differential model based on a different utilization of the Finger tensor. A step strain in the deformation, dominated by convection, is assumed. Setting $\boldsymbol{q} = \boldsymbol{C}_{(t)}^{-1/2}$, the polymeric stress is written as

$$\boldsymbol{\Xi}_p = G \frac{\boldsymbol{q}}{\{\boldsymbol{q}\}} . \tag{5.215}$$

Taking the time derivative of Eq. (5.215) yields (note that the time derivative involved here is the instantaneous rate of change)

$$\dot{\boldsymbol{\Xi}}_p = G \left(\frac{\dot{\boldsymbol{q}}}{\{\boldsymbol{q}\}} - \frac{\boldsymbol{q}\,\{\dot{\boldsymbol{q}}\}}{\{\boldsymbol{q}\}^2} \right) . \tag{5.216}$$

This last equation provides the dynamics of the stress with respect to the deformation. To find the governing equation for $\dot{\boldsymbol{q}}$, recall that $\boldsymbol{C}_{(t)}^{-1} = \boldsymbol{q}^2$, and Eq. (5.85) yields

$$\boldsymbol{q}\dot{\boldsymbol{q}} + \dot{\boldsymbol{q}}\boldsymbol{q} = \boldsymbol{L}\boldsymbol{q}^2 + \boldsymbol{q}^2\boldsymbol{L}^T \,. \tag{5.217}$$

With Eq. (5.215), Eq. (5.216) can be written as

$$\dot{\boldsymbol{\Xi}}_p = G\frac{\dot{\boldsymbol{q}}}{\{\boldsymbol{q}\}} - \boldsymbol{\Xi}_p\frac{\{\dot{\boldsymbol{q}}\}}{\{\boldsymbol{q}\}} \,. \tag{5.218}$$

Pre- and post-multiplying (5.218) by $\boldsymbol{\Xi}_p$ and summing yields

$$\boldsymbol{\Xi}_p\dot{\boldsymbol{\Xi}}_p + \dot{\boldsymbol{\Xi}}_p\boldsymbol{\Xi}_p = G\frac{\boldsymbol{\Xi}_p\dot{\boldsymbol{q}} + \dot{\boldsymbol{q}}\boldsymbol{\Xi}_p}{\{\boldsymbol{q}\}} - 2\boldsymbol{\Xi}_p^2\frac{\{\dot{\boldsymbol{q}}\}}{\{\boldsymbol{q}\}} \,. \tag{5.219}$$

The numerator in the fraction is directly related to $\boldsymbol{q}\dot{\boldsymbol{q}} + \dot{\boldsymbol{q}}\boldsymbol{q}$, so that by taking Eq. (5.217) into account, Eq. (5.219) gives

$$\boldsymbol{\Xi}_p\dot{\boldsymbol{\Xi}}_p + \dot{\boldsymbol{\Xi}}_p\boldsymbol{\Xi}_p = \boldsymbol{L}\boldsymbol{\Xi}_p^2 + \boldsymbol{\Xi}_p^2\boldsymbol{L}^T - 2\boldsymbol{\Xi}_p^2\frac{\{\dot{\boldsymbol{q}}\}}{\{\boldsymbol{q}\}} \,. \tag{5.220}$$

In order to compute $\{\boldsymbol{q}\}$, Eq. (5.217) is premultiplied by $\boldsymbol{q}^{-1}$ which yields

$$\dot{\boldsymbol{q}} + \boldsymbol{q}^{-1}\dot{\boldsymbol{q}}\boldsymbol{q} = \boldsymbol{q}^{-1}\boldsymbol{L}\boldsymbol{q}^2 + \boldsymbol{q}\boldsymbol{L}^T \,, \tag{5.221}$$

with the trace being given by

$$\{\dot{\boldsymbol{q}}\} = \{\boldsymbol{L}\boldsymbol{q}\} \,. \tag{5.222}$$

The combination of Eqs. (5.220) and (5.221) produces the relation

$$\boldsymbol{\Xi}_p\dot{\boldsymbol{\Xi}}_p + \dot{\boldsymbol{\Xi}}_p\boldsymbol{\Xi}_p = \boldsymbol{L}\boldsymbol{\Xi}_p^2 + \boldsymbol{\Xi}_p^2\boldsymbol{L}^T - 2\boldsymbol{\Xi}_p^2\frac{\{\boldsymbol{L}\boldsymbol{\Xi}_p\}}{G} \,. \tag{5.223}$$

Equation (5.223) is the exact representation of the integral equation (5.200) for the assumed strain jump. The final differential equation of the Doi-Edwards model is obtained by addition of a relaxation term to Eq. (5.223),

$$\boldsymbol{\Xi}_p\dot{\boldsymbol{\Xi}}_p + \dot{\boldsymbol{\Xi}}_p\boldsymbol{\Xi}_p = \boldsymbol{L}\boldsymbol{\Xi}_p^2 + \boldsymbol{\Xi}_p^2\boldsymbol{L}^T - 2\boldsymbol{\Xi}_p^2\frac{\{\boldsymbol{L}\boldsymbol{\Xi}_p\}}{G} - \frac{2}{\lambda}\boldsymbol{\Xi}_p\left(\boldsymbol{\Xi}_p - \frac{G}{3}\boldsymbol{I}\right) \,, \tag{5.224}$$

or in a more conventional notation in terms of the square of the polymeric stress as

$$\frac{D\boldsymbol{\Xi}_p^2}{Dt} = \boldsymbol{L}\boldsymbol{\Xi}_p^2 + \boldsymbol{\Xi}_p^2\boldsymbol{L}^T - 2\boldsymbol{\Xi}_p^2\frac{\{\boldsymbol{L}\boldsymbol{\Xi}_p\}}{G} - \frac{2}{\lambda}\left(\boldsymbol{\Xi}_p^2 - \frac{G}{3}\boldsymbol{\Xi}_p\right) \,. \tag{5.225}$$

5.12.3 Pom-Pom Model

The presence in polymer melts of long-chain branches calls for a novel approach, especially as they offer strain-hardening in extensional flows and shear-thinning

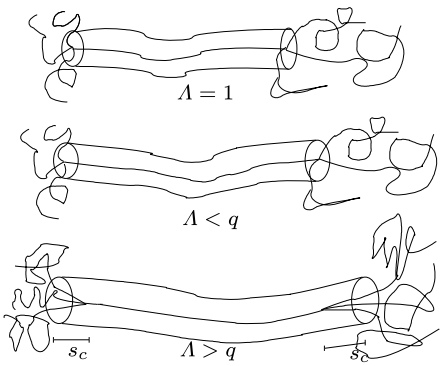

Fig. 5.10 The pom-pom model

in shear flows. This task has been undertaken in a paper by McLeish and Larson (1998) where they propose an idealized branched polymer architecture that will exhibit strain-hardening in extension and strain-softening in shear. The key ingredient of such branching structure is the use of multiple branch points on the same polymer molecule. The model is constructed by a backbone segment that connects two identical pom-poms, each composed of q arms (cf. Fig. 5.10). As in the Doi-Edwards model, the backbone is considered inserted in a tube of diameter d formed by other neighboring pieces. The pom-pom with its q arms attached to each branch point is dangling and contributes to the representation of the rheological properties of highly-entangled polymer melts. Because of the backbone confinement, the chain segment cannot move more than the tube diameter in the transverse direction. Therefore, the polymer chain deforms and moves more in the other direction where, through reptation, it diffuses and by elastic entropy, may also retract. The tube model impedes the unlimited stretching of the segments. The Brownian force on every free chain composing the pom-pom has the value $k_B\theta/d$ and maintains the curved chain segment inside the tube. For the pom-pom shown on Fig. 5.10, with $q = 3$ arms, the backbone stretches to a maximum length corresponding to the maximum tension $3k_B\theta/d$. In the analysis to follow, the dimensionless stretch ratio Λ of the backbone length to its equilibrium value will be used as the time dependent variable. When the backbone segment is in full extension (note that it is finitely extensible), the arms of the pom-pom are withdrawn into the tube (Fig. 5.10) and give rise to the retraction phenomenon. A second dynamical variable s_c defines the dimensionless length of the withdrawal of the branch point inside the tube.

Two other parameters, s_a and s_b, that are the lengths of the entangled paths of the arms and the backbone, respectively, are introduced. The characteristic arm relaxation time can be evaluated as

$$\lambda_a(x) = \lambda_0 \exp\left[\frac{15}{4}s_a\frac{(1-x)^2}{2} - (1-\varphi_b)\frac{(1-x)^3}{3}\right], \quad x = \frac{s_c}{s_a}, \tag{5.226}$$

where φ_b is the fraction of molecular weight contained in the backbone. The parameter λ_0 is a characteristic time scale featuring a deep retraction of the arm. The

characteristic time for the backbone relaxation is obtained through an Einstein diffusion argument and leads to

$$\lambda_b = \frac{4}{\pi^2} s_b^2 \varphi_b \lambda_a(0) q \ . \tag{5.227}$$

For the stress model, the tube segment assumption of Doi-Edwards is taken, and the relation (5.198), based on the orientation tensor (5.199), is used

$$\boldsymbol{\Xi}_p = \frac{15}{4} G_0 <\mathbf{u} \otimes \mathbf{u}> \ , \tag{5.228}$$

where G_0 is the relaxation modulus at the initial time. The brackets denote an average of the distribution of the tube-segment orientation vectors $\mathbf{u}$. The timescales associated with the arm and backbone relaxations are very disparate and separated. This induces a wide range of deformation rates between λ_b^{-1} and $\lambda_a^{-1}(0)$ which is the source of the nonlinear behavior generated essentially by the backbone material. The arms contribute to the Newtonian background viscosity. The relevant variables are related to the backbone orientation and stretch considering that some arm material becomes part of the backbone in the withdrawal process. Therefore, the modified stress is

$$\boldsymbol{\Xi}_p = \frac{15}{4} \varphi_b^2 G_0 <\mathbf{u} \otimes \mathbf{u}>, \quad \varphi_b = \frac{s_b}{s_b + 2q s_a} \ . \tag{5.229}$$

This stress must still take into account flows that stretch the backbone ($\Lambda > 1$), or produce branch-point withdrawal ($s_c > 0$). In case of backbone stretching, it is obvious that the stress depends linearly on Λ. Furthermore, the thermodynamic force is also linear with the stretch, and the overall effect is to generate a stress contribution from the backbone that is quadratic in Λ. Let us define the orientation tensor $\boldsymbol{Q}$ as,

$$\boldsymbol{Q} = <\mathbf{u} \otimes \mathbf{u}> \ , \tag{5.230}$$

where the brackets denote the average over the distribution space. Equation (5.229) then generalizes to

$$\boldsymbol{\Xi}_p = \frac{15}{4} \varphi_b G_0 \left(\varphi_b \Lambda^2 + \frac{2q s_b}{s_b + 2q s_a} \right) \boldsymbol{Q} \ . \tag{5.231}$$

5.12.3.1 Dynamical Equation for the Orientation Tensor

The integral form of the orientation tensor $\boldsymbol{Q}$ is inspired by the Lagrangian representation (5.200) of the Doi-Edwards model and uses the expression of the memory function given by Eq. (5.214). This yields

$$\boldsymbol{Q}(t) = \int_{-\infty}^{t} \frac{1}{\lambda_b(t')} \exp\left(- \int_{t'}^{t} \frac{dt''}{\lambda_b(t'')} \right) \boldsymbol{Q}(t') \mathrm{d}t' \ , \tag{5.232}$$

with the definition

$$\boldsymbol{Q}(t') = \left\langle \frac{\mathbf{u}' \otimes \mathbf{u}'}{u'^2} \right\rangle \ , \tag{5.233}$$

where $\mathbf{u}$ is the orientation unit vector before deformation at time t', and $\mathbf{u}'$ the deformed unit vector at the present time t such that

$$\mathbf{u}' = \boldsymbol{\mathcal{F}}_{(t)}(t')\mathbf{u}(t') \ . \tag{5.234}$$

5.12.3.2 Dynamical Equation for the Stretch

The (molecular) dynamics for the backbone stretch is governed by the local equilibrium of the dissipative drag mainly exerted on the tube, and the elastic recovery of the backbone with effective spring constant $k_B\theta/(s_b d^2)$. From Eq. (3.9), the relation of the time derivative of deformation tensor at the present time $\dot{\boldsymbol{\mathcal{F}}} = \boldsymbol{L}\boldsymbol{\mathcal{F}}(t)$ is deduced. The average length increase per unit length of the tube is then given by $\boldsymbol{L}\,\boldsymbol{Q}$ and therefore the increase of the relative tube velocity is given by $\Lambda\{\boldsymbol{L}\,\boldsymbol{Q}\}$ and the dynamical equation for the stretch becomes

$$\frac{\mathrm{d}\Lambda}{\mathrm{d}t} = \Lambda\{\boldsymbol{L}\,\boldsymbol{Q}\} - \frac{1}{\lambda_s}(\Lambda - 1) \quad \text{for} \quad \Lambda < q \ , \tag{5.235}$$

with the stretch relaxation time scale given by

$$\lambda_s = s_b \lambda_a(0) q \ . \tag{5.236}$$

5.12.3.3 Dynamical Equation for the Arm Withdrawal

When $\Lambda > q$ the transient relation for s_c is very similar to Eq. (5.235), that is

$$\frac{\mathrm{d}s_c}{\mathrm{d}t} = \left(q\frac{s_b}{2} + s_c\right)\{\boldsymbol{L}\,\boldsymbol{Q}\} - \frac{1}{2\lambda_a(s_c)} \ , \tag{5.237}$$

where the term $qs_b/2$ is a consequence of the backbone stretching by a factor $\Lambda_{max} = q$ before the branch-point withdrawal enters in action. The pom-pom set of equations is therefore given by Eqs. (5.231), (5.232), (5.235), (5.237), (5.227), (5.226) and (5.236). This set represents a formidable computational task to integrate numerically and consequently McLeish and Larson (1998) designed an approximate differential model.

5.12.3.4 The Approximate Differential Pom-Pom Model

The orientation tensor is approximated by $\boldsymbol{Q}_A$ that is defined as

$$\boldsymbol{Q}_A = \frac{\boldsymbol{c}}{\{\boldsymbol{c}\}} \ . \tag{5.238}$$

The suggested differential equation is

$$\overset{\triangledown}{\boldsymbol{c}} + \frac{1}{\lambda_b}\left(\boldsymbol{c} - \frac{\boldsymbol{I}}{3}\right) = 0 \ . \tag{5.239}$$

Note that the tensor $\boldsymbol{c}$ is closely related to the configuration tensor. Instead of (5.228), Rubio and Wagner (1999) showed that the correct relation for the polymeric stress is

$$\boldsymbol{\Xi}_p = 3G_0\varphi_b^2\Lambda^2 < \boldsymbol{Q}_A > , \tag{5.240}$$

when Eq. (5.239) is used. The factor 3 replaces the former ratio 15/4.

5.12.4 The Extended Pom-Pom Model

The pom-pom model has three identifiable flaws: steady state solutions in elongation show discontinuities; the equation for orientation is unbounded for high strain rates; and the second normal stress difference does not exist for shear flows. Verbeeten et al. (2001) further considered the backbone as a structure made of dimensionless connector vectors $\mathbf{r}_i$ of dimensionless stretch Λ_i and direction $\mathbf{u}_i$, the unit tangent vector to the backbone. One can then write

$$\mathbf{r}_i = |\mathbf{r}_i|\mathbf{u}_i = \Lambda_i \mathbf{u}_i \ . \tag{5.241}$$

The subscript i is needed to identify the various parts of the backbone; however for the sake of simplicity we will omit it in the sequel. The dynamic equation for the connector is then given by a non-affine motion

$$\dot{\mathbf{r}} = (\boldsymbol{L} - \boldsymbol{B})\,\mathbf{r} \ , \tag{5.242}$$

a generalization of (5.206), where $\boldsymbol{B}$ is a tensor that is still to be defined and will specify the slippage of the backbone with respect to the neighboring continuum and is aptly named the slip tensor. The dot is the time derivative in Eulerian or Lagrangian representation. Defining the dimensionless length of the connector as

$$|\mathbf{r}| = (\mathbf{r}\cdot\mathbf{r})^{1/2} \ , \tag{5.243}$$

the time evolution of the stretch can be evaluated as

$$|\dot{\mathbf{r}}| = \dot{\Lambda} = \frac{1}{2}(\mathbf{r}\cdot\mathbf{r})^{-1/2}(\dot{\mathbf{r}}\cdot\mathbf{r} + \mathbf{r}\cdot\dot{\mathbf{r}}) \ . \tag{5.244}$$

Using (5.242) and the definition (5.241) in Eq. (5.244), an evolution equation for Λ is obtained

$$\dot{\Lambda} = \Lambda\{(\boldsymbol{L} - \boldsymbol{B})(\mathbf{u}\otimes\mathbf{u})\} = \Lambda\{(\boldsymbol{D} - \boldsymbol{B})(\mathbf{u}\otimes\mathbf{u})\} \ . \tag{5.245}$$

Again combining Eqs. (5.242), (5.241) and (5.245), one gets

$$\dot{\mathbf{u}} = (\boldsymbol{L} - \boldsymbol{B})\,\mathbf{u} - \{(\boldsymbol{D} - \boldsymbol{B})(\mathbf{u}\otimes\mathbf{u})\}\mathbf{u} \ . \tag{5.246}$$

The dynamic equation for the connector length can be redefined by taking its average,

$$\dot{\Lambda} = \Lambda\{(\boldsymbol{D} - \boldsymbol{B})\,\boldsymbol{Q}\} \ . \tag{5.247}$$

With the help of (5.246), the relation for $\dot{\boldsymbol{Q}}$

$$\dot{\boldsymbol{Q}} = <\dot{\mathbf{u}} \otimes \mathbf{u} + \mathbf{u} \otimes \dot{\mathbf{u}}> , \tag{5.248}$$

and the assumption that the closure approximation $<\mathbf{u} \otimes \mathbf{u} \otimes \mathbf{u} \otimes \mathbf{u}> \simeq \boldsymbol{Q}^2$ holds, the evolution equation for the orientation tensor becomes

$$\overset{\triangledown}{\boldsymbol{Q}} + \boldsymbol{B}\,\boldsymbol{Q} + \boldsymbol{Q}\boldsymbol{B}^T + 2\{(\boldsymbol{D} - \boldsymbol{B})\,\boldsymbol{Q}\}\,\boldsymbol{Q} = 0 . \tag{5.249}$$

With the proposed model (5.240), the form of the slip tensor, as a function of the averaged stress tensor, is chosen as

$$\boldsymbol{B} = c_1 \boldsymbol{\Xi}_p + c_2 \boldsymbol{I} - c_3 \boldsymbol{\Xi}_p^{-1} = c_1 3 G_0 \varphi_b^2 \Lambda^2 <\boldsymbol{Q}_A> + c_2 \boldsymbol{I} - \frac{c_3}{3 G_0 \varphi_b^2 \Lambda^2} <\boldsymbol{Q}_A>^{-1} , \tag{5.250}$$

where the coefficients c_i, $i = 1, 2, 3$ are still to be defined. It is easy to check that the substitution of Eq. (5.250) into Eq. (5.249) yields a relation that depends only on c_1 and c_3. In order to obtain a non-vanishing second normal stress coefficient, Verbeeten et al. (2001) proposed that c_1 and c_3 be chosen in a Giesekus form (see also Peters and Baaijens 1997) such that

$$c_1 = \frac{\alpha}{2 G_0 \lambda_{0b}}, \qquad c_3 = \frac{G_0 (1 - \alpha)}{2 \lambda_{0b}} , \tag{5.251}$$

where α is a parameter monitoring the anisotropy of the model and λ_{0b} is the relaxation time for the tube orientation of the backbone. Imposing that the dynamic equation for the stretch (5.235) is exactly satisfied, the coefficient c_2 is computed by the substitution of (5.250) into (5.247)

$$c_2 = \frac{1 - \alpha - 3\alpha \lambda^4 \{\boldsymbol{\Xi}_p^2\}}{2 \lambda_{0b} \lambda^2} + \frac{1}{\lambda_s} \left(1 - \frac{1}{\Lambda} \right) . \tag{5.252}$$

The slip tensor becomes

$$\boldsymbol{B} = \frac{3\alpha \Lambda^2}{2\lambda_{0b}} <\boldsymbol{Q}_A> + \left[\frac{1 - \alpha - 3\alpha \Lambda^4 \{\boldsymbol{\Xi}_p^2\}}{2 \lambda_{0b} \Lambda^2} + \frac{1}{\lambda_s} \left(1 - \frac{1}{\Lambda} \right) \right] \boldsymbol{I} - \frac{(1 - \alpha)}{6 \lambda_{0b} \Lambda^2} <\boldsymbol{Q}_A>^{-1} . \tag{5.253}$$

The dynamic equations for the orientation tensor and the stretch are

$$\overset{\triangledown}{\boldsymbol{Q}} + 2\{(\boldsymbol{D} - \boldsymbol{Q})\,\boldsymbol{Q}\}\,\boldsymbol{Q} + \frac{1}{\lambda_{0b} \Lambda^2} \left[3\alpha \Lambda^4 \boldsymbol{Q}_A^2 + (1 - \alpha - 3\alpha \Lambda^4 \{\boldsymbol{\Xi}_p^2\}\,\boldsymbol{Q}_A - \frac{1 - \alpha}{3} \boldsymbol{I} \right] = 0 \tag{5.254}$$

and

$$\dot{\Lambda} = \Lambda \{\boldsymbol{D}\,\boldsymbol{Q}\} - \frac{1}{\lambda_s} (\Lambda - 1) , \quad \lambda_s = \lambda_{0s} e^{-\nu(\Lambda - 1)}, \quad \nu = \frac{2}{q} . \tag{5.255}$$

The model can be rewritten as a single equation if Eq. (5.107) is adopted for the conformation tensor. The extra-stress tensor is therefore

$$\boldsymbol{\Xi} = G_0 \left(3\Lambda^2 \boldsymbol{Q}_A - \boldsymbol{I} \right) . \tag{5.256}$$

Carrying through the time derivative of (5.256), the dynamic equation for the stress is

$$\overset{\nabla}{\boldsymbol{\Xi}} + \boldsymbol{B}\boldsymbol{\Xi} + \boldsymbol{\Xi}\boldsymbol{B}^T + G_0 \left(\boldsymbol{B} + \boldsymbol{B}^T \right) = 2G_0 \boldsymbol{D} . \tag{5.257}$$

Inserting Eq. (5.253) into Eq. (5.257) yields

$$\overset{\nabla}{\boldsymbol{\Xi}} + \frac{1}{\lambda(\boldsymbol{\Xi})} \boldsymbol{\Xi} = 2G_0 \boldsymbol{D} , \tag{5.258}$$

where

$$\frac{1}{\lambda(\boldsymbol{\Xi})} = \frac{1}{\lambda_{0b}} \left[\frac{\alpha}{G_0} \boldsymbol{\Xi} + f(\boldsymbol{\Xi})^{-1} \boldsymbol{I} + G_0 [f(\boldsymbol{\Xi})^{-1} - 1] \boldsymbol{\Xi}^{-1} \right] , \tag{5.259}$$

$$\frac{f(\boldsymbol{\Xi})^{-1}}{\lambda_{0b}} = \frac{2}{\lambda_s} \left(1 - \frac{1}{\Lambda} \right) + \frac{1}{\lambda_{0b} \Lambda^2} \left(1 - \frac{\alpha \{\boldsymbol{\Xi}_p^2\}}{3G_0^2} \right) , \tag{5.260}$$

with

$$\Lambda = \sqrt{1 + \frac{\{\boldsymbol{\Xi}\}}{3G_0}} . \tag{5.261}$$

5.12.5 *Linear Entangled Polymer Chains and the Rolie-Poly Equation*

Because the Doi-Edwards model fails to predict the correct shear stress in moderately nonlinear flows, two remedies were brought by consideration of chain stretch and constraint release as was already observed in previous sections. A microscopic theory based on the tube model of Doi and Edwards was elaborated by Milner et al. (2001) who were able to take four motions into account: reptation, flow convection, retraction and convection constraint release by a Rouse type (isotropic) motion. To this end, a stochastic dynamic equation describes the tube motion. Let us introduce the stochastic vector $\mathbf{R}(s,t)$ that gives the vector position of the tube segment under consideration. The variable s is the dimensionless curvilinear abscissa along the tube and $s \in [0, Z]$ where the symbol Z is the number of segments in the chain. The stochastic equation is written as

$$\begin{aligned} \mathbf{R}(s, t + \Delta t) = \mathbf{R}(s + \Delta\xi(t) \\ + \Delta t \left(\boldsymbol{L}\mathbf{R} + \frac{3}{2} \frac{\nu}{|\mathbf{R}'|} \mathbf{R}'' + \mathbf{g}(s,t) + \frac{1}{2\pi^2 \tau_e} \frac{(\mathbf{R}'' \cdot \mathbf{R}')\mathbf{R}'}{\mathbf{R}'^2} \right) \end{aligned} \tag{5.262}$$

where the notation $\mathbf{R}' = \partial\mathbf{R}/\partial s$ is now used for ease of notation. On the right-side of (5.262), $\mathbf{R}(s + \Delta\xi, t)$ describes reptation; the next term is the advection by the flow; the third and fourth terms concern the convection constraint release; the last term is the model of the reptation generated by the stretch evolution. The term $\Delta\xi(t)$ is the random noise due to the Brownian forces that generate reptation. The function $\mathbf{g}(s, t)$ is connected to the constraint release events. These two random variables have zero mean while the second moments are

$$<\Delta\xi(t)\Delta\xi(t')> = 2D_c\delta(t - t') \,, \tag{5.263}$$

$$<\boldsymbol{g}(s, t)\boldsymbol{g}(s', t')> = \nu a^2\delta(s - s')\delta(t - t')\boldsymbol{I} \,, \tag{5.264}$$

where ν is the constraint release frequency, and D_c the diffusion constant characterizing the reptation of one entanglement segment

$$D_c = \frac{1}{3Z\pi^2\tau_e} \,, \tag{5.265}$$

with τ_e, the Rouse relaxation time for one segment. The solution of Eq. (5.262) is sought in terms of the tangent correlation function

$$\boldsymbol{f}(s, s', t) = <\mathbf{R}'(s) \otimes \mathbf{R}'(s')> \,. \tag{5.266}$$

Using appropriate averages of (5.262) with the second moments, one is led (after a few pages of algebra (sic)) to the equation

$$\begin{aligned}\frac{\partial \boldsymbol{f}}{\partial t} &= \boldsymbol{L}\boldsymbol{f} + \boldsymbol{f}\boldsymbol{L}^T + D_c\left(\frac{\partial}{\partial s} + \frac{\partial}{\partial s'}\right)^2 \boldsymbol{f} \\ &+ \frac{3\nu}{2}\left[\frac{\partial}{\partial s}\left(\frac{1}{\sqrt{\{\boldsymbol{f}(s,s)\}}}\frac{\partial}{\partial s}(\boldsymbol{f} - \boldsymbol{f}_{eq})\right) + \frac{\partial}{\partial s'}\left(\frac{1}{\sqrt{\{\boldsymbol{f}(s',s')\}}}\frac{\partial}{\partial s'}(\boldsymbol{f} - \boldsymbol{f}_{eq})\right)\right] \\ &+ \frac{1}{2\pi^2\tau_e}\left[\frac{\partial}{\partial s}\left(\boldsymbol{f}(s,s')\frac{\partial}{\partial s}\ln\{\boldsymbol{f}(s,s')\}\right) + \frac{\partial}{\partial s'}\left(\boldsymbol{f}(s,s')\frac{\partial}{\partial s'}\ln\{\boldsymbol{f}(s,s')\}\right)\right] .\end{aligned} \tag{5.267}$$

At equilibrium when there is no flow,

$$\boldsymbol{f}_{eq} = \frac{a^2}{3}\delta(s - s')\boldsymbol{I} \,, \tag{5.268}$$

and the polymeric stress is then given by

$$\boldsymbol{\Xi}_p = \frac{3G_e}{Z}\int_0^Z \boldsymbol{f}(s, s)\mathrm{d}s \,, \tag{5.269}$$

where G_e is the plateau modulus $k_B\theta$ per displaced volume of an entanglement segment.

The Rolie-Poly model, aimed at an easier computational treatment, was designed by Likhtman and Graham (2003). The one-mode equation is a simplified version of the full model (5.267), and can be obtained through several routes. The simplest one is to drop the dependencies with respect to s in $\boldsymbol{f}(s, s')$ to generate the polymeric stress in terms of G_e units

$$\frac{D\boldsymbol{\Xi}_p}{Dt} = \boldsymbol{L}\boldsymbol{\Xi}_p + \boldsymbol{\Xi}_p\boldsymbol{L}^T - \frac{1}{\lambda_d}(\boldsymbol{\Xi}_p - \boldsymbol{I}) - f_{retr}(\{\boldsymbol{\Xi}_p\})\boldsymbol{\Xi}_p - f_{ccr}(\{\boldsymbol{\Xi}_p\})(\boldsymbol{\Xi}_p - \boldsymbol{I}) \,. \tag{5.270}$$

The third term on the right-side of Eq. (5.270) is a diffusion term characterizing reptation and relaxation towards equilibrium with the time scale λ_d. The fourth and fifth terms are retraction and CCR terms with both of them depending on the stretch given by $\{\boldsymbol{\Xi}_p\}$. Two limiting regimes are considered: small stretch with $\{\boldsymbol{\Xi}_p\} - 3 \ll 1$ and large stretch $\{\boldsymbol{\Xi}_p\} - 3 \gg 1$ which correspond to situations where the deformation is slower or faster than the stretch given by the Rouse relaxation time $\lambda_R = Z^2\lambda_e$. By a careful construction of the functions f_{retr} and f_{ccr} (the details are omitted here, but the interested reader may find them in Likhtman and Graham 2003), and an appropriate choice of the interpolation functions between the two regimes to match the full theory, one is led to the Rolie-Poly constitutive equation (ROuse LInear Entangled POLYmers)

$$\frac{D\boldsymbol{\Xi}_p}{Dt} = \boldsymbol{L}\boldsymbol{\Xi}_p + \boldsymbol{\Xi}_p\boldsymbol{L}^T - \frac{(\boldsymbol{\Xi}_p - \boldsymbol{I})}{\lambda_d} - \frac{2(1 - \sqrt{3/\{\boldsymbol{\Xi}_p\}})}{\lambda_R}\left[\boldsymbol{\Xi}_p + \beta\left(\frac{\{\boldsymbol{\Xi}_p\}}{3}\right)^{\delta}(\boldsymbol{\Xi}_p - \boldsymbol{I})\right] , \tag{5.271}$$

where β is of the order of unity and δ is a negative power close to one half. When $\lambda_R \to 0$, the former non-stretching theory is recovered. The factor in the last term of (5.271) goes to the following limit

$$\frac{2(1 - \sqrt{(3/\{\boldsymbol{\Xi}_p\}))}}{\lambda_R} \to \frac{2}{3}\{\boldsymbol{L}\boldsymbol{\Xi}_p\} \,. \tag{5.272}$$

Consequently, the non-stretching form of the Rolie-Poly equation is given by

$$\frac{D\boldsymbol{\Xi}_p}{Dt} = \boldsymbol{L}\boldsymbol{\Xi}_p + \boldsymbol{\Xi}_p\boldsymbol{L}^T - \frac{1}{\lambda_{eff}}(\boldsymbol{\Xi}_p - \boldsymbol{I}) - \frac{2}{3}\{\boldsymbol{L}\boldsymbol{\Xi}_p\}\boldsymbol{\Xi}_p \,, \tag{5.273}$$

where

$$\frac{1}{\lambda_{eff}} = \frac{1}{\lambda_d} + \frac{2}{3}\beta\{\boldsymbol{L}\boldsymbol{\Xi}_p\} \,. \tag{5.274}$$

Chapter 6
Turbulent Flows

One can arguably assume that the start of turbulence research as we view it within the context of conservation equations and statistical correlations began in the late nineteenth century. The seminal papers of Boussinesq (1877) and Reynolds (1895) dealing with turbulent momentum transfer and statistical averages of turbulent fluctuations still lie at the core of the research being conducted today. Not until the middle of the last century did texts on the subject begin to appear in the form of monographs focused on either homogeneous turbulence (Batchelor 1953) where theoretical analysis was tractable or turbulent shear flows (Townsend 1956) where the emphasis shifted to the extensive experimental results that had been gathered up to that point. These early monographs were soon augmented with texts (Hinze 1959; Lumley 1970a; Monin and Yaglom 1971) dealing more rigorously with the (statistical) theoretical aspects. The first text directed mainly at introducing students to the subject was Tennekes and Lumley (1972) and this marked the beginning of an era that continues today where numerical solutions have become as, or sometimes more, important in turbulence research as physical experiments. A recent presentation including modeling and simulation considerations is given in the book by Pope (2000). Although the primary focus in this chapter is on the incompressible flows and Newtonian fluids, there has also been much effort directed toward high-speed flows and compressible turbulence and now, within the last decade, to viscoelastic, polymeric fluids.

6.1 Homogeneity and the Spectral Cascade

Before embarking within the continuum mechanics framework to modeling of complex turbulent motion that often involve spatial inhomogeneities and (statistical) unsteadiness, it is useful to highlight some aspects of the simpler case of homogeneous turbulence. Though amenable to analytical scrutiny through Fourier analysis, important insight into the spectral cascade underlying even more "complex" turbulent fields has been gained for well over half a century. The assumption of spatial homogeneity naturally leads to a Fourier decomposition of the primitive variables

M.O. Deville, T.B. Gatski, *Mathematical Modeling for Complex Fluids and Flows*,
DOI 10.1007/978-3-642-25295-2_6,

governed by the Navier-Stokes equations. Of course, such analysis avoids the crucial difficulties induced by the presence of solid boundaries in most engineering applications and replaces differential operators by wavenumber multiplications in spectral space. Nevertheless, these Fourier tools yield direct access to spectra that are convenient and reliable theoretical instruments to interpret the physical phenomena. As might be expected, the field has been extensively explored and exploited by several authors arguably starting with the monograph by Batchelor (1953). Over the intervening decades there have been several reviews and these are nicely highlighted by McComb (1990) and Lesieur (2008). In the following, only a brief overview is provided, and the interested reader is referred to these texts for a more thorough discussion.

Let us approximate the velocity field by the following Fourier series given in a 2π periodic box

$$\mathbf{v}(\mathbf{x},t) = \sum_{\mathbf{k}} \mathbf{u}(\mathbf{k},t)\exp(i\mathbf{k}\cdot\mathbf{x}) \,, \tag{6.1}$$

where the wavevector $\mathbf{k}$ goes from $-\infty$ to ∞. Inserting (6.1) in the Navier-Stokes (5.170) with $\boldsymbol{\Xi}_p = \mathbf{0}$, one obtains

$$\left(\frac{\partial}{\partial t} + \nu k^2\right) u_\alpha(\mathbf{k},t) = \frac{i}{2} P_{\alpha\beta\gamma}(\mathbf{k}) \sum_{\mathbf{p}+\mathbf{q}=\mathbf{k}} u_\beta(\mathbf{p},t) u_\gamma(\mathbf{q},t) \,, \tag{6.2}$$

with the solenoidal condition $k_\alpha u_\alpha(\mathbf{k},t) = 0$, and where the projector operator $P_{\alpha\beta\gamma}$ is

$$P_{\alpha\beta\gamma}(\mathbf{k}) = k_\beta\left(\delta_{\alpha\gamma} - \frac{k_\alpha k_\gamma}{|\mathbf{k}|^2}\right) + k_\gamma\left(\delta_{\alpha\beta} - \frac{k_\alpha k_\beta}{|\mathbf{k}|^2}\right) . \tag{6.3}$$

The physical space nonlinearity inherent in the Navier-Stokes equations is now replaced in spectral space with a model interaction given by the projection operator $P_{\alpha\beta\gamma}$. Correspondingly, the turbulent stress spectrum tensor $\boldsymbol{\Phi}_{\alpha\beta}(\mathbf{k})$ can be constructed,

$$\Re\left[\overline{u_\alpha(\mathbf{k},t) u^*_\beta(\mathbf{k}',t)}\right] = \delta\left(\mathbf{k}-\mathbf{k}'\right)\boldsymbol{\Phi}_{\alpha\beta}(\mathbf{k}) \,, \tag{6.4}$$

where as indicated the real part is taken, * designates complex conjugate, and $\delta(\mathbf{k}-\mathbf{k}')$ is a scalar delta function dependent on the wavevectors $\mathbf{k}$ and $\mathbf{k}'$. If $\boldsymbol{\Phi}_{\alpha\beta}(\mathbf{k})$ is only a function of the magnitude of $\mathbf{k}$ then a spherical symmetry exists and an integration over the radius $|\mathbf{k}|$ yields an expression for the physical space turbulent kinetic energy,

$$\begin{aligned} K &= 2\pi \int_0^\infty \boldsymbol{\Phi}_{\alpha\alpha}(\kappa)\kappa^2 \mathrm{d}\kappa \\ &= \int_0^\infty E(\kappa)\mathrm{d}\kappa \end{aligned} \tag{6.5}$$

where the wavenumber $\kappa = |\mathbf{k}|$ ($|\mathbf{k}|^2 = \mathbf{k}\cdot\mathbf{k}$), and $E(\kappa)$ is the energy spectral density. The theory associated with the behavior of $E(k)$ in the inertial range of spectral

scales is due to Kolmogorov (1941a, 1941b) and has been a major cornerstone of turbulence theory and an implicit, underlying factor in turbulent model development.

The evolution of the turbulent kinetic energy is often the starting point in describing the behavior of a turbulent flow. In spectral space this is also the case since it provides important information about the spectral cascade. From the Navier-Stokes equations in Eq. (6.2), an evolution equation for the energy density $E(\kappa)$ can be obtained using Eq. (6.4). Multiplying Eq. (6.2) by u_α^* and adding the resulting equation to its complex conjugate and averaging yields

$$\left(\frac{\mathrm{d}}{\mathrm{d}t} + 2\nu\kappa^2\right) E(\kappa) = T(\kappa) \ , \tag{6.6}$$

where the term on the right, derivable from the spectral nonlinearly term,

$$T(\kappa) = \pi\kappa^2 i \Bigg[u_\alpha^* P_{\alpha\beta\gamma}(\mathbf{k}) \sum_{\mathbf{p}+\mathbf{q}=\mathbf{k}} u_\beta(\mathbf{p},t) u_\gamma(\mathbf{q},t) - u_\alpha P_{\alpha\beta\gamma}(\mathbf{k}) \sum_{\mathbf{p}+\mathbf{q}=\mathbf{k}} u_\beta^*(\mathbf{p},t) u_\gamma^*(\mathbf{q},t) \Bigg] \ , \tag{6.7}$$

represents the transfer of energy in spectral space. Interestingly, integrating Eq. (6.6) over all wavenumbers yields

$$\frac{\mathrm{d}K}{\mathrm{d}t} + 2\nu \int_0^\infty \kappa^2 E(\kappa)\mathrm{d}\kappa = \int_0^\infty T(\kappa)\mathrm{d}\kappa \ . \tag{6.8}$$

The second term on the left is a turbulent energy dissipation rate,

$$\varepsilon = 2\nu \int_0^\infty \kappa^2 E(\kappa)\mathrm{d}\kappa \ , \tag{6.9}$$

that represents the ultimate sink of energy in the spectral cascade. As Eq. (6.8) suggests, for a homogeneous (isotropic) turbulence no production mechanism exists so $\int_0^\infty T(\kappa)\mathrm{d}\kappa = 0$ and the turbulence simply decays. Thus $T(\kappa)$ is a transfer mechanism through the spectral cascade from large to small "scales". Much more can extracted from this simple set of equations as different spectral regions are explored (see Durbin and Petterson Reif 2010). Nevertheless, a complete description of the spectral evolution can only be made once an accurate closure for $T(\kappa)$ is obtained; however, since $T(\kappa)$ is proportional to the velocity third-moments, the challenge of an accurate representation is formidable.

Irrespective of the inherent difficulties, there have been noteworthy attempts at closing Eq. (6.6). Some involved representations based on a spectral eddy viscosity, and others involved a quasi-normal approximation for the fourth moments which was the basis for the Direct Interaction Approximation (DIA) (e.g. Kraichnan 1964) approach and the Eddy Damped Quasi-Normal Markovian (EDQNM) model (Orszag 1970). Unfortunately, a detailed discussion of these topics is beyond the scope here and the reader is referred to the book by McComb (1990) for details and additional references.

Before proceeding onto the more engineering based modeling most commonly used for complex turbulent flow fields, it is worth making note of the renormalization group (RG or RNG) model developed by Yakhot and Orszag (1986) (see also McComb 1990; Lesieur 2008) for turbulent flow prediction, and was adapted from that proposed by Wilson (1971). In the turbulence problem, the goal of RG theory is to provide a quantitative description of the small scales, and inherent in this description (Yakhot and Orszag 1986) is the assumption of the universality of the Kolmogorov $-5/3$ form of the $E(k)$ spectrum. The details of the RG mathematical formulation are cumbersome and as seen are a worthy monograph topic in themselves so any detailed development is outside the scope of this monograph. However, a brief description of the underlying ideas are worthwhile since many of the ideas become relevant to the development of hybrid methodologies where varying spectral cutoffs are requisite for model development.

The basic idea behind RG consists in choosing a wavenumber dependent eddy viscosity $\nu_e(\mathbf{k})$ as the renormalized variable. A wavenumber cutoff k_{c1} is chosen in the energy spectrum such that $k_{c1} < k_d$, where k_d is the largest wavenumber corresponding to the Kolmogorov scale. As proposed by Yakhot and Orszag (1986), the RG method works in two major steps. First, the Fourier transformed Navier-Stokes equations in the range $k_{c1} \leq k \leq k_d$ are solved. The resulting solution is introduced into the Navier-Stokes equations dealing with $0 \leq k \leq k_{c1}$. This process takes the influence of the high wavenumbers into account and modifies the effective viscosity such that $\nu_{new} := \nu + \delta\nu_e(\mathbf{k})$. Second, the primitive variables are rescaled in order that the Navier-Stokes equations on the lower modes $0 \leq k \leq k_{c1}$ are similar to the original equations on the full spectrum. The method is iterated by choosing a second wavenumber cut-off $k_{c2} \leq k_{c1} \leq k_m$ and the process is repeated until convergence toward a fixed point. Yakhot and Orszag (1986) demonstrated the existence of such fixed point. Additionally, Yakhot et al. (1989) also showed that RG theory is a way to build up LES models (Yakhot et al. 1989). There have been several critical questions raised about the details of the formalism used in the Yakhot and Orszag (1986) development (see, for example, Eyink 1994); however, the closure model within the K–ε framework (for example Yakhot et al. 1992) is one of the more popular models used in CFD applications.

Leaving now homogeneous fields, Fourier space and related considerations, the focus of the remainder of this chapter turns to inhomogeneous flows and the primary numerical methodologies and modeling strategies based on the Navier-Stokes equations.

6.2 Numerical Solution Methodologies

A common hierarchy of numerical solution methods based on the Navier-Stokes equations consists of direct simulations, scale resolving simulations and averaged-equation computations. The reader may be more familiar with the other more common terminology, that is, direct numerical simulation (DNS), large-eddy simulation (LES) and Reynolds-averaged Navier-Stokes (RANS). Over the last decade,

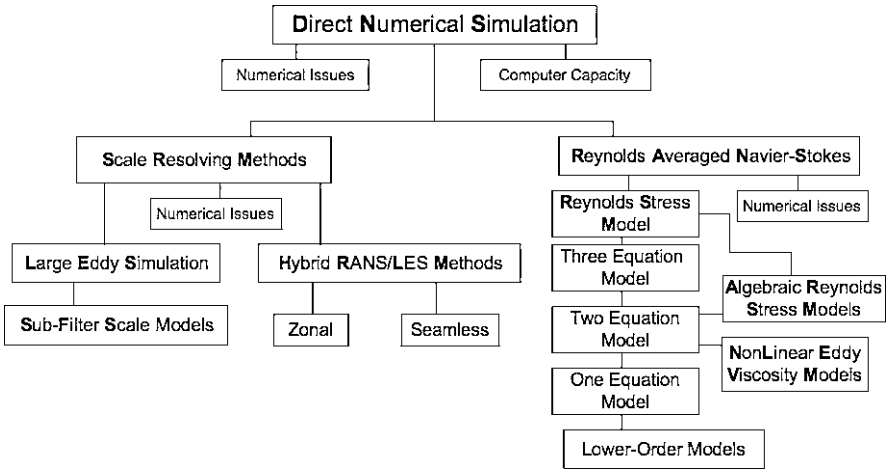

Fig. 6.1 Hierarchy of turbulent flow solution methods

however, there has been an increased need for engineering relevant, unsteady flow field computations. Although methodologies such as LES are generally applicable to these flows, scale resolution limitations arise as the Reynolds number increases. This has necessitated the development of hybrid methods that combine features of the LES method with features of RANS methods. This has then additionally led to critically examining the relationship between quantities obtained from filtered-variable equations and those obtained from averaged-variable equations. These hybrid methods have thus led to scale resolving simulations that are only capable of directly computing a limited range of spectral motions. Fortunately, such methods have some success in automatically adjusting the spectral cut-off within the flow field that allows for more rapid and memory efficient numerical solutions. Figure 6.1 gives a hierarchical sketch of the various solution methods that are most commonly used currently. The list reflects the more traditional, continuum mechanics approach to turbulent flow field solutions within the engineering community. However, as was presented in Sect. 1.5, an alternative route is through a molecular dynamics approach using, for example, a lattice Boltzmann method. This latter approach will be discussed in Chap. 7.

As Chap. 4 suggested, a primary interest in this book is the development of constitutive equations applicable to complex fluids and complex flows. Chapter 5 has focused on the complex fluids, and in this chapter the emphasis turns to complex flows—that is turbulent flows. The need for such constitutive equations, or closure models as they are termed in the turbulence community, can be seen from a brief discussion of the three solution methodologies alluded to in the previous paragraph. The reader is alerted to the fact that this change in topical focus brings about some changes in notation. Primarily the reader will notice that the rate of strain tensor which previously had been denoted by $\boldsymbol{D}$ or D_{ij} will now be replaced by $\boldsymbol{S}$ and S_{ij} when the discussion relates to either filtered or mean variables.

6.2.1 Direct Numerical Simulation (DNS)

As the name implies, direct numerical simulations (DNS) simply involve the numerical solution of the full three-dimensional Navier-Stokes equations as described, for incompressible flows, by Eqs. (3.73) and (3.77).[1] With sufficiently accurate spatial mesh resolution, time step integration and algorithm, it should be possible to capture all the scales of motion through to the Kolmogorov length scale η. Both internal (channel flow) and external (boundary layer) flows under a variety of conditions have been investigated. For incompressible simulations, higher-order spatial and temporal accuracy of the algorithm is often required. These requirements can vary depending on the flow under consideration and a full discussion of such algorithmic issues is not the intent here. Of interest, is the imposed physical limitations due to the broad spectrum of scales present in such turbulent flows.

Since the range of scales between the characteristic, or integral, scale L of the largest turbulent motions and the Kolmogorov scale η needs to be resolved, it is necessary that the computational domain in each direction must be at least as large as the respective turbulent integral scale. Assuming that L is equal in all directions (an often violated assumption),

$$N\Delta > L \ , \tag{6.10}$$

where N is number of grid points, and Δ is the spatial mesh size (assumed to be equal in all directions as well). As required, Δ must be sufficiently small to resolve the Kolmogorov scale

$$\Delta \leq \eta = \left(\frac{\nu^3}{\varepsilon}\right)^{1/4} \ , \tag{6.11}$$

where ν is the kinematic viscosity, and ε is the energy dissipation rate associated with the smallest turbulent scales. For a Newtonian fluid the viscosity ν is simply the Newtonian viscosity ν_0; however, for generalized Newtonian fluids (GNF) and viscoelastic fluids, the viscosity ν needs to be selected more carefully. In the case of viscoelastic fluids, for example, the total zero-shear viscosity needs to be used.

If an energetic equilibrium is assumed so that the dissipation rate is related to the large scale dynamics, this gives an inertial range estimate of the dissipation rate,

$$\varepsilon \approx \frac{u'^3}{L} \ , \tag{6.12}$$

where u' is an *rms* velocity characteristic of the large scales. Inserting Eq. (6.12) into the definition of η in Eq. (6.11) and combining with Eq. (6.10) yields

$$N^{-1} < \frac{\Delta}{L} \leq Re^{-3/4}, \qquad \text{or} \qquad Re^{3/4} \leq \frac{L}{\Delta} < N \ , \tag{6.13}$$

[1] Note that throughout this chapter the density field is assumed constant and has been assimilated into the pressure field and the viscous stress tensor. It, therefore, will not appear explicitly in any of the differential formulations.

where $Re = u'L/\nu$ is a turbulent Reynolds number. For a full three-dimensional simulation N^3 points are required, and this estimate is given by

$$N^3 \geq Re^{9/4} \,. \tag{6.14}$$

With engineering relevant flows having Reynolds numbers exceeding 10^7, it is easily seen that the number of grid points required can rapidly become prohibitive.

In addition to the potentially very large memory requirements, the computational time required can be large as well. Assuming that an explicit numerical method is used, the Δt must be sufficiently small so that the fluid particle moves only a fraction of the mesh spacing Δ per time step, that is,

$$u' \Delta t < \Delta \,, \tag{6.15}$$

or

$$C = \frac{u' \Delta t}{\Delta} < 1 \,, \tag{6.16}$$

where C is the Courant number. Analogous to the turbulent integral scale L, the integral turbulent time scale τ is given by

$$\tau = \frac{L}{u'} \,. \tag{6.17}$$

The length of time required for a simulation is then some multiple of this time scale so that substituting Eq. (6.16) into Eq. (6.17) yields

$$M = \frac{\tau}{\Delta t} = \frac{L}{C\Delta} \propto Re^{3/4} \,, \tag{6.18}$$

where from Eq. (6.11), $\Delta \sim \mathcal{O}(\eta)$. The number of floating-point operations necessary in the simulation is proportional to number of mesh points, N^3 and number of time steps M, that is

$$\begin{aligned} &\propto N^3 \times M \\ &\propto Re^{9/4} \times Re^{3/4} \,, \end{aligned} \tag{6.19}$$

that is, proportional to Re^3. Even with these cost limitations, numerous benchmark turbulent flow simulations have been performed, albeit at values of Reynolds number usually below those encountered in real situations. Fortunately, for viscoelastic fluids, there does not appear any additional spatial or temporal resolution constraints introduced. The important advantage of the method, even under these low Reynolds number conditions, is the ability to get a broad range of statistical correlations that would otherwise be unattainable or attainable with insufficient accuracy. Nevertheless, currently and for the foreseeable future, it will be necessary for the numerical simulation of practical engineering turbulent flow fields to solve a system of equations for flow variables that represent the motion of a more limited spectral range of scales.

There is no shortage of activity performing direct numerical simulations of turbulent flows of Newtonian fluids across a wide range of speeds spanning both subsonic

and supersonic flows. In contrast, for non-Newtonian, that is viscoelastic, fluids the activity is much more limited and of course constrained to the subsonic regime. Nevertheless, in a little over a decade, large strides have been made in the DNS of such viscoelastic turbulent flows and a great deal of insight into the fluid/flow dynamics has been made. Such simulations have been primarily focused on fully developed channel flow and boundary layer flows. It appears the first DNS of a viscoelastic (FENE-P) fluid was performed by Sureshkumar et al. (1997) at a friction Reynolds number of 125 at friction Weissenberg numbers ranging from 12.5 to 50. Although Oldroyd-B fluids have an historical precedent, their inherent limitations as discussed in Chap. 5 have made them less attractive for such direct simulations. In contrast, the models discussed in Sect. 5.9, specifically the FENE models, where the relevant dependent variable is the conformation tensor $\boldsymbol{c}$, represents both an improved physical fluid model (shear-thinning behavior). In such simulations, the starting point is of course the instantaneous mass (continuity) and momentum conservation equations[2]

$$\frac{\partial v_j}{\partial x_j} = 0 \,, \tag{6.20}$$

and

$$\frac{Dv_i}{Dt} = \frac{\partial v_i}{\partial t} + \frac{\partial}{\partial x_j}(v_i v_j) = -\frac{\partial p}{\partial x_i} + \frac{\partial \Xi_{ij}}{\partial x_j} + f_i \,, \tag{6.21}$$

where the inclusion of the body force term, f_i, may be needed in some numerical simulations. In channel flow simulations, for example, $f_i = f_p \delta_{i1}$ represents the force associated with the pressure drop required to maintain the streamwise flow (Kim et al. 1982; Sureshkumar et al. 1997). For a Newtonian fluid simulation, the stress-strain rate relation $\Xi_{ij} = \Xi^n_{ij} = 2\nu_0 D_{ij}$ is used with ν_0 the Newtonian (solvent) kinematic viscosity. The usual non-dimensional scalings then introduce a Reynolds number Re into the viscous diffusion term. For a viscoelastic (non-Newtonian) simulation the situation is complicated by the need to consider a polymeric contribution as well as a solvent (Newtonian) contribution to the stress field Ξ_{ij}, that is

$$\begin{aligned} \Xi_{ij} &= \Xi^n_{ij} + \Xi^v_{ij} \\ &= 2\nu_0 D_{ij} + \Xi^p_{ij} \,, \end{aligned} \tag{6.22}$$

is the deviatoric part of the sum of the Newtonian fluid stress, $\boldsymbol{\Xi}^n$, and the polymeric stress $\boldsymbol{\Xi}^p$. It is customary for numerical simulations to write Eq. (6.21) in the form

$$\frac{\partial v_i}{\partial t} + \frac{\partial}{\partial x_j}(v_i v_j) = -\frac{\partial p}{\partial x_i} + \frac{\partial \Xi^p_{ij}}{\partial x_j} + \nu_0 \frac{\partial^2 v_i}{\partial x_j^2} \,, \tag{6.23}$$

where the body force term will be dropped in the sequel. The FENE-P dumbbell model has been almost exclusively used in such simulations for over a decade for

[2]The reader will notice that, throughout the chapter, index notation will be predominantly used in the governing equations to be discussed. This notation is more common in the turbulent flow literature.

channel flow (e.g. Sureshkumar et al. 1997; Dimitropoulos et al. 2001; Thais et al. 2010) and boundary layers (e.g. Dimitropoulos et al. 2005, 2006). An exception has been the DNS of Min et al. (2003) who used an Oldroyd-B model (see Eq. (5.54)) for the viscoelastic fluid although at low friction Weissenberg numbers (< 50). Because of its general form and extensive use, the discussion here will focus on the FENE-P fluid.

In such fluids, the viscoelastic polymeric stress Ξ_{ij}^p is given by Eq. (5.152)

$$\Xi_{ij}^p = \nu_{p0} \left(f(\{\boldsymbol{c}\}) c_{ij} - \delta_{ij} \right) , \tag{6.24}$$

where ν_{p0} is the polymeric contribution to the zero-shear viscosity, and $f(\{\boldsymbol{c}\})$ is the Peterlin function given by

$$f(\{\boldsymbol{c}\}) = \frac{L^2}{L^2 - \{\boldsymbol{c}\}} . \tag{6.25}$$

For the Oldroyd-B fluid, the Peterlin function is simply unity, $f(\{\boldsymbol{c}\}) = 1$, so that the polymeric stress is linearly proportional to the conformation tensor. An alternate form of Eq. (6.25) has often been used (for example Sureshkumar et al. 1997; Dimitropoulos et al. 1998; Thais et al. 2010), where the maximum chain extensibility L^2 in the numerator has been replaced with $L^2 - 3$ as originally proposed by Beris and Edwards (1994) (see Eqs. (5.154) and (5.155)). At high chain extensions, this added equilibrium term has minimal effect. An evolution equation for the conformation tensor c_{ij} for a FENE-P fluid, Eq. (5.150), is used and written as

$$\overset{\nabla}{c}_{ij} = -\frac{1}{\lambda} \left[\frac{\Xi_{ij}^p}{\nu_{p0}} \right] . \tag{6.26}$$

Flow field simulations usually introduce a normalization involving the total zero-shear viscosity, ν_{tot}, given by the sum of the solvent viscosity ν_0 and a polymeric (viscoelastic) zero-shear contribution ν_{p0}, and with a value of 0.9 usually taken for the ratio ν_0/ν_{tot}. A notable exception has been the simulation study of Ptasinski et al. (2003) who obtained results for the ratio ν_0/ν_{tot} as low as 0.4. In direct numerical simulations (for example Sureshkumar et al. 1997; Dimitropoulos et al. 1998; De Angelis et al. 2002; Thais et al. 2010), an isotropic diffusive term, proportional to $(1/\mathrm{Pr}_v)(\partial^2 c_{ij}/\partial x_k^2)$, has been introduced ($\mathrm{Pr}_v$ a stress Prandtl number) into Eq. (6.26) for numerical stability (Sureshkumar and Beris 1995). For channel flow simulations, values of friction Reynolds number as high as 1000 (Thais et al. 2011) have been achieved with maximum extensibility of $L = 200$ (Li et al. 2006) and friction Weissenberg numbers of 120 (Dubief et al. 2004), and for boundary layer simulations values of momentum thickness Reynolds number of 775 with $L = 100$ and friction Weissenberg numbers of 50 (Dimitropoulos et al. 2005, 2006) have been attained.

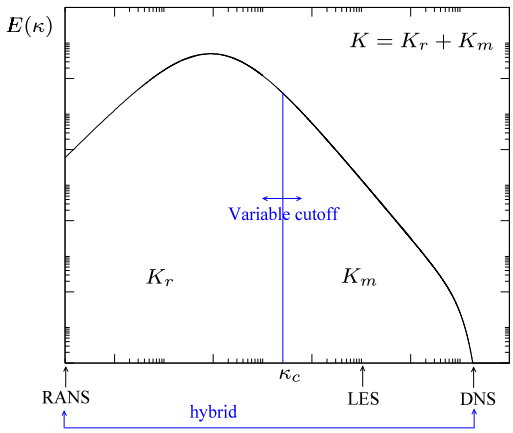

Fig. 6.2 Sketch of spectral energy cascade and wavenumber cutoff for direct and scale resolving simulation methods; K_r the resolved turbulent kinetic energy, K_m the modeled (unresolved) turbulent kinetic energy, and κ_c the filter wavenumber cutoff

6.2.2 Scale Resolving Simulations

An obvious remedy to the broad scale range requirement of the DNS methodology is to model those scales that are not resolvable by the simulation. The sketch in Fig. 6.2 illustrates the spectral partitioning that is required in such scale resolving (or eddy resolving) strategies. In order to extract this subset range of spectral scales, a filtering process needs to be introduced and applied to the dependent flow variables, such as the velocity and pressure. For a flow variable f, for example, this filtering process can be defined as a subset of the general operation

$$F(\mathbf{x},t) = \mathcal{G} * f = \int \mathcal{G}(\mathbf{x}-\mathbf{x}',t-t')\; f(\mathbf{x}',t')\; \mathrm{d}\mathbf{x}'\; \mathrm{d}t' \;, \tag{6.27}$$

where different forms for the convolution kernel $\mathcal{G}(\mathbf{x}-\mathbf{x}',t-t')$ can be associated with the different solution methodologies. In the discussion of the scale resolving simulations, the overbar notation will imply a filtering operation applied to the instantaneous variable. This process effectively partitions the dependent variables into a resolved part and an unresolved or subfilter part,

$$f(\mathbf{x},t) = F(\mathbf{x},t) + f'(\mathbf{x},t) \;, \tag{6.28}$$

where F $(:= \overline{f})$ is the resolved part and f' the unresolved or subfilter part. It will be shown that through this convolution process, it is possible to provide a unified treatment between a scale resolving methodology, such as a large eddy simulation (LES), and a methodology based on statistical means, such as RANS. This is useful in the development of alternative methodologies, such as the hybrid RANS/LES methods, currently being used.

6.2.2.1 Spatial and Temporal Filtering

Large eddy simulation (LES) has been, until recently, the primary scale resolving methodology used. It has been traditionally based on a spatial filtering approach and

was originally formulated for geophysical (atmospheric) applications (Smagorinsky 1963; Lilly 1966; Deardorff 1970). The formalism behind the requisite spatial filters is well-established and documented (e.g. Berselli et al. 2006; Sagaut 2006). For the most part, the top-hat, Gaussian, and spectral filters are the three convolution filters most commonly employed for the spatial scale partitioning. A top-hat filter, for example, with a spatial filter cut-off length of $\mathbf{\Delta}$, would then have a corresponding (centered) filter kernel given by

$$\mathcal{G}(\mathbf{x},t) = G_{\mathbf{\Delta}}(\mathbf{x};\mathbf{\Delta})G(t) = \frac{\mathcal{H}\left(\frac{\Delta_i}{2} - |x_i|\right)}{\Delta_i}\delta(t)\ , \tag{6.29}$$

with $\mathcal{H}$ representing the Heaviside function and $\delta(t)$ the Dirac delta function. Note that the filter width $\mathbf{\Delta}$ is written here as a vector to emphasize that the spatial filtering process needs, in general, to be inhomogeneous. For the most part, the filter width is usually taken as isotropic and equated to a value associated with the local grid spacing. Accounting for non-uniform grids leads, however, to several additional considerations (e.g. Sagaut 2006) that are beyond the intent and scope of the discussion here. For filters that are homogeneous and isotropic, a filtered quantity $\overline{f}$ can then be constructed from Eq. (6.27), using Eq. (6.29) as

$$F_{\Delta}(t;\Delta) = \mathcal{G}_{\Delta} * f = \frac{1}{\Delta}\int_{x-\frac{\Delta}{2}}^{x+\frac{\Delta}{2}} f(\mathbf{x}',t)\,d\mathbf{x}'\ . \tag{6.30}$$

Although currently not a common formalism for the scale resolving simulation methodology, the Eulerian temporal filtering of flow variables is a straightforward extension of the filtering concepts under discussion. Some recent work (Pruett 2000; Pruett et al. 2003) suggests it might be an effective alternative to the common spatial filtering process. Causal time domain filters are used since they are applicable to real time processes and only depend on past and present inputs. In this case, the filter kernel function in Eq. (6.27) is then given by

$$\mathcal{G}(\mathbf{x},t) = G(\mathbf{x})G_{\Delta_t}(t;\Delta_t) = \delta(\mathbf{x})\frac{\mathcal{H}(\Delta_t + t)}{\Delta_t}\ , \tag{6.31}$$

where Δ_t is a temporal filter width. The filtered quantity F can then be constructed in an analogous manner to Eq. (6.30), so that

$$F_{\Delta_t}(\mathbf{x};\Delta_t) = \mathcal{G}_{\Delta_t} * f = \frac{1}{\Delta_t}\int_{t-\Delta_t}^{t} f(\mathbf{x},t')\,dt'\ . \tag{6.32}$$

As will be discussed further in Sect. 6.2.3, the mean and moment equation approaches had been applied mainly to statistically steady (stationary) inhomogeneous flows. Since the Reynolds-averaged function $F(\mathbf{x})$ used in these mean and moment methods is the limit of the temporally-filtered function F_{Δ_t} when the temporal filter width Δ_t goes to infinity, suggests that within the realm of temporal filtering, it is possible to develop a linkage between the scale resolving methods, such as LES, and the mean and moment methods (Pruett et al. 2003). Within the context of spatial filtering, such a linkage can only be formally established in homogeneous flows. Nevertheless, it should also be recognized that an inherent linkage will always exist between any temporal filtering process and a corresponding spatial one.

6.2.2.2 Large Eddy Simulations

In large eddy simulation (LES), the goal is to simulate the resolved scales correctly by accurately replicating the unresolved scales and appropriately dissipating the energy of the unresolved scales. Whether spatial or temporal filters are used, application of the convolution operator given in Eq. (6.27) to the Navier-Stokes equations, Eqs. (3.73) and (3.77), results in the same form, and are given by

$$\frac{\partial V_j}{\partial x_j} = 0 \,, \tag{6.33}$$

$$\frac{DV_i}{Dt} = \frac{\partial V_i}{\partial t} + \frac{\partial}{\partial x_j}(V_i V_j) = -\frac{\partial P}{\partial x_i} + \frac{\partial \overline{\Xi}_{ij}}{\partial x_j} - \frac{\partial R_{ij}}{\partial x_j} \,, \tag{6.34}$$

where $\overline{\Xi}_{ij}$ is the filtered stress tensor Ξ_{ij} and R_{ij} is called the residual or subgrid stress tensor,

$$R_{ij} = \overline{v_i v_j} - V_i V_j \,. \tag{6.35}$$

Since there has been very limited application (see Sect. 6.2.2.3) of the LES approach to viscoelastic fluids, the focus in this section will be on Newtonian fluids with $\overline{\boldsymbol{\Xi}}$ given by the Newtonian form $2\nu_0 \boldsymbol{S}$, where $\boldsymbol{S}$ is now the filtered rate of strain tensor, $\boldsymbol{S} = \overline{\boldsymbol{D}}$. In this form, the large scale resolved motion ($\kappa < \kappa_c$) is computed directly, and the residual stress, which represents the contribution to the total turbulent stress from the unresolved motion ($\kappa > \kappa_c$), needs to be modeled in order to solve the equation system. The residual stress tensor plays an essential role in the dynamic balance that arises when a large eddy simulation methodology is employed. In the absence of any numerical dissipation effects (the ideal case), it is essential to include the effect of R_{ij}. If neglected, for example, the absence of any small (unresolved) scale dissipation results in an accumulation of kinetic energy near the cutoff wavenumber initially and which eventually spreads throughout the whole range of spectral scales—eventually destroying the simulation.

Since the velocity field shown in Eq. (6.35) is the total field, it can be partitioned as given in Eq. (6.28), so that Eq. (6.35) can be expanded as

$$R_{ij} = \underbrace{\overline{V_i V_j} - V_i V_j}_{L_{ij}} + \underbrace{\overline{V_i v_j'} + \overline{V_j v_i'}}_{C_{ij}} + \underbrace{\overline{v_i' v_j'}}_{\tau_{ij}} \,, \tag{6.36}$$

where L_{ij} is the Leonard tensor which represents the interactions between resolved scales, C_{ij} is a cross tensor which represents the interactions between resolved and unresolved scales, τ_{ij} is the unresolved (subfilter) turbulent stress tensor which represents the interaction between the unresolved small scales. The different energetic mechanisms contributing to the total turbulent stress are clearly distinguished by these tensors. In addition, the Leonard stress term is a consequence of the fact that the filtering process is not, in general, idempotent, that is $\mathcal{G} * F \neq F$ which consequently leads to $\mathcal{G} * f' \neq 0$. This will be discussed in more detail shortly in Sect. 6.2.3.1. One such filter that does retain the idempotent property is the spectral

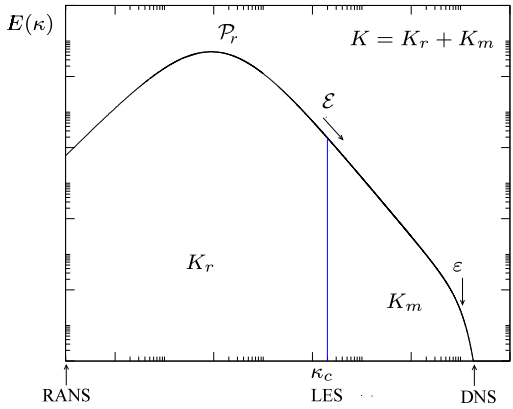

Fig. 6.3 LES spectral energy cascade and dynamic balance; K_r is the resolved turbulent kinetic energy and K_m is the modeled (unresolved) turbulent kinetic energy

cutoff filter. In this case, $L_{ij} = 0$ and $C_{ij} = 0$, so that the residual stress tensor is only attributed to the subfilter scale motions τ_{ij}. Even though the decomposition in Eq. (6.36) suggests that each term can be modeled separately, most often global models for R_{ij} are used.

Returning to the important role played by the subgrid scale (SGS) stress in the energetic dynamics, it might be expected that a solution methodology dependent on a spectral partitioning of an energy cascade requires modeling strategies capable of replicating the correct energy transfer mechanisms. The transport equation for the resolved scale kinetic energy $K_V = V_i V_i/2$ can be obtained directly from Eq. (6.34) and is given by

$$\frac{DK_V}{Dt} = -\frac{\partial\,(V_i P)}{\partial x_i} + \nu_0 \frac{\partial^2 K_V}{\partial x_j^2} - \nu_0 \frac{\partial V_i}{\partial x_j}\frac{\partial V_i}{\partial x_j} - \frac{\partial\left(R_{ij} V_i\right)}{\partial x_j} - \mathcal{E}\,. \tag{6.37}$$

The last term on the right $\mathcal{E}$ $(= -R_{ij}S_{ji})$ is a subgrid dissipation term and plays an important role in energy transfer from resolved to unresolved scales. Overall, the energy cascade is from resolved to subgrid scales ($R_{ij}S_{ji} < 0$); however, a local transfer of energy from subgrid to resolved scales (backscatter, $R_{ij}S_{ji} > 0$) can also occur. An important criterion to be used in formulating a suitable model for R_{ij} in total, or for the individual terms given in Eq. (6.36), can be readily identified by considering the case of homogeneous turbulence in energetic equilibrium $DK/Dt = 0$. For a homogeneous turbulence, the equilibrium energetic balance is simply one between production $\mathcal{P}$ and turbulent energy dissipation ε (see Fig. 6.3). Since the turbulent energy production $\mathcal{P}$ is dominated by the large (resolved) scales, $\mathcal{P} \approx \mathcal{P}_r$, the corresponding subgrid dissipation that governs the energy cascade to the small scales ($\kappa > \kappa_c$) is $\mathcal{E}$ (see Fig. 6.3). Thus an energetic equilibrium, with a production-to-dissipation rate balance, can only be achieved if $\mathcal{E} = \varepsilon$ $(= \mathcal{P}_r)$, and the subgrid scale model for the residual stress R_{ij} must be able to mimic the effect of the molecular dissipation rate ε.

In general, two types of modeling approaches are followed. One type is functional modeling where the divergence of the residual stress tensor $\partial R_{ij}/\partial x_j$ is modeled, and the other type is structural modeling where the residual stress tensor itself R_{ij} is modeled. In the former case, the strategy is to model the effect of the unresolved scales on the resolved scales; whereas, in the latter case there is no assumption about the interaction of the resolved and unresolved scales. Mixed models that combine the two approaches have also been developed, but the most widely used models are the functional models.

Not surprisingly, the hierarchy of closures for the subgrid stress field parallels that for the turbulent stress field found in the Reynolds-averaged approaches. The simplest and probably the most used SGS models are based on a scalar (unresolved scale) Newtonian eddy viscosity $\nu_t(\mathbf{x}, t)$ used in a Boussinesq-type relation

$$R_{ij} = \frac{\delta_{ij}}{3} R_{kk} - 2\nu_t S_{ij} \ . \tag{6.38}$$

With this form, the subgrid scale dissipation rate $\mathcal{E} = -R_{ij} S_{ji}$ then becomes

$$\mathcal{E} = \nu_t (2 S_{ij} S_{ji}) \ , \tag{6.39}$$

which further emphasizes its role as a resolved scale dissipation. In this type formulation, the isotropic part of Eq. (6.38) is usually assimilated into the scalar pressure field so that a modified pressure,

$$P_m = P + \frac{R_{kk}}{3} \ , \tag{6.40}$$

is introduced. The inherent drawback of such a combination is that the filtered pressure P is not available directly since the pressure field computed is P_m. The closer the spectral cutoff κ_c is to the wavenumber range of the peak (resolved) energy production, the greater the difference between the P_m and P pressure fields since the residual stress plays a larger role in the dynamic balance. Nevertheless, as noted this type of formulation is popular, and is exemplified by the Smagorinsky model and the associated dynamic procedure.

Smagorinsky Model The inclusion of a dynamic balance involving an eddy viscosity ν_t assumes that a characteristic velocity u' and length scale L can be found such that

$$\nu_t \propto u' L = v_c \Delta_c \ , \tag{6.41}$$

where v_c and Δ_c are a velocity and length scales, respectively, associated with spectral cutoff κ_c. Since the subgrid scale dissipation $\mathcal{E}$ represents a rate of energy transfer from the large to the small scales, it also can be estimated from these characteristic velocity and length scales, that is,

$$\mathcal{E} \propto \frac{v_c^3}{\Delta_c} \ . \tag{6.42}$$

Equation (6.42) is simply an inertial estimate for an energy dissipation rate and is simply a combination of an energy estimate (v_c^2) and a time scale estimate (Δ_c/v_c).

Recall that the subgrid scale dissipation $\mathcal{E}$ is given by $-R_{ij}S_{ji}$, so that when coupled with Eqs. (6.38) and (6.42), a relationship between the characteristic velocity and length scales is found,

$$\frac{v_c^3}{\Delta_c} \propto v_c \Delta_c (2S_{ij}S_{ji}) \,, \tag{6.43a}$$

or

$$v_c \propto \Delta_c \sqrt{2S_{ij}S_{ji}} \,. \tag{6.43b}$$

This yields directly a model (Smagorinsky 1963) for the subgrid scale eddy viscosity given by

$$\nu_t = (C_s \Delta_c)^2 \sqrt{2S_{ij}S_{ji}} \,, \tag{6.44}$$

where C_s is the Smagorinsky constant ($C_s \approx 0.15$–0.18). An estimate for the Smagorinsky constant can be easily obtained from the turbulent energy spectrum.

The Kolmogorov spectrum (energy spectral density) is given by the well-known $\kappa^{-5/3}$ distribution,

$$E(\kappa) = C_k \, \varepsilon^{2/3} \kappa^{-5/3} \,, \tag{6.45}$$

where $C_k = 1.41$. It is then assumed that the resolved scale rate of strain product $S_{ij}S_{ji}$ can be extracted from this assumed spectrum through

$$S_{ij}S_{ji} \approx \int_0^{\kappa_c} \kappa^2 E(\kappa) \, \mathrm{d}\kappa = C_k \, \varepsilon^{2/3} \int_0^{\kappa_c} \kappa^{1/3} \, \mathrm{d}\kappa \tag{6.46}$$

$$= \frac{3}{4} C_k \, \varepsilon^{2/3} \, (\pi/\Delta_c)^{4/3} \,, \tag{6.47}$$

where the integration is assumed valid to $\kappa_c = 0$ and $\kappa_c = \pi/\Delta_c$. With the assumption of a spectral equilibrium again invoked, $\mathcal{E} = \varepsilon$, Eqs. (6.39) and (6.47) can be combined to yield

$$C_s = \frac{1}{\pi} \left(\frac{2}{3C_k} \right)^{3/4} \approx 0.18 \,. \tag{6.48}$$

The model has been applied to a wide variety of flows, but even in a simple wall-bounded flow, such as channel flow, the optimal value for C_s that has been found is 0.065. Such variations in the closure coefficient highlights the weakness of the calibration and brings into question the universality of the model.

A Dynamic Procedure Even though the Smagorinsky model for the residual stress field is based on an isotropic eddy viscosity closure, the primary deficiency is the utilization of a fixed calibration coefficient C_s. A remedy for the lack of universality of C_s has been found by utilizing a dynamic procedure that determines C_s from the simulated resolved field without calibration (Germano et al. 1991; Lilly 1992). The underlying assumption is based on a scale-similarity hypothesis that assumes the behavior of the smallest resolved scales is similar to the subgrid (unresolved) scales being modeled.

For the Smagorinsky model a second filter, the *test filter*, of the same type as the first, but with $\widetilde{\kappa}_c < \kappa_c$ ($\widetilde{\Delta}_c > \Delta_c$) is introduced. This second filtering operation is designated here by $\widetilde{\ }$. The residual stress tensor associated with the double-filtered velocity can then be written as

$$\mathcal{R}_{ij} = \widetilde{\overline{v_i v_j}} - \widetilde{V}_i \widetilde{V}_j \ , \tag{6.49}$$

so that

$$\begin{aligned} \mathcal{L}_{ij} = \mathcal{R}_{ij} - \widetilde{R}_{ij} &= \widetilde{\overline{v_i v_j}} - \widetilde{V}_i \widetilde{V}_j - \left(\widetilde{\overline{v_i v_j}} - \widetilde{\overline{V_i V_j}} \right) \\ &= \widetilde{\overline{V_i V_j}} - \widetilde{V}_i \widetilde{V}_j \ . \end{aligned} \tag{6.50}$$

Equation (6.50) is composed of explicit terms only and is known as *Germano's identity*.

Consistent with the scale-similarity hypothesis, the dynamic procedure requires that $\mathcal{R}_{ij}$ and R_{ij} retain the same functional relationship with the corresponding strain rate field, that is, for the Smagorinsky model

$$R_{ij} - \frac{\delta_{ij}}{3} R_{kk} = -C_d \beta_{ij} \ , \tag{6.51a}$$

$$\mathcal{R}_{ij} - \frac{\delta_{ij}}{3} \mathcal{R}_{kk} = -C_d \alpha_{ij} \ , \tag{6.51b}$$

with

$$\beta_{ij} = \Delta_c^2 \sqrt{2 S_{pq} S_{qp}} \ S_{ij} \ , \tag{6.52}$$

$$\alpha_{ij} = \widetilde{\Delta}_c^2 \sqrt{2 \widetilde{S}_{pq} \widetilde{S}_{qp}} \ \widetilde{S}_{ij} \ , \tag{6.53}$$

and the proportionality coefficient C_d for the two residual stress fields is assumed the same. In terms of the Germano identity, Eqs. (6.51a), (6.51b) become

$$\mathcal{L}_{ij} - \frac{\delta_{ij}}{3} \mathcal{L}_{kk} = \widetilde{C_d \beta_{ij}} - C_d \alpha_{ij} \ , \tag{6.54}$$

with C_d now taken as a function of space and time, $C_d = C_d(\mathbf{x}, t)$. With the explicit appearance of the term $\widetilde{C_d \beta_{ij}}$, Eq. (6.54) is an integral equation which makes the determination of C_d problematic. The problem can be alleviated by assuming that C_d is constant over the filter length and determining it, for example, from a minimization of the residual error

$$e_{ij} = \mathcal{L}_{ij} - \frac{\delta_{ij}}{3} \mathcal{L}_{kk} + C_d \alpha_{ij} - C_d \widetilde{\beta}_{ij} \ , \tag{6.55}$$

where now the determination of C_d is algebraic. If the filter length is too large, the assumption of constant C_d can become problematic so that the choice $\widetilde{\Delta}_c = 2\Delta_c$ is usually made. Equation (6.55) is an over-determined system for C_d since the equation represents the six components of e_{ij}. A scalar relation can be easily formulated using a least-squares approach, such that $\partial e_{ij} e_{ji} / \partial C_d = 0$, which then yields

$$C_d = -\frac{1}{2} \left(\mathcal{L}_{ij} - \frac{\delta_{ij}}{3} \mathcal{L}_{kk} \right) \frac{m_{ji}}{m_{kl} m_{lk}} \ , \tag{6.56}$$

where $m_{ij} = \alpha_{ij} - \widetilde{\beta}_{ij}$. While certainly a resolved scale sensitive approach to the determination of the closure coefficient C_d, the fact that its instantaneous value is closely coupled to the behavior of a (resolved scale) turbulent velocity makes the procedure susceptible to numerical instabilities. Averaging either locally, in space or time, or in homogeneous directions can improve the robustness of the method.

Scale-Similarity Model The scale-similarity hypothesis used in developing a dynamic procedure assumed an equality between eddy viscosities associated with the residual stress R_{ij} and the residual stress associated with the double-filtered velocity $\mathcal{R}_{ij}$ (Bardina et al. 1980). A stronger scale-similarity assumption can also be made by assuming that the residual stress R_{ij} itself is related to the double-filtered velocity. In contrast to the Smagorinsky model that exemplified the functional modeling approach, such a scale-similarity model, where the residual stress itself is modeled, is representative of a structural modeling approach. (Recall that in the Germano identity, Eq. (6.50), $\mathcal{L}_{ij}$ was related to the double-filtered velocity.) The subgrid scale stress can then be written as

$$R_{ij} = \widetilde{\widetilde{V_i}\widetilde{V_j}} - \widetilde{V}_i \widetilde{V}_j \ , \tag{6.57a}$$

or if the second-filter is the same as the first, as

$$R_{ij} = \overline{V_i V_j} - \overline{V}_i \overline{V}_j \ . \tag{6.57b}$$

The effect of the double-filtering process is to better identify the largest unresolved scales to be modeled. This can be seen by considering the decomposition of the velocity field $V_i - \overline{V}_i$ into

$$V_i - \overline{V}_i = \overline{V_i + v_i'} - \overline{V}_i \tag{6.58}$$

$$= \overline{V}_i + \overline{v_i'} - \overline{V}_i \tag{6.59}$$

$$= \overline{v_i'} \ , \tag{6.60}$$

where $\overline{v_i'}$ can be seen as representative of the larger scale motions of the unresolved field. This approach provides a higher level of local and instantaneous correlation with the exact R_{ij} than eddy-viscosity models; however, the model does not ensure the correct SGS dissipation so that numerical instabilities arise.

Approximate Deconvolution Method Deconvolution methods are based upon defiltering the filtered flow fields and can be linked with the scale-similarity process already discussed. For the convolution operation described in Eq. (6.27), the corresponding approximate deconvolution for the velocity field can be written as

$$v_i^* = \mathcal{G}_a^{-1} V_i \ , \tag{6.61}$$

where $\mathcal{G}_a^{-1}$ is an approximation to the exact inverse $\mathcal{G}^{-1}$ of the convolution operation. A variety of deconvolution procedures have been proposed (see Sagaut 2006), but an explicit series approximation due to van Cittert, such as

$$\mathcal{G}_a^{-1} = I_d + (I_d - \mathcal{G}) + (I_d - \mathcal{G})^2 + \ldots + (I_d - \mathcal{G})^n \ , \tag{6.62}$$

has the advantage of having terms only involving multiple filters (here I_d is the identity operator). The resulting velocity reconstruction is of the form

$$v_i \approx v_i^* = \mathcal{G}_a^{-1} V_i = \sum_{n=0}^{N} c_n V^{(n+1)} \,, \tag{6.63}$$

where the c_n coefficients can be determined from the binomial formula, and $V^{(n+1)}$ is the $n+1$ filtered velocity field v_i, that is

$$\begin{aligned} v_i^* = V_i \quad (n=0), \qquad v_i^* = 2V_i - \overline{V}_i \quad (n=1) \,, \\ v_i^* = 3V_i - 3\overline{V}_i + \overline{\overline{V}}_i \quad (n=2) \,. \end{aligned} \tag{6.64}$$

Using this type of reconstruction, Stolz et al. (2001a) (see also Stolz and Adams 1999; Stolz et al. 1999, 2001b) proposed a model for the subgrid scale stress R_{ij} given by

$$R_{ij} = \overline{v_i^* v_j^*} - \overline{v}_i^* \overline{v}_j^* \,, \tag{6.65}$$

where v_i^* is given in Eq. (6.63). A comparison of Eqs. (6.57b) and (6.65) shows that the approximate deconvolution method (ADM) with $n = 0$ reduces to the originally proposed scale-similarity model. Not surprisingly the ADM, while capable of spectrally reconstructing an important portion of the unresolved motion, cannot accurately account for the smaller scale dissipative motion. Accordingly, the ADM, like the simple scale-similarity model discussed previously, suffers from a lack of dissipation necessary to ensure stable numerical simulations. These deficiencies necessitate a combination with subgrid scale stress models that include the necessary dissipative behavior. This requirement then leads to the introduction of mixed models to be discussed next.

Mixed Models As was just noted for both the scale-similarity model and the ADM, a common deficiency is the lack of subgrid scale dissipation and resulting deterioration of numerical stability. For the scale-similarity model in Eq. (6.57b), a common remedy for such a deficiency is straightforward and simply employs a linear combination of the scale-similarity model with a more dissipative functional eddy viscosity model such as the Smagorinsky model given in Eq. (6.44). The resulting mixed model is given by

$$R_{ij} - \frac{\delta_{ij}}{3} R_{kk} = \frac{1}{2} \left(\mathcal{L}_{ij} - \frac{\delta_{ij}}{3} \mathcal{L}_{kk} - 2\nu_t S_{ij} \right) \tag{6.66}$$

with

$$\mathcal{L}_{ij} = \overline{V_i V_j} - \overline{V}_i \overline{V}_j, \quad \nu_t = (C_s \Delta_c)^2 \sqrt{2 S_{ij} S_{ji}} \,. \tag{6.67}$$

Of course, instead of the Smagorinsky model eddy viscosity, a model based on the dynamic procedure could have also been used.

For the ADM, the mixed model is not formulated as simply as the linear combination just described. Stolz et al. (2001a) introduced a relaxation term, or secondary

regularization, into the filtered momentum equation to properly account for the energy transfer to the unresolved scales. This regularization term is given by

$$-\psi \left(I_d - \mathcal{G}_a^{-1} * \mathcal{G} \right) V_i \ , \tag{6.68}$$

where ψ is an inverse relaxation time. The term is dissipative and acts as an additional filter on V_i every $1/\psi \Delta t$ (Δt is the numerical integration time step). In contrast to the simple scale-similarity model, the dissipative modification used in the ADM is not based on any type of eddy viscosity concept, but rather on an enhancement of certain scales of motion obtained through the filtering of the instantaneous velocity field.

While certainly not as scale encompassing as a DNS, LES does directly simulate the resolved scales unsteady motion of the flow. It is not as computationally intensive as a DNS and, in general, the scales to be modeled are somewhat spectrally removed from the large or resolved scales and may therefore have a more universal (flow independent) character. As might be expected, closure models not dependent on boundary conditions or relatively decoupled from the large scale features of the flow should be more easily developed. Nevertheless, the computational cost can be high depending on the geometry and Reynolds number of flow and the fact that the simulation, by necessity must be three-dimensional. Although the algorithmic requirements can be reduced to second-order in space and time, it is often not possible to ascertain the influence of the numerical scheme on the results. In addition to the book by Sagaut (2006), the interested reader is referred to the books by Geurts (2004) and Lesieur et al. (2005) for additional references and discussion.

Even though this simulation technique was first adapted to engineering turbulent flows over 30 years ago (Reynolds 1976), the above issues, particularly those associated with computational requirements for wall-bounded flows, have prevented it from becoming a common engineering tool. This has led to the development of zonal or global hybrid models to help alleviate the computational overhead. Such complex flows have been computed in the past by solving equations for the (steady) statistical moments. This is the commonly known Reynolds-averaged approach which will be discussed next.

6.2.2.3 Viscoelastic Turbulent Fluid Simulations

Although direct numerical simulations have rapidly reached a high level of maturity for some viscoelastic fluid models, such as the FENE-P model, little has been done in the area of large eddy simulations for such fluids. An inherent problem lies in the complexity of a filtered conformation tensor evolution equation. A filtered form of the conformation tensor equation, Eq. (6.26), can be written as

$$\begin{aligned} &\frac{\partial \overline{c}_{ij}}{\partial t} + \frac{\partial}{\partial x_k}\left(V_k \overline{c}_{ij}\right) - \frac{\partial V_i}{\partial x_k}\overline{c}_{kj} - \frac{\partial V_j}{\partial x_k}\overline{c}_{ki} + \frac{1}{\lambda}\left[\frac{\Xi_{ij}^{\overline{c}}}{\nu_{p0}}\right] \\ &\quad = -\frac{\partial N_{ijk}}{\partial x_k} + P_{ij} - \frac{1}{\lambda}\left[\frac{T_{ij}^p}{\nu_{p0}}\right] \ , \end{aligned} \tag{6.69}$$

and the filtered polymeric stress relation, Eq. (6.24), as

$$\Xi_{ij}^{\overline{c}} = \nu_{p0}\left(f(\{\overline{\boldsymbol{c}}\})\overline{c}_{ij} - \delta_{ij}\right) . \tag{6.70}$$

Written in this form, the left side of Eq. (6.69) describes the evolution of the part of the conformation tensor associated with the large scale motions. The various subgrid or subfilter terms associated with the filtered conformation tensor equation are then given by

$$N_{ijk} = \overline{v_k c_{ij}} - V_k\,\overline{c}_{ij} , \tag{6.71a}$$

$$P_{ij} = \overline{\frac{\partial v_i}{\partial x_k} c_{kj}} + \overline{\frac{\partial v_j}{\partial x_k} c_{ki}} - \left(\frac{\partial V_i}{\partial x_k}\,\overline{c}_{kj} + \frac{\partial V_j}{\partial x_k}\,\overline{c}_{ki}\right) , \tag{6.71b}$$

$$T_{ij}^{p} = \overline{\Xi}_{ij}^{p} - \Xi_{ij}^{\overline{c}} , \tag{6.71c}$$

with Ξ_{ij}^{p} given by Eq. (6.24). Additionally, in Eq. (6.34) a filtered polymeric contribution $\overline{\Xi}_{ij}^{p}$ would now appear. Observe that the isotropic diffusive term mentioned in the discussion of DNS has been omitted here as well for consistency of presentation.

Obviously, large eddy simulations of viscoelastic fluids requires a broad scope of knowledge about the flow dynamics. Nevertheless, there are subfilter closure methodologies that minimize the need for physical rationalizations in order to proceed. A scale-similarity procedure or, more specifically, an approximate deconvolution approach (see Sect. 6.2.2.2) may be best adapted. The ADM relies on a partial reconstruction of the unresolved scales of motion through a deconvolution of the resolved field. Its shortcoming is that it is not sufficiently dissipative to properly account for the smallest unresolved, which can be accounted for through a secondary regularization process in the governing evolution equation. Thus, such a formulation minimizes the need for physical arguments related to the detailed dynamics to close the equations. Such an approach has been followed by Thais et al. (2010) where a temporal approximate decomposition approach has been followed. Although those simulations were limited to friction Reynolds numbers of 180 with $L = 100$ and friction Weissenberg numbers up to 115, the results were consistent with those obtained by direct numerical simulations. From this initial study, it does appear a systematic scale-resolving simulation approach can be applied to such viscoelastic turbulent flows, and as more detailed knowledge of the flow physics emerges from the direct simulations it may be possible to apply other subgrid scale closures to such flows.

6.2.3 Mean Equation Methods

This is the oldest approach applied to the solution of turbulent flow. It is based on the fact that the stochastic processes inherent in a turbulent motion has some statistical mean and that higher-order moments of the corresponding random variables exist.

Originally, the processes involved can be stationary or non-stationary, and/or homogeneous or inhomogeneous. The mean equation method has been the predominant means of solving for turbulent flow fields and is still a very important methodology for high Reynolds number flows and engineering flows in general. Within the last decade, the maturity of scale resolving methods and the need to remedy some inherent deficiencies in the mean equation methods has led to a more generalized interpretation of the mean and moment equations solved.

6.2.3.1 Reynolds Average

The commonly known Reynolds decomposition partitions the flow field variables into a form given by Eq. (6.28). Within the context of a Reynolds average, this means that F is a (ensemble) mean quantity and f' is a random fluctuating quantity. In general, this averaging procedure should satisfy the following four properties, or so-called "Reynolds axioms" (Kampé de Fériet and Betchov 1951): (i) $\mathcal{G} * (f+g) = F+G$; (ii) $\mathcal{G} * (\alpha f) = \alpha F$; (iii) $\mathcal{G} * (Fg) = FG$; (iv) $\mathcal{G} * (\lim f_n) = \lim F_n$ (this last condition ensures that convolution of any limiting process of a function f_n is equivalent to the same limiting process of the convolution function F_n). For $g = 1$ and with Eq. (6.28), it follows from (iii) that $F - \mathcal{G} * F = 0 = \mathcal{G} * f'$ which is an idempotent property that shows that the turbulent fluctuating quantity f' is centered about its mean value. Property (iv) ensures that the mean value of a partial derivative can be replaced by the partial derivative of a mean value. It is often additionally assumed that the mean was constant in either time (stationary) or space (homogeneous). For engineering flows, the former case of stationary, inhomogeneous turbulence was the norm so that F was only a function of spatial variables. In such cases, with the ergodic hypothesis used, the mean is then interpreted as a (long) time mean.

Until recently, there was little effort to try to reconcile the filtering operation given in Eq. (6.27) with Reynolds averaging. However, the emergence of hybrid models which merge both a scale resolving method, such as LES, with an averaged method, such as RANS, has provided the necessary incentive to explore this relationship. Consider the case where time mean variables are needed. The filter function (Gatski et al. 2007) in Eq. (6.27) is then given by

$$\begin{aligned} \mathcal{G}(\mathbf{x}' - \mathbf{x}, t' - t) &= G(\mathbf{x}' - \mathbf{x}) G_{\Delta_T}(t - t'; \Delta_T) \\ &= \delta(\mathbf{x}' - \mathbf{x})\, \mathcal{H}(t - t') \frac{\mathcal{H}(t' - t + \Delta_T)}{\Delta_T} , \end{aligned} \tag{6.72}$$

so that

$$F_{\Delta_T}(\mathbf{x}; \Delta_T) = \mathcal{G}_{\Delta_T} * f = \frac{1}{\Delta_T} \int_{t-\Delta_T}^{t} f(\mathbf{x}, t') \mathrm{d}t' . \tag{6.73}$$

With such filter kernels, the process is a time average over all scales of motion. This implies that the entire spectral range of scales (the subfilter part f') would need to be modeled when such "filters" are applied. This process is then equivalent to a

Reynolds average when the filter width Δ_T extends over several characteristic, or integral, time scales of the flow, that is

$$F(\mathbf{x}) = \lim_{\Delta_T \to \infty} F_{\Delta_T}(\mathbf{x}; \Delta_T)$$
$$= \lim_{\Delta_T \to \infty} \left(\mathcal{G}_{\Delta_T} * f\right) = \lim_{\Delta_T \to \infty} \frac{1}{\Delta_T} \int_0^{\Delta_T} f(\mathbf{x}, t)\, dt \ . \tag{6.74}$$

It is worth noting that if the limiting process were expressed as

$$F(\mathbf{x}) = \left(\lim_{\Delta_T \to \infty} \mathcal{G}_{\Delta_T} \right) * f \ , \tag{6.75}$$

then it could not be interpreted as a convolution filter since $\lim_{\Delta_T \to \infty} \mathcal{G}_{\Delta_T}(t) = 0$. However, as shown by Eq. (6.74) and recognized very early by Kampé de Fériet and Betchov (1951), the Reynolds average, as given in Eq. (6.74), can be expressed as a series of "truncated" functions obtained by convolution. As a practical matter, Reynolds averaging is evaluated as long-time averaging, where "long-time" implies long compared to the integral time scale. As just shown, Reynolds averaging can then be associated with the convolution (top-hat) filter $\mathcal{G}_{\Delta_T}$ with a sufficiently large Δ_T. Once this is established, the important condition that the Reynolds-average is idempotent ($\mathcal{G} * F = F$) holds, and fluctuations are centered about the mean value, $\mathcal{G} * f' = 0$. Note, however, that in spectral space the sharp cut-off, or spectral, filters possesses the idempotent property as well.

Irrespective of the formalism involved in applying a filtering/averaging operator to any flow variable, the resultant partitioning is then expressed in terms of mean and fluctuating parts, given formally by Eq. (6.28), which is called a Reynolds decomposition. If the turbulence field is statistically steady or stationary, ergodicity is usually assumed and a (long) time average over many turbulent time scales corresponds to an ensemble average. Similarly, if the turbulence is statistically homogeneous a spatial average over many turbulent length scales corresponds to an ensemble average.

6.2.3.2 Reynolds-Averaged Equations

When a filtering/averaging operator is applied to the Navier-Stokes equations, Eqs. (3.73), (3.77), and (3.87), the resulting system of equations is the well-known Reynolds-averaged Navier-Stokes (RANS) equations, which are given by

$$\frac{\partial V_j}{\partial x_j} = 0 \ , \tag{6.76}$$

$$\frac{DV_i}{Dt} = \frac{\partial V_i}{\partial t} + \frac{\partial}{\partial x_j}(V_i V_j) = -\frac{\partial P}{\partial x_i} + \frac{\partial}{\partial x_j}\left(\overline{\Xi}_{ij} - \tau_{ij}\right) \ , \tag{6.77}$$

where

$$\overline{\Xi}_{ij} = \overline{\Xi}^n_{ij} = 2\nu_0 S_{ij} \ , \tag{6.78}$$

is the deviatoric part of the viscous stress contribution, and

$$\tau_{ij} = \overline{v_i' v_j'} \tag{6.79}$$

is the Reynolds stress tensor. This Reynolds stress represents the contribution of all the fluctuating scales of motion to the turbulent stress field (it is also the subfilter stress where now the subfilter scales are all the fluctuating scales of motion). Statistical time variation of the velocity field is retained in the averaged momentum equation in order to recognize that some statistical unsteadiness (unsteady RANS or URANS) can be accommodated within this solution method. It is clear that the form-invariance exists between Eqs. (6.76) and (6.77) and Eqs. (6.33) and (6.34), but the dependent variables represent completely different scales of motion in the flow. What distinguishes the two flow field solutions are the imposed boundary conditions and the type of closure developed for R_{ij} and τ_{ij}. These two variables are responsible for accounting for the unresolved motions of the flow. For stationary flows ($\partial V_i/\partial t = 0$), which have long been the type of flows where RANS equations are applied, the approach is the computationally least intensive since issues associated with grid resolution of the turbulent scales do not apply. Thus, second-order numerical methods in space and time are generally sufficient and grid points numbering $\mathcal{O}(10^7)$ adequate except in the most complex geometric configurations. In addition, due to the decoupling between grid size and physical scales of motion, it is also possible to accurately assess numerical convergence issues associated with grid-resolved solutions.

For a Newtonian fluid, this Reynolds stress represents the contribution of all the fluctuating scales of motion to the turbulent stress field; however, when turbulent flow of dilute polymer solutions are considered the formulation is more complex. For a generalized Newtonian fluid (see Pinho 2003), for example, the non-Newtonian effects are included in the fluid viscosity as discussed in Sect. 5.2. (Recall that in this chapter, for ease of notation and the fact incompressible fluid flows are considered, the density ρ is assimilated into the different variables and does not appear explicitly.) For such fluids, the right side of Eq. (6.77) is altered so $\overline{\Xi}_{ij} - \tau_{ij}$ now becomes

$$\overline{\Xi}_{ij} - \tau_{ij} = 2\overline{\nu} S_{ij} + 2\overline{\nu' s_{ij}'} - \tau_{ij} \ , \tag{6.80}$$

with s_{ij}' the fluctuating rate of strain tensor. With the inclusion of shear rate effects into the viscosity for a GNF, fluctuations in the fluid viscosity appear in the correlation $\overline{\nu' s_{ij}'}$ and require closure. In general, the quantity $\overline{\nu}$ will be a combination of the (viscoelastic) shear viscosity contribution and an averaged molecular viscosity (see, for example, Pinho 2003; Cruz et al. 2004).

For polymeric fluid models, the right side of Eq. (6.77) becomes

$$\overline{\Xi}_{ij} - \tau_{ij} = 2\nu_0 S_{ij} + \overline{\Xi}_{ij}^{p} - \tau_{ij} \ , \tag{6.81}$$

where $\overline{\Xi}_{ij}^{p}$ represents a direct polymeric influence on the total (mean) stress Ξ_{ij}. At the lowest order, the polymeric stress can be represented by an isotropic linear relationship with the mean rate of strain tensor $\boldsymbol{S}$. At the next order a rate of change

variation of the strain rate tensor can be included. An immediate first choice would be a second-order fluid given by

$$\overline{\Xi}^{p}_{ij} = \nu_{p1} S_{ij} + \nu_{p2} \overset{\nabla}{S}_{ij} + \nu_{p12} S^2_{ij} \, . \tag{6.82}$$

Pinho et al. (2008b) have considered a truncated version of Eq. (6.82) with $\nu_{p12} = 0$ and $\nu_{p1} = \nu_{p2}$. For this second-order fluid Pinho et al. (2008b) formulated a one-equation model applicable to fully developed two-dimensional flow. The sole model equation was for the turbulent kinetic energy and required closure for the polymeric work associated with the $\overset{\nabla}{S}_{ij}$ term in Eq. (6.82). As was discussed in Sects. 5.2 and 5.5, such constitutive equations suffer from inherent deficiencies; although, the studies associated with such modeling strategies are very useful in establishing a procedure for the RANS computation of drag reducing flows.

Beyond such models lie the more complex nonlinear dumbbell models such as the FENE-P model. This has been used extensively in direct numerical simulations and, therefore, provides an important database for any RANS-type model development. In such fluids, it is necessary to examine the transport equation for the mean conformation tensor. This equation can be written as (cf. Eq. (6.69))

$$\begin{aligned} \overset{\nabla}{\overline{c}}_{ij} &= \frac{\partial \overline{c}_{ij}}{\partial t} + V_k \frac{\partial \overline{c}_{ij}}{\partial x_k} - \frac{\partial V_i}{\partial x_k} \overline{c}_{kj} - \frac{\partial V_j}{\partial x_k} \overline{c}_{ki} \\ &= -\frac{1}{\lambda} \left[\frac{\overline{\Xi}^{p}_{ij}}{\nu_{p0}} \right] - \frac{\partial}{\partial x_k} \left(\overline{v'_k c'_{ij}} \right) + \left(\overline{c'_{ik} \frac{\partial v'_j}{\partial x_k}} + \overline{\frac{\partial v'_i}{\partial x_k} c'_{kj}} \right) , \end{aligned} \tag{6.83}$$

or in terms of the symmetric mean rate of strain and skew-symmetric mean rate of rotation tensors as (cf. Eqs. (4.34a), (4.34b))

$$\begin{aligned} \frac{D\overline{c}_{ij}}{Dt} &= \frac{\partial \overline{c}_{ij}}{\partial t} + V_k \frac{\partial \overline{c}_{ij}}{\partial x_k} \\ &= \left(\overline{c}_{ik} S_{kj} + S_{ik} \overline{c}_{kj} \right) - \left(\overline{c}_{ik} W_{kj} - W_{ik} \overline{c}_{kj} \right) - \frac{1}{\lambda} \left[\frac{\overline{\Xi}^{p}_{ij}}{\nu_{p0}} \right] \\ &\quad - \frac{\partial}{\partial x_k} \left(\overline{v'_k c'_{ij}} \right) + \left(\overline{c'_{ik} \frac{\partial v'_j}{\partial x_k}} + \overline{\frac{\partial v'_i}{\partial x_k} c'_{kj}} \right) . \end{aligned} \tag{6.84}$$

The mean conformation tensor equation is written in this form to emphasize the form-similarity with the Reynolds stress tensor equation (cf. Eq. (6.90)). For a FENE-P fluid, the relationship with the polymeric stress is complicated by the Peterlin function; however, one can make qualitative comparisons of the various grouping of terms and the dynamic role played. Within this context, the first two grouping of terms, which include the mean rate of strain and rate of rotation tensors are the analog of the stress production terms. They differ only in sign, but their origin is inherently different, with the mean conformation tensor terms coming from terms representing the fluid element deformation and those that appear in the turbulent stress equation, Eq. (6.90), originating from translational motion of the element. Based

on channel flow simulation data (see Housiadas et al. 2005), the turbulent transport term associated with the $\overline{v_k' c_{ij}'}$ correlation has been found to be small throughout most of the channel with the exception of region in proximity to the wall. The nonlinear term associated with the fluctuating velocity gradients has also been analyzed and a closure model proposed by Pinho et al. (2008b). The only remaining term is the averaged polymeric stress. Using Eq. (6.24), an expression for this term can be written as (cf. Eq. (6.70))

$$\begin{aligned}\overline{\Xi}_{ij}^{p} &= \nu_{p0}\left\{\overline{\left[f(\{\boldsymbol{c}\})c_{ij} - \delta_{ij}\right]}\right\} \\ &= \nu_{p0}\left\{\left[\overline{f(\{\boldsymbol{c}\})}\,\overline{c}_{ij} - \delta_{ij}\right] + \overline{f(\{\boldsymbol{c}\})c_{ij}'}\right\}\ , \end{aligned} \tag{6.85}$$

where in the above the Reynolds decomposition $\boldsymbol{c} = \overline{\boldsymbol{c}} + \boldsymbol{c}'$ has been applied. From Eq. (6.85), it is apparent that the correct forms of the Peterlin function, given in Eq. (6.25), need to be used in evaluating this expression. It is worth highlighting that in order to get the mean polymeric stress it is necessary in general to provide a closure model for $\overline{f(\{\boldsymbol{c}\})c_{ij}'}$. Pinho et al. (2008b) have assessed the relative importance of this term using DNS data and found that it can be neglected relative to the first term in Eq. (6.85). Such closure issues become relevant when analysis of kinetic and elastic energies are of interest. For linear spring models such as the Oldroyd-B fluid, the elastic energy ($\propto \overline{\Xi}_{ii}^{p}$) is straightforward to obtain since the relevant viscoelastic equation is for the viscoelastic stress itself which is linearly proportional to the conformation tensor. For the FENE-P nonlinear fluid model, Eq. (6.85) shows the situation to be complicated by the multiplicative factor of $\overline{f(\{\boldsymbol{c}\})}$ and the higher-order correlation $\overline{f(\{\boldsymbol{c}\})c_{ij}'}$. Only very recently, has the FENE-P equation come under investigation for RANS model development (Resende et al. 2011). Additional studies should follow, so it is anticipated progress in obtaining RANS models and suitable closures will be made in the relatively near future. For example, recent studies using direct simulation data from fully developed channel flow (Housiadas et al. 2005; Li et al. 2006) have shown that the turbulent transport term associated with $\overline{v_k' c_{ij}'}$ can be neglected relative to the other terms in Eq. (6.84).

The major drawback to the RANS formulation for Newtonian fluids lies in the fact that τ_{ij} must accurately represent the effect of all the turbulence on the resultant mean motion; whereas, for viscoelastic fluids the situation is compounded by the need to close higher-order correlations for solution at the mean flow level. Such complexity does not preclude proceeding with the formalism necessary to have closure and obtain solutions; however, development of models capable of yielding accurate solutions over a wide parameter range will require development time.

6.3 Mean Equation Closure

Although the scale resolved and averaged equations eliminate the need to resolve all the scales of the turbulent motion required by direct numerical simu-

lations, they each are burdened with the need to determine higher-order correlations, such as R_{ij} and τ_{ij} for Newtonian fluids, that appear in the respective momentum equations. For viscoelastic, polymeric fluids, the difficulties are further compounded, and in these cases closure model development is at the early stages. For this reason, little detail of such viscoelastic modeling will be presented. However, the reader is encouraged to pursue such topics in the cited literature.

As was discussed in Sect. 6.2.2.2 for the LES methodology, there are generally two broad approaches used in solving the closure problem; the functional modeling approach and the structural modeling approach. While this terminology has usually been associated with the scale resolving or LES approach, it is easily extended to include the mean equation approach. For the scale resolving method, the mathematical focus of the functional modeling approach is to represent the net effect of the subfilter scales on the resolved motion by a suitable model for $\partial R_{ij}/\partial x_j$. The dynamic details of the interactions, such as represented by the decomposition in Eq. (6.36), are not considered. For the mean equation method, where all the scales of motion are modeled, this same qualitative description and underlying motivation for functional modeling is directly applicable. For structural modeling, the goal is to model the turbulent stress tensor itself, τ_{ij}. In this type of modeling approach, it is apparent that the details of the modeling for the scale resolving (LES) method and the mean equation method would differ substantially. The structural models that have been proposed for the LES method have been confined primarily to a scale similarity assumption which in its simplest form exploits a dynamic coupling between the smallest resolved scales and the unresolved scales, and as shown there are deconvolution methods where a portion of the subfilter scale motion is reconstructed from the simulated resolved scales (see Sagaut 2006). Such approaches have minimal connection to the utilization of a "constitutive equation" to describe the dynamic motion of a turbulent stress tensor.

For the mean equation method, the structural modeling approach has traditionally been focused on such a "constitutive equation" concept (Rivlin 1957; Crow 1967, 1968; Lumley 1970b). From a physical standpoint, the task is to characterize the turbulence, and one obvious characterization is to adequately describe the evolution of the representative turbulent velocity and length or time scales, an idea that originated over 60 years ago (Kolmogorov 1942). This task has been most directly approached through equations for the velocity correlations and either algebraic or differential specification of a characteristic length or time scale. Starting from the transport equation for the velocity second-moment τ_{ij}, a hierarchy of models (see Fig. 6.1) can be deduced from this differential transport equation through a variety of simplifying assumptions (see Gatski 1996). In the next section, this Reynolds stress transport equation is derived and from that a series of turbulence models can be extracted. The reader may also consult the very recent book by Hanjalić and Launder (2011) that is devoted to second-moment closures.

6.3.1 Reynolds Stress Tensor

A straightforward approach to finding the appropriate closure for τ_{ij} is to simply form the second-moment equation and attempt to find models for the higher order correlations in the equation. The starting point for developing the second moment or the Reynolds stress transport equations is the fluctuating momentum equation, which is obtained by using the Reynolds decomposition (6.28) and subtracting the mean momentum equation (6.77) from the instantaneous momentum equation (3.77). The resulting fluctuating momentum equation for v_i' is given by

$$\mathcal{L}v_i' = \frac{\partial v_i'}{\partial t} + V_k\frac{\partial v_i'}{\partial x_k} + v_k'\frac{\partial v_i'}{\partial x_k} + v_k'\frac{\partial V_i}{\partial x_k} + \frac{\partial p'}{\partial x_i} - \frac{\partial \Xi_{ik}'}{\partial x_k} - \frac{\partial \tau_{ik}}{\partial x_k} = 0 \quad (6.86)$$

and the corresponding second-moment formed from

$$\overline{v_i'\mathcal{L}v_j'} + \overline{v_j'\mathcal{L}v_i'} = 0\,. \quad (6.87)$$

Note that in Eq. (6.86), the Ξ_{ij}' represents the fluctuating component of the deviatoric part of the Cauchy stress tensor. As was seen in Sect. 6.2.3.2, for fluid constitutive equations beyond the Newtonian form, the fluctuating stress tensor Ξ_{ij}' leads to higher-order correlations appearing in the Reynolds-averaged formulation. For example, for a simple generalized Newtonian fluid, the fluctuating stress is

$$\Xi_{ij}' = 2\left(\nu' S_{ij} + \overline{\nu} s_{ij}'\right)\,. \quad (6.88)$$

For more complex constitutive equations ($\Xi_{ij} = \Xi_{ij}^n + \Xi_{ij}^p$), such as those for the second-order fluids (see, for example, Pinho et al. 2008b, Eqs. (11) and (12)), and the FENE-P fluids, that involve the upper convective derivative, the form of the fluctuating polymeric stress can be complex, for example,

$$\Xi_{ij}'^{p} = \nu_{p0}\left\{\left[f(\{\boldsymbol{c}\})c_{ij} - \overline{f(\{\boldsymbol{c}\})}\,\overline{c}_{ij}\right] - \overline{f(\{\boldsymbol{c}\})c_{ij}'}\right\}\,, \quad (6.89)$$

and $\overline{\boldsymbol{\Xi}'^{p}} = \mathbf{0}$. The resulting transport equation for the velocity second-moment, or Reynolds stress tensor τ_{ij}, can then be written as

$$\begin{aligned}\frac{D\tau_{ij}}{Dt} &= \frac{\partial \tau_{ij}}{\partial t} + V_k\frac{\partial \tau_{ij}}{\partial x_k}\\ &= \underbrace{-\left(\tau_{ik}S_{kj} + S_{ik}\tau_{kj}\right) + \left(\tau_{ik}W_{kj} - W_{ik}\tau_{kj}\right) - \varepsilon_{ij}}_{\text{Production and Destruction}}\\ &\quad + \underbrace{\left(\Pi_{ij} + D_{ij}^t + \nu_0\frac{\partial^2\tau_{ij}}{\partial x_k^2}\right)}_{\text{Redistribution and Transport and Diffusion}}\\ &\quad + \underbrace{\left(D_{p\cdot ij}^t - \varepsilon_{p\cdot ij}\right)}_{\text{Polymeric Contribution}}\,,\end{aligned} \quad (6.90)$$

where the first two collection of terms on the right side represent Newtonian contributions and the third $D^t_{p\cdot ij} - \varepsilon_{p\cdot ij}$ is a purely polymeric contribution ($D^t_{p\cdot ij}$ and $\varepsilon_{p\cdot ij}$ are the ij components of the tensors $\boldsymbol{D}^t_p$ and $\boldsymbol{\varepsilon}_p$). The Newtonian contributions have been examined extensively and these will discussed more fully shortly. It may be tempting to at least make a qualitative comparison between the production terms in Eq. (6.90) and those in Eq. (6.84). Aside from the difference in sign, there is a fundamental difference in their origin. For the Reynolds stress transport equation, the origin is the material derivative and within the material derivative operator it is the contribution from the spatial movement of the fluid element (as described in Sect. 3.2.1). The subsequent Reynolds decomposition then yields these production terms. In contrast, the "production terms" originate from contributions in the convective derivative associated with the time dependence of the relative deformation gradient of the fluid element (see Sect. 4.3.2.1). While both are linked to the material fluid element, the Reynold stress production is linked to the proper description of the movement of the fluid element; whereas, the conformation (or polymeric stress) tensor production is linked to a rate of (relative) deformation of the fluid element.

The polymeric contributions,

$$D^t_{p\cdot ij} = \frac{\partial}{\partial x_k}\left(\overline{v'_i \Xi'^p_{jk}} + \overline{v'_j \Xi'^p_{ik}}\right), \tag{6.91}$$

$$\varepsilon_{p\cdot ij} = \left(\overline{\Xi'^p_{ik}\frac{\partial v'_j}{\partial x_k}} + \overline{\frac{\partial v'_i}{\partial x_k}\Xi'^p_{kj}}\right) \tag{6.92}$$

are, of course, unique to the study of viscoelastic flows, and represent polymeric transport effects, $D^t_{p\cdot ij}$, and polymeric dissipative effects, $\varepsilon_{p\cdot ij}$, that is work associated with the viscoelastic stress on the deformation of the fluid element. Pinho et al. (2008b) have further analyzed these terms using the available channel flow simulation data and found that each can be approximated by

$$D^t_{p\cdot ij} \approx \nu_{p0}\frac{\partial}{\partial x_k}\left[f(\{\overline{\boldsymbol{c}}\})\left(\overline{v'_i c'_{jk}} + \overline{v'_j c'_{ik}}\right)\right], \tag{6.93}$$

$$\varepsilon_{p\cdot ij} \approx \nu_{p0} f(\{\overline{\boldsymbol{c}}\})\left[\overline{c'_{ik}\frac{\partial v'_j}{\partial x_k}} + \overline{\frac{\partial v'_i}{\partial x_k}c'_{kj}}\right]. \tag{6.94}$$

Pinho et al. (2008b) (see Resende et al. 2011, for additional details) has developed closure models for these terms that are rather complex so the reader is referred to their study for details. It should be cautioned that while great strides have been very recently made in the development of RANS closure models for these viscoelastic fluids, the available database is limited and certainly constrained to simple geometries. As such the range of validity of such models still needs to be verified.

Equation (6.90) represents six independent tensor components that constitute an incompressible Reynolds stress transport equation applicable to viscoelastic fluid flows. The first two terms on the right side of Eq. (6.90) are the turbulent production terms due to the mean velocity gradients and the third term is the viscous diffusion term. For both the turbulent production and viscous diffusion, the terms are exact

and require no modeling. The remaining terms on the right in Eq. (6.90) are higher-order correlations and require modeling in order to close the equation. These terms are the pressure-strain rate correlation, Π_{ij},

$$\Pi_{ij} = \overline{p'\left(\frac{\partial v_i'}{\partial x_j} + \frac{\partial v_j'}{\partial x_i}\right)} = \overline{p'\left(s_{ij}' + s_{ji}'\right)}\,, \tag{6.95a}$$

the turbulent transport due to velocity and pressure fluctuations

$$D_{ij}^t = -\frac{\partial}{\partial x_k}\left[\overline{v_i' v_j' v_k'} + \left(\overline{p' v_i'}\delta_{jk} + \overline{p' v_j'}\delta_{ik}\right)\right]\,, \tag{6.95b}$$

and the turbulent dissipation rate,

$$\begin{aligned}\varepsilon_{ij} &= 2\nu_0 \overline{\frac{\partial v_i'}{\partial x_k}\frac{\partial v_j'}{\partial x_k}} \\ &= 2\nu_0\left[2\overline{w_{ij}'^2} + 2\overline{s_{ik}' w_{kj}'} - \overline{\frac{\partial v_i'}{\partial x_k}\frac{\partial v_k'}{\partial x_j}}\right]\,,\end{aligned} \tag{6.95c}$$

with w_{ij}' the fluctuating rate of rotation tensor. Both the turbulent transport tensor D_{ij}^t and the turbulent dissipation rate tensor ε_{ij} can be decomposed into isotropic and deviatoric parts (the pressure-strain rate correlation tensor Π_{ij} represents the deviatoric part since the trace vanishes in incompressible flows), given by

$$D_{ij}^t = D_{kk}^t\left(\frac{\delta_{ij}}{3} + d_{ij}^t\right)\,, \tag{6.96}$$

$$\varepsilon_{ij} = \varepsilon_{kk}\left(\frac{\delta_{ij}}{3} + d_{ij}^\varepsilon\right)\,, \tag{6.97}$$

where d_{ij}^t is the turbulent transport anisotropy and d_{ij}^ε is the dissipation rate anisotropy. These quantities play a role in the formulation of closure models for turbulent flows along with the corresponding decomposition of the turbulent stress tensor τ_{ij}, given by

$$\tau_{ij} = 2K\left(\frac{\delta_{ij}}{3} + b_{ij}\right)\,, \tag{6.98}$$

where b_{ij} is the turbulent stress anisotropy and $K = \tau_{kk}/2$ is the turbulent kinetic energy. The tensor anisotropies just introduced are useful since they provide a quantitative measure of deviation from the isotropic or equilibrium state. This can also provide a measure of any inhomogeneities if the isotropic state is associated with turbulence homogeneity.

A useful diagnostic in assessing the behavior of the turbulent anisotropy tensor was first proposed by Lumley (1978), who examined the limiting values of the invariants associated with b_{ij} in incompressible flows. These invariants are given by (see Eqs. (2.30)–(2.32)), $\mathrm{I}_2(\boldsymbol{b}) = -b_{ij}b_{ji}/2$ and $\mathrm{I}_3(\boldsymbol{b}) = \det \boldsymbol{b}$ with $\mathrm{I}_1(\boldsymbol{b}) = 0$. For isotropic turbulence, the anisotropies vanish and the corresponding point is the origin of Fig. 6.4 representing the anisotropy invariant map. From the origin, two

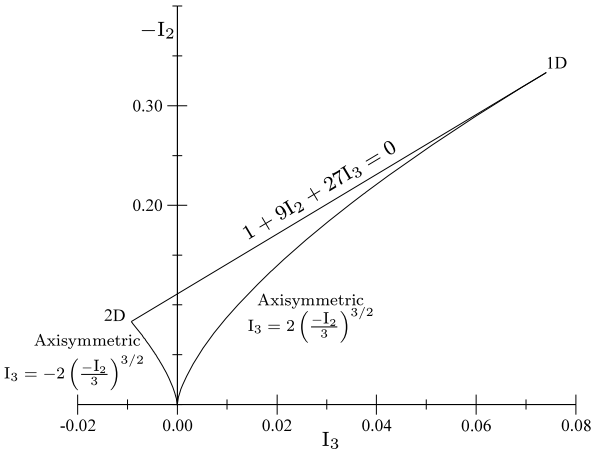

Fig. 6.4 Bounds associated with second and third invariants of anisotropy tensor: 1D—axisymmetric boundary at $(I_3,\ -I_2) = (2/27, 1/3)$; 2D—axisymmetric boundary at $(I_3,\ -I_2) = (-1/108, 1/12)$

other limiting boundaries are shown that are both associated with axisymmetric turbulence. In these cases, two of the diagonal elements are equal and the third is the negative of the sum of the other two (incompressibility) so that the relation $I_3(\boldsymbol{b}) = \pm 2[-I_2(\boldsymbol{b})/3]^{3/2}$ holds. If the two equal diagonal elements are vanishingly small relative to the third, this leads to the one-component state shown in Fig. 6.4 and the relative bounding line is $I_3(\boldsymbol{b}) = +2[-I_2(\boldsymbol{b})/3]^{3/2}$. In contrast, if the third element is vanishingly small relative to the two equal diagonal elements than the two-component limit holds and the bounding line is $I_3(\boldsymbol{b}) = -2(-I_2(\boldsymbol{b})/3)^{3/2}$. As Fig. 6.4 shows, a straight line connects the one-component axisymmetric limit with the two-component axisymmetric limit, so that the boundary of the anisotropy invariant map is delimited by

$$-I_2(\boldsymbol{b}) = 3\left[\frac{I_3(\boldsymbol{b})}{2}\right]^{2/3}, \quad -I_2(\boldsymbol{b}) = 3\left[-\frac{I_3(\boldsymbol{b})}{2}\right]^{2/3}$$
$$\text{and} \quad -I_2(\boldsymbol{b}) = 3\left[I_3(\boldsymbol{b}) + \frac{1}{27}\right]. \tag{6.99}$$

If the principal axes of the stress tensor coincide with the principal axes of the stress anisotropy tensor, the eigenvalues associated with the stress tensor can be easily related to the anisotropy tensor using Eq. (6.98). In principal axes, the stress and anisotropy tensors are diagonal and the invariants are determined from these eigenvalues. The bounding lines of the invariant map then represent different stress ellipsoid shapes (see Simonsen and Krogstad 2005). Although the anisotropy map analysis is well-adapted to the turbulent stress anisotropy, it can generally be applied to other anisotropy tensors, such as d_{ij}^t and d_{ij}^ε. While the mathematical limits may equally apply to these other anisotropy tensors, the physical interpretation of these map boundaries may be different depending on the physical quantity being examined. Nevertheless, as will be shown in Sect. 6.4.1, the invariant map can be useful in assessing the quality of various models needed in the closure of the Reynolds stress transport equation.

The scalar quantities representing the isotropic part appear in the transport equation for the trace of the turbulent stress, the kinetic energy equation, which is directly extracted from Eq. (6.90) as

$$\frac{DK}{Dt} = \mathcal{P} + \nu_0 \frac{\partial^2 K}{\partial x_k \partial x_k} + D^t - \varepsilon + D^t_{p\cdot} - \varepsilon_{p\cdot} \tag{6.100}$$

where $\mathcal{P} = -\tau_{ik} S_{ki}$ is the turbulent kinetic energy production, and D^t and ε, and $D^t_{p\cdot}$ and $\varepsilon_{p\cdot}$ are simply the trace (divided by 2) of the respective expressions given in Eqs. (6.95b) and (6.95c), and Eqs. (6.91) and (6.92), respectively. In addition, isotropic forms of the polymeric contributions in Eqs. (6.91) and (6.92) now appear in the kinetic energy balance. Once again, closure is required for all the turbulent transport and turbulent dissipation rate contributions on the right-side of Eq. (6.100). For generalized Newtonian fluids where the fluctuating stress Ξ'_{ij} is given by Eq. (6.88), both the Reynolds stress transport equation and corresponding kinetic energy equation can become very complex since numerous higher-order correlations appear associated with the spatial and temporal variation of the instantaneous viscosity field. This situation is analogous to that found in strongly compressible flows where the viscosity, dependent on the temperature field, is a function of both space and time. Pinho (2003), Cruz et al. (2004) have analyzed a two equation $K - \varepsilon$ for a generalized Newtonian fluid including order of magnitude estimates for the various terms. Interestingly, the closed form model for the GNF kinetic energy equation originally arrived at by Pinho was the usual Newtonian form but with a spatially dependent mean viscosity. The later study by Cruz et al. (2004) addressed a closure for a new turbulent correlation $\overline{\mu' s'_{ij}}$ (μ' is the fluctuating molecular viscosity).

With the transport equations for either τ_{ij} or K established, the closure problem is now identified in a rather general form. Obviously, over the last four decades of research in this area, innumerable attempts at modeling these correlations have been attempted and are certainly too numerous to detail. The following sections highlight some approaches and identify other strategies that have been used.

6.3.2 Dissipation Rate Tensor

As was shown previously, the evolution of the turbulent velocity field, characterized by either the turbulent Reynolds stress tensor or the scalar turbulent kinetic energy is governed by a corresponding transport equation that requires closure. Additionally, a turbulent length or time scale is required to complete the characterization of the turbulence field. For the most part this remaining length or time scale needed in the characterization can be obtained from a combination of a dissipation rate ε and a kinetic energy K. This energy dissipation rate can be obtained by specifying a length or time scale, or by solving a transport equation analogous to the kinetic energy equation. The former approach was first put forth by Prandtl (1945) who proposed to couple a dissipation rate specification with a K equation. This has since been

adapted to a formulation that utilizes a transport equation for the turbulent viscosity. The latter approach was first proposed by Kolmogorov (1942) who introduced a specific dissipation rate, or "frequency", that was coupled with an equation for the turbulent energy. This two-equation formulation has largely remained the same since; although alternate proposals for the scale equation have emerged. Although the turbulent energy dissipation rate appears directly in the transport equations for the Reynolds stresses (kinetic energy) alternate measures of the energy dissipation have been proposed. In general, the combinations are many and need only take the general form $K^n \varepsilon^m$.

In the following, the approach of developing a transport equation to account for the energy dissipation rate will be discussed. It serves the dual purpose of completing the differential specification of the turbulence closure problem and begins to identify the physical assumptions usually employed in developing turbulence models for other correlations.

There does not appear to have been any attempt to provide a usable transport equation for the tensor dissipation rate ε_{ij} within the context of a second-moment closure. Some limited forms of a differential transport equation have been proposed by Oberlack (1997) and Speziale and Gatski (1997). Speziale and Gatski (1997) also proposed a tensorial representation for d^{ε}_{ij}, not directly linked to the stress anisotropy but derivable from a tensor dissipation equation for homogeneous flows under some weak equilibrium conditions. There have been some attempts at investigating the dissipation rate anisotropy, d^{ε}_{ij}. For d^{ε}_{ij}, some proposals have simply focused on a direct link with the Reynolds stress anisotropy (Hanjalić and Launder 1976) and others on a tensorial expansion in terms of b_{ij} (Hallbäck et al. 1990). Nevertheless, the isotropic dissipation rate has been the subject of study for 40 years and its formulation will be discussed now.

The transport equation for the dissipation rate ε $(= \varepsilon_{ii}/2)$ can be derived from the fluctuating momentum equation (6.86) using

$$\nu_0 \overline{\frac{\partial v_i'}{\partial x_j} \frac{\partial \left(\mathcal{L} v_i'\right)}{\partial x_j}} = 0 \,, \tag{6.101}$$

so that

$$\frac{D\varepsilon}{Dt} = P_\varepsilon^1 + P_\varepsilon^2 + P_\varepsilon^3 + D_\varepsilon + T_\varepsilon - \Upsilon + \Upsilon^p \tag{6.102}$$

where

$$P_\varepsilon^1 = -4\nu_0 \left(\overline{s_{ij}' s_{jk}'} - \overline{w_{ij}' w_{jk}'} \right) S_{ik} \tag{6.103a}$$

is the mean velocity production,

$$P_\varepsilon^2 = -2\nu_0 \left(\overline{v_k' s_{ij}'} \frac{\partial S_{ij}}{\partial x_k} + \overline{v_k' w_{ij}'} \frac{\partial W_{ij}}{\partial x_k} \right) \tag{6.103b}$$

is the mean velocity gradient production,

$$P_\varepsilon^3 = -2\nu_0 \overline{\left(s_{ij}' s_{jk}' - w_{ij}' w_{jk}' \right) s_{ki}'} \tag{6.103c}$$

is the fluctuating velocity production,

$$D_\varepsilon = \nu_0 \frac{\partial^2 \varepsilon}{\partial x_k \partial x_k} \tag{6.103d}$$

is the viscous diffusion,

$$T_\varepsilon = -\nu_0 \frac{\partial}{\partial x_k} \left[\overline{v'_k \left(s'_{ij} s'_{ji} - w'_{ij} w'_{ji} \right)} + 2 \overline{\left(s'_{kj} + w'_{kj} \right) \frac{\partial p'}{\partial x_j}} \right] \tag{6.103e}$$

is the turbulent velocity and pressure transport,

$$\Upsilon = 2\nu_0^2 \left[\overline{\frac{\partial s'_{ij}}{\partial x_k} \frac{\partial s'_{ji}}{\partial x_k}} - \overline{\frac{\partial w'_{ij}}{\partial x_k} \frac{\partial w'_{ji}}{\partial x_k}} \right] \tag{6.103f}$$

is the destruction of dissipation due to the viscous stress, and

$$\Upsilon^p = \nu_0 \overline{\frac{\partial v'_i}{\partial x_n} \frac{\partial}{\partial x_n} \left(\frac{\partial \Xi'^p_{ik}}{\partial x_k} \right)} \tag{6.104}$$

is the destruction of dissipation due to the polymeric stress, and Ξ'^p_{ik} is given by Eq. (6.89).

Although Eq. (6.102) is the exact transport equation for the isotropic dissipation rate extracted from the trace of the transport equation of Eq. (6.95c), the isotropic dissipation rate has often been associated with the mean square vorticity fluctuations through the relation

$$\begin{aligned} \varepsilon &= \nu_0 \overline{\frac{\partial v'_i}{\partial x_k} \frac{\partial v'_i}{\partial x_k}} = 2\nu_0 \left[\overline{w'_{ij} w'_{ij}} - \frac{1}{2} \overline{\frac{\partial v'_i}{\partial x_k} \frac{\partial v'_k}{\partial x_i}} \right] \\ &= \nu_0 \left[\overline{\omega'^2_i} - \overline{\frac{\partial v'_i}{\partial x_k} \frac{\partial v'_k}{\partial x_i}} \right] , \end{aligned} \tag{6.105}$$

where $w'_{ij} (= -e_{ijk} \omega'_k / 2)$ has been used, with ω'_k the fluctuating vorticity vector. The turbulent stress contribution is an inhomogeneous term that is, nevertheless, neglected even in inhomogeneous flow computations.

The form of the individual terms in Eq. (6.102) can be generally grouped into production, destruction, and diffusion of dissipation contributions to the transport equation balance. The lack of rigor associated with the modeling of the individual terms in Eq. (6.102) is an obvious deficiency in the overall closure of the turbulent constitutive equations. Nevertheless, even with the associated problems, the form of isotropic dissipation rate equation that is commonly used is relatively standard. In the present context the high-Reynolds-number form of the modeled isotropic dissipation rate equation is simply written as

$$\frac{\partial \varepsilon}{\partial t} + V_k \frac{\partial \varepsilon}{\partial x_k} = \mathcal{P}_\varepsilon + \mathcal{D}_\varepsilon + \mathcal{T}_\varepsilon - \Upsilon_\varepsilon - \Upsilon^p_\varepsilon , \tag{6.106}$$

with

$$\mathcal{P}_\varepsilon = -C_{\varepsilon 1}\frac{\varepsilon}{K}\tau_{kl}S_{kl}\ , \tag{6.107a}$$

$$\mathcal{D}_\varepsilon = \nu_0\frac{\partial^2\varepsilon}{\partial x_k \partial x_k}\ , \tag{6.107b}$$

$$\mathcal{T}_\varepsilon = C_\varepsilon\frac{\partial}{\partial x_k}\left(\frac{K}{\varepsilon}\tau_{kl}\frac{\partial\varepsilon}{\partial x_l}\right)\ , \tag{6.107c}$$

$$\Upsilon_\varepsilon = C_{\varepsilon 2}\frac{\varepsilon^2}{K}\ , \tag{6.107d}$$

where the right-side of Eq. (6.106) represents the production, viscous diffusion, turbulent transport, and destruction, respectively, and the terms in Eqs. (6.107a)–(6.107d) are the standard high Reynolds number forms for a Newtonian fluid. The remaining term on the right Υ_ε^p is also a destruction term as pointed out earlier and, although Pinho et al. (2008b) neglected this term, Resende et al. (2011) have proposed an model for this term that also included low-Reynolds number corrections. The corresponding high Reynolds number form, however, can be written as

$$\Upsilon_\varepsilon^p = C_\varepsilon^p(\beta, We, L)\frac{\varepsilon\varepsilon_p}{K}\left(f(\{\overline{\boldsymbol{c}}\})\{\overline{\boldsymbol{c}}\}\right)^2\ , \tag{6.108}$$

where the closure coefficient C_ε^p can be a function of the ratio of (zero-shear) polymeric viscosity to total viscosity β, Weissenberg number and polymeric chain length (for FENE-P fluid).

Pinho (2003) carried out an analysis of the isotropic dissipation rate equation similar to the analysis of the turbulent kinetic energy equation for a generalized Newtonian fluid. The resulting modeled form for the dissipation had the usual Newtonian contributions, but now included the material derivative of the mean viscosity. Nevertheless, as expected, the form of the GNF dissipation rate equation had many similarities to the compressible form of the turbulent dissipation rate equation (see Sinha and Candler 2003; Kreuzinger et al. 2006, for example). For Newtonian fluids, the calibration coefficients $C_{\varepsilon 1}$, $C_{\varepsilon 2}$, and C_ε have values that are set in conjunction with the pressure-strain closure, although the value of $C_{\varepsilon 2}$ is chosen close to 1.90 to match the decay rate of isotropic turbulence. Depending on the stress closure model and the values of the coefficients $C_{\varepsilon 1}$ and $C_{\varepsilon 2}$, the closure coefficient C_ε is generally set between the values 0.15–0.18 to have the correct log-law slope in the equilibrium boundary layer (see Launder et al. 1975; Abid and Speziale 1993). More recently Jakirlić and Hanjalić (2002) have proposed a model for the turbulent energy dissipation rate and the dissipation rate anisotropy that is consistent with the constraints imposed by the presence of a wall (see Sect. 6.5.3). The analysis starts with the two-point correlation equation for the fluctuating velocity field and yields a form for the isotropic dissipation rate composed of a dissipation rate associated with a homogeneous flow and an inhomogeneous contribution.

Dissipation Rate Alternatives Although the energy dissipation rate appears as a consequence of the mathematical construction of the Reynolds stress transport equation, the choice of a tensor or scalar quantity capable of replicating the action of destruction (sink) term in the stress transport or turbulent kinetic energy equation is not unique. As was suggested in Sect. 6.3.2 by the recasting of the dissipation rate equation into an equation for the enstrophy, other alternative variables exist which when coupled with the turbulent velocity scale ($\sqrt{K}$), would be equally applicable. As might be expected, numerous proposals have been made for such alternative variables for Newtonian fluids, but the most widespread and possibly more utilized than the energy dissipation rate itself, is the specific dissipation rate $\omega \sim \varepsilon / K$. (The symbol ω used here is the commonly used representation for specific dissipation rate; however, the reader is cautioned not to confuse this with the same variable used elsewhere in this book.)

The specific dissipation rate ω was first proposed for the destruction term in the kinetic energy equation by Kolmogorov (1942), and then reintroduced by Saffman (1970) and popularized by Wilcox (see Wilcox 2006, for a detailed discussion). The corresponding transport equation is more robust for complex flow calculations than the isotropic dissipation rate equation. It is well-suited for wall-bounded flows since its transport equation does not require any wall-proximity corrections as does the dissipation rate equation. This fact has been exploited by Menter (1994) who proposed a blended transport equation utilizing both the specific dissipation rate and dissipation rate. It also has become a popular choice in the solution of complex turbulent flow fields.

It is worth mentioning, albeit briefly, that three equation formulations have also been used; although, the motivation for a third transport equation has varied. One motivation has been to introduce an intermittency function in order to account for any spatial transition region that may be present—particularly in wall-bounded flows, and the other motivation has been to introduce some memory effects into the closure model rather than having the models solely based on the mean velocity field at the present time. This latter trait, a turbulent modeling equivalent to including a principle of determinism constraint into the turbulent constitutive equation has not been extensively pursued; although, many practical flow calculations where there are rapid mean flow distortions suggests it would be an important dynamic feature to include.

Nevertheless, common to all these two, or three, equation models is the requirement that a functional relationship needs to be determined between the Reynolds stress and the mean (velocity) field. Similar to the constitutive requirements discussed in Chap. 4, this relationship is dependent on the (mean) velocity gradient.

6.4 Reynolds Stress Transport Equation Closure

As Eq. (6.90) showed for Newtonian fluids, closure of the Reynolds stress transport equation required the specification of the pressure-strain rate correlation, Π_{ij},

the turbulent transport, D_{ij}^t, and turbulent tensor dissipation rate. The dissipation rate tensor was shown to be generally represented by its isotropic part which was determined by a modeled transport equation, Eq. (6.106). The remaining terms requiring closure, the pressure-strain rate correlation and turbulent transport, are both modeled using tensor representations that are based on known mean flow variables, specifically the mean strain rate and rotation rate tensors, and the Reynolds stress or Reynolds stress anisotropy tensor itself. The viscoelastic terms, as previously noted, have only now come under investigation for closure modeling. As such, only validation across a wide parameter range will reveal in time the inherent accuracy of such models.

6.4.1 Pressure-Strain Rate Correlation

In the development of closure models in the Reynolds stress transport equations, the majority of the effort has been devoted to the formulation of closures for the pressure-strain rate correlation term. The reason for this is that it is of the same order as the production term and acts as a redistribution between the Reynolds stress components since its action on the anisotropy of the stress field diminishes the difference between the normal stress components. In addition, it survives in the simplest of turbulent flows; that is, homogeneous turbulent flows and the closure (expansion) coefficients can be obtained from an *a priori* evaluation of such flows.

The underlying basis for the development of such models has been known for some time (see Chou 1945; Rotta 1951). It is based on the partitioning of the turbulent pressure field p' into slow $p'^{(s)}$ and rapid $p'^{(r)}$ parts. The $p'^{(s)}$ part is the solution of a Poisson equation that involves gradients of the turbulent velocity field; the $p'^{(r)}$ part is the solution of a Poisson equation involving the mean velocity gradients. The former is associated with the "slow" relaxation of the turbulence toward isotropy, and the latter is associated with the "rapid" response of the turbulence to imposed mean velocity gradients. Based on this splitting, a functional form for the pressure-strain rate correlation, Π_{ij}, can be written as (e.g. see Speziale et al. 1991),

$$\frac{\Pi_{ij}}{K} = \frac{\boldsymbol{\Pi}(\boldsymbol{b}, \boldsymbol{S}, \boldsymbol{W}, \tau)}{K} = \tau^{-1}\left(\mathcal{A}_{ij}(\boldsymbol{b}) + \tau \mathcal{M}_{ijkl}(\boldsymbol{b})\frac{\partial V_k}{\partial x_l}\right), \qquad (6.109)$$

where $\mathcal{A}_{ij}(\boldsymbol{b})$ and $\mathcal{M}_{ijkl}(\boldsymbol{b})$ are tensor functions of the anisotropy tensor and are related to integrals over the flow volume derived from the pressure Poisson equation, and $\boldsymbol{S}$ and $\boldsymbol{W}$ are the respective symmetric and skew-symmetric parts of the mean velocity gradient $\partial V_k/\partial x_l$. Note that the explicit inclusion of the scalar variable K (in Π_{ij}/K) is intended to emphasize that the turbulent time scale variable τ can be comprised of any combination of turbulent kinetic energy K and energy destruction scale such ε, ω, etc. The $\mathcal{A}_{ij}(\boldsymbol{b})$ term is associated with the "slow" relaxation part, and the $\mathcal{M}_{ijkl}(\boldsymbol{b})$ term is associated with the "rapid" response to imposed mean velocity gradients.

With the functional dependency outlined in Eq. (6.109), the proper representation for $\boldsymbol{\Pi}/K$ would be generated from the integrity basis given by the invariant

combinations of $\boldsymbol{b}$, $\boldsymbol{S}$, and $\boldsymbol{W}$. A tensorial representation composed of the full integrity basis of these three tensors would consist of 41 terms (see Tables 2.1 and 2.2 and the procedure discussed in Sect. 6.5) which would be unmanageably large. Although the closures to date have not been systematically based on a consistent set of terms extracted from the full tensor basis set, they have been categorized by the power of the anisotropy tensor $\boldsymbol{b}$ appearing in the representation. As such, the proposed models have been linear, quadratic, or cubic in the anisotropy tensor. This truncated form is given by (cf. Sjögren and Johansson 2000)

$$\frac{\boldsymbol{\Pi}(\boldsymbol{b},\boldsymbol{S},\boldsymbol{W},\tau)}{K} = \tau^{-1}\left(\sum_{i=1}^{2}\alpha_i\boldsymbol{\Phi}_i + \tau\sum_{i=3}^{8}\alpha_i\boldsymbol{\Phi}_i\right), \tag{6.110a}$$

with

$$\begin{aligned}
\boldsymbol{\Phi}_1 &= \boldsymbol{b} & \boldsymbol{\Phi}_5 &= \boldsymbol{bW} - \boldsymbol{Wb}\\
\boldsymbol{\Phi}_2 &= \boldsymbol{b}^2 - \tfrac{1}{3}\{\boldsymbol{b}^2\}\boldsymbol{I} & \boldsymbol{\Phi}_6 &= \boldsymbol{b}^2\boldsymbol{S} + \boldsymbol{Sb}^2 - \tfrac{2}{3}\{\boldsymbol{b}^2\boldsymbol{S}\}\boldsymbol{I}\\
\boldsymbol{\Phi}_3 &= \boldsymbol{S} & \boldsymbol{\Phi}_7 &= \boldsymbol{b}^2\boldsymbol{W} - \boldsymbol{Wb}^2\\
\boldsymbol{\Phi}_4 &= \boldsymbol{bS} + \boldsymbol{Sb} - \tfrac{2}{3}\{\boldsymbol{bS}\}\boldsymbol{I} & \boldsymbol{\Phi}_8 &= \boldsymbol{b}^2\boldsymbol{Wb} - \boldsymbol{bWb}^2\,.
\end{aligned} \tag{6.110b}$$

In addition, note that in the above basis there is only a linear dependence on the mean velocity gradient field (through $\boldsymbol{S}$ and $\boldsymbol{W}$) which is consistent with the functional form $\boldsymbol{\Pi}$ given in Eq. (6.109). The terms associated with α_1 and α_2 are previously mentioned slow terms representing the turbulence-turbulence interactions. The remaining terms in the representation are associated with the rapid term and represent a direct response of the turbulence to mean shear.

Even with the truncated representation for Π_{ij}/K, there still remains 8 expansion coefficients that need to be determined, and as noted these can be functions of the flow invariants. For the slow term coefficients, it can be generally assumed that the expansion coefficients associated with these terms are independent of any invariants associated with the mean motion and so the dependence is limited to the Reynolds stress anisotropy invariants $\{\boldsymbol{b}^2\}$ and $\{\boldsymbol{b}^3\}$, and the scalar variable τ. For the linear slow term coefficient α_1, the accepted approach is to determine its value from experimental and simulation data for the return-to-isotropy of an initially, anisotropic homogeneous turbulence. Rotta (1951) was the first to exploit the return-to-isotropy calibration but only focused on a linear decay term. Later Lumley and Newman (1977), Lumley (1978), using invariant theory and associated tensor representations, developed a nonlinear model whose expansion coefficients depended on the anisotropy invariants and turbulent Reynolds number ($\propto K\tau/\nu$) (this is the same scaling as suggested in Eq. (6.109) where K has been factored to the left side). Further refinements have been made (see Haworth and Pope 1986; Sarkar and Speziale 1990), but each has essentially introduced more and more complexity into the expansion coefficients; however, each tends to produce values of $\alpha_1 \approx 3$ (a constant value of 3.4 is often taken) with the variation depending on complexity of the functional form. Additionally, these authors have also suggested values for the coefficient of the nonlinear term, α_2. The choices are more varied and complex than with the α_1 coefficient due to the fact that such nonlinear effects

are much weaker than the dominant linear decay and vary more among the various experiments and simulations.

While the determination of the slow term coefficients was straightforward due to the limited invariant dependency of the expansion coefficients and the limit to quadratic terms in the anisotropy, a more complex situation arises for the remaining six terms representing the rapid part of the Π_{ij}/K correlation. Nevertheless, a noteworthy contribution in this regard was put forth by Crow (1968) who attempted to provide a low-order (one term, $\boldsymbol{S}$) representation for the rapid part of Π_{ij}/K primarily analogous to the development of a viscoelastic constitutive equation. In contrast to the isolation of the slow term, Crow (1968) assumed the slow term to be of higher-order relative to the rapid part and focused solely on this term. The basis of the development was the assumption of an elastic response of the turbulence to an initial, instantaneous imposition of mean shear. Recall that for the determination of the slow term, the problem formulation was the opposite, that is, an anisotropic (homogeneous) turbulence, produced by a mean shear, was allowed to relax back to an isotropic state by an instantaneous removal of the mean shear. In general, the inclusion of a pressure term in the differential formulation would suggest a strong non-local coupling between the turbulent stress field and the mean field. What is then usually invoked is a local action assumption analogous to the principle introduced in fluid constitutive equation development; however, unlike the constitutive local action principle which precludes any effect on the stress from a point a finite distance away, this local action assumption decouples the mean (shear) field from the turbulent stress from a point greater than the (finite) length over which the turbulence is correlated. Crow (1968), using the solution of the pressure Poisson equation, obtained a relationship between the pressure correlation term and the mean shear (that is $\boldsymbol{S}$). (Crow (1968) formed the velocity-pressure gradient correlation rather than the pressure-strain rate correlation, but forming the pressure-strain rate correlation would yield a similar relationship.) The corresponding numerical coefficient, α_3, was found to be 0.8—and is the value most often chosen for this representation term.

As was pointed out in Sect. 4.2.2, the constraint of realizability can be used as a guide to model development. An example of this can be shown in assessing the expansion coefficients for a model of the pressure-strain rate correlation. For a two-dimensional homogeneous shear flow, the evolution of the turbulence stress tensor is given by Eq. (6.90) with the turbulent and molecular transport and diffusion terms vanishing. This leaves a simple time evolution equation comprised of an exact production term, a pressure-strain rate redistribution term, and the turbulent dissipation rate term. Since the mean field is fixed, and therefore decoupled from the turbulent stress evolution, the stress field is described by a set of ordinary differential equations. This system can be integrated over several mean shear time scales, and leads to asymptotic limiting values for the anisotropy tensor components b_{ij}, the invariant $\{\boldsymbol{bS}\}$, and the turbulent time scale K/ε. The limiting values for b_{ij} yield values for $\mathrm{I}_2(\boldsymbol{b})$ and $\mathrm{I}_3(\boldsymbol{b})$ that identify equilibrium points within the invariant triangle in Fig. 6.4. These predicted values can be compared to either numerical simulation or experimental results to assess model performance, which in this simple shear flow is

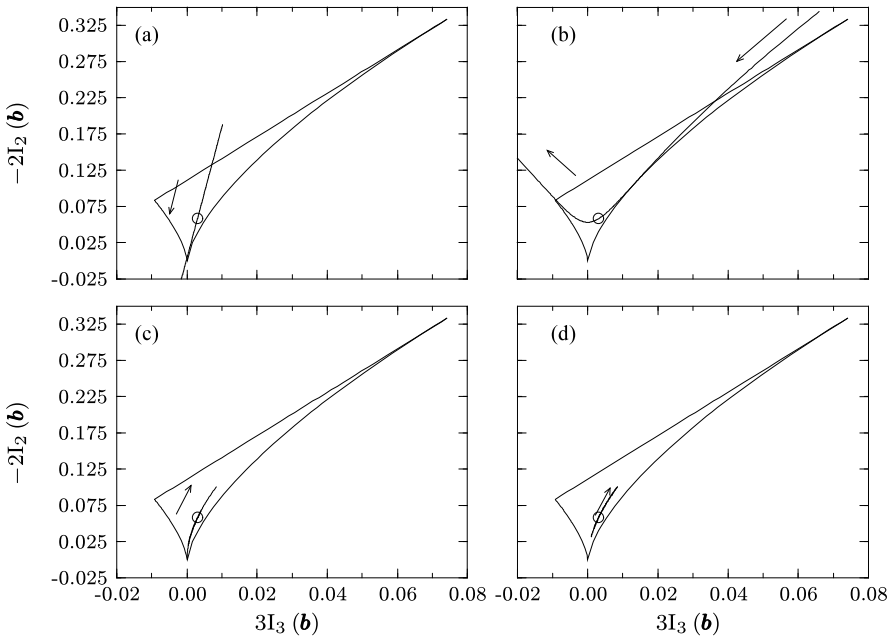

Fig. 6.5 Equilibrium values in the invariant map ($\mathrm{I}_3\,(\boldsymbol{b})$, $-\mathrm{I}_2\,(\boldsymbol{b})$) as a function of the expansion coefficients. The *arrows* indicate the direction of increase of the parameter value: (**a**) Variation of α_3 from -2 to 2; (**b**) Variation of α_4 from -4 to 6; (**c**) Variation of $\{\boldsymbol{bS}\}$ from 0 to 20; (d) Variation of α_1 from 0 to 10; Location corresponding to the SSG model (Speziale et al. 1991) equilibrium value, ○[3]

dependent solely on the pressure-strain rate correlation model. A relatively common model in use is the SSG model (Speziale et al. 1991) in which the expansion coefficients for the linear form are given by $\alpha_1 = 3.4 + 1.8\{\boldsymbol{bS}\}$, $\alpha_3 = 0.8 - 1.3\sqrt{-2\mathrm{I}_2\,(\boldsymbol{b})}$, $\alpha_4 = 1.25$, and $\alpha_5 = 0.4$ (with all others zero). Figure 6.5 shows the effect of varying some of these coefficients and the invariant $\{\boldsymbol{bS}\}$ in the prediction of the anisotropy invariant equilibrium states. As the figure shows, the model tends to be most sensitive to variations in α_3 and α_4 and that it is possible to choose values that force unrealizable solutions. This analysis, coupled with physical constraints that include the decay of isotropic turbulence, the return to isotropy of anisotropic turbulence, and the behavior of the turbulence under rapidly distorted conditions, are the means by which the expansion coefficients should be determined.

As might be expected, an extensive literature base deals with the full range of issues associated with developing specific models (e.g. Hanjalić and Jakirlić 2002). At the next level of complexity beyond the linear rapid term, models quadratic in the stress anisotropy $\boldsymbol{b}$ arise. The expansion coefficients associated with these terms

[3]Figures 6.5 and 6.8 reprinted with permission from: T. Jongen, T.B. Gatski (1999) A unified analysis of planar homogeneous turbulence using single-point closure equations. J Fluid Mech 399:117–150. Copyright Cambridge University Press.

can, in general, be functions of the invariants of the tensors $\boldsymbol{b}$, $\boldsymbol{S}$, and $\boldsymbol{W}$; however, for this combination of tensors, there are 29 invariants comprising this integrity basis (see Tables 2.1 and 2.2). The highest level of closure that have been developed are models that contain terms cubic in the stress anisotropy tensor (Fu et al. 1987; Craft and Launder 1996, 2002). The additional information needed in specifying the expansion coefficients in these higher-order terms are extracted from some benchmark flows where the mean field is fixed in space and time (and either two-dimensional or axisymmetric), and subject to the constraint that the turbulence is realizable (Schumann 1977; Lumley 1978; Johansson and Hallbäck 1994) such that any correlation model proposed will yield non-negative component normal turbulent stresses.

6.4.2 Turbulent Transport

As was discussed in Sect. 6.3.1, the contributions toward turbulent transport in the Reynolds stress transport equation are attributed to the velocity triple-moments and the pressure-velocity correlation. The common procedure in incompressible flows is to partition the velocity-pressure gradient correlation into a traceless pressure-strain rate correlation and a pressure-velocity correlation, with the slow part of the fluctuating pressure field the primary contributor to the pressure-velocity contribution (Lumley 1978). The approach that has been followed in modeling the D_{ij}^t term in Eq. (6.90) is to provide a structural model for the velocity triple-moment and pressure-velocity correlation combination rather than a functional model for the corresponding divergence, that is D_{ij}^t. In the early development of such a model, most authors chose to consider the influence of both the velocity triple-moment and pressure-velocity correlation but to assimilate the respective contributions into the same polynomial representation. In what follows, an attempt will be made to distinguish between the representation associated with the combined velocity triple-moment and pressure-velocity correlation, D_{ijk}^t, and the representation associated solely with the velocity triple-moment, $\overline{v_i' v_j' v_k'}$.

As with the second-moment equations, it is possible to construct a transport equations for $\overline{v_i' v_j' v_k'}$ (see Chou 1945) and attempt a term-by-term approximation of the various unknown turbulence correlations that appear. The obvious difficulty with this approach lies in formulating adequate approximations of the large number of additional unknown higher-order terms that are involved. Even though the exact transport equation for $\overline{v_i' v_j' v_k'}$ (e.g. Hanjalić and Launder 1972) includes production terms associated with the mean velocity gradient, the contributions from S_{ij} and W_{ij} have been excluded from any proposed model (representations). This has been partly predicated on early experimental results for wall-bounded flows (e.g. Hanjalić and Launder 1972) which showed that these production terms were much smaller in proximity to the wall than the associated transport terms in the velocity triple-moment equation. In addition, for homogeneous flows where S_{ij} and W_{ij} do not vanish, there is no contribution to the dynamic balance from turbulent transport.

Such arguments are further augmented by the fact that the turbulent transport term is the divergence of the flux of the Reynold stress and as such should be expressible in terms of the Reynolds stress and related turbulent correlations. Such arguments have led to the functional form of D^t_{ijk} being given by

$$D^t_{ijk} = \mathcal{D}^t_{ijk}\left(\tau_{lm}, \varepsilon\right) \ . \tag{6.111}$$

(Note that the dissipation rate is used here since it was the variable used in the formulation of the representations to be discussed; however, other energy dissipation variables could have been chosen.) What is then desired is a functional series expansion about these dependencies that leads to terms in the representation dependent on the gradients of the arguments, that is, $b_{lm,n} = \partial b_{lm}/\partial x_n$, $K_{,n} = \partial K/\partial x_n$ and $\varepsilon_{,n} = \partial\varepsilon/\partial x_n$ (Lumley and Khajeh-Nouri 1974). Although the dependence on the dissipation rate is allowed, there has been only limited accounting of this term in any representation of either the velocity triple-moment or total transport term (see Cormack et al. 1978; Magnaudet 1993). For the most part, only representations involving the turbulent stress and associated gradients have been used. Although, such functional series expansion can best be placed in the context of deviations from isotropy and homogeneity that are better represented by the anisotropy tensor **b** rather than the stress tensor itself, almost all of the transport term correlations have been expressed in terms of the stress tensor itself. This is the format that will be used in the examples to follow, but it is a straightforward, though tedious, exercise to rewrite each example in terms of the anisotropy tensor itself.

There have been several proposed representations for D^t_{ijk} that have been based solely on the velocity triple-moment term or a combination with the pressure-velocity correlation. In either case, once determined, the spatial gradients (divergence) of D^t_{ijk} represent flux of turbulent stress and pressure by the fluctuating velocity. Probably the earliest published model was that proposed by Daly and Harlow (1970) which is bilinear in the stress and stress gradient. It is given by

$$D^t_{ijk} = -\tau\left(C^1_{DH}\frac{\partial\tau_{ij}}{\partial x_p}\tau_{pk} + C^2_{DH}\tau_{qq}\frac{\partial\tau_{ip}}{\partial x_p}\delta_{jk}\right) \ , \tag{6.112}$$

where both C^1_{DH} and C^2_{DH} were initially assumed to have a turbulent Reynolds number dependence, but are now usually taken as a constant value of ~ 0.22 (Hanjalić 1994). The DH model is probably the most widely used model in calculation methods, but the representation on the right-hand side does not have the same permutation of indices invariance as the left-hand side. This inconsistency is not usually a problem in thin shear layers where the flow direction is known and turbulent transport is primarily in the direction of shear; however, it can be problematic in complex flows where turbulent mixing can be significant in all coordinate directions.

A more complicated, but tensorial admissible expression was proposed by Hanjalić and Launder (1972). It is a model solely for the velocity triple-moments since the experimental results available to them suggested it made a negligible contribution to the turbulent diffusion. The HL model can be written as

$$\overline{v'_i v'_j v'_k} = -\tau C_{HL}\sum \tau_{ij,p}\tau_{pk} \ , \tag{6.113}$$

where the summation, $\sum$, implies a cyclic permutation of the indices i, j, and k. The expansion coefficient C_{HL} was determined from computational calibration based on best reproduction of experimental results, and is now usually taken as 0.11.

An isotropic version of the HL model has been proposed by Mellor and Herring (1973) for the velocity triple-moments and coupled with a gradient of kinetic energy term for the pressure-velocity correlation to obtain

$$D^t_{ijk} = -\tau \left(C^1_{MH} K \sum \tau_{ij,k} + C^2_{MH} \tau_{qq} \frac{\partial \tau_{pp}}{\partial x_i} \delta_{jk} \right) . \tag{6.114}$$

The expansion coefficients C^1_{MH} and C^2_{MH} were assumed proportional to the turbulent integral scale but values of ~ 0.15 are usually used (Hanjalić 1994; Straatman et al. 1998). Shir (1973) also proposed a model $\overline{v'_i v'_j v'_k}$ in the study of atmospheric turbulent flows, but that model only contained the first term in Eq. (6.114) and therefore did not exhibit the correct symmetry properties.

More complex extensions of these simple forms were proposed. Lumley (1978) proposed a model that was bilinear in the tensor product, and attempted to account more rigorously for the pressure-diffusion effects. His analysis was based on the assumption of weakly anisotropic and inhomogeneous turbulence which led to

$$\overline{v'_i v'_j v'_k} = -\tau C^1_L \left[\sum \tau_{ij,p} \tau_{pk} + C^2_L \sum \left(\tau_{pp,q} \tau_{qi} + 2\tau_{ip,q} \tau_{pq} \right) \delta_{jk} \right] , \tag{6.115}$$

for the velocity triple-moments with expansion coefficients $C^1_L = 0.2$ and $C^2_L = 0.13$, and

$$\overline{p' v'_i} \delta_{jk} + \overline{p' v'_j} \delta_{ik} = -\frac{1}{5} \left(\overline{v'_i v'_p v'_p} \delta_{jk} + \overline{v'_j v'_p v'_p} \delta_{ik} \right) , \tag{6.116}$$

for the pressure-diffusion terms (see also Straatman 1999 who suggested a recalibration of the coefficients associated with the pressure-velocity processes).

The most complex model for turbulent transport to be considered has been proposed by Cormack et al. (1978). Their analysis only considered the velocity triple-moment and started with a general representation for the deviatoric part of the stress tensor τ_{ij}, that is $2Kb_{ij}$ rather than the stress tensor itself. Although the representation in terms of the deviatoric part (or anisotropy) is preferable on physical grounds as discussed at the beginning of this section, for ease of comparison with the other models discussed in this section, it is rewritten here in terms of the stress tensor. Their general representation through second-order in the turbulent stresses, can be written as

$$\overline{v'_i v'_j v'_k} = \tau \sum_{\alpha=1}^{3} c_\alpha \Psi^{(\alpha)}_{ijkl} \tau_{pp,l} + \tau^2 \sum_{\beta=1}^{6} c_\beta \Psi^{(\beta)}_{ijkl} \varepsilon_{,l} + \tau \sum_{\gamma=1}^{5} c_\gamma \Phi^{(\gamma)}_{ijk} , \tag{6.117}$$

where c_α, c_β and c_γ are closure coefficients, and Ψ_{ijk} and Φ_{ijk} are third-order symmetric tensor-valued functions given by

$$\begin{aligned}
\Psi^{(1)}_{ijkl} &= \tau_{qq} \textstyle\sum \delta_{ij} \delta_{kl} & \Psi^{(4)}_{ijkl} &= \tau^{-1}_{qq} \textstyle\sum \tau_{ij} \tau_{kl} \\
\Psi^{(2)}_{ijkl} &= \textstyle\sum \tau_{ij} \delta_{lk} & \Psi^{(5)}_{ijkl} &= \tau^{-1}_{qq} \textstyle\sum \tau_{ir} \tau_{rj} \delta_{lk} \\
\Psi^{(3)}_{ijkl} &= \textstyle\sum \delta_{ij} \tau_{lk} & \Psi^{(6)}_{ijkl} &= \tau^{-1}_{qq} \textstyle\sum \delta_{ij} \tau_{lr} \tau_{rk}
\end{aligned} \tag{6.118a}$$

and

$$\begin{aligned} \Phi_{ijk}^{(1)} &= \tau_{qq} \sum \tau_{ij,k} & \Phi_{ijk}^{(4)} &= \sum \tau_{ij,p} \tau_{pk} \\ \Phi_{ijk}^{(2)} &= \tau_{qq} \sum \tau_{ip,p} \delta_{jk} & \Phi_{ijk}^{(5)} &= \sum \left(\tau_{ip,j} + \tau_{jp,i} \right) \tau_{pk} \, . \\ \Phi_{ijk}^{(3)} &= \sum \tau_{ip,p} \tau_{jk} \end{aligned} \tag{6.118b}$$

Their final modeled form was given by

$$\overline{v_i' v_j' v_k'} = -\tau \left[\sum_{\alpha=1}^{3} C_{CLS}^{\alpha} \Psi_{ijkl}^{(\alpha)} \tau_{pp,l} - \tau \sum_{\gamma=1}^{3} C_{CLS}^{\gamma} \Phi_{ijk}^{(\gamma)} \right] . \tag{6.119}$$

The six expansion constants are linear combinations of the original four constants proposed by Cormack et al. (1978) and are: $C_{CLS}^{\alpha=1} = -0.005$, $C_{CLS}^{\alpha=2} = -0.068$, $C_{CLS}^{\alpha=3} = 0.096$ and $C_{CLS}^{\gamma=1} = 0.034$, $C_{CLS}^{\gamma=2} = -0.068$, $C_{CLS}^{\gamma=3} = 0.204$.

Magnaudet (1993) also considered the Cormack et al. model and provided a cross-diffusion extension that included the gradient of the isotropic dissipation rate. The functional form was constrained by the requirements that the model be fully symmetric, realizable and have the proper asymptotic consistency as the velocity triple-moment near solid and free surfaces. The representation can be written as

$$\overline{v_i' v_j' v_k'} = -\tau \left[C_M^{\gamma=3} \Phi_{ijk}^{(3)} + C_M^{\gamma=4} \Phi_{ijk}^{(4)} \right] + \Psi_{ijkl}^{(4)} \left[C_M^{\alpha=4} \tau_{pp,l} + C_M^{\beta=4} \varepsilon_{,l} \right] , \tag{6.120}$$

where the expansion coefficients were determined from an *a priori* evaluation of the model using DNS data for plane channel flow (Kim et al. 1987), and were chosen as $C_M^{\gamma=3} = 0.16$, $C_M^{\gamma=4} = 0.125$, $C_M^{\alpha=4} = 0.03$, $C_M^{\beta=4} = 0.09$. Hanjalić (1994) has evaluated the performance of the Daly and Harlow (1970), Hanjalić and Launder (1972), and Magnaudet (1993) models against the same plane channel flow DNS data, and found that the correct qualitative features were replicated for most of the velocity triple-moments components; although, the magnitude levels were underestimated by the DH and HL models and overestimated by the Magnaudet model.

A similar comparison for plane channel flow is presented in Fig. 6.6 but at a higher value of friction Reynolds number, Re_τ of 590 (Moser et al. 1999). From Fig. 6.6, it is seen that the MH (Mellor and Herring 1973) model performs poorly in predicting any of the triple-moment components; whereas, the HL (Hanjalić and Launder 1972) model appears to perform the best among all the models evaluated. The Lumley (1978) and (linearized) Magnaudet (1993) models yield mixed results. Although the Magnaudet model (1993) shown is a linear truncation of the full model proposed, its predictive capabilities are well below both the HL and Lumley models. Possibly the higher-order terms used in the original model, which are quadratic in the Reynolds stresses, are needed. The Lumley (1978) model yields results that are essentially the same as the HL model suggesting little is gained by the implementing the more complicated form. Clearly, by increasing the Reynolds number to a value which enhances the turbulence dynamics, the behavior of the various models can be altered relative to the flows (lower *Re*) that were used for calibration. This type

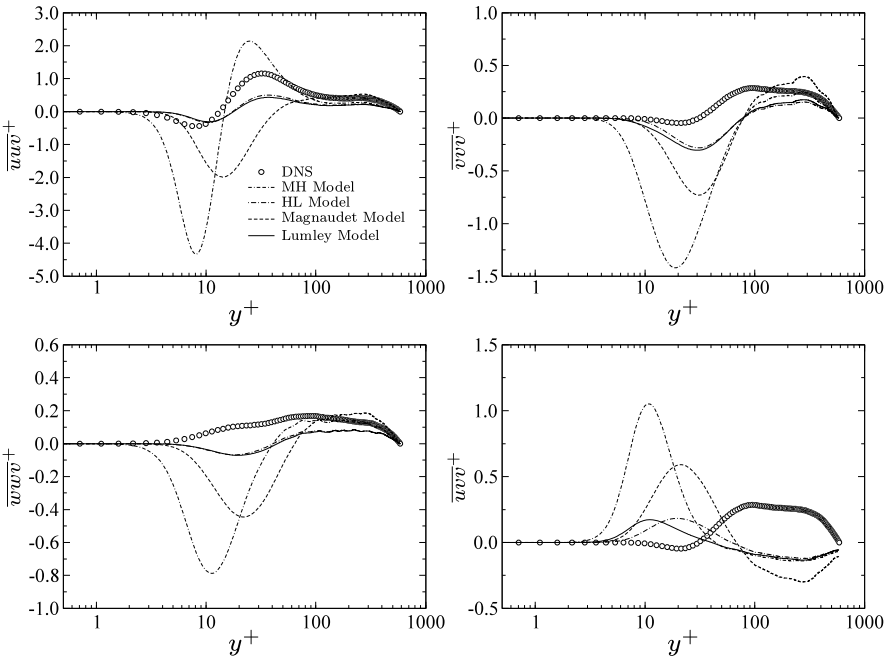

Fig. 6.6 Comparison of velocity triple-moment models with DNS results (Moser et al. 1999) of turbulent channel flow at $Re_\tau = 590$[4]

of behavior highlights the dangers of model calibration and the subsequent range of applicability of such models.

From the continuum mechanics approach, representations for third-order isotropic tensor functions, invariant under the full orthogonal group O_3, were first investigated by Pennisi (1992) and later adapted by Smith (see Appendix in Younis et al. 2000) to the velocity triple-moment representation problem (see also Smith and Younis 2004, for further discussion). The tensorial dependencies of the velocity triple-moment were assumed to be

$$\overline{v_i' v_j' v_k'} = \mathcal{D}^t_{ijk}\left(\tau_{lm}, S_{lm}, W_{lm}, \varepsilon\right) \ . \tag{6.121}$$

This differs significantly with the form given in Eq. (6.111) where there was no dependence on the mean field. (Note that the dissipation rate is used here and which was the variable used in the formulation of the representations to be discussed; however, other dissipation variables could have been chosen.) As has been discussed earlier in this section, such dependencies on the mean field are probably not appropriate on physical grounds, and will not be considered further. With the dependencies in Eq. (6.121), it can be shown that, in general, there are 30 linearly independent terms

[4]Reprinted with permission from: T.B. Gatski (2004) Constitutive equations for turbulent flows. Theor Comput Fluid Dyn 18:345–369. Copyright Springer 2004.

(Younis et al. 2000; Smith and Younis 2004) of degree 2 or less in the representation of a third-order isotropic tensor fully symmetric in its indices. Elimination of the dependencies on S_{ij} and W_{ij} reduces this number to 14, and with scaling redundancies accounted for, the final number is 11. The resulting functional form and tensor representation for $\overline{v_i' v_j' v_k'}$ is given by

$$\begin{aligned}\overline{v_i' v_j' v_k'} &= \mathcal{D}_{ijk}^t \left(\tau_{lm}, \tau_{lm,n}, \tau\right) \\ &= -\tau \sum_{\gamma=1}^{11} c_\gamma \Theta_{ijk}^{(\gamma)} ,\end{aligned} \tag{6.122}$$

where c_γ are the expansion coefficients, and $\Theta_{ijk}^{(\gamma)}$ are the third-order symmetric tensor-valued functions (cf. Younis et al. 2000; Smith and Younis 2004)

$$\begin{aligned}
\Theta_{ijk}^{(1)} &= \tau_{qq} \sum \tau_{ij,k} & \Theta_{ijk}^{(7)} &= \sum \left(\tau_{ip,j} + \tau_{jp,i}\right) \tau_{pk} \\
\Theta_{ijk}^{(2)} &= \tau_{qq} \sum \tau_{pp,i} \delta_{jk} & \Theta_{ijk}^{(8)} &= \sum \tau_{pp,q} \tau_{qi} \delta_{jk} \\
\Theta_{ijk}^{(3)} &= \tau_{qq} \sum \tau_{ip,p} \delta_{jk} & \Theta_{ijk}^{(9)} &= \sum \tau_{ip,q} \tau_{qp} \delta_{jk} \\
\Theta_{ijk}^{(4)} &= \sum \tau_{ij,p} \tau_{pk} & \Theta_{ijk}^{(10)} &= \sum \tau_{pq,i} \tau_{qp} \delta_{jk} \\
\Theta_{ijk}^{(5)} &= \sum \tau_{pp,i} \tau_{jk} & \Theta_{ijk}^{(11)} &= \sum \tau_{pq,p} \tau_{qi} \delta_{jk} \, . \\
\Theta_{ijk}^{(6)} &= \sum \tau_{ip,p} \tau_{jk}
\end{aligned} \tag{6.123}$$

It is of interest to compare the forms in Eq. (6.123) with those that were obtained previously and from more physical considerations although, in general, maintaining the proper tensorial dependencies. As mentioned in the discussion of the DH model, while it is a popular engineering model in thin-shear flows, it does not retain the proper index permutation properties. Nevertheless, from a comparison of Eq. (6.112) it is seen that the first term is a component of $\Theta_{ijk}^{(4)}$ and the second term is a component of $\Theta_{ijk}^{(3)}$. In contrast, the HL model, Eq. (6.113), possesses the correct index permutation properties and corresponds to basis tensor $\Theta_{ijk}^{(4)}$. Of the early transport models that were considered, the MH model, Eq. (6.114), is based on the two lowest-order basis tensors, $\Theta_{ijk}^{(1)}$ and $\Theta_{ijk}^{(2)}$. It is easy to see with this retrospective look the various similarities and hierarchal ordering inherent in these early models. While their calibration differed, the underlying polynomial representations followed a consistent increase in complexity and, at the time, better predictive capability.

The next set of proposed representations, based on the Lumley model Eq. (6.115), were comprised of three of the basis tensors given in Eq. (6.123), $\Theta_{ijk}^{(4,8,9)}$. The most complex model that was proposed was the Cormack et al. model given in Eq. (6.119). It contained the basis tensors $\Theta_{ijk}^{(2,5,8)}$ which represented gradients involving the turbulent kinetic energy, and the basis tensors, $\Theta_{ijk}^{(1,3,6)}$, which represented terms involving the stress tensor components.

It may not be surprising that some studies have found little real difference in model performance across a wide range of benchmark turbulent shear flows (see

Cormack et al. 1978; Schwarz and Bradshaw 1994). There are a number of flows that have a ratio of turbulence kinetic energy production to dissipation rate near unity, and hence the divergence of the turbulent transport can make only a modest contribution to the overall budget of the Reynolds stresses. In such flows, defects in modeling the velocity triple-moments and/or pressure-velocity correlation are easily concealed by shortcomings in the closure of the other unknown correlations appearing in Eq. (6.90). In other flows, such as in the self-similar wake behind a bluff body, the ratio of production to dissipation is only about 10%, with the remainder of the balance provided by the divergence of the turbulent transport. It is in these "weakly sheared" flows that current turbulence transport closures become problematic.

6.5 Polynomial Representations of the Turbulent Stress Tensor

The formulation of representations for the pressure-strain rate correlation (Sect. 6.4.1) and the turbulent transport (Sect. 6.4.2), coupled with a transport equation representing the rate of turbulent energy dissipation (Sect. 6.3.2), results in a differential system of seven transport equations that can be solved to provide the turbulent stress field for inclusion in the mean field equations. While such mathematical formalism may have a fundamental appeal from an academic perspective, over the last four decades such full transport equation approaches have received less and less attention. The more common and acceptable approach has been confined to two transport equations consisting almost exclusively of the turbulent kinetic energy equation, Eq. (6.100), and a rate of energy dissipation scale equation. The lowest-order tensor representation for the Reynolds stress tensor that has been used in such formulations has been given by the one-term representation,

$$\boldsymbol{b} = -C_\mu \tau \boldsymbol{S} \,, \tag{6.124a}$$

or

$$\boldsymbol{\tau} = \frac{2}{3} K \delta_{ij} - 2\nu_t \boldsymbol{S} \,. \tag{6.124b}$$

and which is commonly referred to as the Boussinesq relationship between the Reynolds stress and mean strain rate field. Since the turbulent eddy viscosity is $\nu_t = C_\mu \tau K$, such a representation is termed an isotropic turbulent eddy viscosity model with C_μ a closure constant. Note that for the eddy viscosity ν_t, the proportionality is with a turbulent velocity scale (through K) and a turbulent velocity time scale, $\tau \propto K/\varepsilon$ or $\tau \propto \omega^{-1}$. The closure coefficient C_μ can, in general, be complex functions of the invariants of the mean field (see Sect. 6.5.2). For completeness, it is worth noting that an alternative approach to determining the eddy viscosity is to solve a transport equation directly for the eddy viscosity ν_t (Spalart and Allmaras 1994). Such a one-equation model, though based primarily on empiricism and on dimensional analysis, is popular among industrial users due to its ease of implementation and relatively inexpensive cost. The major conceptual limitation of the

low-order forms is the isotropy of the eddy viscosity but, in contrast, the important practical advantage is the highly desirable property of an added diffusive-type behavior into the governing equations since an eddy viscosity associated with the turbulence is much larger than the viscosity of the (Newtonian) fluid. Of course, introduction of a viscoelastic fluid can complicate this simple relationship. Using DNS data from channel flow simulations Li et al. (2006) extracted the behavior of the viscoelastic turbulent eddy viscosity for a FENE-P fluid using Eqs. (6.124a), (6.124b) for the shear stress component. Various drag reduction regimes were analyzed and a linear relationship between the Newtonian and viscoelastic fluids in different regions of the channel was established.

In general, in order to potentially augment the predictive capability of such closures it is necessary to go to higher-order representations that effectively include more dynamics into the parameterization. The remainder of this section will deal with such representations; although, the primary focus will once again be on Newtonian fluids.

6.5.1 Turbulent Stress of a Simple Fluid

At the outset, one can appeal to the discussion on constitutive equation development given in Chap. 4, where it was shown that the Cauchy stress field is a functional of the relative deformation gradient and consequently to the right Cauchy-Green tensor (see Eq. (4.3)). While there are inherent differences between the turbulent stress that is associated with second-moment velocity correlations and the material stress associated with a fluid element as discussed in Sects. 4.2.1 and 4.2.2, there are some kinematic similarities that can be used in providing a suitable polynomial representation of the turbulent stress tensor. For example, it has long been established that the turbulent stress is a functional of the history of the deformation. The large scale turbulence responds to the mean field with an inherent time scale of τ ($= K/\varepsilon$, for example). If this (ensemble) mean field is unchanging over several τ time scales then the ratio $S\tau$ is small (where S is a characteristic mean deformation rate); however, should any (ensemble) mean field changes occur rapidly then $S\tau$ can be large and this is a rapid distortion. It is clear then that the stress field does in some way depend on this mean deformation just as the pressure-strain rate correlation had a mean deformation dependency. In the absence of any such deformation for a long period (relative to the time scale τ) the turbulent stress simply relaxes to an isotropic state. As suggested in Sect. 4.2.2 and further elaborated on here, the determinism principle does apply and could be used to formulate a tensorial expansion for the turbulent stress field.

Based on these comments, it does seem appealing to attempt to further adapt the constitutive equation formalism discussed in Chap. 4 to the turbulent stress field, so that analogous to Eq. (4.3)

$$\boldsymbol{\tau}(\boldsymbol{X}, t) = \mathfrak{S}(\boldsymbol{C}_{(t)}(t-s); \boldsymbol{X}, t), \qquad \forall s \geq 0\,. \tag{6.125}$$

Such was the approach first proposed by Lumley (1967) in providing a polynomial relationship for the turbulent stress tensor. The approach was based on the attempt to construct a (mathematically) rational sequence of approximations about an isotropic state (undistorted state) and a homogeneous field. The functional describing the stress had a "fading memory" to account for the response of the turbulent stress to the (ensemble) mean distortion and a "limited awareness" to restrict the spatial region about which a fluid element can be influenced. The latter spatial constraint suggested an approximation procedure about a homogeneous field. Analogous questions also arise in the study of viscoelastic fluids and constitutive equation formulation where the extra-stress is constrained by fading memory effects. This problem was addressed by Coleman and Noll (1961) who developed an approximation theorem that provided a tensorial expansion for the "retarded history" functional that described the extra-stress field. Consistent with the determinism principle, the functional $\mathfrak{S}$ is assumed sufficiently analytic and differentiable to allow a series expansion in the parameter s about the local time t. This series expansion is then given by

$$\boldsymbol{\tau}(\boldsymbol{X},t)=\mathfrak{S}\left(\boldsymbol{C}_{(t)}(t)+\sum_{n}\frac{s^n}{n!}\frac{\partial^n \boldsymbol{C}_{(t)}(t-s)}{\partial s^n}\bigg|_{\boldsymbol{X},s=0};\boldsymbol{X},t\right),\quad n=1,2,\ldots\,. \tag{6.126}$$

From Eqs. (3.55a), (3.55b) the resulting representation is in terms of the Rivlin-Ericksen tensors and can be written as

$$\boldsymbol{b}=\tau\alpha_1\boldsymbol{A}_1+\tau^2\left[\alpha_2(\mathrm{tr}\,\boldsymbol{A}_2)\boldsymbol{I}+\alpha_3\boldsymbol{A}_2+\alpha_4(\mathrm{tr}\,\boldsymbol{A}_1^2)\boldsymbol{I}+\alpha_5\boldsymbol{A}_1^2\right]+O(\tau^3)\,, \tag{6.127}$$

where $\boldsymbol{A}_i$, $i=1,2,3\ldots$ are the Rivlin-Ericksen tensors. Lumley (1967) identified the expansion parameter s with the turbulent time scale τ and proceeded to write the above expansion to third order. In addition, as noted the expansion Lumley proposed also included a spatial contribution to account for inhomogeneous effects and this resulted in terms involving second-order spatial gradients of $\boldsymbol{A}_1$ where $\boldsymbol{A}_1$ is the rate of strain tensor. A comparison with Eqs. (6.124a), (6.124b) shows that the lowest order term in Eq. (6.127) is simply the form taken for a isotropic linear eddy viscosity model. In general here, the α_1 can be functions of the flow invariants.

While the proposed expansion given in Eq. (6.127) was appealing, it soon was recognized to have some inherent deficiencies. Lumley (1970b) made two modifications to his earlier considerations. The first was to abandon the constraint associated with local awareness since there was clear evidence from studies of turbulent flows that the turbulence could be correlated on lengths corresponding to the (spatial) integral scale of the flow. This had limited impact on his earlier considerations since the retarded memory aspect was a more important consideration rather than inhomogeneity effects. Of much more critical importance was the assumed sole dependence on the mean deformation through $\boldsymbol{C}_{(t)}(t)$. This was a consequence of the assumption that the principle of material indifference held also for a turbulent flow (Lumley 1967). Although this was and continues to be a source of discussion in the fluid turbulence field, it is now taken that this principle does not hold for a turbulent

flow and that some account needs to be made, not just for the deformation rate, but also for the rotation rate of the material element. With the abandonment of the order fluid constitutive equation expansion, the focus was directed to representations constructed from flow invariants. This has been more successful and closure models derived in this manner are still in use.

6.5.2 Turbulent Stress from Invariant Bases

From the discussion and polynomial representation of the last section, Sect. 6.5.1, as well as from the determination of the polynomial representation for the pressure-strain rate correlation in Sect. 6.4.1, it is reasonable to assume at the outset that a polynomial representation for the stress anisotropy tensor $\boldsymbol{b}$ must include both the symmetric rate of strain tensor and the skew-symmetric rate of rotation tensor. Thus, what is first needed is a representation for a symmetric tensor function of a symmetric and skew-symmetric tensor. This tensor function was examined previously in Sect. 2.4.1.2, with the expansion coefficient integrity basis invariants given in Eq. (2.68), and the associated basis tensors given in Eq. (2.70). For the particular case here, where $\boldsymbol{A} = \boldsymbol{S}$ and $\boldsymbol{X} = \boldsymbol{W}$, the expansion coefficients can be functions of the 6 invariants ($\mathrm{tr}\,\boldsymbol{S} = 0$, incompressible flow)

$$\mathrm{tr}\,\boldsymbol{S}^2, \quad \mathrm{tr}\,\boldsymbol{W}^2, \quad \mathrm{tr}\,\boldsymbol{S}^3, \quad \mathrm{tr}\,(\boldsymbol{W}^2\boldsymbol{S}), \quad \mathrm{tr}\,(\boldsymbol{S}^2\boldsymbol{W}^2), \quad \mathrm{tr}\,(\boldsymbol{S}^2\boldsymbol{W}^2\boldsymbol{S}\boldsymbol{W})\,, \tag{6.128}$$

with the corresponding ten-term tensor basis $\boldsymbol{\Phi}_k$ given by

$$\begin{aligned}
&\boldsymbol{\Phi}_1 = \boldsymbol{S} && \boldsymbol{\Phi}_6 = \boldsymbol{W}^2\boldsymbol{S} - \tfrac{1}{3}\{\boldsymbol{W}^2\boldsymbol{S}\}\boldsymbol{I} \\
&\boldsymbol{\Phi}_2 = \boldsymbol{S}\boldsymbol{W} && \boldsymbol{\Phi}_7 = \boldsymbol{W}\boldsymbol{S}\boldsymbol{W}^2 \\
&\boldsymbol{\Phi}_3 = \boldsymbol{S}^2 - \tfrac{1}{3}\{\boldsymbol{S}^2\}\boldsymbol{I} && \boldsymbol{\Phi}_8 = \boldsymbol{S}\boldsymbol{W}\boldsymbol{S}^2 \\
&\boldsymbol{\Phi}_4 = \boldsymbol{W}^2 - \tfrac{1}{3}\{\boldsymbol{W}^2\}\boldsymbol{I} && \boldsymbol{\Phi}_9 = \boldsymbol{W}^2\boldsymbol{S}^2 - \tfrac{1}{3}\{\boldsymbol{W}^2\mathbf{S}^2\}\mathbf{I} \\
&\boldsymbol{\Phi}_5 = \boldsymbol{W}\boldsymbol{S}^2 && \boldsymbol{\Phi}_{10} = \boldsymbol{W}\boldsymbol{S}^2\boldsymbol{W}^2\,.
\end{aligned} \tag{6.129}$$

In Eq. (6.129), the trace has been subtracted out where necessary to ensure that each basis tensor term is traceless. For a complete representation of $\boldsymbol{b}$ for a three-dimensional flow, the polynomial representation will include all the basis tensors in Eq. (6.129) such that

$$\boldsymbol{b} = \frac{1}{2}\sum_{k=1}^{10} I_k \left(\boldsymbol{\Phi}_k + \boldsymbol{\Phi}_k^T\right)\,, \tag{6.130}$$

with the expansion coefficients I_k, in general being functions of the six invariants given in Eq. (6.128). The functional dependency of the stress anisotropy tensor on only the rate of strain and rate of rotation tensors is the simplest situation that can occur. Even in incompressible flows, more complex effects can arise such as accounting for wall-normal effects, and if thermal effects are considered, dependency on the heat flux would need to be considered. Such additional dependencies could

significantly augment the number of invariants and basis tensors that would need to be considered. It is sufficient here, where the intent is to describe the methodology in developing such a turbulent constitutive equation to restrict the attention to this simple case of sole dependency on one symmetric and one skew-symmetric tensor related to the mean velocity gradient.

There are two types of turbulent constitutive equations or models that have been extracted from such integrity basis polynomial representations. Both use the tensor bases given in Eq. (6.130), but are distinguished by the manner in which the expansion coefficients are determined. In the remainder of this section, these two types of turbulent models, one called a nonlinear eddy viscosity model (NLEVM) and the other called an explicit algebraic Reynolds stress model (EARSM) will be discussed.

6.5.2.1 Nonlinear Eddy Viscosity Model (NLEVM)

As was shown in Eq. (6.129), the term $\boldsymbol{\Phi}^{(1)}$ is the basis tensor in the linear eddy viscosity model (LEVM) of Eqs. (6.124a), (6.124b). Since the remaining terms $\boldsymbol{\Phi}^{(n)}$ $(n \geq 2)$ in the polynomial expansion are nonlinear terms, it readily follows that a model that contains a subset of these basis tensor terms is often labeled a nonlinear eddy viscosity model (NLEVM). For a nonlinear eddy viscosity model, the expansion coefficients are based on calibrations with experimental or numerical data, and on some physical consistency constraints.

As might be expected, there have been a significant number of nonlinear eddy viscosity models proposed. Some early attempts included the models of Yoshizawa (1984) (see also Nisizima and Yoshizawa 1987), Myong and Kasagi (1990) and Rubinstein and Barton (1990). The functional forms of the representations were expressed in terms of the mean velocity gradients and were not formulated based on integrity basis representations. Yoshizawa (1984) derived a model based on the Direct Interaction Approximation (DIA); whereas, Rubinstein and Barton (1990) derivation was based on the renormalization group (RNG) approach. Myong and Kasagi (1990) used a similar functional form as Nisizima and Yoshizawa (1987), but provided a wall-proximity modification. As for the corresponding expansion coefficients, they were primarily chosen in these studies by validation against fully developed two-dimensional flows such as plane channel flow. These examples serve to show that a variety of approaches can be used to generate polynomial representations for the turbulent stress that do not follow the usual guidelines for constitutive equation development. In addition, even though representations using a mean velocity gradient tensor can be rewritten in terms of the tensor bases in Eq. (6.129), such velocity gradient tensor representations both complicate the appearance and rational ordering of the terms. In what follows, turbulent stress tensor representations that have been developed primarily from tensor basis ideas will be discussed in some detail. Since it is not possible to list or discuss all of these tensor representation based models, the intent then is to highlight a few models that represent the variety of assumptions required in identifying the expansion coefficients I_k. By construction,

these nonlinear eddy viscosity models contain terms of degree 2 or 3 included in the complete representation given in Eq. (6.129).

Consider first the quadratic representation proposed by Shih et al. (1995),

$$\boldsymbol{b} = \sum_{k=1}^{4} I_k^{SZL} \left(\boldsymbol{\Phi}_k + \boldsymbol{\Phi}_k^T \right) , \tag{6.131}$$

where the basis tensors are extracted from the list in Eq. (6.129). The four expansion coefficients, I_k^{SZL} are determined by the imposition of physical constraints on the turbulent stress anisotropy field. For example, for an isotropic turbulence under a rapid mean rotation, there is no effect on the turbulence field which requires that $\boldsymbol{b} = 0$ when $\boldsymbol{S} = 0$. This leads immediately to the requirement that $I_4^{SZL} = 0$. Another fundamental constraint is imposed through the condition of realizability which requires that the turbulent normal stress components be positive definite and that Schwarz' inequality holds between the turbulent stress components, that is

$$\tau_{\beta\beta} \geq 0, \qquad \text{and} \qquad \tau_{\beta\gamma}^2 \leq \tau_{\beta\beta}\tau_{\gamma\gamma} \text{ (no sum)} , \tag{6.132}$$

where the first constraint requires that $b_{\beta\beta} \geq -1/3$ and the second requires that the corresponding correlation coefficient be ≤ 1. An analysis of the limiting cases of axisymmetric expansion and contraction led to the choice $I_3^{SZL} = 0$ which resulted in a two-term representation ($k = 2$) that was bilinear in the tensors $\mathbf{S}$ and $\boldsymbol{W}$. The remaining coefficients I_1^{SZL} and I_2^{SZL} were optimized by further comparison with experiment and numerical simulation of homogeneous shear flow and the equilibrium log-layer, and were functions of the mean flow invariants $\text{tr}\,\boldsymbol{S}^2$ and $\text{tr}\,\boldsymbol{W}^2$. Initial validation studies were run on rotating homogeneous shear flow, backward-facing step flows, and confined jets with overall improved predictions over the linear eddy viscosity models. A similar functional form was also used by Lien and Leschziner (1995) to study high-lift airfoil flows; although, the coefficient values used for the corresponding K and ε transport equations were different. Irrespective of the calibration process, an inherent deficiency associated with this functional form arises in the case of simple unidirectional shear flow (say $S_{ij}\delta_{i1}\delta_{j2}$). In this case, $b_{11} = -b_{22}$, and $b_{33} = 0$ always—which is inconsistent with observed behavior of such flows. It is also possible to show (Gatski and Jongen 2000) that, similar to a linear representation (LEVM), a quadratic representation that omits the $\boldsymbol{\Phi}_3$ term yields the condition $\text{I}_3\,(\boldsymbol{b}) = 0$ in any two-dimensional flow. As Fig. 6.7 shows, such models yield predictions for plane channel flow that are inconsistent with the direct numerical simulation data (Kim et al. 1987) as well as predictions from a differential Reynolds stress model (RSM) (So et al. 1996).

While quadratic models have been widely used, there have been some higher-order representations proposed in order to better predict flows with complex strain fields. Craft et al. (1996) considered a model of the form,

$$\boldsymbol{b} = \sum_{k=1}^{6} I_k^{CLS} \left(\boldsymbol{\Phi}_k + \boldsymbol{\Phi}_k^T \right) , \tag{6.133}$$

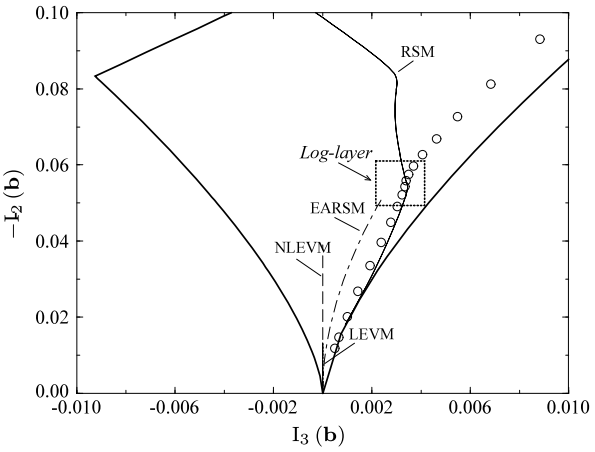

Fig. 6.7 Wall-normal variation of the turbulent stress in the anisotropy invariant map for fully developed plane channel flow: ◯, DNS (Kim et al. 1987); ···, LEVM; - - - -, NLEVM (Shih et al. 1995); -·-·-, EARSM; —, RSM (So et al. 1996)[5]

where the basis tensors are extracted from the list in Eq. (6.129). Aside from the inclusion of the terms of degree 3 from Eq. (6.129) in the representation, the expansion coefficients each retained a dependency on the mean flow invariants as in the quadratic representation just discussed. Calibration of the closure coefficients was based on an optimization over a wide range of flows including: plane channel flow, circular pipe flow, axially rotating pipe flow, fully developed curved channel flow, and impinging jet flows. Due to the redundant appearance of factors in the cubic terms, the calibration optimization led to $I_6^{CLS} = 0$. Since there was no comparison to rapidly rotating isotropic turbulence, the basis tensor $\boldsymbol{\Phi}_4$ was retained which would lead to erroneous predictions in such flows (Speziale 1998a). In order to improve the predictive capability of the NLEVM in the near-wall region where the two-component limit of turbulence applies (see Sect. 6.3.1), Craft et al. (1997) introduced a transport equation for the trace of the Reynolds stress anisotropy $\mathrm{tr}\,\boldsymbol{b}^2$. The consequence of introducing this transport equation was to provide an additional constraint on the turbulent stress anisotropy that was directly related to the flow dynamics through the Reynolds stress anisotropy transport equation. Although implemented differently, inclusion of such a dynamic transport equation constraint into the construction of the polynomial representation for the turbulent anisotropy will be the characterizing feature of the explicit algebraic stress models to be discussed in Sect. 6.5.2.2.

The two examples just presented showed representations of $\boldsymbol{b}$ based solely on a tensor invariant theory construction. While this leads to the correct functional forms for the various representations, it is also devoid of any dynamic condition. Speziale (1987) attempted to impose such a dynamic condition by imposing the constraint of material frame-indifference in the limit of two-dimensional turbulence on the representation of $\boldsymbol{b}$. As was discussed in Chap. 4, the MFI condition does not

[5]Figure 6.7 reprinted with permission from: T.B. Gatski, T. Jongen (2000) Nonlinear eddy viscosity and algebraic stress models for solving complex turbulent flows. Prog Aerosp Sci 36:655–682. Copyright Elsevier 2000.

generally hold except for this limiting case of two-dimensional turbulence. With this constraint, it is necessary that the representation be form-invariant under a change of frame. The inclusion of the skew-symmetric rate of rotation tensor precludes such an invariant property so it is necessary to modify the functional dependency of the anisotropy tensor $\boldsymbol{b}$. Speziale (1987) proposed that the tensorial dependency of $\boldsymbol{b}$ be given by

$$\boldsymbol{b} = \boldsymbol{b}\left(\boldsymbol{S}, \boldsymbol{W}, \overset{\nabla}{\boldsymbol{S}}\right) , \tag{6.134}$$

where $\overset{\nabla}{\boldsymbol{S}}$ is the Oldroyd upper convective derivative of the rate of strain tensor (cf. Eqs. (4.33a), (4.33b)),

$$\overset{\nabla}{\boldsymbol{S}} = \frac{D\boldsymbol{S}}{Dt} - 2\boldsymbol{S}^2 + \boldsymbol{S}\boldsymbol{W} - \boldsymbol{W}\boldsymbol{S} . \tag{6.135}$$

Such a modeling proposal is analogous to the second-order fluid model proposed for viscoelastic fluids and given in Eq. (6.82). The resulting polynomial representation proposed by Speziale (1987) was then

$$\boldsymbol{b} = \sum_{k=1}^{3} I_k^S \left(\boldsymbol{\Phi}_k + \boldsymbol{\Phi}_k^T\right) + I_\nabla \left(\overset{\nabla}{\boldsymbol{S}} - \frac{1}{3}\{\overset{\nabla}{\boldsymbol{S}}\}\boldsymbol{I}\right) , \tag{6.136}$$

which, as written, is a representation composed of frame-invariant basis tensors. In the calibration of the model in fully developed channel flow, it was determined that $I_3^S = I_\nabla$. This then allows Eq. (6.136) to be written as

$$\boldsymbol{b} = \sum_{k=1}^{3} I_k^S \left(\boldsymbol{\Phi}_k + \boldsymbol{\Phi}_k^T\right) + I_\nabla \frac{D\boldsymbol{S}}{Dt} , \tag{6.137}$$

with $I_2^S = I_\nabla$ as well. It is interesting to point out that while Eqs. (6.136) and (6.137) are equivalent, the frame-invariance of Eq. (6.137) is much less obvious since the material derivative D/Dt is restricted to only Galilean invariance. Not surprisingly, validation studies on rectangular duct flow and backstep flow yielded improved predictions over LEVM results.

These nonlinear representations of the turbulent stress anisotropy are necessarily coupled with scalar transport equations for the turbulent kinetic energy and a dissipation scale variable ($K-\varepsilon$, $K-\omega$, ...). As might be expected, a wide variety of scale equations have been used in the application of these representations to a variety of inhomogeneous flows. As the preceding discussion showed, the tensor representations themselves are simply dictated by invariance considerations and the functional dependency of the Reynolds stresses. The influence of any flow dynamics is (indirectly) confined to the calibration process associated with the expansion coefficients and the choice of differential scale equations to be solved in conjunction with the polynomial representations. Both the calibration process and choice of scale equations can have a significant influence on the model predictions, especially if the key dynamics is dictated by factors other than the anisotropy of the turbulence.

6.5.2.2 Explicit Algebraic Reynolds Stress Model

The final type of polynomial representation that has been developed for the turbulent Reynolds stress (anisotropy) is the same as that discussed in the previous section with the same basis tensors as those given in Eq. (6.129). The unique characteristic of an explicit algebraic Reynolds stress model is that it utilizes the dynamic constraint provided by a weak-equilibrium form of the modeled transport equation for the Reynolds stress anisotropy itself. This is in contrast to the procedure used in the identification of the expansion coefficients for nonlinear eddy viscosity models where the imposition of constraints dictated by the limiting case of homogeneous flows or calibration with inhomogeneous flows was used. The starting point is then the stress anisotropy transport equation obtained from the definition of the turbulent stress anisotropy given in Eq. (6.98), and the relevant stress and kinetic energy equations in Eqs. (6.90) and (6.100), respectively. The resulting $\boldsymbol{b}$ transport equation is then

$$\frac{D\boldsymbol{b}}{Dt} - \frac{D^t}{K}\left[\boldsymbol{d}^t - \boldsymbol{b}\right] = (2\tau\{\boldsymbol{bS}\} + 1)\,\frac{\boldsymbol{b}}{\tau} - \frac{2}{3}\boldsymbol{S} + \frac{\boldsymbol{\Pi} - \boldsymbol{d}^\varepsilon}{2K} - \left[\boldsymbol{bS} + \boldsymbol{Sb} - \frac{2}{3}\{\boldsymbol{bS}\}\boldsymbol{I}\right] + (\boldsymbol{bW} - \boldsymbol{Wb}) \ , \tag{6.138}$$

where the anisotropy definitions for $\boldsymbol{d}^t$ and $\boldsymbol{d}^\varepsilon$ are given in Eqs. (6.96) and (6.97), respectively, and $D^t = D^t_{kk}/2$. In light of the extensive proposals for the pressure-strain rate correlation, a modeled form for $\boldsymbol{\Pi}/K$ is used in Eq. (6.139). Without loss of generality, a linear model is assumed for the purposes here, so that from Eq. (6.110b), the basis tensors $\boldsymbol{\Phi}_i$ $(i = 1, 3, 4, 5)$ are chosen for the pressure-strain rate representation. Equation (6.138) can then be written as

$$\frac{D\boldsymbol{b}}{Dt} - \frac{D^t}{K}\left[\boldsymbol{d}^t - \boldsymbol{b}\right] = \left(2\tau\{\boldsymbol{bS}\} + 1 + \frac{\alpha_1}{2}\right)\frac{\boldsymbol{b}}{\tau} - \frac{1}{2}\left(\frac{4}{3} - \alpha_3\right)\boldsymbol{S} - \frac{\boldsymbol{d}^\varepsilon}{2K} - \frac{1}{2}(2 - \alpha_4)\left[\boldsymbol{bS} + \boldsymbol{Sb} - \frac{2}{3}\{\boldsymbol{bS}\}\boldsymbol{I}\right] + \frac{1}{2}(2 - \alpha_5)\,(\boldsymbol{bW} - \boldsymbol{Wb}) \ , \tag{6.139}$$

or, in the more compact form, as

$$\frac{D\boldsymbol{b}}{Dt} = \boldsymbol{F}\left(\boldsymbol{b}, \boldsymbol{S}, \boldsymbol{W}, \boldsymbol{d}^t, \boldsymbol{d}^\varepsilon\right) \ , \tag{6.140}$$

where the scalar dependencies have been omitted for brevity.

The weak-equilibrium form results from the assumption of a weak anisotropy variation in the turbulent fluid coupled with an assumption of a weakly inhomogeneous flow. The imposition of these two constraints on the anisotropy transport equation results in an implicit algebraic equation for **b**. Although the detailed form of this implicit algebraic equation is dependent on closure provided by the representations of pressure-strain rate correlation, it nevertheless provides a direct dynamic constraint on the polynomial representation for $\boldsymbol{b}$. As a first step it is necessary to

discuss in some detail the weak-equilibrium conditions that need to be applied to the **b** transport equation.

Weak-Equilibrium Conditions The term weak-equilibrium can be interpreted in slightly different ways, but with the same underlying meaning which is related to constant or nearly constant behavior of the turbulent stress anisotropy. By construction, any equilibrium (constant) of the turbulent stress rate is a weaker assumption than requiring the individual stress component rates and kinetic energy rate to be in equilibrium. Alternately, one can also assume that the turbulence field is only weakly anisotropic and that some sequence of approximations around an isotropic state would be sufficient to describe the turbulence. Whichever, physical basis is used, the practical requirement necessitates a replacement of the anisotropy stress rate with an algebraic polynomial with terms inclusive of $\boldsymbol{b}$, $\boldsymbol{S}$ and/or $\boldsymbol{W}$. Similarly, these same ideas need to be applied to the turbulent transport and dissipation rate anisotropies as a means of relating these quantities to the stress anisotropy.

In the absence of domain boundary effects or imposed forces, it is not unreasonable to assume as a first approximation that the dissipation rate anisotropy, $\boldsymbol{d}^{\varepsilon}$, vanishes. The small dissipation scales of the turbulence are least influenced by the mean strain fields and the large scale anisotropies associated with it. The situation is less clear with the turbulent transport anisotropy. As a practical matter, the turbulent transport contribution can vanish by simply assuming an equality between the turbulent transport anisotropy, $\boldsymbol{d}^{t}$, and the turbulent stress anisotropy, $\boldsymbol{b}$. Rodi (1972, 1976) assumed the Daly-Harlow (Daly and Harlow 1970) model for the turbulent transport and showed that for a homogeneous distribution of the turbulent stress anisotropy that $\boldsymbol{d}^{t} = \boldsymbol{b}$. Recall, however, that the Daly-Harlow model did not have the correct index permutation properties and so was not generally admissible to flows other than thin shear flows. Since the higher-order models discussed in Sect. 6.4.2 do not yield this same simple relationship between the turbulent transport anisotropy $\boldsymbol{d}^{t}$ and $\boldsymbol{b}$, its range of validity is questionable. Nevertheless, despite all these limitations it is the common assumption invoked in extracting an implicit algebraic equation from Eq. (6.139). With the assumptions $\boldsymbol{d}^{t} = \boldsymbol{b}$ and $\boldsymbol{d}^{\varepsilon} = 0$, Eq. (6.139) is then reduced to the functional form

$$\begin{aligned}\frac{D\boldsymbol{b}}{Dt} &= a_0\boldsymbol{b} - a_1\boldsymbol{S} - a_2\left[\boldsymbol{bS} + \boldsymbol{Sb} - \frac{2}{3}\{\boldsymbol{bS}\}\boldsymbol{I}\right] + a_3\left(\boldsymbol{bW} - \boldsymbol{Wb}\right) \\ &= \boldsymbol{F}\left(\boldsymbol{b}, \boldsymbol{S}, \boldsymbol{W}\right) \ , \end{aligned} \tag{6.141}$$

where the a_i coefficients are identified by direct comparison to Eq. (6.139). In contrast to the somewhat speculative approach in providing weak-equilibrium relationships for the turbulent transport anisotropy $\mathbf{d}^{t}$ and dissipation rate anisotropy $\boldsymbol{d}^{\varepsilon}$, a more rational and general approach can be taken in specifying the weak-equilibrium condition for turbulent anisotropy stress rate.

In rectilinear flow fields, such as homogeneous planar flows, where the fluid element paths are parallel, the turbulent anisotropy stress rate $D\boldsymbol{b}/Dt$ will vanish if the imposed mean deformation persists over several turbulent time scales. Impos-

ing this weak-equilibrium condition, $D\boldsymbol{b}/Dt = \boldsymbol{0}$, in Eq. (6.141) yields the implicit algebraic Reynolds stress equation

$$\boldsymbol{F}\left(\boldsymbol{b}, \boldsymbol{S}, \boldsymbol{W}\right) = 0\,. \tag{6.142}$$

This condition has been verified for a variety of planar homogeneous flows where $\boldsymbol{b}$ reaches a time independent value, and in inhomogeneous flows such as planar boundary layers, where the wall-normal distribution of $\boldsymbol{b}$ values show no streamwise variation. Of course, it is possible to solve the implicit algebraic equation system in Eq. (6.142) directly for the five (independent) stress anisotropy components if the model for the pressure strain rate correlation is bilinear in the functional dependencies given by $\boldsymbol{F}(\boldsymbol{b}, \boldsymbol{S}, \boldsymbol{W})$ (Rodi 1972, 1976); however, no polynomial representation is used in such an approach and this will not be considered further.

The fluid motion described by Eq. (6.142) represents a simple motion of a material element associated with a (locally) homogeneous deformation along a (rectilinear) path where the principal directions of the rate of strain tensor do not change. The question that arises is whether the weak-equilibrium condition given by the vanishing of $D\boldsymbol{b}/Dt$ is generally applicable to more complex motions. The answer is yes, but the choice of frame where the condition is applied is important. Two types of flows are of interest within this context. The first corresponds to non-inertial flow fields where rotational effects are present and the second to flow fields with curvature. In engineering flows, the former case is often identified with turbomachinery flows, and the latter case is often associated with changes of geometry, such as in a curved channel and duct, backstep or diffuser flow. In both types of flows, the underlying assumption is that the material rate of change of $\boldsymbol{b}$ vanishes in the frame moving with the turbulent fluid element.

For the first case, a rotating flow, the frame of reference where the flow variables are required is the rotating frame itself. This only then requires that Eq. (6.139) be transformed to a non-inertial frame, which leads to

$$\frac{D\boldsymbol{b}^*}{Dt} + \left(\boldsymbol{b}^*\boldsymbol{\Omega}^{(r)} - \boldsymbol{\Omega}^{(r)}\boldsymbol{b}^*\right) = \boldsymbol{F}\left(\boldsymbol{b}^*, \boldsymbol{S}^*, \boldsymbol{W}_a^*\right)\,, \tag{6.143}$$

where the usual transformation rules are used, for example, $\boldsymbol{b}^* = \boldsymbol{Q}\boldsymbol{b}\boldsymbol{Q}^T$, $\boldsymbol{\Omega}^{(r)}$ is the imposed rotation rate of the non-inertial frame, and $\boldsymbol{W}_a^* = \boldsymbol{W}^* - \boldsymbol{\Omega}^{(r)}$ is the (objective) absolute (or intrinsic) vorticity tensor ($\boldsymbol{\Omega}^{(r)}$ is the spin of the starred frame as measured in the unstarred frame). The equilibrium condition imposed on the turbulent stress anisotropy is a physical constraint and should be independent of frame. In this example, the frame rotation has been isolated into the terms ($\boldsymbol{b}^*\boldsymbol{\Omega}^{(r)} - \boldsymbol{\Omega}^{(r)}\boldsymbol{b}^*$) on the left and the absolute vorticity tensor on the right, so that the correct weak-equilibrium condition is $D\boldsymbol{b}^*/Dt = \boldsymbol{0}$ in this frame, and the implicit algebraic equation for $\boldsymbol{b}^*$ is

$$\boldsymbol{F}\left(\boldsymbol{b}^*, \boldsymbol{S}^*, \boldsymbol{W}_a^*\right) - \left(\boldsymbol{b}^*\boldsymbol{\Omega}^{(r)} - \boldsymbol{\Omega}^{(r)}\boldsymbol{b}^*\right) = 0\,. \tag{6.144}$$

Rotating homogeneous shear flow and rotating channel flow (spanwise rotation) are often studied in order to understand the influence of non-inertial effects on turbulence dynamics. As noted above, in these studies the observer is in the (reference) non-inertial frame so no additional transformations are required to analyze

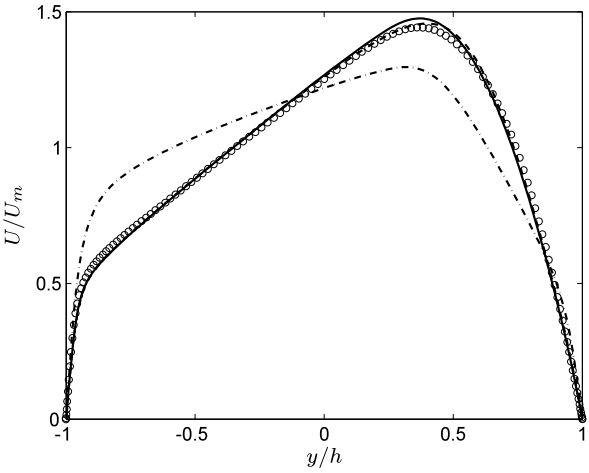

Fig. 6.8 Mean velocity distribution across rotating channel flow for $Ro = 0.77$ ($= 2\Omega^{(r)}h/U_m$, U_m, mean bulk velocity; h, channel half-width) and $Re_\tau = 180$ (no rotation). Computations using EARSM applying $D\boldsymbol{b}^*/Dt = 0$ (—) in Eq. (6.143) compared to the corresponding DRSM (- - -) and the EARSM applying $D\boldsymbol{b}/Dt = 0$ (···). DNS of Alvelius (1999), ∘. Reprinted with permission from Gatski and Wallin (2004)

results obtained. The consequences of choosing an incorrect equilibrium condition is exemplified for the case of a rotating channel flow. In Fig. 6.8 the mean velocity distribution is shown for a spanwise rotating channel. As the figure shows, the equilibrium condition $D\boldsymbol{b}^*/Dt = 0$ condition applied in Eq. (6.143) closely replicates the results from the differential Reynolds stress model; however, the condition $D\boldsymbol{b}/Dt = 0$ yields an erroneously prediction even though the algebraic expression $\boldsymbol{F}(\boldsymbol{b}^*, \boldsymbol{S}^*, \boldsymbol{W}_a^*)$ only contains objective variables.

The second type of motion to be examined is the case of a turbulent flow with curvature. In such flows, the fluid element is undergoing a motion comprised of both a rigid-body rotation and a deformation; however, the frame of reference where the flow variables are required is an inertial frame. As the example of rotating turbulent flow shows, the effects of any rotational effects need to be accounted for in establishing a suitable weak-equilibrium condition. For a flow with curvature, this suggests that some measure, $\boldsymbol{\Omega}^{(c)}$, of the rigid-body rotation of the fluid element motion be established. In a non-inertial frame, with rotation rate $\boldsymbol{\Omega}^{(c)}$, the motion is once again described by Eq. (6.143) with the imposed frame rotation $\boldsymbol{\Omega}^{(r)}$ now replaced by $\boldsymbol{\Omega}^{(c)}$ characterizing the flow curvature. Nevertheless, the same equilibrium condition $D\boldsymbol{b}^*/Dt = 0$ holds (now in a frame that provides a measure of the fluid element rotation induced by the flow curvature) and Eq. (6.144) applies now with $\boldsymbol{\Omega}^{(r)} = \boldsymbol{\Omega}^{(c)}$. However, as noted above, such flow fields usually require a knowledge of the flow variables in an inertial frame so that Eq. (6.144) needs to be transformed back to an inertial frame.[6] This transformation yields an implicit algebraic equation for $\boldsymbol{b}$ ($= \boldsymbol{Q}^T\boldsymbol{b}^*\mathbf{Q}$) given by

[6] In general, the inertial frame of relevance in this curved flow case may not necessarily be the one from which Eq. (6.143) was obtained originally. For example, a fixed relative rotation between the two inertial frames can occur. Nevertheless, since the essence of the discussion here is the proper choice of equilibrium condition and appropriate measure of effect of curvature, the transformation back to the inertial frame is simply based on the orthogonal transformation tensor $\boldsymbol{Q}$.

$$\boldsymbol{F}\left(\boldsymbol{b}, \boldsymbol{S}, \boldsymbol{W}_a\right) + \left(\boldsymbol{b}\boldsymbol{\Omega}^{(c)} - \boldsymbol{\Omega}^{(c)}\boldsymbol{b}\right) = 0\,, \tag{6.145}$$

where $\boldsymbol{\Omega}^{(c)}$ ($D\,\boldsymbol{Q}/Dt = \boldsymbol{\Omega}^{(c)}\,\boldsymbol{Q}$) is the rotational measure of the flow curvature relative to the inertial frame, and $\boldsymbol{W}_a = \boldsymbol{W} + \boldsymbol{\Omega}^{(c)}$ is the absolute vorticity tensor relative to the inertial frame. The task is to identify a frame where the rigid-body rotations of the fluid element can be isolated and to determine $\boldsymbol{\Omega}^{(c)}$.

As noted, the fluid elements in curved flows are undergoing a deformation consisting of both fluid element stretching and fluid element rigid-body rotation. However, as Eq. (4.37) showed, the rotation rate tensor is a combination of both a rotational component associated with the deformation gradient tensor and a component related to the stretching associated with the deformation gradient tensor. It was shown in Sect. 4.3.2.3, that if the frame of motion of the fluid element is aligned with the principal directions of the rate of strain tensor, the deformation is partitioned into a part solely representing the fluid element extension (the rate of strain tensor) and a part representing the fluid element rigid-body rotation (the rate of rotation tensor). This latter part, representing the rotation rate of the principal axes of the strain rate tensor (relative to the inertial frame) is $\boldsymbol{\Omega}^{(c)}$.

Calculations of turbulent flows with curvature, such as curved channels or ducts, are usually performed in inertial coordinate frames. It is then necessary to modify the governing equations as suggested above, and holds for both differential and algebraic formulations. Since such flow fields are inhomogeneous, the orientation of the principal directions varies with spatial position so that the orientation angle of these principal directions also varies relative to some base frame orientation. The rotation rate $\boldsymbol{\Omega}^{(c)}$ is then given by the material rate of change of this orientation angle.

Expansion Coefficient Determination from Invariants As was mentioned at the beginning of this section, the primary difference between an explicit algebraic Reynolds stress model and a nonlinear eddy viscosity model is in the former model, a dynamic constraint introduced by the implicit algebraic Reynolds stress equation is directly used in the determination of the expansion coefficients. A direct strategy involves the solution of the implicit algebraic transport equation, Eq. (6.142), using the tensor basis given in Eq. (6.129) (Wallin and Johansson 2000). A linear system of equations for the five independent anisotropy components can be obtained by successive use of the Cayley-Hamilton theorem and a coupling with a nonlinear equation for invariant related to the stress anisotropy and rate of strain invariant $\{\boldsymbol{bS}\}$.

An alternative approach, and the one first used by Pope (1975) for a two-dimensional three-term tensor basis and later by Gatski and Speziale (1993) for a complete ten-term basis, involved a partitioning of the implicit algebraic equation, Eq. (6.141), into the form

$$a_0 \sum_{k=1}^{\mathrm{N}} g_k \boldsymbol{T}_k - a_2 \sum_{k=1}^{\mathrm{N}} g_k \sum_{\gamma=1}^{\mathrm{N}} H_{k\gamma}\boldsymbol{T}_\gamma + a_3 \sum_{k=1}^{\mathrm{N}} g_k \sum_{\gamma=1}^{\mathrm{N}} J_{k\gamma}\boldsymbol{T}_\gamma = a_1 \boldsymbol{S}\,, \tag{6.146}$$

with the expansion coefficients $H_{k\gamma}$ and $H_{k\gamma}$ given by

$$\sum_{k=1}^{\mathrm{N}} g_k \boldsymbol{T}_k = \boldsymbol{b} \ , \tag{6.147a}$$

$$\sum_{\gamma=1}^{\mathrm{N}} H_{k\gamma} \boldsymbol{T}_\gamma = \boldsymbol{T}_k \boldsymbol{S} + \boldsymbol{S}\boldsymbol{T}_k - \frac{2}{3}\{\boldsymbol{T}_k \boldsymbol{S}\}\boldsymbol{I} \ , \tag{6.147b}$$

$$\sum_{\gamma=1}^{\mathrm{N}} J_{k\gamma} \boldsymbol{T}_\gamma = \boldsymbol{T}_k \boldsymbol{W} - \boldsymbol{W}\boldsymbol{T}_k \ , \tag{6.147c}$$

where

$$\boldsymbol{T}_k = \frac{1}{2}\left(\boldsymbol{\Phi}_k + \boldsymbol{\Phi}_k^T\right) \ , \tag{6.148}$$

with $\boldsymbol{\Phi}_k$ the basis tensors given in Eq. (6.129), and it is assumed that the appropriate weak-equilibrium condition on $D\boldsymbol{b}/Dt$ has been applied. Since the basis tensors are linearly independent, the coefficients of the tensor basis $\boldsymbol{T}_k$ can be cast into a $\mathrm{N} \times \mathrm{N}$ linear system of equations for the unknown coefficient vector g_k, and written in the form

$$\left[a_0 \delta_{\gamma k} - a_2 H_{\gamma k} + a_3 J_{\gamma k}\right] g_k = a_1 \delta_{\gamma 1} \ , \tag{6.149}$$

with $\gamma = 1, \ldots, \mathrm{N}$. It is important to recognize that there has been no restriction invoked on the number of terms in the polynomial representation for the turbulent anisotropy tensor (other than the integrity basis of invariants is formed based on second-order tensor products), so that in general, the number could vary from 1 to 10. A closer examination of Eq. (6.149) and the coefficients a_0 (see Eqs. (6.139) and (6.141)) reveals a dependency on an invariant formed between the turbulent anisotropy tensor $\boldsymbol{b}$ and the rate of strain tensor $\boldsymbol{S}$ $(= \boldsymbol{T}_1)$, that is

$$a_0 = \left(2\tau\{\boldsymbol{b}\boldsymbol{S}\} + 1 + \frac{\alpha_1}{2}\right) \ . \tag{6.150}$$

Since the a_i coefficients are dependent on the expansion coefficients used in the closure representation for the pressure-strain rate correlation, any of the a_i can contain invariants formed from the anisotropy tensor $\boldsymbol{b}$. The form for the a_0 coefficient shown in Eq. (6.150) is the simplest form that can arise but the invariant $\{\boldsymbol{b}\boldsymbol{S}\}$ is always present and is an artifact of the construction of the anisotropy equation itself. Although the early representations (Pope 1975; Taulbee 1992; Gatski and Speziale 1993) did not account for this implicit dependence in deriving their tensorial representations, the form of the expansion coefficients g_k was valid, but the representations were not fully explicit. The representation can be made fully explicit by forming the invariant $\{\boldsymbol{b}\boldsymbol{S}\}$ using the representation given in Eq. (6.147a) (Ying and Canuto 1996; Girimaji 1996),

$$\{\boldsymbol{b}\boldsymbol{S}\} = \sum_{k=1}^{\mathrm{N}} g_k \{\boldsymbol{T}_k \boldsymbol{S}\} \ , \tag{6.151}$$

and solving the resulting polynomial equation for $\{\boldsymbol{b}\boldsymbol{S}\}$ in terms of the flow invariants given in Eq. (6.128). Not surprisingly, in the general case of a ten-term

representation, this can be problematic due to the complex form of the resulting polynomial equation for $\{\boldsymbol{bS}\}$. However, as the following example shows, the case of a two-dimensional mean flow field can be easily handled and is illustrative of the general procedure.

Consider a two-dimensional mean flow field (in the absence of any curvature and rotation effects). The turbulent stress anisotropy, rate of strain and rate of rotation tensors now have the component form,

$$[b] = \begin{pmatrix} b_{11} & b_{12} & b_{13} \\ b_{12} & b_{22} & b_{23} \\ b_{31} & b_{32} & b_{33} \end{pmatrix}, \qquad [S] = \begin{pmatrix} S_{11} & S_{12} & 0 \\ S_{12} & -S_{11} & 0 \\ 0 & 0 & 0 \end{pmatrix},$$
$$[W] = \begin{pmatrix} 0 & W_{12} & 0 \\ -W_{12} & 0 & 0 \\ 0 & 0 & 0 \end{pmatrix}, \tag{6.152}$$

where the trace of each vanishes, and the symmetric and skew-symmetric properties of $\boldsymbol{b}$, $\boldsymbol{S}$ and $\boldsymbol{W}$ have been introduced. For such a two-dimensional flow, the higher-degree basis tensors $k \geq 4$ in Eq. (6.129) can be rewritten in terms of the basis tensors $\boldsymbol{\Phi}_1$, $\boldsymbol{\Phi}_2$, and $\boldsymbol{\Phi}_3$.[7] Substituting the corresponding three-term polynomial representation of basis tensors $\boldsymbol{T}_k$ into Eq. (6.146), and equating coefficients of each basis term, yields a set of three equations in the three unknown expansion coefficients g_1, g_2, and g_3 given by Eq. (6.149) in the form

$$\begin{pmatrix} a_0 & -4\mathrm{I}_2(\boldsymbol{W})\, a_3 & \frac{2}{3}\mathrm{I}_2(\boldsymbol{S})\, a_2 \\ a_3 & a_0 & 0 \\ -2a_2 & 0 & a_0 \end{pmatrix} \begin{pmatrix} g_1 \\ g_2 \\ g_3 \end{pmatrix} = \begin{pmatrix} a_1 \\ 0 \\ 0 \end{pmatrix}. \tag{6.153}$$

This yields the solution

$$g_1 = a_1 a_0 \left[a_0^2 + 4\mathrm{I}_2(\boldsymbol{W})\, a_3^2 + \frac{4}{3}\mathrm{I}_2(\boldsymbol{S})\, a_2^2 \right]^{-1},$$
$$g_2 = -\left(\frac{a_3}{a_0}\right) g_1, \quad g_3 = 2\left(\frac{a_2}{a_0}\right) g_1 . \tag{6.154}$$

In obtaining this solution for the expansion coefficients, an incomplete three-term tensor basis was assumed. The same result would have also been obtained (Gatski and Speziale 1993) by considering the complete ten-term basis and applying the two-dimensional form of $\boldsymbol{S}$ and $\boldsymbol{W}$ and the corresponding reduction of invariants in Eq. (6.128) to

$$\mathrm{tr}\, \boldsymbol{S}^2, \quad \mathrm{tr}\, \boldsymbol{W}^2, \quad \mathrm{tr}(\boldsymbol{S}^2\boldsymbol{W}^2) = \frac{1}{2}\mathrm{tr}\, \boldsymbol{S}^2\, \mathrm{tr}\, \boldsymbol{W}^2 . \tag{6.155}$$

[7] For the two-dimensional case, the basis tensor $\boldsymbol{\Phi}_3$ is reduced to the form

$$\boldsymbol{\Phi}_3 = \frac{1}{3}\boldsymbol{I} - \frac{1}{2}\boldsymbol{I}^{(2)},$$

by the Cayley-Hamilton theorem where $\boldsymbol{I}^{(2)}$ is the two-dimensional Kronecker delta.

As explained, the resulting three-term representation is not yet fully explicit since the a_0 coefficient is a function of $\{\boldsymbol{bS}\}$. From Eq. (6.151), the invariant $\{\boldsymbol{bS}\}$ is obtained from the solution of

$$\begin{aligned} &4\tau^3\{\boldsymbol{bS}\}^3 + 4\tau^2\left(1+\frac{\alpha_1}{2}\right)^2\{\boldsymbol{bS}\}^2 \\ &\quad + \left[\tau\left(1+\frac{\alpha_1}{2}\right)^2 + 4\tau^3\left(a_1+\frac{a_2^2}{3}\right)\mathrm{I}_2(\boldsymbol{S}) + 4\tau^3 a_3^2\mathrm{I}_2(\boldsymbol{W})\right]\{\boldsymbol{bS}\} \\ &\quad + 2\tau^2 a_1\left(1+\frac{\alpha_1}{2}\right)\mathrm{I}_2(\boldsymbol{S}) = 0 \end{aligned} \tag{6.156}$$

where Eqs. (6.150) and (6.154) have been used. The correct root to be chosen is the one with the largest (positive) real part (Jongen and Gatski 1999).

Another equivalent approach to obtaining an explicit representation follows directly from the system of equations described in Eq. (6.149). This system was obtained by requiring that the coefficients of each tensor basis term vanish. Rivlin and Ericksen (1955) showed that the same solution could be obtained by forming scalar invariants comprised of factors from the polynomial representations basis. Additionally, they also showed how the procedure could be adapted when not all the members of the representation were linearly independent. Equation (6.146) is now replaced by

$$\sum_{k=1}^{\mathrm{N}} g_k\left[a_0\{\boldsymbol{T}_k\boldsymbol{T}_\gamma\} - 2a_2\{\boldsymbol{T}_k\boldsymbol{S}\boldsymbol{T}_\gamma\} + 2a_3\{\boldsymbol{T}_k\boldsymbol{W}\boldsymbol{T}_\gamma\}\right] = a_1\{\boldsymbol{S}\boldsymbol{T}_\gamma\}\,, \tag{6.157}$$

with $\gamma = 1, \ldots, \mathrm{N}$. This can be written in a form analogous to Eq. (6.149) given by

$$\left[a_0\{\boldsymbol{T}_\gamma\boldsymbol{T}_k\} - 2a_2\{\boldsymbol{T}_\gamma\boldsymbol{S}\boldsymbol{T}_k\} - 2a_3\{\boldsymbol{T}_\gamma\boldsymbol{W}\boldsymbol{T}_k\}\right] g_k = a_1\{\boldsymbol{S}\boldsymbol{T}_\gamma\}\,, \tag{6.158}$$

where the invariants $\{\boldsymbol{T}_\gamma\boldsymbol{T}_k\}$, $\{\boldsymbol{T}_\gamma\boldsymbol{S}\boldsymbol{T}_k\}$, and $\{\boldsymbol{T}_k\boldsymbol{W}\boldsymbol{T}_\gamma\}$ will consist of combinations of the invariants given in Eq. (6.128).

In order to see the equivalence of the two approaches just presented, consider once again the two-dimensional mean flow example with the turbulent stress anisotropy, rate of strain and rate of rotation tensors given by Eq. (6.152), with only the three basis tensors $\boldsymbol{\Phi}_1$, $\boldsymbol{\Phi}_2$, and $\boldsymbol{\Phi}_3$ taken. Equation (6.158) can then be written in the matrix form

$$\begin{pmatrix} a_0 & 4\mathrm{I}_2(\boldsymbol{W})\,a_3 & \frac{2}{3}\mathrm{I}_2(\boldsymbol{S})\,a_2 \\ -4\mathrm{I}_2(\boldsymbol{W})\,a_3 & 4\mathrm{I}_2(\boldsymbol{W})\,a_0 & 0 \\ \frac{2}{3}\mathrm{I}_2(\boldsymbol{S})\,a_2 & 0 & -\frac{1}{3}\mathrm{I}_2(\boldsymbol{S})\,a_0 \end{pmatrix} \begin{pmatrix} g_1 \\ g_2 \\ g_3 \end{pmatrix} = \begin{pmatrix} a_1 \\ 0 \\ 0 \end{pmatrix}\,, \tag{6.159}$$

and which is equivalent to the expression given in Eq. (6.153).

It should be clear from the formulation of such explicit algebraic turbulent stress anisotropy representations that the imposition of any physical constraints is placed on development of a suitable pressure-strain rate correlation model and the relationships used for the turbulent transport and dissipation rate anisotropies. The resulting implicit algebraic anisotropy equation and subsequent explicit polynomial representation are direct consequences of correctly formulating a properly invariant model through an established set of mathematical manipulations. This has the advantage of

minimizing any inherent bias in choice of calibration flow field. The disadvantage is that the complexity of the implicit transport equation and the subsequent number of basis tensors can increase rapidly and yield very complex representations. Fortunately, imposition of a two-dimensional flow field restriction has resulted in many generally applicable models for a variety of complex (three-dimensional) flow fields.

6.5.3 Constraints Imposed by Solid Boundaries

Although flows such as jets and wakes are of great interest and have important technological applications for propulsion and aeroacoustics, for example, a more common link between turbulent flows of both Newtonian and viscoelastic fluids lies within wall-bounded flows. An important dynamic link is the suppression of the wall-normal component of the turbulent Reynolds stress for both Newtonian and polymeric fluids due to the blocking effect of the wall. This has a strong and similar influence on the anisotropy levels for both the turbulent Reynolds stress and the polymeric stress fields. Such modeling efforts have sometimes been called low-Reynolds number modeling; however, the choice here is to use near-wall or wall-proximity modeling to distinguish it from the separate problem of models for transition prediction.

For turbulence modeling of Newtonian fluids that account for wall-proximity effects, the approaches have varied from the early empirical, though physically rational, van Driest damping function (van Driest 1956) to the current level of sophistication using an elliptic relaxation approach (Durbin 1991, 1993; Manceau and Hanjalić 2000a, 2000b; Manceau et al. 2002). For modeling of turbulent polymeric fluids, the historical record is much shorter and the approach focusing mainly viscoelastic modified damping functions (Cruz and Pinho 2003; Pinho 2003; Cruz et al. 2004; Li et al. 2006; Pinho et al. 2008a, 2008b; Resende et al. 2011). Since the viscoelastic wall-proximity modeling has been limited and has not reached maturity, the comments in the remainder of this section will focus on the near-wall turbulent Newtonian fluid modeling. Overall, the issue of near-wall modeling is at least as complex as the issue of developing the high-Reynolds-number models, and unfortunately less precise.

Earlier modeling efforts have been reviewed by So et al. (1991) and Hanjalić (1994), the primary focus for a mathematical framework has been the elliptic relaxation method just referred to. In its general form, this approach introduces a tensor function representing the combined effects of a near-wall velocity-pressure gradient correlation and anisotropic dissipation rate. The tensor function asymptotes to a high Reynolds number form away from solid boundaries through an elliptic relaxation equation. It is worthwhile to briefly highlight some of the aspects of this approach.

In Eq. (6.90) the combination of pressure-strain rate and turbulent transport terms, given by Eqs. (6.95a) and (6.95b) respectively, is redefined and replaced by

$$\phi_{ij} = -\overline{v_i' \frac{\partial p'}{\partial x_j}} - \overline{v_j' \frac{\partial p'}{\partial x_i}} + \frac{2}{3} \frac{\partial \overline{p' v_k'}}{\partial x_k} \delta_{ij} \ , \tag{6.160a}$$

$$D_{ij}^t = -\frac{\partial}{\partial x_k} \left(\overline{v_i' v_j' v_k'} + \frac{2}{3} \overline{p' v_k'} \delta_{ij} \right) \ . \tag{6.160b}$$

In the elliptic relaxation method, the behavior of the dissipation rate anisotropy d_{ij}^{ε} in the wall-proximity region is taken into account. This is accomplished by a relaxation of the dissipation rate anisotropy to its wall value, which is assumed to be equal to b_{ij}. With this assumption, $\phi_{ij} - \varepsilon_{ij}$ can be written as

$$\phi_{ij} - \varepsilon_{ij} = \varepsilon K f_{ij} - 2 \left(b_{ij} + \frac{\delta_{ij}}{3} \right) \varepsilon \ , \tag{6.161a}$$

or in terms of the relaxation function f_{ij} as

$$\varepsilon K f_{ij} = \phi_{ij} - 2\varepsilon \left(d_{ij}^{\varepsilon} - b_{ij} \right) \ . \tag{6.161b}$$

The system is closed through the solution of a relaxation equation for f_{ij} given by

$$\left(1 - \ell^2 \nabla^2 \right) f_{ij} = \frac{1}{\varepsilon K} \left(\Pi_{ij} + 2\varepsilon_c b_{ij} \right) \ , \tag{6.162}$$

where ∇^2 is the Laplacian operator and Π_{ij} can be any of the high Reynolds forms given in Eq. (6.110a). The elliptic relaxation equation is driven by the high Reynolds number form of the pressure-strain rate correlation $\boldsymbol{\Pi}$ and a contribution from the Reynolds stress anisotropy $\boldsymbol{b}$ (away from the wall the dissipation rate is assumed to be isotropic $d_{ij}^{\varepsilon} = 0$). Consistent with this approach is the recognition that as solid boundaries are approached, length and time scales are limited by the smallest turbulent scales, the Kolmogorov scales. For consistency, these limits are introduced, so that a composite dissipation rate is

$$\varepsilon_c = \frac{K}{\tau_c} \ , \tag{6.163}$$

with associated composite length and time scales defined by

$$\tau_c = \max \left[\tau, C_{\tau_K} \left(\frac{\nu}{\varepsilon} \right)^{1/2} \right] \ , \tag{6.164a}$$

$$\ell = C_\ell \max \left[\frac{K^{3/2}}{\varepsilon}, C_{\ell_K} \left(\frac{\nu}{\varepsilon} \right)^{1/4} \right] \ , \tag{6.164b}$$

where C_{τ_K}, C_ℓ, and C_{ℓ_K} are closure coefficients. As distance from the solid boundary increases, both the composite length and time scales asymptote to the inertial scales $K^{3/2}/\varepsilon$ and K/ε, respectively. The viscosity ν appearing in Eqs. (6.164a) and (6.164b) is intentionally left without a subscript. Of course, for Newtonian fluids $\nu = \nu_0$, but for viscoelastic fluid flows the selection of ν is altered. Obviously, a first choice could be the total zero-shear viscosity $\nu_0 + \nu_{p0}$ but various constraints involving the near-wall polymeric behavior could easily alter the choice.

A simplification of the elliptic relaxation approach has been proposed by Manceau and Hanjalić (2000a). It is an elliptic blending approach where a wall-proximity form for the velocity-pressure gradient correlation and tensor dissipation rate are merged with the high Reynolds number forms for each. The relevant blending function is a scalar quantity satisfying an elliptic relaxation equation analogous to Eq. (6.162). The approach introduces wall unit-normals into the formulation through the specification of the wall-proximity form for the velocity-pressure gradient correlation. Manceau and colleagues (see Oceni et al. 2010) have exploited this by forming outer products of these wall unit-normal vectors that result in an additional symmetric tensor dependency of the Reynolds stress anisotropy tensor $\boldsymbol{b}$. This additional tensor dependency can be coupled with the symmetric rate of strain tensor $\boldsymbol{S}$ and the skew-symmetric rate of rotation tensor $\boldsymbol{W}$ to form a set of basis tensors used in the representation of the Reynolds stress developed using the procedure discussed in Sect. 6.5.2.2.

6.6 Hybrid Methodologies

As the discussion throughout this chapter has shown, both the scale resolving methods, that is both spatial and temporal LES, and the mean and moment equation methods focus on distinct aspects of the turbulent flow field. Suitably averaged, the scale resolving solutions can yield mean quantities that are directly computed with a mean and moment method such as RANS; however, if only the mean is needed, the expense associated with a scale resolving method such as LES is not the most cost effective. In addition, each method has associated deficiencies that limit their respective range of applicability. Both fundamental and applied research in the development of closure models for R_{ij} and τ_{ij} have been going on for several decades. In particular, the development of models for τ_{ij} has probably been the most active area of research in the development and enhancement of the RANS methodology (Speziale 1991).

With the recent need to compute more dynamically and geometrically complex turbulent flows, a new type of methodology has emerged that essentially blends a scale resolving method with a mean and moment method. This hybrid methodology was initially motivated by the inability of LES methods to accurately model the near-wall dynamics unless the resolution was at or near that of a DNS; whereas, RANS models have been successfully developed to effectively treat the wall-proximity behavior. This has led to methods, such as hybrid RANS/LES, that blend the system of equations characterizing each method into a new set applicable over the whole flow domain. Figures 6.2 and 6.3 showed a sketch of the turbulent energy density spectrum and the typical wavenumber cutoffs associated with an LES solution and relationship with the DNS and RANS limits. Figure 6.9 further illustrates the situation by highlighting the various overlap regions that can occur in performing scale resolving simulations. For example, if models are used based on scale similarity ideas, Fig. 6.9 shows that the resolved scale motion obtained by a direct solution

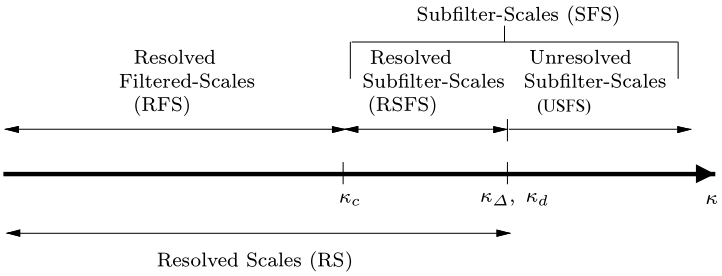

Fig. 6.9 Sketch of wavenumber partitioning over spectral range of turbulent motion: κ_c is the wavenumber cutoff of the simulation filter; κ_Δ is the wavenumber cutoff of the spatial grid; κ_d is high wavenumber cutoff where the energy content is negligible $\kappa_d \leq \kappa_\eta$, κ_η Kolmogorov wavenumber

of the filtered momentum equations in turn influences the dynamics of the subgrid-scales. For hybrid methods, the cutoff wavenumber κ_c can move significantly left or right on the axis and the importance of the subgrid dynamics can vary greatly. For a cutoff located at very high wavenumbers, essentially all the dynamic scales are resolved scales and a DNS is at hand. In contrast, if the cutoff moves to very low wavenumbers, then almost all the scales are on unresolved and subgrid scale. An inherent problem with such scale similarity methods, if adapted for hybrid methods, is that less and less resolved motion is available as the RANS limit is approached so that the burden of modeling the subgrid scale motion falls to the USFS model chosen. There are numerous issues associated with the development of hybrid methods and many of these are detailed in the book by Sagaut et al. (2006). Two major issues are associated with the development of a successful blending methodology at least for Newtonian flows. The first, which has received the most attention, is the way the respective methodologies are applied within the computational domain, and the second is the development of a turbulent stress model that readily blends the characterizing features of the residual stress tensor R_{ij} and the Reynolds stress tensor τ_{ij}. In the first case, the two alternatives are either the zonal or non-zonal, or seamless, approaches. For the zonal approach, either an LES method or a RANS method is applied to a specific region of the flow depending on the solution method required in that region. The challenge then being the smooth merging of the interfacial boundaries between the two methodologies. In the second case, a sufficiently high fidelity model is developed that is sensitized to the dynamics in the region and suitably modifies the turbulent stress field model. For this seamless approach, the form-invariance of the scale resolving filtered equations and the mean equations is exploited so that a single system of equations can be solved throughout the whole domain as long as a model that is capable of adapting to the different scale resolving requirements of each method is used.

A comparison of the defining relations for R_{ij} in Eq. (6.36) and τ_{ij} in Eq. (6.79) reveals two main differences between the two stress tensors. The first is the fact that the overbar in each relation is different. For R_{ij}, the overbar represents a low-pass filter in space and/or time, and for τ_{ij} the overbar represents a mean value. If a

temporal filtering procedure is used, it is possible to show that in the limit of a large filter width, and stationary statistics, the filtering procedure can lead to a mean value for the filtered quantity. The second difference is readily apparent from a comparison of the forms given in Eqs. (6.36) and (6.79). The residual stress tensor necessarily includes a contribution from the resolved field, L_{ij}, and a contribution from the interaction between the resolved scale motion and the subfilter scale motion, C_{ij}, as well as a contribution solely based on the subfilter scale motions, τ_{ij}. In the limit, when the temporal filter operator tends to the Reynolds average operator, the idempotent property of the averaging operator holds so that both L_{ij} and C_{ij} vanish and R_{ij} and τ_{ij} are equivalent.

The first, and the simplest in concept, hybrid model was the Detached Eddy Simulation model proposed by Spalart et al. (1997). It consisted of a simple one-equation RANS model (see Fig. 6.1) for the turbulent eddy viscosity ν_t, the S-A model (Spalart and Allmaras 1994), which contained a destruction of proportional to distance from the wall, d. By simply replacing the distance to the wall with the minimization function $\min(d, C_{DES}\Delta)$, where Δ is representative of the spatial grid spacing and C_{DES} an adjustable constant, the model effectively acted like a Smagorinsky-type LES model away from the wall and the RANS S-A model near the wall. This DES-type approach is arguably the most popular of the hybrid methods currently being used and has been updated for enhanced predictive capability (see Shur et al. 2008). Another early proposal by Speziale (1998c) is worth highlighting since it was a more rational mathematical approach to merging the LES and RANS methodologies. It simply assumed that the residual or subgrid stress tensor R_{ij} (see Eq. (6.35)) could be modeled as

$$R_{ij} = \left[1 - \exp(-\beta\Delta/L_K)\right]^n \tau_{ij} \ , \tag{6.165}$$

where τ_{ij} is the turbulent Reynolds stress, L_K is the Kolmogorov length scale, and β and n are constants. Relative to the Kolmogorov length, in the limit of fine grids, the residual stress vanishes and the ensuing simulation is a DNS; whereas, for large grid spacings the residual stress acts like the Reynolds stress. Inherent in the performance of the model is a intelligent construction of the computational grid in order for the model to be properly sensitized to the flow dynamics. The hybrid modeling proposed in Eq. (6.165) has been the basis for the Flow Simulation Methodology used by Fasel and colleagues for over a decade (see Fasel et al. 2006, for example).

Chapter 7
The Boltzmann Equation

For about two decades, the lattice Boltzmann method (LBM) has made a major breakthrough in the numerical solution of fluid flow problems and has become a real and efficient alternative with respect to the traditional route of CFD tools and software. Seen from afar, the method looks like a toy algorithm that is easily written as a one page program to solve, for example, the square cavity problem. However, if a more careful and thorough analysis is undertaken, the method reveals itself as a very acute and deep instrument to simulate the behavior of complex fluid motion. LBM represents the motion of virtual particles that collide according to some simple rules and then stream and move across a computational grid named the lattice. These particles mimic the fluid flow and yield excellent results for many difficult problems. The design of the underlying model is made at the mesoscopic scale, that is, at an intermediate scale between the continuous representation and the nanoscale. Nevertheless a multi-scale analysis using the Chapman-Enskog expansion produces the well known (weakly compressible) Navier-Stokes equations.

To start, recall the basic essentials of the kinetic theory leading to the Boltzmann equation. These considerations lead to an equation that governs the evolution of the particle velocity distribution function in phase space. The full Boltzmann equation contains on the right hand side a collision operator that involves all the nonlinearities. A simplifying hypothesis called the BGK approximation yields a collision form that is linear, and can be handled in a much simpler setting. A clear and precise way is then described for generating higher-order approximations of the continuous Boltzmann equation. A systematic construction that was introduced by Shan et al. (2006) is followed here, and is based on Hermite functions. With these approximations, a Galerkin method is designed to produce, through a Chapman-Enskog analysis, the dynamical relations. The lattice Boltzmann method results from the discretization in velocity space. The LBM is then formulated for viscoelastic fluids and turbulent flows.

M.O. Deville, T.B. Gatski, *Mathematical Modeling for Complex Fluids and Flows*,
DOI 10.1007/978-3-642-25295-2_7,

7.1 Kinetic Theory

Truesdell and Muncaster (1980) developed the kinetic theory from thermodynamics considerations. The interested reader may consult their book and will find a thorough presentation of the material covered here by following another path. In that respect the book by Woods (1993) is found very illuminating and useful.

7.1.1 Generalities

Consider a light gas composed of molecules. At the position $P(\mathbf{x}, t)$ is centered an infinitesimal volume $\mathrm{d}\mathbf{x}$ $(= \mathrm{d}x_1\mathrm{d}x_2\mathrm{d}x_3)$ that contains a large number of the gas particles, and let the number density of the molecules be denoted by $n(\mathbf{x}, t)$ as a continuous variable. The fluid density is then defined as

$$\rho(\mathbf{x}, t) = n(\mathbf{x}, t)\, m \ , \tag{7.1}$$

where m is the molecular mass of the particles. Denoting by $\boldsymbol{\xi}$ the particle velocity in the elementary volume, the macroscopic fluid velocity can be computed as the continuous variable $\mathbf{v} = <\boldsymbol{\xi}>$, where the operator $< >$ is the average value obtained for all the particles in $\mathrm{d}\mathbf{x}$. The expected or average value of a generic variable $\phi(\boldsymbol{\xi})$ is given by an ensemble average

$$<\phi> = \frac{1}{n}\int \phi(\mathbf{x}, \boldsymbol{\xi}, t) f(\mathbf{x}, \boldsymbol{\xi}, t)\, \mathrm{d}\boldsymbol{\xi} := \frac{1}{n}\int \phi\, f \mathrm{d}\boldsymbol{\xi} \ . \tag{7.2}$$

The large value of the Avogadro number $(6.0220 \times 10^{23}/\mathrm{mol})$ precludes writing the Newton's equation of motion for each molecule. Furthermore, a knowledge of the behavior of each particle is not of interest, but rather on their collective performance. One then has to resort to a statistical description using the particle velocity distribution function $f(\mathbf{x}, \boldsymbol{\xi}, t)$ operating in a six-dimensional phase space that results from the combination of the spatial and velocity spaces. Now the number density is obtained by integrating over the velocity space,

$$n(\mathbf{x}, t) = \int f(\mathbf{x}, \boldsymbol{\xi}, t)\, \mathrm{d}\boldsymbol{\xi} \ , \tag{7.3}$$

so that the density of the fluid ρ and the momentum $\rho\mathbf{v}$ are therefore evaluated by

$$\rho = \int m f \, \mathrm{d}\boldsymbol{\xi}, \quad \rho\mathbf{v} = \int m\boldsymbol{\xi} f \, \mathrm{d}\boldsymbol{\xi} \ , \tag{7.4}$$

with m the particle mass. Next, a relative velocity of the molecule with respect to that of the gas is introduced; it is called the microscopic velocity

$$\mathbf{c} = \boldsymbol{\xi} - \mathbf{v} \ , \tag{7.5}$$

with the consequence that

$$<\mathbf{c}> = 0 \ . \tag{7.6}$$

The concept of pressure is central to the kinetic theory. For the sake of simplicity, imagine that a beam of (non-colliding between themselves) particles strike a surface $\mathrm{d}\mathcal{S}$ of unit normal vector $\mathbf{n}$. The average collision rate is proportional to a probability factor of the collision times $n\mathbf{n}\cdot\mathbf{c}\,\mathrm{d}\mathcal{S}$. As soon as the particles hit the wall, they stop instantaneously and each particle incurs a loss of impulse $m\mathbf{c}$. By the impulse-momentum theorem, the force exerted on the surface is

$$\mathbf{f} = \rho\mathbf{n}<\mathbf{c}\otimes\mathbf{c}> := \mathbf{n}\boldsymbol{P} = \mathbf{n}\int m(\mathbf{c}\otimes\mathbf{c})\,f\,\mathrm{d}\boldsymbol{\xi}\ , \tag{7.7}$$

where the tensor $\boldsymbol{P}$ is called the pressure tensor in kinetic theory, but is nothing less than the Cauchy stress tensor $-\boldsymbol{\Sigma}$ of continuum mechanics with a negative sign. The hydrodynamic pressure p results from the trace of $\boldsymbol{P}$ such that $p = \{\boldsymbol{P}\}/3$. Therefore we have still the traceless extra-stress tensor $\boldsymbol{\Xi}$ such that similarly to Eq. (1.7), the following relation holds

$$\boldsymbol{P} = p\boldsymbol{I} - \boldsymbol{\Xi}\ . \tag{7.8}$$

The expected kinetic energy is given by

$$\rho K_E = \frac{m}{2}<\mathbf{c}\cdot\mathbf{c}> = \frac{m}{2}\int f|\mathbf{c}|^2\,\mathrm{d}\boldsymbol{\xi} = \frac{3}{2}n\,k_B\theta\ , \tag{7.9}$$

and defines the absolute temperature θ.

The usual scalar pressure field is related to the absolute temperature by the equation of state

$$p = n\,k_B\,\theta = \rho R\theta\ , \tag{7.10}$$

where $R = k_B/m$ is called the gas constant. The internal energy per unit mass is given as

$$e = \frac{3}{2}R\theta\ . \tag{7.11}$$

In the case of an ideal gas, it can be shown that the specific entropy is

$$s = c_v\ln\theta - R\ln\rho + const\ . \tag{7.12}$$

where c_v is the specific heat at constant volume, $c_v := \partial e/\partial\theta$, obtained from (7.11). With (7.10), (7.12) and the definition for c_v, Eq. (7.12) can be rewritten as

$$\rho s = -k_B n\ln n + \frac{3}{2}k_B n\ln\theta + const\ . \tag{7.13}$$

Taking into account (7.3), and absorbing the second term into the constant (isothermal condition), the relation

$$\rho s = -k_B\int f\ln f\,\mathrm{d}\boldsymbol{\xi} \tag{7.14}$$

is obtained. If at the macroscopic level the physical system goes to equilibrium, so that the spatial gradients $\nabla\mathbf{v} = \nabla\theta = \mathbf{0}$, then the entropy reaches a maximum value, and the corresponding distribution f takes the equilibrium value $f^{(0)}$. After some

algebra to compute the entropy variation that vanishes, the equilibrium velocity distribution is given by the Maxwell-Boltzmann relation

$$f^{(0)} = n\left(\frac{m}{2\pi k_B\theta}\right)^{3/2}\exp\left(-\frac{m}{2k_B\theta}c^2\right) . \tag{7.15}$$

7.1.2 Continuous Boltzmann Equation

In phase space, the total differential of any scalar function $f(\mathbf{x}, \boldsymbol{\xi}, t)$ is

$$\mathrm{d}f = \left(\frac{\partial f}{\partial t}\right)_{\mathbf{x},\boldsymbol{\xi}}\mathrm{d}t + \left(\frac{\partial f}{\partial \mathbf{x}}\right)_{\boldsymbol{\xi},t}\mathrm{d}\mathbf{x} + \left(\frac{\partial f}{\partial \boldsymbol{\xi}}\right)_{\mathbf{x},t}\mathrm{d}\boldsymbol{\xi} , \tag{7.16}$$

and the rate of change of f is a generalization of the continuous material time derivative given by

$$\frac{D_B f}{Dt} := \frac{\partial f}{\partial t} + \boldsymbol{\xi}\frac{\partial f}{\partial \mathbf{x}} + \mathbf{g}\frac{\partial f}{\partial \boldsymbol{\xi}} , \tag{7.17}$$

where $\mathbf{g}$ is an external force per unit mass (acceleration).

The density of the molecules with given position $\mathbf{x}$ and velocity $\boldsymbol{\xi}$ at time t changes by the combined effect of the motions the molecules undergo under the action of the force $\mathbf{g}$ (for example gravity), and the motions induced by the intermolecular forces. The Boltzmann equation can then be written as

$$\frac{D_B f}{Dt} = \mathcal{C}[f, f] , \tag{7.18}$$

where the collision operator $\mathcal{C}[f, f]$ represents the rate of change of f due to the collisions. The notation $\mathcal{C}[f, f]$, emphasizes the nonlinearity of the operator. Maxwell gave the following expression for two colliding particles

$$\mathcal{C}[f, f] = \int \mathbf{u}(f' f'^* - f f^*)\,\mathrm{d}\mathcal{S}\mathrm{d}\boldsymbol{\xi}^* , \tag{7.19}$$

where $\mathbf{u} = \boldsymbol{\xi}^* - \boldsymbol{\xi}$ is the relative velocity when the collision occurs. The particles before the collision have respective velocities $\boldsymbol{\xi}$ and $\boldsymbol{\xi}^*$, and after the collision their respective velocities are $\boldsymbol{\xi}'$ and $\boldsymbol{\xi}'^*$. The integration is performed on the surface $\mathrm{d}\mathcal{S}$ which is orthogonal to the relative velocity.

The distribution function f satisfies the H-theorem that is a characteristic feature of the thermodynamic irreversibility. The quantity H is defined by the relation

$$H = \int f \ln f \,\mathrm{d}\mathbf{x}\mathrm{d}\boldsymbol{\xi} , \tag{7.20}$$

which is linked to the entropy by

$$\int \rho s \mathrm{d}\mathbf{x} = -k_B H + const . \tag{7.21}$$

It then follows from the H-theorem that

$$\frac{\mathrm{d}H}{\mathrm{d}t} \leq 0 \,, \tag{7.22}$$

independently of the collision operator. Note that the H-theorem is the cornerstone of a lattice Boltzmann modeling based on thermodynamics considerations (Succi et al. 2002).

7.1.3 Boltzmann-BGK Based Continuous Equations

The Boltzmann equation (7.18) is a nonlinear integro-partial differential equation that is notoriously difficult to solve. This is the reason why Bhatnagar et al. (1954) proposed a simplified version of the collision operator assuming that the particles would return to equilibrium within a relaxation time τ. Equation (7.18) then becomes the Boltzmann-BGK equation

$$\frac{D_B f}{Dt} = -\frac{1}{\tau}\left(f - f^{(0)}\right) \,, \tag{7.23}$$

where the equilibrium distribution $f^{(0)}$ is

$$f^{(0)} = \rho\left(\frac{m}{2\pi k_B \theta}\right)^{3/2} \exp\left(-\frac{m}{2k_B\theta}c^2\right) \,. \tag{7.24}$$

Let us define an average in velocity space of a generic variable $\mathcal{A}(\mathbf{x}, \boldsymbol{\xi}, t)$ (which could be a scalar, vector or tensor function) by

$$\langle \mathcal{A}(\mathbf{x}, t)\rangle = \frac{1}{\rho}\int \mathcal{A} f \,\mathrm{d}\boldsymbol{\xi} \,. \tag{7.25}$$

Multiplying Eq. (7.23) through by $\mathcal{A}$ and integrating over the velocity space, the dynamic equation for $\langle \mathcal{A}\rangle$ is obtained

$$\begin{aligned} -\frac{\rho}{\tau}\left(\langle\mathcal{A}\rangle - \langle\mathcal{A}\rangle^{\mathrm{eq}}\right) = \frac{\partial}{\partial t}\left(\rho\langle\mathcal{A}\rangle\right) + \boldsymbol{\nabla}_{\mathbf{x}}\cdot\left(\rho\langle\boldsymbol{\xi}\mathcal{A}\rangle\right) - \rho\langle\boldsymbol{\xi}\boldsymbol{\nabla}_{\mathbf{x}}\mathcal{A}\rangle \\ - \rho\left\langle\mathcal{A}\boldsymbol{\nabla}_{\boldsymbol{\xi}}\cdot\mathbf{g}\right\rangle - \rho\left\langle\mathbf{g}\boldsymbol{\nabla}_{\boldsymbol{\xi}}\mathcal{A}\right\rangle \,, \end{aligned} \tag{7.26}$$

with $\boldsymbol{\nabla}_{\mathbf{x}}\cdot$ the divergence in physical space and $\boldsymbol{\nabla}_{\boldsymbol{\xi}}\cdot$ the divergence in velocity space and

$$\langle\mathcal{A}\rangle^{\mathrm{eq}} = \frac{1}{\rho}\int \mathcal{A} f^{(0)} d\boldsymbol{\xi} \,. \tag{7.27}$$

The mass, momentum and energy conservation laws require that the expectation value of these three fields be the same either with the use of f or the equilibrium distribution $f^{(0)}$, so that

$$\rho = \rho\langle 1\rangle = \rho\langle 1\rangle^{\mathrm{eq}} \,, \tag{7.28}$$

$$\rho\mathbf{v} = \rho\langle\boldsymbol{\xi}\rangle = \rho\langle\boldsymbol{\xi}\rangle^{\mathrm{eq}} \,, \tag{7.29}$$

$$\rho K_E = \frac{\rho}{2}\langle c^2\rangle = \frac{\rho}{2}\langle c^2\rangle^{\mathrm{eq}} \,. \tag{7.30}$$

Setting $\mathcal{A} = (1, \boldsymbol{\xi}, \boldsymbol{\xi}^2/2)$ in turn in (7.26), the three well known conservation equations for mass, momentum and energy are generated

$$\frac{\partial \rho}{\partial t} + \nabla \cdot (\rho \mathbf{v}) = 0 \,, \tag{7.31a}$$

$$\frac{\partial \rho \mathbf{v}}{\partial t} + \nabla \cdot (\rho \mathbf{v}\mathbf{v}) = -\nabla \cdot \boldsymbol{P} + \rho \mathbf{g} \,, \tag{7.31b}$$

$$\frac{\partial}{\partial t}\left(\rho K_E + \frac{1}{2}\rho \mathbf{v}^2\right) + \nabla \cdot \left[\mathbf{v}\left(\rho K_E + \frac{1}{2}\rho \mathbf{v}^2\right)\right] = -\nabla \cdot (\boldsymbol{P}\mathbf{v} + \mathbf{q}) \,, \tag{7.31c}$$

where the pressure tensor was defined in Eq. (7.7) and the energy flux is defined as

$$\mathbf{q} = \frac{1}{2}\int \mathbf{c}\, c^2 f \, \mathrm{d}\mathbf{c} \,. \tag{7.32}$$

The system of equations, (7.31a)–(7.31c), requires constitutive equations for the pressure tensor and energy flux to be closed and solvable. Grad (1949a, 1949b) proposed to project the solutions of the BGK equation (7.23) on a Hermite basis. Two sets of equations are then produced for the stress tensor and the heat flux. The full set of partial differential equations for ρ, $\rho\mathbf{v}$, ρK_E, $\boldsymbol{P}$, and $\mathbf{q}$ are known as Grad's 13-moment equations. This set is sufficiently complicated that it has resisted all attempts to solve it in closed form. Using the Hermite basis and the associated projection method, a set of kinetic equations can be obtained by writing the Hermite expansion coefficients and truncating the function approximations (Shan et al. 2006). Note that the choice of Hermite polynomials is suggested by the exponential nature of the equilibrium distribution function. In the following, the presentation will follow that detailed in Malaspinas (2009), Malaspinas et al. (2010).

7.2 Hermite Function Approximation

The velocity distribution function is written as an expansion in terms of Hermite polynomials, more precisely of the Hermite functions

$$f(\mathbf{x}, \boldsymbol{\xi}, t) = \omega(\boldsymbol{\xi}) \sum_{n=0}^{\infty} \frac{1}{n!} \boldsymbol{\mathcal{H}}^{(n)}(\boldsymbol{\xi}) \boldsymbol{a}^{(n)}(\mathbf{x}, t) \,, \tag{7.33}$$

where $\omega(\boldsymbol{\xi})$ is the Hermite weight function and $\boldsymbol{\mathcal{H}}^{(n)}$ and $\boldsymbol{a}^{(n)}$ denote the Hermite polynomial of degree n and the expansion coefficient of degree n, respectively (see the Appendix for the definition of $\boldsymbol{\mathcal{H}}^{(n)}$). The quantities $\boldsymbol{\mathcal{H}}^{(n)}(\boldsymbol{\xi})$ ($\mathcal{H}_{\boldsymbol{\alpha}}$) and $\boldsymbol{a}^{(n)}(\mathbf{x}, t)$ ($a_{\boldsymbol{\alpha}}$) are both tensors of order n and the product of the tensor in Eq. (7.33) involves full contraction of the indices (note that the vector $\boldsymbol{\alpha}$ is multi-indexed $\alpha_1 \ldots \alpha_n$ and Einstein's convention for the summation over all repeated indices in $\boldsymbol{\alpha}$ is assumed). The expansion coefficients are obtained by taking the scalar product of f with the Hermite basis polynomials

$$\boldsymbol{a}^{(n)}(\mathbf{x}, t) = \int f(\mathbf{x}, \boldsymbol{\xi}, t)\, \boldsymbol{\mathcal{H}}^{(n)}(\boldsymbol{\xi})\, \mathrm{d}\boldsymbol{\xi} \,. \tag{7.34}$$

Using the first moments of f,

$$\rho = \int f \, \mathrm{d}\boldsymbol{\xi}, \quad \rho \mathbf{v} = \int \boldsymbol{\xi} f \, \mathrm{d}\boldsymbol{\xi} \, , \tag{7.35}$$

and the definitions (7.7) of the second-order pressure tensor $\boldsymbol{P}$ and (7.34), $\boldsymbol{a}^{(n)}$ $(n = 0, \ldots, 4)$ can be evaluated as

$$a^{(0)} = \rho \, , \tag{7.36a}$$

$$a_{\alpha}^{(1)} = \rho v_{\alpha} \, , \tag{7.36b}$$

$$a_{\alpha_1\alpha_2}^{(2)} = P_{\alpha_1\alpha_2} + \rho \left(v_{\alpha_1} v_{\alpha_2} - \delta_{\alpha_1\alpha_2} \right) \, , \tag{7.36c}$$

$$\begin{aligned} a_{\alpha_1\alpha_2\alpha_3}^{(3)} = {} & Q_{\alpha_1\alpha_2\alpha_3} + v_{\alpha_1} a_{\alpha_2\alpha_3}^{(2)} + v_{\alpha_2} a_{\alpha_1\alpha_3}^{(2)} + v_{\alpha_3} a_{\alpha_1\alpha_2}^{(2)} \\ & + (1 - D) \rho v_{\alpha_1} v_{\alpha_2} v_{\alpha_3} \, , \end{aligned} \tag{7.36d}$$

$$\begin{aligned} a_{\alpha_1\alpha_2\alpha_3\alpha_4}^{(4)} = {} & R_{\alpha_1\alpha_2\alpha_3\alpha_4} - \left(P_{\alpha_1\alpha_2} \delta_{\alpha_3\alpha_4} + P_{\alpha_1\alpha_3} \delta_{\alpha_2\alpha_4} + P_{\alpha_1\alpha_4} \delta_{\alpha_2\alpha_3} \right. \\ & \left. + P_{\alpha_2\alpha_3} \delta_{\alpha_1\alpha_4} + P_{\alpha_2\alpha_4} \delta_{\alpha_3\alpha_1} + P_{\alpha_3\alpha_4} \delta_{\alpha_1\alpha_2} \right) \\ & + \left(\delta_{\alpha_1\alpha_2} \delta_{\alpha_3\alpha_4} + \delta_{\alpha_1\alpha_3} \delta_{\alpha_2\alpha_4} + \delta_{\alpha_1\alpha_4} \delta_{\alpha_2\alpha_3} \right) \, , \end{aligned} \tag{7.36e}$$

where the quantities $\boldsymbol{Q}$ and $\boldsymbol{R}$ are defined by

$$\boldsymbol{Q} = \int (\mathbf{c} \otimes \mathbf{c} \otimes \mathbf{c}) f \, \mathrm{d}\mathbf{c}, \quad \boldsymbol{R} = \int (\mathbf{c} \otimes \mathbf{c} \otimes \mathbf{c} \otimes \mathbf{c}) f \, \mathrm{d}\mathbf{c} \, , \tag{7.37}$$

and the integrands $\mathbf{c} \otimes \mathbf{c} \otimes \mathbf{c}$ and $\mathbf{c} \otimes \mathbf{c} \otimes \mathbf{c} \otimes \mathbf{c}$ are third- and fourth-order tensor products. The internal energy tensor flux, $\boldsymbol{Q}$, is related to the energy flux $\mathbf{q}$ by

$$q_{\alpha_1} = Q_{\alpha_1\alpha_2\alpha_2} \, . \tag{7.38}$$

Due to the orthogonality property of the Hermite functions, the leading moments of the distribution function f up to order N are preserved by truncating the high-order terms in its Hermite series. This is well known in numerical methods and corresponds to a spectral approximation where one uses a finite series for the unknown

$$f(\mathbf{x}, \boldsymbol{\xi}, t) \cong f_N(\mathbf{x}, \boldsymbol{\xi}, t) = \omega(\boldsymbol{\xi}) \sum_{n=0}^{N} \frac{1}{n!} \boldsymbol{\mathcal{H}}^{(n)}(\boldsymbol{\xi}) \boldsymbol{a}^{(n)}(\mathbf{x}, t) \, . \tag{7.39}$$

The approximation f_N will produce the same velocity moments as the original f. The governing partial differential equations that will be obtained are based only on truncated Hermite expansions. Note that Grad's 13-moment equations correspond to a truncation with $N = 4$.

In order to analyze the effect of the loss of information due to the truncation at a certain order, the Chapman-Enskog expansion (see Chapman and Cowling 1960) will be used.

7.3 Galerkin Method

The Galerkin method is designed to obtain the dynamical equations driving the evolution of the coefficients of the expansion of f_N, namely Eq. (7.39). Observe first that the Boltzmann-BGK equation (7.23) is a first-order partial differential equation with the quadratic nonlinearity of the collision operator having been discarded by the BGK approximation. There is no need to carry out an integration by parts of Eq. (7.23), and the Galerkin method can be applied as usual where the test functions are chosen equal to the basis functions. The Galerkin method has already been applied by Tölke et al. (2000) in a simpler setting with $N = 2$.

Since it will be needed later, the expansion of the equilibrium distribution is computed first, and is given by

$$f^{(0)} = \omega \sum_{n=0}^{\infty} \frac{1}{n!} \mathcal{H}^{(n)} \boldsymbol{a}_0^{(n)} \,, \tag{7.40}$$

$$\boldsymbol{a}_0^{(n)} = \int f^{(0)} \mathcal{H}^{(n)} \mathrm{d}\boldsymbol{\xi} \,. \tag{7.41}$$

The coefficients $\boldsymbol{a}_0^{(n)}$ up to order four are straightforwardly to compute using Gaussian integration and are given by

$$a_0^{(0)} = \rho \,, \tag{7.42a}$$

$$a_{0\alpha_1}^{(1)} = \rho v_{\alpha_1} \,, \tag{7.42b}$$

$$a_{0\alpha_1\alpha_2}^{(2)} = \rho v_{\alpha_1} v_{\alpha_2} + \rho(\theta_B - 1)\delta_{\alpha_1\alpha_2} \,, \tag{7.42c}$$

$$\begin{aligned} a_{0\alpha_1\alpha_2\alpha_3}^{(3)} &= \rho v_{\alpha_1} v_{\alpha_2} v_{\alpha_3} \\ &\quad + \rho(\theta_B - 1)(\delta_{\alpha_1\alpha_2} v_{\alpha_3} + \delta_{\alpha_1\alpha_3} v_{a_2} + \delta_{\alpha_2\alpha_3} v_{\alpha_1}) \,, \end{aligned} \tag{7.42d}$$

$$\begin{aligned} a_{0\alpha_1\alpha_2\alpha_3 a\alpha_4}^{(4)} &= \rho v_{\alpha_1} v_{\alpha_2} v_{\alpha_3} v_{\alpha_4} \\ &\quad + \rho(\theta_B - 1)^2(\delta_{\alpha_1\alpha_2}\delta_{\alpha_3\alpha_4} + \delta_{\alpha_1\alpha_3}\delta_{\alpha_2\alpha_4} + \delta_{\alpha_1\alpha_4}\delta_{\alpha_2\alpha_3}) \\ &\quad + \rho(\theta_B - 1)(\delta_{\alpha_1\alpha_2} v_{\alpha_3} v_{\alpha_4} + \delta_{\alpha_1\alpha_3} v_{\alpha_2} v_{\alpha_4} + \delta_{\alpha_1\alpha_4} v_{\alpha_2} v_{\alpha_3} \\ &\quad + \delta_{\alpha_2\alpha_3} v_{\alpha_1} v_{\alpha_4} + \delta_{\alpha_2\alpha_4} v_{\alpha_1} v_{\alpha_3} + \delta_{\alpha_3\alpha_4} v_{\alpha_1} v_{\alpha_2}) \,, \end{aligned} \tag{7.42e}$$

where $\theta_B = k_B\theta/m$ (cf. Eq. (7.10)).

The BGK equation (7.23), written as

$$\partial_t f + \boldsymbol{\xi}\nabla_{\mathbf{x}} f + \mathbf{g}\nabla_{\boldsymbol{\xi}} f = -\frac{1}{\tau}\left(f - f^{(0)}\right) \,, \tag{7.43}$$

is projected onto the Hermite basis. Using the relations of the Appendix, particularly Eq. (A.5), the first transport term is projected as

$$\int \mathcal{H}^{(n)} \boldsymbol{\xi} \nabla_{\mathbf{x}} f \mathrm{d}\boldsymbol{\xi} = \nabla_{\mathbf{x}} \cdot \boldsymbol{a}^{(n+1)} + \left(\nabla_{\mathbf{x}} \boldsymbol{a}^{(n-1)} + \mathrm{perm}\right) \,, \tag{7.44}$$

where "perm" represents all the cyclic index permutations.

Using Eq. (A.2), the second transport term, that is the gradient in the velocity space, can be evaluated as

$$\nabla_{\boldsymbol{\xi}} f = \sum_{n=0}^{\infty} \frac{1}{n!} \boldsymbol{a}^{(n)} \nabla_{\boldsymbol{\xi}} \left[\omega(\boldsymbol{\xi}) \boldsymbol{\mathcal{H}}^{(n)} \right] = \sum_{n=0}^{\infty} \frac{(-1)^n}{n!} \boldsymbol{a}^{(n)} \nabla_{\boldsymbol{\xi}}^{n+1} \omega(\boldsymbol{\xi})$$
$$= -\omega(\boldsymbol{\xi}) \sum_{n=0}^{\infty} \frac{1}{n!} \boldsymbol{a}^{(n)} \boldsymbol{\mathcal{H}}^{(n+1)} = -\omega(\boldsymbol{\xi}) \sum_{n=1}^{\infty} \frac{n}{n!} \boldsymbol{a}^{(n-1)} \boldsymbol{\mathcal{H}}^{(n)} \,. \tag{7.45}$$

The body force term yields the expansion

$$\mathbf{G}(\boldsymbol{\xi}) \equiv \int (\mathbf{g} \nabla_{\boldsymbol{\xi}} f) \boldsymbol{\mathcal{H}}^{(n)} \mathrm{d}\boldsymbol{\xi} = \mathbf{g} \boldsymbol{a}^{(n-1)} + \text{perm} \,, \tag{7.46}$$

where $\mathbf{G}$ denotes the force term. Collecting all contributions, the Hermite-Galerkin equations yield

$$\partial_t \boldsymbol{a}^{(n)} + \nabla_{\mathbf{x}} \cdot \boldsymbol{a}^{(n+1)} + \left(\nabla_{\mathbf{x}} \boldsymbol{a}^{(n-1)} + \text{perm} \right) - \left(\mathbf{g} \boldsymbol{a}^{(n-1)} + \text{perm} \right)$$
$$= -\frac{1}{\tau} \left(\boldsymbol{a}^{(n)} - \boldsymbol{a}_0^{(n)} \right) \,, \tag{7.47}$$

where here and in the sequel the abbreviated notation ∂_ϕ is substituted for the full partial derivative $\partial / \partial \phi$. Inspection of (7.47) reveals that to compute $\boldsymbol{a}^{(n)}$ we need the Hermite coefficients of $\boldsymbol{a}^{(n+1)}$ in the divergence term. This is the reason why in the next section we will compute the time derivative till $n = 3$ that involve coefficients up to $\boldsymbol{a}^{(4)}$ we did compute e.g. in Eqs. (7.42a)–(7.42e).

7.4 Chapman-Enskog Expansion

The Chapman-Enskog analysis is carried out to find an expression for the pressure tensor and the heat flux. The expansion is based on the Knudsen number, $\mathrm{Kn} = \lambda / L$, which is defined as the ratio of the mean free path λ to the characteristic length L of the problem. The theory we elaborate is valid for small values of Kn, typically $\mathrm{Kn} < 0.1$. The traditional analysis of Chapman and Cowling (1960) consists in expanding the distribution function f in power series of Kn like

$$f = \sum_{i=0}^{\infty} \mathrm{Kn}^i \, f^{(\mathrm{i})} \tag{7.48}$$

where $f^{(0)}$ is the Maxwell-Boltzmann equilibrium distribution. In this procedure the time and space derivatives are also expressed in terms of powers of Kn

$$\partial_t = \mathrm{Kn} \, \partial_t^{(0)} + \mathrm{Kn}^2 \, \partial_t^{(1)} + \ldots, \quad \text{and} \quad \nabla = \mathrm{Kn} \, \nabla \,. \tag{7.49}$$

The classical Chapman-Enskog analysis is rather cumbersome and to avoid heavy developments we will adopt the procedure used by Huang (1987).

7.4.1 Zero Order Approximation

Assume that the distribution function is given by its equilibrium value $f^{(0)}$. The BGK equation (7.43) can be written as

$$\partial_t f^{(0)} + \boldsymbol{\xi}\nabla_{\boldsymbol{x}} f^{(0)} + \mathbf{g}\nabla_{\boldsymbol{\xi}} f^{(0)} = 0\,, \tag{7.50}$$

where Eq. (7.46) has been taken into account.

The Hermite-Galerkin equations, Eq. (7.47), reduce to the following relations

$$\partial_t \boldsymbol{a}_0^{(n)} + \nabla_{\mathbf{x}} \cdot \boldsymbol{a}_0^{(n+1)} + \left(\nabla_{\mathbf{x}} \boldsymbol{a}_0^{(n-1)} + \text{perm}\right) - \left(\mathbf{g}\boldsymbol{a}_0^{(n-1)} + \text{perm}\right) = 0\,. \tag{7.51}$$

Choosing $n = 0, 1$, one finds

$$\partial_t \rho + \nabla \cdot (\rho \mathbf{v}) = 0\,, \tag{7.52}$$

$$\partial_t (\rho \mathbf{v}) + \nabla \cdot (\rho \theta_B \boldsymbol{I} + \rho \mathbf{v} \otimes \mathbf{v}) = \rho \mathbf{g}\,. \tag{7.53}$$

For $n = 2$, the trace of Eq. (7.51) is taken and leads to

$$\partial_t (\rho K_E) - \mathbf{v} \cdot \nabla(\rho\theta_B) + \left(\frac{D+2}{2}\right) \nabla \cdot (\rho \theta_B \mathbf{v}) = 0\,. \tag{7.54}$$

D is the dimension of space. This approximation generates the Euler equations for inviscid fluids.

7.4.2 First Order Approximation

Assume now that f is no longer exactly at equilibrium and is perturbed by a small term. One writes

$$f = f^{(0)} + f^{(1)}, \quad |f^{(1)}| \ll |f^{(0)}|\,. \tag{7.55}$$

Let us evaluate the order of magnitude of the "off-equilibrium" part $f^{(1)}$ by dimensional analysis. Assuming that the characteristic speed of the particles is the speed of sound, c_s, the total time derivative of the BGK equation (7.43) can be approximated as

$$\frac{\mathrm{d}f}{\mathrm{d}t} \sim \frac{c_s}{L} f = -\frac{1}{\tau}\left(f - f^{(0)}\right)\,. \tag{7.56}$$

With the multiscale expansion of f in (7.55), Eq. (7.56) can be written as

$$f^{(0)} \sim -\frac{L}{c_s \tau} f^{(1)}\,, \tag{7.57}$$

where $|f^{(1)}| \ll |f^{(0)}|$ has been used. As $c_s\tau$ is the mean free path λ, the previous estimate shows that

$$|f^{(1)}| \sim \mathrm{Kn}\,|f^{(0)}| \tag{7.58}$$

in agreement with the assumption that the perturbation expansion is valid in the limit $\mathrm{Kn} \ll 1$.

In order to obtain the off-equilibrium contribution, consider Eq. (7.43) written as

$$\partial_t f^{(0)} + \boldsymbol{\xi}\nabla_{\boldsymbol{x}} f^{(0)} + \mathbf{g}\nabla_{\boldsymbol{\xi}} f^{(0)} = -\frac{1}{\tau} f^{(1)} \,. \tag{7.59}$$

With the Hermite basis, Eq. (7.59) becomes

$$-\frac{1}{\tau}\boldsymbol{a}_1^{(n)} = \partial_t \boldsymbol{a}_0^{(n)} + \nabla_{\mathbf{x}} \cdot \boldsymbol{a}_0^{(n+1)} + \left(\nabla_{\mathbf{x}} \boldsymbol{a}_0^{(n-1)} + \text{perm}\right) - \left(\mathbf{g}\boldsymbol{a}_0^{(n-1)} + \text{perm}\right) \,, \tag{7.60}$$

where $\boldsymbol{a}_1^{(n)}$ is defined by

$$\boldsymbol{a}_1^{(n)} = \int f^{(1)} \boldsymbol{\mathcal{H}}^{(n)} \mathrm{d}\boldsymbol{\xi} \,. \tag{7.61}$$

Recall that the Hermite coefficients of the equilibrium distribution are given in terms of the conserved moments, namely the mass ρ, the momentum $\mathbf{j} = \rho\mathbf{v}$, and the internal energy $e = \rho K_E$. The time derivative in Eq. (7.60) can be expressed as

$$\begin{aligned} \partial_t \boldsymbol{a}_0^{(n)} &= \partial_\rho \boldsymbol{a}_0^{(n)} \partial_t \rho + \partial_{\mathbf{j}} \boldsymbol{a}_0^{(n)} \cdot \partial_t(\rho\mathbf{v}) + \partial_e \boldsymbol{a}_0^{(n)} \partial_t e & (7.62)\\ &= -\partial_\rho \boldsymbol{a}_0^{(n)} \nabla \cdot (\rho\mathbf{v}) + \partial_{\mathbf{j}} \boldsymbol{a}_0^{(n)} \cdot \left[\rho\mathbf{g} - \nabla \cdot (\rho\theta_B \boldsymbol{I} + \rho\mathbf{v}\otimes\mathbf{v})\right] \\ &\quad + \partial_e \boldsymbol{a}_0^{(n)} \left[(\mathbf{v}\cdot\nabla)\rho\theta_B - \left(\frac{D+2}{2}\right)\nabla\cdot(\rho\theta_B\mathbf{v})\right] \,, & (7.63) \end{aligned}$$

where in the last line the "conservation laws" computed in Eqs. (7.52)–(7.54) are used to replace the time derivatives by space derivatives. With Eqs. (7.42a)–(7.42e) the "conserved moment derivatives" for $a_0^{(n)}$, $n = 0, \ldots, 3$, can be computed,

$$\begin{aligned} \partial_\rho a_0^{(0)} = 1, \quad \partial_\rho a_{0\alpha_1}^{(1)} &= 0 \,, \\ \partial_\rho a_{0\alpha_1\alpha_2}^{(2)} &= -v_{\alpha_1} v_{\alpha_2} - \delta_{\alpha_1\alpha_2} \,, \\ \partial_\rho a_{0\alpha_1\alpha_2\alpha_3}^{(3)} &= -2 v_{\alpha_1} v_{\alpha_2} v_{\alpha_3} \\ &\quad - \theta_B(\delta_{\alpha_1\alpha_2} v_{\alpha_3} + \delta_{\alpha_1\alpha_3} v_{\alpha_2} + \delta_{\alpha_2\alpha_3} v_{\alpha_1}), \end{aligned} \tag{7.64a}$$

$$\begin{aligned} \partial_{j_{\alpha_1}} a_0^{(0)} = 0, \quad \partial_{j_{\alpha_2}} a_{0\alpha_1}^{(1)} &= \delta_{\alpha_1\alpha_2}, \\ \partial_{j_{\alpha_3}} a_{0\alpha_1\alpha_2}^{(2)} &= \delta_{\alpha_1\alpha_3} v_{\alpha_2} + \delta_{\alpha_2\alpha_3} v_{\alpha_1} \,, \\ \partial_{j_{\alpha_4}} a_{0\alpha_1\alpha_2\alpha_3}^{(3)} &= v_{\alpha_1} v_{\alpha_2} \delta_{\alpha_3\alpha_4} + v_{\alpha_1} v_{\alpha_3} \delta_{\alpha_2\alpha_4} + v_{\alpha_2} v_{\alpha_3} \delta_{\alpha_1\alpha_4} \\ &\quad + (\theta_B - 1)(\delta_{\alpha_1\alpha_2}\delta_{\alpha_3\alpha_4} + \delta_{\alpha_1\alpha_3}\delta_{\alpha_2\alpha_4} + \delta_{\alpha_2\alpha_3}\delta_{\alpha_1\alpha_4}) \,, \end{aligned} \tag{7.64b}$$

$$\begin{aligned} \partial_e a_0^{(0)} = \partial_e a_{0\alpha_1}^{(1)} = 0, \quad \partial_e a_{0\alpha_1\alpha_2}^{(2)} &= \frac{2}{D}\delta_{\alpha_1\alpha_2} \,, \\ \partial_e a_{0\alpha_1\alpha_2\alpha_3}^{(3)} &= \frac{2}{D}(\delta_{\alpha_1\alpha_2} v_{\alpha_3} + \delta_{\alpha_1\alpha_4} v_{\alpha_2} + \delta_{\alpha_2\alpha_3} v_{\alpha_1}) \,. \end{aligned} \tag{7.64c}$$

A straightforward computation yields the first-order coefficients

$$a_1^{(0)} = a_{1\alpha_1}^{(1)} = a_{1\alpha_1\alpha_1}^{(2)} = 0\,, \tag{7.65a}$$

$$a_{1\alpha_1\alpha_2}^{(2)} = -\tau\rho\theta_B \Lambda_{\alpha_1\alpha_2}\,, \tag{7.65b}$$

$$\begin{aligned} a_{1\alpha_1\alpha_2\alpha_3}^{(3)} = &-\tau\rho\theta_B \big[\Lambda_{\alpha_1\alpha_2} v_{\alpha_3} + \Lambda_{\alpha_1\alpha_3} v_{\alpha_2} + \Lambda_{\alpha_2\alpha_3} v_{\alpha_1} \\ &+ \big(\delta_{\alpha_1\alpha_2}\partial_{\alpha_3}\theta_B + \delta_{\alpha_1\alpha_3}\partial_{\alpha_2}\theta_B + \delta_{\alpha_2\alpha_3}\partial_{\alpha_1}\theta_B\big)\big]\,, \end{aligned} \tag{7.65c}$$

where

$$\Lambda_{\alpha_1\alpha_2} = \partial_{\alpha_1} v_{\alpha_2} + \partial_{\alpha_2} v_{\alpha_1} - \frac{2}{D}\partial_{\alpha_3} v_{\alpha_3}\delta_{\alpha_1\alpha_2}\,. \tag{7.66}$$

Note that Eqs. (7.65a)–(7.65c) is a consequence of the mass, momentum and energy conservation laws. The off-equilibrium distribution function can therefore be constructed as

$$f^{(1)} = \sum_{n=0}^{3} \frac{1}{n!} \boldsymbol{\mathcal{H}}^{(n)} \boldsymbol{a}_1^{(n)} \tag{7.67a}$$

$$\begin{aligned} &= \Big(\frac{1}{2}\mathcal{H}_{\alpha_1\alpha_2}^{(2)} a_{1\alpha_1\alpha_2}^{(2)} + \frac{1}{6}\mathcal{H}_{\alpha_1\alpha_2\alpha_3}^{(3)} a_{1\alpha_1\alpha_2\alpha_3}^{(3)}\Big) \\ &= -\tau\rho\theta_B \Big\{\frac{1}{2}\mathcal{H}_{\alpha_1\alpha_2}^{(2)}\Lambda_{\alpha_1\alpha_2} + \frac{1}{6}\mathcal{H}_{\alpha_1\alpha_2\alpha_3}^{(3)}\big[\Lambda_{\alpha_1\alpha_2} v_{\alpha_3} + \Lambda_{\alpha_1\alpha_3} v_{\alpha_2} \\ &\quad + \Lambda_{\alpha_2\alpha_3} v_{\alpha_1} + \big(\delta_{\alpha_1\alpha_2}\partial_{\alpha_3}\theta_B + \delta_{\alpha_1\alpha_3}\partial_{\alpha_2}\theta_B + \delta_{\alpha_2\alpha_3}\partial_{\alpha_1}\theta_B\big)\big]\Big\}\,. \end{aligned} \tag{7.67b}$$

In order to close Eqs. (7.31b) and (7.31c), the stress tensor $\boldsymbol{P}$ and the heat flux vector $\mathbf{q}$ need to be computed. In the same spirit as the perturbation expansion for f, we split $\boldsymbol{P}$ and $\mathbf{q}$ as

$$\boldsymbol{P} = \boldsymbol{P}^{(0)} + \boldsymbol{P}^{(1)}, \quad \mathbf{q} = \mathbf{q}^{(0)} + \mathbf{q}^{(1)}\,. \tag{7.68}$$

From Eqs. (7.7) and (7.32), $\boldsymbol{P}^{(n)}$ and $\mathbf{q}^{(n)}$ can be computed using (A.4c) and (A.4d),

$$\begin{aligned} P_{\alpha_1\alpha_2}^{(n)} = \int \mathrm{d}\boldsymbol{\xi} \Big[&\mathcal{H}_{\alpha_1\alpha_2}^{(2)} - \mathcal{H}_{\alpha_1}^{(1)} v_{\alpha_2} - \mathcal{H}_{\alpha_2}^{(1)} v_{\alpha_1} \\ &+ (\delta_{\alpha_1\alpha_2} + v_{\alpha_1} v_{\alpha_2})\mathcal{H}^{(0)}\Big] f^{(n)}\,, \end{aligned} \tag{7.69}$$

$$\begin{aligned} q_{\alpha_1}^{(n)} = \frac{1}{2}\int \mathrm{d}\boldsymbol{\xi} \Big[&\mathcal{H}_{\alpha_1\alpha_2\alpha_2}^{(3)} - 2\mathcal{H}_{\alpha_1\alpha_2}^{(2)} v_{\alpha_2} - \mathcal{H}_{\alpha_2\alpha_2}^{(2)} v_{\alpha_1} + \mathcal{H}_{\alpha_1}^{(1)} v_{\alpha_2} v_{\alpha_2} \\ &+ 2\mathcal{H}_{\alpha_2}^{(1)} v_{\alpha_1} v_{\alpha_2} - \mathcal{H}^{(0)}(v_{\alpha_1} v_{\alpha_2} v_{\alpha_2} + (D+2) v_{\alpha_1})\Big] f^{(n)}\,. \end{aligned} \tag{7.70}$$

It then follows from Eq. (7.40) truncated to $n = 3$ and (7.64a), (7.64b), (7.64c) that

$$\mathbf{q}^{(0)} = 0, \quad P_{\alpha_1\alpha_2}^{(0)} = \rho\theta_B\delta_{\alpha_1\alpha_2}\,. \tag{7.71}$$

Taking into account that $f^{(1)}$ involves only $\mathcal{H}_{\alpha_1\alpha_2}^{(2)}$ and $\mathcal{H}_{\alpha_1\alpha_2\alpha_3}^{(3)}$ (cf. (7.67a), (7.67b)), and Eqs. (7.69)–(7.70), the next terms $\boldsymbol{P}^{(1)}$ and $\mathbf{q}^{(1)}$ are then given by,

$$P^{(1)}_{\alpha_1\alpha_2} = \int \mathrm{d}\boldsymbol{\xi}\mathcal{H}^{(2)}_{\alpha_1\alpha_2} f^{(1)} \,, \tag{7.72}$$

$$q^{(1)}_{\alpha_1} = \frac{1}{2}\int \mathrm{d}\boldsymbol{\xi}\left(\mathcal{H}^{(3)}_{\alpha-1\alpha_2\alpha_2} - 2v_{\alpha_2}\mathcal{H}^{(2)}_{\alpha_1\alpha_2}\right) f^{(1)} \,. \tag{7.73}$$

Using the orthogonality properties of the Hermite polynomials (see the Appendix), these integrals yield

$$\boldsymbol{P}^{(1)} = -\tau\rho\theta_B\boldsymbol{\Lambda} \,, \tag{7.74}$$

$$\mathbf{q}^{(1)} = -\tau\rho\theta_B\left(\frac{D+2}{2}\right)\boldsymbol{\nabla}\theta_B \,. \tag{7.75}$$

The Navier-Stokes equations are obtained

$$\partial_t\rho + \boldsymbol{\nabla}\cdot(\rho\mathbf{v}) = 0 \,, \tag{7.76}$$

$$\rho\frac{D\mathbf{v}}{Dt} + \boldsymbol{\nabla}\cdot(p\boldsymbol{I} - \mu_s\boldsymbol{\Lambda}) = \rho\mathbf{g} \,, \tag{7.77}$$

$$\rho\frac{DK_E}{Dt} + \{(p\boldsymbol{I} - \mu_s\boldsymbol{\Lambda})\,\boldsymbol{L}\} - \left(\frac{D+2}{2}\right)\boldsymbol{\nabla}\cdot(\kappa\boldsymbol{\nabla}\theta_B) = 0 \,, \tag{7.78}$$

where the pressure p refers to (7.10). The dynamic viscosity μ_s and thermal diffusivity κ are given by

$$\mu_s = \kappa = \rho\theta_B\tau \,. \tag{7.79}$$

Equations (7.76)–(7.78) constitute the non-isothermal compressible Navier-Stokes equations. Unfortunately, the model is not general enough as it only allows the viscosity to be equal to the thermal diffusivity with a vanishing bulk viscosity. These defects come from the fact the model contains the relaxation time τ as the unique transport parameter. Therefore it cannot represent correctly all the macroscopic transport coefficients. To obtain a shear viscosity different from the diffusivity coefficient, a multiple relaxation time model has to be designed (Shan and Chen 2007).

The BGK Boltzmann equation approximated to first-order terms in the small Knudsen number limit leads to the compressible Navier-Stokes equations. If we incorporate second-order terms in the development of f, we are led to the Burnett equations (see for example, Burnett 1935; Balakrishnan 2004).

It should be emphasized that in order to recover the macroscopic limit, namely the Navier-Stokes equations, only the truncation of the velocity distribution function up to order four in Hermite polynomials was needed. If this series is truncated to a lower order, different models are generated. For example, the truncation to third order gives back the compressible Navier-Stokes equations as above; however, the heat flux is different and cannot be used for non-isothermal flows.

The truncation to second-order Hermite polynomials has dominated the lattice Boltzmann model theory over the last two decades (Chen and Doolen 1998; Succi 2001; Wolf-Gladrow 2000). The development holds for low Mach number flows where the fluid is weakly compressible. The equilibrium distribution function is given by

$$f^{(0)} = \omega(\boldsymbol{\xi})\rho\left(1 + \boldsymbol{\xi}\cdot\mathbf{v} + \frac{1}{2}\mathcal{H}^{(2)}_{\alpha_1\alpha_2}v_{\alpha_1}v_{\alpha_2}\right) \,, \tag{7.80}$$

with the pressure tensor

$$P_{\alpha_1\alpha_2} = \rho\delta_{\alpha_1\alpha_2} - 2\mu_s S_{\alpha_1\alpha_2} \,, \tag{7.81}$$

and dynamic viscosity $\mu_s = \rho\tau$. The associated governing equations are

$$\begin{aligned} &\partial_t \rho + \boldsymbol{\nabla}\cdot(\rho\mathbf{v}) = 0 \,, \\ &\rho\frac{D\mathbf{v}}{Dt} + \boldsymbol{\nabla}\cdot(p\boldsymbol{I} - 2\mu_s\boldsymbol{S}) = \rho\mathbf{g} \,. \end{aligned} \tag{7.82}$$

7.5 Lattice Boltzmann Method

The lattice Boltzmann method (LBM) is a numerical implementation of the Boltzmann-BGK model designed to run on a Cartesian mesh with equally spaced grid points, the so-called lattice. These lattices are named $DxQy$, where x is the space dimension D and y the number of lattice velocities. At each grid point, virtual particles collide and after the collision, they stream in imposed directions. The numerical method is a direct consequence of the Hermite-Galerkin approximation. To this end, the continuous integrals defined in the velocity space are replaced by numerical quadratures, and in the Hermite framework it is customary to choose Gauss-Hermite (GH) rules. Therefore, the Hermite coefficients (7.34) are obtained by the relation

$$\boldsymbol{a}^{(n)}(\boldsymbol{x},t) = \int \mathrm{d}\boldsymbol{\xi}\; f_N(\boldsymbol{x},\boldsymbol{\xi},t)\boldsymbol{\mathcal{H}}^{(n)}(\boldsymbol{\xi}) = \int \mathrm{d}\boldsymbol{\xi}\; \omega(\boldsymbol{\xi}) r(\boldsymbol{x},\boldsymbol{\xi},t) \,, \tag{7.83}$$

where $r(\boldsymbol{x},\boldsymbol{\xi},t)$ is a polynomial function of $\boldsymbol{\xi}$ of degree not greater than $2N$. Taking full advantage of the GH rules to integrate Eq. (7.83) exactly (cf. the Appendix), $\boldsymbol{a}^{(n)}(\boldsymbol{x},t)$ can be written as

$$\boldsymbol{a}^{(n)}(\boldsymbol{x},t) = \sum_{i=0}^{P-1} w_i r(\boldsymbol{x},\boldsymbol{\xi}_i,t) = \sum_{i=0}^{P-1} \frac{w_i}{\omega(\boldsymbol{\xi}_i)} f_N(\boldsymbol{x},\boldsymbol{\xi}_i,t)\boldsymbol{\mathcal{H}}^{(n)}(\boldsymbol{\xi}_i) \,, \tag{7.84}$$

where $w_i, \boldsymbol{\xi}_i, i = 0, \ldots, P-1$, are the weights and abscissae of the GH quadrature chosen with a degree $\geqslant 2N$. From Eq. (7.84), the discretized $f_N(\boldsymbol{x},\boldsymbol{\xi}_i,t)$ $(i = 0, \ldots, P-1)$ completely determine $f_N(\boldsymbol{x},\boldsymbol{\xi},t)$ and its moments because of the high accuracy (or in some cases, of the exactness) of the quadrature rule. As shown in the Appendix, the GH quadrature nodes are not equally spaced with a unit step length as should be the case in the standard LBM. In order to be consistent with these models, all the velocities are normalized by a scaling factor c_l, which is a lattice sound speed. For example, in the D2Q9 and D3Q27 lattices, the distance between nodes is given by $\sqrt{3}$ and the scaling factor $1/\sqrt{3}$ can be interpreted as the adiabatic index γ, the ratio of the specific heat coefficients at constant pressure and constant volume. Recall that for compressible fluids, the speed of sound squared is linearly proportional to the temperature through a product of the gas constant and specific heat ratio γ.

This rescaling procedure slightly affects the various Hermite polynomials and expansion coefficients. Nevertheless, in the following this rescaling will be used in order to present the correct implementation formulas (see the Appendix). The expansion coefficients $a_0^{(0)}$ and $a_{0\alpha}^{(1)}$ are unchanged and are given by Eqs. (7.42a)–(7.42b) respectively; however, the other expansion coefficients of $f^{(0)}$ are changed and given by

$$a_{0\,\alpha_1\alpha_2}^{(2)} = \rho v_{\alpha_1} v_{\alpha_2} + c_l^2 \rho(\theta_B - 1)\delta_{\alpha_1\alpha_2} \,, \tag{7.85a}$$

$$\begin{aligned} a_{0\,\alpha_1\alpha_2\alpha_3}^{(3)} &= \rho v_{\alpha_1} v_{\alpha_2} v_{\alpha_3} \\ &\quad + c_l^2 \rho(\theta_B - 1)(\delta_{\alpha_1\alpha_2} v_{\alpha_3} + \delta_{\alpha_1\alpha_3} v_{\alpha_2} + \delta_{\alpha_2\alpha_3} v_{\alpha_1}) \,, \end{aligned} \tag{7.85b}$$

$$\begin{aligned} a_{0\,\alpha_1\alpha_2\alpha_3\alpha_4}^{(4)} &= \rho v_{\alpha_1} v_{\alpha_2} v_{\alpha_3} v_{\alpha_4} \\ &\quad + c_l^4 \rho(\theta_B - 1)^2(\delta_{\alpha_1\alpha_2}\delta_{\alpha_3\alpha_4} + \delta_{\alpha_1\alpha_3}\delta_{\alpha_2\alpha_4} + \delta_{\alpha_1\alpha_4}\delta_{\alpha_2\alpha_3}) \\ &\quad + c_l^2 \rho(\theta_B - 1)(\delta_{\alpha_1\alpha_2} v_{\alpha_3} v_{\alpha_4} + \delta_{\alpha_1\alpha_3} v_{\alpha_2} v_{\alpha_4} + \delta_{\alpha_1\alpha_4} v_{\alpha_2} v_{\alpha_3} \\ &\qquad + \delta_{\alpha_2\alpha_4} v_{\alpha_1} v_{\alpha_4} + \delta_{\alpha_2\alpha_4} v_{\alpha_1} v_{\alpha_3} + \delta_{\alpha_3\alpha_4} v_{\alpha_1} v_{\alpha_2}) \,. \end{aligned} \tag{7.85c}$$

With f_i defined as

$$f_i(\boldsymbol{x}, t) := \frac{w_i}{\omega(\boldsymbol{\xi}_i)} f(\boldsymbol{x}, \boldsymbol{\xi}_i, t) \,, \tag{7.86}$$

the discretized equilibrium distribution function, truncated to fourth-order is

$$\begin{aligned} f_i^{(0)} &= w_i \sum_{n=0}^{4} \frac{1}{c_l^{2n} n!} \boldsymbol{a}_0^{(n)} \boldsymbol{\mathcal{H}}_i^{(n)} \\ &= w_i \rho \left\{ 1 + \frac{\boldsymbol{\xi}_i \cdot \mathbf{v}}{c_l^2} + \frac{1}{2c_l^4} \left[(\boldsymbol{\xi}_i \cdot \mathbf{v})^2 - c_l^2 \mathbf{v}^2 + c_l^2(\theta_B - 1)(\xi_i^2 - c_l^2 D) \right] \right. \\ &\quad + \frac{\boldsymbol{\xi}_i \cdot \mathbf{v}}{6c_l^6} \left[(\boldsymbol{\xi}_i \cdot \mathbf{v})^2 - 3c_l^2 \mathbf{v}^2 + 3c_l^2(\theta_B - 1)(\xi_i^2 - c_l^2(D+2)) \right] \\ &\quad + \frac{1}{24c_l^8} \Big[(\boldsymbol{\xi}_i \cdot \mathbf{v})^4 - 6c_l^2 \mathbf{v}^2 (\boldsymbol{\xi}_i \cdot \mathbf{v})^2 + 3c_l^4 \mathbf{v}^4 \\ &\quad + 6c_l^2(\theta_B - 1) \left((\boldsymbol{\xi}_i \cdot \mathbf{v})^2 (\xi_i^2 - c_l^2(D+4)) + c_l^2 \mathbf{v}^2 (c_l^2(D+2) - \boldsymbol{\xi}_i^2) \right) \\ &\quad \left. + 3c_l^4(\theta_B - 1)^2 \left(\xi_i^4 - 2c_l^2(D+2)\xi_i^2 + c_l^4 D(D+2) \right) \Big] \right\} \,, \end{aligned} \tag{7.87}$$

with $\mathcal{H}_i^{(n)}$ the discretized Hermite polynomials. With these definitions, the discretized force term, G_i, from Eq. (7.46) can be written as

$$G_i = w_i \sum_{n=1}^{3} \frac{1}{n! c_l^{2n}} \boldsymbol{\mathcal{H}}_i^{(n)} \boldsymbol{a}_0^{(n)}$$

$$
\begin{aligned}
&= w_i \rho \left[\frac{\xi_{i\alpha_1} g_{\alpha_1}}{c_l^2} + \frac{\mathcal{H}^{(2)}_{i\alpha_1\alpha_2}}{c_l^4} g_{\alpha_1} v_{\alpha_2} \right. \\
&\quad \left. + \frac{\mathcal{H}^{(3)}_{i\alpha_1\alpha_2\alpha_3}}{2c_l^6} g_{\alpha_1} \left(v_{\alpha_2} v_{\alpha_3} + c_l^2 (\theta_B - 1) \delta_{\alpha_2\alpha_3} \right) \right] \\
&= w_i \rho \left\{ \frac{\boldsymbol{\xi}_i \cdot \mathbf{g}}{c_l^2} + \frac{1}{2c_l^4} \left[(\boldsymbol{\xi}_i \cdot \mathbf{v})(\boldsymbol{\xi}_i \cdot \boldsymbol{g}) - c_l^2 (\mathbf{g} \cdot \mathbf{v}) \right] \right. \\
&\quad + \frac{1}{6c_l^6} \left[(\boldsymbol{\xi}_i \cdot \mathbf{g}) \left((\boldsymbol{\xi}_i \cdot \mathbf{v})^2 + c_l^2 \boldsymbol{\xi}_i^2 (\theta_B - 1) \right) \right. \\
&\quad - c_l^2 \left[(\boldsymbol{\xi}_i \cdot \mathbf{v}) \left(2(\mathbf{g} \cdot \mathbf{v}) + (\mathbf{v}^2 + c_l^2 (\theta_B - 1) D) \right) \right. \\
&\quad \left. \left. \left. + 2c_l^2 (\theta_B - 1)(\boldsymbol{\xi}_i \cdot \mathbf{g}) \right] \right] \right\} . \qquad (7.88)
\end{aligned}
$$

The off-equilibrium term of the distribution function then becomes

$$
\begin{aligned}
f_i^{(1)} = -w_i \frac{\tau \rho \theta_B}{c_s^2} \left\{ \frac{1}{2} \mathcal{H}^{(2)}_{i\alpha_1\alpha_2} \Lambda_{\alpha_1\alpha_2} + \frac{1}{6c_s^2} \mathcal{H}^{(3)}_{i\alpha_1\alpha_2\alpha_3} \left[\Lambda_{\alpha_1\alpha_2} v_{\alpha_3} + \Lambda_{\alpha_1\alpha_3} v_{\alpha_2} \right. \right. \\
\left. \left. + \Lambda_{\alpha_2\alpha_3} v_{\alpha_1} + c_s^2 \left(\delta_{\alpha_1\alpha_2} \partial_{\alpha_3} \theta_B + \delta_{\alpha_1\alpha_3} \partial_{\alpha_2} \theta_B + \delta_{\alpha_2\alpha_3} \partial_{\alpha_1} \theta_B \right) \right] \right\} . \qquad (7.89)
\end{aligned}
$$

The BGK equation, discretized in velocity space, for f_N (the subscript N will be omitted in the sequel), is

$$
\partial_t f_i + \boldsymbol{\xi}_i \cdot \boldsymbol{\nabla} f_i = -\frac{1}{\tau} \left(f_i - f_i^{(0)} \right) + G_i . \qquad (7.90)
$$

The different moments used to describe the hydrodynamic variables are no longer computed as integrals over the infinite velocity set, but as weighted sums over the finite number of discrete velocities that corresponds to the number of local quadrature nodes

$$
\rho = \sum_{i=0}^{P-1} f_i , \qquad (7.91a)
$$

$$
\rho \mathbf{v} = \sum_{i=0}^{P-1} \boldsymbol{\xi}_i f_i , \qquad (7.91b)
$$

$$
\rho K_E = \frac{1}{2} \sum_{i=0}^{P-1} \boldsymbol{c}_i^2 f_i , \qquad (7.91c)
$$

$$
\boldsymbol{P} = \sum_{i=0}^{P-1} \boldsymbol{c}_i \boldsymbol{c}_i f_i , \qquad (7.91d)
$$

$$
\mathbf{q} = \frac{1}{2} \sum_{i=0}^{P-1} \boldsymbol{c}_i \boldsymbol{c}_i^2 f_i , \qquad (7.91e)
$$

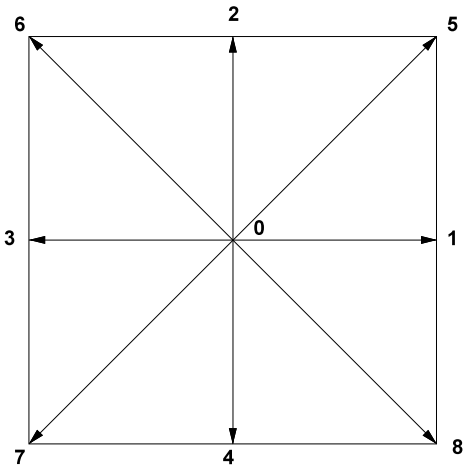

Fig. 7.1 D2Q9 velocity model for the Newtonian case

where $\mathbf{c}_i = \boldsymbol{\xi}_i - \mathbf{v}$ is the discrete microscopic velocity vector in the moving frame. Note that because of the renormalization of the Hermite basis, the viscosity, thermal diffusivity and the perfect gas law are given by

$$\mu_s = c_l^2 \rho \theta_B \tau, \quad \kappa = c_l^4 \rho \theta_B \tau, \quad p = c_l^2 \rho \theta_B \ . \tag{7.92}$$

The choice of the quadrature rule and the associated accuracy dictates the number of nodes to be used in order to exactly evaluate the Hermite coefficients, and depending on the physics of the problem, a different number of these coefficients will need to be computed exactly. In the incompressible case, $N = 2$ is needed, but in the thermal compressible case $N = 4$ is needed. Thus, for incompressible viscous fluids, as $N = 2$ is needed in the Hermite approximation, this implies three interpolation points. The 1D GH rule is therefore $Q^3_{1,5}$ (cf. the Appendix). The 2D and 3D extensions are the degree five quadratures (the standard lattices) $Q^9_{2,5}$ or $Q^{19}_{3,5}$. These quadrature rules are strongly linked to the geometrical or topological lattices $DxQy$. Figure 7.1 shows the $D2Q9$ arrangement of the nine velocities ξ_i, the node zero at the origin containing a particle at rest. More precisely, $\xi_0 = (0, 0)$, $\xi_1 = (1, 0)$, $\xi_2 = (0, 1)$, $\xi_3 = (-1, 0)$, $\xi_4 = (0, -1)$, $\xi_5 = (1, 1)$, $\xi_6 = (-1, 1)$, $\xi_7 = (-1, -1)$, $\xi_8 = (1, -1)$. The speed of sound is $c_s = 1/\sqrt{3}$ and the lattice weights are $w_0 = 4/9$, $w_{1,2,3,4} = 1/9$, $w_{5,6,7,8} = 1/36$.

Equation (7.90) is a linear advection-diffusion equation. Setting $f_i^{\mathrm{eq}} := f_i^{(0)} + \tau G_i$ the BGK Boltzmann equation is

$$\frac{\mathrm{d}f_i}{\mathrm{d}t} = -\frac{1}{\tau}\left(f_i - f_i^{\mathrm{eq}}\right) \ . \tag{7.93}$$

Integrating in time with a trapezoidal rule, yields for Eq. (7.93)

$$\overline{f}_i(\mathbf{x} + \boldsymbol{\xi}_i, t+1) - \overline{f}_i(\mathbf{x}, t) = -\frac{1}{\overline{\tau}}\left(\overline{f}_i(\mathbf{x}, t) - f_i^{\mathrm{eq}}(\mathbf{x}, t)\right) \ , \tag{7.94}$$

where

$$\overline{f}_i(\mathbf{x}, t) = f_i(\mathbf{x}, t) + \frac{1}{2\tau}\left(f_i(\mathbf{x}, t) - f_i^{\mathrm{eq}}(\mathbf{x}, t)\right) \tag{7.95}$$

is the new variable and the time step Δt is chosen equal to unity. The scheme in (7.94) is explicit with a modified relaxation time defined as

$$\overline{\tau} = \tau + \frac{1}{2} \,. \tag{7.96}$$

The use of the $\overline{f}_i(\mathbf{x}, t)$ slightly modifies the definition of the velocity in physical space which is now obtained from

$$\mathbf{v} = \overline{\mathbf{v}} + \frac{\mathbf{g}}{2} \,. \tag{7.97}$$

Dropping the overbar on both the relaxation time and the velocity distribution for ease of notation, the Navier-Stokes LBM approach can be summarized for isothermal flows (no temperature variation), $\theta_B = 1$, and incompressible fluids, so the cut-off value $N = 2$ is used in the Hermite approximation. From Eqs. (7.42a)–(7.42c) and (7.65a)–(7.65b), the Hermite coefficients are

$$a_0^{(0)} = \rho, \quad a_{0\alpha_1}^{(1)} = \rho v_{\alpha_1}, \quad a_{0\alpha_1\alpha_2}^{(2)} = \rho v_{\alpha_1} v_{\alpha_2} \,, \tag{7.98a}$$

$$a_1^{(0)} = 0, \quad a_{1\alpha_1}^{(1)} = 0, \quad a_{1\alpha_1\alpha_2}^{(2)} = -2\tau\rho S_{\alpha_1\alpha_2} \,. \tag{7.98b}$$

The contributions to Eq. (7.94), $f_i^{(0)}$, $f_i^{(1)}$ and G_i, are given by

$$f_i^{(0)} = w_i \rho \left(1 + \frac{\boldsymbol{\xi}_i \cdot \mathbf{v}}{c_l^2} + \frac{1}{2c_l^4} \mathcal{H}_{i\alpha_1\alpha_2}^{(2)} v_{\alpha_1} v_{\alpha_2} \right) \,, \tag{7.99a}$$

$$f_i^{(1)} = -\frac{w_i \rho}{c_l^2} \mathcal{H}_{i\alpha_1\alpha_2}^{(2)} S_{\alpha_1\alpha_2} \,, \tag{7.99b}$$

$$G_i = w_i \rho \left(\frac{\boldsymbol{\xi}_i - \mathbf{v}}{c_l^2} - \frac{(\boldsymbol{\xi}_i \cdot \mathbf{v}) \boldsymbol{\xi}_i}{c_l^4} \right) \cdot \mathbf{g} \,, \tag{7.99c}$$

where $\mathbf{v}$ is the physical velocity of Eq. (7.97), and the pressure tensor is given by

$$\boldsymbol{P}^{(0)} = c_l^2 \rho \boldsymbol{I}, \quad \boldsymbol{P}^{(1)} = -\frac{\tau}{2c_l^4} \boldsymbol{S} \,. \tag{7.100}$$

The numerical scheme is finally given by

$$f_i(\mathbf{x} + \boldsymbol{\xi}_i, t + 1) - f_i(\mathbf{x}, t) = -\frac{1}{\tau} \left(f_i(\mathbf{x}, t) - f_i^{(0)}(\rho, \mathbf{v}) \right) + \left(1 - \frac{1}{2\tau} \right) G_i \,. \tag{7.101}$$

The algorithm is split into two steps: collision and streaming (or propagation). Defining f_i^{in} and f_i^{out} as the f_i's before and after the collision, the two stages are

1. The collision:

$$f_i^{\text{out}}(\mathbf{x}, t) = f_i^{\text{in}}(\mathbf{x}, t) - \frac{1}{\tau} \left(f_i^{\text{in}}(\mathbf{x}, t) - f_i^{(0)}(\rho, \mathbf{v}) \right) + \left(1 - \frac{1}{2\tau} \right) G_i \,. \tag{7.102}$$

2. The propagation:

$$f_i^{\text{in}}(\mathbf{x} + \boldsymbol{\xi}_i, t + 1) = f_i^{\text{out}} \,. \tag{7.103}$$

Each step is applied to the whole system before the next one can start. The collision is a completely local operation while the propagation only communicates with a few neighbors. This "locality" of the scheme is particularly efficient for parallelization.

The reader will find in Yu et al. (2003) a review of the possibilities offered by LBM to tackle difficult applications as well as the discussion of the boundary conditions on solid walls which are traditionally handled by the bounce-back condition.

7.6 Multiple Relaxation Time Boltzmann Equation

For the sake of simplicity, let us assume that the force field vanishes, namely $\mathbf{g} = \mathbf{0}$. The Boltzmann equation (7.18) then becomes

$$\frac{\partial f}{\partial t} + \boldsymbol{\xi} \cdot \frac{\partial f}{\partial \boldsymbol{x}} = \mathcal{C}[f, f] \,. \tag{7.104}$$

7.6.1 Linearized Boltzmann Equation

In order to build a multiple relaxation time (MRT) model, the collision operator is first linearized. Cercignani (1988) proposed to expand the pdf f as a series expressed with the small parameter ϵ as

$$f = \sum_{n=0}^{\infty} \epsilon^n \, f^{(n)} \,, \tag{7.105}$$

so that the collision operator becomes

$$\mathcal{C}[f, f] = \sum_{n=0}^{\infty} \epsilon^n \sum_{k=0}^{n} \mathcal{C}[f^{(k)}, f^{(n-k)}] := \sum_{n=0}^{\infty} \epsilon^n \mathcal{C}^{(n)} \,. \tag{7.106}$$

Since the equilibrium pdf implies $\mathcal{C}[f^{(0)}, f^{(0)}] = 0$, $\mathcal{C}^{(0)}$ vanishes, and the remainder is given by

$$\mathcal{C}^{(n)} = 2\mathcal{C}[f^{(0)}, f^{(n)}] + \sum_{k=1}^{n-1} \mathcal{C}[f^{(k)}, f^{(n-k)}] \,. \tag{7.107}$$

For ϵ small, the last term under the summation is negligible with respect to the first one. Setting $f^{(n)} = f^{(0)} h(\mathbf{x}, \boldsymbol{\xi}, t)$ (this last expression corresponds to approximate $f = f^{(0)}[1 + h]$), the collision operator (7.19) reduces to the linearized expression

$$\mathcal{L}h := 2(f^{(0)})^{-1} \mathcal{C}[f^{(0)}, f^{(0)} h] = \int \mathbf{u} f^{(0)*} (h'^* + h' - h^* - h) \, \mathrm{d}S \mathrm{d}\boldsymbol{\xi}^* \,. \tag{7.108}$$

This linearized operator may be analyzed by analytical means, and the reader is referred to the paper by Gross and Jackson (1959) where the eigenvectors and eigenvalues are determined. As the $\mathcal{L}$ operator is self-adjoint all the eigenvalues are nonpositive.

7.6.2 MRT Lattice Boltzmann Method

When discretized in the velocity space, the linearized Boltzmann equation produces the relationship

$$\partial_t f_i + \boldsymbol{\xi}_i \cdot \boldsymbol{\nabla} f_i = -\Omega_{ij}\left(f_j - f_j^{(0)}\right) , \tag{7.109}$$

where Ω_{ij} is the collision matrix coming from the collision operator, namely

$$\Omega_{ij} = \frac{\partial \mathcal{C}_i}{\partial f_j}\left(f^{(0)}\right) . \tag{7.110}$$

Note that the BGK method is recovered if $\boldsymbol{\Omega} = \boldsymbol{I}/\tau$. Expressed in lattice units, the numerical scheme integrating (7.109) can be written as

$$f_i(\mathbf{x} + \boldsymbol{\xi}_i, t+1) - f_i(\mathbf{x}, t) = -\Omega_{ij}\left(f_j - f_j^{(0)}\right) . \tag{7.111}$$

In matrix form, Eq. (7.111) can be written as

$$\underline{f}^{in} = \underline{f} - [\Omega]\left(\underline{f} - \underline{f}^{(0)}\right) \tag{7.112}$$

where $\underline{f}^{in}$ is a vector of q unknowns made of the $f_i(\mathbf{x} + \boldsymbol{\xi}_i, t+1)$ at the end of the streaming step.

Let us focus our attention on the matrix-vector product $[\Omega]\underline{f}$ and carry out a similarity transform such that as the matrix $[\Omega]$ is diagonalized, there exists a regular matrix $[M]$ made of the eigenvectors of $[\Omega]$ and a diagonal matrix $[\Lambda]$ made of its eigenvalues so that

$$[\Omega] = [M]^{-1}[\Lambda][M] . \tag{7.113}$$

Combining (7.112) and (7.113) leads to the relation

$$\underline{f}^{in} = \underline{f} - [M]^{-1}[\Lambda][M]\left(\underline{f} - \underline{f}^{(0)}\right) . \tag{7.114}$$

In a moment space representation, more precisely with quantities generated by the variable transformation $\underline{F} := [M]\underline{f}$, Eq. (7.114) becomes

$$\underline{F}^{in} = \underline{F} - [\Lambda]\left(\underline{F} - \underline{F}^{(0)}\right) . \tag{7.115}$$

The discrete approach of the MRT LBM was first proposed by d'Humières (1992). The moments are separated into two groups: the hydrodynamic moments that correspond to conserved variables like density, momentum and energy and the kinetic non-conserved moments. In the moment space, the base vectors $\boldsymbol{\xi}_i$ are constructed through a Gram-Schmidt orthogonalization procedure conducted in a carefully chosen order. Then the moments M_i are generated by projecting the population vector $\underline{F}$ onto the $\boldsymbol{\xi}_i$. These moments are related to physical quantities like the density, energy, components of momentum, components of the stress tensor, etc. The collision operator is built up in such a way that its eigenvectors are the M_i and the corresponding eigenvalues are the inverse of the relaxation times towards equilibrium. Therefore, the collision process is computed in the moment space spanned

by the eigenspace of the collision matrix. The P eigenvalues of the diagonalized $[\Omega]$ are in between 0 and 2 for stability and separation of scales, and the relaxation times of the non-conserved quantities are faster than the hydrodynamic time scales. The theoretical tools to investigate the best choice of the adjustable parameters of the generalized lattice Boltzmann equation (LBE) are given by Lallemand and Luo (2000) where the linear analysis of the LBE evolution operator is carried out. The generalized hydrodynamics of the LBE model provides the user with some deep insight into dispersion, dissipation, isotropy and stability of the model. It is shown that the separate relaxations for the kinetic modes improves the stability with respect to the LBM BGK model.

In recent years, MRT-LB models have been proposed (Bouzidi et al. 2001; d'Humières et al. 2001, 2002) for rectangular grids and three-dimensional computations. The related three-dimensional velocity models are the D3Q13 by d'Humières et al. (2001), the D3Q15 and D3Q19 by d'Humières et al. (2002). Dellar (2003) introduced "ghost" variables and using them produces an MRT-LB model.

7.7 LBM for Viscoelastic Fluids

MRT-LB models are able to produce non-Newtonian models and linear viscoelastic fluids (Giraud et al. 1997, 1998; Wagner et al. 2000; Lallemand et al. 2003). The paper by Lallemand et al. (2003) gives the state-of-the-art of MRT-LBM applied to viscoelastic fluids. A major assumption of the MRT line of reasoning, namely that the tensors related to the stresses are traceless is not met in general for viscoelastic fluids. However the stress is indeed traceless in linear viscoelasticity and therefore the MRT approach reproduces the linear Jeffreys model

$$\boldsymbol{\Xi} + \lambda_1 \frac{D\boldsymbol{\Xi}}{Dt} = 2\mu_1 \left(\boldsymbol{D} + \lambda_2 \frac{D\boldsymbol{\Xi}}{Dt} \right). \tag{7.116}$$

Kehrwald (2005) combines a Cross model for the viscosity of a shear-thinning fluid and a 3D MRT-LBM with good results for a simple benchmark problem. Then the molding of a liquid composite is simulated and results are compared with experiments. The LBM demonstrates real capabilities to solve the industrial problem.

More recently, several papers addressed the LBM counterpart of the Oldroyd-B and FENE-P continuous models (Onishi et al. 2005, 2006). The published numerical results do not yet allow for any firm conclusions on the ability of LBM to effectively deal with strongly non-linear viscoelastic effects. In the next section, a methodology is developed that allows for full incorporation of the viscoelastic configuration tensor. To this end, an advection-diffusion model with a source term is developed (see Guo et al. 2002; Latt 2007; Chopard et al. 2009, for further details and applications).

7.7.1 Advection-Diffusion Equation with a Source Term

The BGK equation is modified by adding an "external source" term $\mathcal{S}_\mathrm{e}$

$$\partial_t f + \boldsymbol{\xi}\cdot\boldsymbol{\nabla} f = -\frac{1}{\tau}\left(f - f^{(0)}\right) + \frac{1}{\rho}\mathcal{S}_\mathrm{e} f \ . \tag{7.117}$$

It is assumed that the momentum flux, $\mathbf{j}$, computed from f is different from that computed by $f^{(0)}$, i.e. $\mathbf{j} = \int \mathrm{d}\boldsymbol{\xi}\,\boldsymbol{\xi} f \neq \int \mathrm{d}\boldsymbol{\xi}\,\boldsymbol{\xi} f^{(0)}$. Carrying through the same procedure as in Sect. 7.1.3 applied to Eq. (7.117), the generic mass conservation equation obtained with $\mathcal{A} = 1$ is

$$\partial_t \rho + \boldsymbol{\nabla}\cdot\mathbf{j} = \mathcal{S}_\mathrm{e} \ . \tag{7.118}$$

In order to evaluate $\mathbf{j}$, a Chapman-Enskog expansion needs to be performed. The Maxwell-Boltzmann equilibrium distribution $f^{(0)}$ is expanded up to order one in Hermite polynomials

$$f^{(0)} = \omega(\boldsymbol{\xi})\left(\rho + \boldsymbol{\xi}\cdot(\rho\mathbf{v})\right) \ . \tag{7.119}$$

Replacing f by $f^{(0)}$ in Eq. (7.117) and projecting on the Hermite basis, one gets

$$\partial_t \boldsymbol{a}_0^{(n)} + \boldsymbol{\nabla}\cdot\boldsymbol{a}_0^{(n+1)} + \left(\boldsymbol{\nabla}\boldsymbol{a}_+^{(n-1)}\mathrm{perm}\right) = \frac{\mathcal{S}_\mathrm{e}}{\rho}\boldsymbol{a}_0^{(n)} \ , \tag{7.120}$$

with the usual meaning for "perm". For $n = 0$, a relation very similar to Eq. (7.51) is produced

$$\partial_t \rho + \boldsymbol{\nabla}\cdot(\rho\mathbf{v}) = \mathcal{S}_\mathrm{e} \ . \tag{7.121}$$

The multiscale decomposition (7.55) is used in Eq. (7.117) and is projected onto the Hermite basis in a similar way as for Eq. (7.60),

$$\partial_t \boldsymbol{a}_0^{(n)} + \boldsymbol{\nabla}\cdot\boldsymbol{a}_0^{(n+1)} + \left(\boldsymbol{\nabla}\boldsymbol{a}_0^{(n)} + \mathrm{perm}\right) = -\frac{1}{\tau}\boldsymbol{a}_1^{(n)} + \frac{\mathcal{S}_\mathrm{e}}{\rho}\boldsymbol{a}_0^{(n)} \ . \tag{7.122}$$

Because of the orthogonality properties of the Hermite polynomials, $a_0^{(n)}$ vanishes for $n \geq 2$. Therefore, for $n = 1$ Eq. (7.122) becomes

$$\begin{aligned} -\frac{1}{\tau}\boldsymbol{a}_1^{(1)} &= \partial_t \boldsymbol{a}_0^{(1)} + \boldsymbol{\nabla}\boldsymbol{a}_0^{(0)} - \frac{\mathcal{S}_\mathrm{e}}{\rho}\boldsymbol{a}_0^{(1)} \\ &= \partial_t(\rho\mathbf{v}) + \boldsymbol{\nabla}\rho - \mathcal{S}_\mathrm{e}\mathbf{v} \\ &= \rho\partial_t\mathbf{v} - \mathbf{v}\boldsymbol{\nabla}\cdot(\rho\mathbf{v}) + \boldsymbol{\nabla}\rho \ , \end{aligned} \tag{7.123}$$

where in the last line Eq. (7.121) is used. The flux $\mathbf{j} = \mathbf{j}^{(0)} + \mathbf{j}^{(1)}$ is therefore given by

$$\mathbf{j} = \rho\mathbf{v} - \tau\left(\rho\partial_t\mathbf{v} - \mathbf{v}\boldsymbol{\nabla}\cdot(\rho\mathbf{v})\right) \ . \tag{7.124}$$

The following macroscopic equation is eventually obtained

$$\partial_t \rho + \boldsymbol{\nabla}\cdot(\rho\mathbf{v}) = \mathcal{S}_\mathrm{e} + \kappa_p\boldsymbol{\nabla}^2\rho + \boldsymbol{\nabla}\cdot\left[\tau\left(\rho\partial_t\mathbf{v} - \mathbf{v}\boldsymbol{\nabla}\cdot(\rho\mathbf{v})\right)\right] \ , \tag{7.125}$$

where $\kappa_p = \tau$ represents the diffusivity coefficient. In comparison with the classical form of an advection-diffusion equation, the last term under the divergence operator in Eq. (7.125) is an extra contribution we will discuss later.

To discretize the velocity space using the Hermite-Galerkin method, the GH quadrature needs to be exact up to the third polynomial degree (see the Appendix). Following the same procedure as in Sect. 7.5, the equilibrium distribution function $f_i^{(0)}$ is given by

$$f_i^{(0)} = w_i \rho \left(1 + \frac{\boldsymbol{\xi}_i \cdot \mathbf{v}}{c_l^2}\right) , \tag{7.126}$$

and due to the rescaling of the quadrature abscissae, the coefficient $a_1^{(1)}$ is modified in the following way

$$a_1^{(1)} = -\tau \left(\rho \partial_t \mathbf{v} - \mathbf{v}\nabla \cdot (\rho \mathbf{v}) + c_l^2 \nabla \rho\right) . \tag{7.127}$$

As a consequence, the macroscopic Eq. (7.125) remains unchanged, but the diffusivity, κ_p is rescaled so that $\kappa_p = c_l^2 \tau$. Finally, the off-equilibrium distribution function, $f_i^{(1)}$ is reconstructed as

$$f_i^{(1)} = -\frac{w_i \tau}{c_l^2} \boldsymbol{\xi}_i \cdot \left(\rho \partial_t \mathbf{v} - \mathbf{v}\nabla \cdot (\rho \mathbf{v}) + c_l^2 \nabla \rho\right) . \tag{7.128}$$

To discretize Eq. (7.117) in time, the same procedure as in Sect. 7.5 is applied. For that purpose, an "effective equilibrium" distribution function is defined and given by

$$f_i^{\text{eq}} := f^{(0)} + \tau \frac{\mathcal{S}_\text{e}}{\rho} f_i^{(0)} . \tag{7.129}$$

With the change of variables of Eq. (7.95), this leads to the discrete equation

$$\begin{aligned} \overline{f}_i(\mathbf{x} + \boldsymbol{\xi}_i, t+1) - \overline{f}_i(\mathbf{x}, t) = &-\frac{1}{\overline{\tau}} \left(\overline{f}_i(\mathbf{x}, t) - f_i^{(0)}(\rho, \mathbf{v})\right) \\ &+ \left(1 - \frac{1}{2\overline{\tau}}\right) \frac{\mathcal{S}_\text{e}}{\rho} f_i^{(0)}(\rho, \mathbf{v}) , \end{aligned} \tag{7.130}$$

where $\overline{\tau} = \tau - 1/2$. The change of variable affects the diffusivity κ_p,

$$\kappa_p = c_l^2 \left(\overline{\tau} - \frac{1}{2}\right) , \tag{7.131}$$

and the computation of the physical density ρ

$$\rho = \overline{\rho} + \frac{\mathcal{S}_\text{e}}{2} . \tag{7.132}$$

The physical velocity $\mathbf{v}$ will not be computed by the advection-diffusion equation but will result as an external field determined by the solution of the Navier-Stokes equations, and will remain unaffected by the change of variables.

7.7.2 Computation of the Constitutive Equation

The evolution of each component of the conformation tensor $\boldsymbol{c}$ is obtained by a separate "advection-diffusion with source" lattice Boltzmann model. Defining $f_{i\alpha_1\alpha_2}$ as the distribution functions that describe the components of the conformation tensor, $c_{\alpha_1\alpha_2}$ and $\mathcal{S}_{e\alpha_1\alpha_2}$ the components of the source term, we set in a similar way as in Eq. (7.132)

$$c_{\alpha_1\alpha_2} = \sum_i f_{i\alpha_1\alpha_2} + \frac{\mathcal{S}_{e\alpha_1\alpha_2}}{2} \,. \tag{7.133}$$

We the rewrite the equilibrium distribution function as

$$f^{(0)}_{i\alpha_1\alpha_2} = c_{\alpha_1\alpha_2}\left(1 + \frac{\boldsymbol{\xi}_i \cdot \mathbf{v}}{c_l^2}\right) \,. \tag{7.134}$$

The macroscopic equations are obtained by replacing ρ by $c_{\alpha_1\alpha_2}$ in (7.125)

$$\begin{aligned}\partial_t c_{\alpha_1\alpha_2} + (\mathbf{v}\cdot\boldsymbol{\nabla})c_{\alpha_1\alpha_2} = \kappa_p \boldsymbol{\nabla}^2 c_{\alpha_1\alpha_2} + \mathcal{S}_{e\alpha_1\alpha_2} \\ + \frac{\kappa_p}{c_l^2}\boldsymbol{\nabla}\cdot\left(c_{\alpha_1\alpha_2}\partial_t\mathbf{v} - \mathbf{v}\boldsymbol{\nabla}\cdot(c_{\alpha_1\alpha_2}\mathbf{v})\right) \,,\end{aligned} \tag{7.135}$$

where $\mathcal{S}_{e\alpha_1\alpha_2}$ depends on the constitutive equation. For the Oldroyd-B and the FENE-P models from Eqs. (5.113) and (5.152),

$$\mathcal{S}_{e\alpha_1\alpha_2} = -\frac{1}{\lambda}\left(c_{\alpha_1\alpha_2} - \delta_{\alpha_1\alpha_2}\right) + c_{\alpha_1\alpha_3}\partial_{\alpha_3}u_{\alpha_2} + \partial_{\alpha_3}u_{\alpha_1}c_{\alpha_3\alpha_2} \,, \tag{7.136a}$$

$$\mathcal{S}_{e\alpha_1\alpha_2} = -\frac{1}{\lambda}\left(hc_{\alpha_1\alpha_2} - b\delta_{\alpha_1\alpha_2}\right) + c_{\alpha_1\alpha_3}\partial_{\alpha_3}u_{\alpha_2} + \partial_{\alpha_3}u_{\alpha_1}c_{\alpha_3\alpha_2} \,, \tag{7.136b}$$

with the definitions

$$h = \frac{r_0^2}{r_0^2 - \{\boldsymbol{c}\}}, \quad b = \frac{r_0^2}{r_0^2 - 3} \,. \tag{7.137}$$

The comparison of (7.135) with (5.113) shows the presence of a "diffusive term" and two "error terms" in the macroscopic equation obtained from the Boltzmann equation. However El-Kareh and Leal (1989) showed that this diffusive term is present in real fluids, albeit very small. Therefore making the diffusivity very small ($\tau \to 1/2$) will also make the error terms negligible, and typically $\kappa_p/\mu_p \sim 10^{-6}$ is chosen.

For this advection-diffusion model, the Gauss-Hermite quadrature is only needed to be exact up to order three, so that only the D2Q5 or D3Q7 lattices (see the Appendix) are needed. As these two lattices are not standard, we give the associated microscopic velocities. For D2Q5, $\xi_0 = (0,0)$, $\xi_1 = (-1,0)$, $\xi_2 = (0,-1)$, $\xi_3 = (1,0)$, $\xi_4 = (0,1)$ and D3Q7, $\xi_0 = (0,0,0)$, $\xi_1 = (-1,0,0)$, $\xi_2 = (0,-1,0)$, $\xi_3 = (0,0,-1)$, $\xi_4 = (1,0,0)$, $\xi_5 = (0,1,0)$, $\xi_6 = (0,0,1)$. The D2Q5 speed of sound is $c_l = 1/\sqrt{3}$ and the lattice weights are $w_0 = 1/3$, $w_{1,2,3,4} = 1/6$, while the D3Q7 speed of sound is $c_l = 1/2$ and the lattice weights are $w_0 = 1/4$, $w_{1,2,3,4,5,6} = 1/8$.

7.7.3 Description of the Algorithm

The macroscopic equations that are solved are the incompressible solenoidal constraint, the governing generalized Navier-Stokes equations and the dynamic constitutive equation for the conformation tensor,

$$\nabla \cdot \mathbf{v} = 0 \,, \tag{7.138}$$

$$\partial_t \mathbf{v} + (\mathbf{v} \cdot \nabla)\mathbf{v} = -\nabla \cdot \left(-p\boldsymbol{I} + 2\mu_s \boldsymbol{S} - \boldsymbol{\Xi}_p\right) \,, \tag{7.139}$$

$$\partial_t \boldsymbol{c} + (\mathbf{v} \cdot \nabla)\boldsymbol{c} = -\frac{1}{\lambda}(\boldsymbol{c} - \boldsymbol{I}) + \boldsymbol{c}\boldsymbol{L} + \boldsymbol{L}^T\boldsymbol{c} \,. \tag{7.140}$$

The numerical algorithm evolves in a decoupled fashion such that the Navier-Stokes and the constitutive equations are solved independently at each time cycle. At time t the conformation tensor $\boldsymbol{c}$ is computed and converted into the viscoelastic stress tensor $\boldsymbol{\Xi}_p$ according to Eqs. (5.108) or (5.151). Then, using a second-order centered finite difference scheme, $\nabla \cdot \boldsymbol{\Xi}_p$ is evaluated and considered as a force that is sent to the Navier-Stokes equation according to Eq. (7.139). In turn, the velocity gradient is determined by a finite-difference scheme once the Navier-Stokes equations are solved for the velocity field and used as given data in the constitutive equations according to Eq. (5.113).

The computational algorithm of one time step is composed of four distinct operations. The first and the second steps compute the solution of the incompressible Navier-Stokes and of the constitutive equations (see Eqs. (7.138), (7.139) and (5.113)). The third step is a coupling between the bulk of the two schemes: the advection-diffusion process with source will receive the velocity field and the "source" term (see Eq. (7.136a))

$$\mathcal{S}_{e\alpha_1\alpha_2} = -\frac{1}{\lambda}\left(c_{\alpha_1\alpha_2} - \delta_{\alpha_1\alpha_2}\right) + c_{\alpha_1\alpha_3}\partial_{\alpha_3}u_{\alpha_2} + \partial_{\alpha_3}u_{\alpha_1}c_{\alpha_3\alpha_2} \,, \tag{7.141}$$

from the Navier-Stokes scheme, and the Navier-Stokes solver will receive the external forcing term

$$\rho\mathbf{g} = \nabla \cdot \boldsymbol{\Xi}_p = \nabla \cdot \left[-\frac{\mu_p}{\lambda}(\boldsymbol{c} - \boldsymbol{I})\right] \,, \tag{7.142}$$

computed from the advection-diffusion with the source scheme. A more detailed explanation of the procedure can be found below. For the sake of simplicity, the 2D case is discussed.

1. Collision and propagation of the advection-diffusion with source scheme (see Eq. (7.130))

$$f_{i\alpha_1\alpha_2}(\mathbf{x} + \boldsymbol{\xi}_i, t+1) = f_{i\alpha_1\alpha_2}(\mathbf{x}, t) - \frac{1}{\tau}\left(f_{i\alpha_1\alpha_2}(\mathbf{x}, t) - f^{(0)}_{i\alpha_1\alpha_2}(c_{\alpha_1\alpha_2}, \mathbf{v})\right) + \left(1 - \frac{1}{2\tau}\right)\frac{\mathcal{S}_{e\alpha_1\alpha_2}}{c_{\alpha_1\alpha_2}} f_i^{(0)}(c_{\alpha_1\alpha_2}, \mathbf{v}) \,. \tag{7.143}$$

2. Collision and propagation of the forced Navier-Stokes scheme (see Eq. (7.101))

$$f_i(\mathbf{x}+\boldsymbol{\xi}_i, t+1) - f_i(\mathbf{x}, t) = -\frac{1}{\tau}\left(f_i(\mathbf{x}, t) - f_i^{(0)}(\rho, \mathbf{v})\right) + \left(1 - \frac{1}{2\tau}\right) G_i \ , \tag{7.144}$$

with $\rho\mathbf{g} = \boldsymbol{\nabla} \cdot \boldsymbol{\Xi}_p$.

3. Coupling of the bulk of the two schemes. On the one hand, with the Navier-Stokes scheme, the velocity and its gradients that will be used for the computation of the equilibrium and the source of the advection-diffusion scheme, are computed. The velocity gradients are computed with a centered finite-difference scheme. On the other hand, the advection-diffusion scheme gives the conformation tensor, that is transformed into the viscoelastic stress tensor, $\boldsymbol{\Xi}_p$ by the relation

$$\boldsymbol{\Xi}_p = -\frac{\mu_1}{\lambda}(\boldsymbol{c} - \boldsymbol{I}) \ . \tag{7.145}$$

The divergence of $\boldsymbol{\Xi}_p$ is computed using a centered finite-difference scheme and $\rho\mathbf{g} = \boldsymbol{\nabla} \cdot \boldsymbol{\Xi}_p$ is transferred to the Navier-Stokes solver.

4. Coupling of the boundaries of the two schemes.

7.8 LBM for Turbulent Flows

Flows of engineering interest are often turbulent, and the LBM has made inroads into incompressible turbulent flow simulations, especially in phenomena associated with car aerodynamics. LBM is vulnerable to the same deficiencies as its Navier-Stokes counterpart. One such vulnerability being the inability to directly simulate high Reynolds number flows on a reasonable discretized system size. This is mainly due to the fact that the lattice size is about the same as the grid size in standard methods like finite differences, finite volumes or finite elements. Nevertheless, within the last decade there have been studies to assess the feasibility of performing both direct numerical simulations (DNS) and large eddy simulations (LES) within the LBM framework.

As with the Navier-Stokes DNS (NS-DNS) approach, the burden lies in being able to provide sufficient numerical accuracy and resolution in order to capture the important dynamics over a broad (spectral) range of scales. As with the counterpart Navier-Stokes over two decades ago, the starting point in assessing the capability of LBM-DNS are the homogeneous turbulent flows with and without shear. An early direct simulation of isotropic decaying turbulence (Yu et al. 2005b, 2005a) was able to replicate the correct kinetic energy power-law decay as well as the correct low-wavenumber energy spectrum scaling. Including non-inertial effects (which is introduced as a force term in the lattice Boltzmann equation) into the simulations, also resulted in the correct suppression of energy in the spectral cascade. For the homogeneous shear case (Yu and Girimaji 2005a), comparisons with NS-DNS (and experiment) for a variety of initial conditions and experiments validated the accuracy

of the LBM-DNS. These latter simulations have also been extended to the case of periodic homogeneous shear where both BGK-LBM and MRT-LBM have been used Yu and Girimaji (2006). In these cases of simple shear, grids on the order of 128^3 have been used with a D3Q19 lattice. Overall improved statistical results were obtained with the MRT model. Channel flow DNS using the BGK-LBM and the D3Q19 model have also been performed (Lammers et al. 2006); although, at low friction Reynolds numbers of 180. Nevertheless, an important aspect of the study was the validation of the accuracy of the LBM (BGK) statistical predictions relative to the usual pseudo-spectral predictions used in such flow fields.

As within the Navier-Stokes framework, where the large eddy simulation (LES) approach has emerged as a intermediary between direct simulation and averaged-based methodologies, within the LBM framework an LES based methodology can also be developed. The starting point is to apply a filtering operation as defined in Eq. (6.27) to the particle distribution function f in Eq. (7.104) to obtain

$$\frac{\partial \overline{f}}{\partial t} + \boldsymbol{\xi} \cdot \frac{\partial \overline{f}}{\partial \boldsymbol{x}} = \overline{\mathcal{C}[f, f]} = \mathcal{G} * \mathcal{C}[f, f] \,, \tag{7.146}$$

or, in a form that introduces a subgrid scale term, as (cf. Eq. (6.34))

$$\frac{D\overline{f}}{Dt} - \mathcal{C}[\overline{f}, \overline{f}] = \overline{\mathcal{C}[f, f]} - \mathcal{C}[\overline{f}, \overline{f}] \,, \tag{7.147}$$

where the right-side is the subgrid scale term (cf. Eq. (6.35)). Correspondingly, the filtered density and momentum are defined by the relations

$$\overline{\rho} = \int \overline{f} \, \mathrm{d}\boldsymbol{\xi}, \quad \overline{\rho \boldsymbol{v}} = \int \boldsymbol{\xi} \overline{f} \, \mathrm{d}\boldsymbol{\xi} \,. \tag{7.148}$$

Following the same rationale as in the development of the LBM for unfiltered variables, the LBM-BGK model is used for simplicity so that Eq. (7.147) then reduces to

$$\frac{D\overline{f}}{Dt} = -\frac{1}{\tau^*} \left(\overline{f} - \overline{f^{(0)}} \right) \,, \tag{7.149}$$

where

$$\overline{f^{(0)}} = \rho \left(\frac{m}{2\pi k_B \theta} \right)^{3/2} \exp\left(-\frac{m}{2k_B \theta} \overline{c}^2 \right) \neq \mathcal{G} * f^{(0)} \,, \tag{7.150}$$

with $\overline{c}^2 = \overline{\mathbf{c}} \cdot \overline{\mathbf{c}}$ ($\overline{\mathbf{c}} = \boldsymbol{\xi} - \overline{\mathbf{v}}$), and τ^* is the relaxation time scale characterizing the filtered model (and is the sum of the relaxation time associated with the molecular viscosity and the eddy viscosity). For the case of isotropic decaying turbulence, Yu et al. (2005a) found in comparison with LBM-DNS that the LBM-LES was able to capture the large scale motion; although, a smaller Smagorinsky constant ($C_s = 0.1$) than the NS-LES yielded better results (cf. Eq. (6.44)). Both BGK-LBE and MRT-LBE have been used in the LES of turbulent flows; although, some results in more complex turbulent flows, such as square and rectangular jets (Yu and Girimaji 2005b; Yu et al. 2006), suggest that the MRT formulation (see also Krafczyk et al. 2003) is necessary in order to obtain the required accuracy. Such jet studies

have involved grids on the order of 5×10^6 and have used a D3Q19 LBE model. Sagaut (2010) has surveyed both the adaptation of the subgrid scale eddy viscosity approach (Smagorinsky model, see Sect. 6.2.2.2) and the adaptation of the (scale similarity) approximate deconvolution approach (ADM) (see Sect. 6.2.2.2) for the LBM. Both BGK-LBE and MRT-LBE have been used in the LES of turbulent flows; although, in most cases the Smagorinsky model has been used to model the subgrid scales. An extensive additional discussion of the LBM-LES method for wall-bounded flows has been given by Premnath et al. (2009a, 2009b).

Appendix
Properties of the Hermite Polynomials

In this appendix, the properties of the Hermite polynomials are recapitulated with some results summarizing the work by Grad (1949a). First, the relations in the continuous case are given and then in the discretized case.

Continuous Case

In a D dimensional space, Rodrigues' formula gives the Hermite polynomial of degree n as a nth rank symmetric tensor whose components are

$$\mathcal{H}^{(n)}_{\alpha_1\ldots\alpha_n}(\boldsymbol{\xi}) := (-1)^n\, e^{\xi^2/2}\, \frac{\partial}{\partial \xi_{\alpha_1}} \ldots \frac{\partial}{\partial \xi_{\alpha_n}} e^{-\xi^2/2}\,, \tag{A.1}$$

or in vector and tensor notation,

$$\boldsymbol{\mathcal{H}}^{(n)}(\boldsymbol{\xi}) = \frac{(-1)^n}{\omega(\boldsymbol{\xi})} \boldsymbol{\nabla}^n_{\boldsymbol{\xi}} \omega(\boldsymbol{\xi})\,, \tag{A.2}$$

where the definition of the weight function $\omega(\boldsymbol{\xi})$ associated with the Hermite polynomials is

$$\omega(\boldsymbol{\xi}) = \frac{e^{-\xi^2/2}}{(\sqrt{2\pi})^D}\,, \tag{A.3}$$

with $\xi^2 = \boldsymbol{\xi}\cdot\boldsymbol{\xi}$.

Here, the Hermite polynomials up to order four will be used, and from the previous definitions, are readily given by

$$\mathcal{H}^{(0)} = 1\,, \tag{A.4a}$$

$$\mathcal{H}^{(1)}_{\alpha} = \xi_\alpha\,, \tag{A.4b}$$

$$\mathcal{H}^{(2)}_{\alpha_1\alpha_2} = \xi_{\alpha_1}\xi_{\alpha_2} - \delta_{\alpha_1\alpha_2}\,, \tag{A.4c}$$

$$\mathcal{H}^{(3)}_{\alpha_1\alpha_2\alpha_3} = \xi_{\alpha_1}\xi_{\alpha_2}\xi_{\alpha_3} - \left(\delta_{\alpha_1\alpha_2}\xi_{\alpha_3} + \delta_{\alpha_1\alpha_3}\xi_{\alpha_2} + \delta_{\alpha_2\alpha_3}\xi_{\alpha_1}\right)\,, \tag{A.4d}$$

M.O. Deville, T.B. Gatski, *Mathematical Modeling for Complex Fluids and Flows*,
DOI 10.1007/978-3-642-25295-2,

$$\mathcal{H}^{(4)}_{\alpha_1\alpha_2\alpha_3\alpha_4} = \xi_{\alpha_1}\xi_{\alpha_2}\xi_{\alpha_3}\xi_{\alpha_4} - \big(\delta_{\alpha_1\alpha_2}\xi_{\alpha_3}\xi_{\alpha_4} + \delta_{\alpha_1\alpha_3}\xi_{\alpha_2}\xi_{\alpha_4} + \delta_{\alpha_1\alpha_4}\xi_{\alpha_2}\xi_{\alpha_3} + \delta_{\alpha_2\alpha_3}\xi_{\alpha_1}\xi_{\alpha_4} + \delta_{\alpha_2\alpha_4}\xi_{\alpha_1}\xi_{\alpha_3} + \delta_{\alpha_3\alpha_4}\xi_{\alpha_1}\xi_{\alpha_2}\big) + \big(\delta_{\alpha_1\alpha_2}\delta_{\alpha_3\alpha_4} + \delta_{\alpha_1\alpha_3}\delta_{\alpha_2\alpha_4} + \delta_{\alpha_1\alpha_4}\delta_{\alpha_2\alpha_3}\big) \ . \tag{A.4e}$$

There exists a three-term recurrence relation between the polynomials

$$\xi_{\alpha_0}\mathcal{H}^{(n)}_{\alpha_1\ldots\alpha_n} = \mathcal{H}^{(n+1)}_{\alpha_0\ldots\alpha_n} + \sum_{i=1}^{n}\delta_{\alpha_0\alpha_i}\mathcal{H}^{(n-1)}_{\alpha_1\ldots\alpha_{i-1}\alpha_{i+1}\ldots\alpha_n} \ , \tag{A.5}$$

where the superscript is now explicitly retained to highlight the recursive nature of the relation. Using Eq. (A.3), the expression $\nabla_{\boldsymbol{\xi}}(\omega\boldsymbol{\mathcal{H}}^{(n)})$ can be rewritten as

$$\nabla_{\boldsymbol{\xi}}(\omega\boldsymbol{\mathcal{H}}^{(n)}) = (-1)^n\nabla^{n+1}_{\boldsymbol{\xi}}\omega = -\omega\boldsymbol{\mathcal{H}}^{(n+1)} \ . \tag{A.6}$$

The Hermite polynomials form an orthonormal basis in the Hilbert space of functions $f(\boldsymbol{\xi})$, with a scalar product defined by

$$(f,g) = \int fg\,\omega \mathrm{d}\boldsymbol{\xi} \ . \tag{A.7}$$

Denoting by $\boldsymbol{\alpha}$ the multi-index $\alpha_1\ldots\alpha_n$, the orthogonality property yields the identity

$$\int \omega(\boldsymbol{\xi})\boldsymbol{\mathcal{H}}^{(m)}_{\boldsymbol{\alpha}}(\boldsymbol{\xi})\boldsymbol{\mathcal{H}}^{(n)}_{\boldsymbol{\beta}}(\boldsymbol{\xi})d\boldsymbol{\xi} = \delta_{mn}\boldsymbol{\delta}^n_{\boldsymbol{\alpha\beta}} \ , \tag{A.8}$$

where $\boldsymbol{\delta}^n_{\boldsymbol{\alpha\beta}}$ is equal to one if the indices $\alpha_1\ldots\alpha_n$ are a permutation of $\beta_1\ldots\beta_n$, and in all other cases, $\boldsymbol{\delta}^n_{\boldsymbol{\alpha\beta}} = 0$.

Within the Galerkin framework, it is usual to approximate a regular function $f(\boldsymbol{\xi})$ by an infinite series in terms of the Hermite polynomials

$$f(\boldsymbol{\xi}) = \sum_{n=0}^{\infty}\boldsymbol{a}^{(n)}_{\boldsymbol{\alpha}}\boldsymbol{\mathcal{H}}^{(n)}_{\boldsymbol{\alpha}}(\boldsymbol{\xi}) \ , \tag{A.9}$$

or, in index notation,

$$f(\boldsymbol{\xi}) = a^{(0)}\mathcal{H}^{(0)} + a_{\alpha_1}\mathcal{H}^{(1)}_{\alpha_1} + a_{\alpha_1\alpha_2}\mathcal{H}^{(2)}_{\alpha_1\alpha_2} + a_{\alpha_1\alpha_2\alpha_3}\mathcal{H}^{(3)}_{\alpha_1\alpha_2\alpha_3} + \ldots \ . \tag{A.10}$$

Multiplying (A.9) by $\omega(\boldsymbol{\xi})\boldsymbol{\mathcal{H}}^{(n)}_{\boldsymbol{\beta}}(\boldsymbol{\xi})$ and integrating, the relation

$$\int \omega(\boldsymbol{\xi})f(\boldsymbol{\xi})\boldsymbol{\mathcal{H}}^{(n)}_{\boldsymbol{\beta}}(\boldsymbol{\xi})d\boldsymbol{\xi} = \boldsymbol{a}^{(n)}_{\boldsymbol{\alpha}}\boldsymbol{\delta}^n_{\boldsymbol{\alpha\beta}} = n!\,\boldsymbol{a}^{(n)}_{\boldsymbol{\beta}} \tag{A.11}$$

is obtained since there are $n!$ distinct permutations of the multi-index $\boldsymbol{i} = (i_1, i_2, \ldots, i_n)$ and $\boldsymbol{a}^{(n)}_{\boldsymbol{\alpha}}$ is symmetric.

It has been recognized over the last decade that from a numerical standpoint it is more stable to work with the Hermite functions $\omega(\boldsymbol{\xi})\boldsymbol{\mathcal{H}}^{(n)}(\boldsymbol{\xi})$ and to express the function f as

$$f(\boldsymbol{\xi}) = \omega(\boldsymbol{\xi})\sum_{n=0}^{\infty}\frac{1}{n!}\boldsymbol{a}^{(n)}\boldsymbol{\mathcal{H}}^{(n)}(\boldsymbol{\xi}) \ , \tag{A.12}$$

with the spectral coefficients then given by

$$\boldsymbol{a}^{(n)} = \int f(\boldsymbol{\xi})\boldsymbol{\mathcal{H}}^{(n)}(\boldsymbol{\xi})d\boldsymbol{\xi} \ . \tag{A.13}$$

Gauss-Hermite Quadrature Rule

In the discrete case one resorts to the Gauss-Hermite (GH) quadrature rule. The integral is replaced by a finite series of nodal values $f(\xi_i), i = 0, \ldots, M-1$ multiplied by the weights w_i. For the one-dimensional (1D) case, one has

$$\int_a^b \omega(\xi) f(\xi) d\xi \approx \sum_{k=0}^{M-1} w_i f(\xi_i) \ . \tag{A.14}$$

A theorem of numerical analysis on Gauss integration (cf. for example Deville et al. 2002) proves that the M point Gaussian quadrature is optimal when the quadrature nodes ξ_i are the roots of the M-th corresponding orthogonal polynomial p_M, and the weights are given by a normalized scalar product

$$w_i = \frac{(p_{M-1}, p_{M-1})}{p_{M-1}(\xi_i)p'_M(\xi_i)} \ , \tag{A.15}$$

where $p'_M = \mathrm{d}p_M/\mathrm{d}\xi$. With these relations, the Gaussian rule integrates exactly to a polynomial of degree $2M-1$. For the GH rule, the quadrature nodes are the zeroes of $\boldsymbol{\mathcal{H}}^{(n)}$. As the first derivative of (A.2) is

$$\frac{\mathrm{d}\mathcal{H}^{(n)}}{\mathrm{d}\xi} = \xi\mathcal{H}^{(n)} - \mathcal{H}^{(n+1)} = n\mathcal{H}^{(n-1)} \ , \tag{A.16}$$

with the help of (A.5), and using (A.8), the corresponding weights are

$$w_i = \frac{M!}{[M\mathcal{H}^{(M-1)}(\xi_i)]^2} \ . \tag{A.17}$$

For higher dimensions, the GH quadratures may be constructed as tensor products of the 1D rules as it is usually done in spectral methods. Other quadratures may be set up and the reader is referred to Shan et al. (2006) and Nie et al. (2008) for full details.

The Gauss-Hermite quadrature weights and abscissae for regular lattices up to exact algebraic degree of 9 are given for the two-dimensional and three-dimensional cases in Tables A.1 and A.2, respectively. The reader is referred to Abramowitz and Stegun (1972) for full mathematical and numerical details on 1D GH quadratures. The subscript *FS* represents a fully symmetric set of velocities. The quadrature rule $Q^P_{D,E}$ is defined in D space dimensions, is exact for a polynomial degree E, and involves P points or quadrature nodes. Note that for the one-dimensional case $D = 1$, $E = 2M-1$, $P = M$. The standard lattices for weakly compressible fluids are D2Q9, D3Q15, D3Q19 and D3Q27, which are nearest neighbors lattices, as well as extended neighborhood lattices that can be used for isothermal and (non iso-)

Table A.1 Gauss-Hermite quadrature formulae in two dimensions

Rule	Lattice	$\boldsymbol{\xi}_i$	w_i
$Q_{2,3}^5$	D2Q5	$(0,0)$	$1-2c_l^2$
		$(c_l,0)_{FS}$	$c_l^2/2$
			$c_l<\sqrt{1/2}$
$Q_{2,5}^7$	D2Q7	$(0,0)$	$1/2$
		$2(\cos\frac{n\pi}{3},\sin\frac{n\pi}{3})$	$1/12$
			$n=1,\ldots,6$
$Q_{2,5}^9$	D2Q9	$(0,0)$	$4/9$
		$(\sqrt{3},0)_{FS}$	$1/9$
		$(\pm\sqrt{3},\pm\sqrt{3})$	$1/36$
$Q_{2,7}^{17}$	D2Q17	$(0,0)$	$(575+193\sqrt{193})/8100$
		$(c_l,0)_{FS}$	$(5555-91\sqrt{193})/18000$
		$(\pm c_l,\pm c_l)$	$(655+17\sqrt{193})/27000$
		$(\pm 2c_l,\pm 2c_l)$	$(685-49\sqrt{193})/54000$
		$(3c_l,0)_{FS}$	$(1445-101\sqrt{193})/162000$
			$c_l=\sqrt{(125+5\sqrt{193})/72}$
$Q_{2,9}^{37}$	D2Q37	$(0,0)$	0.23315066913235250228650
		$(c_l,0)_{FS}$	0.10730609154221900241246
		$(\pm c_l,\pm c_l)$	0.05766785988879488203006
		$(2c_l,0)_{FS}$	0.01420821615845075026469
		$(\pm 2c_l,\pm 2c_l)$	0.00101193759267357547541
		$(3c_l,0)_{FS}$	0.00024530102775771734547
		$(c_l,2c_l)_{FS}$	0.00535304900051377523273
		$(c_l,3c_l)_{FS}$	0.00028341425299419821740
			$c_l=1.196979770393074358972 39$

thermal compressible fluids. Also we list the D2Q5 and D3Q7 lattices that do not have enough isotropy to correctly represent fluids, but are adequate for advection-diffusion schemes.

Discrete Case

The $\xi_i, i=1,\ldots,M$ of the GH quadrature rule must be rescaled in order to recover the standard formulation of the lattice Boltzmann method which is expressed on an equally spaced grid. This rescaling has the effect of modifying the discrete Hermite polynomials by the appearance of the coefficient c_l that is a lattice sound speed. In that way Eqs. (A.4a)–(A.4e) become

Table A.2 Gauss-Hermite quadrature formulae in three dimensions

Rule	Lattice	$\boldsymbol{\xi}_i$	w_i
$Q_{3,3}^{7}$	D3Q7	$(0,0,0)$	$1-3c_l^2$
		$(c_l,0,0)_{FS}$	$c_l^2/2$
			$c_l<\sqrt{1/3}$
$Q_{3,5}^{15}$	D3Q15	$(0,0,0)$	$2/9$
		$(\sqrt{3},0,0)_{FS}$	$1/9$
		$(\pm\sqrt{3},\pm\sqrt{3},\pm\sqrt{3})$	$1/72$
$Q_{3,5}^{19}$	D3Q19	$(0,0,0)$	$1/3$
		$(\sqrt{3},0,0)_{FS}$	$1/18$
		$(\sqrt{3},\sqrt{3},0)_{FS}$	$1/36$
$Q_{3,5}^{27}$	D3Q27	$(0,0,0)$	$8/27$
		$(\sqrt{3},0,0)_{FS}$	$2/27$
		$(\sqrt{3},\sqrt{3},0)_{FS}$	$1/54$
		$(\pm\sqrt{3},\pm\sqrt{3},\pm\sqrt{3})$	$1/216$
$Q_{3,7}^{39}$	D3Q39	$(0,0,0)$	$1/12$
		$(c_l,0,0)_{FS}$	$1/12$
		$(\pm c_l,\pm c_l,\pm c_l)$	$1/27$
		$(2c_l,0,0)_{FS}$	$2/135$
		$(2c_l,2c_l,0)_{FS}$	$1/432$
		$(3c_l,0,0)_{FS}$	$1/1620$
			$c_l=\sqrt{3/2}$
$Q_{3,9}^{121}$	D3Q121	$(0,0,0)$	0.03059162202948600642469
		$(c_l,0,0)_{FS}$	0.09851595103726339186467
		$\pm c_l,\pm c_l,\pm c_l$	0.02752500532563812386479
		$(c_l,2c_l,0)_{FS}$	0.00611102336683342432241
		$(2c_l,2c_l,0)_{FS}$	0.00042818359368108406618
		$(3c_l,0,0)_{FS}$	0.00032474752708807381296
		$(2c_l,3c_l,0)_{FS}$	0.00001431862411548029405
		$(\pm 2c_l,\pm 2c_l,\pm 2c_l)$	0.00018102175157637423759
		$(c_l,3c_l,0)_{FS}$	0.00010683400245939109491
		$(\pm 3c_l,\pm 3c_l,\pm 3c_l)$	0.00000069287508963860285
			$c_l=1.19697977039307435897239$

$$\mathcal{H}_i^{(0)} = 1 \,, \tag{A.18a}$$

$$\mathcal{H}_{i\alpha_1}^{(1)} = \xi_{i\alpha_1} \,, \tag{A.18b}$$

$$\mathcal{H}_{i\alpha_1\alpha_2}^{(2)} = \xi_{i\alpha_1}\xi_{i\alpha_2} - c_l^2\delta_{\alpha_1\alpha_2} \,, \tag{A.18c}$$

$$\mathcal{H}_{i\alpha_1\alpha_2\alpha_3}^{(3)} = \xi_{i\alpha_1}\xi_{i\alpha_2}\xi_{i\alpha_3} - c_l^2\left(\delta_{\alpha_1\alpha_2}\xi_{i\alpha_3} + \delta_{\alpha_1\alpha_3}\xi_{i\alpha_2} + \delta_{\alpha_2\alpha_3}\xi_{i\alpha_1}\right) \,, \tag{A.18d}$$

$$\begin{aligned}\mathcal{H}_{i\alpha_1\alpha_2\alpha_3\alpha_4}^{(4)} = {} & \xi_{i\alpha_1}\xi_{i\alpha_2}\xi_{i\alpha_3}\xi_{i\alpha_4} - c_l^2\left(\delta_{\alpha_1\alpha_2}\xi_{i\alpha_3}\xi_{i\alpha_4} + \delta_{\alpha_1\alpha_3}\xi_{i\alpha_2}\xi_{i\alpha_4}\right. \\ & \left. + \delta_{\alpha_1\alpha_4}\xi_{i\alpha_2}\xi_{i\alpha_3} + \delta_{\alpha_2\alpha_3}\xi_{i\alpha_1}\xi_{i\alpha_4} + \delta_{\alpha_2\alpha_4}\xi_{i\alpha_1}\xi_{i\alpha_3} + \delta_{\alpha_3\alpha_4}\xi_{i\alpha_1}\xi_{i\alpha_2}\right) \\ & + c_l^4\left(\delta_{\alpha_1\alpha_2}\delta_{\alpha_3\alpha_4} + \delta_{\alpha_1\alpha_3}\delta_{\alpha_2\alpha_4} + \delta_{\alpha_1\alpha_4}\delta_{\alpha_2\alpha_3}\right) \,.\end{aligned} \tag{A.18e}$$

The orthogonality of the basis vectors then leads to

$$\sum_i w_i \mathcal{H}_{\alpha_1\ldots\alpha_m}^{(m)} \mathcal{H}_{\beta_1\ldots\beta_n}^{(n)} = \delta_{mn} c_l^{2m}\left(\delta_{\alpha_1\beta_1}\cdots\delta_{\alpha_m\beta_n} + \text{perm}\right) \,, \tag{A.19}$$

where "perm" yields all the α_i permutations in the first index and β_i permutations in the second index of the $\delta_{\alpha_i\beta_i}$. In particular, for the non-vanishing products, we have

$$\sum_i w_i \mathcal{H}_i^{(0)}\mathcal{H}_i^{(0)} = 1 \,, \tag{A.20a}$$

$$\sum_i w_i \mathcal{H}_{i\alpha_1}^{(1)}\mathcal{H}_{i\alpha_2}^{(1)} = c_l^2\delta_{\alpha_1\alpha_2} \,, \tag{A.20b}$$

$$\sum_i w_i \mathcal{H}_{i\alpha_1\alpha_2}^{(2)}\mathcal{H}_{i\alpha_3\alpha_4}^{(2)} = c_l^4\left(\delta_{\alpha_1\alpha_3}\delta_{\alpha_2\alpha_4} + \delta_{\alpha_1\alpha_3}\delta_{\alpha_2\alpha_4}\right) \,, \tag{A.20c}$$

$$\begin{aligned}\sum_i w_i \mathcal{H}_{i\alpha_1\alpha_2\alpha_3}^{(3)}\mathcal{H}_{i\alpha_4\alpha_5\alpha_6}^{(3)} = {} & c_l^6\left[\delta_{\alpha_1\alpha_4}\left(\delta_{\alpha_2\alpha_5}\delta_{\alpha_3\alpha_6} + \delta_{\alpha_2\alpha_6}\delta_{\alpha_3\alpha_5}\right)\right. \\ & + \delta_{\alpha_1\alpha_5}\left(\delta_{\alpha_2\alpha_4}\delta_{\alpha_3\alpha_6} + \delta_{\alpha_2\alpha_6}\delta_{\alpha_3\alpha_4}\right) \\ & \left. + \delta_{\alpha_1\alpha_6}\left(\delta_{\alpha_2\alpha_4}\delta_{\alpha_3\alpha_5} + \delta_{\alpha_2\alpha_5}\delta_{\alpha_3\alpha_4}\right)\right] \,.\end{aligned} \tag{A.20d}$$

Finally, the expansion in Hermite polynomials of a discrete quantity f_i is

$$f_i = w_i \sum_{n=0}^{\infty} \frac{1}{c_l^{2n} n!} \mathcal{H}_i^{(n)} a^{(n)} \,, \tag{A.21}$$

where $a^{(n)} = \sum_i w_i \mathcal{H}_i^{(n)} f_i$ is the expansion coefficient of order n.

References

Abid R, Speziale CG (1993) Predicting equilibrium states with Reynolds stress closures in channel flow and homogeneous shear flow. Phys Fluids A 5:1776–1782

Abramowitz M, Stegun IA (1972) Handbook of mathematical functions with formulas, graphs, and mathematical tables, 10th edn. Wiley, New York

Alvelius K (1999) Studies of turbulence and its modelling through large eddy- and direct numerical simulation. PhD thesis, Department of Mechanics, KTH, Stockholm, Sweden

Astarita G (1979) Objective and generally applicable criteria for flow classification. J Non-Newton Fluid Mech 6:69–76

Astarita G, Marucci G (1974) Principles of non-Newtonian fluid mechanics. McGraw-Hill, Maidenhead

Balakrishnan R (2004) An approach to entropy consistency in second-order hydrodynamic equations. J Fluid Mech 503:201–245

Bardina J, Ferziger JH, Reynolds WC (1980) Improved subgrid scale models for large eddy simulation. Paper no. 80-1357, AIAA

Barnes HA, Hutton JF, Walters K (1987) An introduction to rheology. Wiley, New York

Batchelor GK (1953) Homogeneous turbulence. Cambridge University Press, Cambridge

Benjamin TB (1978) Bifurcation phenomena in steady flows of a viscous fluid. II. Philos Trans R Soc A 359:27–43

Beris AN, Edwards BJ (1994) Thermodynamics of flowing systems with internal microstructure. Oxford University Press, New York

Berselli LC, Iliescu T, Layton WJ (2006) Mathematics of large eddy simulation of turbulent flows. Springer, Berlin

Bhatnagar PL, Gross EP, Krook M (1954) A model for collision processes in gases. I. Small amplitude processes in charged and neutral one-component systems. Phys Rev 94:511–525

Bingham EC (1916) An investigation of the laws of plastic flow. US Bur Stand Bull 13:309–353

Bird RB, Armstrong RC, Hassager O (1987a) Dynamics of polymeric liquids, vol 1: Fluid mechanics. Wiley, New York

Bird RB, Curtiss CF, Armstrong RC, Hassager O (1987b) Dynamics of polymeric liquids, vol 2: Kinetic theory. Wiley, New York

Boger DV, Walters K (1993) Rheological phenomena in focus. Elsevier, Amsterdam

Botsis J, Deville M (2006) Mécanique des milieux continus: une introduction. Presses Polytechniques et Universitaires Romandes, Lausanne

Boussinesq J (1877) Essai sur la théorie des eaux courantes. Mém Acad Sci Inst Fr 23:46–50

Bouzidi M, d'Humières D, Lallemand P, Luo L-S (2001) Lattice Boltzmann equation on a two-dimensional rectangular grid. J Comput Phys 172:704–717

Burnett D (1935) The distribution of velocities and mean motion in a slight nonuniform gas. Proc Lond Math Soc 39:385–430

M.O. Deville, T.B. Gatski, *Mathematical Modeling for Complex Fluids and Flows*,
DOI 10.1007/978-3-642-25295-2, © Springer-Verlag Berlin Heidelberg 2012

Carreau PJ (1972) Rheological equations from molecular network theories. Trans Soc Rheol 16:99–127
Cercignani C (1988) The Boltzmann equation and its applications. Springer, Berlin
Chandrasekhar S (1943) Stochastic problems in physics and astronomy. Rev Mod Phys 15:1–89
Chapman S, Cowling TG (1960) The mathematical theory of nonuniform gases. Cambridge University Press, Cambridge
Chen S, Doolen GD (1998) Lattice Boltzmann method for fluid flows. In: Annual review of fluid mechanics. Annual Reviews, New York, pp 329–364
Chilcott MD, Rallison JM (1988) Creeping flow of dilute polymer solutions past cylinders and spheres. J Non-Newton Fluid Mech 29:381–432
Chopard B, Falcone J-L, Latt J (2009) The lattice Boltzmann advection-diffusion model revisited. Eur Phys J 171:245–249
Chou PY (1945) On velocity correlations and the solutions of the equations of turbulent fluctuation. Q Appl Math 3:38–54
Coleman B, Markowitz H, Noll W (1966) Viscometric flows of non-Newtonian fluids. Springer Tracts in Natural Philosophy, vol 5. Springer, Berlin
Coleman BD, Noll JM (1960) An approximation theorem for functionals, with applications in continuum mechanics. Arch Ration Mech Anal 6:355–370
Coleman BD, Noll JM (1961) Recent results in the continuum theory of viscoelastic fluids. Ann NY Acad Sci 89:672–714
Coles D (1965) Transition in circular Couette flow. J Fluid Mech 21:385–425
Collyer AA, Fischer PJ (1976) The Kaye effect revisited. Nature 261:682
Cormack DE, Leal LG, Seinfeld JH (1978) An evaluation of mean Reynolds stress turbulence models: the triple velocity correlation. J Fluids Eng 100:47–54
Craft TJ, Launder BE (1996) A Reynolds stress closure designed for complex geometries. Int J Heat Fluid Flow 17:245–254
Craft TJ, Launder BE (2002) Closure modelling near the two-component limit. In: Launder B, Sandham N (eds) Closure strategies for turbulent and transitional flows. Cambridge University Press, Cambridge, pp 102–126
Craft TJ, Launder BE, Suga K (1996) Development and application of a cubic eddy-viscosity model of turbulence. Int J Heat Fluid Flow 17:108–115
Craft TJ, Launder BE, Suga K (1997) Prediction of turbulent transitional phenomena with a nonlinear eddy-viscosity model. Int J Heat Fluid Flow 18:15–28
Cross MM (1965) Rheology of non-Newtonian fluids: a new flow equation for pseudo-plastic systems. J Colloid Sci 20:417–437
Crow SC (1967) Visco-elastic character of fine-grained isotropic turbulence. Phys Fluids 10:1587–1589
Crow SC (1968) Visco-elastic properties of fine-grained incompressible turbulence. J Fluid Mech 33:1–20
Cruz DOA, Pinho FT (2003) Modeling the new stress for improved drag reduction predictions of viscoelastic pipe flow. J Non-Newton Fluid Mech 114:109–148
Cruz DOA, Pinho FT, Resende PR (2004) Modeling the new stress for improved drag reduction predictions of viscoelastic pipe flow. J Non-Newton Fluid Mech 121:127–141
Daly BJ, Harlow FH (1970) Transport equations of turbulence. Phys Fluids 13:2634–2649
De Angelis E, Casciola CM, Piva R (2002) DNS of wall turbulence: dilute polymers and self-sustaining mechanisms. Comput Fluids 31:495–507
Deardorff JW (1970) Turbulence measurements in supersonic two-dimensional wake. J Fluid Mech 41:453–480
de Gennes PG (1971) Reptation of a polymer chain in the presence of fixed obstacles. J Chem Phys 55:572–579
Dellar PJ (2003) Incompressible limits of lattice Boltzmann equations using multiple relaxation times. J Comput Phys 190:351–370
den Toonder JMJ, Nieuwstadt FTM, Kuiken GDC (1995) The role of elongational viscosity in the mechanism of drag reduction by polymer additives. Appl Sci Res 54:95–123

Deville MO, Fischer PF, Mund EH (2002) High-order methods for incompressible fluid flow. Cambridge University Press, Cambridge
d'Humières D (1992) Generalized lattice-Boltzmann equations. In: Shizgal BD, Weaver DP (eds) Rarefied gas dynamics: theory and applications. Progress in astronautics and aeronautics, vol 159. AIAA, Washington, pp 450–458
d'Humières D, Bouzidi M, Lallemand P (2001) Thirteen-velocity three-dimensional lattice Boltzmann model. Phys Rev E 63:066702
d'Humières D, Ginzburg I, Krafczyk M, Lallemand P, Luo L-S (2002) Multiple-relaxation-time lattice Boltzmann models in three-dimensions. Philos Trans R Soc Lond A 360:437–451
Dimitropoulos CD, Sureshkumar R, Beris AN (1998) Direct numerical simulation of viscoelastic turbulent channel flow exhibiting drag reduction: effect of the variation of rheological parameters. J Non-Newton Fluid Mech 79:433–468
Dimitropoulos CD, Sureshkumar R, Beris AN, Handler RA (2001) Budgets of Reynolds stress, kinetic energy and streamwise enstrophy in viscoelastic turbulent channel flow. Phys Fluids 13(4):1016–1024
Dimitropoulos CD, Dubief Y, Shakfeh ESG, Moin P, Lele SK (2005) Direct numerical simulation of polymer-induced drag reduction in turbulent boundary layer flow. Phys Fluids 17:011705
Dimitropoulos CD, Dubief Y, Shakfeh ESG, Moin P (2006) Direct numerical simulation of polymer-induced drag reduction in turbulent boundary layer flow of inhomogeneous polymer solutions. J Fluid Mech 566:153–162
Doi M, Edwards SF (1978a) Dynamics of concentrated polymer systems, part 1. Brownian motion in the equilibrium state. J Chem Soc Faraday Trans 74:1789–1801
Doi M, Edwards SF (1978b) Dynamics of concentrated polymer systems, part 2. Molecular motion under flow. J Chem Soc Faraday Trans 74:1802–1817
Doi M, Edwards SF (1978c) Dynamics of concentrated polymer systems, part 3. The constitutive equation. J Chem Soc Faraday Trans 74:1818–1832
Doi M, Edwards SF (1979) Dynamics of concentrated polymer systems, part 4. Rheological properties. J Chem Soc Faraday Trans 75:38–54
Doi M, Edwards SF (1988) The theory of polymer dynamics. Oxford University Press, Oxford
Dubief Y, White CM, Terrapon VE, Shakfeh ESG, Moin P, Lele SK (2004) On the coherent drag-reducing and turbulence-enhancing behaviour of polymers in wall flows. J Fluid Mech 514:271–280
Durbin PA (1991) Near-wall turbulence closure modeling without 'damping functions'. Theor Comput Fluid Dyn 3:1–13
Durbin PA (1993) A Reynolds stress model for near-wall turbulence. J Fluid Mech 249:465–498
Durbin PA, Petterson Reif BA (2010) Statistical theory and modeling for turbulent flows, 2nd edn. Wiley, New York
El-Kareh AW, Leal LG (1989) Existence of solutions for all Deborah numbers for a non-Newtonian model modified to include diffusion. J Non-Newton Fluid Mech 33:257–287
Ericksen JL (1960) Transversely isotropic fluids. Kolloid Z 173:117–122
Eringen AC (1980) Mechanics of continua. Krieger, New York
Eyink L (1994) The renormalization group method in statistical hydrodynamics. Phys Fluids 6:3063–3078
Fasel HF, von Terzi DA, Sandberg RD (2006) A methodology for simulating compressible turbulent flows. J Appl Mech 73:405–412
Fattal R, Kupferman R (2004) Constitutive laws for the matrix-logarithm formulation of the conformation tensor. J Non-Newton Fluid Mech 123:281–285
Fenstermacher PR, Swinney HL, Gollub JP (1979) Dynamical instabilities and the transition to chaotic Taylor vortex flow. J Fluid Mech 94:103–128
Fosdick RL, Serrin J (1979) On the impossibility of linear Cauchy and Piola-Kirchhoff constitutive theories for stress in solids. J Elast 9:83–89
Frewer M (2009) More clarity on the concept of material frame-indifference in classical continuum mechanics. Acta Mech 202:213–246
Fu S, Launder BE, Tselepidakis DP (1987) Accommodating the effects of high strain rates in modelling the pressure-strain correlation. Technical report TFD/87/5, UMIST

Gatski TB (1996) Turbulent flows: model equations and solution methodology. In: Peyret R (ed) Handbook of computational fluid dynamics. Academic Press, London, pp 339–415
Gatski TB, Jongen T (2000) Nonlinear eddy viscosity and algebraic stress models for solving complex turbulent flows. Prog Aerosp Sci 36:655–682
Gatski TB, Speziale CG (1993) On algebraic stress models for complex turbulent flows. J Fluid Mech 254:59–78
Gatski TB, Wallin S (2004) Extending the weak-equilibrium condition for algebraic Reynolds stress models to rotating and curved flows. J Fluid Mech 518:147–155
Gatski TB, Rumsey CL, Manceau R (2007) Current trends in modelling research for turbulent aerodynamic flows. Philos Trans R Soc A 365:2389–2418
Germano M, Piomelli U, Moin P, Cabot WH (1991) A dynamic subgrid-scale eddy viscosity model. Phys Fluids A 3:1760–1765
Geurts BJ (2004) Elements of direct and large-eddy simulation. Edwards, Philadelphia
Giesekus H (1966) Die elastizität von flüssgkeiten. Rheol Acta 5:29–35
Giesekus H (1982) A simple constitutive equation for polymer fluids based on the concept of deformation-dependent tensorial mobility. J Non-Newton Fluid Mech 11:69–109
Giraud L, d'Humières D, Lallemand P (1997) A lattice-Boltzmann model for visco-elasticity. Int J Mod Phys C 8:805–815
Giraud L, d'Humières D, Lallemand P (1998) A lattice Boltzmann model for Jeffreys viscoelastic fluid. Europhys Lett 42:625–630
Girimaji SS (1996) Fully explicit and self-consistent algebraic Reynolds stress model. Theor Comput Fluid Dyn 8:387–402
Gordon RJ, Schowalter WR (1972) Anisotropic fluid theory: a different approach to the dumbbell theory of dilute polymer solutions. Trans Soc Rheol 16:79–97
Grad H (1949a) Note on the N-dimensional Hermite polynomials. Commun Pure Appl Math 2:325–330
Grad H (1949b) On the kinetic theory of rarefied gases. Commun Pure Appl Math 9:331–407
Green AI, Naghdi PM (1965) A general theory of an elastic-plastic continuum. Arch Ration Mech Anal 18:251–281
Groisman A, Steinberg V (2000) Elastic turbulence in a polymer solution flow. Nature 405:53–55
Groisman A, Steinberg V (2004) Elastic turbulence in curvilinear flows of polymer solutions. New J Phys 6:29. doi:10.1088/1367-2630/6/1/029
Gross EP, Jackson EA (1959) Kinetic models and the linearized Boltzmann equation. Phys Fluids 2:432–441
Guo Z, Shi B, Zheng C (2002) A coupled lattice BGK model for the Boussinesq equations. Int J Numer Methods Fluids 2:325–342
Hallbäck M, Groth J, Johansson AV (1990) An algebraic model for nonisotropic turbulent dissipation rate in Reynolds stress closures. Phys Fluids A 2:1859–1866
Hanjalić K (1994) Advanced turbulence closure models: a view of current status and future prospects. Int J Heat Fluid Flow 15:178–203
Hanjalić K, Jakirlić S (2002) Second-moment turbulence closure modelling. In: Launder B, Sandham N (eds) Closure strategies for turbulent and transitional flows. Cambridge University Press, Cambridge, pp 47–101
Hanjalić K, Launder BE (1972) A Reynolds stress model of turbulence and its application to thin shear flows. J Fluid Mech 52:609–638
Hanjalić K, Launder BE (1976) Contribution towards a Reynolds-stress closure for low-Reynolds-number turbulence. J Fluid Mech 74:593–610
Hanjalić K, Launder BE (2011) Modelling turbulence in engineering and the environment: second-moment routes to closure. Cambridge University Press, Cambridge
Harnoy A (1976) Stress relaxation in elastico-viscous lubricants in gears and rollers. J Fluid Mech 76:501–517
Hasimoto H, Sano O (1980) Stokeslet and eddies in creeping flow. Annu Rev Fluid Mech 12:335–363
Haworth DC, Pope SB (1986) A generalized Langevin model for turbulent flows. Phys Fluids 29:387–405

Herschel WH, Bulkley R (1926) Konsistenzmessungen von gummi-benzollösungen. Kolloid Z 39:291–300
Hinze JO (1959) Turbulence. McGraw-Hill, New York
Housiadas KD, Beris AN (2003) Polymer-induced drag reduction: effects of the variations in elasticity and inertia in turbulent viscoelastic channel flow. Phys Fluids 15:2369–2384
Housiadas KD, Beris AN, Handler RA (2005) Viscoelastic effects on higher order statistics and on coherent structures in turbulent channel flow. Phys Fluids 17:035106
Huang K (1987) Statistical mechanics, 2nd edn. Wiley, New York
Huilgol RR, Phan-Thien N (1997) Fluid mechanics of viscoelasticity. Elsevier, Amsterdam
Hulsen MA, van Heel APG, van den Brule BHAA (1997) Simulation of viscoelastic flows using Brownian configuration fields. J Non-Newton Fluid Mech 70:79–101
Ianniruberto G, Marrucci G (1996) On compatibility of the Cox–Merz rule with the model of Doi and Edwards. J Non-Newton Fluid Mech 65:241–246
Ianniruberto G, Marrucci G (2000) Convective orientational renewal in entangled polymers. J Non-Newton Fluid Mech 95:363–374
Ianniruberto G, Marrucci G (2001) A simple constitutive equation for entangled polymers with chain stretch. J Rheol 45:1305–1318
Itô K (1951) On stochastic differential equations. Mem Am Math Soc 4:1–51
Jakirlić S, Hanjalić K (2002) A new approach to modelling near-wall turbulence energy and stress dissipation. J Fluid Mech 459:139–166
James DF (2009) Boger fluids. In: Annual review of fluid mechanics. Annual Reviews, New York, pp 129–142
Jaumann G (1911) Geschlossenes system physikalischer und chemischer differentialgesefze. Sitz Zer Akad Wiss Wien 120:385–530
Jeffreys H (1965) Cartesian tensors. Cambridge University Press, Cambridge
Jeffreys H (1976) The earth: its origin, history and physical constitution, 6th edn. Cambridge University Press, Cambridge
Johansson AV, Hallbäck M (1994) Modelling of rapid pressure-strain in Reynolds-stress closures. J Fluid Mech 269:143–168
Jongen T, Gatski TB (1999) A unified analysis of planar homogeneous turbulence using single-point closure equations. J Fluid Mech 399:117–150
Jongen T, Gatski TB (2005) Tensor representations and solutions of constitutive equations for viscoelastic fluids. Int J Eng Sci 43:556–588
Joseph DD (1990) Fluid dynamics of viscoelastic liquids. Springer, Berlin
Jovanović J, Pashtrapanska M, Frohnapfel B, Durst F, Koskinen J, Koskinen K (2006) On the mechanism responsible for turbulent drag reduction by dilute addition of high polymers: theory, experiments, simulations and predictions. J Fluids Eng 128:118–130
Kampé de Fériet J, Betchov R (1951) Theoretical and experimental averages of turbulent functions. Proc K Ned Akad Wet 53:389–398
Kaye A (1963) A bouncing liquid stream. Nature 197:1001
Kehrwald D (2005) Lattice Boltzmann simulation of shear-thinning fluids. J Stat Phys 121:223–237
Keunings R (2004) Micro-macro methods for the multiscale simulation of viscoelastic flow using molecular models of kinetic theory. In: Rheology reviews 2004. British Society of Rheology, London, pp 67–98
Kim J, Moin P, Moser RD (1982) Numerical investigation of turbulent channel flow. J Fluid Mech 118:341–377
Kim J, Moin P, Moser RD (1987) Turbulence statistics in fully developed channel flow at low Reynolds number. J Fluid Mech 177:133–186
Kolmogorov AN (1941a) The local structure of turbulence in incompressible viscous fluid for very large Reynolds numbers. Dokl Akad Nauk SSSR 30:301–305
Kolmogorov AN (1941b) On degeneration of isotropic turbulence in an incompressible viscous fluid. Dokl Akad Nauk SSSR 31:538–541
Kolmogorov AN (1942) Equations of turbulent motion in an incompressible fluid. Izv Akad Nauk SSSR, Ser Fiz 6:56–58

Koschmieder EL (1993) Bénard cells and Taylor vortices. Cambridge University Press, Cambridge
Krafczyk M, Tölke J, Luo L-S (2003) Large-eddy simulations with a multiple-relaxation-time LBE model. Int J Mod Phys 17:33–39
Kraichnan RH (1964) Kolmogorov's hypothesis and Eulerian turbulence theory. Phys Fluids 7:1723–1734
Kreuzinger J, Friedrich R, Gatski TB (2006) Compressibility effects in the solenoidal dissipation rate equation: a priori assessment and modeling. Int J Heat Fluid Flow 27:696–706
Lallemand P, Luo L-S (2000) Theory of the lattice Boltzmann method: dispersion, dissipation, isotropy, Galilean invariance, and stability. Phys Rev E 61:6546–6562
Lallemand P, d'Humières D, Luo LS, Rubinstein R (2003) Theory of the lattice Boltzmann method: three-dimensional model for linear viscoelastic fluids. Phys Rev E 67:021203
Lammers P, Beronov KN, Volkert R, Brenner G, Durst F (2006) Lattice BGK direct numerical simulation of fully developed turbulence in incompressible plane channel flow. Comput Fluids 35:1137–1153
Larson RG (1988) Constitutive equations for polymer melts and solutions. Butterworth, Boston
Larson RJ (1983) Convection and diffusion of polymer network strands. J Non-Newton Fluid Mech 13:279–308
Latt J (2007) Hydrodynamic limit of lattice Boltzmann equations. PhD dissertation, University of Geneva, Geneva, Switzerland. http://www.unige.ch/cyberdocuments/theses2007/LattJ/meta.html
Launder BE, Reece GJ, Rodi W (1975) Progress in the development of a Reynolds-stress turbulence closure. J Fluid Mech 68:537–566
Lesieur M (2008) Turbulence in fluids, 4th edn. Springer, Dordrecht
Lesieur M, Métais O, Comte P (2005) Large-eddy simulations of turbulence. Cambridge University Press, Cambridge
Li CF, Gupta VK, Sureshkumar R, Khomami B (2006) Turbulent channel flow of dilute polymeric solutions: drag reduction scaling and an eddy viscosity model. J Non-Newton Fluid Mech 139:177–189
Lien FS, Leschziner MA (1995) Modelling 2D separation from a high lift aerofoil with a non-linear eddy-viscosity model and second-moment closure. Aeronaut J 99:125–144
Liepmann HW (1962) Free turbulence. In: Favre A (ed) Mécanique de la turbulence. Colloques Internationaux du CNRS, vol 108, pp 211–227
Likhtman AE, Graham RS (2003) Simple constitutive equation for linear polymer melts derived from molecular theory: Rolie-Poly equation. J Non-Newton Fluid Mech 114:1–12
Lilly DK (1966) On the application of the eddy-viscosity concept in the inertial sub-range of turbulence. Manuscript 123, NCAR
Lilly DK (1992) A proposed modification of the Germano subgrid-scale closure method. Phys Fluids A 4:633–635
Lozinski A, Owens RG, Phillips TN (2011) The Langevin and Fokker-Planck equations in polymer rheology. In: Ciarlet PG, Glowinski R, Xu J (eds) Numerical methods for non-Newtonian fluids. Handbook of numerical analysis. Elsevier, Amsterdam, pp 211–303
Lumley JL (1967) Rational approach to relations between motions of differing scales in turbulent flows. Phys Fluids 10:1405–1408
Lumley JL (1970a) Stochastic tools in turbulence. Academic Press, New York
Lumley JL (1970b) Toward a turbulent constitutive relation. J Fluid Mech 41:413–434
Lumley JL (1978) Computational modeling of turbulent flows. Adv Appl Mech 18:123–176
Lumley JL (1983) Turbulence modeling. J Appl Mech 50:1097–1103
Lumley JL, Khajeh-Nouri B (1974) Computational modeling of turbulent transport. In: Turbulent diffusion in environmental pollution. Academic Press, New York, pp 237–248
Lumley JL, Newman GR (1977) The return to isotropy of homogeneous turbulence. J Fluid Mech 82:161–178
Magnaudet J (1993) Modelling of inhomogeneous turbulence in the absence of mean velocity gradients. Appl Sci Res 51:525–531

Malaspinas O (2009) Lattice Boltzmann method for the simulation of viscoelastic fluid flows. PhD dissertation, number 4505. EPFL, Lausanne, Switzerland
Malaspinas O, Fiétier N, Deville M (2010) Lattice Boltzmann method for the simulation of viscoelastic fluid flows. J Non-Newton Fluid Mech 165:1637–1653
Manceau R, Hanjalić K (2000a) Elliptic blending model: a new near-wall Reynolds stress turbulence closure. Phys Fluids 14:744–754
Manceau R, Hanjalić K (2000b) A new form of the elliptic relaxation equation to account for wall effects in RANS modeling. Phys Fluids 12:2345–2351
Manceau R, Carlson JR, Gatski TB (2002) A rescaled elliptic relaxation approach: neutralizing the effect on the log layer. Phys Fluids 14:3868–3879
Marrucci G, Greco F, Ianniruberto G (2001) Integral and differential constitutive equations for entangled polymers with simple versions of CCR and force balance on entanglements. Rheol Acta 40:98–103
Marshall JS, Naghdi PM (1991) Consequences of the second law for a turbulent fluid flow. Contin Mech Thermodyn 3:65–77
McComb WD (1990) The physics of fluid turbulence. Clarendon, Oxford
McLeish TCB, Larson RG (1998) Molecular constitutive equations for a class of branched polymers: the pom-pom polymer. J Rheol 42:81–110
Mellor GL, Herring HJ (1973) A survey of the mean turbulent field closure models. AIAA J 11:590–599
Menter F (1994) Two-equation eddy-viscosity turbulence models for engineering applications. AIAA J 32:1598–1605
Milner ST, McLeish TCB, Likhtman AE (2001) Microscopic theory of convective constraint release. J Rheol 45:539–563
Min T, Yoo JY, Choi H, Joseph DD (2003) Drag reduction by polymer additives in a turbulent channel flow. J Fluid Mech 486:213–238
Mompean G (2002) On predicting abrupt contraction flows with differential and algebraic viscoelastic models. Comput Fluids 31:935–956
Mompean G, Thais L (2007) Assessment of a general equilibrium assumption for development of algebraic viscoelastic models. J Non-Newton Fluid Mech 145:41–51
Mompean G, Jongen T, Deville MO, Gatski TB (1998) On algebraic extra-stress models for the simulation of viscoelastic flows. J Non-Newton Fluid Mech 79:261–281
Mompean G, Thompson RL, Souza Mendes PR (2003) A general transformation procedure for differential viscoelastic models. J Non-Newton Fluid Mech 111:151–174
Mompean G, Thais L, Tomé MF, Castelo A (2011) Numerical prediction of three-dimensional time-dependent viscoelastic extrudate swell using differential and algebraic models. Comput Fluids 44:68–78
Monin AS, Yaglom AM (1971) Statistical fluid mechanics, vols 1 and 2. MIT Press, Boston
Morozov AN, van Saarloos W (2007) An introductory essay on subcritical instabilities and the transition to turbulence in visco-elastic parallel shear flows. Phys Rep 447:112–143
Moser RD, Kim J, Mansour NN (1999) Direct numerical simulation of turbulent channel flow up to $Re_\tau = 590$. Phys Fluids 11:943–945
Myong HK, Kasagi N (1990) Prediction of anisotropy of the near-wall turbulence with an anisotropic low-Reynolds-number k–ε turbulence model. J Fluids Eng 112:521–524
Nelson E (2001) Dynamical theories of brownian motion. Princeton University Press, Princeton. www.math.princeton.edu/~nelson/books/bmotion.pdf
Nie XB, Shan X, Chen H (2008) Galilean invariance of lattice Boltzmann models. Europhys Lett 81(3):34005 (6 pp)
Nisizima S, Yoshizawa A (1987) Turbulent channel and Couette flows using an anisotropic k–ε model. AIAA J 25:414–420
Noll W (1962) Motions with constant stretch history. Arch Ration Mech Anal 11:97–105
Noll W (1976) The representation of monotonous processes by exponentials. Indiana Univ Math J 25:209–214
Oberlack M (1997) Non-isotropic dissipation in non-homogeneous turbulence. J Fluid Mech 350:351–374

Oceni AG, Manceau R, Gatski TB (2010) Introduction of wall effects in explicit algebraic stress models through elliptic blending. In: Stanislas M, Jimenez J, Marusic I (eds) Progress in wall turbulence: understanding and modelling. Springer, Heidelberg, pp 275–283
Oldroyd JG (1950) On the formulation of rheological equations of state. Proc R Soc Lond Ser A 200:523–541
Oldroyd JG (1958) Non-Newtonian effects in steady motion of some idealized elastico-viscous liquids. Proc R Soc Lond Ser A 245:278–297
Onishi J, Chen Y, Ohashi H (2005) A lattice Boltzmann model for polymeric liquids. Prog Comput Fluid Dyn 5:75–84
Onishi J, Chen Y, Ohashi H (2006) Dynamic simulation of multi-component viscoelastic fluids using the lattice Boltzmann method. Physica A 362:84–92
Orlandi P (1995) A tentative approach to the direct simulation of drag reduction by polymers. J Non-Newton Fluid Mech 60:277–301
Orszag SA (1970) Analytical theories of turbulence. J Fluid Mech 41:59–82
Öttinger H-C (1996) Stochastic processes in polymeric fluids: tools and examples for developing simulation algorithms. Springer, Berlin
Owens RG, Phillips TN (2002) Computational rheology. Imperial College Press, London
Pennisi S (1992) On third order tensor-valued isotropic functions. Int J Eng Sci 30:679–692
Peterlin A (1966) Hydrodynamics of macromolecules in a velocity field with longitudinal gradient. J Polym Sci, Polym Phys 4:287–291
Peters GWM, Baaijens FPT (1997) Modelling of non-isothermal viscoelastic flows. J Non-Newton Fluid Mech 68:205–224
Phan-Thien N (2002) Understanding viscoelasticity basics of rheology. Springer, Berlin
Phan-Thien N, Tanner RI (1977) A new constitutive equation derived from network theory. J Non-Newton Fluid Mech 2:353–365
Pinho FT (2003) A GNF framework for turbulent flow models of drag reducing fluids and proposal for a k–ε type closure. J Non-Newton Fluid Mech 121:127–141
Pinho FT, Li CF, Younis BA, Sureshkumar R (2008a) A low Reynolds number turbulence closure for viscoelastic fluids. J Non-Newton Fluid Mech 154:89–108
Pinho FT, Sadanandan B, Sureshkumar R (2008b) One equation model for turbulent channel flow with second order viscoelastic corrections. Flow Turbul. Combust. doi:10.1007/s10494-008-9134-6
Pope SB (1975) A more general effective viscosity hypothesis. J Fluid Mech 72:331–340
Pope SB (2000) Turbulent flows. Cambridge University Press, Cambridge
Prandtl L (1945) Über ein neues formelsystem für die ausgebildete turbulenz. In: Nachr. Akad. Wiss. Göttingen. van den Loerck und Ruprecht, Göttingen, pp 6–19
Premnath KN, Pattison MJ, Banerjee S (2009a) Dynamic simulation of multi-component viscoelastic fluids using the lattice Boltzmann method. Physica A 388:2640–2658
Premnath KN, Pattison MJ, Banerjee S (2009b) Dynamic simulation of multi-component viscoelastic fluids using the lattice Boltzmann method. Phys Rev E 362:026703
Pruett CD (2000) On Eulerian times-domain filtering for spatial large-eddy simulation. AIAA J 38:1634–1642
Pruett CD, Gatski TB, Grosch CE, Thacker WD (2003) The temporally filtered Navier-Stokes equations: properties of the residual stress. Phys Fluids 15:2127–2140
Ptasinski PK, Boersma BJ, Nieuwstadt FTM, Hulsen MA, Van den Brule HAA, Hunt JCR (2003) Turbulent channel flow near maximum drag reduction: simulations, experiments and mechanisms. J Fluid Mech 490:251–291
Reiner M (1964) The Deborah number. Phys Today 62
Resende PR, Kim K, Younis BA, Sureshkumar R, Pinho FT (2011) A FENE-P k–ε turbulence model for low and intermediate regimes of polymer-induced drag reduction. J Non-Newton Fluid Mech 166:639–660
Reynolds O (1895) On the dynamical theory of incompressible viscous fluids and the determination of the criterion. Philos Trans R Soc Lond A 186:123–164
Reynolds WC (1976) Computation of turbulent flows. In: Annual review of fluid mechanics. Annual Reviews, New York, pp 183–208

Rivlin RS (1955) Further remarks on the stress-deformation relations for isotropic materials. J Ration Mech Anal 4:681–702
Rivlin RS (1957) The relation between the flow of non-Newtonian fluids and turbulent Newtonian fluids. Q Appl Math 15:212–215
Rivlin RS, Ericksen JL (1955) Stress-deformation relations for isotropic materials. Arch Ration Mech Anal 4:323–425
Rivlin RS, Smith GF (1975) On identities for 3×3 matrices. Rend Mat 8:348–353
Rodi W (1972) The prediction of free turbulent boundary layers by use of a two-equation model of turbulence. PhD thesis, University of London, London
Rodi W (1976) A new algebraic relation for calculating the Reynolds stresses. Z Angew Math Mech 56:219–221
Rotta JC (1951) Statistiche theorie nichthomogener turbulenz. Z Phys 129:547–572
Rubinstein R, Barton JH (1990) Nonlinear Reynolds stress models and the renormalization group. Phys Fluids A 2:1472–1476
Rubio P, Wagner MH (1999) Letter to the editor: A note added to Molecular constitutive equations or a class of branched polymers: the pom-pom polymer (J. Rheol., 42:81–110, 1998). J Rheol 43:1709–1710
Sadiki A, Hutter K (1996) On the frame dependence and form invariance of the transport equations for the Reynolds stress tensor and the turbulent heat flux vector: its consequences on closure models in turbulence modelling. Contin Mech Thermodyn 8:341–349
Saffman PG (1970) A model for inhomogeneous turbulence. Proc R Soc Lond Ser A 317:417–433
Sagaut P (2006) Large eddy simulation for incompressible flows. Springer, Berlin
Sagaut P (2010) Toward advanced subgrid models for lattice-Boltzmann-based large-eddy simulation: theoretical formulations. Comput Math Appl 59:2191–2199
Sagaut P, Cambon C (2008) Homogeneous turbulence dynamics. Cambridge University Press, Cambridge
Sagaut P, Deck S, Terracol M (2006) Multiscale and multiresolution approaches in turbulence. Imperial College Press, London
Sarkar S, Speziale CG (1990) A simple nonlinear model for the return to isotropy in turbulence. Phys Fluids 29:84–93
Schmid PJ, Henningson DS (2001) Stability and transition in shear flows. Springer, New York
Schumann U (1977) Realizability of Reynolds stress models. Phys Fluids 20:721–725
Schwarz WR, Bradshaw P (1994) Term-by-term tests of stress-transport turbulence models in a three-dimensional boundary layer. Phys Fluids 6:986–998
Shan X, Chen H (2007) A general multiple-relaxation-time Boltzmann collision model. Int J Mod Phys C 18:635–643. doi:10.1017/S0022112005008153
Shan X, Yuan X-F, Chen H (2006) Kinetic theory representation of hydrodynamics: a way beyond the Navier Stokes equation. J Fluid Mech 550:413–441. doi:10.1017/S0022112005008153
Shaqfeh ESG (1996) Purely elastic instabilities in viscometric flows. In: Annual review of fluid mechanics. Annual Reviews, New York, pp 129–185
Shih T-H, Zhu J, Lumley JL (1995) A new Reynolds stress algebraic equation model. Comput Methods Appl Mech Eng 125:287–302
Shir CC (1973) A preliminary numerical study of atmospheric turbulent flows in the idealized planetary boundary layer. J Atmos Sci 30:1327–1339
Shur ML, Spalart PR, Strelets MK, Travin AK (2008) A hybrid RANS-LES approach with delayed-DES and wall-modelled LES capabilities. Int J Heat Fluid Flow 29:1638–1649
Simonsen AJ, Krogstad P-Å (2005) Turbulent stress invariant analysis: clarification of existing terminology. Phys Fluids 17:088103
Sinha K, Candler GV (2003) Turbulent dissipation-rate equation for compressible flows. AIAA J 41:1017–1021
Sjögren T, Johansson AV (2000) Development and calibration of algebraic nonlinear models for terms in the Reynolds stress transport equations. Phys Fluids 12:1554–1572
Smagorinsky I (1963) General circulation experiments with the primitive equations. I. The basic experiment. Mon Weather Rev 91:99–164

Smith GF (1965) On isotropic integrity bases. Arch Ration Mech Anal 18:282–292
Smith GF (1994) Constitutive equations for anisotropic and isotropic materials. Mechanics and physics of discrete systems, vol 3. North Holland, Amsterdam
Smith GF, Younis BA (2004) Isotropic tensor-valued polynomial function of second-order and third-order tensors. Int J Eng Sci 43:447–456
So RMC, Lai YG, Zhang HS, Hwang BC (1991) Second-order near-wall turbulence closures: a review. AIAA J 29:1819–1835
So RMC, Aksoy H, Yuan SP, Sommer TP (1996) Modeling Reynolds-number effects in wall-bounded turbulent flows. J Fluids Eng 118:260–267
Spalart PR, Allmaras SR (1994) A one-equation turbulence model for aerodynamic flows. Rech Aérosp 1:5–21
Spalart PR, Jou W-H, Strelets M, Allmaras SR (1997) Comments on the feasibility of LES for wings, and on a hybrid RANS/LES approach. In: Liu C, Liu Z (eds) Advances in DNS/LES. Greyden Press, Columbus, pp 137–147
Spencer AJM (1965) Isotropic integrity bases for vectors and second-order tensors, part II. Arch Ration Mech Anal 18:51–82
Spencer AJM (1971) Theory of invariants. Academic Press, New York, pp 239–353
Spencer AJM (2004) Continuum mechanics. Dover, Mineola
Spencer AJM, Rivlin RS (1959) The theory of matrix polynomials and its application to the mechanics of isotropic continua. Arch Ration Mech Anal 2:309–336
Spencer AJM, Rivlin RS (1962) Isotropic integrity bases for vectors and second-order tensors, part I. Arch Ration Mech Anal 9:45–63
Speziale CG (1981) Some interesting properties of two-dimensional turbulence. Phys Fluids 24:1425–1427
Speziale CG (1987) On nonlinear k–l and k–ε models of turbulence. J Fluid Mech 178:459–475
Speziale CG (1991) Analytical methods for the development of Reynolds-stress closures in turbulence. In: Annual review of fluid mechanics. Annual Reviews, New York, pp 107–157
Speziale CG (1998a) A consistency condition for non-linear algebraic Reynolds stress models in turbulence. Int J Non-Linear Mech 33:579–584
Speziale CG (1998b) A review of material frame-indifference in mechanics. Appl Mech Rev 51:489–504
Speziale CG (1998c) Turbulence modeling for time-dependent RANS and VLES: a review. AIAA J 36:173–184
Speziale CG, Gatski TB (1997) Analysis and modelling of anisotropies in the dissipation rate of turbulence. J Fluid Mech 344:155–180
Speziale CG, Sarkar S, Gatski TB (1991) Modelling the pressure-strain correlation of turbulence: an invariant dynamical systems approach. J Fluid Mech 227:245-27
Stolz S, Adams NA (1999) An approximate deconvolution procedure for large-eddy simulation. Phys Fluids 11:1699–1701
Stolz S, Adams NA, Kleiser L (1999) The approximate deconvolution model applied to turbulent channel flow. In: Voke P, Sandham N, Kleiser L (eds) Direct and large eddy simulation III. Kluwer Academic, Dordrecht, pp 163–174
Stolz S, Adams NA, Kleiser L (2001a) An approximate deconvolution model for large-eddy simulation with application to wall-bounded incompressible flows. Phys Fluids 13:997–1015
Stolz S, Adams NA, Kleiser L (2001b) An approximate deconvolution model for large-eddy simulations of compressible flows and its application to shock-turbulent-boundary-layer interaction. Phys Fluids 13:2985–3001
Straatman AG (1999) A modified model for diffusion in second-moment turbulence closures. J Fluids Eng 121:747–756
Straatman AG, Stubley GD, Raithby GD (1998) Examination of diffusion modeling using zero-mean-shear turbulence. AIAA J 36:929–935
Succi S (2001) The lattice Boltzmann equation for fluid dynamics and beyond. Oxford University Press, Oxford
Succi S, Karlin IV, Chen H (2002) Colloquium: role of the H theorem in lattice Boltzmann hydrodynamic simulations. Rev Mod Phys 74:1203–1220

Sureshkumar R, Beris AN (1995) Effect of artificial stress diffusivity on the stability of numerical calculations and the dynamics of time-dependent viscoelastic flows. J Non-Newton Fluid Mech 60:53–80
Sureshkumar R, Beris AN, Handler RA (1997) Direct numerical simulation of the turbulent channel flow of a polymer solution. Phys Fluids 9:743–755
Tanner RI (1989) Engineering rheology. Clarendon, Oxford
Taulbee DB (1992) An improved algebraic Reynolds stress model and corresponding nonlinear stress model. Phys Fluids A 4:2555–2561
Taylor GI (1923) Stability of a viscous liquid contained between two rotating cylinders. Philos Trans R Soc A 223:289–343
Tennekes H, Lumley JL (1972) A first course in turbulence. MIT Press, Boston
Thais L, Tejada-Martínez AE, Gatski TB, Mompean G (2010) Direct and temporal large eddy numerical simulations of FENE-P drag reduction flows. Phys Fluids 22:013103. doi:10.1063/1.3294574
Thais L, Tejada-Martínez AE, Gatski TB, Mompean G (2011) A massively parallel hybrid scheme for direct numerical simulation of turbulent viscoelastic channel flow. Comput Fluids 43:134–142
Thrasher M, Jung S, Pang YK, Chuu C-P, Swinney H (2007) The bouncing jet: a Newtonian liquid rebounding off a free surface. Phys Rev E 76:056319
Tölke J, Krafczyk M, Schulz M, Rank E (2000) Discretization of the Boltzmann equation in velocity space using a Galerkin approach. Comput Phys Commun 129:91–99
Toms BA (1949) Some observations on the flow of linear polymer solutions through straight tubes at large Reynolds numbers. In: Proc. of the 1st international congress of rheology, vol 2, pp 135–141
Townsend AA (1956) The structure of turbulent shear flows. Cambridge University Press, Cambridge
Trouton FT (1906) On the coefficient of viscous traction and its relation to that of viscosity. Proc R Soc Lond Ser A 77:426–440
Truesdell C (1955) The simplest rate theory of pure elasticity. Commun Pure Appl Math 8:123–132
Truesdell C (1960) The principles of continuum mechanics. Colloquium lectures in pure and applied sciences, vol 5. Socony Mobil Oil Co, Fairfax County
Truesdell C (1965) Rational mechanics of deformation and flow. In: Proceedings of the 4th international congress on rheology. Wiley, New York
Truesdell C (1991) A first course in rational continuum mechanics, vol 1, 2nd edn. Academic Press, Boston
Truesdell C, Muncaster RG (1980) Fundamentals of Maxwell's kinetic theory of monatomic gas, treated as a branch of rational mechanics. Academic Press, New York
Truesdell C, Noll W (1992) The nonlinear field theories of mechanics, 2nd edn. Springer, Berlin
Truesdell C, Rajagopal KR (2000) An introduction to the mechanics of fluids. Birkhäuser, Boston
van Driest ER (1956) On turbulent flow near a wall. J Aeronaut Sci 23:1007–1011
Verbeeten WMH, Peters GWM, Baaijens FPT (2001) Differential constitutive equations for polymer melts: the extended pom-pom model. J Rheol 45:823–843
Versluis M, Blom C, van der Meer D, van der Weele K, Lohse D (2006) Leaping shampoo and the stable Kaye effect. J Stat Mech P07007
Wagner AJ, Giraud L, Scott CE (2000) Simulation of a cusped bubble rising in a viscoelastic fluid with a new numerical method. Comput Phys Commun 129:227–232
Wallin S, Johansson AV (2000) An explicit algebraic Reynolds stress model for incompressible and compressible turbulent flows. J Fluid Mech 403:89–132
Wang C-C (1965) A representation theorem for the constitutive equation of a simple material in motions with constant stretch history. Arch Ration Mech Anal 20:329–340
Wang C-C (1970) A new representation theorem for isotropic functions. Arch Ration Mech Anal 36:166–223
Warner HR (1972) Kinetic theory and rheology of dilute suspensions of finitely extendible dumbbells. Ind Eng Chem Fundam 11:379–387

Wilcox DC (2006) Turbulence modeling for CFD, 3rd edn. DCW Industries, La Cañada
Wilson HJ (2011) Graduate lectures on polymeric fluids. University College of London, London. http://www.ucl.ac.uk/~ucahhwi/GM05/index.html
Wilson KG (1971) Renormalization group and critical phenomena. 1. Renormalization group and Kadanoff scaling picture. Phys Rev B 4:3174–3183
Wolf-Gladrow DA (2000) Lattice-gas cellular automata and lattice Boltzmann models: an introduction. Lecture notes in mathematics, vol 1725. Springer, Berlin
Woods LC (1993) An introduction to the kinetic theory of gases and magnetoplasmas. Oxford University Press, Oxford
Yakhot A, Orszag SA, Yakhot V, Israeli M (1989) Renormalisation group formulation for large-eddy simulation. J Sci Comput 4:139–159
Yakhot A, Orszag SA, TB Gatski ST, Speziale CG (1992) Development of turbulence models for shear flows by a double expansion technique. Phys Fluids A 4:1510–1520
Yakhot V, Orszag SA (1986) Renormalisation group analysis of turbulence. I. Basic theory. J Sci Comput 1:3–51
Yamamoto M (1956) Anisotropic fluid theory: a different approach to the dumbbell theory of dilute polymer solutions. J Phys Soc Jpn 11:413–421
Ying R, Canuto VM (1996) Turbulence modeling over two-dimensional hills using an algebraic Reynolds stress expression. Bound-Layer Meteorol 77:69–99
Yoshizawa A (1984) Statistical analysis of the deviation of the Reynolds stress from its eddy-viscosity representation. Phys Fluids 27:1377–1387
Younis BA, Gatski TB, Speziale CG (2000) Towards a rational model for the triple velocity correlations of turbulence. Proc R Soc Lond A 456:909–920
Yu H, Girimaji SS (2005a) DNS of homogeneous shear turbulence revisited with the lattice Boltzmann method. J Turbul 6:N6. doi:10.1080/14685240500103200
Yu H, Girimaji SS (2005b) Near-field turbulent simulations of rectangular jets using lattice Boltzmann method. Phys Fluids 17:125106
Yu H, Girimaji SS (2006) Direct numerical simulations of homogeneous turbulence subject to periodic shear. J Fluid Mech 566:117–151
Yu H, Mei R, Luo L-S, Shyy W (2003) Viscous flow computations with the method of lattice Boltzmann equations. Prog Aerosp Sci 39:329–367
Yu H, Girimaji SS, Luo L-S (2005a) DNS and LES of decaying isotropic turbulence with and without frame rotation using the lattice Boltzmann method. J Comput Phys 209:599–616
Yu H, Girimaji SS, Luo L-S (2005b) Lattice Boltzmann simulations of decaying homogeneous isotropic turbulence. Phys Rev E 71:061708
Yu H, Luo L-S, Girimaji SS (2006) LES of turbulent square jet flow using an MRT lattice Boltzmann model. Comput Fluids 35:957–965

Index

M.O. Deville, T.B. Gatski, *Mathematical Modeling for Complex Fluids and Flows*,
DOI 10.1007/978-3-642-25295-2, © Springer-Verlag Berlin Heidelberg 2012